Max-Planck-Institut
für Kohlenforschung

technische universität
dortmund

# Molybdän- und Wolfram-Katalysatoren mit Tripodalen Liganden für die Alkin-Metathese

# &

# Isolierung eines homoleptischen Mo(V) Alkoxid Komplexes

## Dissertation

zur Erlangung des akademischen Grades

Doktor der Naturwissenschaften

(Dr. rer. nat.)

Fakultät für Chemie und Chemische Biologie

Technische Universität Dortmund

vorgelegt von

**M. Sc. Julius Vincent Hillenbrand**

geboren am 10.04.1994

in Nördlingen

Mülheim an der Ruhr, 2021

# Eidesstattliche Versicherung (Affidavit)

Hillenbrand, Julius Vincent
Name, Vorname
(Surname, first name)

208551
Matrikel-Nr.
(Enrolment number)

Belehrung:

Wer vorsätzlich gegen eine die Täuschung über Prüfungsleistungen betreffende Regelung einer Hochschulprüfungsordnung verstößt, handelt ordnungswidrig. Die Ordnungswidrigkeit kann mit einer Geldbuße von bis zu 50.000,00 € geahndet werden. Zuständige Verwaltungsbehörde für die Verfolgung und Ahndung von Ordnungswidrigkeiten ist der Kanzler/die Kanzlerin der Technischen Universität Dortmund. Im Falle eines mehrfachen oder sonstigen schwerwiegenden Täuschungsversuches kann der Prüfling zudem exmatrikuliert werden, § 63 Abs. 5 Hochschulgesetz NRW.

Die Abgabe einer falschen Versicherung an Eides statt ist strafbar.

Wer vorsätzlich eine falsche Versicherung an Eides statt abgibt, kann mit einer Freiheitsstrafe bis zu drei Jahren oder mit Geldstrafe bestraft werden, § 156 StGB. Die fahrlässige Abgabe einer falschen Versicherung an Eides statt kann mit einer Freiheitsstrafe bis zu einem Jahr oder Geldstrafe bestraft werden, § 161 StGB.

Die oben stehende Belehrung habe ich zur Kenntnis genommen:

Official notification:

Any person who intentionally breaches any regulation of university examination regulations relating to deception in examination performance is acting improperly. This offence can be punished with a fine of up to EUR 50,000.00. The competent administrative authority for the pursuit and prosecution of offences of this type is the chancellor of the TU Dortmund University. In the case of multiple or other serious attempts at deception, the candidate can also be unenrolled, Section 63, paragraph 5 of the Universities Act of North Rhine-Westphalia.

The submission of a false affidavit is punishable.

Any person who intentionally submits a false affidavit can be punished with a prison sentence of up to three years or a fine, Section 156 of the Criminal Code. The negligent submission of a false affidavit can be punished with a prison sentence of up to one year or a fine, Section 161 of the Criminal Code.

I have taken note of the above official notification.

Mülheim, 27.01.2021
Ort, Datum
(Place, date)

Unterschrift
(Signature)

Titel der Dissertation:
(Title of the thesis):

Molybdän- und Wolfram-Katalysatoren mit Tripodalen Liganden für die Alkin-Metathese & Isolierung eines homoleptischen Mo(V) Alkoxid Komplexes

Ich versichere hiermit an Eides statt, dass ich die vorliegende Dissertation mit dem Titel selbstständig und ohne unzulässige fremde Hilfe angefertigt habe. Ich habe keine anderen als die angegebenen Quellen und Hilfsmittel benutzt sowie wörtliche und sinngemäße Zitate kenntlich gemacht.
Die Arbeit hat in gegenwärtiger oder in einer anderen Fassung weder der TU Dortmund noch einer anderen Hochschule im Zusammenhang mit einer staatlichen oder akademischen Prüfung vorgelegen.

I hereby swear that I have completed the present dissertation independently and without inadmissible external support. I have not used any sources or tools other than those indicated and have identified literal and analogous quotations.

The thesis in its current version or another version has not been presented to the TU Dortmund University or another university in connection with a state or academic examination.*

*Please be aware that solely the German version of the affidavit ("Eidesstattliche Versicherung") for the PhD thesis is the official and legally binding version.

Mülheim, 27.01.2021
Ort, Datum
(Place, date)

Unterschrift
(Signature)

1. Berichterstatter: Prof. Dr. Alois Fürstner
2. Berichterstatter: Prof. Dr. Norbert Krause

Die vorliegende Arbeit entstand unter der Anleitung von Prof. Dr. Alois Fürstner in der Zeit von Januar 2018 bis Januar 2021 am Max-Planck-Institut für Kohlenforschung in Mülheim an der Ruhr. Teile dieser Arbeit wurden bereits in folgenden Beiträgen veröffentlicht:

J. Hillenbrand, M. Leutzsch, C. P. Gordon, C. Copéret, A. Fürstner, "$^{183}$W NMR Spectroscopy Guides the Search for Tungsten Alkylidyne Catalysts for Alkyne Metathesis", *Angew. Chem. Int. Ed.* **2020**, *59*, 21758–21768.

J. Hillenbrand, M. v. Gastel, E. Bill, F. Neese, A. Fürstner, "Isolation of a Homoleptic Non-Oxo Mo(V) Alkoxide Complex: Synthesis, Structure and Electronic Properties of Penta-*tert*-Butoxymolybdenum", *J. Am. Chem. Soc.* **2020**, 142, 38, 16392–16402.

J. Hillenbrand, M. Leutzsch, E. Yiannakas, C. P. Gordon, C. Wille, N. Nöthling, C. Copéret, A. Fürstner, "Canopy Catalysts" for Alkyne Metathesis: Molybdenum Alkylidyne Complexes with a Tripodal Ligand Framework" *J. Am. Chem. Soc* **2020**, *142*, 25, 11279-11294.

J. Hillenbrand, M. Leutzsch, A. Fürstner, "Molybdenum Alkylidyne Complexes with Tripodal Silanolate Ligands: The Next Generation of Alkyne Metathesis Catalysts" *Angew. Chem. Int. Ed.* **2019**, *58*, 15690.

Die praktischen Arbeiten entstanden zum Teil in Zusammenarbeit mit Dr. Takahiro Fukino, Nepomuk Korber, Christopher Rustemeier, Christian Wille und Ektoras Yiannakas. NMR-spektroskopische Messungen wurden in enger Zusammenarbeit mit Dr. Markus Leutzsch durchgeführt. Theoretische Berechnungen wurden in Zusammenarbeit mit Christopher Gordon und Prof. Dr. Christophe Copéret durchgeführt. UV/Vis, MCD, IR und EPR Spektroskopie und theoretische Berechnungen wurden in Zusammenarbeit mit Dr. Maurice van Gastel, Dr. Eckhard Bill und Prof. Dr. Frank Neese durchgeführt. Die Einkristallstrukturanalysen wurden von Nils Nöthling, Dr. Richard Goddard und Jörg Rust durchgeführt. Die beschriebenen Ergebnisse bilden eine vollständige Darstellung dieser gemeinsamen Arbeiten. Die von diesen Mitarbeitern alleinverantwortlich erzielten Ergebnisse wurden als solche an entsprechender Stelle vermerkt.

## Danksagung

An erster Stelle möchte ich meinem Doktorvater, Prof. Dr. Alois Fürstner, für das entgegengebrachte Vertrauen und die stetige Unterstützung bei dieser herausfordernden Dissertation bedanken. Dabei hat besonders die gestattete wissenschaftliche Freiheit und die exzellente Forschungsinfrastruktur des Instituts zum Erfolg dieser Arbeit als auch zu meiner persönlichen Weiterentwicklung beigetragen. Für die freundliche Übernahme des Koreferats danke ich Prof. Dr. Norbert Krause.

Für die erfolgreiche Zusammenarbeit auf dem Alkin-Metathese-Projekt danke ich Nepomuk Korber, Christopher Rustemeier, Christian Wille und Ektoras Yiannakas. Ein besonderer Dank geht an Dr. Markus Leutzsch, für die hervorragende NMR-spektroskopischen Untersuchungen und die enge Zusammenarbeit auf verschiedenen Projekten. Des Weiteren danke ich Dr. Eckhard Bill, Prof. Dr. Christophe Copéret, Dr. Maurice van Gastel, Dr. Chistopher P. Gordon, Dr. Alexander Haack, und Prof. Dr. Frank Neese für die erfolgreiche Zusammenarbeit auf mehreren spektroskopischen und theoretischen Projekten. Für die Durchführung und Auswertung zahlreicher Kristallstrukturanalysen danke ich Elke Dreher, Dr. Richard Goddard, Prof. Dr. Christian W. Lehmann, Nils Nöthling, Jörg Rust und Heike Schucht.

Ein besonderer Dank gilt allen Festangestellten der Abteilung Fürstner, namentlich Sebastian Auris, Andrea Bosserhoff, Roswitha Leichtweiß, Monika Lickfeld, Karin Radkowski, Christopher Rustemeier, Saskia Schulthoff und Christian Wille, für die tatkräftige Unterstützung bei administrativen als auch wissenschaftlichen Angelegenheiten. An dieser Stelle möchte ich allen Mitarbeitern des Instituts für die hilfsbereite Unterstützung danken.

Für die sorgfältige und zügige Korrektur dieser Arbeit möchte ich Tobias Biberger, Stephan Hess, Kyria Liendo Grau und Daniel Rütter meinen Dank aussprechen. Bei allen aktuellen und ehemaligen Mitgliedern der Arbeitsgruppe bin ich für die Hilfsbereitschaft und gute Arbeitsatmosphäre sehr dankbar. Insbesondere danke ich meinen langjährigen Büro- und Boxkollegen: Dr. Felix Anderl, Tobias Biberger, Dr. Lee R. Collins, Stephan Hess, Dr. John Murphy, Dr. Yonghoon Kwon, Lorenz Löffler, Dr. Sorin-Claudiu Rosca, Saskia Schulthoff, Simon Spohr, Dr. Bernhard Wölfl und Raphael Zachmann.

Mein ganz besonderer Dank gilt meiner Familie für die stetige Unterstützung und ihren Rückhalt während meiner Ausbildung. Ihnen möchte ich diese Arbeit widmen.

*Meiner Familie*

*“Imagination is more important than knowledge. Knowledge is limited. Imagination encircles the world.”*

**Albert Einstein**

## Zusammenfassung

Eine neue Generation an Molybdän-Alkylidin-Katalysatoren für die Alkinmetathese wurde entwickelt. Zuvor waren wohldefinierte Molybdän-Alkylidin-Katalysatoren mit einem tripodalen Ligandensystem nicht zugänglich, weshalb diese Arbeit einen wichtigen Meilenstein auf dem Gebiet der Alkinmetathese markiert. Ein neu entwickelter tripodaler Silanolatligand und eine verbesserte Komplexierungsmethode ermöglichen nun den Zugang zu diesen Katalysatoren im Gramm-Maßstab. Das modulare Liganden-Design bot die Möglichkeit verschiedene Katalysator Variationen herzustellen, um die wichtigen Parameter für die Katalyse zu untersuchen.

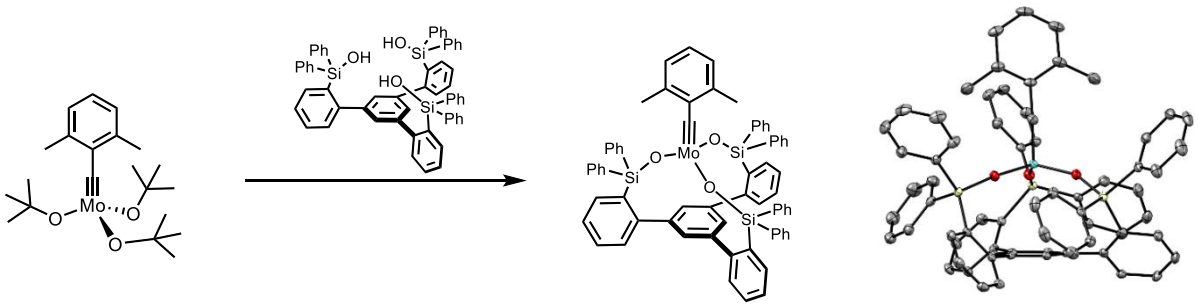

Eine systematische $^{95}$Mo-NMR Studie lieferte wertvolle Einblicke in die elektronische Struktur dieser Komplexe und erwies sich als sehr nützliche Methode für die Optimierung des Liganden- und Katalysatordesigns. Die chemische Verschiebungstensoranalyse des Alkylidin-Kohlenstoffatoms wies eine erhöhte Elektrophilie nach, die durch die tripodale Ligandensphäre vermittelt wird. Das Benchmarking der katalytischen Aktivität mit einer Reihe verschiedener Katalysatoren zeigte, dass der Komplex mit Methyl-substituierten tripodalen Silanolatliganden der aktivste Katalysator ist. Die Isolation eines Molybdän-Metallacyclobutadien-Komplexes mit Triphenylsilanolat-Liganden und eine umfangreiche Studie zur Bildung von Molybdän-Metallatetrahedranen mit tripodaler Ligandensphäre bewies, dass beide Intermediate reversibel zugänglich sind und miteinander im Gleichgewicht stehen. Darüber hinaus erzeugt die tripodale Ligandensphäre zwei verschiedene Molybdän-Metallacyclobutadienformen, die eine Pseudorotation für das Durchlaufen des katalytischen Zyklus benötigen. Die neu entwickelten Katalysatoren weisten eine unübertroffene Toleranz gegenüber funktionellen Gruppen auf, tolerierten protische Gruppen wie ungeschützte Alkohole, und zeigten sogar eine gewisse Stabilität gegenüber Wasser. Zusätzlich wurde das ausgezeichnete Anwendungsprofil an verschiedenen, herausfordernden Ringschluss-Alkinmetathese Reaktionen für die Naturstoffsynthese erfolgreich unter Beweis gestellt. Daher haben wir für die neu entwickelten Molybdän-Alkylidin-Katalysatoren die Bezeichnung „canopy catalysts“ eingeführt.

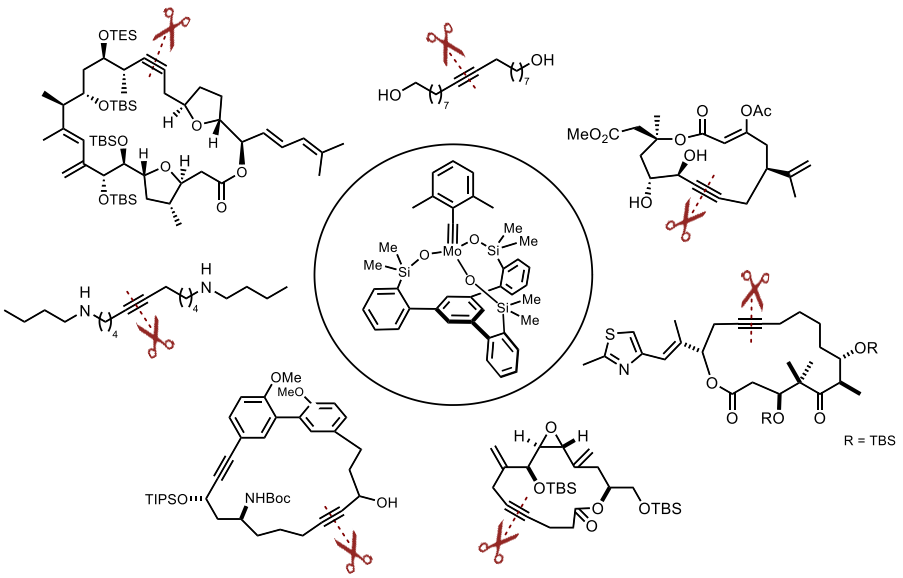

Im zweiten Teil dieser Arbeit haben wir eine Vielzahl an tripodalen Wolfram-Alkylidin-Komplexen hergestellt und dabei einen neuen Katalysator für die Alkinmetathese entwickelt, der den klassischen Schrock-Katalysator bei Weitem übertrifft. Eine detaillierte spektroskopische, kristallographische und theoretische Untersuchung dieser Wolfram-Alkylidin-Komplexe lieferte Einblicke in deren geometrische sowie elektronische Struktur. In diesem Kontext zeigte die $^{183}$W-NMR Spektroskopie eindrücklich, dass der tripodale Silanolatligand den Wolfram-Komplex besonders Lewis-sauer macht. Dadurch wird das Wolfram-Metallacyclobutadien-Intermediat soweit stabilisiert, dass die katalytische Aktivität zum Erliegen kommt.

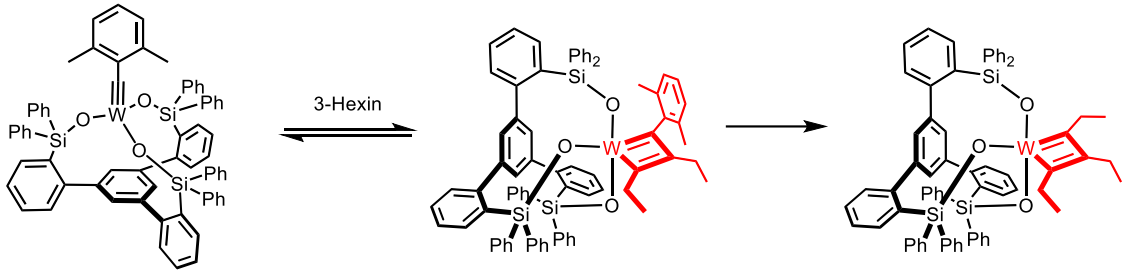


Alle hergestellten Wolfram Komplexe mit tripodalen Silanolatliganden oder auch literatur-bekannte Wolfram-Katalysatoren ergaben enttäuschende Ergebnisse bei einfachen Metathese-Testreaktionen. Die schwächeren Donoreigenschaften der Silanolatliganden führten am Wolframalkylidin nur zu geringer katalytischer Aktivität. Dies hat uns dazu verleitet, einen tripodalen Alkoxid-Liganden zu entwickeln, der durch Komplexierung den entsprechenden Wolfram Komplex in sehr guten Ausbeuten und im Gramm-Maßstab zugänglich macht. Dieser Wolfram Komplex übertrifft alle anderen getesteten Katalysatoren hinsichtlich Aktivität und Selektivität.

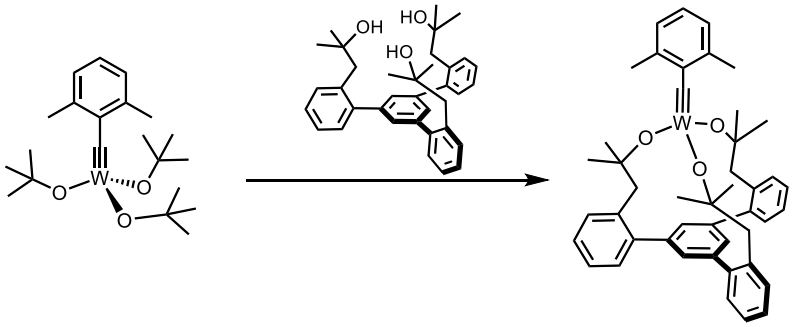

Im dritten Kapitel berichten wir über die Isolierung des ersten, monomeren, homoleptischen, fünffach koordinierten Alkoxid-Mo(V)-Komplexes. Hochvalente Molybdänkomplexe mit Alkoxid-Liganden sind dafür prädestiniert Molybdän-Oxo-Komplexe zu bilden und/oder zu dimerisieren. Der isolierte [Mo(O*t*Bu)$_5$] Komplex ist das erste Beispiel einer völlig neuen Klasse an hochvalenten Molybdänkomplexen. Ebenso ist es uns gelungen einen Molybdän-Nitrido-Komplex mit *tert*-Butoxid-Liganden zu isolieren. Vorhergehende Arbeiten zeigten, dass *tert*-Butoxid-Liganden niedervalente Mo(III)-Komplexe nicht ausreichend vor der konkurrierenden Dimerisierung schützen können, wodurch deren Reaktivität im Unbekannten blieb. Interessanterweise wird der Molybdän-Nitrido-Komplex durch die Aktivierung eines Acetonitril-Moleküls am Mo(III)-Alkoxid-Komplex gebildet.

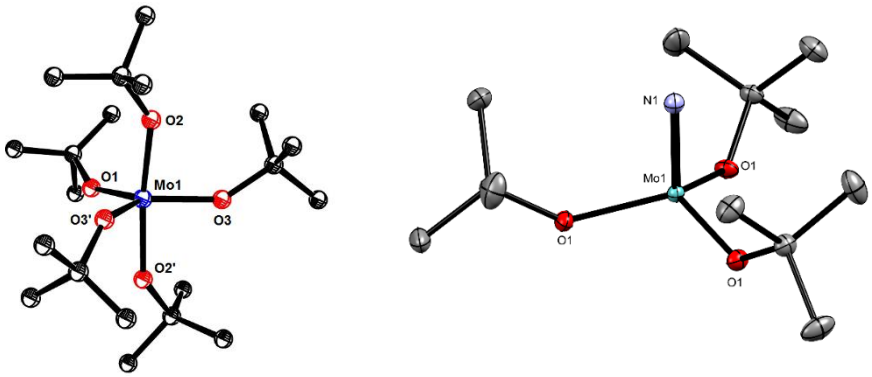

## Abstract

A new generation of molybdenum alkylidyne catalysts for alkyne metathesis is presented. Previously, well-defined molybdenum alkylidyne complexes with a tripodal ligand framework have been elusive. Therefore, this work marks an important milestone in the field of alkyne metathesis. A newly developed tripodal silanolate ligand and an improved complexation method gave access to these catalysts on scale. Moreover, the modular ligand design allowed us to prepare a library of different catalysts and to investigate the critical parameter for catalysis.

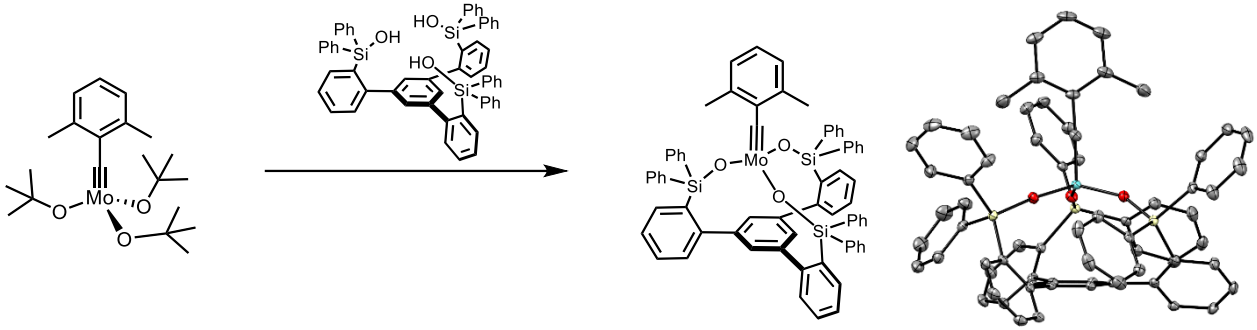

A systematic $^{95}$Mo NMR study provided valuable insights into the electronic structure of these complexes and turned out to be a very useful tool for catalyst design. Chemical shift tensor analysis of the alkylidyne carbon atom revealed an increased electrophilicity imparted by the tripodal ligand sphere. Benchmarking of the catalytic activity of a series of different catalysts showed that the catalyst with a methyl substituted silanolate ligand is by far the most active catalyst in the entire new series. Isolation of a molybdenacyclobutadiene complex endowed with triphenylsilanolates and extensive investigations on molybdenatetrahedranes with tripodal silanolate ligands proved that both intermediates are accessible and reversibly interconverting. The tripodal ligand sphere generates two distinct molybdenacyclobutadiene forms, which need to pass through a pseudorotation for productive alkyne metathesis. The newly developed catalysts revealed an unrivaled functional group tolerance, tolerate protic functional groups such as unprotected alcohols and even entailed a certain stability towards water. Furthermore, the excellent application profile has been demonstrated on challenging ring-closing alkyne metathesis reactions for polyfunctionalized (natural) products. Therefore, we termed the newly developed molybdenum alkylidyne complexes with a tripodal ligands sphere “canopy catalysts”.

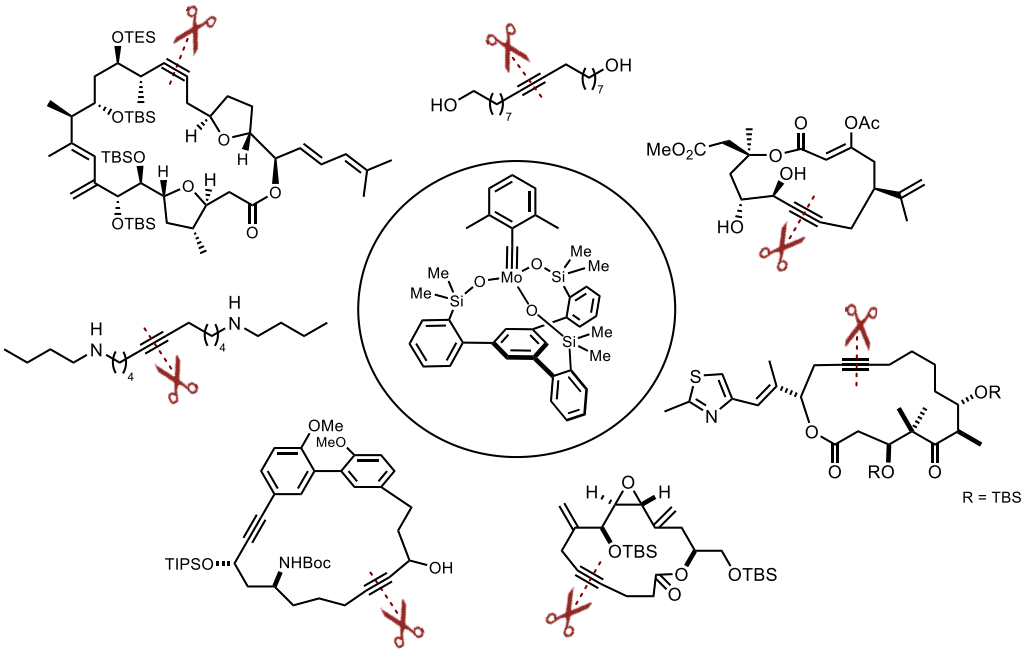

In the second part of this work, we extended the coverage to tripodal tungsten alkylidyne complexes and developed a new competent tungsten based catalyst for alkyne metathesis that outperformed the classical Schrock catalyst. Isolation of a mixed tungstenacyclobutadiene complex provided compelling evidence that tripodal silanolate ligands on tungsten result in poor catalytic performance. A combined spectroscopic, crystallographic, and computational study provided insights into the structure and electronic character of tungsten alkylidyne complexes. $^{183}$W NMR spectroscopy revealed that tripodal silanolate ligands upregulate the Lewis acidity of tungsten alkylidyne complexes, in that the tungstenacyclobutadiene intermediate gets over-stabilized and catalytic activity is lost.

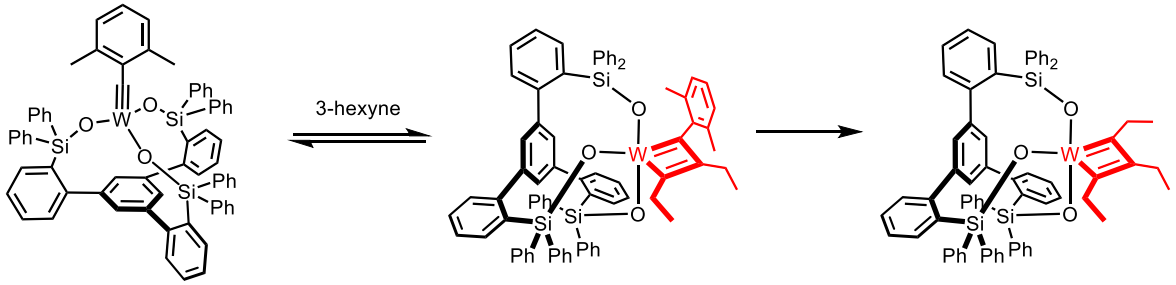


All tungsten alkylidyne complexes with tripodal silanolate ligands as well as several literature-known catalysts gave disappointing results in simple homo-metathesis reactions. Therefore, we developed a more strongly donating tripodal alkoxide ligand, which upon complexation gave the corresponding tungsten complex in quantitative yield on scale. The newly developed catalyst outperformed all other tungsten-based catalysts in terms of activity and selectivity.

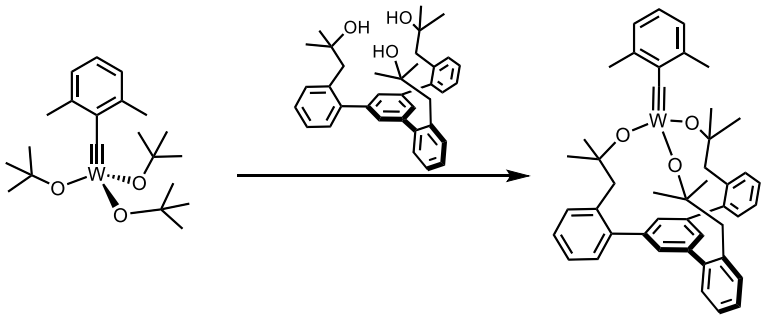

In the third chapter, we report the isolation of the first monomeric, homoleptic, five-coordinated alkoxide, non-oxo 4d$^1$ Mo(V) complex. High-valent molybdenum complexes endowed with alkoxide ligands are prone to dimerize and/or form molybdenum-oxo-complexes. [Mo(O*t*Bu)$_5$] represents the first example of an entirely new class of high-valent molybdenum complexes. In addition, we isolated a molybdenum nitrido complex endowed with *tert*-butoxide ligands. Previously, low-valent Mo(III) alkoxide complexes have not been sufficiently shielded to suppress dimerization and their reactivity for small molecule activation is unknown. Intriguingly, the molybdenum nitrido complex is formed by activation of acetonitrile by the low-valent Mo(III) alkoxide complex.

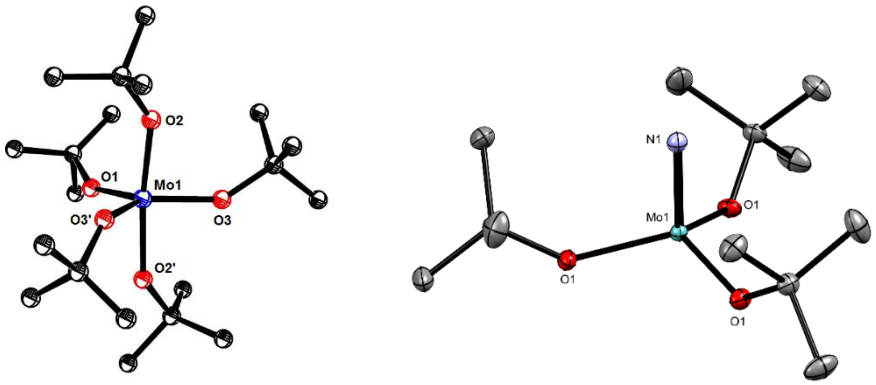

Max-Planck-Institut
für Kohlenforschung

technische universität
dortmund

# Molybdenum and Tungsten Alkylidyne Complexes with a Tripodal Ligand Sphere for Alkyne Metathesis

# &

# Isolation of a Homoleptic Non-oxo Mo(V) Alkoxide Complex

# Table of Contents

# 1 Introduction

## 1.1 Catalytic Metathesis Reactions

Alkene and alkyne metathesis have emerged as very powerful methods for the cleavage and formation of carbon-carbon multiple bonds.[1, 2] Metathesis (*greek* = transposition) constitutes the scrambling of carbon-carbon double or triple bonds with the help of transition metal alkylidene or alkylidyne catalysts (**Scheme 1**). The advent of well-defined alkene metathesis catalysts with high activity, good functional group tolerance and user-friendliness, has propelled their application in academia and industry.[3-5] [6] In comparison, alkyne metathesis has received less attention by the community and the impact remained limited. However, in the past two decades new alkyne metathesis catalysts have been developed, which combine high activity, bench-stability and remarkable functional-group tolerance.[7-9] In 2005, the Royal Swedish Academy of Sciences has awarded the Nobel Prize in chemistry to Yves Chauvin, Robert. H. Grubbs, and Richard R. Schrock for their fundamental work in elucidating the mechanism of metathesis and the discovery of highly active metathesis catalysts.[10-12]

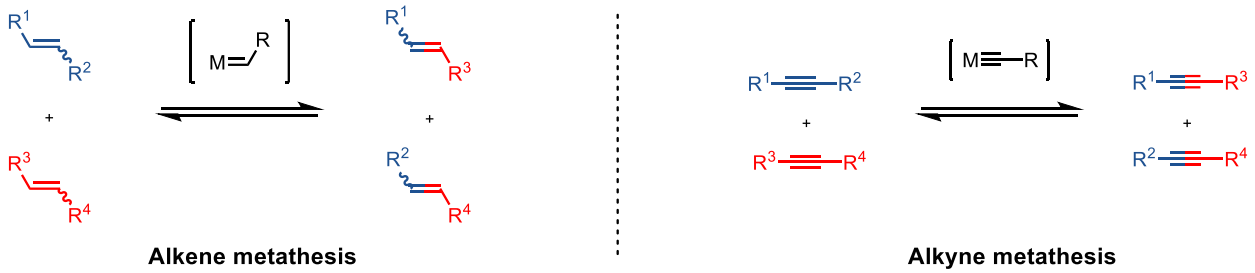


**Scheme 1.** Alkene and alkyne metathesis.

## 1.2 Alkyne Metathesis

The first alkyne metathesis reaction was described by Pennella et al. in 1968, who discovered that supported tungsten oxide catalyzes the scrambling of 2-pentyne to give 2-butyne and 3-hexyne under forcing conditions (200 °C - 450 °C).[13-15] Shortly after the initial discovery, Mortreux and Blanchard developed a homogenous catalyst system based on $[Mo(CO)_6]$ (**2**) and resorcinol (**Scheme 2**). Heating this mixture to 160 °C allowed for the equilibration metathesis of methyltolane (**1**).[16] Although this catalyst system is relatively simple and many efforts have been devoted to improve it, the need for elevated temperatures and the limited functional group tolerance led only to few applications in organic synthesis.[17-36]

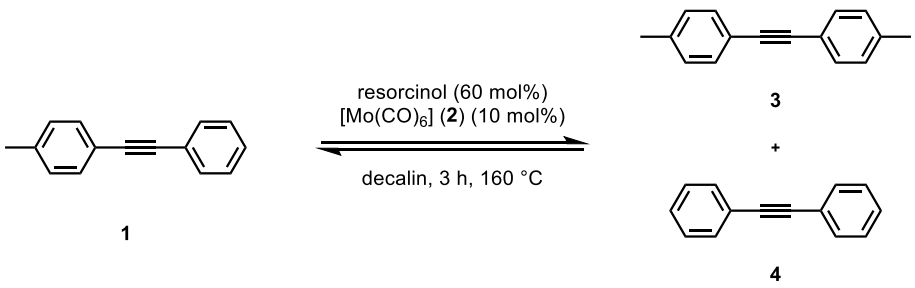


**Scheme 2.** The first homogenous catalyzed alkyne metathesis by Mortreux.[16]

Until today, the catalytically active species of the *in situ* generated Mortreux system remains unclear. Several mechanistic scenarios had been considered and the mechanism of alkyne metathesis has been of great debate.[37-40] In 1975, Katz came up with a mechanism for alkyne metathesis that is

closely related to the mechanism of alkene metathesis proposed by Chauvin.[41] In this proposal, species **A** with a metal-carbon triple bond undergoes a [2+2] cycloaddition with the alkyne to give metallacyclobutadiene **B**. Intermediate **B** is in resonance to structure **B'** and undergoes a [2+2] cycloreversion to release the product and regenerate a catalytically active species (**Scheme 3**). By that time no "metal carbynes" were known to catalyze the metathesis reaction of alkynes in the proposed mechanistic cycle.[42]

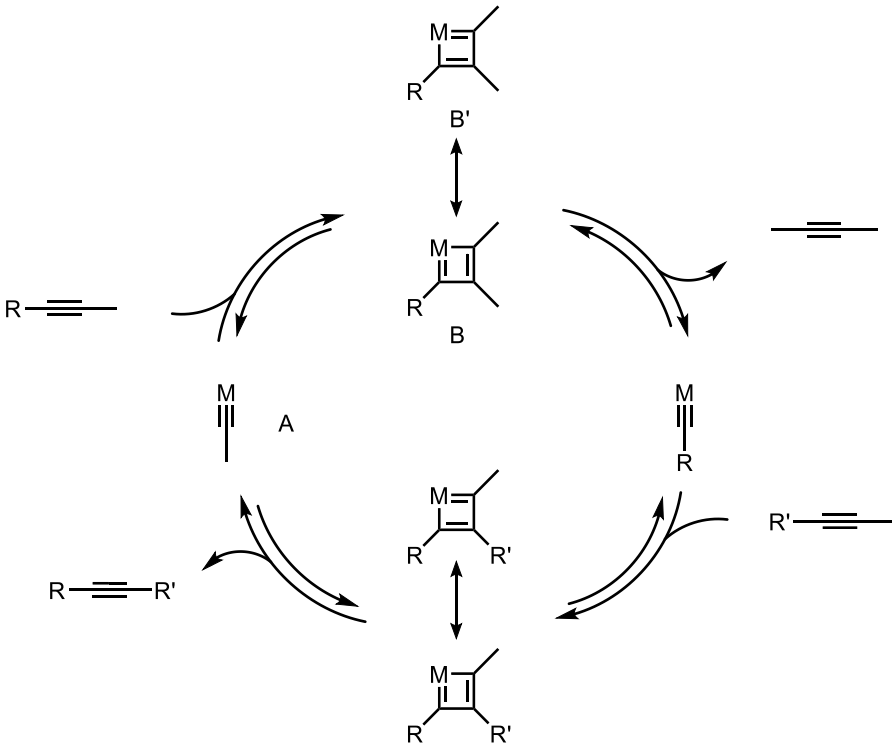


**Scheme 3.** Catalytic cycle of alkyne metathesis.

The breakthrough discovery of a new class of high oxidation state metal complexes containing multiple metal carbon bonds by Schrock and co-workers opened up a new chapter in organometallic chemistry.[1] The first high oxidation state alkylidene and alkylidyne complexes were described for tantalum, which are very different from the classical Fischer-type carbene or carbyne complexes.[43, 44] Unlike carbyne complexes, Schrock alkylidyne complexes are in their highest possible oxidation state and the alkylidyne ligand is, formally considered, trianionic. The metal carbon triple bond is polarized in that the metal is positive and the carbon negative. In 1981, Schrock and co-workers described the first well-defined alkyne metathesis catalyst [$W(CCMe_3)(O\mathit{t}Bu)_3$] (**5**), which catalyzed the metathesis of aliphatic and aromatic alkynes at room temperature with remarkable ease.[45] This initial discovery marked the beginning of the increased interest in the development of ever more efficient alkyne metathesis catalysts.

## 1.3 Tungsten Alkylidyne Catalysts

The tungsten alkylidyne complex **5** can be prepared by two different routes (**Scheme 4**). The classical route proceeded *via* the tris(neopentyl)neopentylidyne complex **7**, which was initially prepared by a double intramolecular α-hydrogen atom abstraction reaction by alkylating [$WCl_6$] with neopentyl magnesium chloride.[46] However, this protocol was only low-yielding since [$WCl_6$] is very easy to reduce and various undesired side reactions occur simultaneously.[47] Therefore, [$(MeO)_3WCl_3$] (**6**) was chosen as a more suitable W(VI) precursor. The methoxide ligands render the metal less

susceptible to reduction, which resulted in good overall yield for complex **7**. Treatment with HCl in 1,2-dimethoxyethane gave complex **7**, which underwent ligand exchange with the desired alkoxide to afford complex **5**.[48] A different route proceeds *via* the metathetic cleavage of the tungsten-tungsten triple bond of complex **11** with neoheptyne.[49-51] Although the metathesis reaction of dinuclear complex **11** and an alkyne only occured with sterically demanding *tert*-butoxide ligands, it demonstrated a new route to access alkylidyne complex **5**.[52, 53]

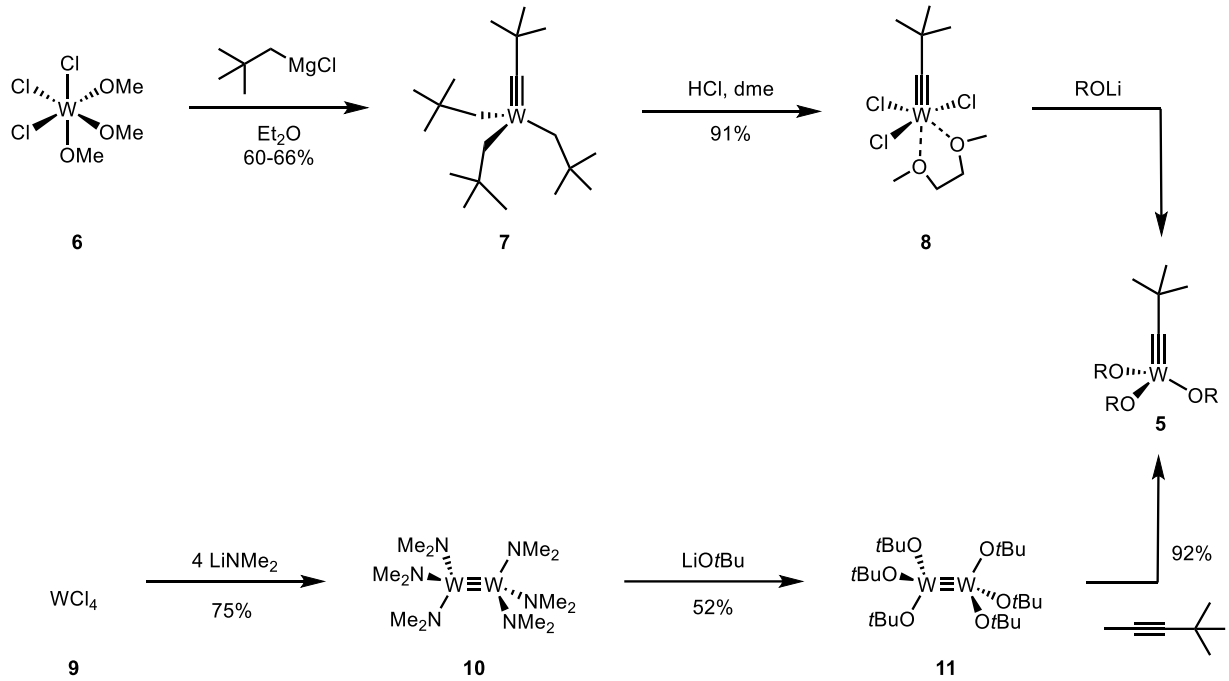


6 7 8 5

9 10 11

**Scheme 4.** Preparative routes to tungsten alkylidyne complexes of type **5**.

A much more scalable and efficient synthesis, which has been extensively used in recent years, started with zero-valent $[W(CO)_6]$ (**12**).[54-58] Nucleophilic addition of an aryl lithium species to carbonyl complex **12** provided the Fischer carbene **13**. Oxidation with oxalyl bromide and subsequent bromination gave access to Schrock alkylidyne **14**. Ligand exchange with the desired alkoxide afforded complex **15** (**Scheme 5**).

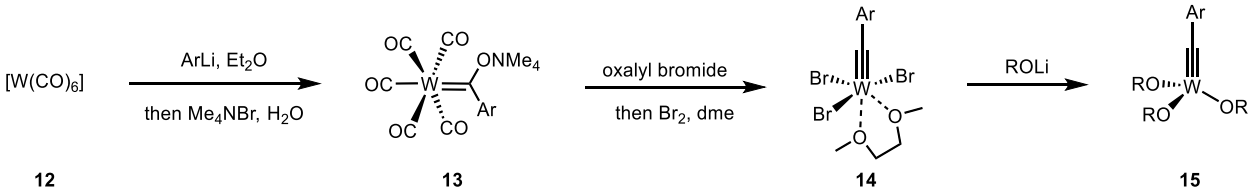


12 13 14 15

**Scheme 5.** Scalable synthesis of tungsten alkylidyne complex **15**.

Over the years, a number of different ligands were tested to uncover the critical parameters for efficient alkyne metathesis. Complex **7** and **8** showed no catalytic activity for the metathesis of internal alkynes.[40, 45, 59, 60] Although complex **8** did not metathesize alkynes catalytically, it reacted with one equivalent 3-hexyne to give a tungstenacyclobutadiene complex and provided evidence for the proposed mechanism. The addition of excess 3-hexyne to complex **8** afforded the cyclopentadienyl complex instead.[61] Sterically demanding amides, sulfides or carboxylates as ancillary ligand also failed to give competent catalysts.[62, 63] In contrast, bulky *tert*-butoxide ligands or 2,6-diisopropylphenoxide ligands afforded active catalysts for alkyne metathesis (**Figure 1**).[64, 65] The

steric bulk around the metal center was necessary to prevent the formation of dimers or oligomers and to shut down any bimolecular decomposition pathways.[64, 66] Addition of two equivalents of 3-hexyne to complex **5b** at ambient temperature gave the corresponding metallacyclobutadiene complex quantitatively.[64]

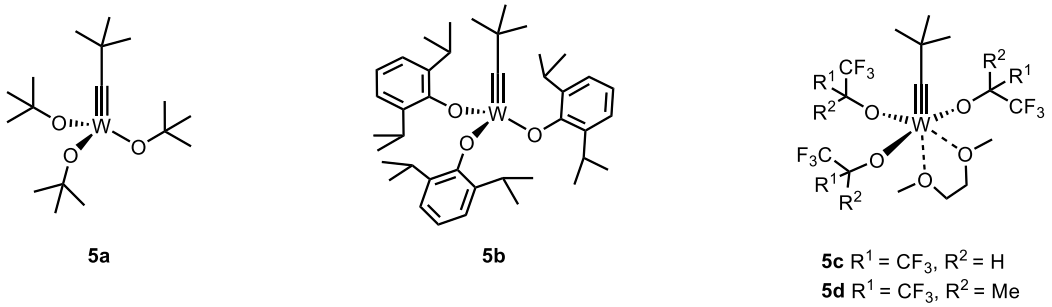


**Figure 1.** Competent tungsten alkylidyne complexes for alkyne metathesis.

The crystal structure of the metallacyclobutadiene complex resembles a trigonal bipyramidal coordination geometry and the four-membered ring lies in the trigonal plane. A kinetic study revealed that loss of the alkyne from the tungstenacyclobutadiene ring is rate-limiting.[64] Nevertheless, complexes of type **5b** are inherently nucleophilic at the alkylidyne carbon atom and react with nucleophiles such as aldehydes or ketones in a Wittig-like reaction to release the olefinic product after hydrolysis.[67] Alkylidyne complexes of type **5** readily decompose in the presence of moisture to tungsten-oxo alkyl complexes.[68, 69]

Since alkoxides were shown to be efficient ligands for alkyne metathesis, the research community has put much effort in balancing the Lewis acidity of the metal center by installing different fluorinated alkoxides. Complexes **5c** and **5d** were claimed to demonstrate good catalytic activity and react rapidly with internal alkynes to give the corresponding tungstenacyclobutadiene complex (**Figure 1**).[70] Interestingly, catalyst **5d** proceed through a dissociative mechanism wherein the alkyne is released from the metallacyclobutadiene **17** and reforms the alkylidyne complex **19** (**Scheme 6**). In contrast, catalyst **5c** reacts through an associative mechanism wherein an additional alkyne is coordinated to the metallacyclobutadiene **17** and forms **20**. The mechanistic dichotomy was reasoned to arise from subtle changes of the steric environment within the tungstenacyclobutadiene complex. The smaller hexafluoroisopropoxide ligand allowed a second alkyne to coordinate and insert into the tungstenacyclobutadiene complex **20** to give tungstenacyclohexatriene complex **21**. Further ring expansions and protonolysis would give access to polymerized substrate. Interestingly, Schrock and co-workers have indeed observed a significant amount of polymer during metathesis reactions catalyzed by complex **5c**.[70] Another known decomposition pathway is the formation of the cyclopentadienyl complex **22** which formed upon reductive elimination from tungstenacyclohexatriene complex **21**.[60]

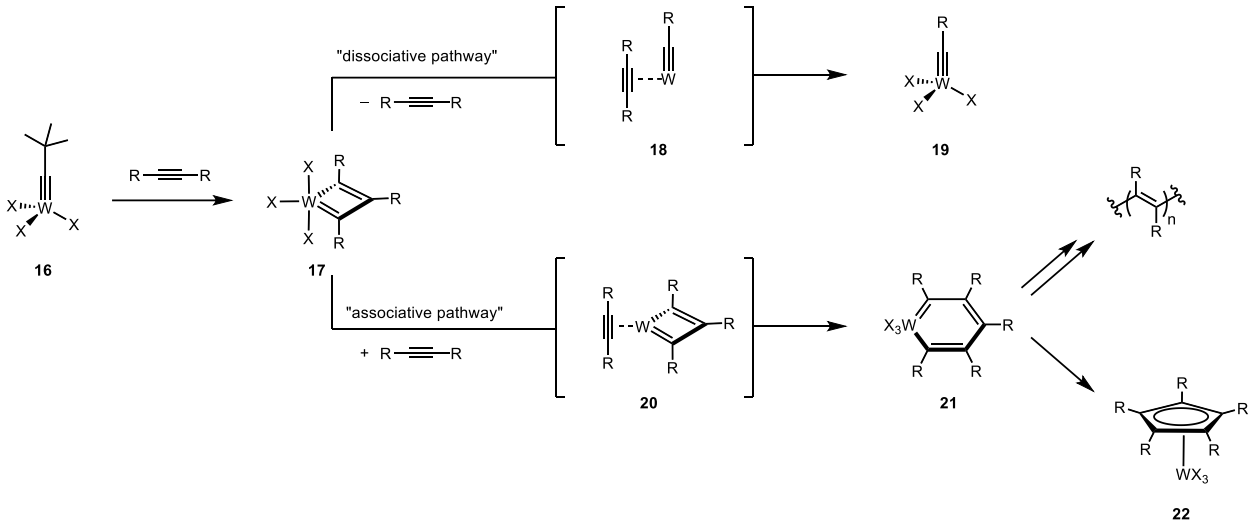


**Scheme 6.** Mechanistic dichotomy in tungsten alkylidyne complexes.

Besides the formation of planar trigonal bipyramidal metallacyclobutadiene complexes, it is also possible to access the tautomeric form of it, a metallatetrahedrane complex (W(VI), trianionic $C_3R_3^{3-}$ fragment), or a $\eta^3$-cyclopropenyl complex (W(IV), monoanionic $C_3R_3^-$ fragment). The addition of 2-butyne or 3-hexyne to carboxylate tungsten complex **23** gave metallatetrahedrane **24** with a pentagonal-bipyramidal coordination geometry (**Scheme 7**). Replacing the ligands by simple *tert*-butoxides destabilized the metallatetrahedrane and released the corresponding alkylidyne complexes **25** and **5a**.[63] Metallatetrahedranes were even accessible by adding a σ-donor ligand (pyridine or tmeda) to tungstenacyclobutadiene complex **25**. Again, ligand exchange with *tert*-butoxide resulted in formation of alkylidyne complex **26**. In contrast to the cyclopentadienyl ring formation, the formation of metallatetrahedrane complexes is reversible.[60] Schrock and co-workers have postulated that metallatetrahedranes are not able to lose an alkyne from the non-planar core and are therefore not involved in productive alkyne metathesis. In this context, a tungsten complex has been isolated that is halfway between a planar and a tetrahedral form and gave exclusively a tungstenatetrahedrane complex upon addition of a phosphine ligand.[71, 72]

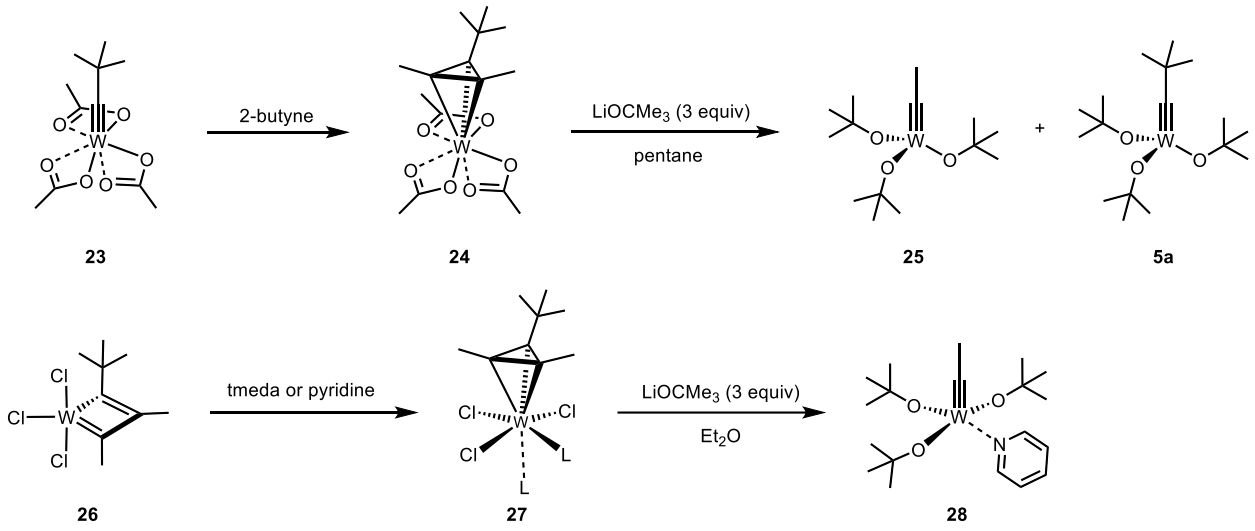


**Scheme 7.** Formation of tungstenametallatetrahedrane complexes; L = pyridine or tmeda.

In light of the high Lewis acidity of tungsten alkylidyne complexes endowed with fluorinated alkoxides, several heteroleptic push/pull ligand systems **29-30** have been reported (**Figure 2**).[57, 73-78] The Tamm group also prepared a new homoleptic siloxy-based catalyst **31** that engaged in the catalytic metathesis of conjugated diynes.[79, 80] Inspired by the high catalytic activity of

cationic alkene metathesis catalysts, Buchmeiser and co-workers recently reported on cationic tungsten alkylidyne complexes such as **32**. All cationic tungsten alkylidyne complexes of type **32** showed only low activity for alkyne metathesis and decomposed by a bimolecular pathway.[81, 82]

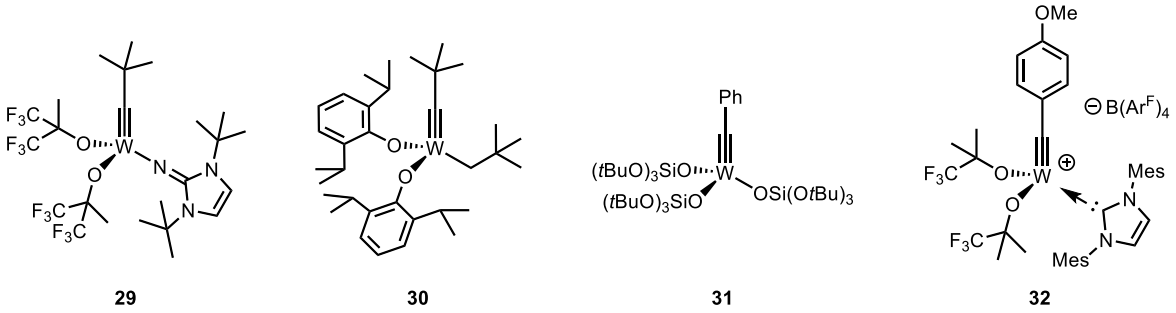


**Figure 2**. Recent ligand designs on tungsten alkylidyne complexes.

The pioneering work of Mayer and co-workers demonstrated that low-valent ("Fischer-type") tungsten alkylidyne complexes **33** are also capable to undergo stoichiometric alkyne metathesis to give the alkyne complex **35** (***Scheme 8***).[83-85] In contrast to high oxidation state $d^0$ alkylidyne complexes, complexes of type **33** possess two d-electrons and engage in significant π-backbonding into the π*-orbitals of π-acidic ligands such as alkynes, alkenes or CO. The electron-rich σ-donating phosphine ligands render the tungsten metal center even more electron rich. Carbyne ligands are amongst the strongest π-accepting ligands and will typically coordinate *trans* to the strongest π-donating ligand or weakest π-accepting ligands such as halides.[86] It is particularly interesting to discuss the electronic structure of these complexes, since they can be viewed as Fischer carbynes with a $CR^+$ fragment (one filled σ-orbital and two empty π*-orbitals) stabilizing filled d-orbitals or as Schrock alkylidynes with a $CR^{3-}$ ligand mixing with empty d-orbitals. In both classifications, the $d_{xy}$-orbital is filled with two electrons and is nonbonding. The alkyne complex **34** faces a "π-conflict" in both descriptions: If the carbyne is viewed as $CR^+$ then the metal d-orbitals are filled and π-donation by the alkyne is diminished. In the alkylidyne case, the $CR^{3-}$ fragment and the alkyne are equally competing for bonding to empty metal d-orbitals, which in turn explains the lower stability and increased reactivity of alkylidyne alkyne complexes.[85] The addition of an alkyne to complex **33** resulted in substitution of two phosphine ligands and gave a five-coordinated alkyne complex **34**. The formation of a five-coordinate complex over an octahedral species has been rationalized by the aforementioned "π-conflict" in octahedral complexes. The fact that this alkyne-adduct **34** is observable is likely due to the π-backdonation of the filled d-orbitals into the π*-orbitals of the alkyne. Therefore, the alkyne needs to be perpendicular to the carbon metal triple bond in order to efficiently overlap with the filled $d_{xy}$-orbital. In consequence, this builds up a substantial rotational barrier to form the metallacyclobutadiene intermediate for productive alkyne metathesis and renders the reaction particularly slow.

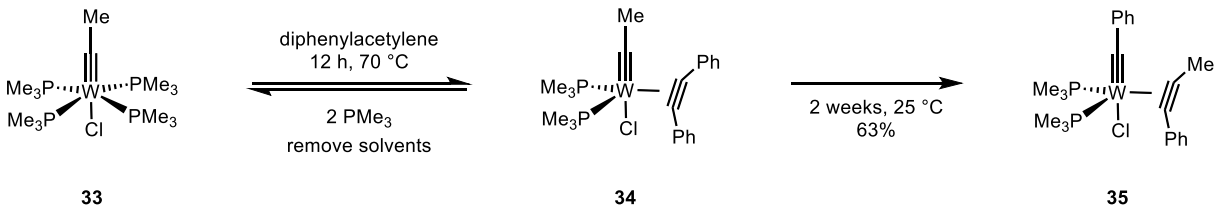


**Scheme 8.** Stoichiometric alkyne metathesis reaction of low-valent tungsten complex **33**.

Terminal alkynes are difficult substrates for classical high-valent Schrock alkylidyne catalysts due to the propensity to deprotonation of the metallacyclobutadiene primarily formed and other side reactions leading to polymer (*vide infra*). Low-valent tungsten complex **33** reacted in a stoichiometric fashion with terminal alkynes to give complex **37**. Although propyne was not observed in the NMR experiment, the reaction showed no indication for polymerization nor deprotonation of the metallacyclobutadiene intermediate (**Scheme 9**).[84]

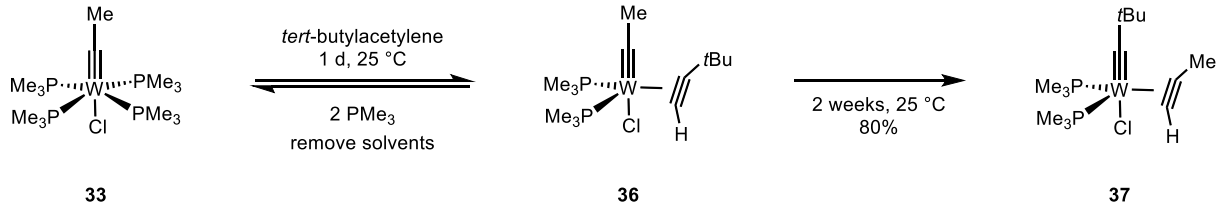


**Scheme 9.** Stoichiometric alkyne metathesis of low-valent tungsten complex **33** with terminal alkynes.

Overall, this suggests the following aspects to be considered to enable catalytic metathesis activity in Fischer-type complexes: strong π-donors and weak σ-donating phosphines; sterically encumbered ligands suppress the unfavorable π-backdonation and favor the [2+2] cycloaddition.

Beside the well-known alkyne cross-metathesis (ACM), Johnson and co-workers reported on the catalytic nitrile-alkyne cross-metathesis (NACM) in which a nitrile such as **38** reacts with sacrificial 3-hexyne to give symmetrical alkynes **39** (**Scheme 10**). This reaction is catalyzed by tungsten-nitrido complexes **40a** and **40b**, which reversibly interconvert to the corresponding alkylidyne complex **19** through an intermediate azametallacyclobutadiene complex **41**. As a consequence thereof, nitrido and the alkylidyne complexes need to be isoenergetic in order to efficiently engage in ACM and NACM to give symmetric alkyne **39**.[87]

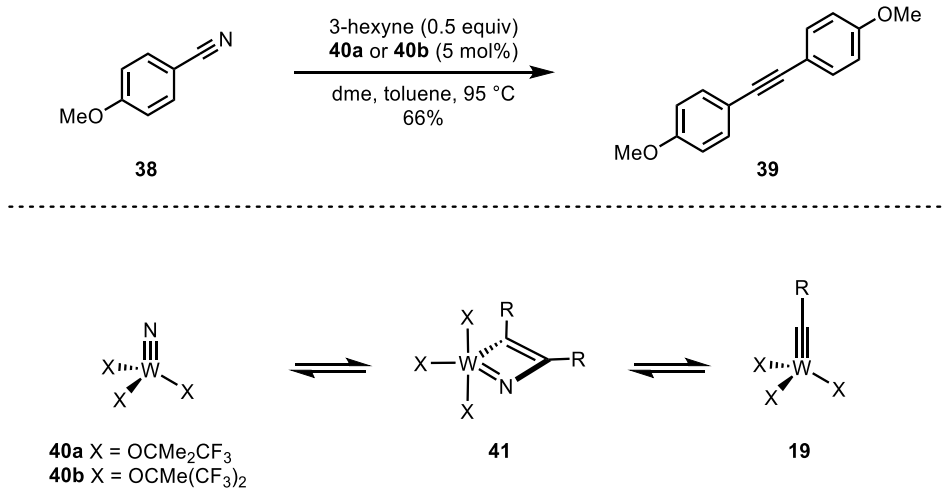


**Scheme 10.** Reversible interconversion of nitrido complexes **40** and alkylidyne complexes **19** through an intermediate azametalacyclobutadiene complex **41.**

In general, the more polarized M≡N bond is thermodynamically favored over the alkylidyne unit when the metal is more electropositive. The charge density at the metal center is largely influenced by the ancillary ligand set. Interestingly, theoretical investigations have shown that catalyst **40a** prefers the alkylidyne ligation whereas catalyst **40b** favors the nitrido resting state.[88]

## 1.4 Rhenium Alkylidyne Catalysts

Beside the well-known $d^0$-tungsten and molybdenum catalysts, Schrock and co-workers also reported on $d^0$-rhenium complexes for alkynes metathesis. Although monoimido bisalkoxide alkylidyne complex **43** reacted with internal alkynes to give fluxional rhenacyclobutadiene complexes, only bulky acetylenes were readily lost again to give productive turnovers (**Scheme 11**).[89] In contrast to symmetric ligand spheres, the heterotopic ligand enabled the substrate to approach the metal from two different faces in which only one metallacyclobutadiene intermediate was productive for alkyne metathesis. Rhenium(VII) metallacyclobutadiene complexes are unstable in the presence of excess acetylene and were ultimately reduced to rhenium(V) complexes.[90]

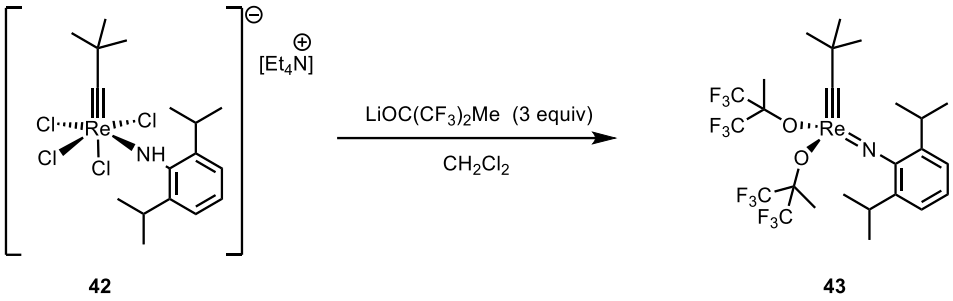


**42** **43**

**Scheme 11.** Preparation of monoimido bisalkoxide rhenium(VII) alkylidyne complex **43**.

Jia and co-workers recently showed that the air-stable $d^2$-Re(V) complex **44** underwent stoichiometric, reversible alkyne metathesis to give complex **45** (**Scheme 12**).[91, 92]

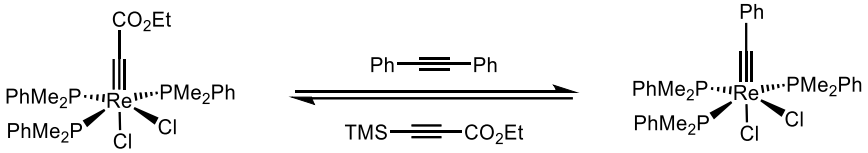

**44** **45**

**Scheme 12.** Stoichiometric, reversible alkyne metathesis of rhenium(V) alkylidyne complex **44**.

Further ligand variations led to the discovery that $d^2$-Re(V) complex **48** is a competent catalyst for alkyne metathesis when bidentate phosphine-phenoxide ligand **47** was employed (**Scheme 13**).[93] The catalyst is resistant to heat, air, and moisture and showed a broad substrate scope, tolerating even challenging functional groups such as alcohols, amines and even carboxylic acids.

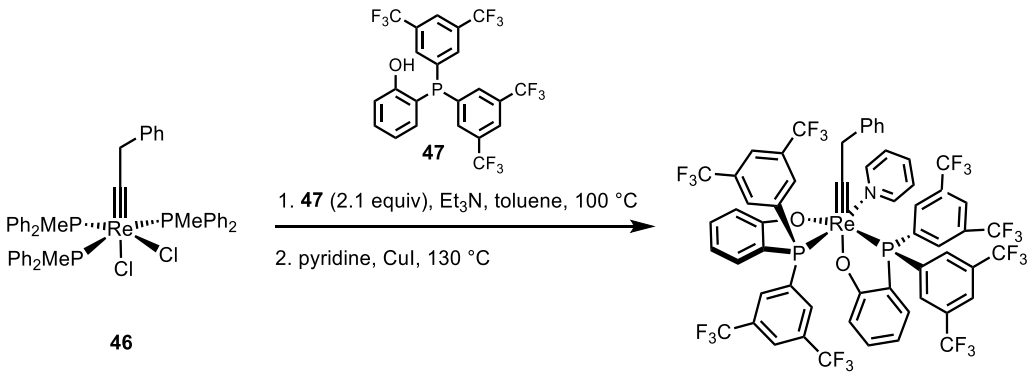


**46** **48**

**Scheme 13.** Preparation of catalytically active Re(V) alkylidyne complex **48**.

After dissociation of pyridine the active catalyst reacts with the alkyne and will proceed through the coordination numbers five and six for productive turnover (**Figure 3**).

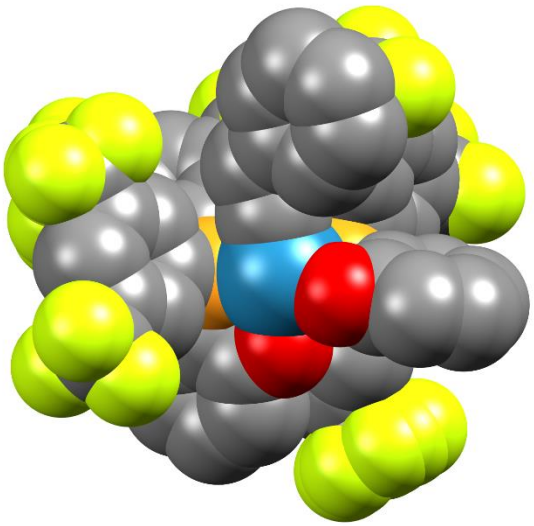

**Figure 3.** Spacefilling representation of solid state structure of Re(V) catalyst **48**; hydrogen and pyridine omitted for clarity.

## 1.5 Molybdenum Alkylidyne Catalysts

In parallel to the development of tungsten alkylidyne complexes, Schrock and co-workers also developed molybdenum alkylidyne complexes for alkyne metathesis. Again, sterically demanding fluorinated alkoxides, 2,6-diisopropylphenoxide or adamantoxide proved to be competent ligands for molybdenum catalysts **49-52** (**Figure 4**). In stark contrast, neopentylidyne complexes endowed with *tert*-butoxide ligands did not react with simple alkynes such as 3-heptyne or diphenylacetylene.[94-97]

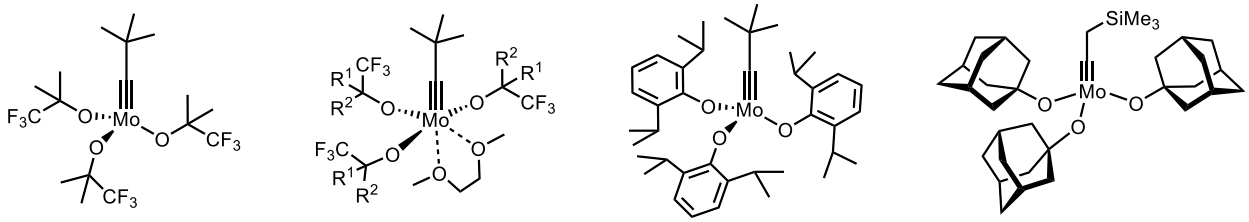


**Figure 4.** Early molybdenum alkyne metathesis catalysts.

The classical preparation of these catalysts from [$MoCl_5$] was problematic and the more scalable and efficient synthesis starting from [$Mo(CO)_6$] (**2**) was preferred in recent years (**Scheme 14**).[57, 78, 98] Nucleophilic addition of mesityl lithium to carbonyl complex **2** gave Fischer carbene **53**. Oxidation with oxalyl bromide and bromine gave access to Schrock alkylidyne **54**. Substitution with *tert*-butoxide or fluorinated alkoxides gave complexes of type **55**.[99, 100] The influence of the different fluorinated alkoxides on the catalytic activity was examined for the simple homo metathesis of 1-phenyl-1-propyne and revealed that all complexes are catalytically active at ambient temperature. In contrast to Schrock's findings, complex **55a** endowed with *tert*-butoxide ligands is an active catalyst, although it showed the slowest conversion of the starting material. Intriguingly, the catalytic

performance increased with an increasing degree of fluorination from **55a** to **55c** and decreased from **55c** to **55d**. More fluorine atoms increased the electrophilicity of **55** until the metallacyclobutadiene intermediate becomes overly stable and the [2+2] cycloreversion becomes rate-determining.[101]

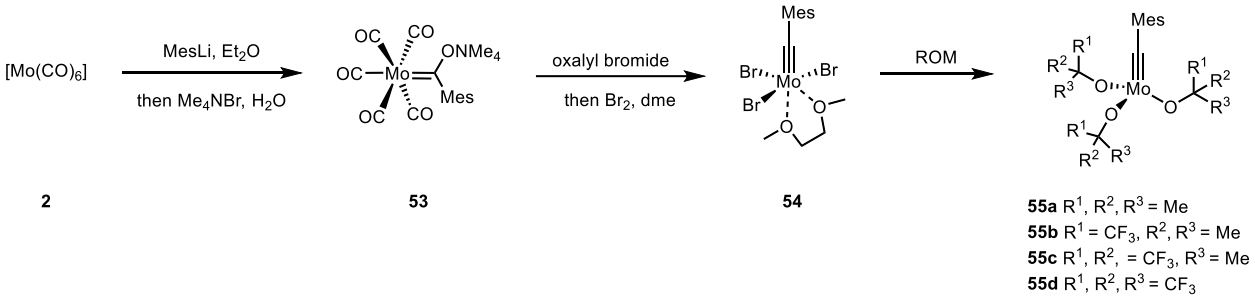


**Scheme 14.** Scalable synthesis of molybdenum alkylidyne complexes **55**.

In 1999, Fürstner and co-workers discovered a new catalytic system for alkyne metathesis (**Scheme *15***).[102] Dissolving complex **58** in toluene and addition of $CH_2Cl_2$ (25 equivalents) generated a mixture of terminal alkylidyne complex **59** and trisamido-molybdenum(IV) chloride **60**, which effectively catalyzed alkyne metathesis. Complex **58** was prepared by reacting $[MoCl_3(THF)_3]$ (**56**) with two equivalents of lithium salt **57**.[103] The highly reactive molybdenum(III) complex **58** is known for various small-molecule activation reactions including the stoichiometric cleavage of the N≡N triple bond of dinitrogen.[104] Due to the high sensitivity of complex **58**, the synthesis requires rigorous Schlenk techniques and argon atmosphere. A detailed mechanistic study revealed that both separately prepared complexes **59** and **60** engage in alkyne metathesis. In agreement with the known decomposition pathways for methylidyne complexes (*vide supra*), complex **59** was inactive after only one turnover. In contrast, trisamido-molybdenum(IV) chloride **60** proved to be particularly active. To this end, it remains unclear through which mechanism complex **60** generates the actual catalytically competent species.[105]

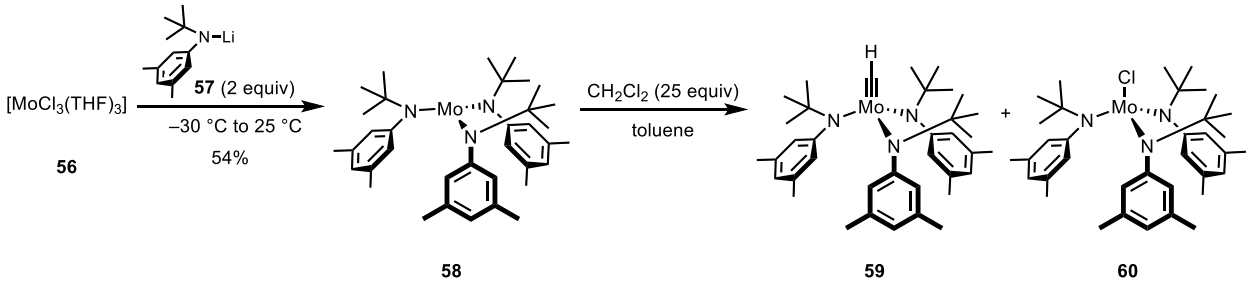


**Scheme 15.** Methylene chloride activation by complex **58** gives catalytically active mixture of **59** and **60**.

Moore and co-workers further improved the protocol by treating complex **54** with higher *gem*-dichlorides and coupling the procedure to a reductive cycle (**Scheme 16**). [106, 107] With this strategy, trisamido-molybdenum(IV) chloride **56** was fully converted to propylidyne catalyst **57**. [103]

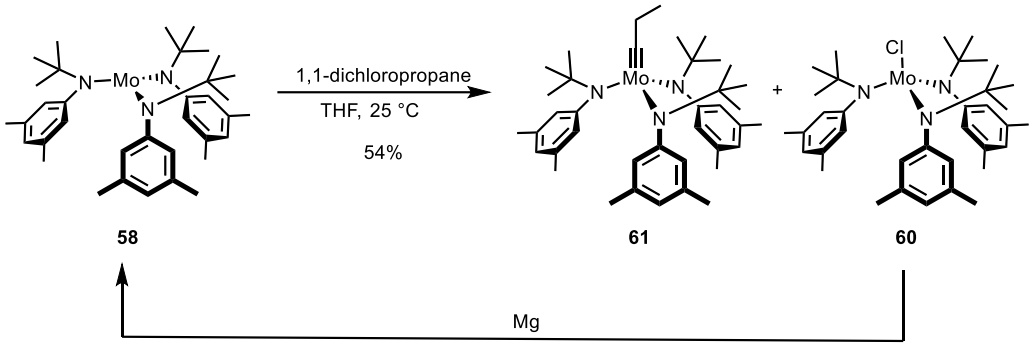


**Scheme 16.** Reductive cycle strategy to access catalyst **61**.

The new catalyst system was successfully applied to several natural product syntheses, which stand witness for the improved functional group tolerance over to the more Lewis acidic tungsten catalyst **5a**. Numerous polar groups, basic amines, thioethers and polyether chains were well tolerated.[108]

### 1.5.1 Molybdenum Nitrido Precatalyst

In sharp contrast to tungsten nitrido complexes, the corresponding molybdenum complexes **62** showed no or only low activity for nitrile-alkyne cross-metathesis (NACM) even under forcing conditions. The conversion of molybdenum nitrido to alkylidyne **63** is known for complexes **62**, which can be prepared by azide decomposition followed by ligand substitution.[109, 110] The more electronegative molybdenum center favors the alkylidyne ligation and the reverse reaction has never been observed (**Scheme 17**).[111]

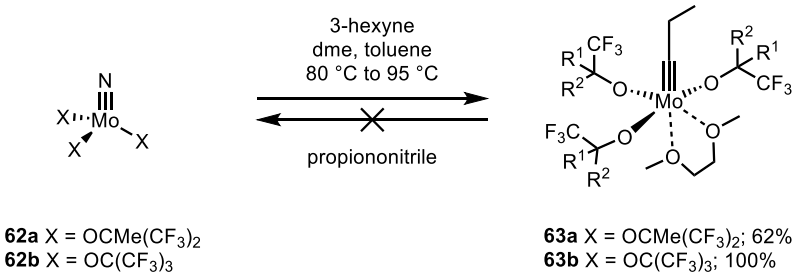


**Scheme 17.** Molybdenum nitrido to alkylidyne conversion.

In 2009, Fürstner and co-workers reported that molybdenum nitrido complex **67** endowed with triphenylsilanolate ligands is an active precursor for alkyne metathesis. A more convenient and scalable synthesis of nitrido complex **67** was developed. Simple heating of inexpensive sodium molybdate (**64**) with TMSCl in dme afforded dioxo-complex **65**. The addition of LiHMDS and protonolysis with $Ph_3SiOH$ gave access to nitrido complex **67** (**Scheme 18**). It was anticipated that precatalyst **67** reacts with alkynes to form the actual active alkylidyne species **68**, although it has not been possible to confirm this by NMR studies.[112] Furthermore, the user-friendliness could be improved by complexation to pyridine or 1,10-phenanthroline. Pyridine adduct **69** is stable enough to be weighed in air and releases the active species by heating to 80 °C, whereas the phenanthroline adduct **70** is air-stable for years and can be reactivated by addition of metal salts (e.g. $MnCl_2$).

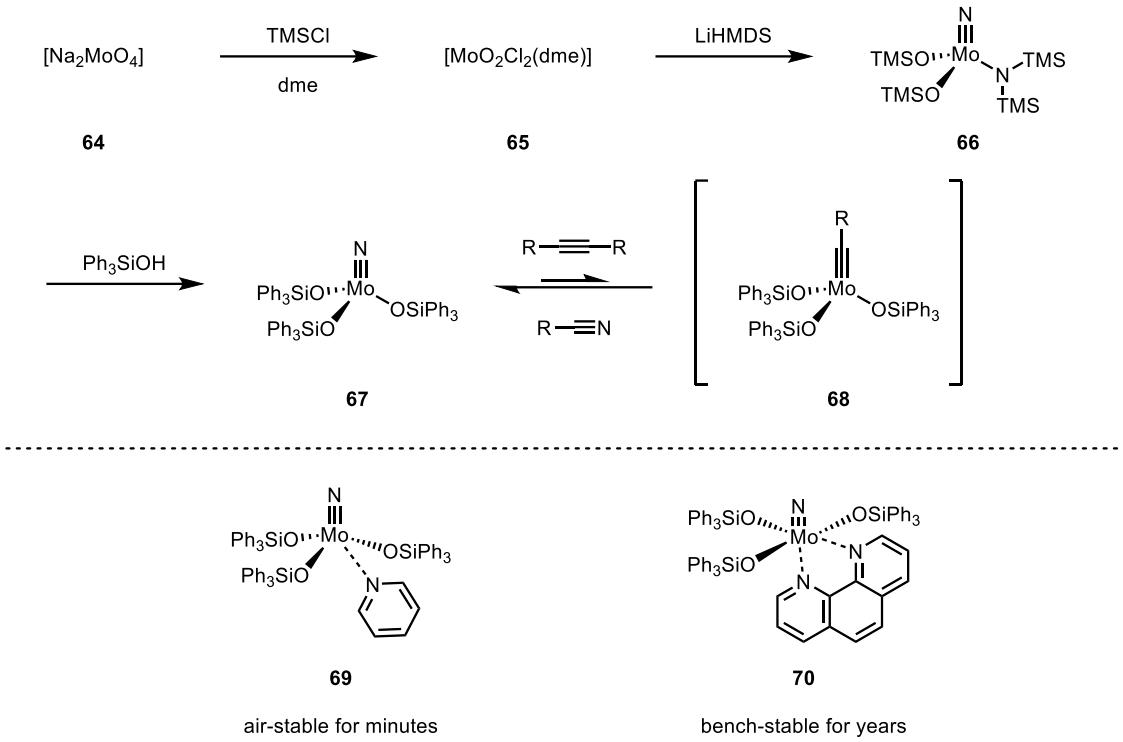


**Scheme 18.** Molybdenum nitrido complexes with triphenylsilanolate ligands for alkyne metathesis.

### 1.5.2 Molybdenum Alkylidyne Complexes with Siloxy Ligands

Nitrido complex **67** was successfully applied to several natural product syntheses.[7] However, high catalyst loadings were necessary to release the actual active alkylidyne complex **68**. Therefore, an independent synthetic route was developed to uncover the full potential of alkylidyne complex **72** (**Scheme 19**).[58, 113]

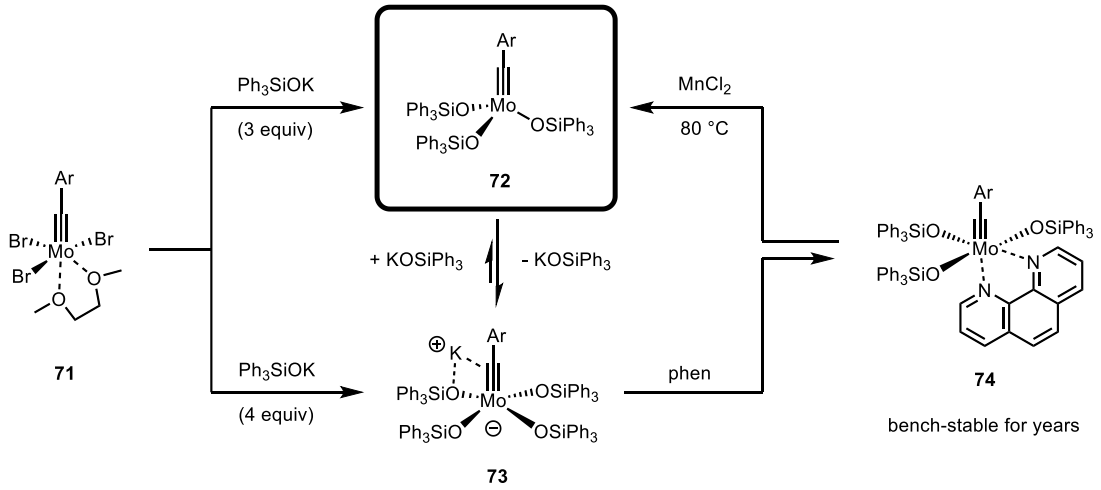


**Scheme 19.** Preparation of molybdenum alkylidyne complexes with siloxy ligands.

Slow addition of a solution of a triphenylsilanolate salt (3 equiv) to precursor **71** gave access to neutral alkylidyne complex **72**. Due to the high Lewis acidity of these complexes, addition of excess ligand salt resulted in the formation of the ate complex **73**. Addition of 1,10-phenanthroline replaced one ligand and formed the bench-stable adduct **74**, which can be reactivated by addition of metal salts (e.g. $MnCl_2$) at 80 °C. Alkylidyne complex **72** showed very high activity for the simple homo-metathesis of 1-phenyl-1-propyne in comparison to the classical Schrock catalyst **5a**. In less than

5 min, 1 mol% of catalyst quantitatively converted the substrate to the product at ambient temperature, whereas **5a** did not reach 20% conversion after 1 h. The high catalytic activity of triphenylsilanolate ligands on molybdenum alkylidyne complex **72** has been attributed to their adaptive ligand properties. Silanolates are weaker σ- and π-donors than alkoxides.[114] Facile bending and stretching of the Mo–O–Si bond angles will alter the hybridization of the oxygen atoms and therefore the degree of π-donation of the oxygen lone-pairs to the metal center. This allows to modulate the Lewis acidity of the metal center while passing through the catalytic cycle (**Scheme 20**).[7]

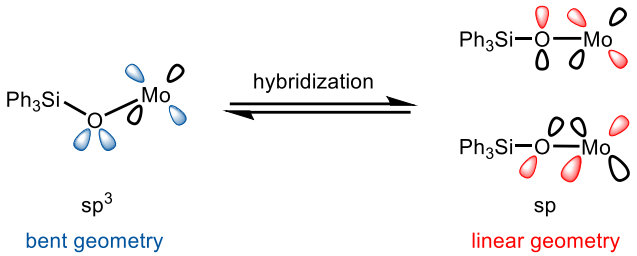


**Scheme 20.** Linear and bent silanolate geometries modulate the Lewis acidity of the molybdenum center.

Furthermore, bulky triphenylsilanolates disfavor bimolecular decomposition and are thermally more robust than alkoxides. A well-known decomposition pathway of metal-ligated alkoxides is the C–O bond cleavage to release a tertiary carbocation or tertiary radical, which does not apply to silanolates.[115, 116] Overall, catalysts of type **72** combine outstanding catalytic activity, unrivaled functional group tolerance, ready availability and user-friendliness.

### 1.5.3 Molybdenum Alkylidyne Complexes with Chelate Ligands

Although molybdenum alkylidyne catalysts of type **72** set new standards, some important limitations remained. Densely decorated diynes represent difficult substrates for the ring-closing alkyne metathesis reaction with triphenylsilanolate-based catalysts and generally led to homodimerization.[117, 118] Due to the high Lewis acidity of Mo(VI) as well as the inherent nucleophilicity and basicity of Schrock alkylidynes, simple protic substrates, such as unhindered primary alcohol, bring productive alkyne metathesis to a hold. Water is ultimately detrimental and requires reactions to be carried out under anhydrous conditions. Even the bench-stable phenanthroline adduct **74** decomposed in $CD_2Cl_2$ containing 10 ppm water.[113]

In recent years, several groups addressed the issues by using tridentate ligand sets instead of a monodentate ligand (**Scheme 21**). Under catalytic conditions, a large excess of substrate is present and will eventually replace the monodentate ligand. Due to the chelate effect, a tridentate ligand is bound more tightly to the metal (enthalpy and entropy), which makes it less likely to be replaced by a single molecule of substrate. In 2011, Zhang and co-workers reported on an amine-tethered phenol ligand **75** that upon mixing with complex **61** gave a catalytically active mixture.[119] Although a dimeric complex **76** could be isolated and characterized, only the *in situ* generated mixture showed catalytic activity for alkyne metathesis.[120] Further ligand variation tried to reduce the electron density on the metal center by blocking or replacing the additional amine coordination (Z = $(NMe)^+$, SiMe, CH).[121, 122] Overall, the catalytic activity could be improved but the composition of the catalytically active entity remained unclear. In 2016, Fürstner and co-workers used a similar approach and prepared various trisilanol-based ligands **77-78**. *In situ* protonolysis of the metathesis active catalyst **61** with tripodal ligand **78-79** gave only ill-defined mixtures with preserved catalytic activity. In this context, an improved functional group tolerance compared to **72** was noticed.[123]

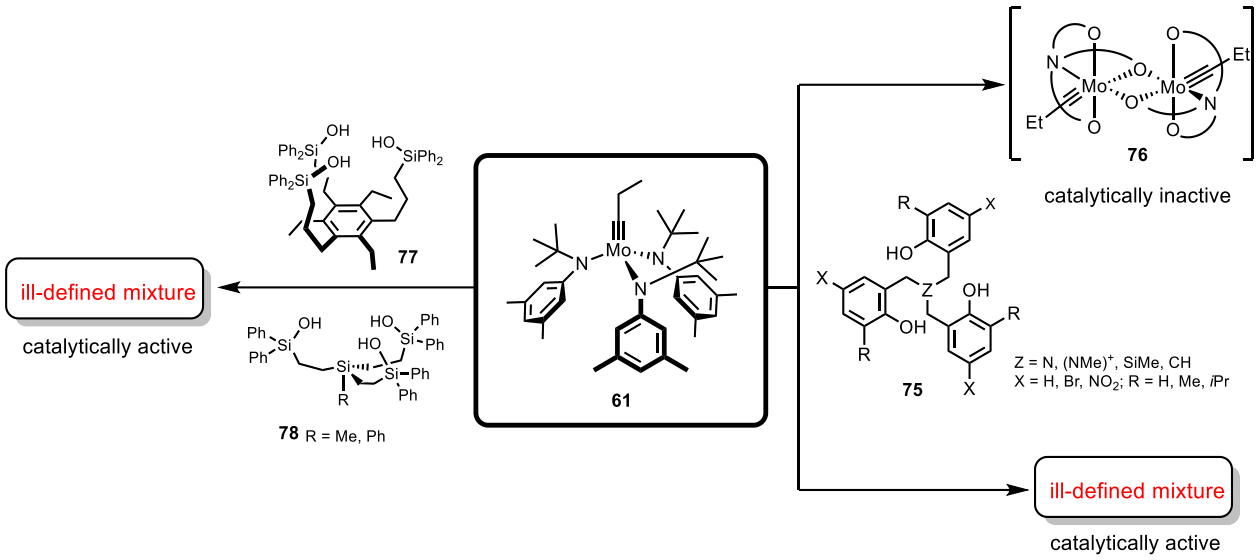


**Scheme 21.** Previous attempts to prepare well-defined molybdenum alkylidyne complexes.

## 1.6 Selected Applications

### 1.6.1 Ring-closing Alkyne Metathesis

The synthetic potential of alkyne metathesis was early recognized by Fürstner and co-workers (**Scheme 22**). Ring-closing alkyne metathesis of diynes and subsequent semi-reduction offers a reliable method for the stereoselective synthesis of (*Z*)-alkenes or (*E*)-alkenes over the conventional ring-closing alkene metathesis which usually led to (*E*, *Z*)-mixtures.[8, 124, 125] Ring-closing metathesis of **79** and subsequent Lindlar hydrogenation/deprotection gave access to macrocyclic (*Z*)-alkene **81**. The complementary reduction to give macrocyclic (*E*)-alkene **84** can been achieved by a catalytic trans-hydrosilylation/desilylation sequence.[126] The high selectivity of alkyne metathesis catalysts for alkynes over alkenes is another remarkable advantage over commonly applied alkene metathesis catalysts and allowed for the orthogonal application in organic synthesis.[7] Recently, this selectivity was challenged by substitution of the benzylidyne of molybdenum catalysts that enabled for the first ring-closing metathesis of alkenes.[127]

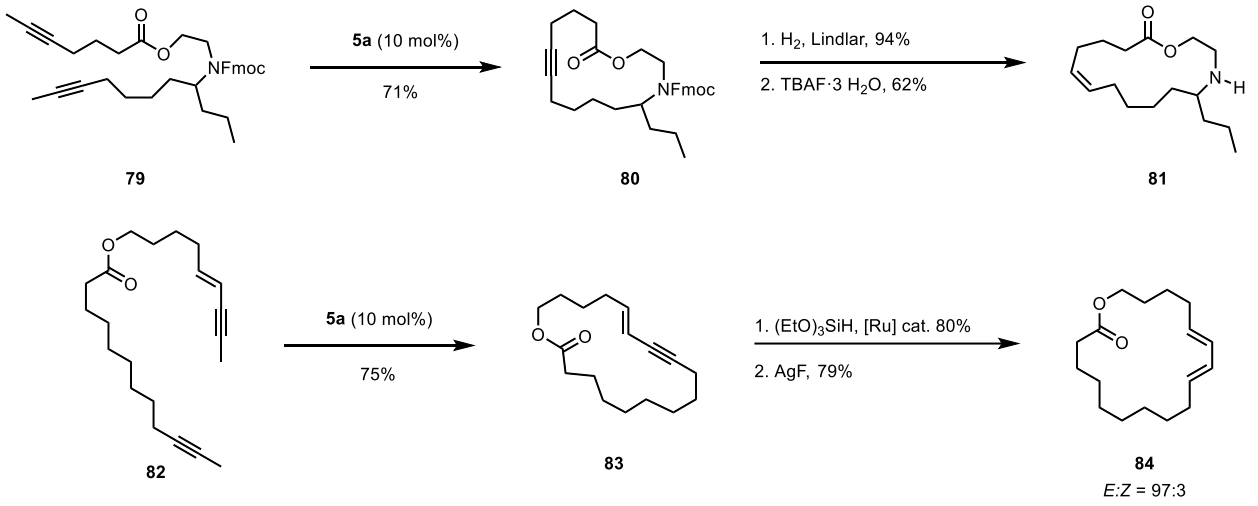


**Scheme 22.** Stereoselective synthesis of macrocyclic (*Z*)- or (*E*)-alkenes.

The excellent application profile and the outstanding functional group tolerance of molybdenum alkylidynes **72** endowed with triphenylsilanolates have been demonstrated in several challenging natural product syntheses (**85**-**88**) (**Figure 5**).[128-131]

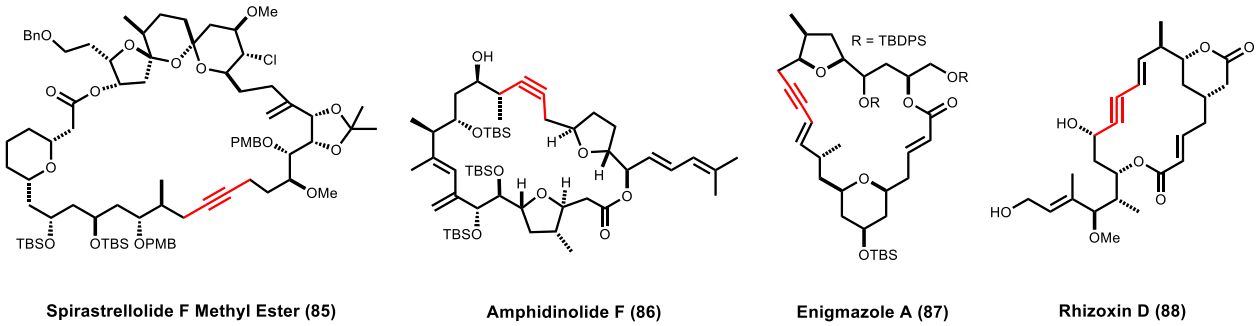


**Figure 5.** Selected examples of ring-closing alkyne metathesis products at the indicated alkyne (red) by relatives of **72**.

Furthermore, propargylic alcohols have emerged as a very useful synthetic linchpin in natural product synthesis (**Scheme 23**). Ring-closing alkyne metathesis of diyne **89** and deprotection of the silyl ether gave propargylic alcohol **90**. Subsequent *cis*-reduction of **90** gave selective access to (*Z*)-isomer **91**. Ruthenium-catalyzed *trans*-hydrostannation of **90** afforded stannane **92**, which in turn can be converted to the natural product **93** by Stille coupling or transformed into a platform of different analogue **94a**-**e**.[132]

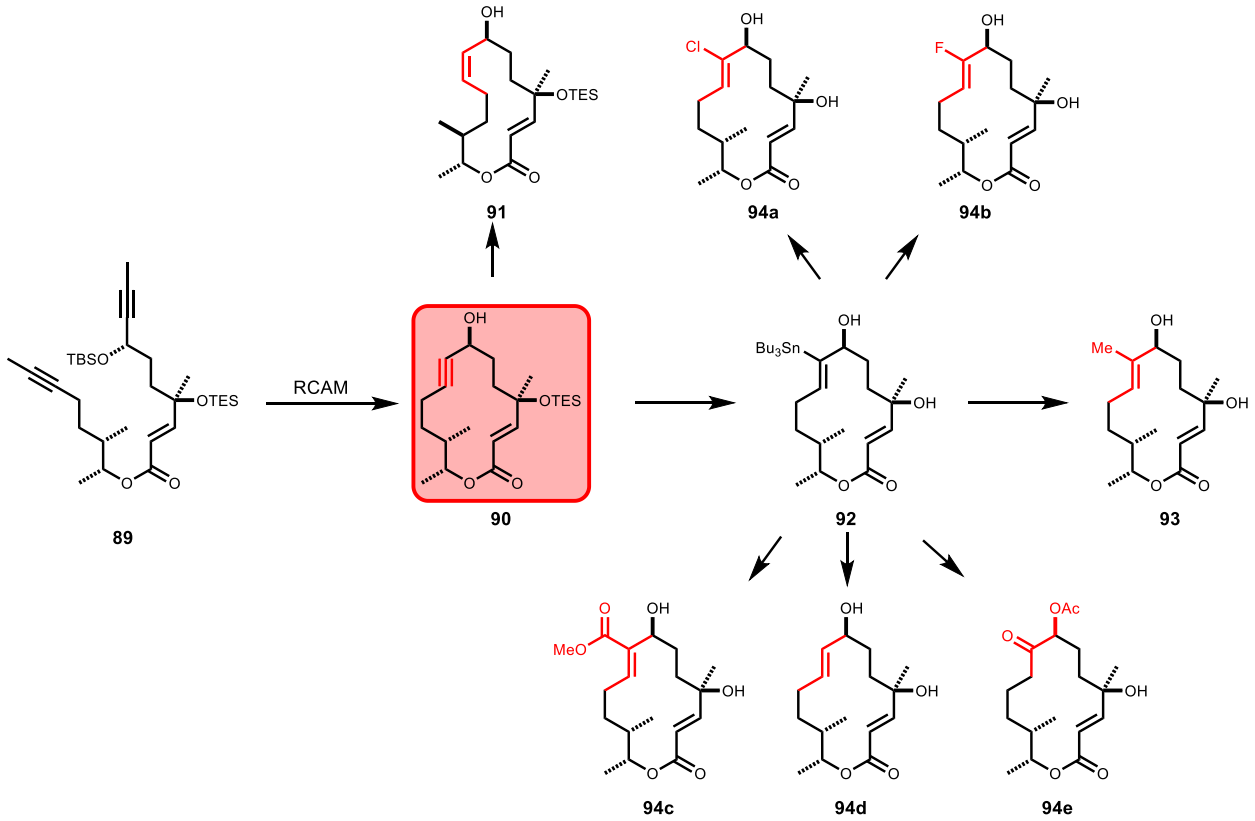


**Scheme 23.** Propargylic alcohols as a synthetic linchpin to streamline the access to various analogues.

## 1.6.2 Terminal Alkyne Metathesis

Terminal alkynes are problematic substrates for alkyne metathesis and there are only few successful examples in the literature. The reasons were quickly elucidated by the isolation of several $\eta^3$-bond deprotio-metallacyclobutadiene complexes **97** of tungsten and molybdenum, which form upon a

transannular C–H activation on the stage of the metallacyclobutadiene complex **96** (**Scheme 24**).[95, 113, 133-135] Rearrangement to an alkynyl-alkylidene unit gave a complex of type **98** for rapid alkyne polymerization. Another likely decomposition pathway involves the dimerization of the methylidyne complex **100** to give dimetallatetrahedrane **101**. Insertion of additional alkynes opened up another competitive channel for polymerization.[136-138]

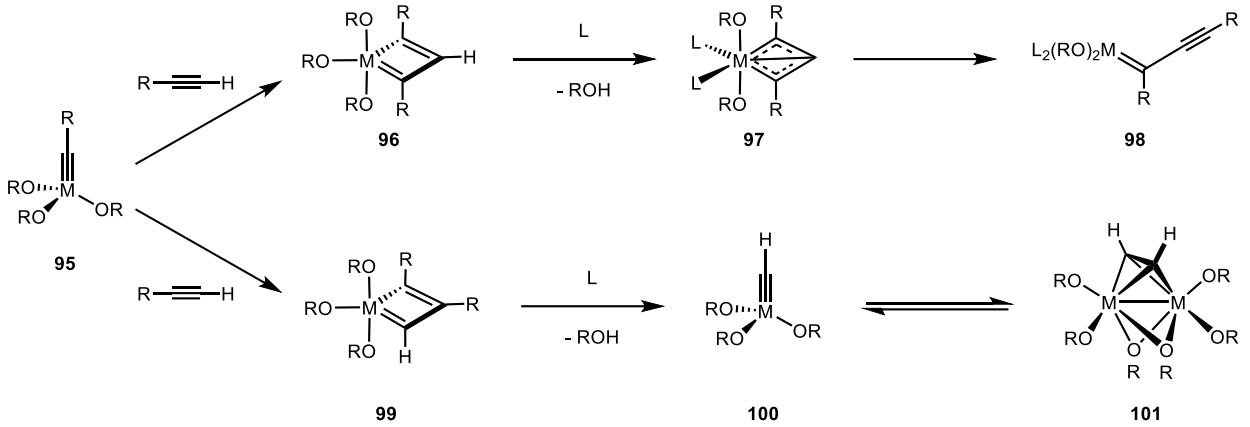


**Scheme 24.** Formation of deprotio-metallacyclobutadiene complex; M = Mo, W, L = neutral ligand.

In recent years, efforts have been made to improve the efficiency of terminal alkyne metathesis. Mortreux and co-workers showed that addition of quinuclidine to tungsten alkylidyne catalyst **5** gave improved selectivity for metathesis of aliphatic terminal alkynes over undesired polymerization.[139] Furthermore, they developed a hemilable bidentate coordinated dinuclear complex that allowed for the metathesis of phenylacetylene.[140] Tamm and co-workers followed up with a molybdenum complex endowed with fluorinated alkoxides that efficiently metathesizes aliphatic terminal alkynes at very high dilution.[98] Fürstner and co-workers reported the first efficient alkyne cross-metathesis (ACM) of terminal alkynes with propynyl(trimethyl)silane.[141]

# 2 Aims and Scope

Since evidence for the formation of a well-defined tripodal catalyst is missing, we encountered several challenges to be addressed for the development of the next generation of alkyne metathesis catalysts. A new tripodal ligand design is required that is more preorganized to prevent competing oligomerization but entails enough flexibility for passing through the catalytic cycle. A silanolate based tripodal ligand is most desirable due to favorable synergy with molybdenum alkylidynes. The ligand synthesis should be facile, modular and scalable. Additionally, a more practical precatalyst is necessary to allow for a better complexation and easier isolation of these catalysts. Furthermore, a tripodal catalyst design would allow the steric and electronic environment around the metal center to be leveraged to a level where catalytic activity and functional group tolerance are well balanced. Finally, we envisioned to extend the coverage to tripodal tungsten alkylidyne catalysts for alkyne metathesis.

# 3 Results

## 3.1 Molybdenum Alkylidyne Complexes for Alkyne Metathesis

### 3.1.1 Ligand Design and Practical Complexation Method

We thought to tackle these challenges by the ligand design shown in **Scheme 25**.[142] A simple three-step sequence converted 2-bromoacetophenone (**102**) into trisilanol **105** on scale. The cyclocondensation of **102** was initially performed in neat triflic acid at 130 °C to afford compound **103** in 59% yield (**Scheme 25**).[143] Later, we discovered that *in situ* release of HCl from $SiCl_4$ and EtOH at 0 °C gave very clean formation of **103** in 90% yield on a 20 g scale. The structure of compound **103** was confirmed by X-ray diffraction (**Figure 6**). Metal-halogen exchange with excess *t*BuLi in diethyl ether at −125 °C and quenching with $Ph_2Si(OMe)_2$ gave access to **104** in 75% yield. As evidenced by the solid state structure, the methoxy groups in compound **104** prevent a $C_3$-symmetric conformation (**Figure 6**). Simple hydrolysis with concentrated, aqueous HCl solution in THF afforded trisilanol **105** in quantitative yield. Colorless crystals suitable for single-crystal X-ray diffraction were grown by storing a concentrated toluene solution of **105** at 5 °C for three days. In the solid state structure of **105** co-crystallized with one water molecule and showed the desired "upward/inward"-orientation of all three Si–OH groups (**Figure 6**). The $C_3$-symmetric conformation is stabilized by a hydrogen-bonding array and sets the necessary level of preorganization to form a well-defined podand complex.

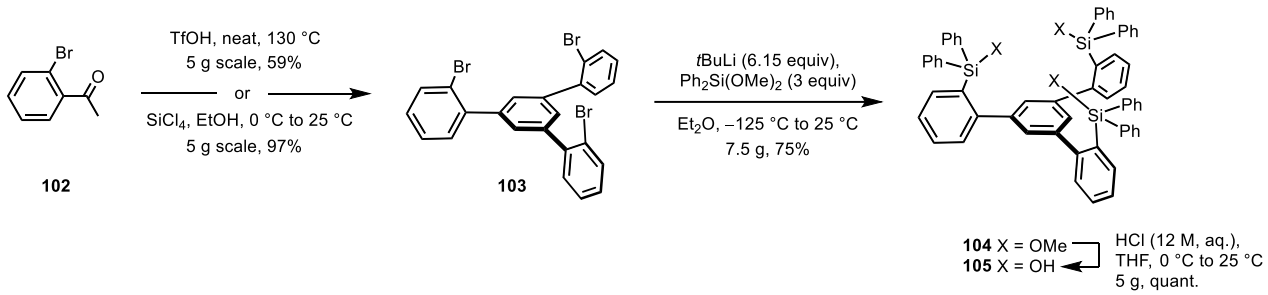


**Scheme 25.** Ligand synthesis of **105** on gram scale.

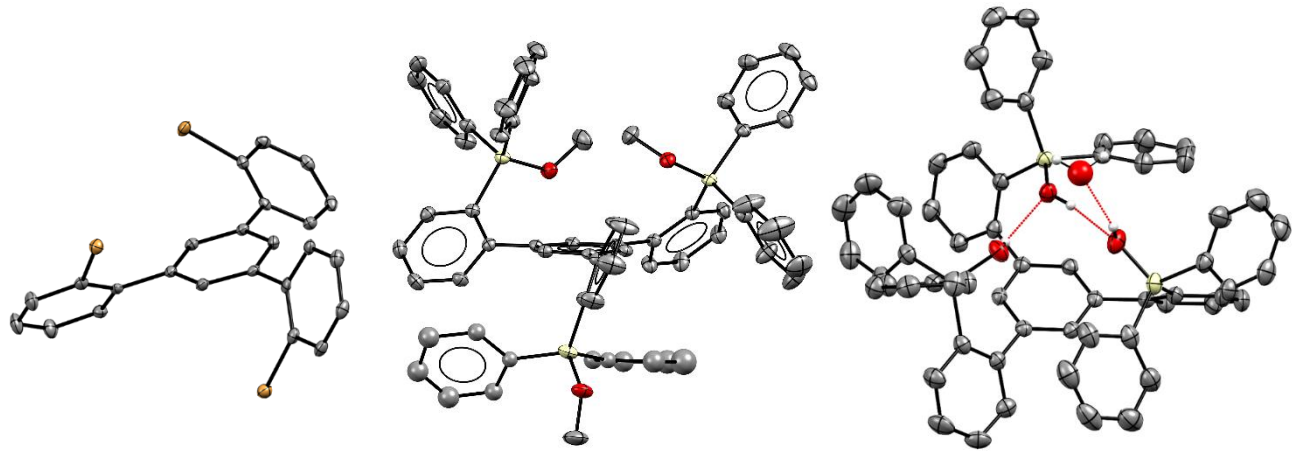

**Figure 6.** Solid state structure of **103, 104** and **105**·$H_2O$; disorder omitted for clarity; only H-atoms involved in hydrogen bonding are shown.

With regard to the actual complexation, we envisioned to use a more practical precatalyst than **61**. Ligand exchange of tribromide complex **106** with sodium *tert*-butoxide provided a very convenient solution to this problem (**Scheme 26**). In contrast to precatalyst **61,** complex **107** was readily accessible on scale. The more basic *tert*-butoxy ligands of **107** will deprotonate triarylsilanol **105** and facilitate the ligand exchange to release *t*BuOH as the only by-product.

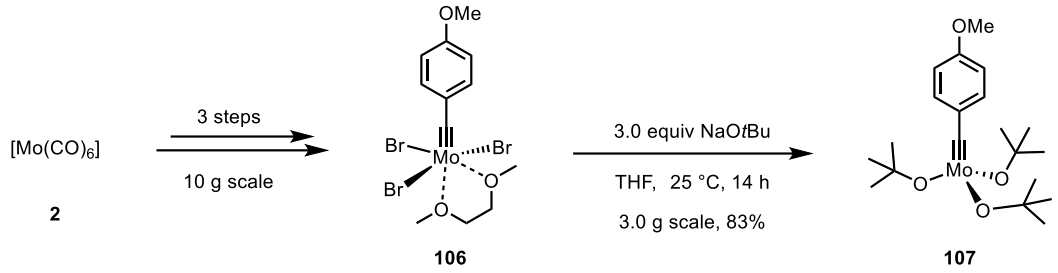


**Scheme 26.** Preparation of molybdenum precatalyst **107** on gram scale.

Stirring of a solution of precatalyst **107** and triarylsilanol **105** in toluene at ambient temperature gave, after evaporation of the released *t*BuOH and solvent in high vacuum, complex [**108**]$_2$ in essentially quantitative yield on a 1 g scale (**Scheme 27**). Complex [**108**]$_2$ was only poorly soluble in [$D_8$]-toluene.

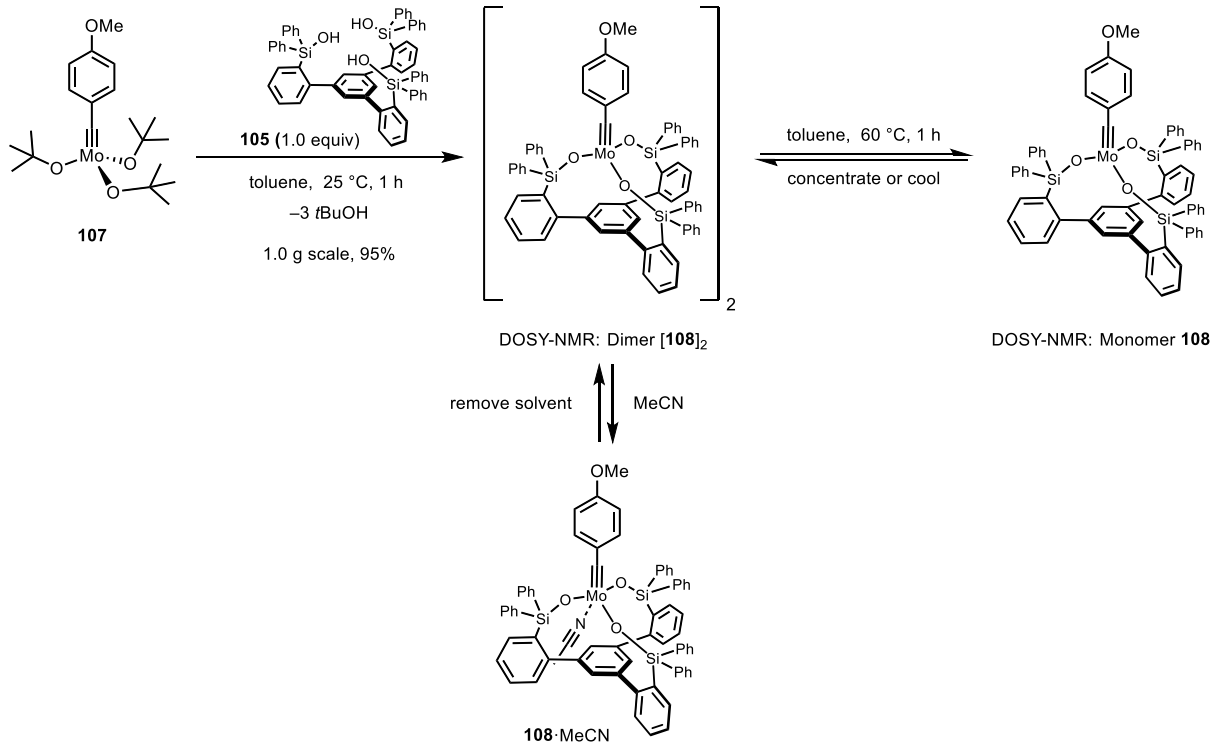


**Scheme 27.** Preparation of structurally well-defined alkyne metathesis catalyst **108**.

Similarly, stirring of a solution of precatalyst **109** and triarylsilanol **105** in toluene at ambient temperature gave complex [**110**]$_2$ in 98% yield on a 1 g scale (**Scheme 28**).

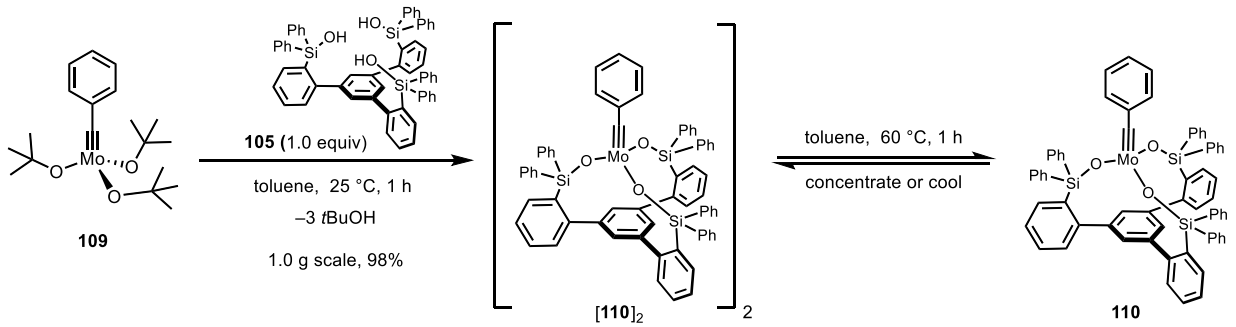


**Scheme 28.** Preparation of structurally well-defined alkyne metathesis catalyst **110**.

### 3.1.2 Aggregation Issue and Isolation of a Tetrameric Molybdenum Complex

Although the NMR signals spoke for a well-defined complex, they did not correspond to the targeted $C_3$-symmetric complex **108**. Heating of a solution of [**108**]$_2$ in [D$_8$]-toluene for 60 min at 60 °C quantitatively formed the monomeric complex **108** (**Figure 7**). Normalized time scale analysis of a simple homo-metathesis reaction confirmed that the reaction has a first-order dependency on the concentration of monomeric complex **108**.[144, 145] Upon evaporation of the solvent or cooling, monomeric complex **108** reverted to [**108**]$_2$. Due to this equilibrium, it has been particularly difficult to obtain a crystal structure and confirm the proposed dimeric structure.

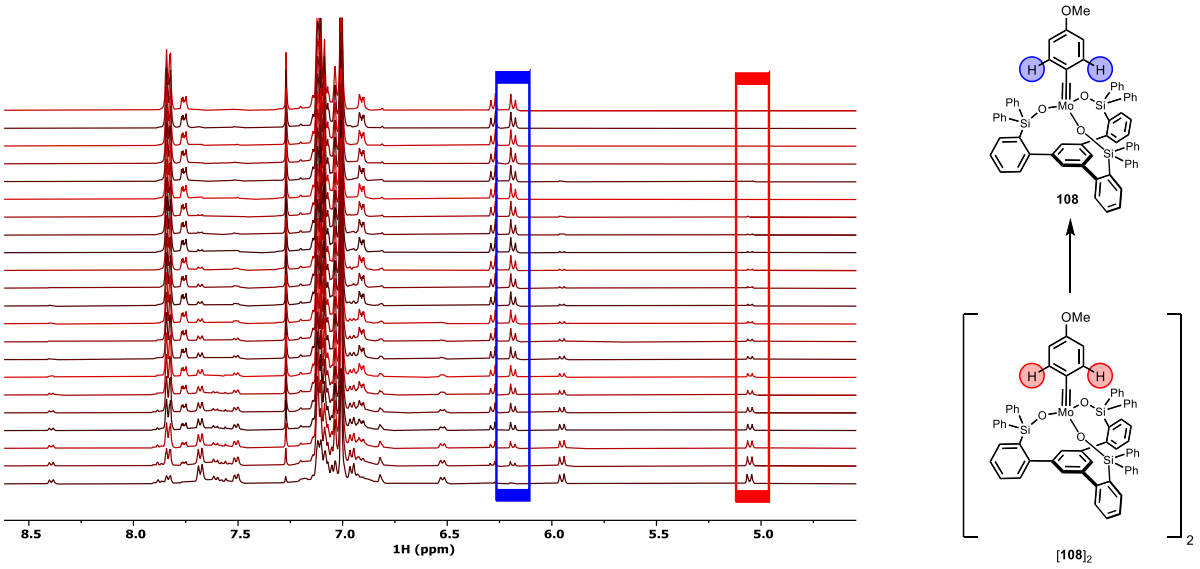


**Figure 7.** $^1$H NMR study of [**108**]$_2$ and **108** recorded in [D$_8$]-toluene at 60 °C over the course of 1 h.

Therefore, we used DOSY NMR to study the different molecular weights and sizes of both molecules. Recently, Evans and co-workers reported on the direct correlation of measured diffusion coefficient with the molecular mass of a molecule (or *vice versa*).[146] Specifically, this method allows to differentiate between monomeric and oligomeric entities that are of different mass. Indeed, when we recorded DOSY spectra of a ≈ 1:1 mixture of both compounds, we observed significantly different diffusion constants (**Table 1**). The predicted *D*-values for the monomer **108** corresponded very well to the experiment and gave confidence in the assignment. The DOSY value of [**108**]$_2$ is smaller and matched to an aggregate of higher molecular weight, likely dimeric or potentially trimeric/tetrameric.

**Table 1.** Measured and predicted diffusion coefficients (*D*) of the different complexes.

| Complex | MW (g·mol$^{-1}$) | $D_{predicted}$ [m$^2$·s$^{-1}$] | $D_{exp.}$ [m$^2$·s$^{-1}$] [a] | Δ |
|---|---|---|---|---|
| **108** | 1113.33 | $5.55\cdot10^{-10} \pm 1.6\cdot10^{-10}$ | $5.557\cdot10^{-10}$ | 0.04% |
| [**108**]$_2$ | 2226.66 | $4.11\cdot10^{-10} \pm 1.0\cdot10^{-10}$ | $3.302\cdot10^{-10}$ | −19.3% |
| [**108**]$_3$ | 3339.99 | $3.47\cdot10^{-10} \pm 1.0\cdot10^{-10}$ | $3.302\cdot10^{-10}$ | −4.47% |
| [**108**]$_4$ | 4453.32 | $3.09\cdot10^{-10} \pm 1.0\cdot10^{-10}$ | $3.302\cdot10^{-10}$ | 7.37% |
| **108**·MeCN | 1154.38 | $5.43\cdot10^{-10} \pm 1.6\cdot10^{-10}$ | $5.458\cdot10^{-10}$ | 0.50% |

Previously, we have noticed that molybdenum silanolate complexes are strongly Lewis acidic and in the presence of excess ligand they tended to form the corresponding ate-complex **73** (*vide supra*). Because aggregates of higher composition have never been observed before, we were committed to clarify the reasons for the formation of [**108**]$_2$. Initially, the strongly shielded *ortho*-benzylidyne protons of [**108**]$_2$ ($\delta_H$ ([D$_6$]-benzene) = 5.00 ppm) directed our attention towards a non-covalent π-interaction. Direct comparison to the monodentate complex **111** ($\delta_H$ ([D$_6$]-benzene) = 5.55 ppm)

showed similarly shielded *ortho*-benzylidyne protons, although this effect seemed to be even stronger in [**108**]$_2$ (**Figure 8**).

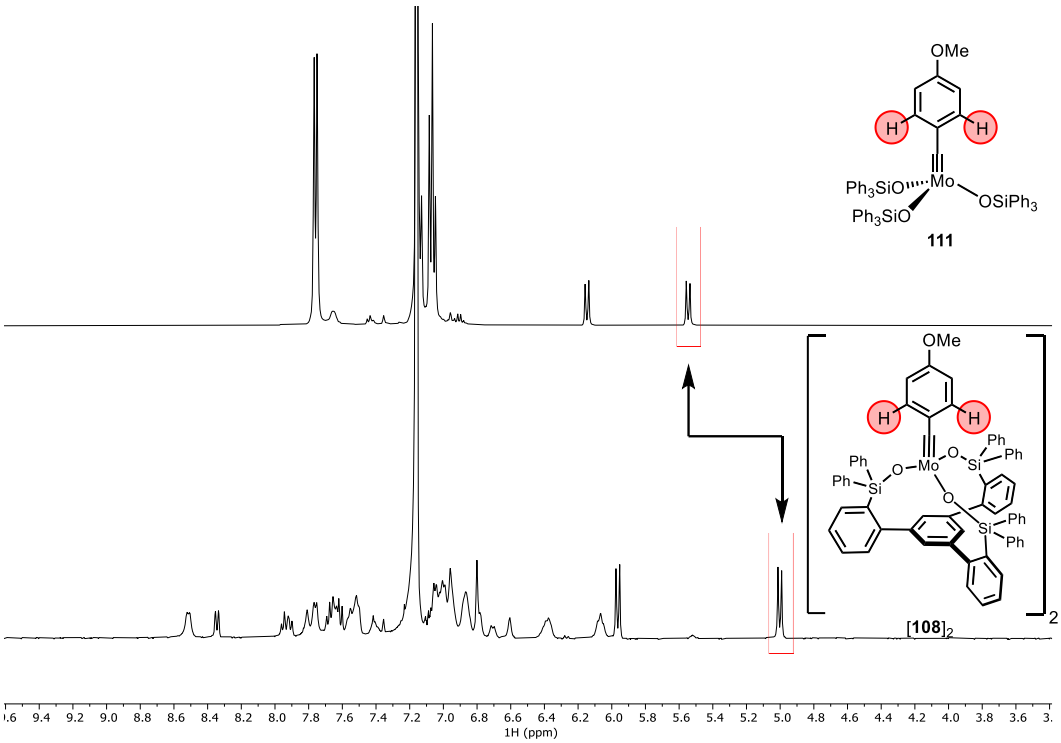


**Figure 8.** $^1$H NMR study of **111** and [**108**]$_2$ in [D$_6$]-benzene at 25 °C.

Upon addition of excess MeCN to a solution of **111** in [D$_8$]-toluene, the *ortho*-benzylidyne protons shifted in the $^1$H NMR spectrum about ~ 0.9 ppm downfield, which signified a disturbance of the peculiar interaction (**Figure 9**).

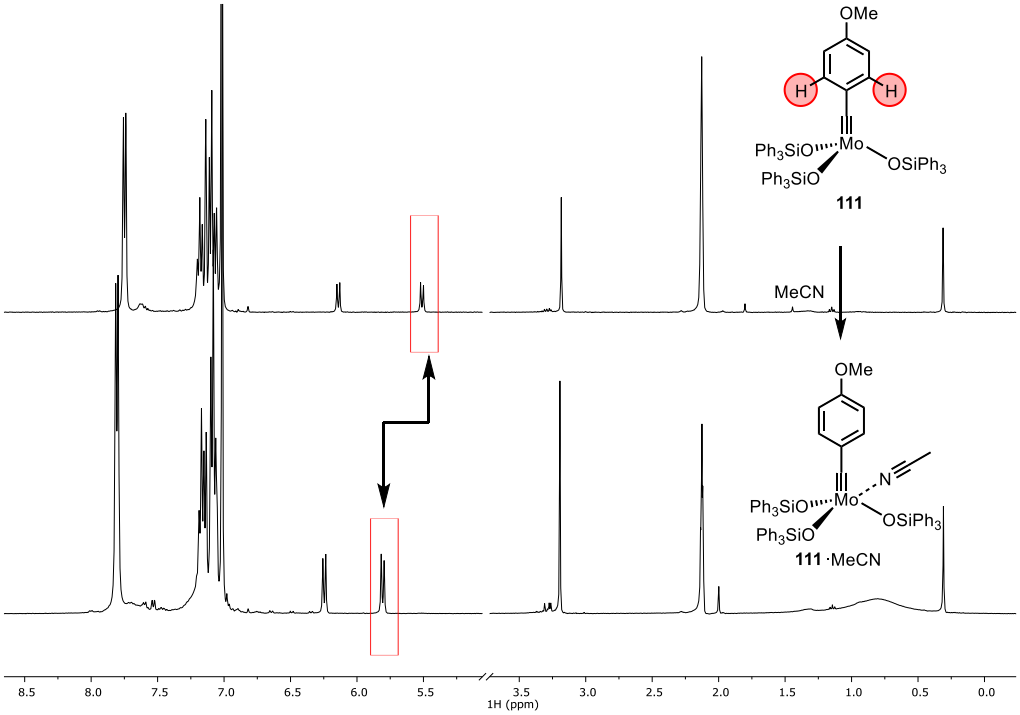


**Figure 9.** $^1$H NMR study: MeCN addition to a solution of **111** in [D$_8$]-toluene at 25 °C.

A detailed NMR study of [**108**]$_2$ intended to clarify the proposed dimeric composition. A solution of [**108**]$_2$ in [D$_8$]-toluene was cooled from 25 °C to −40 °C. Sharp signal sets were observed at −10 °C, which upon further cooling to −40 °C broadened again (**Figure 10**). The strongly shielded dublett (~ 4.9 ppm) arising from the *ortho*-protons on the alkylidyne unit were even more shielded when cooling to −40 °C; this observation supported the proposed anisotropic effect.

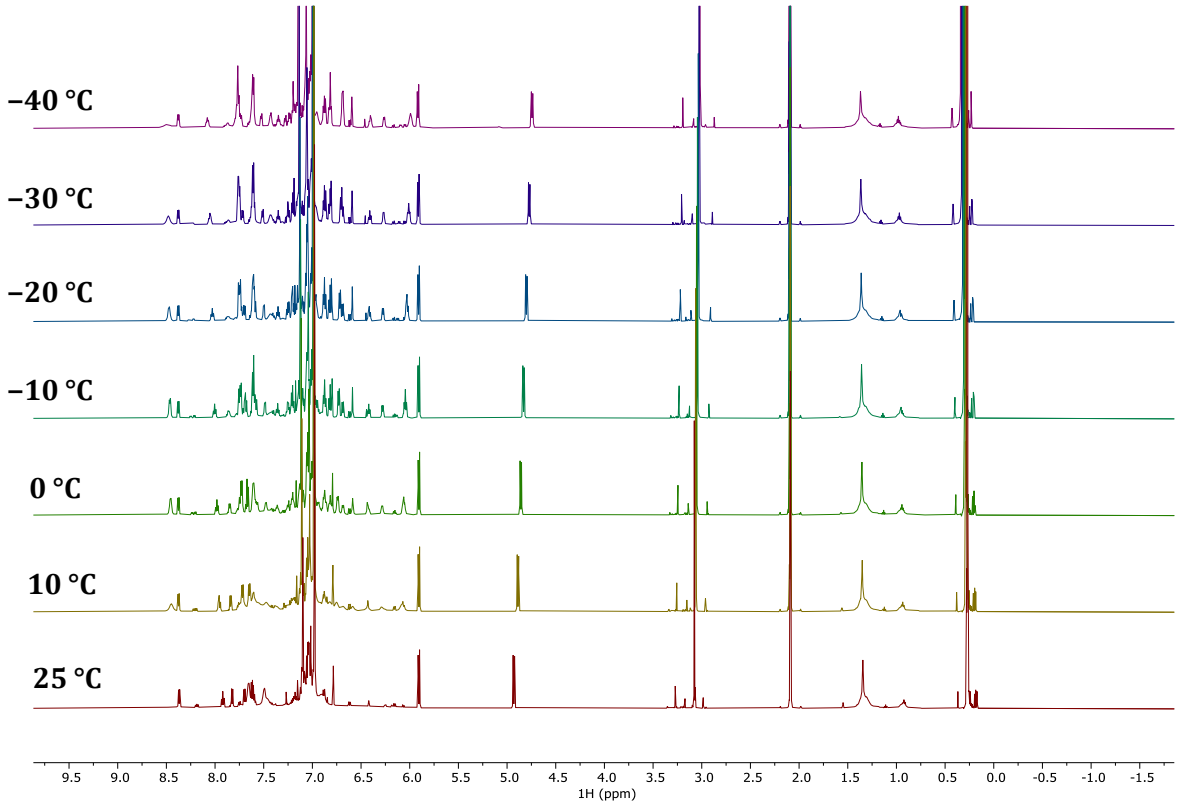


**Figure 10.** VT NMR study of [**108**]$_2$ in [D$_8$]-toluene from 25 °C to −40 °C.

A $^{29}$Si NMR experiment gave three distinct signals for [**108**]$_2$, confirming the asymmetry of this species (**Figure 11**). However, it is not entirely clear, which symmetry tentative [**108**]$_2$ does show and thus the NMR studies did not allow the composition of it to be determined.

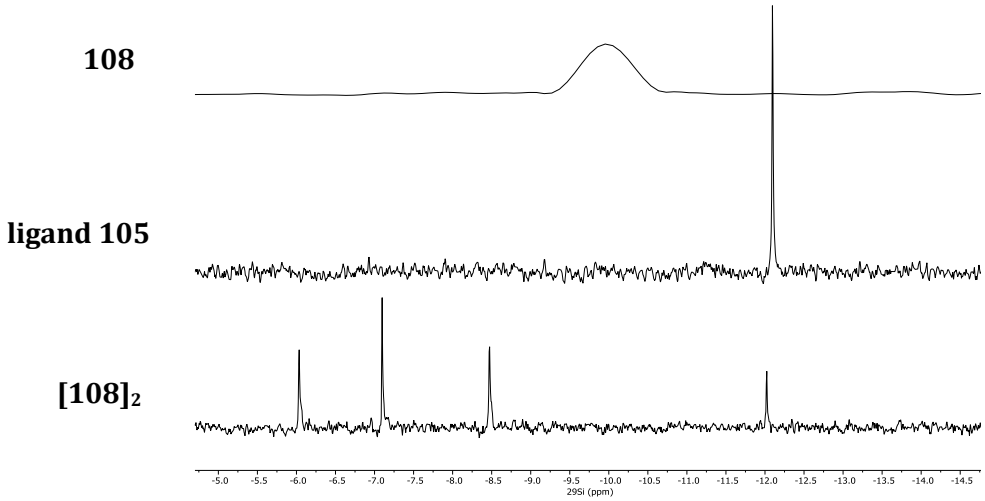


**Figure 11.** $^{29}$Si NMR projection from 2D-measurement of **108** in [D$_8$]-toluene at 25 °C; 1D-$^{29}$Si NMR of free ligand **105** in [D$_8$]-toluene at 25 °C; 1D-$^{29}$Si NMR of [**108**]$_2$ in [D$_8$]-toluene at −10 °C.

The X-ray structure of **111** shows that the *ortho*-benzylidyne protons resides within the anisotropy cone of the adjacent phenyl groups, which nicely explained the strong shielding of the *ortho*-protons (**Figure 12** A). Furthermore, two molecules in the unit cell are in close contact and exhibited several C–H/π and π/π interactions (**Figure 12** B).[113]

A)

B)

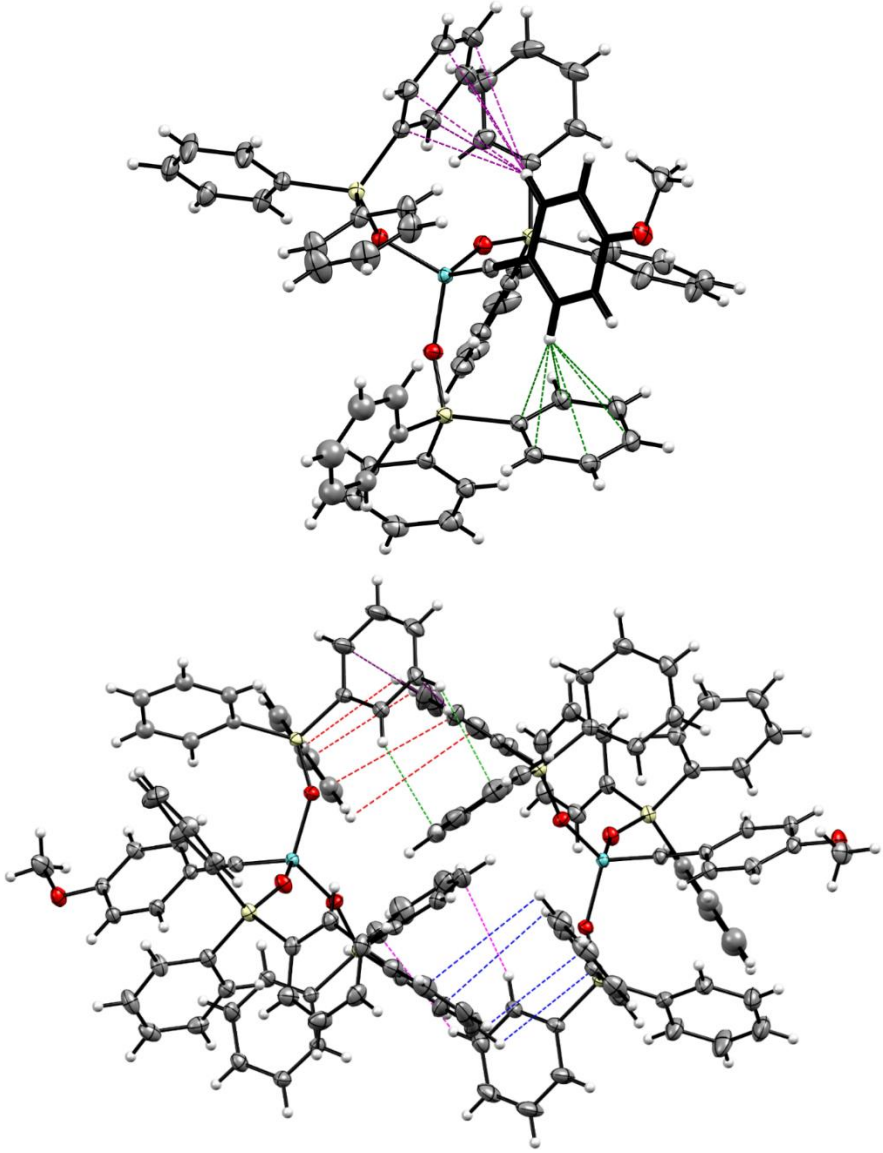

**Figure 12.** A) C–H/π interaction of **111** in the solid state B) Several C–H/π and π/π interaction of [**111**]$_2$ in the solid state.[113]

This dimeric aggregate [**111**]$_2$ of the solid state was also present in concentrated solution as judged by DOSY NMR (**Table 2**). Under catalytic conditions, it was fully dissociated to the monomeric complex **111** even without heating.

**Table 2.** Measured and predicted diffusion coefficients (D) of **111** and [**111**]$_2$.

| Complex | MW [g mol$^{-1}$] | $D_{predicted}$ [$10^{-10}$ m$^2$s$^{-1}$] | | $D_{exp.}$ [$10^{-10}$ m$^2$ s$^{-1}$] | | Conc. [M] | Δ |
|---|---|---|---|---|---|---|---|
| **111** | 1041.31 | 5.72 | ±1.7 | 6.02 | ±0.12 | 0.006 | 5.2% |
| **[111]$_2$** | 2082.62 | 4.23 | ±1.2 | 4.18 | ±0.04 | 0.16 | -1.3% |
| **111**·MeCN | 1082.36 | 5.6251 | ±1.6 | 5.87 | ±0.22 | 0.016 | 4.3% |

Since we could not grow crystals of suitable quality for X-ray diffraction, we cannot exclude a covalent cross-linking in [**108**]$_2$. We were also not able to determine the composition of presumed [**108**]$_2$ by several high resolution mass spectrometry measurements with either THF, MeCN or pyridine as the solvent (only monomeric **108** was detected). However, we could confirm the structure of monomeric molybdenum alkylidyne complex **108** by adding MeCN. Dissolving [**108**]$_2$ in benzene/MeCN (1:2) and carefully layering this solution with excess *n*-pentane gave, after three days at ambient temperature, dark blue crystals of adduct **108**·MeCN, which reverted to [**108**]$_2$ upon evaporation of the solvent (**Scheme 27**). The solid state structure of **108**·MeCN shows the expected monomeric podand-like molybdenum alkylidyne complex bearing an "end-on" bound MeCN ligand (**Figure 13**). The diffusion coefficient of **108**·MeCN determined by DOSY spectroscopy is very similar to that of **108**, which confirmed the notion that **108** itself is a monomeric species formed by dissociation of an aggregate. The solid state structure is best described as a square pyramidal coordinate geometry. The "end-on" coordinated MeCN ligand deviated strongly from linearity as the Mo-N-C angle is notably bent (163.2(2)°). This might result from π-backdonation from the filled molybdenum alkylidyne orbitals into the empty π* orbitals of the N≡C triple bond. The coordination *trans* to the alkylidyne can be excluded since the podand ligand blocks this coordination site by the basal phenyl ring.[113] Although, the basal phenyl ring is far away from the molybdenum atom (3.5–4.0 Å), we cannot exclude a through-space orbital interaction.[147, 148] The Mo≡C bond distance of 1.742(2) Å and the Mo≡C-Ar bond angle of 161.4(2)° are in the range of known molybdenum alkylidyne complexes.[113] Further analysis revealed that the Si–O–Mo bond angles ($<_{avg.}$ = 162.7(3)°) are more obtuse in comparison to those of the similar monodentate complex **68**·MeCN ($<_{avg.}$ = 156.3(5)°).[113] Previously, the outstanding cooperativity of molybdenum triphenylsilanolates has been attributed to the flexible bending and stretching of the Mo–O–Si hinges. However, the rigidified new podand complex does not preclude alkyne metathesis from occurring and teaches us a fundamental lesson about the necessary parameters for catalytic performance.

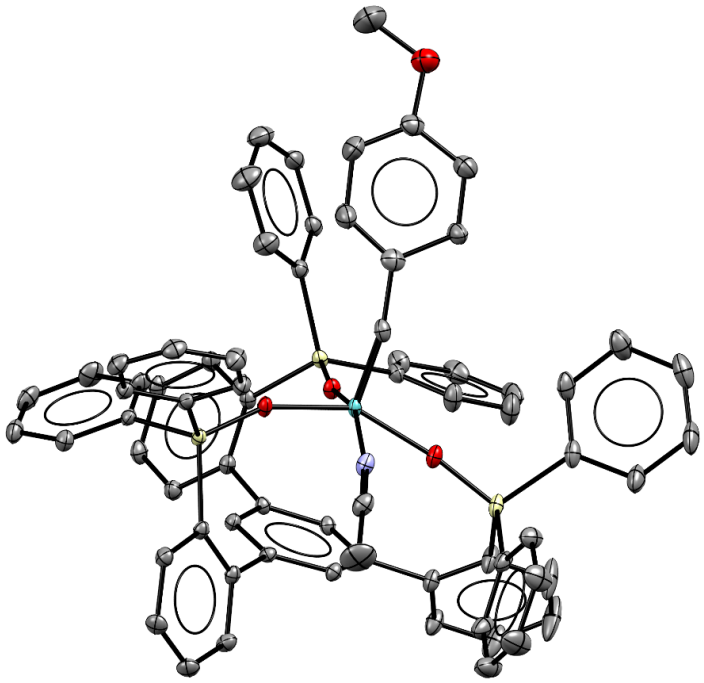

**Figure 13.** Solid state structure of catalyst **108**·MeCN.

Next, we prepared the more electron-donating trisilanol **112**. Dimethoxybis(4-methoxyphenyl)silane (**113**) was made by double substitution of tetramethyl orthosilicate with aryl

Grignard reagent.[149] Compound **113** was subjected to the previously established lithiation/quenching sequence to furnish protected trisilanol **114** in 12% yield. Hydrolysis with concentrated, aqueous HCl gave trisilanol **112** in 99% yield (**Scheme 29**).

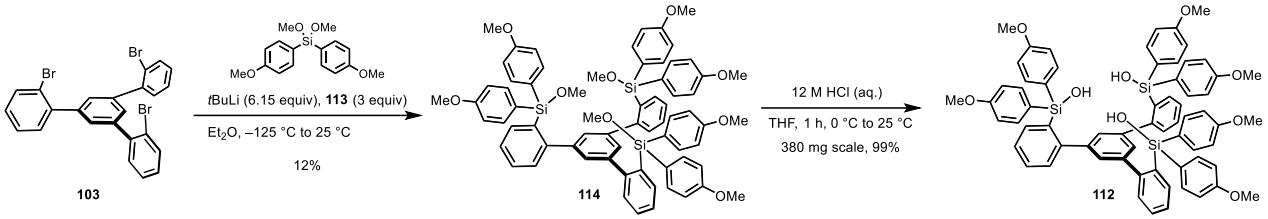


**Scheme 29.** Preparation of trisilanol **112**.

The reason for the low-yielding first step was the formation of the constitution isomer **115** as the major side-product, which was isolated in 43% yield after preparative HPLC separation (**Figure 14**). The NMR department confirmed the connectivity and structure of **115**, which is likely the result of an intra- or intermolecular C–H metalation (see **Figure 14**). Variation of the temperature or the order of addition did not improve the selectivity for the desired compound **112**. In order to prevent the formation of the constitutional isomer **115**, it might be worthwhile to reduce **113** to the corresponding Si–H compound and then subject it to the lithiation/quenching sequence.

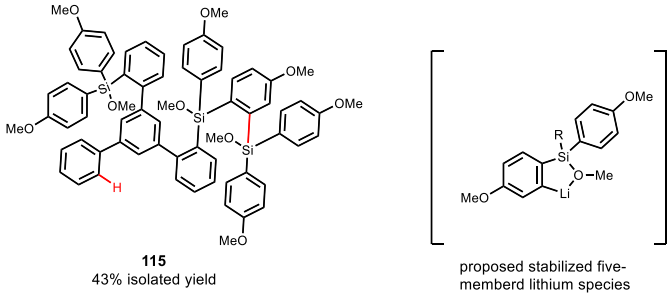


**Figure 14.** Isolated major side-product **115** and proposed five-membered intermediate.

The solid state structure of ligand **112** confirmed the $C_3$-symmetric conformation, which is stabilized by a hydrogen-bonding array and sets the necessary level of preorganization to form a well-defined podand complex (**Figure 15**).

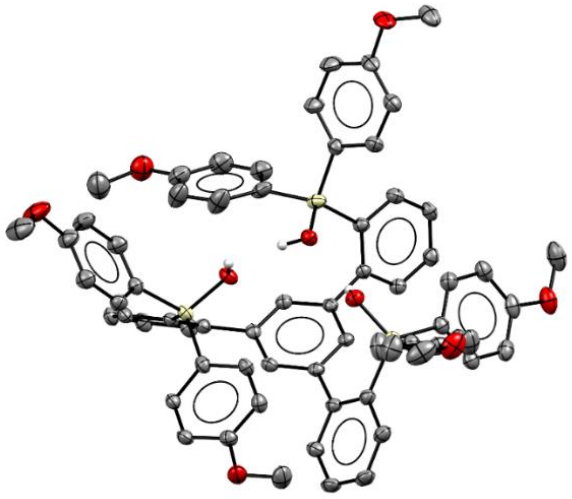

**Figure 15.** Solid state structure of **112**; disorder omitted for clarity and only H-atoms involved in hydrogen bonding are shown.

Stirring of a solution of precatalyst **107** and triarylsilanol **112** in toluene at ambient temperature and evaporation of the solvent gave complex [**116**]$_2$ as a yellow solid in 76% yield (**Scheme 30**). Similarly, monomeric complex **116** formed quantitatively after heating a solution of complex [**116**]$_2$ in toluene for 60 min at 60 °C (**Figure 16**). Several high resolution mass spectrometry measurements of a solution of [**116**]$_2$ in either THF or MeCN detected only monomeric **116**.

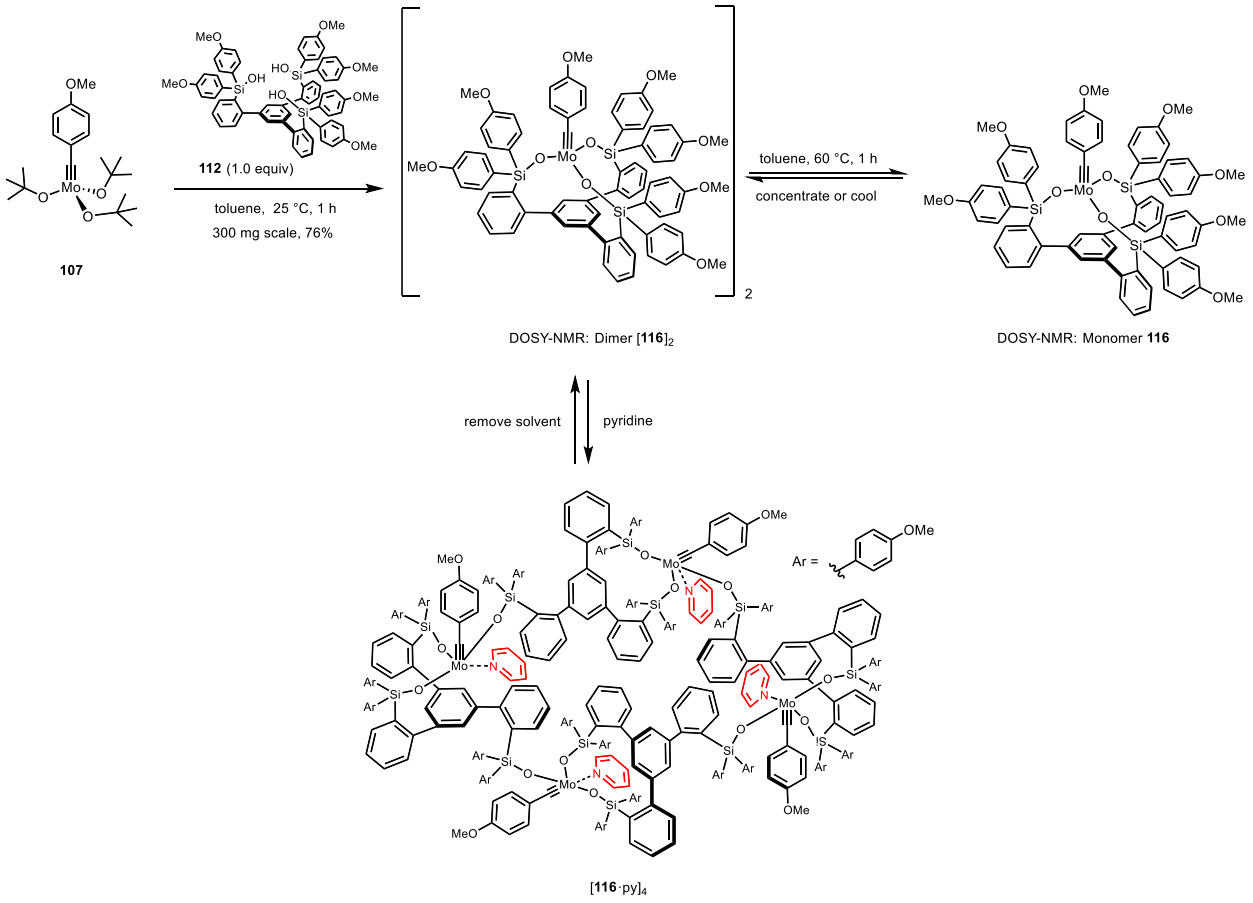


**Scheme 30.** Preparation of structurally well-defined alkyne metathesis catalyst **116** and isolation of [**116**·py]$_4$.

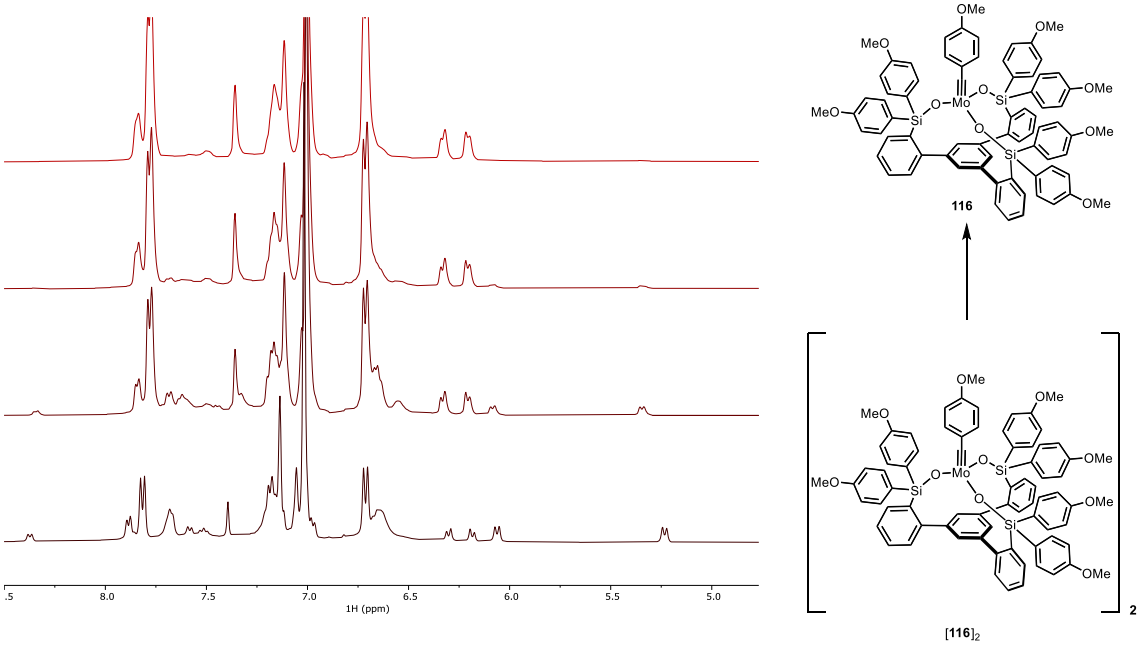


**Figure 16.** $^1$H NMR study of conversion of [**116**]$_2$ to [**116**] recorded in [D$_8$]-toluene at 60°C over the course of 1 h.

Again, we recorded DOSY spectra of a ≈ 1:1 mixture of both compounds and observed significantly different diffusion constants (**Table 3**). The predicted *D*-values for the monomer **116** corresponded very well to the experiment. The DOSY value of [**116**]$_2$ matched to an aggregate of higher molecular weight, most likely a tetrameric structure.

**Table 3.** Measured and predicted diffusion coefficients (*D*) of complexes.

| Complex | MW (g·mol$^{-1}$) | $D_{predicted}$ [m$^2$·s$^{-1}$] | $D_{exp.}$ [m$^2$·s$^{-1}$] [a] | Δ |
|---|---|---|---|---|
| **116** | 1293.48 | $5.20\cdot10^{-10} \pm 1.5\cdot10^{-10}$ | $4.758\cdot10^{-10}$ | −8.47% |
| [**116**]$_2$ | 2586.97 | $3.86\cdot10^{-10} \pm 1.1\cdot10^{-10}$ | $2.959\cdot10^{-10}$ | −23.36% |
| [**116**]$_3$ | 3880.45 | $3.27\cdot10^{-10} \pm 1.1\cdot10^{-10}$ | $2.959\cdot10^{-10}$ | −9.42% |
| [**116**]$_4$ | 5173.92 | $2.91\cdot10^{-10} \pm 1.1\cdot10^{-10}$ | $2.959\cdot10^{-10}$ | −1.73% |

Similarly, we intended to confirm this structure by adding a coordinating solvent such as pyridine to facilitate the dissociation and stabilize the monomeric form. The yellow solid of [**116**]$_2$ was dissolved in pyridine to give a deep purple solution. Layering this solution with *n*-pentane at ambient temperatures gave purple crystals suitable for X-ray diffraction. The solid state structure shows a tetrameric pyridine adduct [**116**·py]$_4$ which was confirmed by several independent crystallization batches (**Figure 17**). The unit cell is huge with a volume of 34696 Å$^3$, four tetrameric molecules occupy one unit cell. Intriguingly, all four molybdenum centers are almost in same distance to each other and form a folded square in that both opposite molybdenum centers are in the same plane (**Figure 18**). Removal of the excess pyridine *in vacuo* and measuring a $^1$H NMR in [D$_8$]-toluene showed monomeric complex **116**, which provided compelling evidence that this process is indeed reversible (**Scheme 30**).

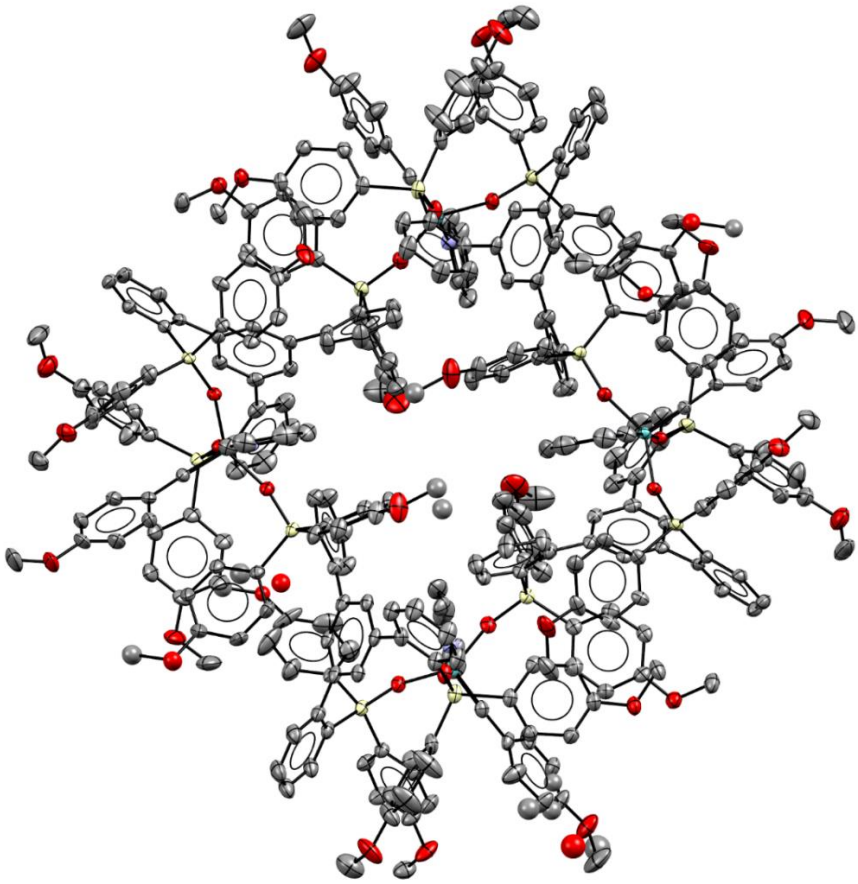

**Figure 17.** Solid state structure of tetrameric [**116**·py]$_4$.

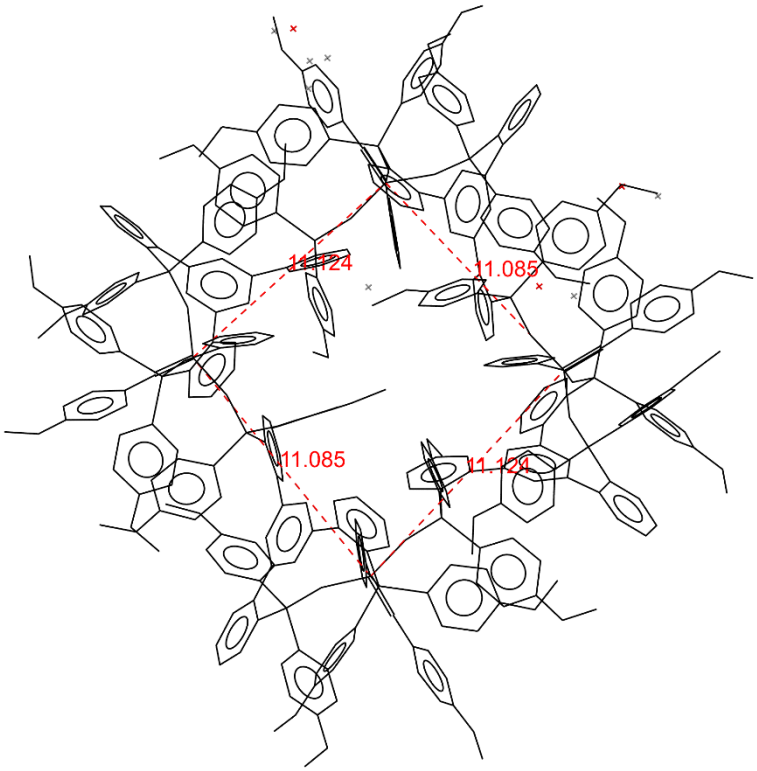


**Figure 18.** Solid state structure of tetrameric [**116**·py]$_4$.

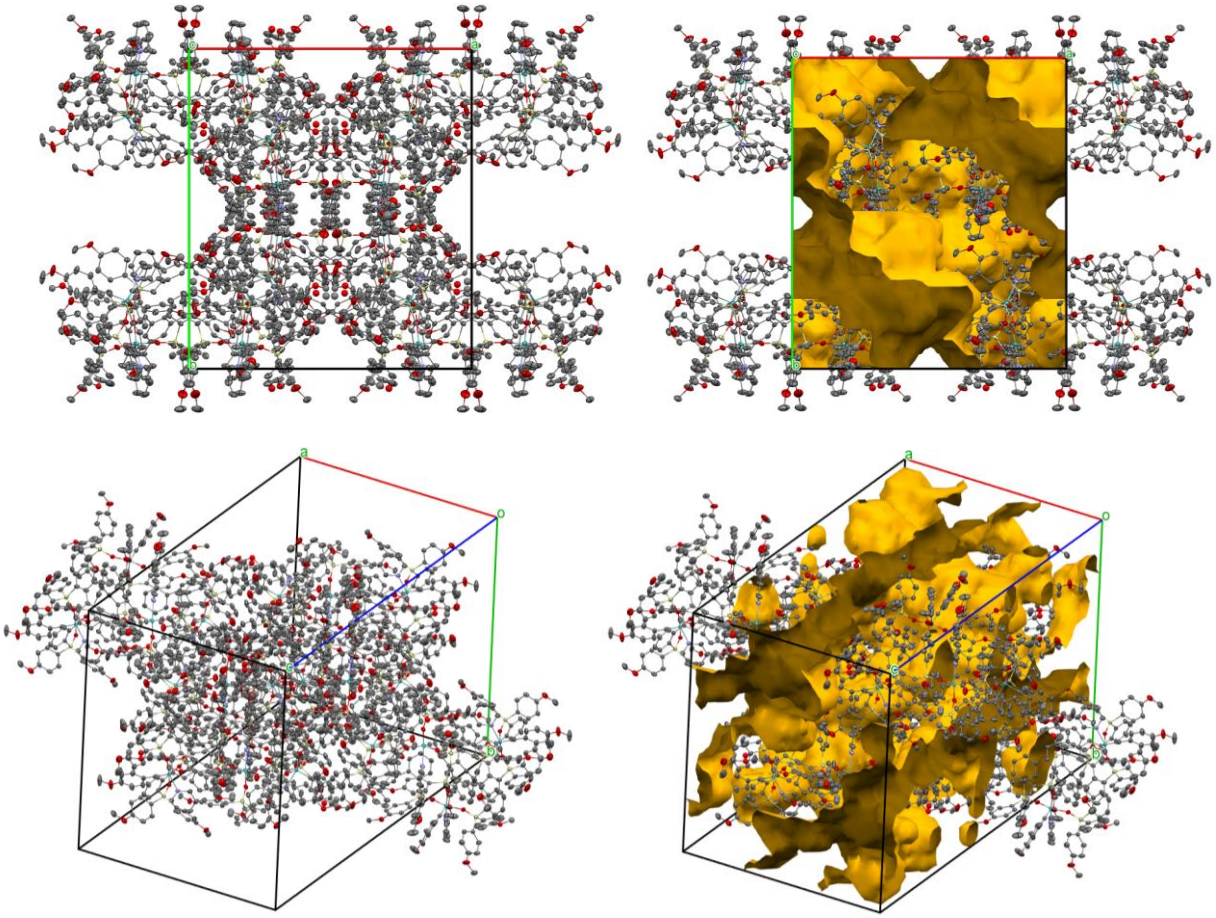

**Figure 19.** Packing of compound [**116**·py]$_4$ in the unit cell. View along the c axis (top left) and in a random orientation (bottom left). Calculated voids (probe radius 1.2 Å, 0.7 Å grid spacing) are shown on the right.

In addition, we were able to confirm the tetrameric structure by high-resolution mass spectrometry (theor. 2589.57955; found: 2589.58989; diff. (ppm) = -1.68) which corresponded to the di-cationic species (2589 = [5493 - 4·(py) + 2·H]$^{2+}$) and represented the tetrameric structure [**116**]$_4$ ($C_{296}H_{258}Mo_4O_4Si_{12}$) upon loss of four molecules of pyridine (**Figure 20**). Elemental analysis of the crystalline material matched well with the theoretical data (anal. calculated for $C_{316}H_{276}Mo_4N_4O_{40}Si_{12}$: C 69.13, H 5.07, N 1.02, 0 11.66, Si 6.14, Mo 6.99; found: C 67.81, H 4.92, N 0.98, Si 6.01, Mo 6.91.).

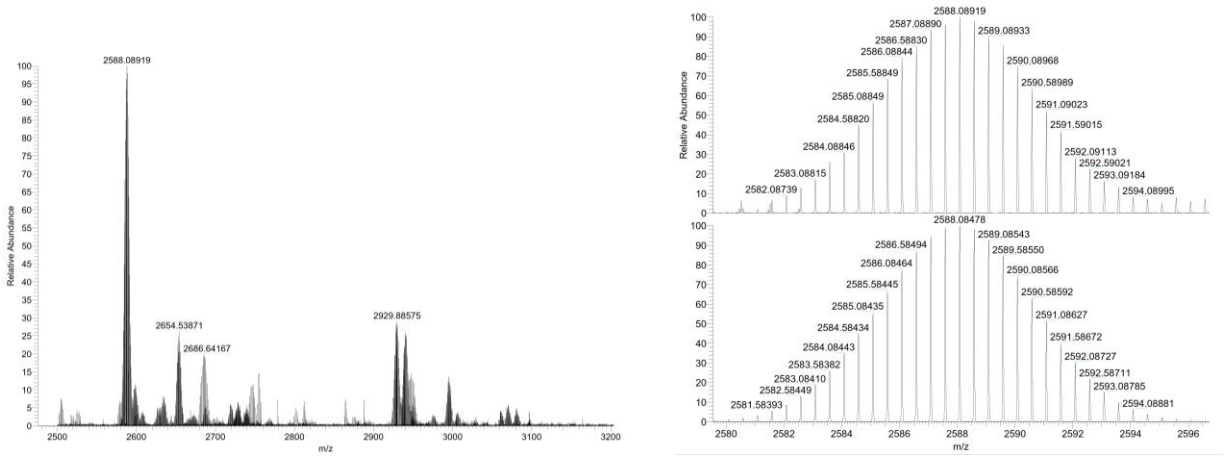


**Figure 20.** High resolution mass spectrometry ESI spectra of [**116**]$_4$.

Overall, the mass spectrometric data and the crystal structure of tetrameric molybdenum alkylidyne complex [**116**·py]$_4$ suggest that tripodal ligand spheres can covalently cross-link to give well-defined tetramers such as [**116**·py]$_4$ and are distinct species in respect to agglomerate [**116**]$_2$. Since mass spectrometry measurements of a solution of [**116**]$_2$ in either THF, MeCN or toluene as the solvent only gave evidence for monomeric **116**, we suppose that [**116**]$_2$ is the result of non-covalent π-interactions (**Figure 21**).

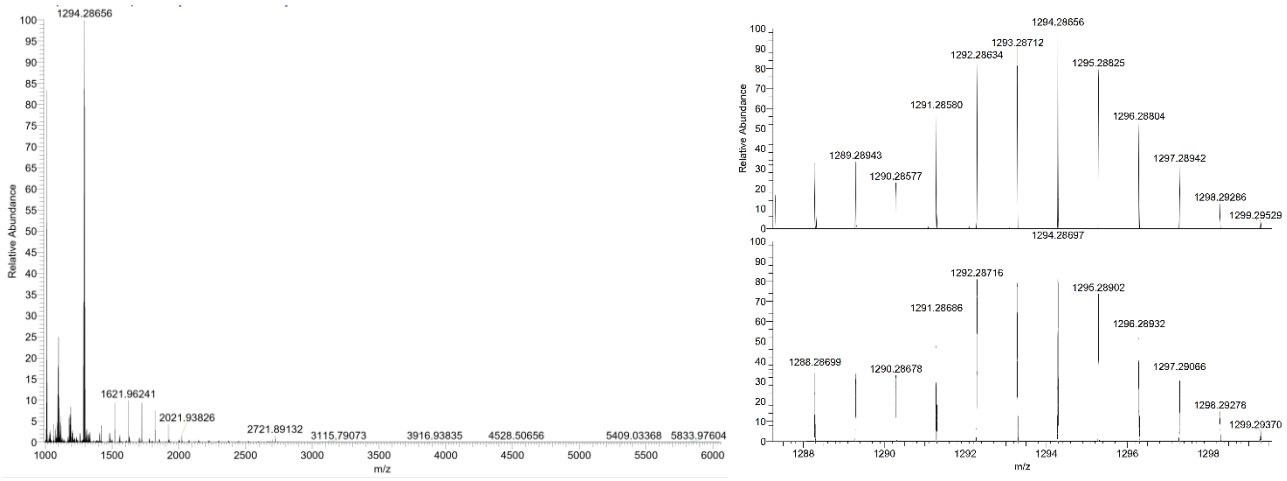


**Figure 21.** High resolution mass spectrometry ESI spectra of [**116**]$_2$.

### 3.1.3 Preparation of a Catalyst Library

Although this aggregation did not prevent alkyne metathesis from occurring (*vide infra*), the poor solubility and the need for heating to release the monomeric species were not ideal for catalysis. We conceived a strategy to circumvent this issue by substituting the *ortho*-benzylidyne protons with sterically bulkier groups or by replacing the phenyl groups on the silanolate ligand (**Figure 22**).

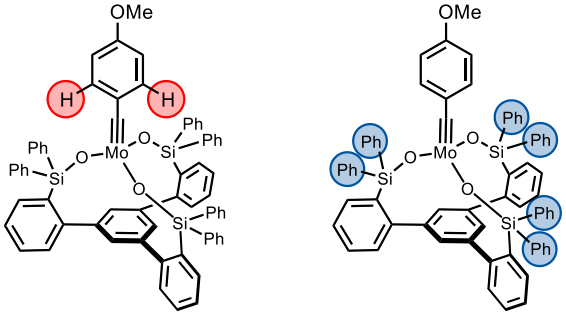


**Figure 22.** Two envisaged strategies to prevent aggregation.

Therefore, we envisioned to prepare the 2,6-dimethylbenzylidyne complex **117** by the literature-known procedure starting from $[Mo(CO)_6]$ (**2**).[150] Metal-halogen exchange at the sterically hindered 2-bromo-1,3-dimethylbenzene site showed no appreciable conversion after 5 h at ambient temperature as judged by GC-MS analysis. Therefore, we adapted the protocol and added excess *t*BuLi at −20 °C to quantitatively form the lithium salt after 1 h (**Scheme 31**).[98] Addition of this lithium species to the carbonyl complex **2** gave, after cation exchange, with tetramethylammonium bromide, Fischer carbene **118**. However, the precipitation of the desired product **118** by addition of an aqueous solution of tetramethylammonium bromide turned out to be difficult and irreproducible. Several independent runs gave low yields between 14–50% yield and product of low purity. Subsequent oxidation with oxalyl bromide and bromine afforded the Schrock alkylidyne **117** in 70% yield (**Scheme 31** A). In contrast, the isolation of the corresponding lithium salt as a diethyl ether adduct **119** (5:3 ratio) provided a convenient solution to this problem. After removal of the solvent, complex **119** was extracted with $CH_2Cl_2$ and precipitated by addition of excess *n*-pentane (under anhydrous conditions) (**Scheme 31** B).

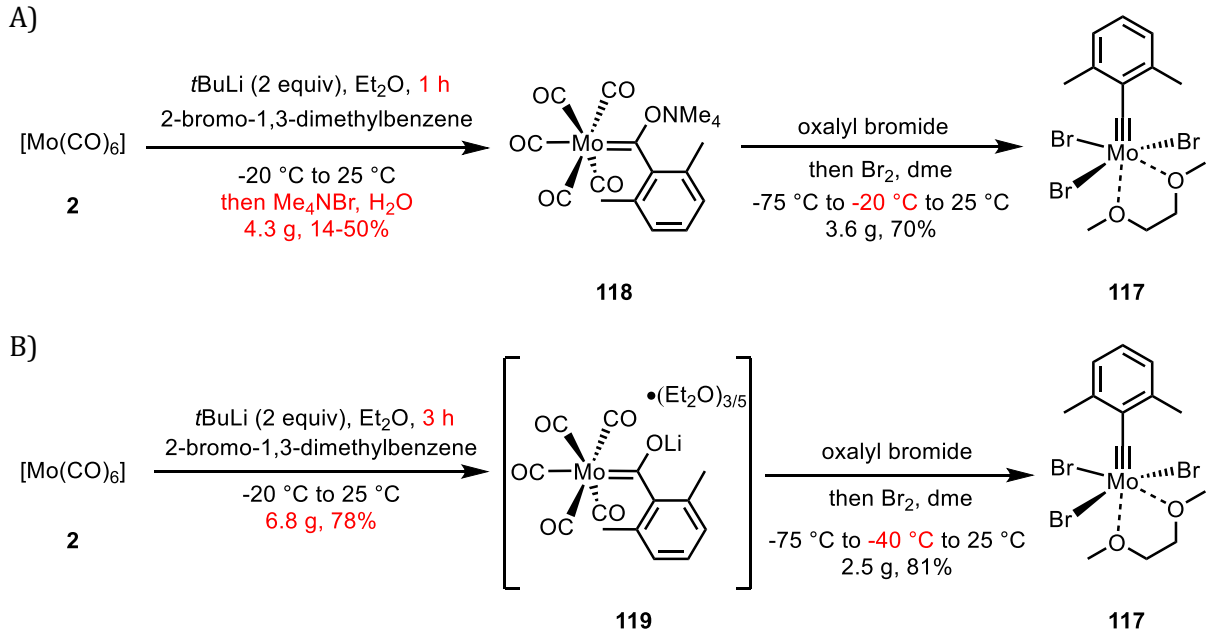


**Scheme 31.** A) Previous procedure to prepare **117**; B) Optimized procedure to prepare **117** on gram scale.

The addition of sodium *tert*-butoxide to a solution of **117** in THF gave access to **120** (**Scheme 32**).

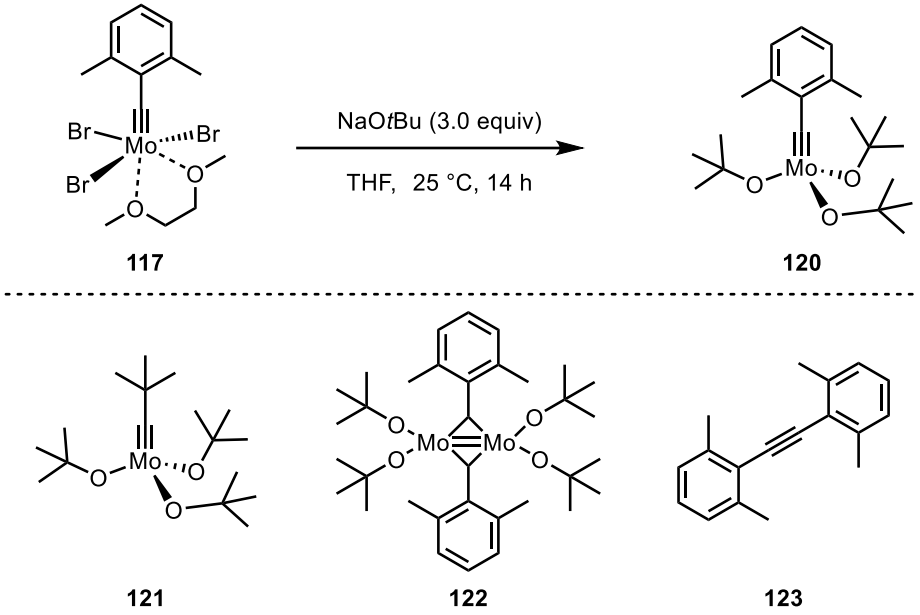


**Scheme 32.** Isolation of minor side products **121**, **122** and alkyne **123**.

However, during the synthesis of **120** we also isolated and characterized three minor side products **121**, **122** and alkyne **123** (**Scheme 32**, **Figure 23**).

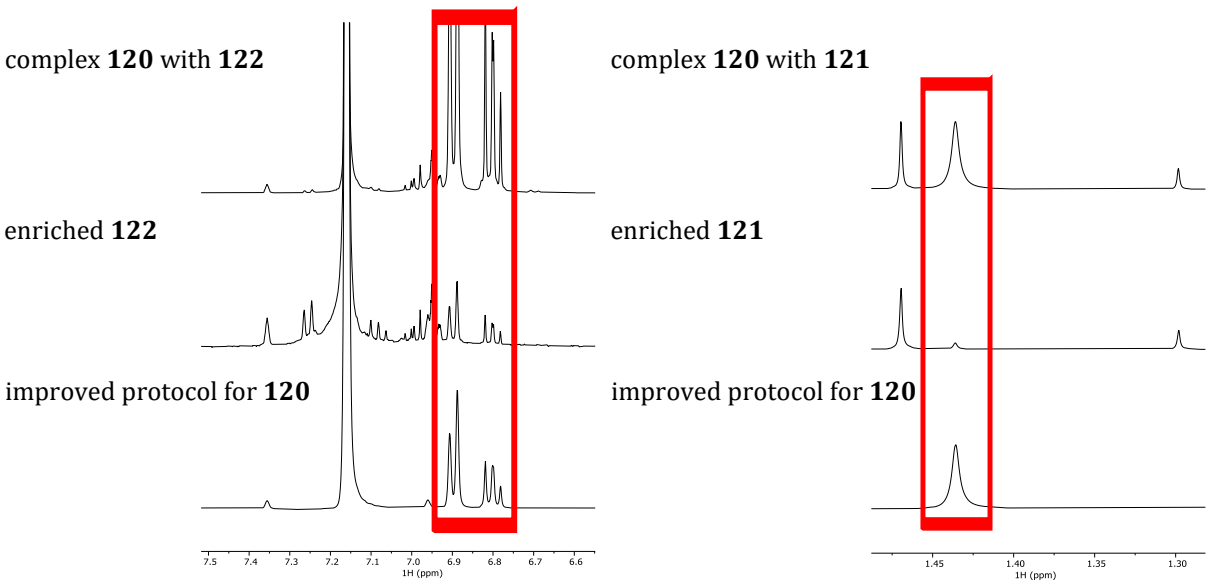


**Figure 23**. $^{1}$H NMR spectra of **120** (red frame) and impurities **121** and **122** in [$D_6$]-benzene at 25 °C.

Therefore, we revisited the entire sequence and optimized it (**Scheme 31** B). Neopentylidyne complex **121** was separated from **120** by sublimation at 60 °C for 3 h under high vacuum ($10^{-3}$ mbar). Intriguingly, compound **121** was most likely formed through nucleophilic attack by the second equivalent of *t*BuLi on [$Mo(CO)_6$] (**2**) and represents a new synthetic route to access neopentylidyne complex **121** (*vide supra*). In order to prevent the formation of complex **121**, it was important to stir the halogen-metal exchange reaction for at least 3 h at –20 °C. This ensured that the second equivalent of *t*BuLi was entirely consumed by reaction with the released *tert*-butyl bromide (**Scheme 31** B). The two other side products complex **122** and alkyne **123** were separated from the main product **120** by recrystallization of an *n*-pentane solution at –85 °C and filtering off the clean

solution of **122** and **123**. Purple crystals suitable for X-ray diffraction were obtained by cooling a concentrated diethyl ether solution of **122** over 10 h from ambient temperature to −75 °C. The measured data confirmed the dinuclear structure of **122** (**Figure 24**). In this batch, we also identified another type of crystal and we obtained the solid state structure of alkyne **123**. Both side products most likely formed during the critical oxidation step of Fischer carbene **118** with oxalyl bromide to form the highly unstable, cationic Fischer carbyne, which is temperature sensitive. Therefore we optimized this step: after the addition of oxalyl bromide to a suspension of **119** in methylene chloride at -78°C, we only warmed the mixture up to −40 °C (internal temperature) instead to -20°C and quickly recooled it to −78 °C. This guaranteed clean conversion to desired complex **117** in 81% yield (**Scheme 31** B).

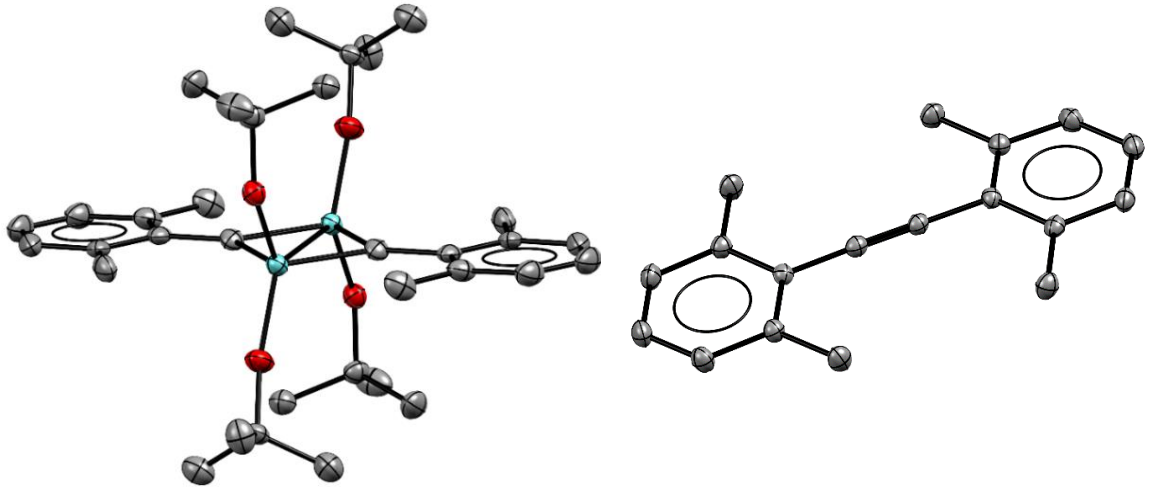

**Figure 24.** Solid state structure of complex **122** and alkyne **123.**

With an optimized protocol for the preparation of **117** in hand (**Scheme 31** B), we treated a solution of complex **117** in THF with sodium *tert*-butoxide to give complex **120** in 83% yield on 800 mg scale (**Scheme 33**).

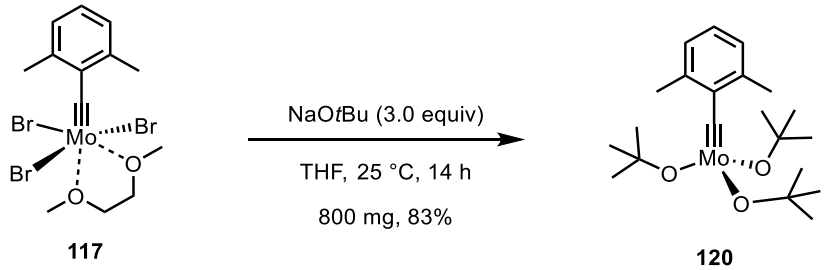


**117** **120**

**Scheme 33.** Preparation of complex **120**.

Now the stage was set to test our hypothesis that 2,6-dimethylbenzylidyne complex **120** prevent the aggregation. Therefore, we stirred a solution of **120** and triarylsilanol **105** in toluene at ambient temperature and removed the solvent to obtain monomeric complex **124** in 65% yield (**Scheme 34**). Yellow crystals suitable for single crystal X-ray diffraction were grown from a concentrated diethyl ether solution of **124** at –20 °C. DOSY NMR and X-ray structure analysis (**Figure 25**) confirmed the monomeric composition of this complex.

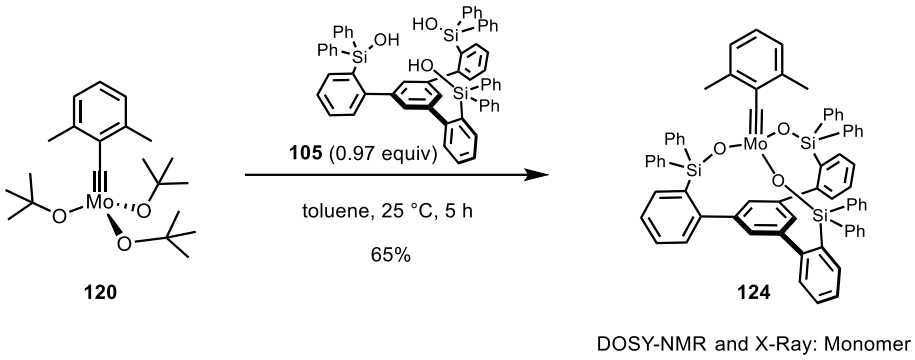


**Scheme 34.** Preparation of the well-defined monomeric complex **124**.

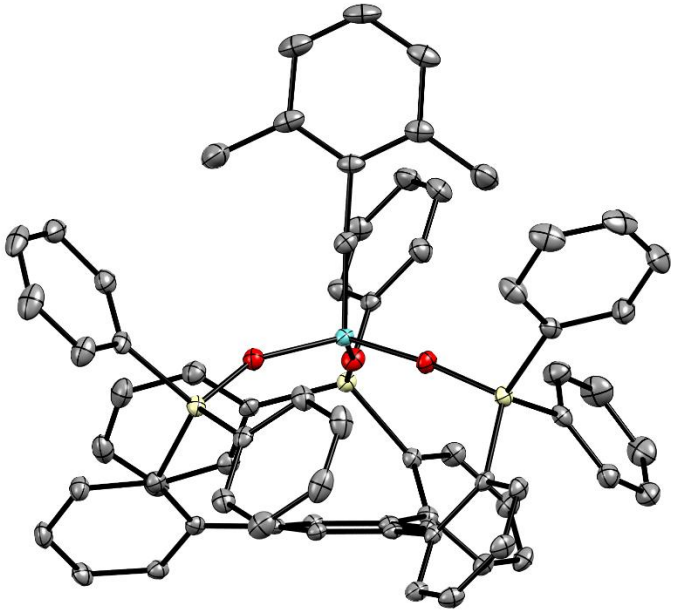

**Figure 25.** Solid state structure of monomeric complex **124**.

The modular ligand design allowed the substitution on the tripodal ligand sphere to be varied in order to study the impact on the catalytic activity (**Scheme 35**). Ligand **127** was synthesized starting from the corresponding fluoride substituted tribromide **125** in 67% yield over two steps. Aliphatic silanolate ligands have been previously shown to be catalytically active but were considered less effective for alkyne metathesis.[113] The new ligands **128–130** were accessible in very good yield over two steps by quenching with electrophile $R_2Si(H)Cl$ (R = Me, *i*Pr) or $R_2SiH_2$ (R = Et) followed by oxidation of the resulting Si–H bond with *meta*-chloroperoxybenzoic acid (*m*CPBA).

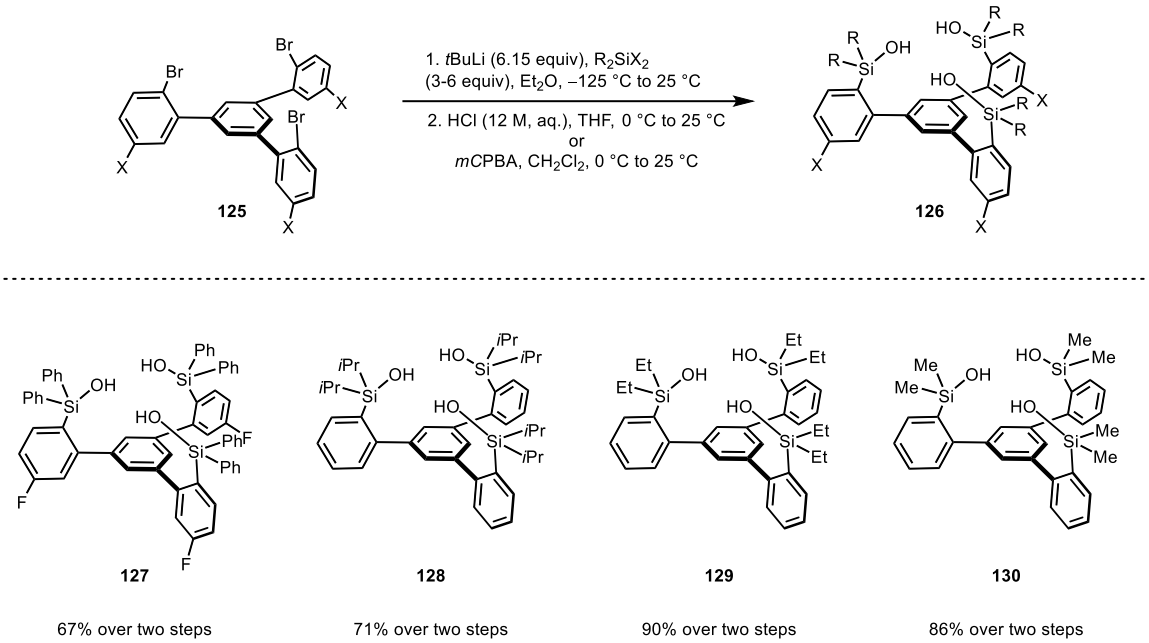


**Scheme 35.** Preparation of various ligands.

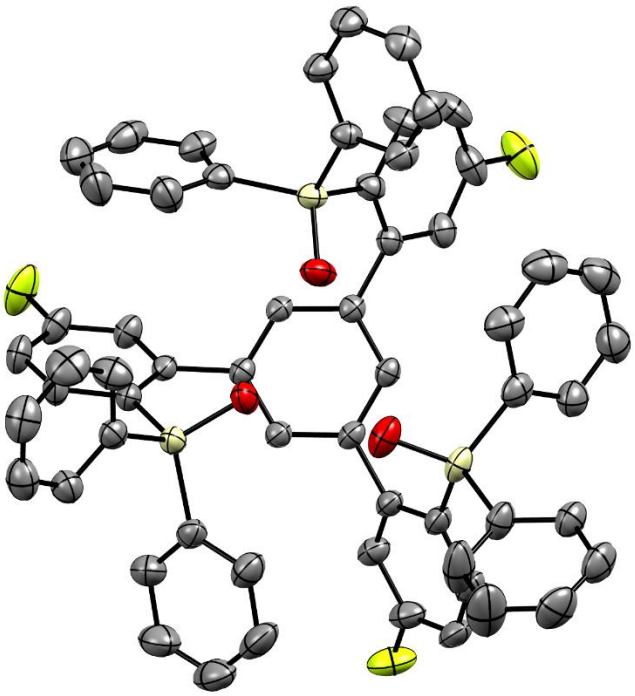

**Figure 26.** Solid state structure of ligand **127**; toluene and H-atoms omitted for clarity.

Stirring of a solution of precatalyst **107** and triarylsilanol **127** in toluene at ambient temperature and evaporation of the solvent gave complex [**131**]$_2$ as a yellow solid in 50% yield (**Scheme 36**).

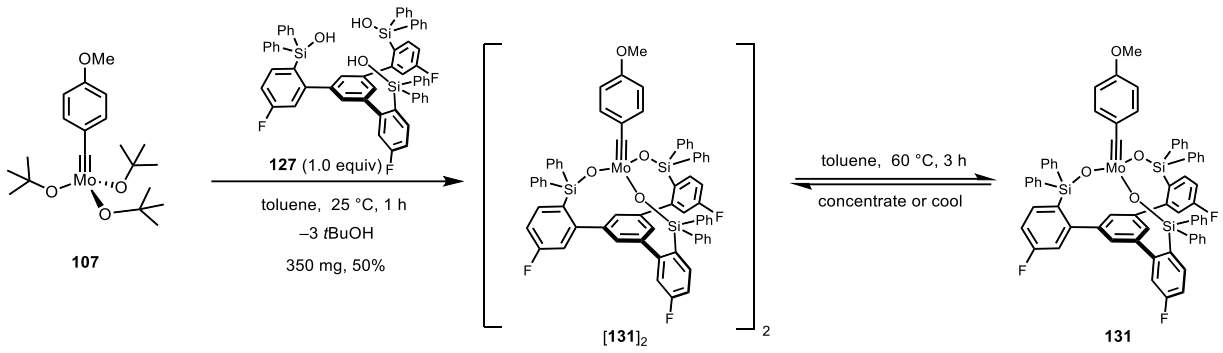


**Scheme 36.** Preparation of structurally well-defined alkyne metathesis catalyst **131**.

With ligand **128** in hand, we tested our second hypothesis that replacing the phenyl groups on the silanolate ligand prevent the aggregation (**Scheme 37**). Stirring of a solution of precatalyst **107** and triarylsilanol **128** in toluene at ambient temperature and removal of the solvent gave monomeric complex **132** in 99% yield.

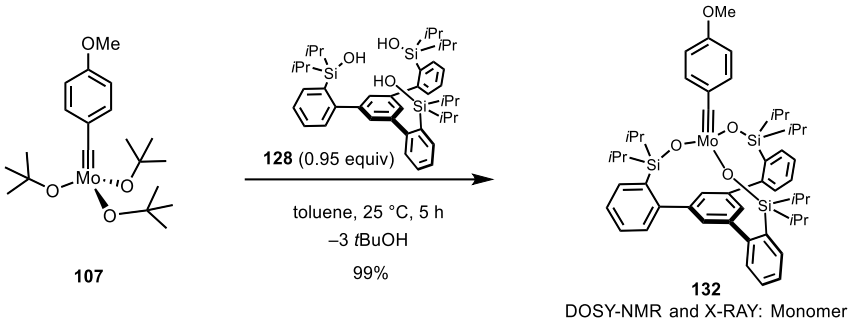


**Scheme 37.** Preparation of well-defined monomeric complex **132**.

Yellow crystals suitable for single-crystal X-ray diffraction were grown from a concentrated diethyl ether solution of **132** at –30 °C. DOSY NMR and X-ray structure analysis (**Figure 27**) confirmed the monomeric composition of complex **132.**

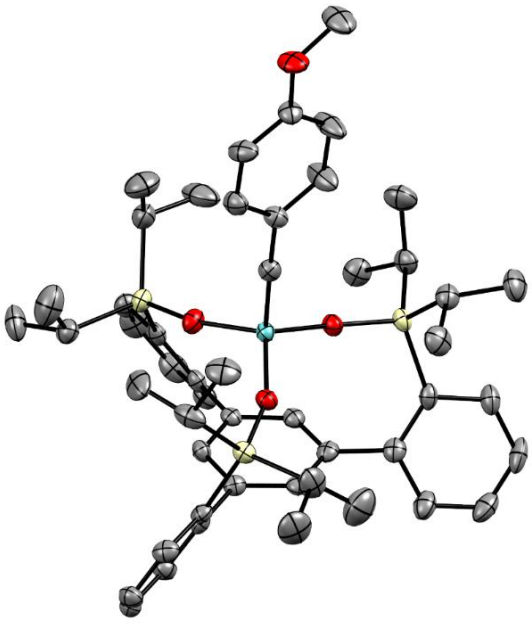

**Figure 27.** Solid state structure of monomeric complex **132**.

In contrast, stirring of a solution of precatalyst **107** and ligand **130** in toluene at ambient temperature failed to give the expected well-defined complex but rather furnished an ill-defined mixture (**Scheme 38**). We concluded that ligand **130** with methyl substituted silanolates is not sterically encumbered enough to prevent competing oligomerization. Based on this assumption, we used the 2,6-dimethyl benzylidyne complex **120** for the complexation. Indeed, stirring of this reaction for 4 h at ambient temperature, removal of the solvent and extraction with *n*-pentane gave the well-defined complex **133** as the major product.

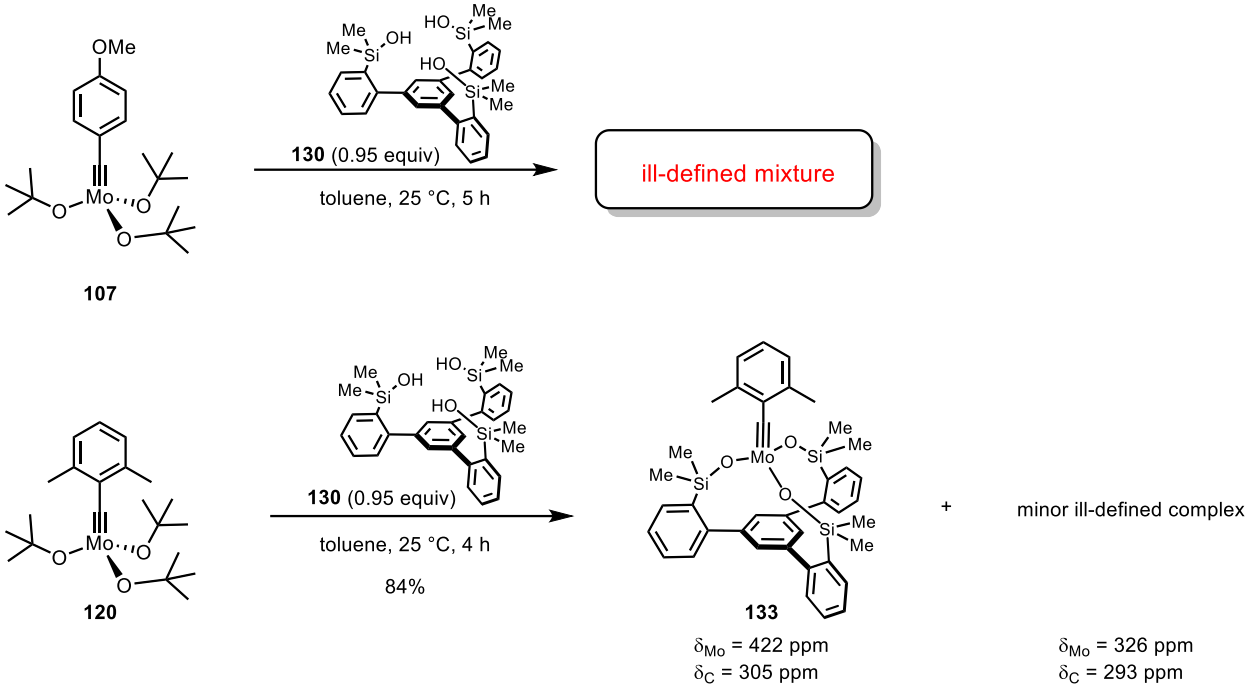


**Scheme 38.** Preparation of well-defined monomeric complex **133**.

$^{95}$Mo NMR and $^{13}$C NMR analysis revealed that there is a minor ill-defined alkylidyne species present, which gave broad NMR signals and had very similar chemical shifts (**Figure 28**).

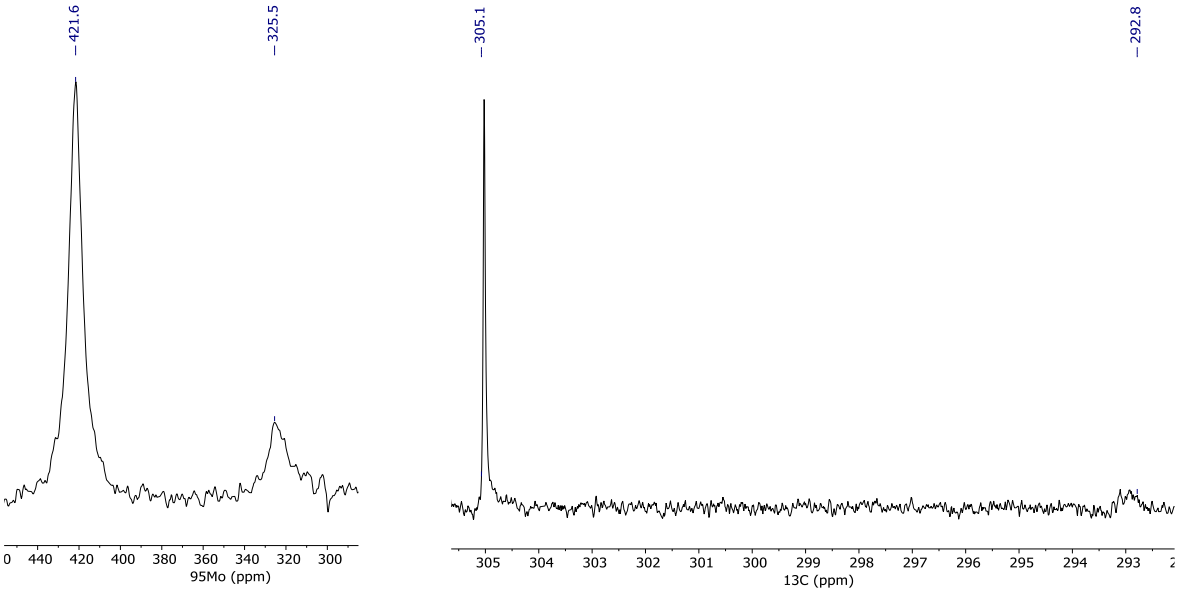


**Figure 28**. $^{95}$Mo NMR and $^{13}$C NMR spectra of **133** and minor ill-defined entity.

Next, we envisioned that an ethyl substituted silanolate ligand should shield the metal center more efficiently and give clean conversion to the desired well-defined complex. Stirring of a solution of precatalyst **120** and ligand **129** in toluene at ambient temperature, removal of the solvent and extraction of the crude product with *n*-pentane gave monomeric complex **134** in 99% yield. Yellow crystals suitable for single-crystal X-ray diffraction were grown from a concentrated *n*-pentane solution of **134** at –20 °C. X-ray structure analysis (**Figure 29**) confirmed the monomeric composition of **134**.

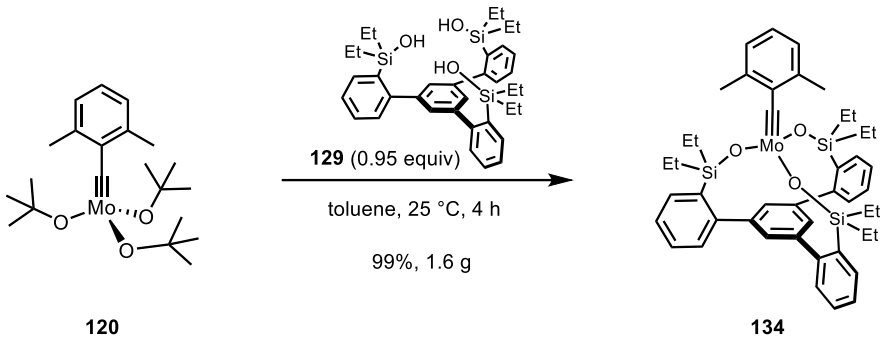


**Scheme 39.** Preparation of the well-defined monomeric complex **134** conducted with Christopher Rustemeier.

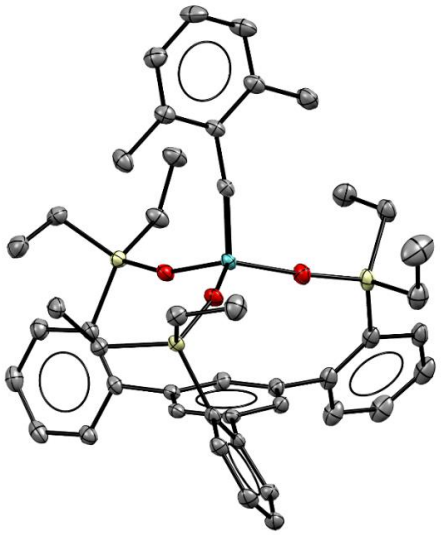

**Figure 29.** Solid state structure of monomeric complex **134**.

Alternatively, we also prepared the analogous carbinol ligand **135** in 78% yield on 2.5 g scale by lithiation of **103** and quenching with benzophenone. The $^{1}$H NMR spectrum of **135** shows dynamic broad signals at ambient temperature and is very different to the NMR spectrum of triarylsilanol **105** (**Figure 30**). Cooling to −50 °C led to sharp signals, which revealed that one alcohol is oriented to the opposite side of the basal phenyl ring.

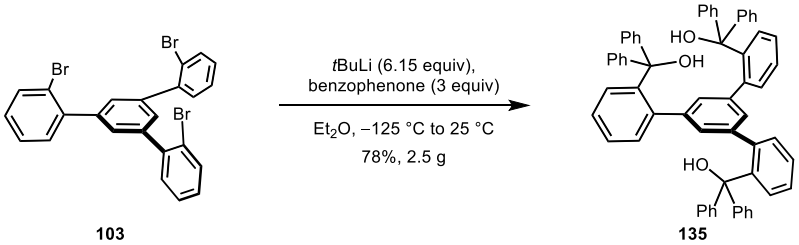


**Scheme 40.** Ligand synthesis of carbinol variant **135** conducted with Ektoras Yiannakas.

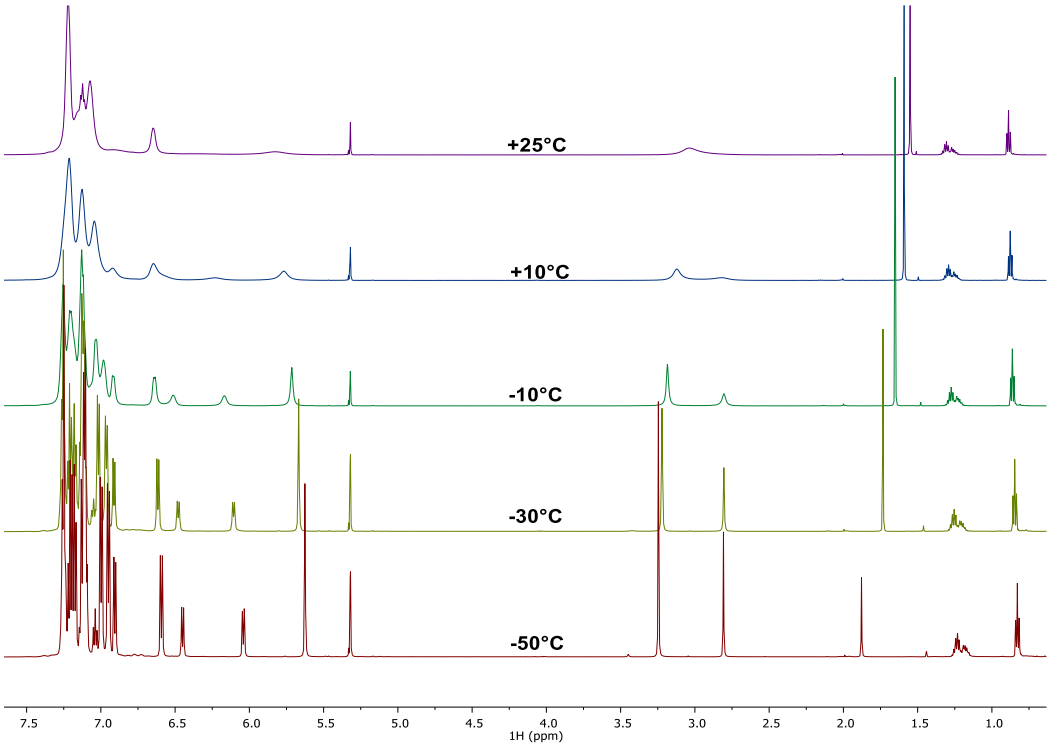


**Figure 30.** VT NMR study of carbinol ligand **135** in $CD_2Cl_2$.

Colorless crystals suitable for single-crystal X-ray diffraction were grown from a concentrated $CH_2Cl_2$ solution of **135** at –75 °C (**Figure 31**). The solid state structure confirmed the presumed two-up/one-down geometry in solution. The necessary $C_3$ symmetry for the formation of podand complexes was not preserved in carbinol ligand **135**. The overall shorter donor bond distances of carbinol ligand **135** ($d(_{O\text{-}C})_{avg.}$ = 1.44(2) Å) in comparison to triarylsilanol ligand **105** ($d(_{O\text{-}Si})_{avg.}$ = 1.64(2) Å), leads to a larger bonding cavity and a less stabilized arrangement. In addition, alcohols are less acidic than silanols and a hydrogen-bonding array is therefore less pronounced.

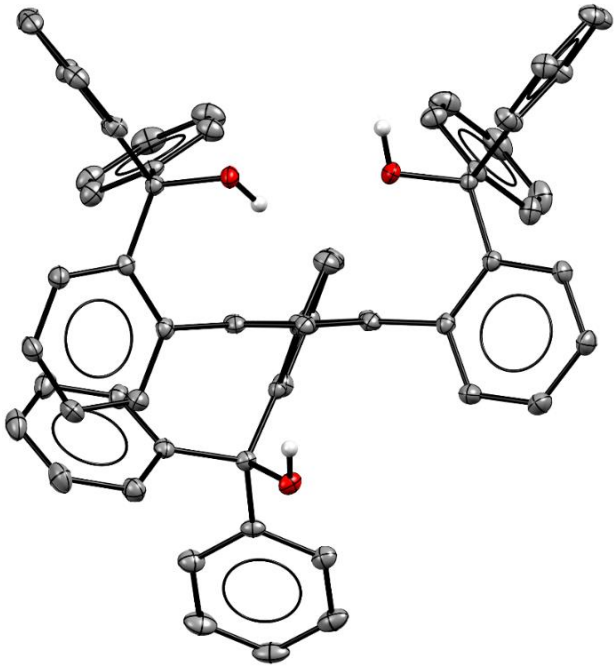

**Figure 31.** Solid state structure of carbinol ligand **135**; $CH_2Cl_2$ omitted for clarity and only H-atoms involved in hydrogen bonding are shown.

Stirring of a solution of precatalyst **107** and carbinol ligand **135** in toluene at ambient temperature and removal of the solvent gave complex **136** in 79% yield (**Scheme 41**). The observed configuration of the carbinol ligand **135** resulted in a bidentate instead of the tridentate binding motif. Two *tert*-butoxide ligands were replaced by ligand **135** whereas the third *tert*-butoxid remained attached to the metal center.

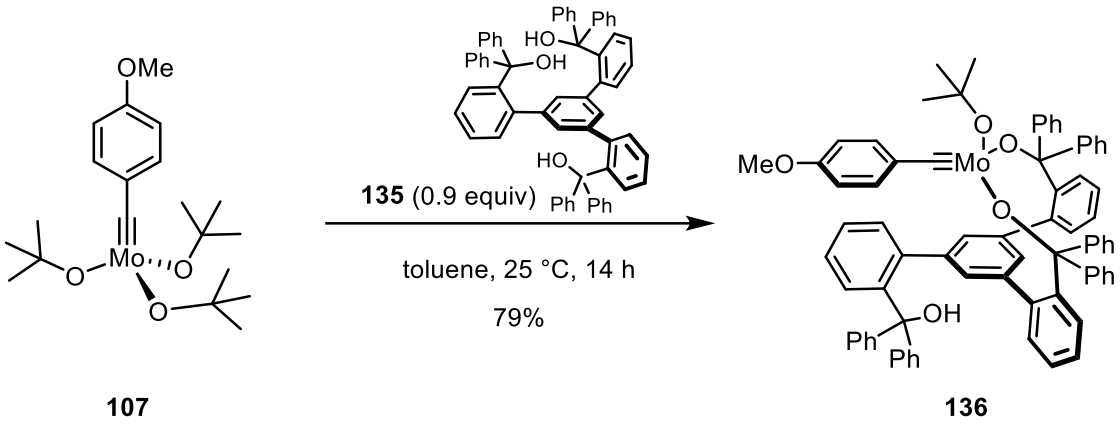


**Scheme 41.** Preparation of bidentate ligated complex **136**.

Heating of a solution of **136** in [$D_8$]-toluene to 60 °C failed to give the $C_3$ symmetric podand complex and resulted in decomposition as evidenced by the formation of isobutylene (**Figure 32**).

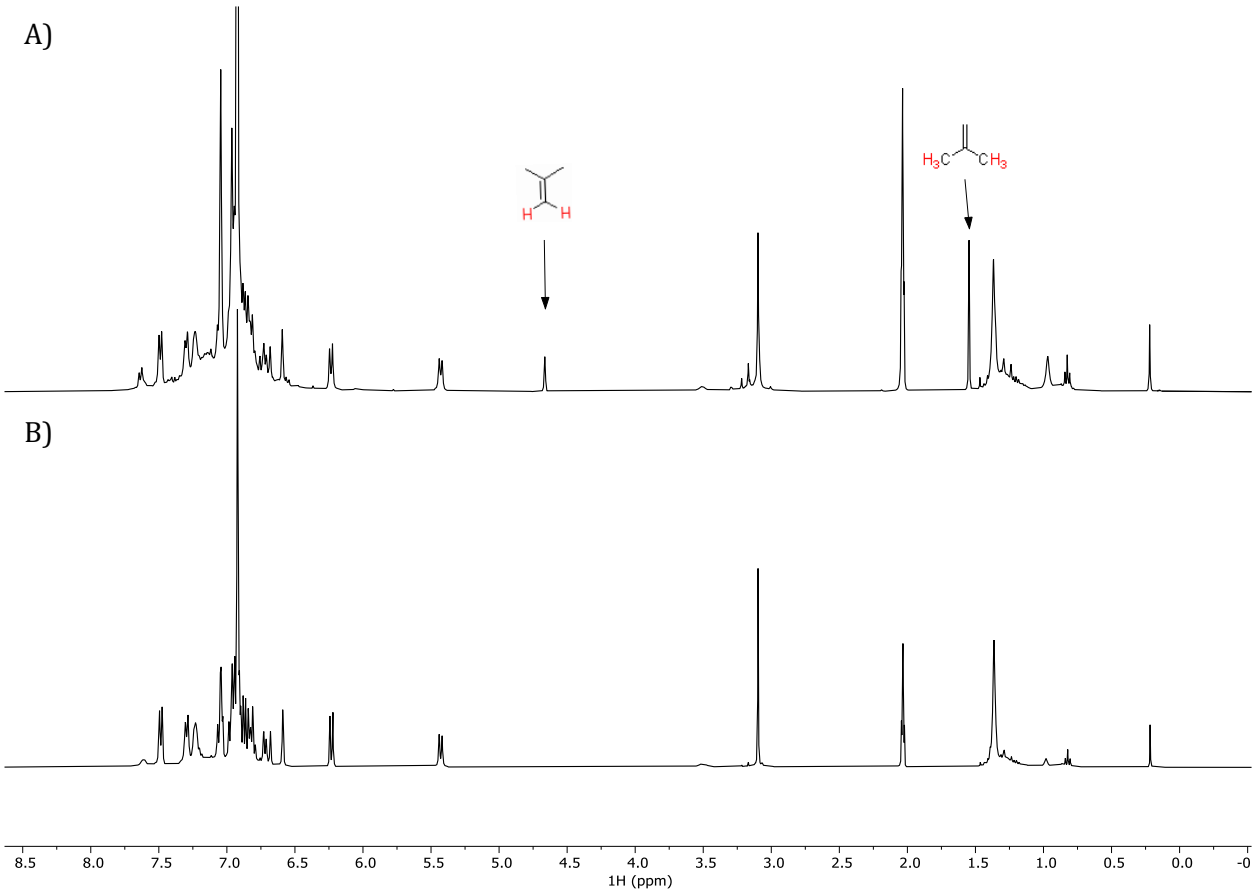


**Figure 32.** Observed decomposition of complex **136** after 6 h heating to 60 °C; A) $^1$H NMR spectrum after heating for 6 h to 60 °C; B) $^1$H NMR spectrum before heating

Another conceivable ligand design meant to favor a $C_3$-symmetric conformation increases the acidity of the carbinol by introducing trifluoromethyl groups. Therefore, we subjected **103** to the standard lithiation sequence and quenched the intermediate with hexafluoroacetone. Although this reaction did not furnish the desired fluorinated ligand **137**, we were able to prepare the new ligand *via* the route depicted in **Scheme 42**. Lithiation and quenching with methylchloroformate gave, after hydrolysis, the corresponding carboxylic acid **138**. Formation of the active ester **139** and subsequent treatment with excess of CsF and $TMSCF_3$ afforded fluorinated carbinol ligand **137**.[151] In contrast to carbinol ligand **135**, the fluorinated variant **137** is $C_3$-symmetric in $CD_2Cl_2$ and only a minor signal set indicated the second rotamer in the $^1H$ NMR spectrum.

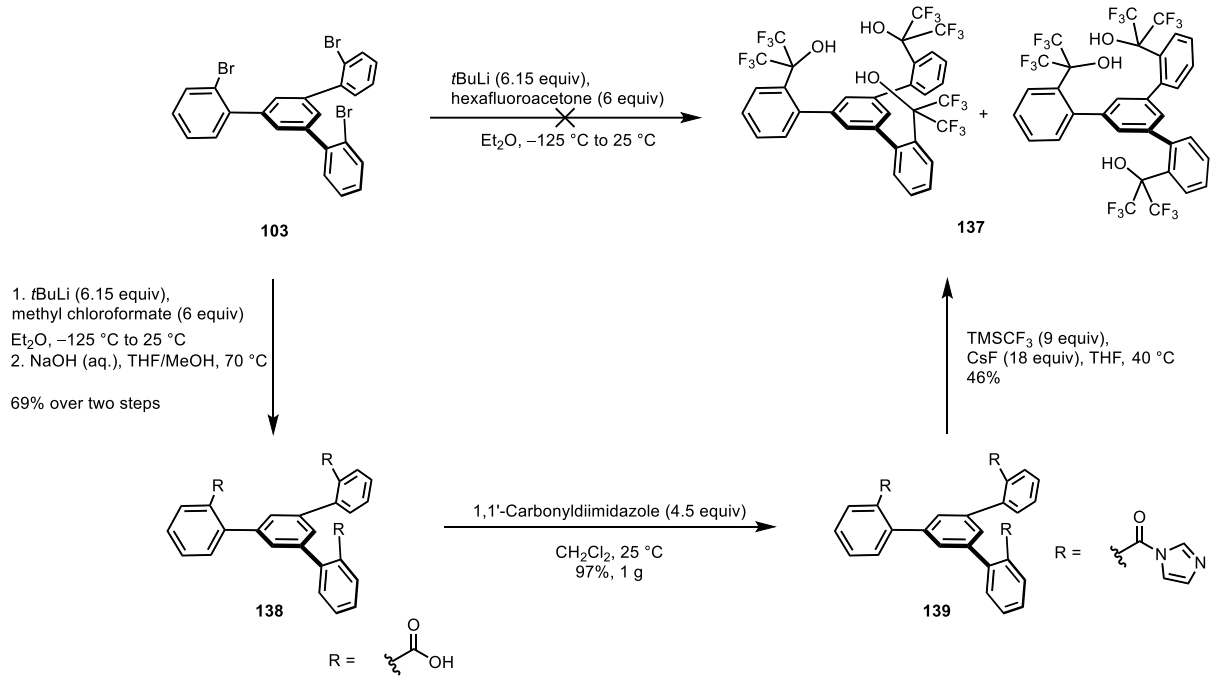


**Scheme 42.** Preparation of fluorinated ligand **137**; conducted with Nepomuk Korber and Ektoras Yiannakas.

However, stirring of a solution of precatalyst **120** and the fluorinated carbinol ligand **137** in toluene at ambient temperature gave again a bidentate complex **138** in 79% yield (**Scheme 43**).

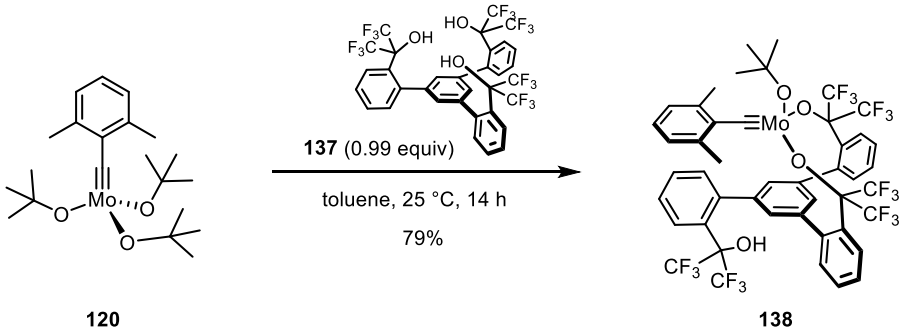


**Scheme 43.** Preparation of bidentate ligated complex **138**.

Slow evaporation of a concentrated solution of complex **138** in benzene afforded yellow crystals suitable for single-crystal X-ray diffraction. The solid state structure confirmed the proposed bidentate coordination environment (**Figure 33**). Although the $C_3$-symmetry of the ligand was preserved in solution, the enlarged bonding cavity did not allow for the formation of the podand complex.

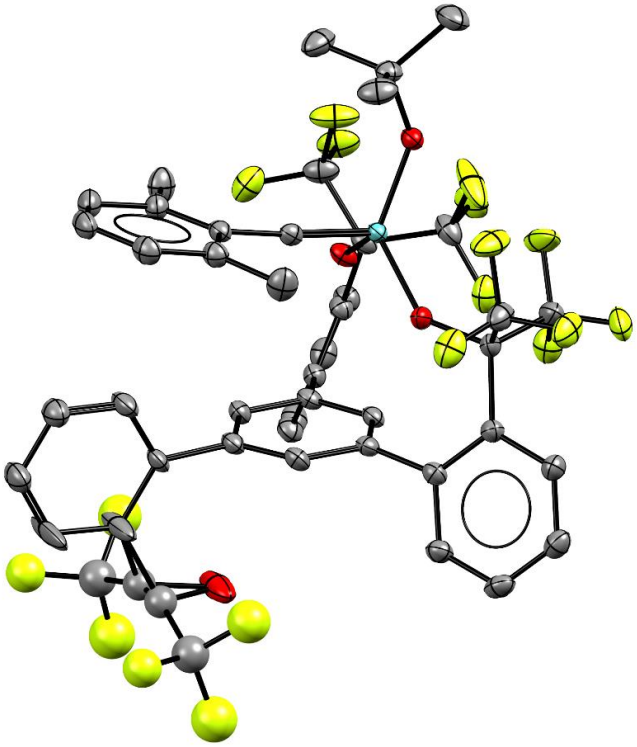

**Figure 33.** Solid state structure of complex **138**; disorder omitted for clarity.

In pursuit of tripodal carbinol complexes, a new ligand design was developed (**Scheme 44**). Treatment of compound **103** with excess *t*BuLi and quenching with six equivalents of 3,3,3-trifluoro-2-(trifluoromethyl)-1,2,-propenoxide (**139**) did not afford the desired ligand **140**, but gave instead the di-substituted compound **141** and **142** as a by-product. Both structures were confirmed by NMR analysis and mass spectrometry. In the literature it has been recognized that the opening of trifluoromethyloxirane with Grignard reagents is particularly slow and addition of catalytic amount of copper(I) iodide facilitates the reaction.[152, 153] Indeed, when copper(I) iodide was added right before the epoxide, ligand **140** became accessible. Yet we have not tried the complexation to the molybdenum alkylidyne.

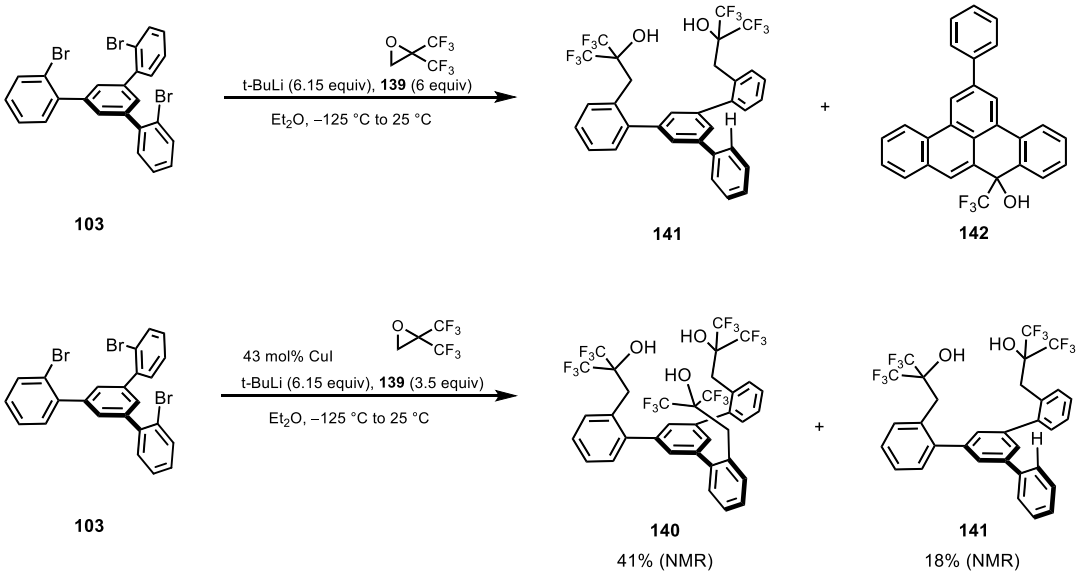


**Scheme 44.** Preparation of ligand **140**; conducted with Christopher Rustemeier.

### 3.1.4 Improved Preparation of Triphenylsilanolate Molybdenum Complexes

The previously reported procedure to prepare triphenylsilanolate based complex **111** *via* salt metathesis of the corresponding Schrock alkylidyne **106** with three equivalents of potassium salt turned out to be difficult to reproduce due to the competing formation of ate complex **73**.[113] Extensive efforts have been directed to improve this protocol.[154] To this end, the solvent was changed from toluene to THF and a solution of potassium triphenylsilanolate salt was added slowly at 0 °C (**Scheme 45**). However, the formed potassium bromide still caused problems during isolation of complex **111**. Therefore, we optimized the isolation procedure on a 1 g scale to guarantee a reproducible protocol. After removal of the THF, the residue was dissolved in toluene and the suspension was filtered through Celite® to remove the microcrystalline potassium bromide. The toluene was removed *in vacuo* and the obtained solid was dissolved in diethyl ether. Stirring of this solution for 30 min at 0 °C resulted in the precipitation of the desired yellow complex **111** that can be isolated by filtration. The improved protocol was repeated seven times on a 1 g scale and gave an average yield of 50% yield.

Alternatively, we considered to take advantage of the newly developed protonolysis protocol that prevents the formation of ate-complex **73** (**Scheme 45**). Ligand exchange with sodium *tert*-butoxide gave access to precatalyst **107**, which can be simply separated from the formed sodium bromide by extraction with n-pentane, in 83% yield on 3 g scale. The addition of a solution of triphenylsilanol to a solution of precatalyst **107** in toluene (or *vice versa*) gave the desired complex **111** and *tert*-butanol, which can be removed by evaporation in high vacuum. The solid was redissolved in diethyl ether and precipitated by addition of excess *n*-pentane. Complex **111** can be isolated by filtration on a 1 g scale in an average yield of 60% yield. In preparative terms, the protonolysis protocol simplified and improved the preparation of complex **111**.

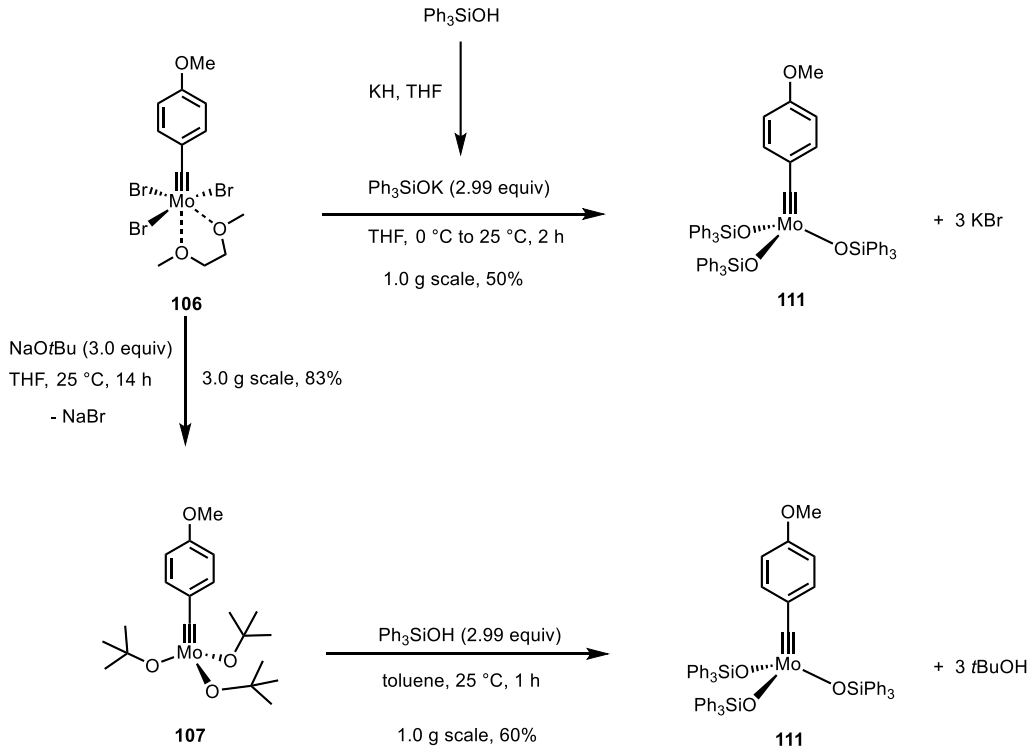


**Scheme 45.** Improved preparation of complex **111** conducted with Christopher Rustemeier.

Additionally, we prepared fluorinated complex **143** in 79% yield by the literature-reported salt metathesis (**Scheme 46**).[98]

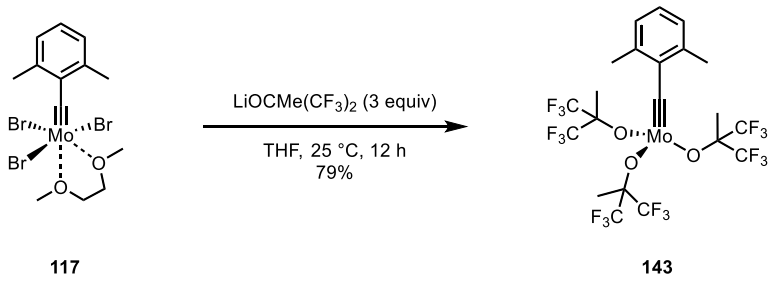


**Scheme 46.** Preparation of complex **143**.

### 3.1.5 $^{95}$Mo NMR Spectroscopy as an Analytical Tool for Catalyst Design

Although $^{95}$Mo NMR spectroscopy has been rarely used for analytical purposes in organometallic chemistry, it carries the potential to investigate the electronic character of molybdenum complexes in solution.[155, 156] The low natural abundance of the $^{95}$Mo isotope (ca. 15.9%), the spin 5/2, the low gyromagnetic ratio, and the quadrupole moment make it particularly difficult to acquire NMR signals of good signal-to-noise ratio. A single study by Enemark and co-workers reported the $^{95}$Mo NMR shifts of [$(Me_3SiCH_2)_3Mo{\equiv}CSiMe_3$] (1845 ppm) and [$(Me_3CCH_2)_3Mo{\equiv}CCMe_3$] (1400 ppm), but failed to record the signal for [$(t$BuO$)_3Mo{\equiv}$CPh].[157]

The few examples of reported $^{95}$Mo NMR shifts encouraged us to investigate this analytical tool in greater detail. Fortunately, we obtained good $^{95}$Mo NMR spectra of complexes **109**, **107** and **120** in [$D_8$]-toluene (~ 0.1 M) at elevated temperature (60 °C) (**Figure 34**). Higher temperature gave sharper $^{95}$Mo NMR signals due to decelerated quadrupole relaxation. The distinct shift difference between **109** ($\delta_{Mo}$ = 62.0 ppm), **107** ($\delta_{Mo}$ = 79.6 ppm) and **120** ($\delta_{Mo}$ = 259 ppm) indicated that the alkylidyne unit has significant orbital overlap to the adjacent phenyl group and the coupling directly influenced the $^{95}$Mo NMR shift.

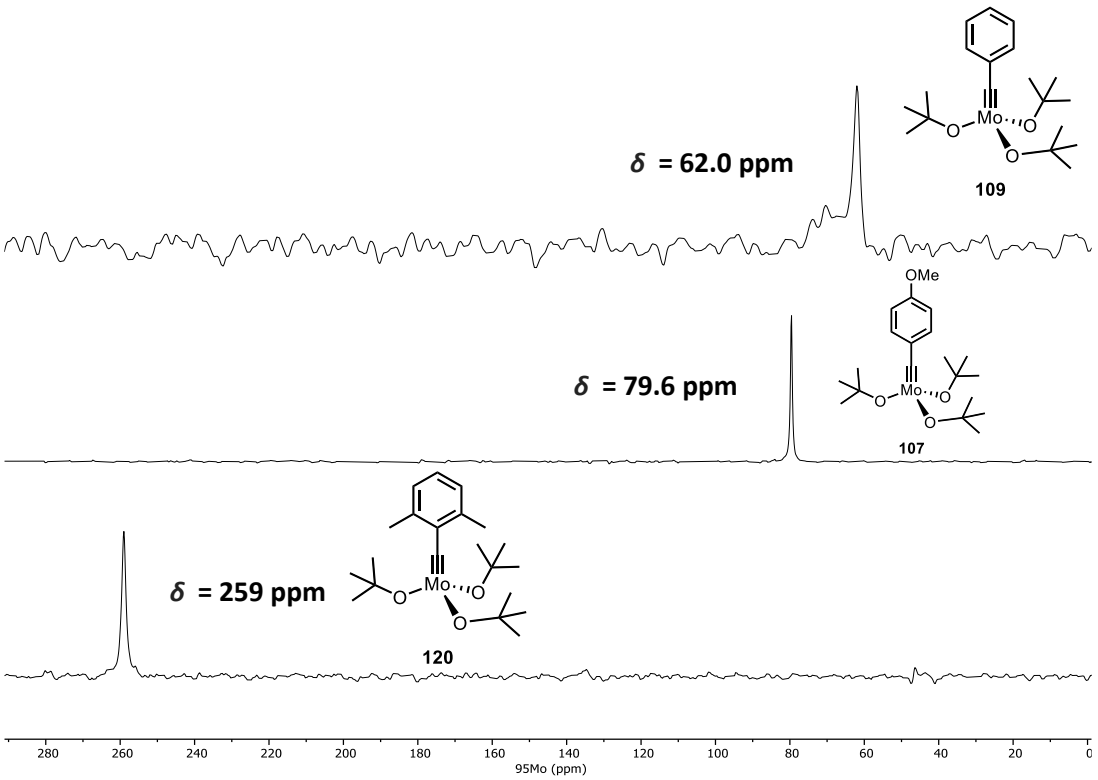


**Figure 34.** $^{95}$Mo NMR spectra of complexes **109**, **107** and **120** differing only in the aryl substituent on the alkylidyne; All spectra were recorded at 60 °C in [$D_8$]-toluene.

Similarly, we observed the same trend in the $^{95}$Mo NMR shift of the corresponding silanolate complexes **110** ($\delta_{Mo}$ = 377 ppm), **108** ($\delta_{Mo}$ = 419 ppm) and **124** ($\delta_{Mo}$ = 467 ppm).

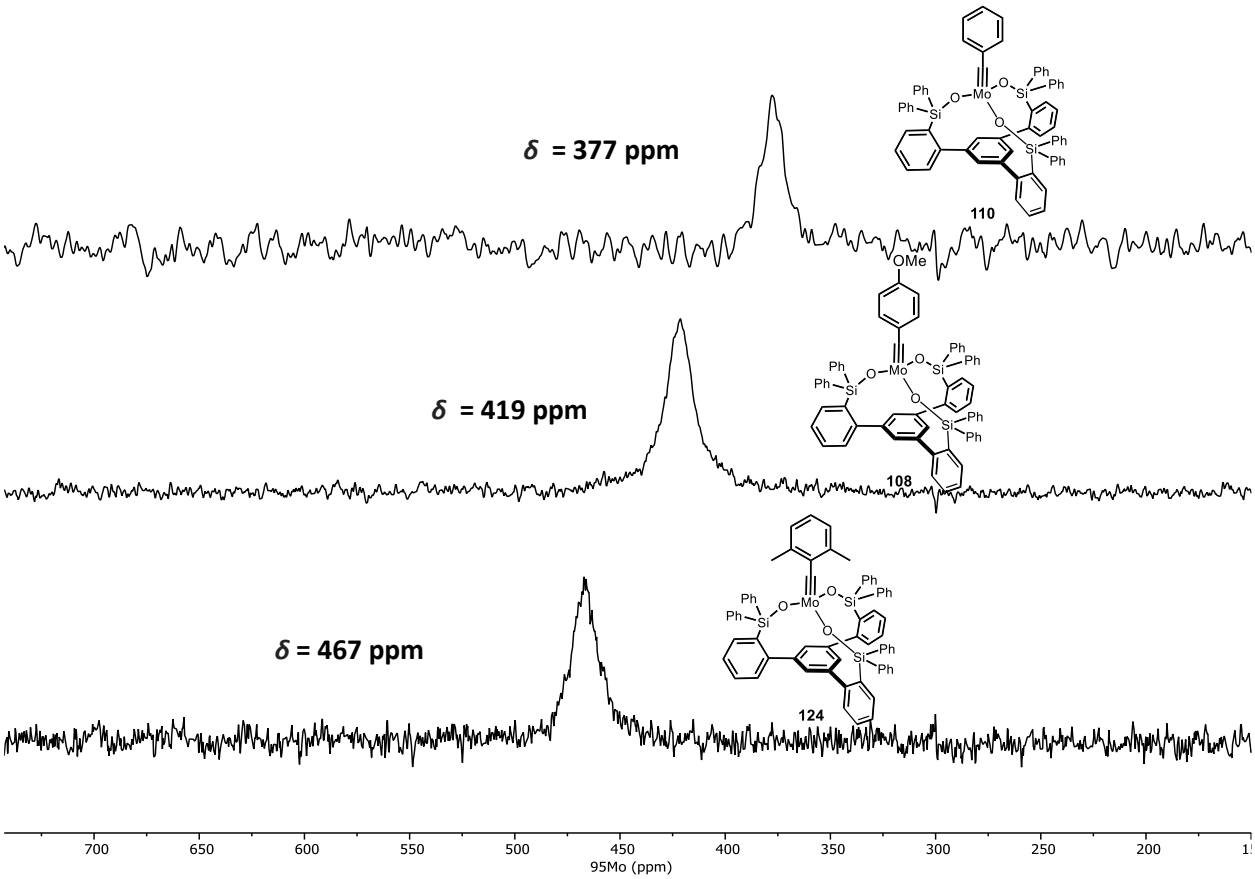


**Figure 35**. $^{95}$Mo NMR spectra of the monomeric canopy complexes **110**, **108** and **124** differing only in the aryl substituent on the alkylidyne; All spectra were recorded at 60 °C in [$D_8$]-toluene.

For this reason, a series of *p*-methoxybenzylidyne complexes with different silanolate or carbinolate ligands were measured to study the electronic influence of the ligand on the molybdenum center. In comparison to the parent complex **108** ($\delta_{Mo}$ = 419 ppm), fluoride substituted complex **131** caused an overall deshielding ($\delta_{Mo}$ = 434 ppm), whereas the MeO substitution of **116** resulted in a $^{95}$Mo NMR signal at higher frequencies ($\delta_{Mo}$ = 414 ppm). The more electron-donating isopropyl substituents in complex **132** gave an even more shielded nucleus ($\delta_{Mo}$ = 359 ppm). Of particular interest is the influence of the overall obtuse Mo–O–Si bonds in tripodal complex **108** in comparison to the monodentate bent Mo–O–Si bonds in complex **111**. Complex **111** resonated at higher frequencies ($\delta_{Mo}$ = 397 ppm) and is hence deemed less Lewis-acidic than complex **108**. The strongly shielded $^{95}$Mo-nuclei of bidentate ligated complex **136** ($\delta_{Mo}$ = 118 ppm) and monodentate complex **107** ($\delta_{Mo}$ = 79.6 ppm) nicely reflected the better donor properties of carbinol ligands. The overall qualitative trend was well pronounced and a careful assessment between electron density on the molybdenum center and $^{95}$Mo NMR shifts can be made (**Figure 36**). We observed a similar trend in the $^{13}$C-alkylidyne and $^{29}$Si NMR shifts (**Table 4**).

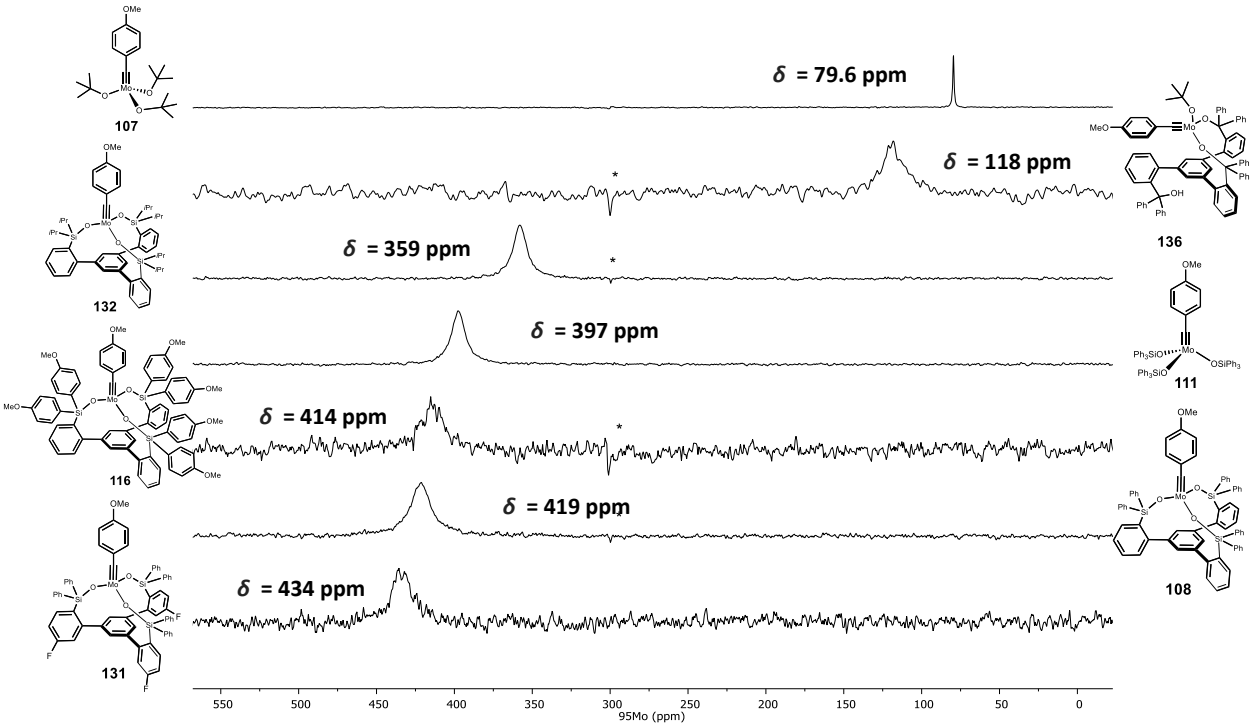


**Figure 36.** $^{95}$Mo NMR spectra of different complexes (all in monomeric form). *Indicates artifacts at the pulse-offset; All spectra were recorded in [$D_8$]-toluene at 60 °C.

**Table 4.** Measured $^{95}$Mo, $^{29}$Si, and $^{13}$C-alkylidyne NMR shifts of the different complexes.

| complex | δ ($^{95}$Mo) [ppm] | δ ($^{29}$Si) [ppm] | δ ($^{13}$C) [ppm] |
|---|---|---|---|
| **14a** | 79.6 | – | 276 |
| **16** | 118 | – | 287 |
| **1d** | 358 | 10.2 | 303 |
| **2a** | 397 | -8.0 | 301 |
| **1c** | 414 | -9.1 | 309 |
| **1a** | 419 | -9.9 | 310 |
| **1b** | 434 | -9.8 | 311 |

We further extended the $^{95}$Mo NMR study to a series of 2,6-dimethylbenzylidyne complexes (**Figure 37**). Interestingly, the opposite trend for the monodentate complex **144**[113] ($\delta_{Mo}$ = 475 ppm) and tripodal complex **124** ($\delta_{Mo}$ = 467 ppm) was observed. Complex **143** with fluorinated alkoxides resonated at much lower field ($\delta_{Mo}$ = 433 ppm), which reflected the weaker donor properties in comparison to the *tert*-butoxide variant **120** ($\delta_{Mo}$ = 259 ppm). The 2,6-dimethylbenzylidyne substitution also allowed the $^{95}$Mo NMR shifts of the "slimmest" tripodal complexes **133** ($\delta_{Mo}$ = 422 ppm) and **134** ($\delta_{Mo}$ = 417 ppm) to be investigated.

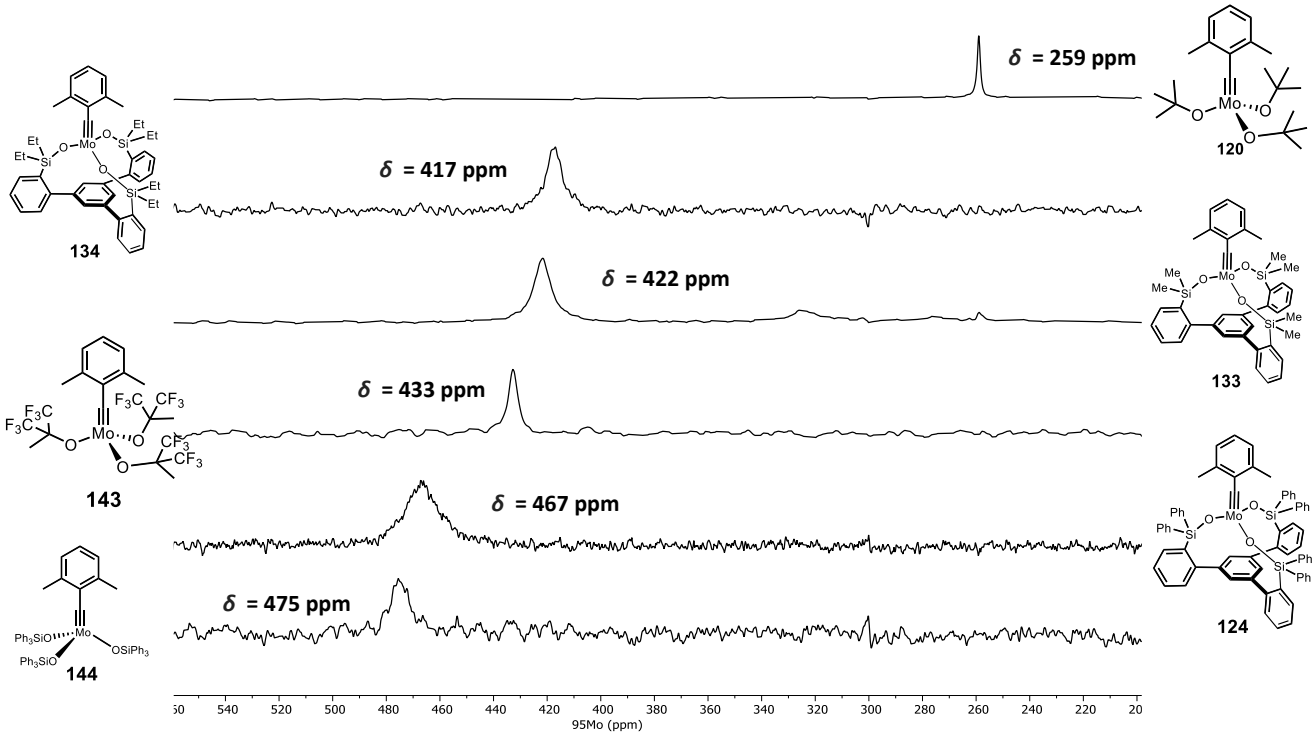


**Figure 37.** $^{95}$Mo NMR spectra of different complexes (all in monomeric form). All spectra were recorded in [$D_8$]-toluene at 60°C.

### 3.1.6 Chemical Shift Tensor Analysis

Overall, $^{95}$Mo NMR spectroscopy proved to be a very sensitive probe to investigate the electronic properties on the metal center and provides a useful spectroscopic tool for catalyst design. As the molybdenum and carbon atom form the operative unit in alkyne metathesis, we envisioned to take advantage of chemical shift tensor (CST) analysis to study the alkylidyne carbon atom in more detail.[158] The chemical shift tensor components ($\delta_{iso} = (\delta_{11} + \delta_{22} + \delta_{33})/3$) obtained by solid state NMR spectroscopy provide insight into the electronic structure of the nucleus. Shielding is an anisotropic property and depends on the orientation of a molecule with respect to the external magnetic field ($B_0$). The shielding tensor $\sigma$ ($\delta_{ii} \approx \sigma_{iso,ref} - \sigma_{ii}$) is accessible by quantum chemical calculations and can be decomposed into diamagnetic and paramagnetic contributions ($\sigma = \sigma_{dia} + \sigma_{para}$). The diamagnetic term ($\sigma_{dia}$) reflects the shielding caused by core orbitals and is fairly insensitive to the large anisotropy of the shielding tensor. However, the paramagnetic term ($\sigma_{para}$) is sensitive to frontier orbitals of the nucleus and causes deshielding, which originates from the coupling of occupied and vacant orbitals. Occupied and vacant molecular orbitals need to be perpendicular to each other and to operator $\hat{L}_i$. When a magnetic field is applied along the i-axis, the angular momentum operator $\hat{L}_i$ leads to a rotation of the orbital 90° about this axis. Strong deshielding for a given nucleus is observed if a high-lying orbital can couple with a low-lying vacant orbital. The most important orbital couplings for a metal alkylidyne are two σ(M–C) orbitals coupling with the low-lying vacant π*(M–C) orbitals and the coupling of occupied π(M–C) orbitals with vacant σ(M–C) orbitals (**Figure 38**).[99]

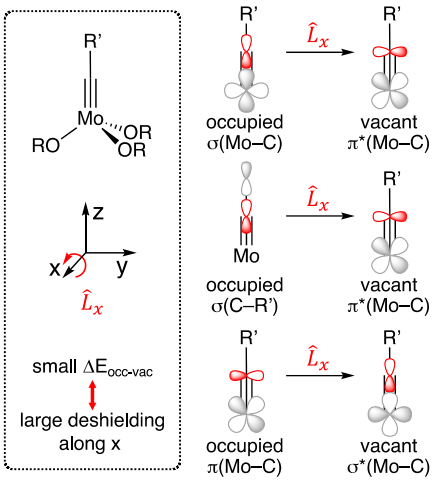


**Figure 38.** Relevant orbital coupling in metal alkylidyne complexes; with Christopher Gordon and Prof. Dr. Christophe Copéret.

Direct comparison of the experimentally measured isotropic alkylidyne $^{13}C$ NMR shift of podand complex **124** ($\delta_C$ = 312 ppm) with the monodentate complex **144** ($\delta_C$ = 303 ppm) showed that the podand complex is more deshielded. The calculated isotropic shifts reproduced the experimental values well: complex **124** ($\delta_C$ = 321 ppm) and complex **144** ($\delta_C$ = 303 ppm). Chemical shift tensor analysis shows that all three components of the shielding tensor contributed to the observed increased deshielding of complex **124** and indicated a lower-lying vacant π*(M–C) orbital (LUMO) and/or a higher-lying occupied σ(M–C) orbital (**Figure *39***). A possible explanation for the alert electronic structure are the obvious obtuse Mo–O–Si bond and the distorted pseudo-tetrahedral coordination sphere in complex **124**. Another likely contribution to the lowered LUMO might arise from the basal phenyl ring, which senses the vacant π*(M–C) orbitals and acts as an acceptor orbital (**Figure 40**).

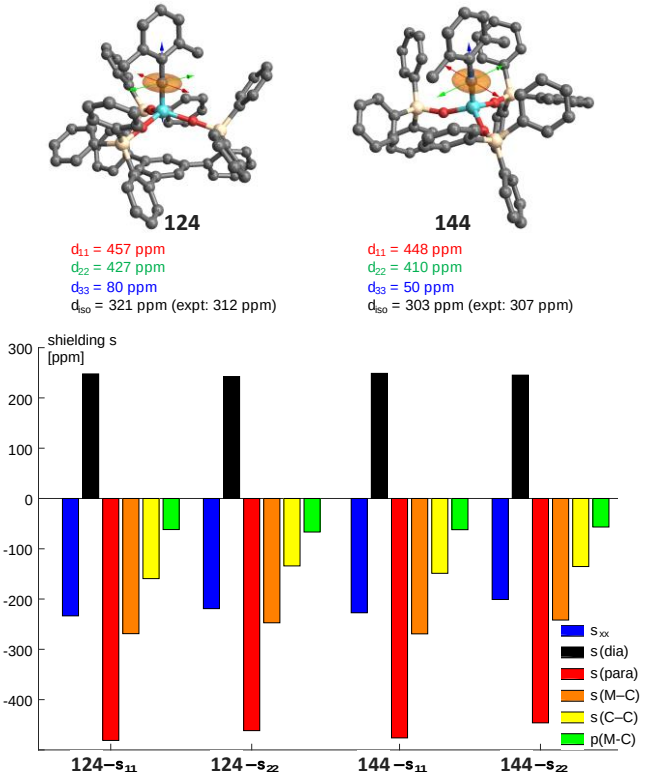


**Figure 39.** Chemical shift tensor analysis of complex **124** and **144**; with Christopher Gordon and Prof. Dr. Christophe Copéret.

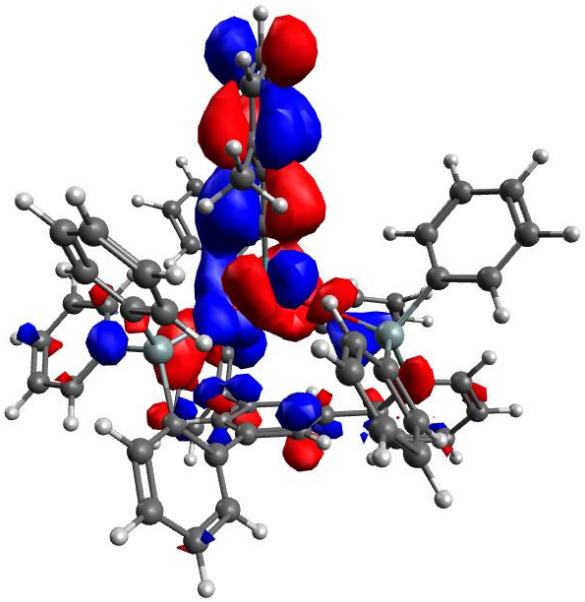

**Figure 40.** Calculated LUMO of complex **124**; with Christopher Gordon and Prof. Dr. Christophe Copéret.

### 3.1.7 Benchmarking of the Catalytic Activity

With numerous complexes in hand (**Figure 41**), we chose the simple homo-metathesis reaction of 1-methoxy-4-(prop-1-yn-1-yl)benzene (**145**) to study the impact of the ligand sphere on the catalytic activity.

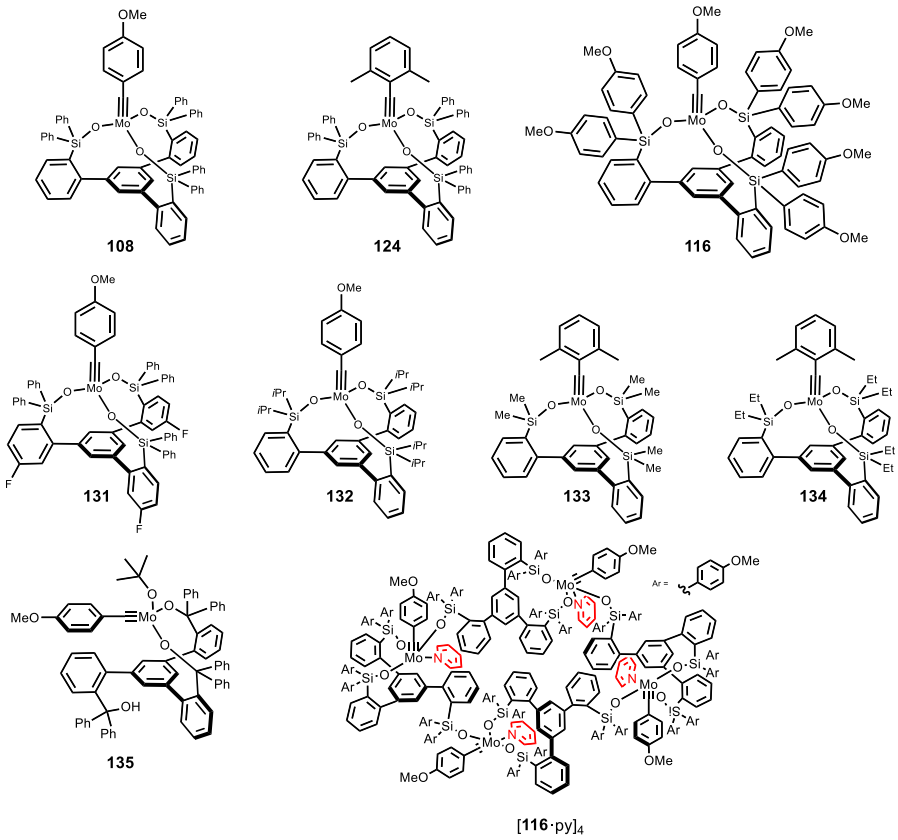


**Figure 41.** Library of prepared complexes for alkyne metathesis.

In the absence of 5 Å molecular sieves the reaction runs only to equilibrium to form equimolar amount of 1,2-bis(4-methoxyphenyl)ethyne (**39**) and 2-butyne (**146**) (**Scheme 47**).

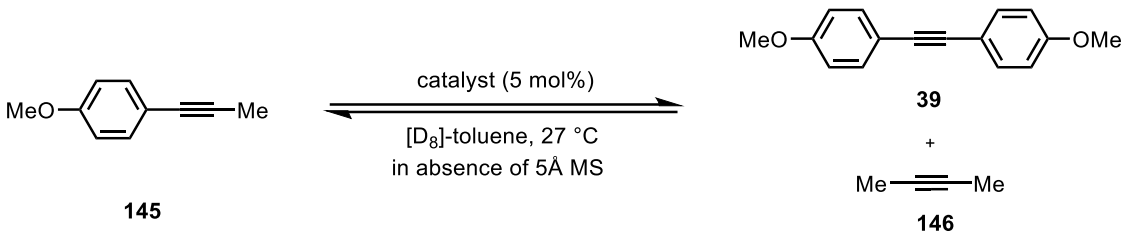


**Scheme 47.** Benchmark catalytic activity of various complexes by $^1$H NMR spectroscopy.

A solution of alkyne **145** in [$D_8$]-toluene was added to a solution of 5 mol% complex **108** in [$D_8$]-toluene. The conversion of the starting material to both products was monitored by $^1$H NMR spectroscopy at 27 °C. The conversion time diagram of catalyst **108** displays a well-behaved reaction profile in which alkyne **145** is consumed until 50% conversion and both products were formed in equal amounts in about 25% yield each (**Figure 42**).

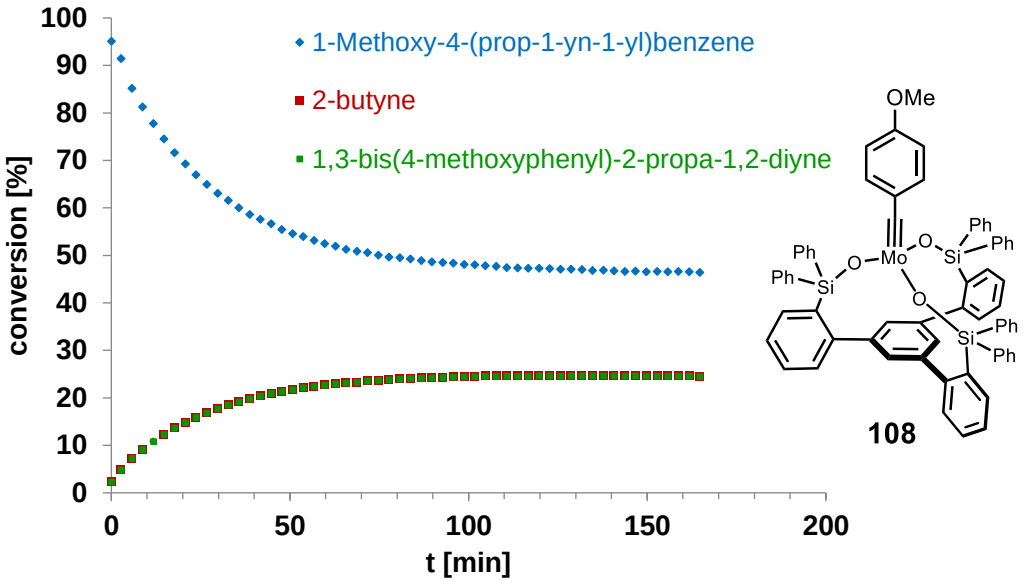


**Figure 42.** Benchmark catalytic activity of complex **108** in [$D_8$]-toluene (0.1 M) by $^1$H NMR spectroscopy at 27 °C.

Next, we tested all complexes for the homo-metathesis of alkyne **145**, monitored the reactions by $^1$H NMR spectroscopy and plotted the data in one conversion-time diagram (**Figure 43**). Catalyst **108** and **131** reached equilibrium in about 150 min. The more electron-rich MeO groups on **116** slowed down the reaction (~250 min). In contrast, complex **124** with the 2,6-dimethyl benzylidyne resulted in significantly slower conversion (~600 min), which indicated an incomplete initiation and a lower effective concentration of the active catalyst in solution. Complex **136** with bidentate carbinol ligand exhibited low activity in comparison to the analogous silanolate complex **108**.

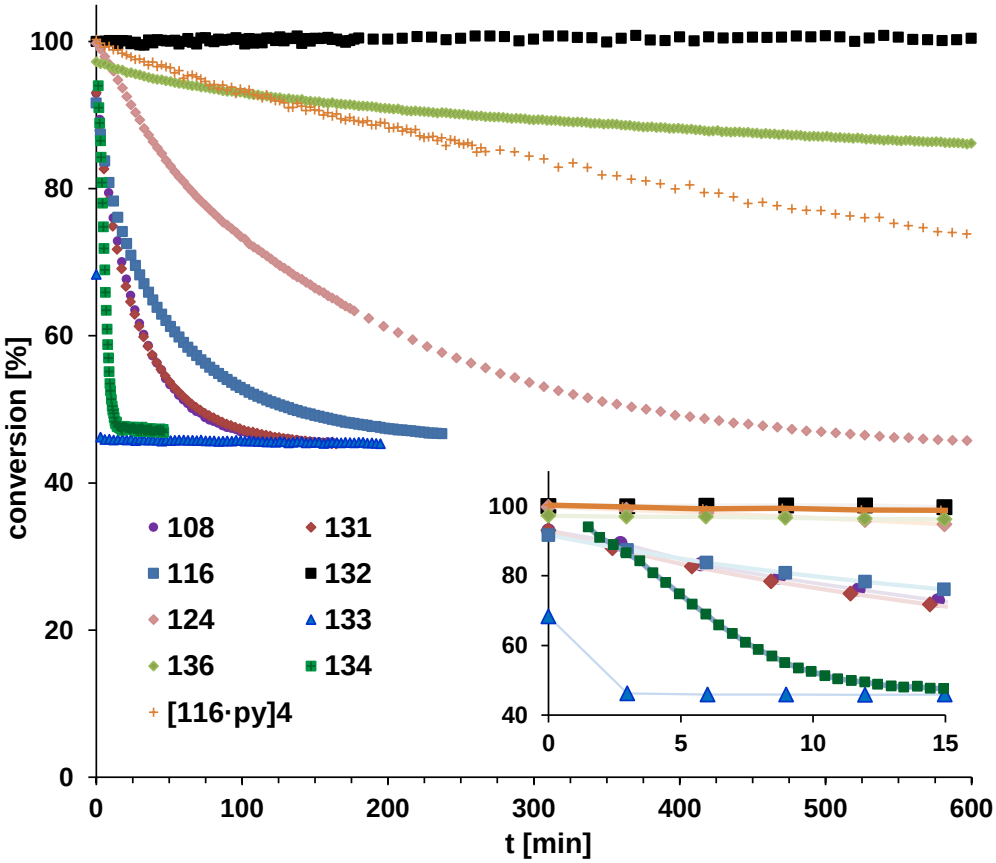


**Figure 43.** Conversion-time diagram of alkyne **145** with various complexes (5 mol% loading) in [$D_8$]-toluene (0.1 M) as monitored by $^1$H NMR spectroscopy at 27 °C.

Intriguingly, cyclotetrameric pyridine adduct [**116**·py]$_4$ is catalytically active and actually faster than complex **136**, demonstrating that even coordinated pyridine does not shut down the catalytic activity. Ligand substitution with aliphatic isopropyl or methyl groups resulted in two surprising observations. Complex **132** did not catalyze the homo-metathesis at 27 °C at all. The crystal structure (*vide supra*) revealed that the isopropyl groups are effectively shielding the molybdenum center and likely prevent any substrate binding, although we observed slow conversion in refluxing toluene. In contrast, the methyl substituted silanolate complex **133** reached equilibrium in less than 5 min and is by far the most active catalyst in the whole series (**Figure 43**, inlet). Similarly, the ethyl variant **134** reached equilibrium in about 12 min.

### 3.1.8 Reactive Intermediates and Mechanism of Alkyne Metathesis

The influence of the different ligand spheres on the catalytic activity is dramatic and we sought to investigate this aspect in more detail. Catalyst **111** with monodentate $Ph_3SiO$ ligands effected alkyne metathesis in less than 10 min, whereas the chelated variant **108** is significantly slower. One possible explanation is the induced higher rigidity of the tripodal ligand sphere, which slowes down the interchange between the two operative coordination geometries during catalysis (pseudo-tetrahedral and trigonal bipyramidal). Another relevant aspect is the exclusive formation of molybdenatetrahedrane **147** upon addition of excess 3-hexyne to **108** at ambient temperature. The Lee group had been the first to report and confirm molybdenatetrahedrane **147** by X-ray crystallography (**Figure 44**).[159]

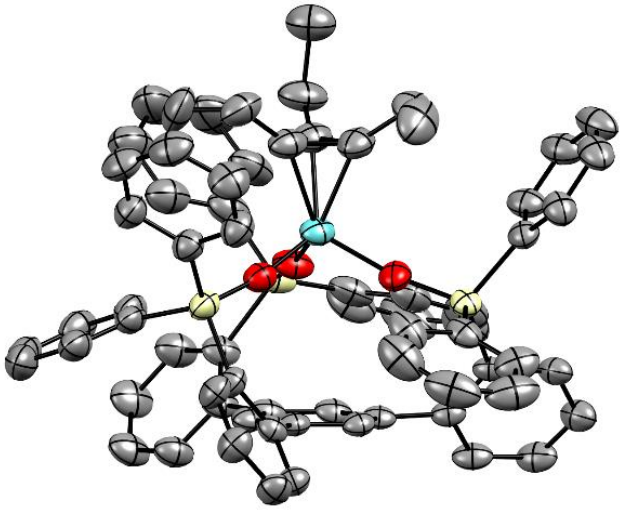

**Figure 44.** Solid state structure of molybdenatetrahedrane **147**; distortion omitted for clarity.[159]

In early studies on the mechanism of alkyne metathesis metallatetrahedranes had been considered as on-cycle intermediates. However, the isolation of several metallacyclobutadiene complexes led to the assumption that metallatetrahedranes are off-cycle intermediates and not involved in the actual catalysis pathway (*vide supra*). The observation that metallatetrahedrane **147** is easily accessible and represents the resting-state when 3-hexyne was added to complex **108**, raised again the question whether or not metallatetrahedranes are competent intermediates for productive metathesis and pass through an alternate [2+1] mechanism (**Scheme 48**).

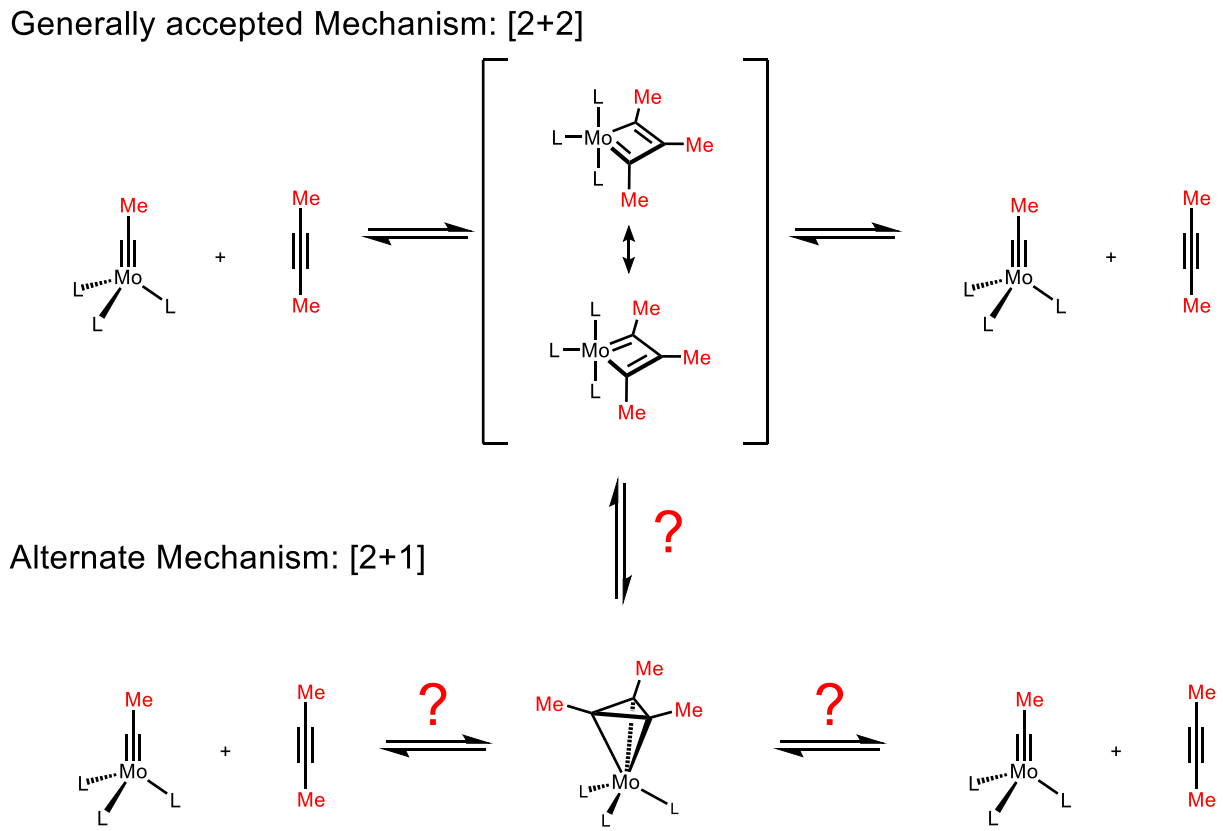


**Scheme 48.** Current mechanistic paradigm for alkyne metathesis and alternate [2+1] mechanism.

To clarify this aspect, we dissolved complex **108** in [$D_8$]-toluene and added five equivalents of 3-hexyne (**Scheme 49**). $^{1}H$ and $^{13}C$ NMR analysis confirmed the formation of molybdenatetrahedrane

**147** in 95%, which gave one characteristic $^{13}C$ NMR signal ($\delta_C$ = 83.8 ppm, 25 °C) for the three carbon atoms directly bound to the molybdenum center. $^{95}Mo$ NMR measurements of a solution of **147** in [$D_8$]-toluene gave no $^{95}Mo$-NMR signal at 25 °C or 60 °C.

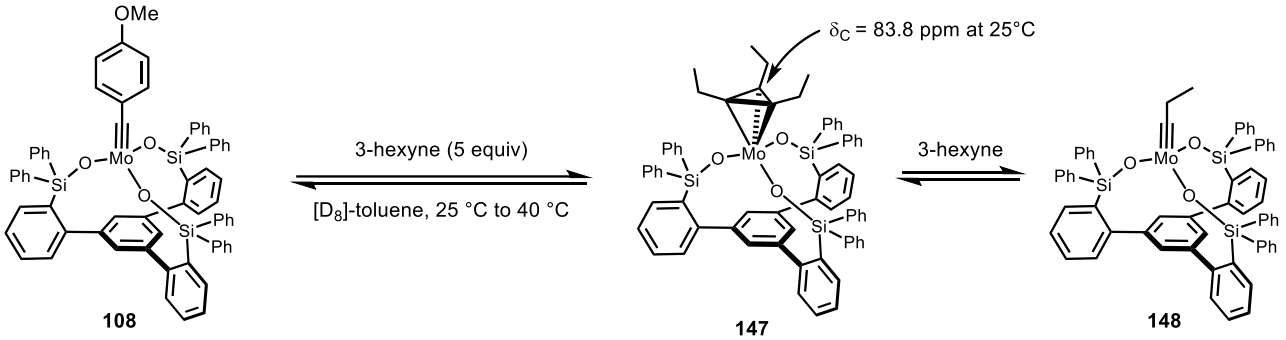


**Scheme 49.** Formation of molybdenatetrahedrane **147**.

EASY-ROESY NMR studies allowed dynamic exchange processes on NMR time scale to be studied. This technique revealed that molybdenatetrahedrane **147** is formed reversibly and is dynamically exchanging with 3-hexyne and propylidyne complex **148** at 25 °C (**Scheme 50**).

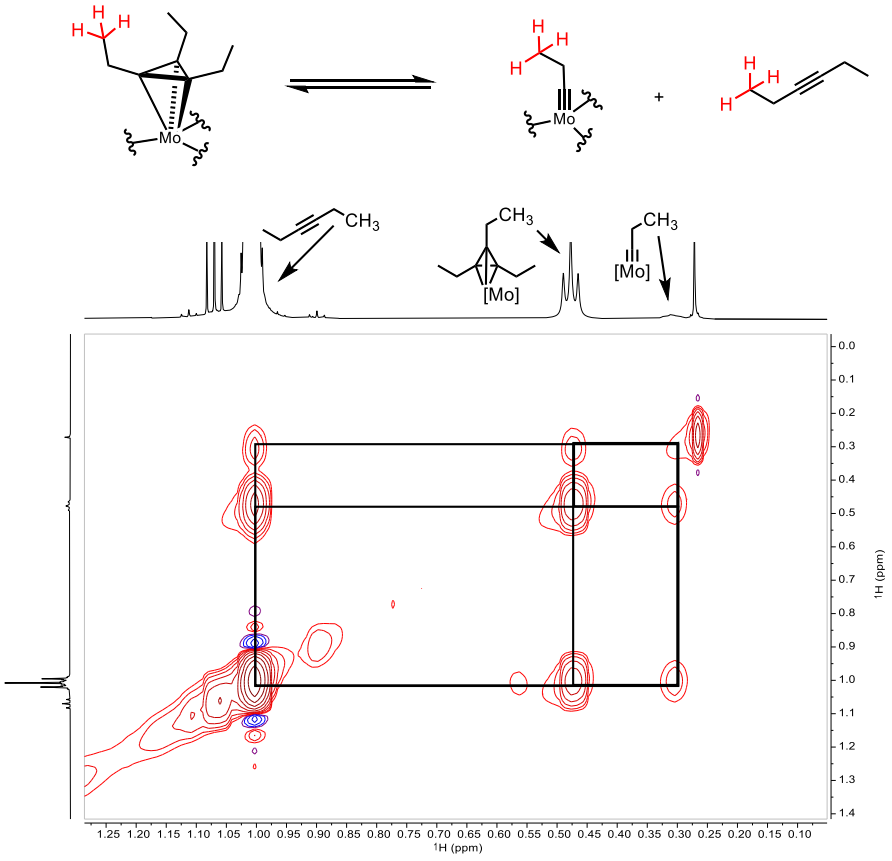


**Scheme 50.** EASY-ROESY NMR study revealed the dynamic, reversible exchange process of **147** with 3-hexyne and **148** at 25 °C. The spin-lock time used for this experiment was 300 ms.

However, molybdenatetrahedrane **147** did not allow to confirm or exclude the proposed alternate [2+1] cycloaddition pathway because it is only in the dynamic exchange with 3-hexyne and propylidyne complex **148**. In contrast, a mixed metallatetrahedran, such as **150**, would be in theory in a dynamic exchange with two alkyne products, that is 3-hexyne and 1-methoxy-4-(but-1-yn-1-yl)benzene **149**. Therefore, we dissolved complex **108** in [$D_8$]-toluene and added five equivalents of

1-methoxy-4-(but-1-yn-1-yl)benzene **149** in order to preferentially form mixed metallatetrahedran **150** and study the [2+1] cycloaddition pathway by exchange NMR experiments (**Scheme 51**).

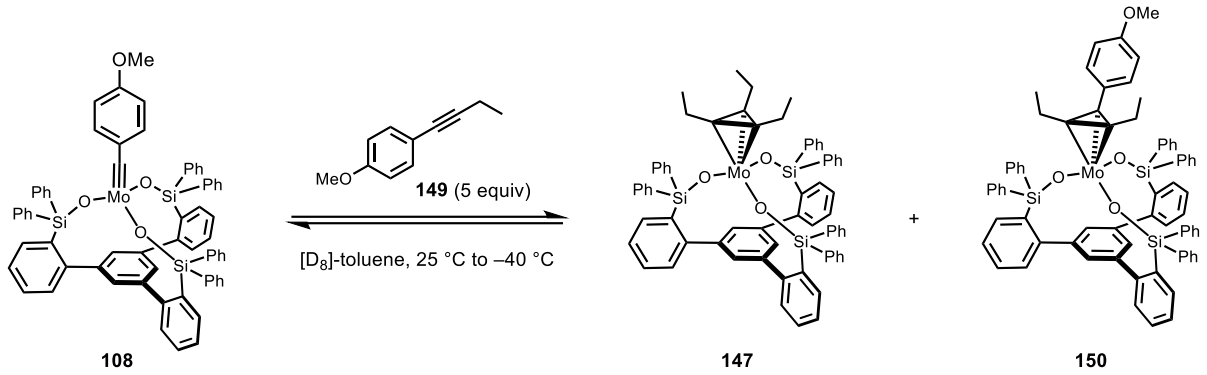


**Scheme 51.** Observation of mixed molybdenatetrahedrane **150**.

By exchange NMR experiments we only observed the exchange between 3-hexyne and mixed molybdenatetrahedrane **150** and the exchange between alkylidyne complex **108** and mixed molybdenatetrahedrane **150**. Consequently, mixed molybdenatetrahedrane **150** can only be formed from 3-hexyne and alkylidyne complex **108** within limits of detection (**Scheme 52**).

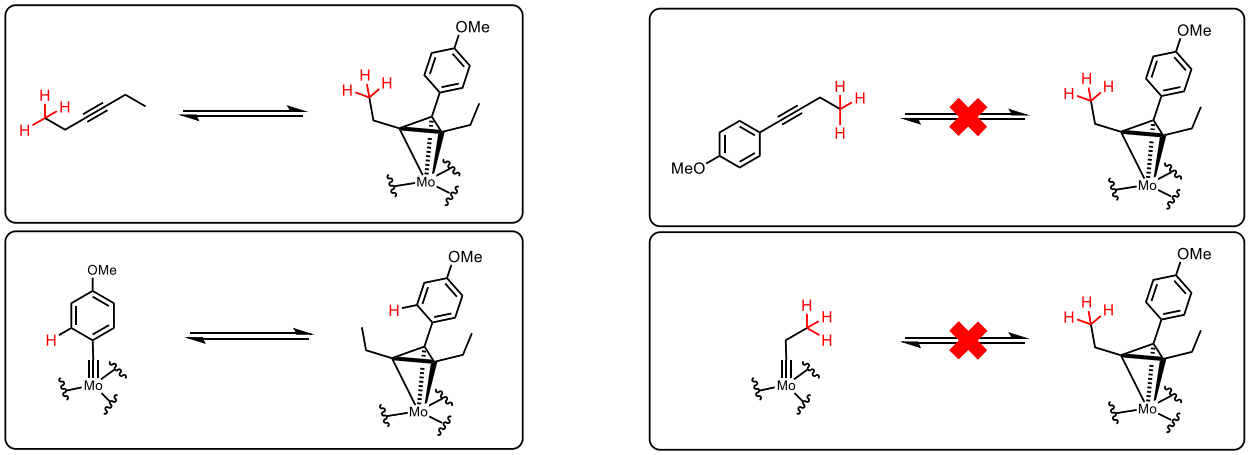


**Scheme 52.** Dynamic exchange processes observed by EXSY NMR spectroscopy.

The privileged exchange pathway might derive from an increased thermodynamic stability of *p*-methoxybenzylidyne complex **108** over the corresponding propylidyne complex **148**. To test this hypothesis we treated complex **110** with excess 4-ocytne to confirm the formation of propyl substituted metallatetrahedrane **151** (**Scheme 53**).

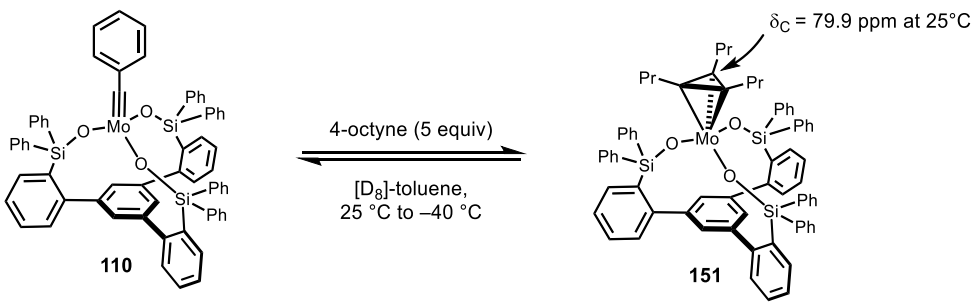


**Scheme 53.** Formation of molybdenatetrahedrane **151**.

The stage was set to run the complementary reaction with 3-hepytne, an asymmetric alkyne bearing an ethyl and propyl group (**Scheme 54**). In theory, we expect to observe the formation of two mixed metallatetrahedranes **152**/**153** and two symmetric metallatetrahedranes **147**/**151**. Indeed, all four metallatetrahedranes were observed and subjected to EASY-ROESY NMR study.

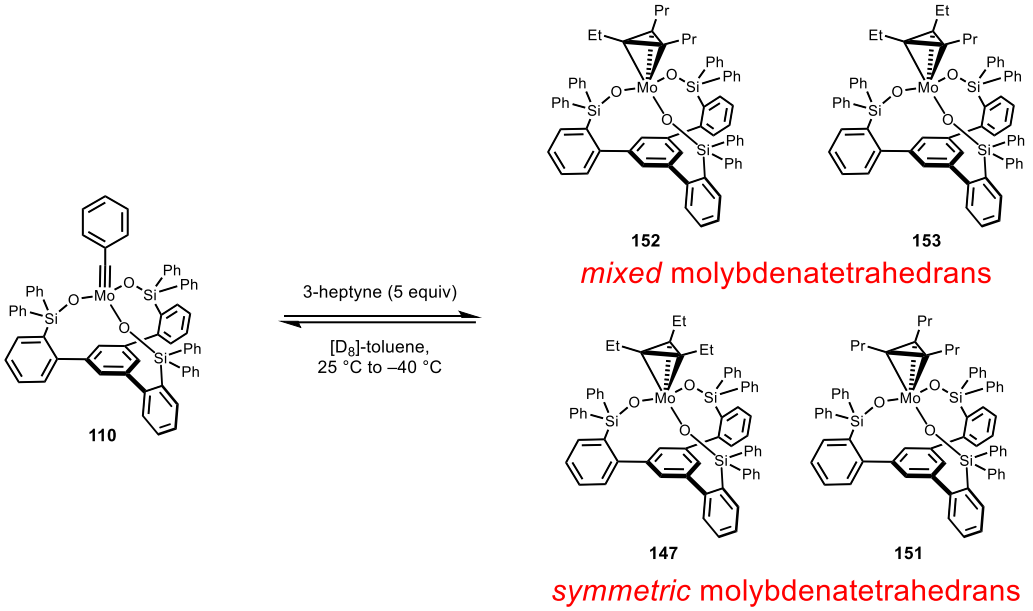


**Scheme 54.** Formation of mixed and symmetric molybdenatetrahedranes.

In contrast to the previous experiment, we observed the exchange process of all ethyl substituted molybdenatetrahedranes with propylidyne complex and the dynamic exchange of all propyl substituted molybdenatetrahedranes with butylidyne complex. In summary, both alkyne products were formed from mixed molybdenatetrahedranes in a formal metathesis reaction (**Scheme 55**). Nevertheless, the experiments did not simply allow us to deduce if metallatetrahedranes participate in a competitive [2+1] mechanism or are off-cycle intermediates.

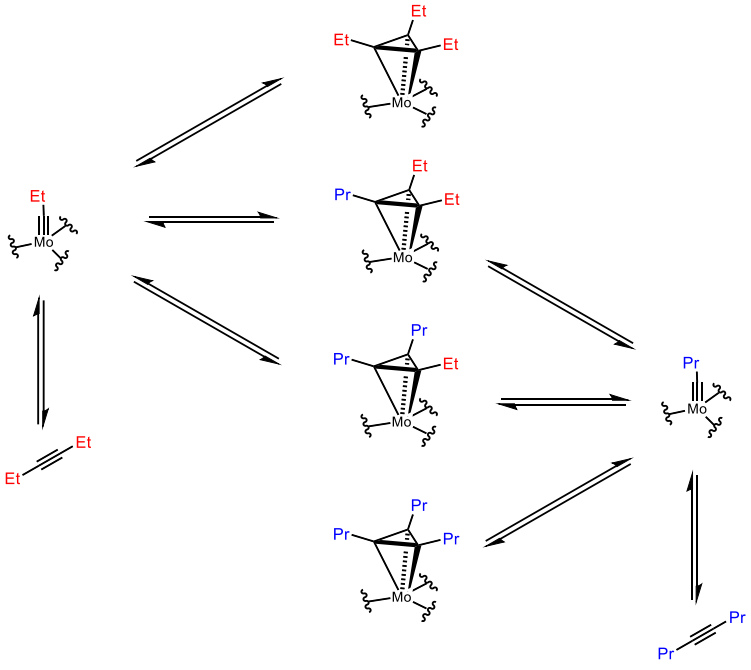

**Scheme 55.** Dynamic exchange processes observed by EXSY NMR spectroscopy.

Driven by curiosity, we conducted the same type of NMR experiment with monodentate complex **111**. Addition of five equivalents of 3-hexyne to a solution of complex **111** in [$D_8$]-toluene gave broad $^1$H NMR signals at ambient temperature, indicating a dynamic exchange process (**Scheme 56**).

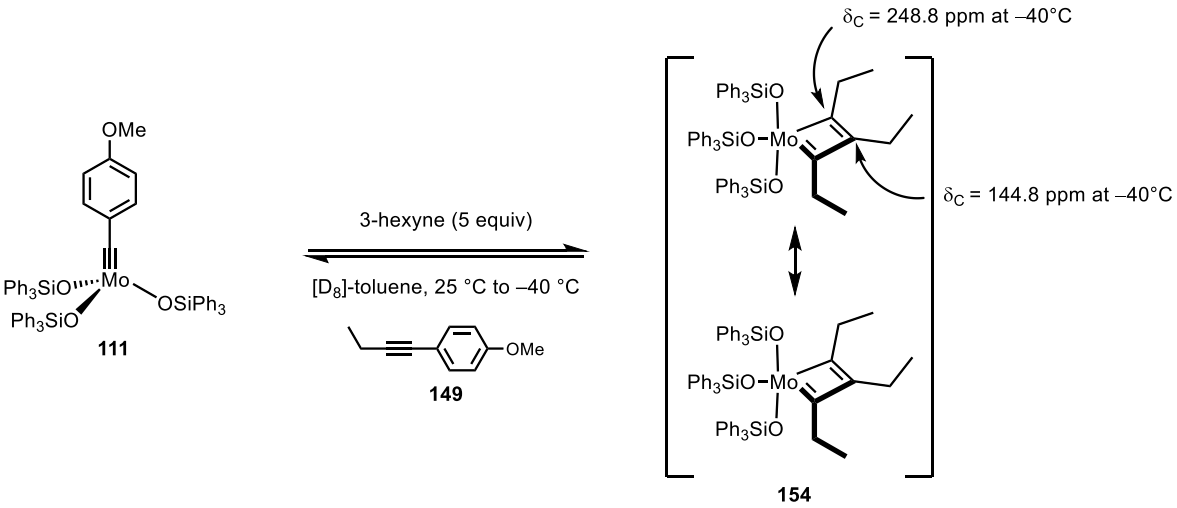


**Scheme 56.** Formation of molybdenacyclobutadiene complex **154**.

Subsequent cooling to −40 °C gave a sharp signal set in the $^1$H NMR spectrum that corresponded to metallacyclobutadiene complex **154** (**Figure 45**), which has one characteristic $^{13}$C NMR shift for both $C_\alpha$ atoms at $\delta_C$ = 248.8 ppm and one $^{13}$C NMR shift for $C_\beta$-atom at $\delta_C$ = 144.8 ppm. Further cooling to −90 °C did not freeze out the two extremes of the metallacyclobutadiene and indicated fast exchange on the NMR timescale.

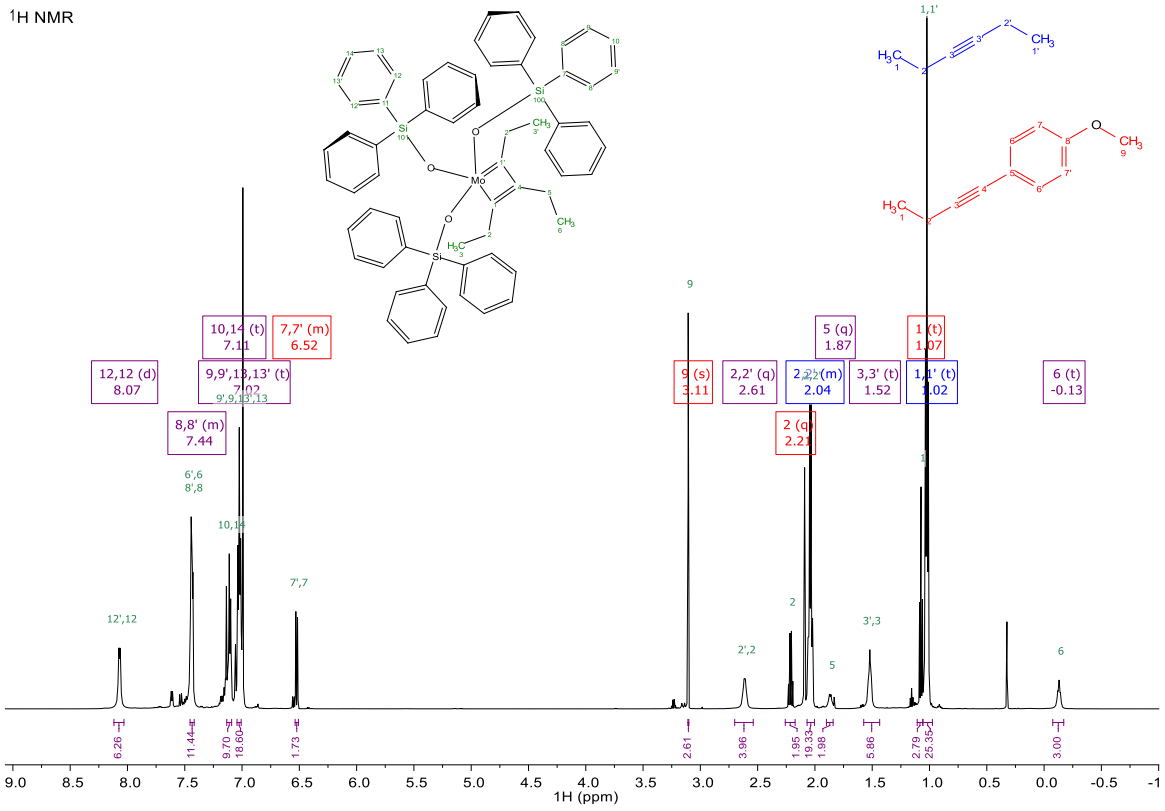


**Figure 45.** $^1$H NMR spectrum of metallacyclobutadiene complex **154** at -40°C in [$D_8$]-toluene.

Molybdenacyclobutadienes are particularly scarce in the literature and the poor quality of X-ray data of competent alkyne metathesis catalysts precluded a detailed structure analysis.[101] In this context, it is remarkable that we obtained the solid state structure of molybdenacyclobutadiene **154**, derived from a very active alkyne metathesis catalyst, in good quality. A solution of metallacyclobutadiene complex **154** in diethyl ether was cooled to −85 °C. After 1 week at this temperature, we obtained steel-blue crystals suitable for single-crystal X-ray diffraction. The X-ray structure shows a distorted trigonal bipyramidal coordination geometry, with the planar molybdenacycle residing in the equatorial plane (**Figure 46**). The bond distances of the molybdenacyclobutadiene core are highly distorted and display one of the two tautomeric extremes in the solid state. The Mo1–C2 bond (1.872(2) Å) is shorter than the Mo1–C3 bond (1.896(2) Å), also the C1–C2 distance (1.476(3) Å) and the C1–C3 distance (1.423(3) Å) are different. The short Mo1–C1 bond (2.117(2) Å) across the four-membered ring indicates a transannular bonding motif.[160]

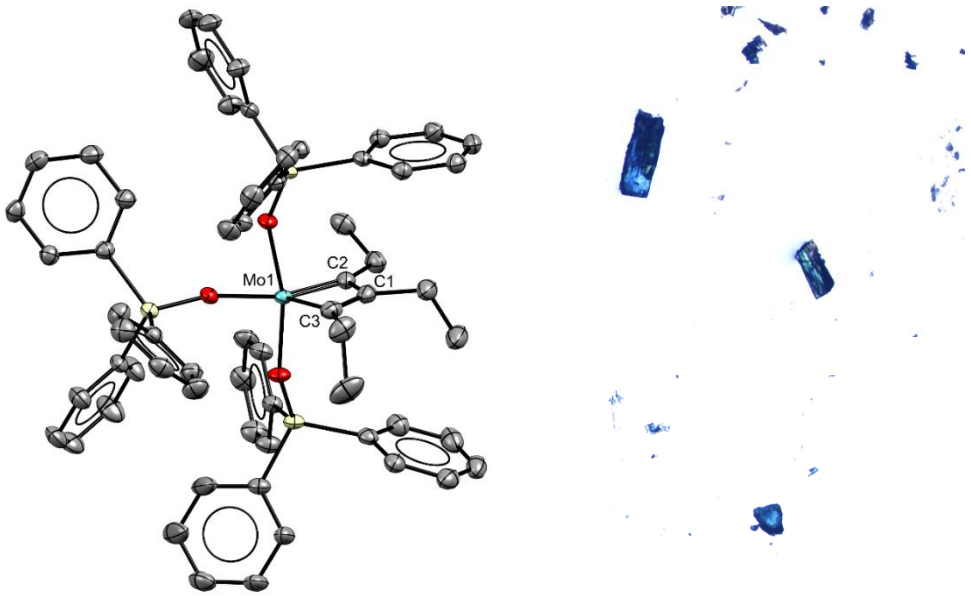


**Figure 46.** A.) Solid state structure of metallacyclobutadiene complex **154**; B.) Steel-blue crystals of complex **154**.

The striking dichotomy between formation of molybdenacyclobutadiene with $Ph_3SiO$ ligands but molybdenatetrahedrane with tridentate ligand **105** encouraged us to study the determining factors. Previously, we noticed that *p*-methoxybenzylidyne complexes exhibited strong C–H π interaction with the adjacent phenyl groups on the silanolates (*vide supra*). Accordingly, molybdenatetrahedrane **147** could be also the result of a stabilizing C–H π interaction of the methylene protons on the ethyl groups to the adjacent phenyl groups. Indeed, at ambient temperature the $^1$H NMR spectrum of **147** shows one broad signal for both methylene protons of the ethyl substituent. This $^1$H NMR signal further broadened on cooling and reached coalescence at -20 °C (**Figure 47** A). Further cooling to -70 °C gave two distinct broad $^1$H NMR signals for both methylene protons ($\Delta_\delta$ = 0.9 ppm) on the ethyl substituent and confirmed the diastereotopic nature of it. This observation was further supported by measuring a 1D selective NOESY NMR experiment at −70 °C. Excitation of the $CH_3$ group on the ethyl substituent showed the coupling to both distinct broad $^1$H NMR signals of both methylene protons ($\Delta_\delta$ = 0.9 ppm) (**Figure 47** B).

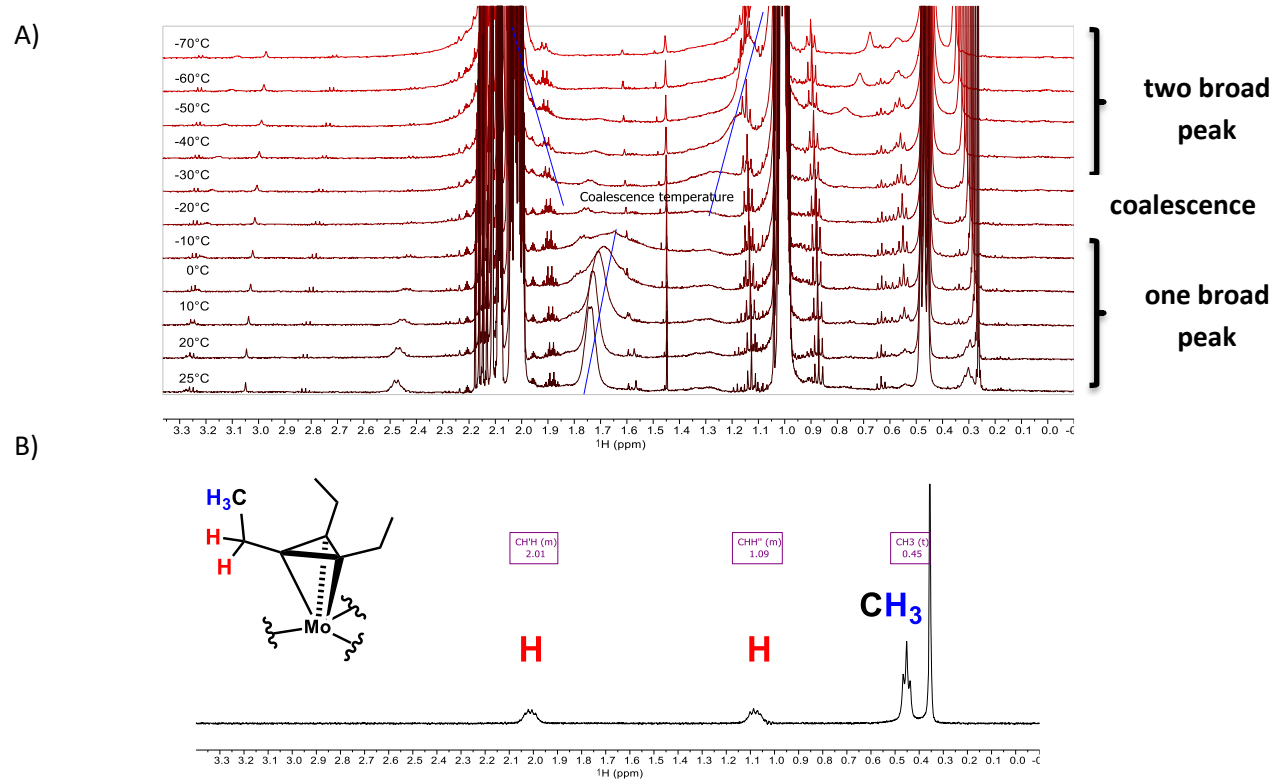


**Figure 47.** A.) Low-temperature NMR study of **147** from 25 °C to −70 °C in [$D_8$]-toluene; B.) 1D selective NOESY NMR of **147** obtained upon excitation of the $CH_3$ group at -70 °C; methylene protons in red; methyl group in blue.

The high catalytic activity of catalyst **133** in comparison to complex **108** raised the question as to which intermediate is formed with catalyst **133** when excess 3-hexyne is added to it (**Figure 48**).

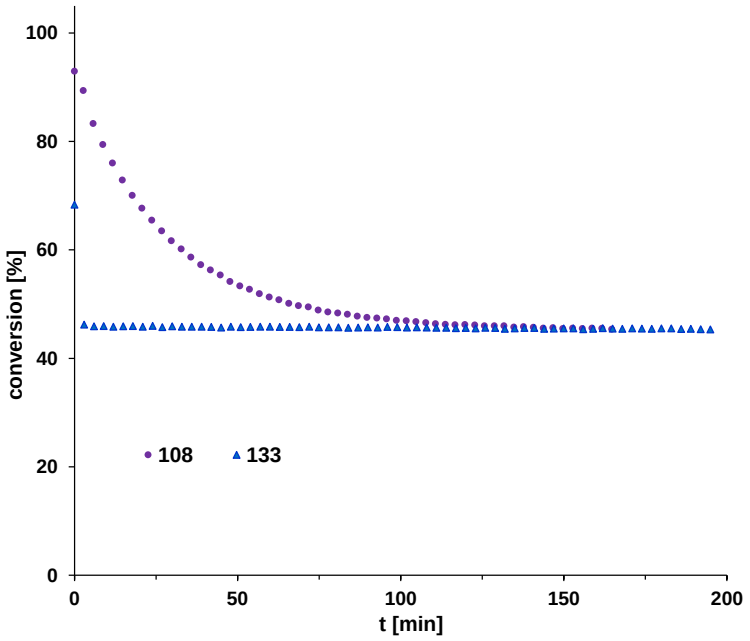


**Figure 48. C**onversion-time diagram of alkyne **145** with complex **108** and **133** (5 mol%) in [$D_8$]-toluene (0.1 M) monitored by $^1$H NMR spectroscopy at 27 °C.

The addition of five equivalents of 3-hexyne to a solution of complex **133** in [$D_8$]-toluene revealed that the major species is dissociated complex **133** and small quantities of a new, dynamic species were detected (**Scheme 57**, **Figure 49** B).

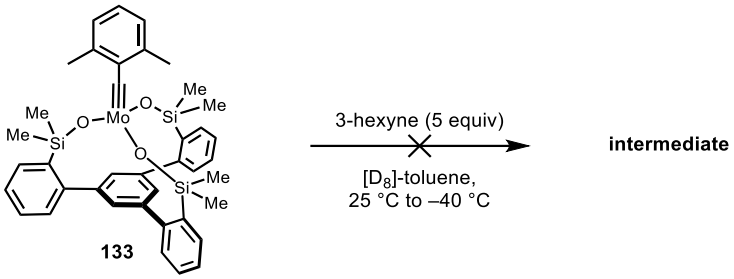


**Scheme 57.** Attempted investigation of intermediates of complex **133** with 3-hexyne.

Although cooling to −40 °C improved the quality of the $^{1}$H NMR signals (3.0 – 3.7 ppm), we were not able to detect any $^{1}$H-, $^{13}$C-HMBC signals to determine the nature of this intermediate (**Figure 49** C and insert).

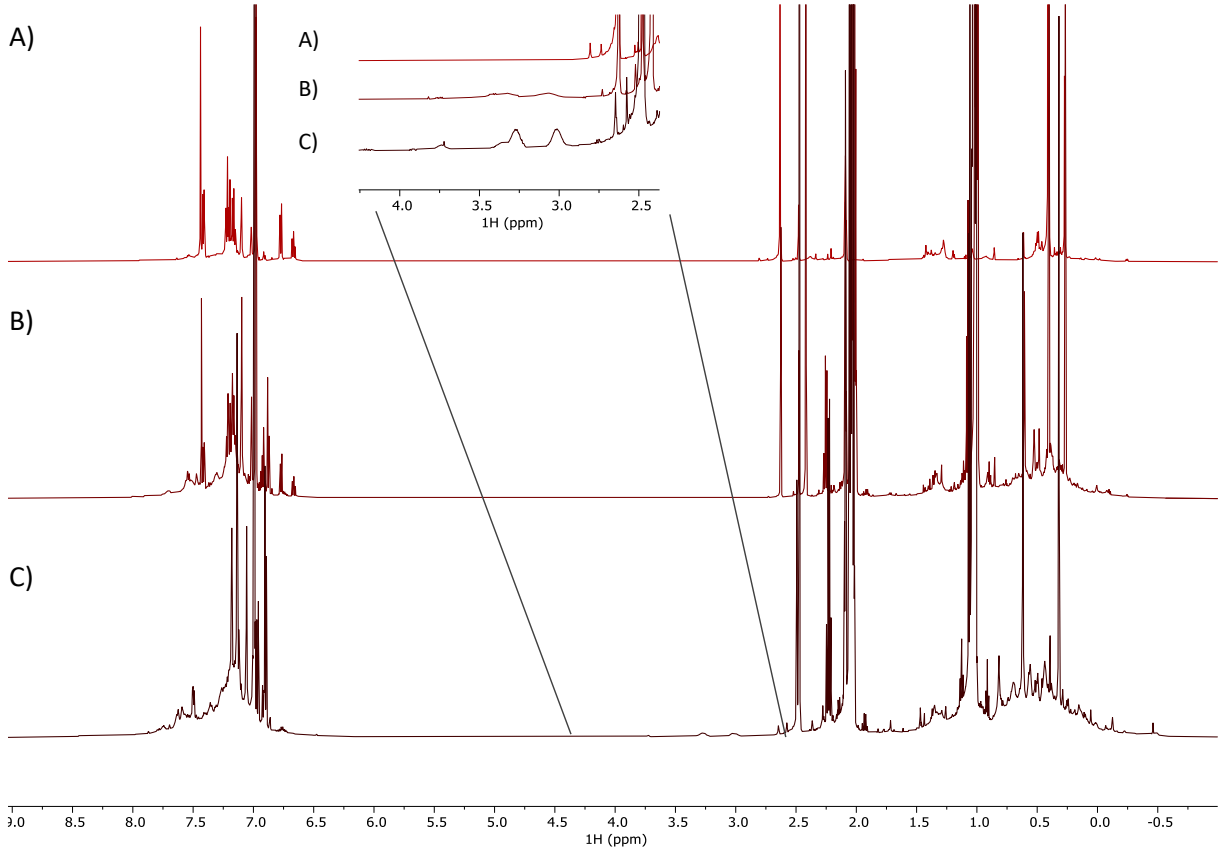


**Figure 49.** A) $^{1}$H NMR of complex **133** in [D$_8$]–toluene at 25 °C. B) $^{1}$H NMR of complex **133** with 5 equiv of 3-hexyne in [D$_8$]-toluene at 25 °C. C) $^{1}$H NMR of complex **133** with 5 equiv of 3-hexyne in [D$_8$]-toluene at −40 °C, insert shows small quantities of a dynamic species.

Since alkylidyne complex **133** appeared to be the resting-state when excess 3-hexyne is added, we concluded that this system is not ideal to study the involved intermediates. Therefore, we changed our strategy and used differently substituted alkyne substrates to investigate subtle changes of the steric and electronic parameters on the stability of the corresponding intermediates. Addition of five equivalents of 2-butyne to a solution of complex **108** in [D$_8$]–toluene at ambient temperature and cooling to −40 °C gave two $^{1}$H NMR signal sets that correspond to molybdenatetrahedrane **155** and molybdenacyclobutadiene complex **156** (**Scheme 58**).

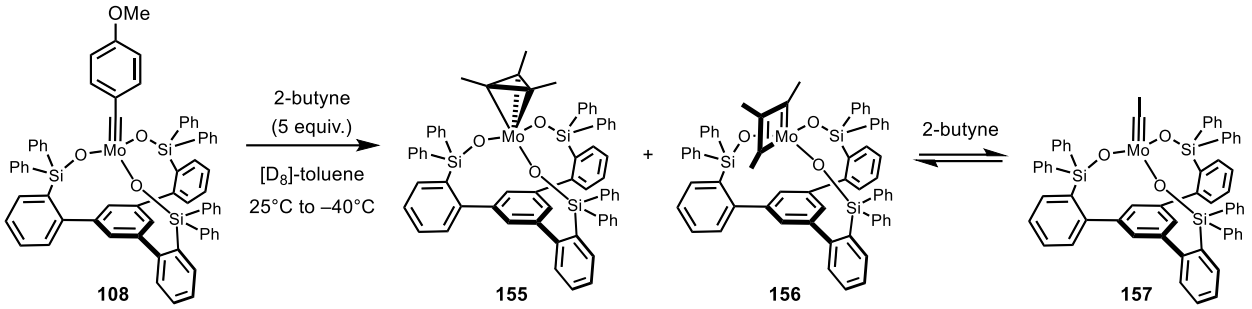


**Scheme 58.** Formation of molybdenacyclobutadiene **156** and molybdenatetrahedrane **155**.

For the first time, we were able to observe a metallatetrahedrane and a metallacyclobutadiene for the same ligand framework. Exchange NMR spectroscopy (ROESY) at −40°C confirmed the mutual interconversion of the methyl substituents at the $C_\alpha/C_{\alpha'}$ positions of **156** and the dynamic exchange process between 2-butyne and **156**. However, we observed neither the exchange between 2-butyne and molybdenatetrahedrane **155** nor ethylidyne complex **157** at all (**Scheme 59**).

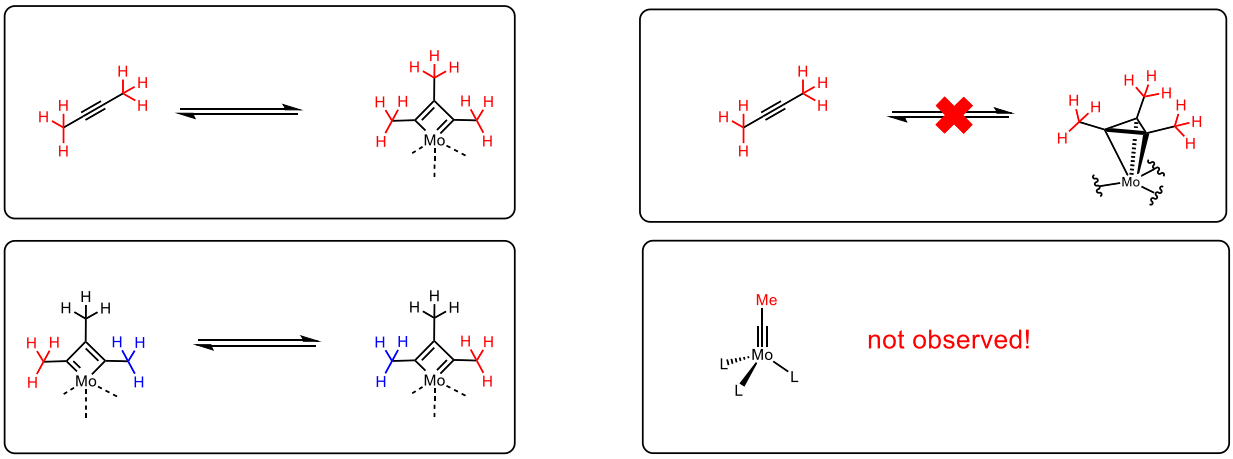


**Scheme 59.** Dynamic exchange processes observed by EXSY NMR spectroscopy at -40 °C.

In contrast, when warming to 0 °C, the exchange between 2-butyne and molybdenatetrahedrane **155** was observed, as was the exchange between both intermediates **155**/**156**, which confirmed that both intermediates are reversibly interconverting on NMR timescale (**Scheme 60**).

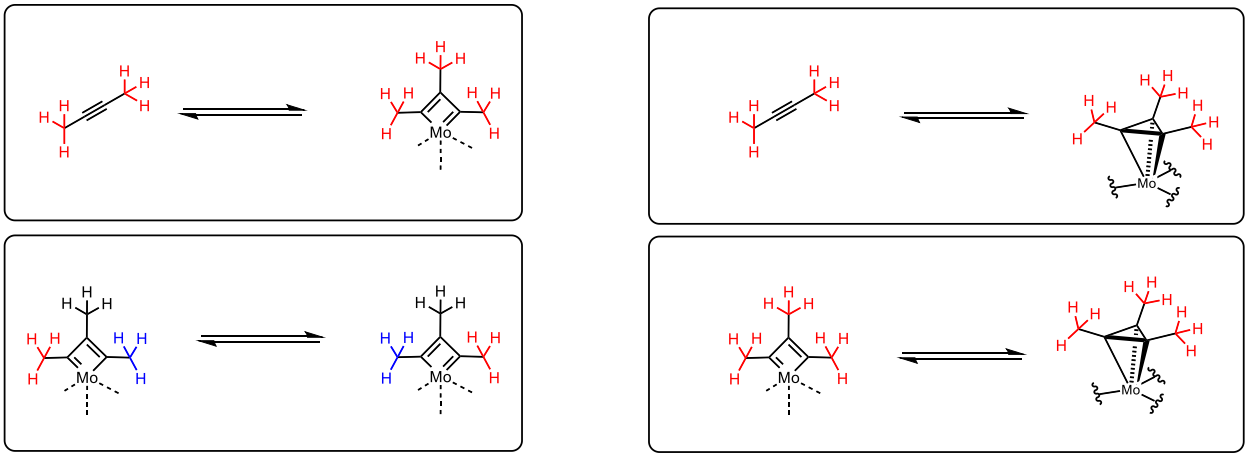

**Scheme 60.** Dynamic exchange processes observed by EXSY NMR spectroscopy at 0 °C.

The three distinct NMR signals were observed for the methyl substituents on the molybdenacyclobutadiene **156**. The strong $^1$H NMR shift difference of the methyl substituent at the $C_\alpha$ position ($\delta_H$ = 2.41 ppm) and the methyl substituent at the $C_{\alpha'}$ position ($\delta_H$ = 1.19 ppm) was attributed to the anisotropic effect and allowed to unambiguously assign the core structure of **156**. Intriguingly, exchange NMR spectroscopy (ROESY) showed the pronounced exchange of 2-butyne with the methyl groups at the $C_{\alpha'}$/$C_\beta$ positions of **156** and a negligible exchange with the methyl group at the $C_\alpha$ position, which again suggested that both [2+2] cycloreversions are not equally likely (**Figure 50**, **Scheme 61**).

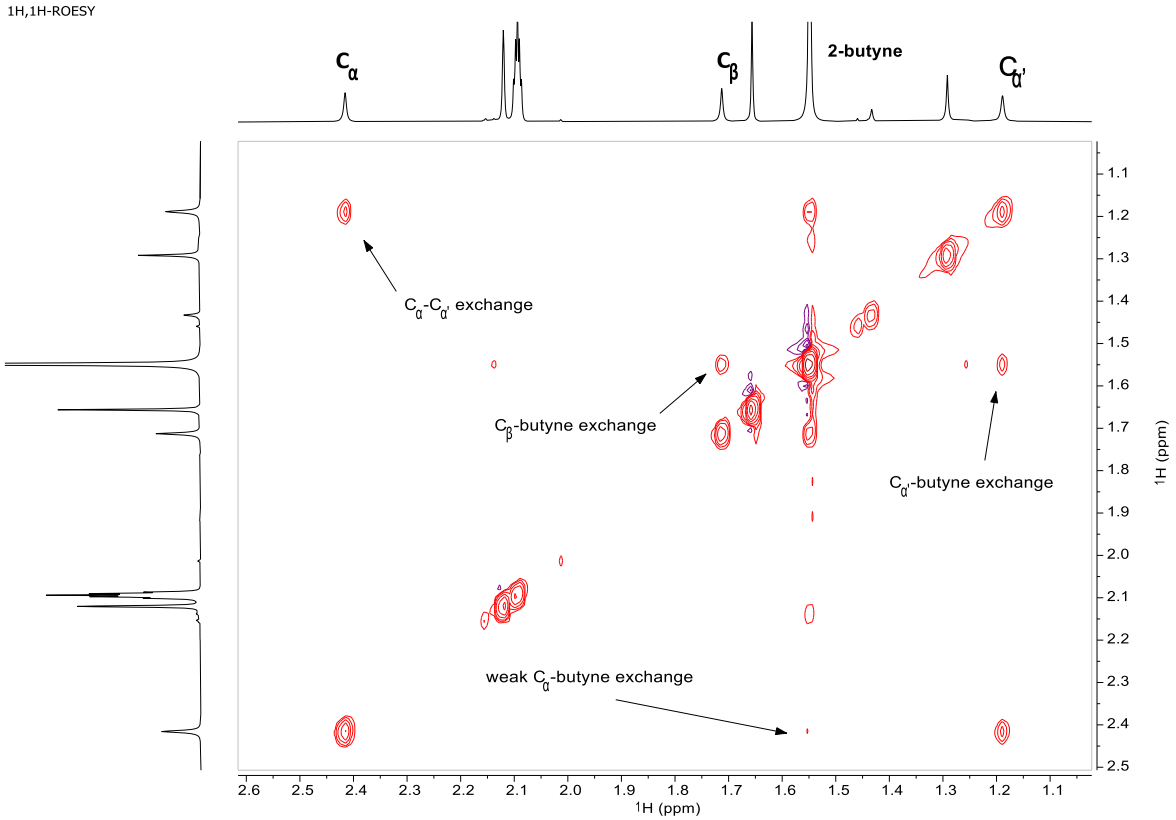


**Figure 50.** Dynamic exchange processes observed by EASY-ROESY NMR spectroscopy in [D$_8$]-toluene at -40 °C.

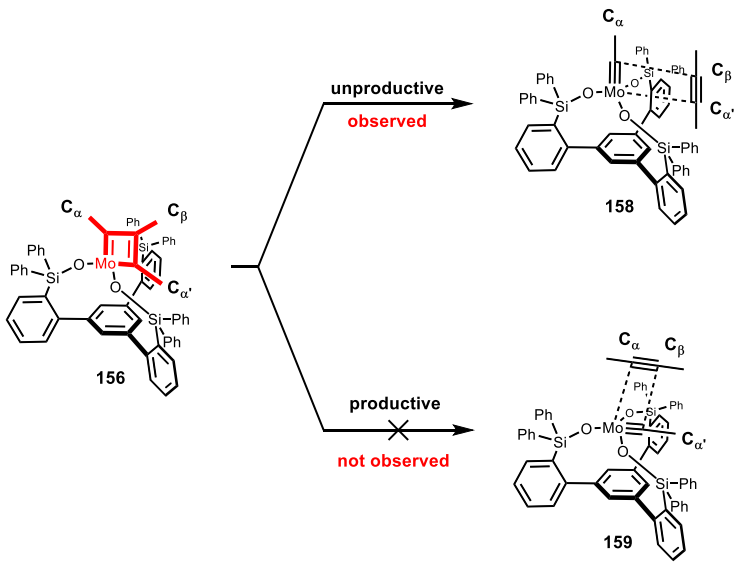


**Scheme 61.** Productive and unproductive [2+2] cycloreversion pathway with canopy catalyst.

The fact that we observe two tautomeric molybdenacyclobutadiene forms, which interconvert on NMR timescale, and that only one [2+2] cycloreversion pathway is productive for metathesis implies that a pseudorotation for each productive turnover is necessary (**Scheme 62**).

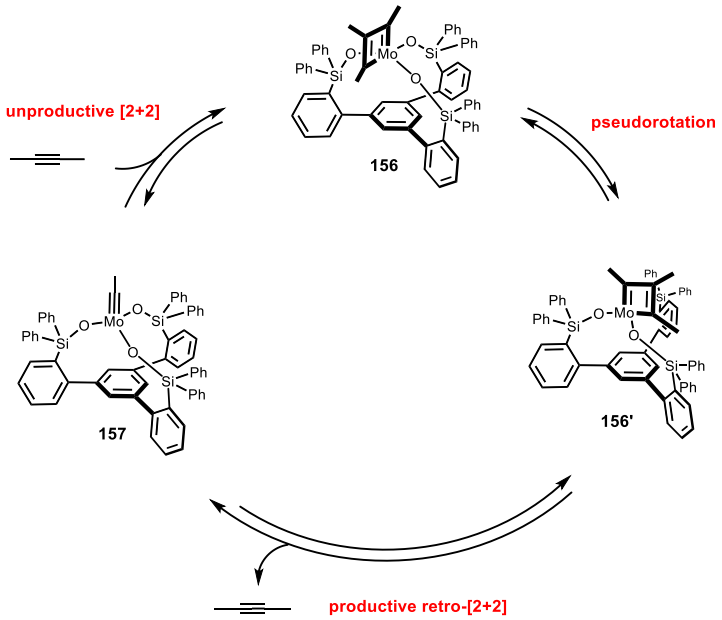


**Scheme 62.** Revised alkyne metathesis mechanism for canopy catalysts.

Overall, the NMR data showed without any doubts that metallatetrahedrane and metallacyclobutadiene are reversibly interconverting. The strong preference of ethyl substituted alkynes to form only metallatetrahedranes and of methyl substituted alkynes to form a mixture of metallatetrahedrane and metallacyclobutadiene, prompted us to determine if metallatetrahedranes are true on-cycle or off-cycle intermediates in alkyne metathesis. Simple homo-metathesis reaction with either methyl or ethyl substituted substrate **145/149** should result in almost identical conversion with 5 mol% of catalyst **108** in the case that the metallatetrahedrane is on-cycle and does not slow down the conversion. On the other hand, if metallatetrahedranes are unreactive sinks and therefore off-cycle intermediates, the conversion of ethyl substituted substrate **149** is excepted to be slower (**Scheme 63**).

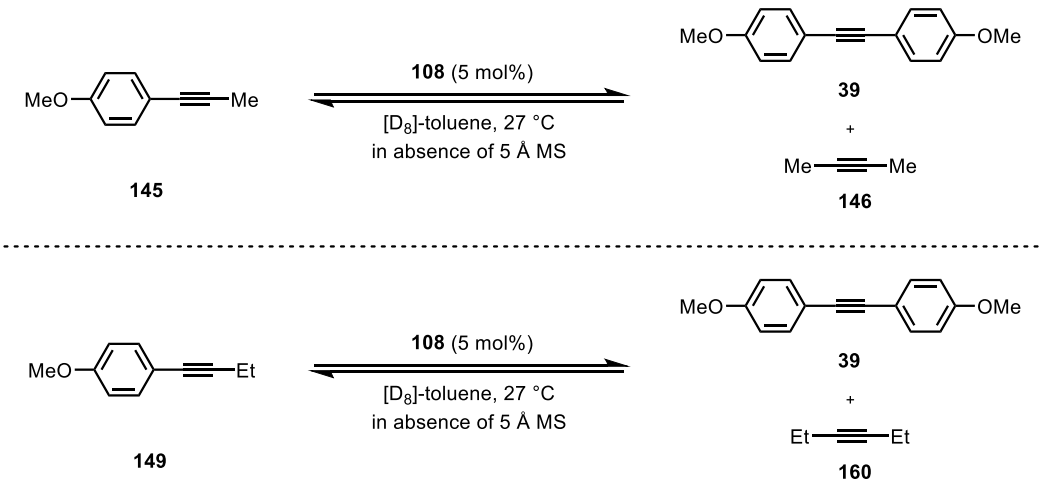


**Scheme 63.** Homo-metathesis reaction of **145** or **149** with catalyst **108** (5 mol% loading) in [$D_8$]-toluene at 27 °C.

Comparison of both reactions in a single conversion-time diagram revealed that both reactions were comparable fast in converting starting material to product. Yet, the conversion-time diagram is not well resolved and an interpretation is therefore not meaningful.

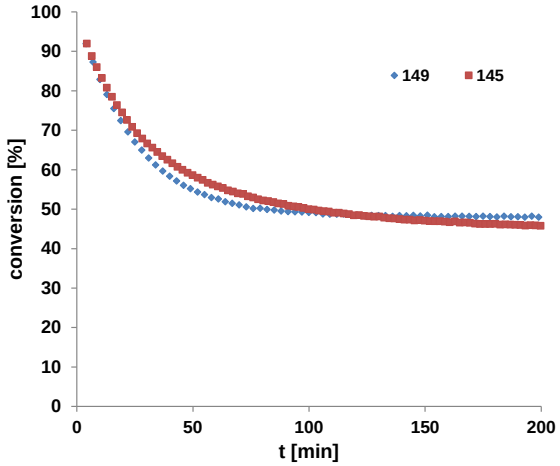


**Figure 51.** Conversion-time diagram of **145** and **149** with catalyst **108** (5 mol% loading) in [$D_8$]-toluene at 27 °C.

### 3.1.9 Scope, Applications and Stability

Next, we investigated the functional group compatibility of catalysts **108** and **133** (**Scheme 64**). Electron-rich and poor tolane derivatives were efficiently converted at ambient temperature or at 60 °C to the desired product **161a,c,d**. Nitro substituted tolane **161f** failed to be metathesized and aldehyde **161g** decomposed in the presence of catalyst **108** or **133**. However, protic phenol **161b** and ketone **161e** did not bring metathesis to a halt. Various basic donor-sites were well tolerated: aromatic and aliphatic thioethers (**162** and **168**), pyridine **163**, thiophene **164**, secondary and tertiary amines (**166** and **167**) or potentially coordinating Weinreb-amide **169**. Also rewarding was the tolerance towards substitution-prone functional groups such as tosylate **170** or primary iodide **171**.

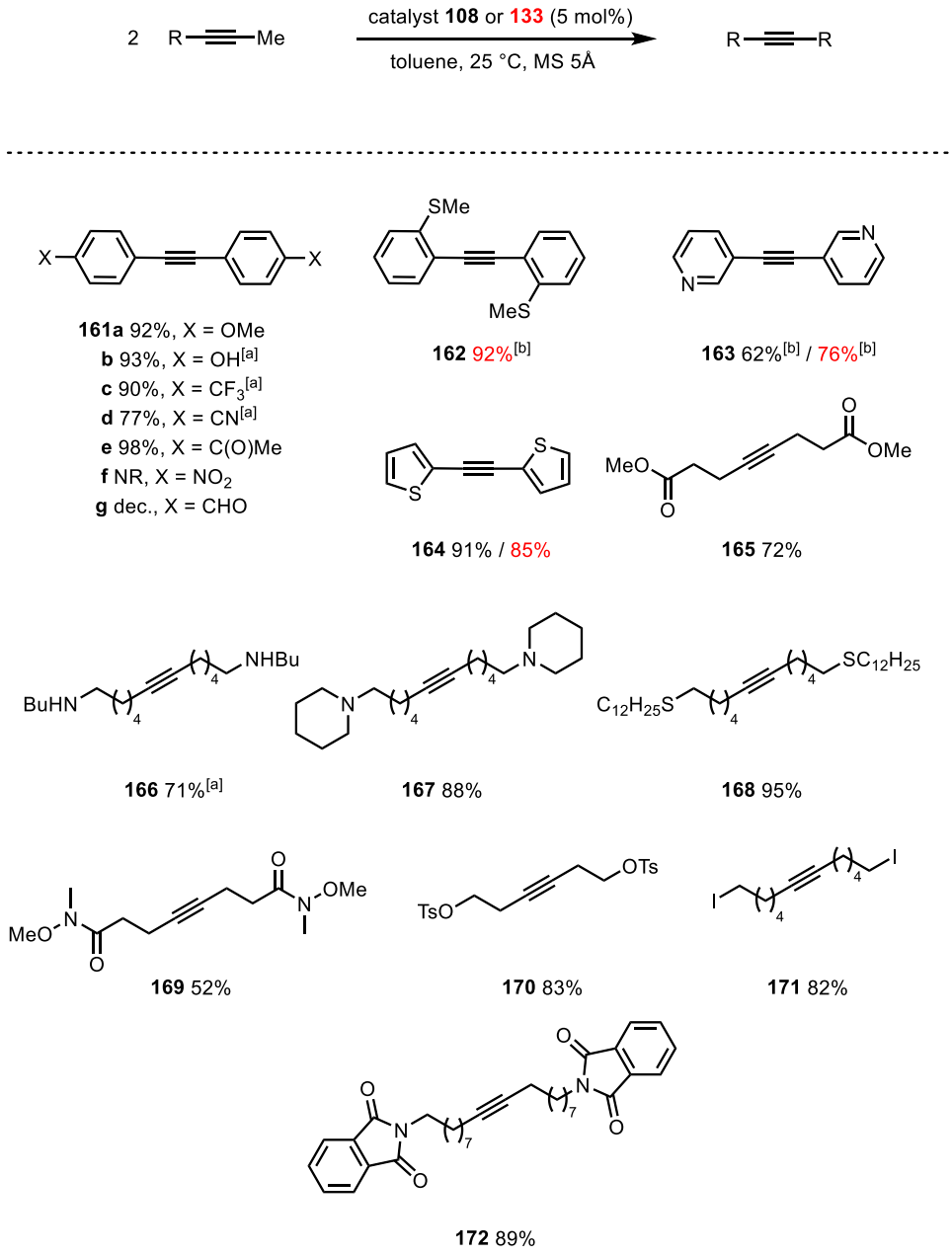


**Scheme 64.** [a]The choice of catalyst is color-coded; at 60 °C. [b]At 90 °C; NR = no reaction

Yet, the functional group compatibility of the newly developed catalysts **108** and **133** towards protic functional groups is most instructive (**Table 5**). Previous monodentate-based catalyst **111** failed to metathesize all primary alcohols **173a-d**, whereas both podand complexes **108** and **133** afforded the desired products. In accordance, with 10 mol% of catalyst **111** only 34% of secondary alcohol **174** was accessible, whereas with catalyst **133** we obtained diol **174** in excellent yield. Intriguingly, only the slimmest variant **133** converted a propargylic alcohol to the desired monomeric macrocycle **175**. The phenyl substituted catalyst **108** mainly gave dimers. Unprotected propargylic –OH groups were not tolerated by catalyst **111** and afforded no product. Similarly, the excellent application profile of catalyst **108** and **133** was demonstrated by the efficient formation of the key intermediates **176** and **177** for two natural product synthesis campaigns.[123, 161]

**Table 5.** Homo-metathesis and ring-closing alkyne metathesis reactions in the presence of unprotected –OH groups[a]

| Substrate | Product | | 111 | 108 | 133 |
|---|---|---|---|---|---|
| 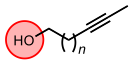 | 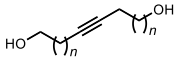 | **173a**, *n* = 4 | 0% | 69% | 73% |
| | | **173b**, *n* = 5 | 0% | 66% | 71% |
| | | **173c**, *n* = 6 | 0% | 83% | 88% |
| | | **173d**, *n* = 7 | 0% | 91% | 87% |
| 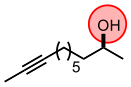 | 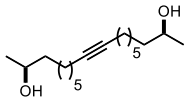 | **174** | 34%[b] | | 94% |
| 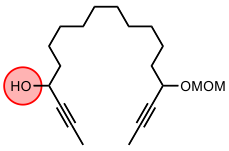 | 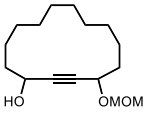 | **175** | 0% | dimers[c] | 68%[d] |
| 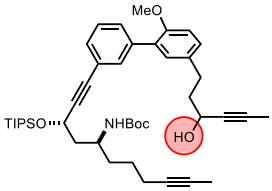 | 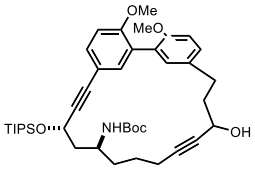 | **176** | 16%[e] | | 66%[f] |
| 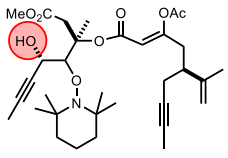 | 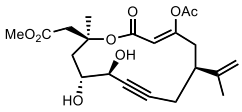 | **177** | 0% | 68%[g] | |

[a]Isolated yields of reactions performed with 5 mol% of catalyst loading in toluene at 25 °C in the presence of MS 5 Å, unless stated otherwise. [b]With 10 mol% of catalyst. [c]Mostly formation of dimers (NMR). [d]With 10 mol% of catalyst at 110 °C. [e]Yield determined by high-performance liquid chromatography (HPLC); in addition, ca. 20% of what appeared to be dimeric products were detected. [f]With 20 mol % of catalyst at 80 °C. [g]Using 30 mol% of catalyst at reflux temperature; yield over two steps (metathetic ring closure and reductive cleavage of the 2,2,6,6-tetramethylpiperidinyl group).

Various CH-acidic functional groups including *β*-ketoesters, malonates, amides, carbamates and sulfones stand witness for the remarkable compatibility towards acidic sites (**Figure 52**).

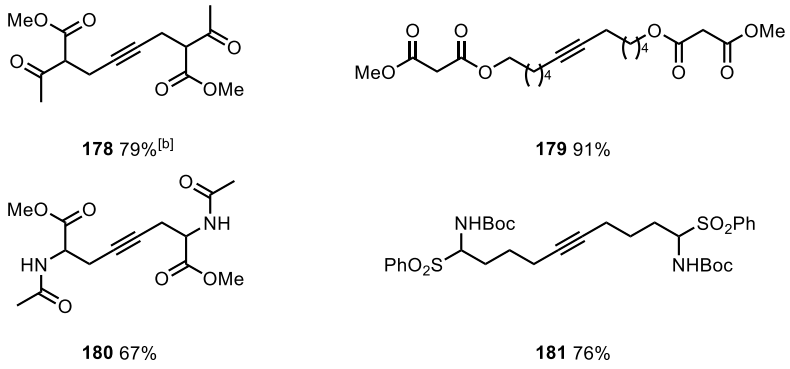


**Figure 52.** [a]The reactions were performed with 5 mol% of **108** in toluene at RT in the presence of MS 5 Å. [b]At 90 °C with 10 mol% of catalyst **108**.

The excellent application profile is also manifested in the ring-closing alkyne metathesis of polyfunctionalized (natural) products carrying sensitive functionalities (**Figure 53**). Macrolactones **182**-**185** of different ring sizes (12, 14, 18, 28) were accessible in good to excellent yield and gave confidence for more advanced applications. The key intermediate **186** for the synthesis of homoepilachnene can be prepared in quantitative yield in the presence of a C–H acidic fluorenyl protecting group.[125] Ring-closing alkyne metathesis was also successfully applied to access cycloalkyne **188** in good yield, which highlights the outstanding functional group tolerance towards heterocycles, ketones and aldol units.[105] In addition, the acid/base sensitive vinyl epoxide and allyl ether found in **187** did not interfere with ring-closing alkyne metathesis and afforded the desired product in 85% yield.[162] The successful formation of cycloalkyne **189** as the key intermediate for the synthesis of natural product amphidinolide F is equally important. Previously, the steric hindrance about the densely functionalized diyne caused preferential formation of dimers either with the monodentate based catalyst **111** or the phenyl substituted catalyst **108** and highlights the synthetic advantage of slim catalyst **133**.

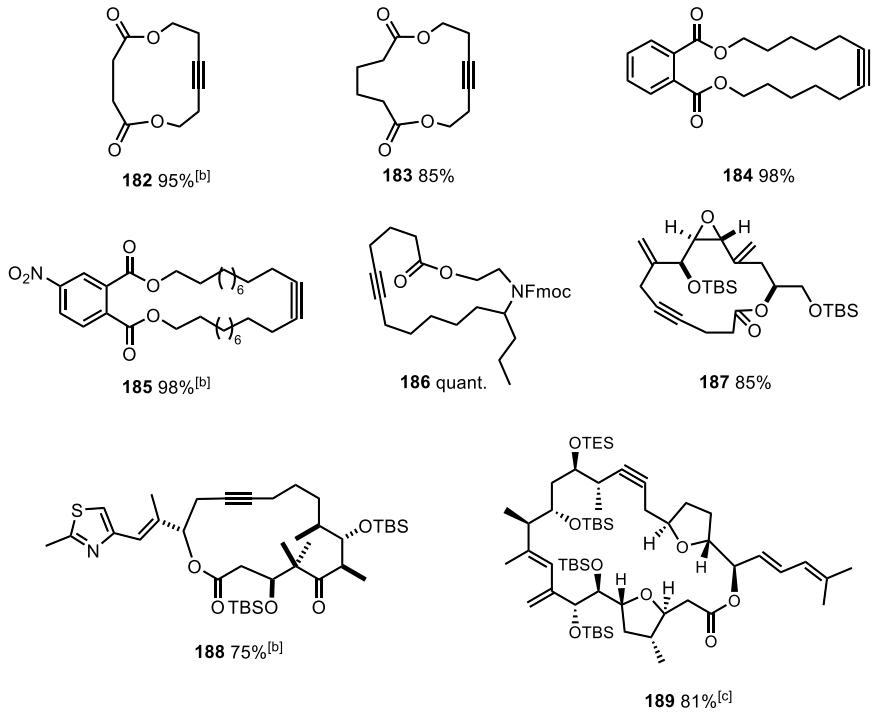


**Figure 53.** Ring-closing alkyne metathesis (RCAM) reactions: [a]Unless stated otherwise, all reactions were performed with **108** (5 mol%) in toluene in the presence of powdered MS 5 Å at 25 °C. [b]At 60 °C. [c]Using 30 mol% of **133** at 80 °C.

Because of the improved functional group tolerance towards protic sites, we termed the newly developed molybdenum alkylidyne complexes with a tripodal ligands sphere "canopy catalysts". The design principle relies on the chelate effect that should prevent the substitution of the silanolate ligand with any protic functional group from occurring. However, the Schrock alkylidyne is inherently nucleophilic and basic at carbon and therefore susceptible for protonation. Since the fate of siloxy-based molybdenum catalysts was previously not investigated in detail, we thought to study this by NMR spectroscopy (**Scheme 65**). Addition of primary alcohol **190** to a solution of catalyst **111** in [$D_8$]-toluene resulted in quantitative hydrolysis and release of free triphenylsilanol in less than 5 min. Although the hydrolysis was accompanied by precipitation of an insoluble brown solid, the $^1$H NMR data gave no evidence for the protonation of the alkylidyne unit.[163-165] It came as no surprise that addition of ten equivalents of water to a solution of catalyst **111** in [$D_8$]-toluene gave the same result. In sharp contrast, canopy catalyst **124** tolerated unhindered primary alcohols and showed improved stability towards water. It took ~9 h in the presence of ten equivalents of water until the tripodal ligand **105** was fully released from catalyst **124** in [$D_8$]-toluene. With these encouraging results, we commenced homo-metathesis reactions in technical grade toluene (84 ppm water) or toluene containing residual EtOH (5300 ppm EtOH). Indeed, in the presence of MS 5 Å which served as a sequestering agent for the generated 2-butyne and is a drying agent itself, we obtained with both contaminated solvents the desired product in almost quantitative yield. In practical terms, this represents a great advantage over previous generations of alkyne metathesis catalysts, where it has been always quintessential to remove residual water or ethanol before running the reactions in toluene.

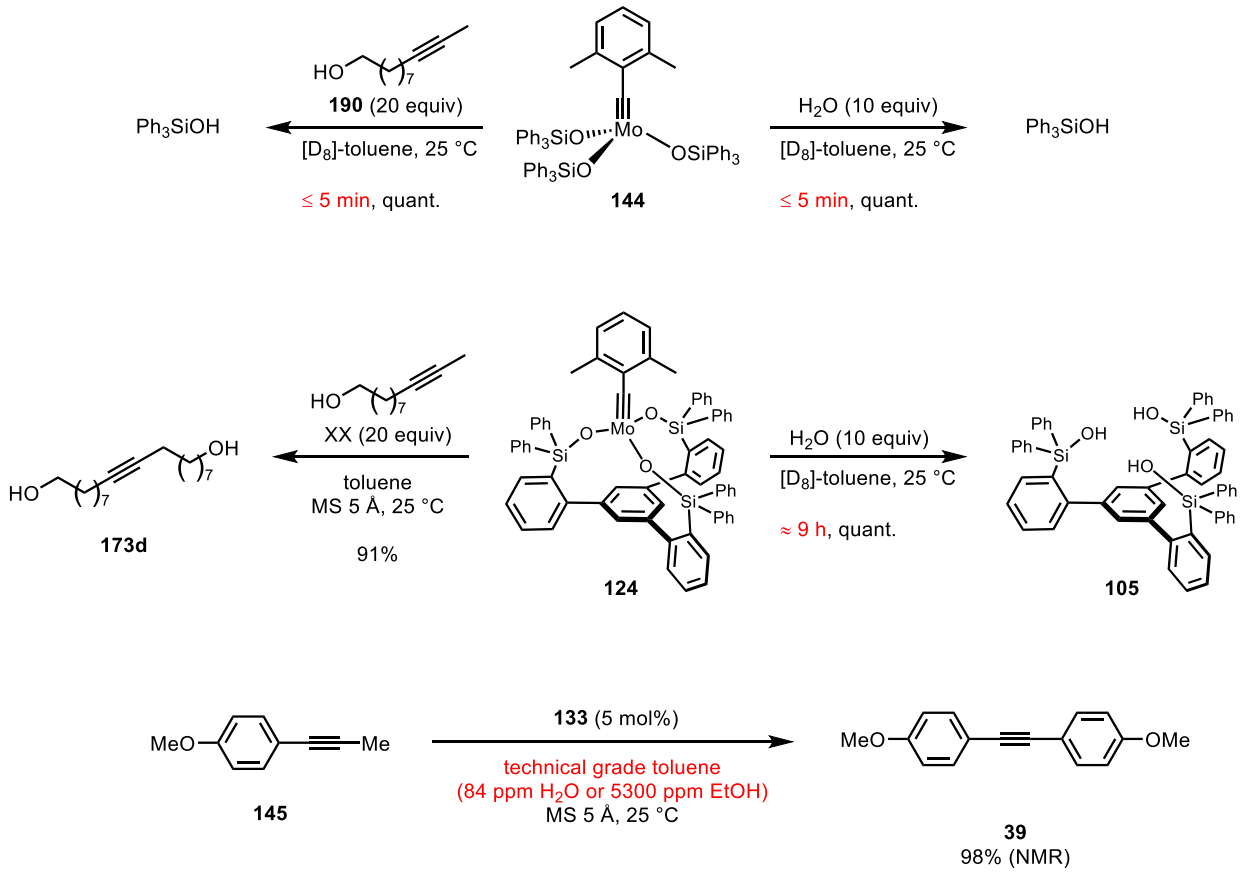


**Scheme 65.** Improved stability towards water.

Next, we tested the stability of solid [**108**]$_2$ in air at ambient temperature. The material is moderately air-sensitive, showing a half-lifetime at ambient temperature of approximately 8 h (**Figure 54**).

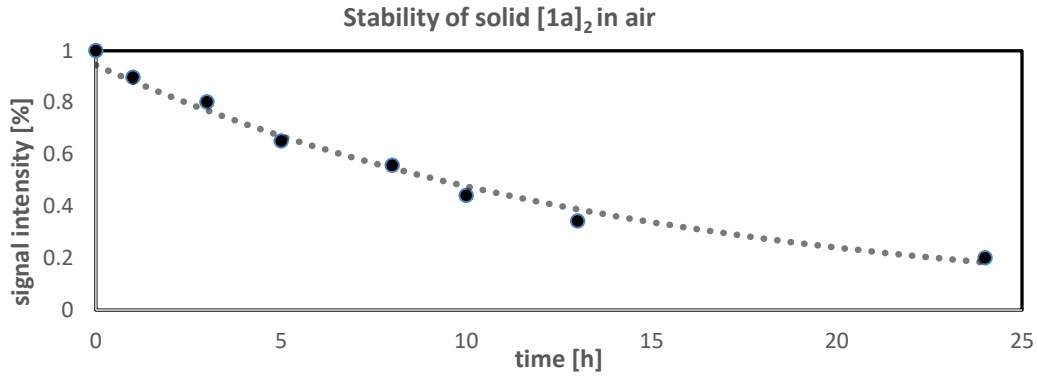


**Figure 54.** Stability of solid [**108**]$_2$ in air at ambient temperature as determined by $^1$H NMR in $C_6D_6$; the signals of the ortho-protons of the *p*-methoxybenzylidyne group were integrated against the signal of the free ligand. The humidity of the air was ≈ 60%.

The temperature stability of monomeric catalyst **108** in [$D_8$]-toluene was monitored for 7 days at 25 °C and for 12 h at 60 °C by NMR spectroscopy. The complex shows excellent thermal stability. No decomposition nor reversion to [**108**]$_2$ was observed.

Overall, an important step in the development of well-defined tripodal alkyne metathesis catalyst has been achieved. These catalysts are easy to make on scale, show remarkable functional group tolerance and carry great potential for advanced applications. This class of complexes might very well mark the advent of the next generation of alkyne metathesis catalysts.

### 3.1.10 Future Directions

Encapsulation of our canopy catalysts similar to alkene metathesis catalysts[166] should facilitate the smooth transition into industrial applications. Likewise, a bench-stable adduct such as **191** or **192** might improve the user-friendliness and simplify the commercialization (**Figure 55**).

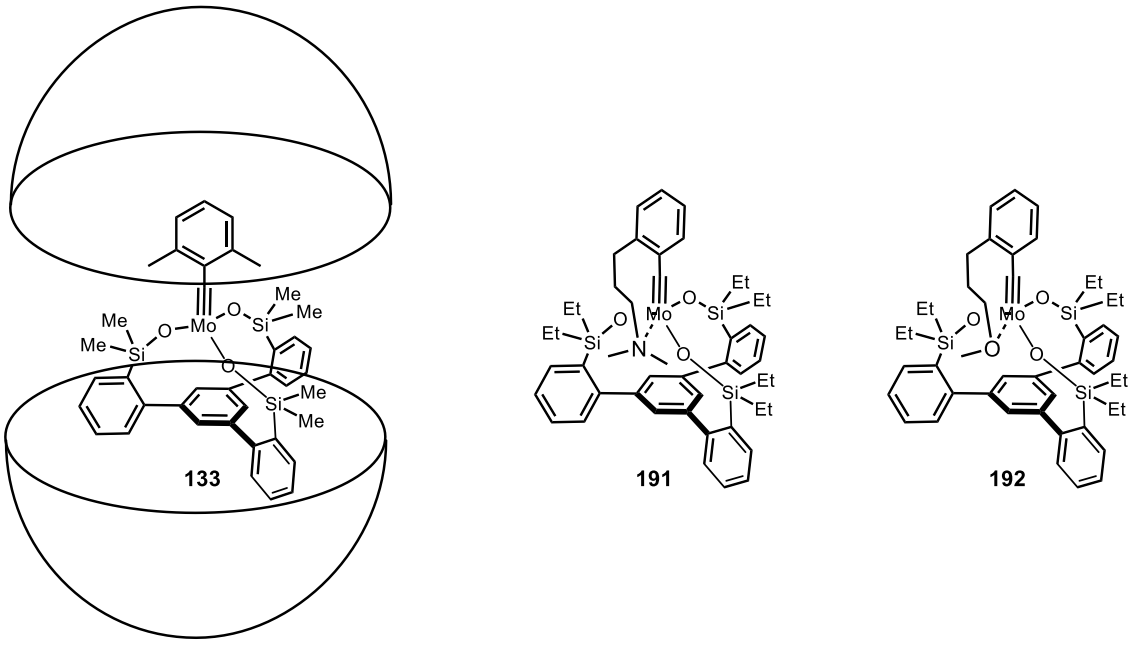


**Figure 55.** Encapsulation of **133** and preparation of a bench-stable adducts **191** and **192**.

## 3.2 Tungsten Alkylidyne Complexes for Alkyne Metathesis

The superior functional group tolerance, the high selectivity and catalytic activity of molybdenum based alkyne metathesis catalysts result in an overall excellent application profile. In contrast, tungsten catalysts for alkyne metathesis are fundamentally different and only few advanced applications are known (*vide supra*). The auspicious results obtained with tripodal ligand spheres on molybdenum alkylidyne complexes encouraged us to prepare and study the corresponding tungsten alkylidyne complexes (**Scheme 66**).

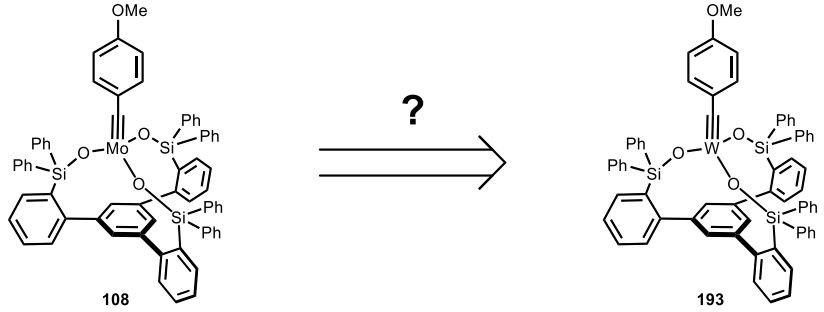


**Scheme 66.** Extend coverage to tripodal tungsten alkylidynes complexes for alkyne metathesis.

### 3.2.1 Preparation of a Catalyst Library

We prepared *p*-methoxybenzylidyne complex **197** by the literature-known procedure starting from $[W(CO)_6]$ (**12**) (**Scheme 67**).[167] Addition of the lithium aryl species to the carbonyl complex **12** gave, after cation exchange with tetramethylammonium bromide, Fischer carbene **194**. Sequential oxidation with oxalyl bromide and bromine afforded the Schrock alkylidyne **196** in 78% yield. Ligand substitution with sodium *tert*-butoxide gave the desired precatalyst **197** in excellent yield.

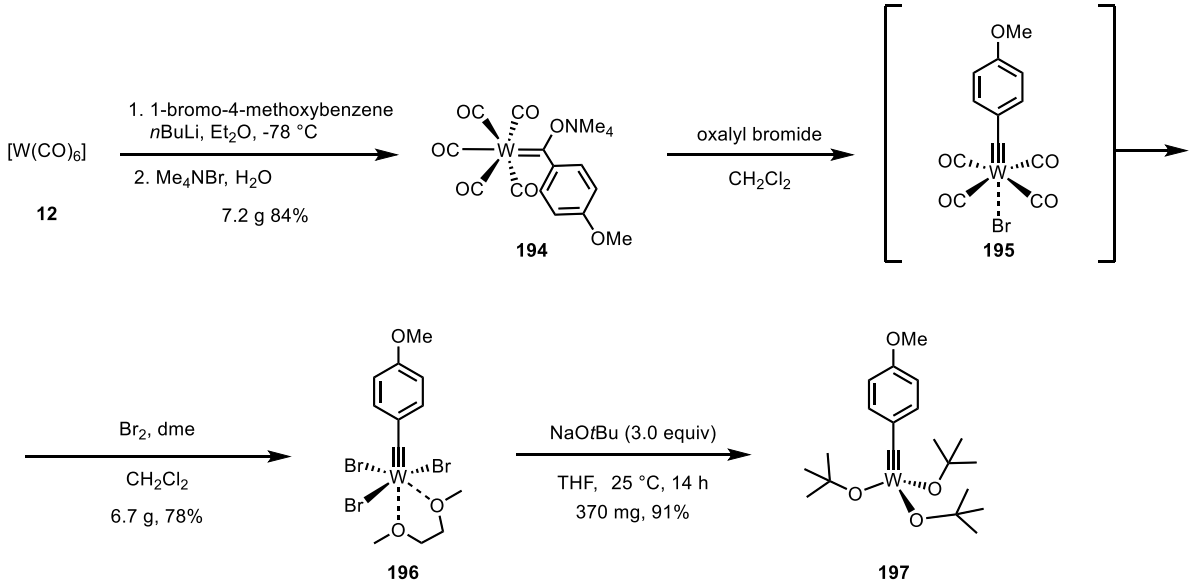


**Scheme 67.** Preparation of precatalyst **197**.

Stirring of a solution of precatalyst **197** and triarylsilanol **105** in toluene at ambient temperature gave, after evaporation of the solvent, only ill-defined mixtures as judged by $^1$H NMR (**Scheme 68**). At this point, it already became clear that tungsten is very much different from molybdenum and entails a higher tendency to expand its coordination sphere to form oligomers.

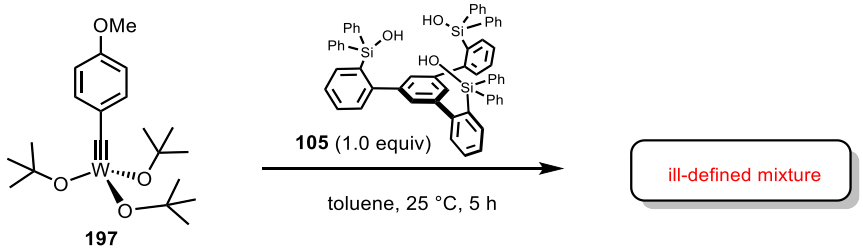


**Scheme 68.** Formation of ill-defined mixtures with precatalyst **197** and **105**.

In consideration thereof, we again took advantage of the 2,6-dimethylbenzyldiyne substitution which had turned out to be ultimately important to access monomeric molybdenum complexes (*vide supra*). In the same manner, we synthesized 2,6-dimethylbenzylidyne complex **201** and, after ligand substitution with sodium *tert*-butoxide, obtained precatalyst **201** in 89% yield (**Scheme 69**).

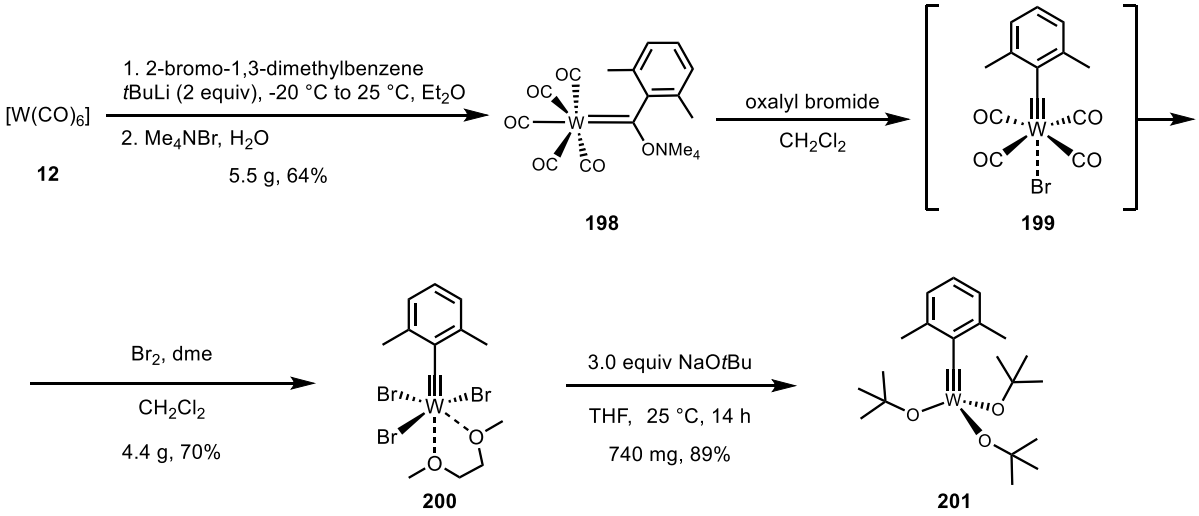


**Scheme 69.** Preparation of precatalysts **201**.

Yellow crystals suitable for single-crystal X-ray diffraction were grown from a concentrated *n*-pentane solution of **201** stored at −85 °C for one week. In the solid state one *tert*-butoxide ligand is orientated "downwards" likely due to steric clash with the 2,6-dimethyl substituent (**Figure 56**).

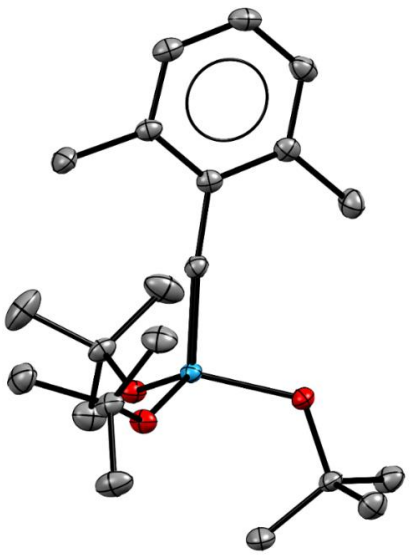

**Figure 56.** Solid state structure of complex **201**.

Stirring of a solution of precatalyst **201** and triarylsilanol **105** in toluene at ambient temperature gave complex **202** in 79% yield (**Scheme 70**). Yellow crystals suitable for single crystal X-ray diffraction were grown from a concentrated diethyl ether solution of **202** at –85 °C. DOSY NMR and X-ray structure analysis (**Figure 57**) confirmed the monomeric composition of this complex. Analysis of the solid state structure reveals that bond distances and angles are largely similar to the analogous molybdenum complex **124**. The shorter bond distance of the W–O 1.879(2) Å (Mo–O 1.886(2) Å) is in accordance with the higher Lewis acidity of tungsten.

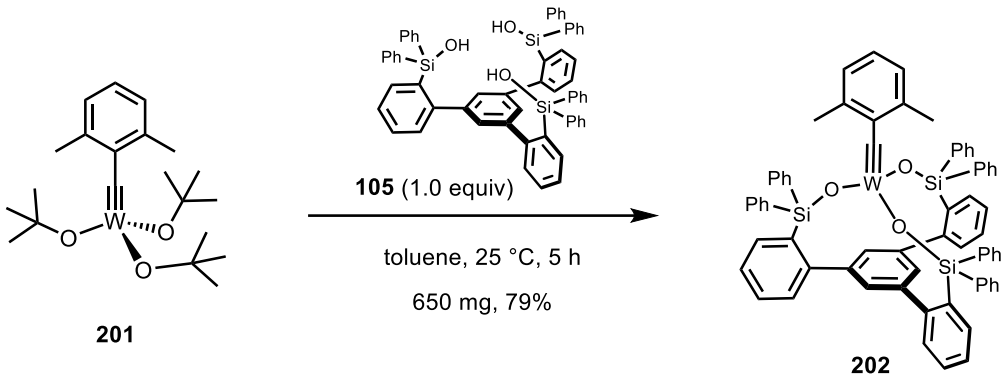


**Scheme 70.** Preparation of tungsten alkylidyne complex **202**.

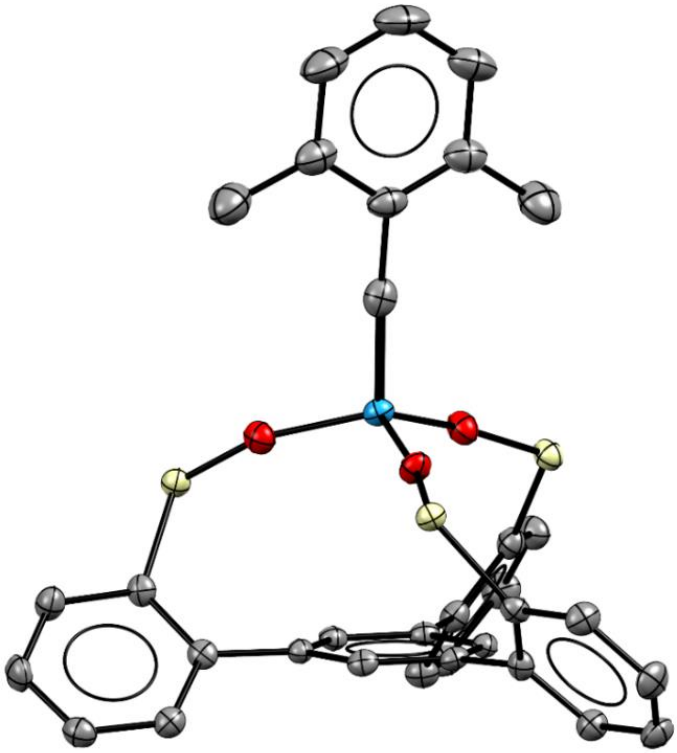

**Figure 57.** Truncated structure of tungsten alkylidyne complex **202**. H-atoms and phenyl rings on the silicon atom were omitted for clarity.

With complex **202** in hand, we tested the catalytic activity and monitored the reaction of **145** by $^{1}$H NMR spectroscopy (**Scheme 71**). Disappointingly, no conversion of the starting material at ambient temperature was observed. Heating to 80 °C in the NMR machine gave broad signals, indicating polymerization.

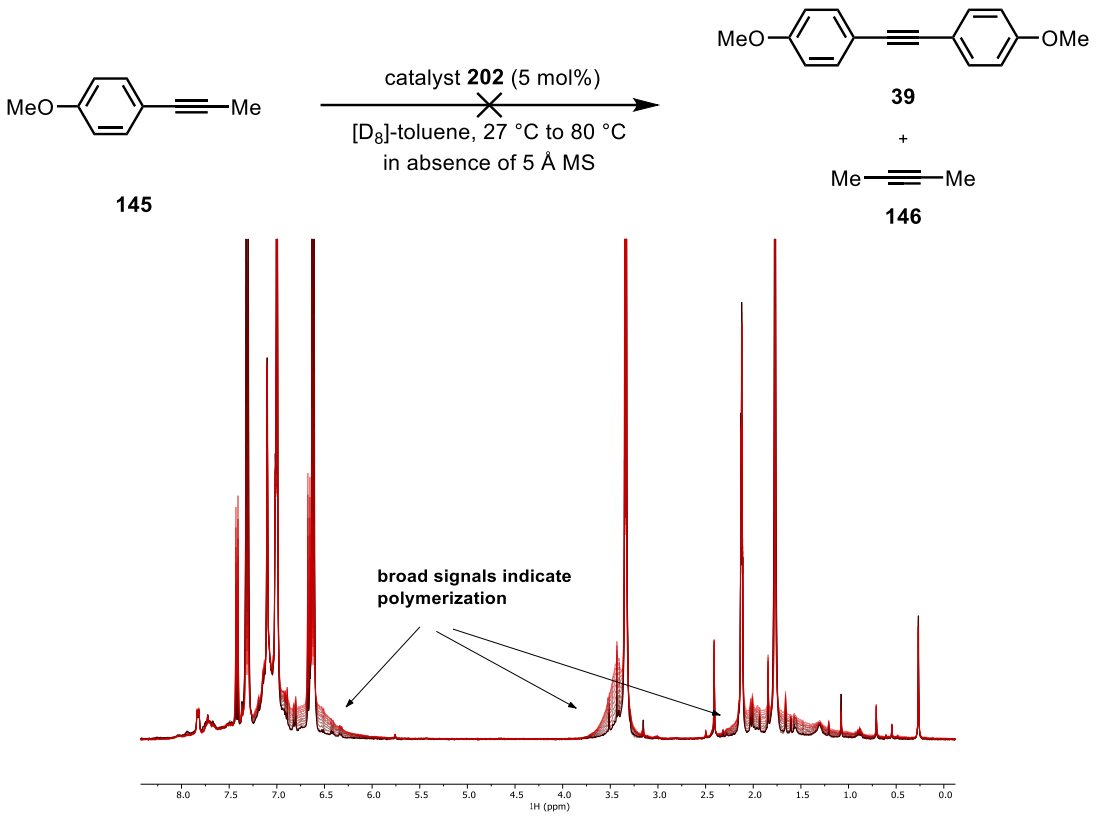


**Scheme 71.** Complex **202** fails to metathesize alkyne **145** in [D8]-toluene at 25 °C and forms broad $^{1}$H NMR signals at 80 °C.

To investigate the reasons for the low catalytic activity, we dissolved complex **202** in [D8]-toluene and obtained a yellow solution (**Scheme 72**). Upon addition of excess 3-hexyne (5 equiv) to this solution, an instant color change to deep red was observed.

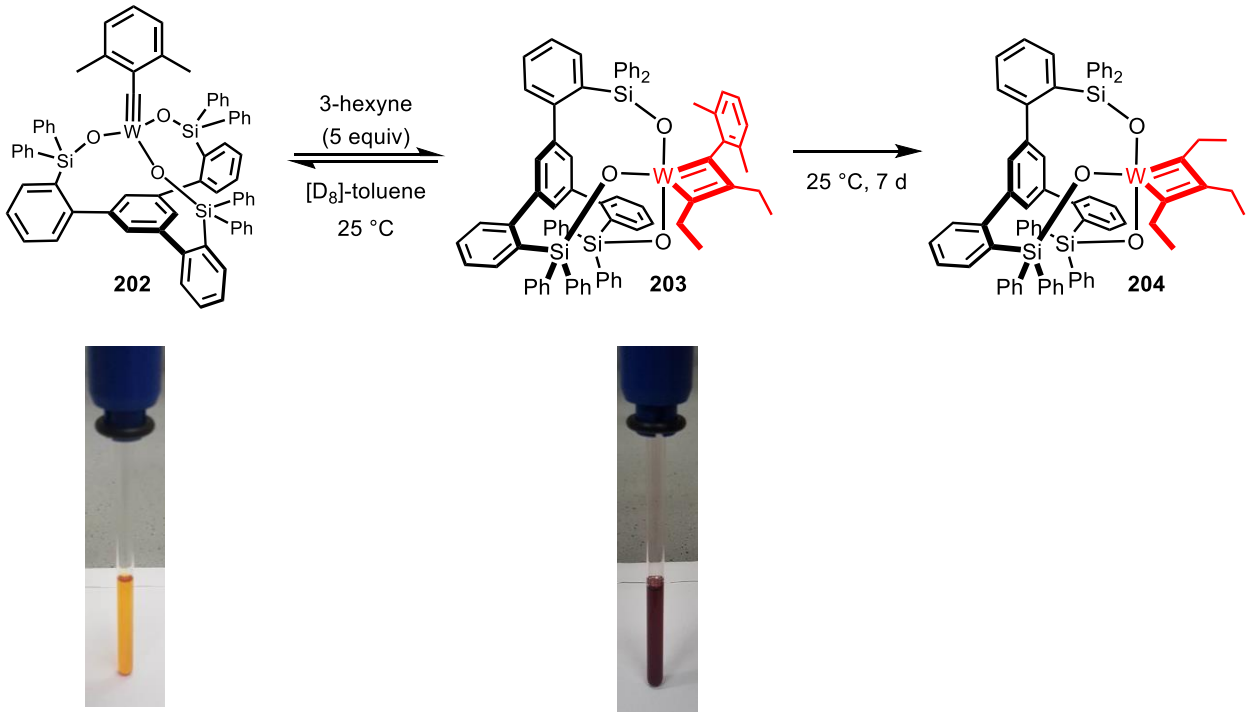


**Scheme 72.** NMR spectroscopy revealed formation of mixed and tri-ethyl substituted tungstenacyclobutadiene complexes **203**/**204** and color change upon addition of 3-hexyne.

Sequential cooling from ambient temperature to –40 °C gave a sharp single set of signals, which could be assigned to the mixed tungstenacyclobutadiene complex **203** (**Figure 58**). Although excess 3-hexyne was present in solution, the mixed metallacyclobutadiene complex **203** was kinetically particularly inert: It took one week to convert it to the more thermodynamically stable tungstenacyclobutadiene complex **204**. The mixed tungstenacyclobutadiene complex **203** is in dynamic exchange with 3-hexyne and alkylidyne complex **202**. As evident by the slow conversion to the triethyl substituted tungstenacyclobutadiene complex **204**, the tungsten center is too Lewis acidic in that the release of alkyne becomes rate-limiting.[64, 70, 101] Remarkably, the analogous molybdenum alkylidyne complex **108** resulted in the exclusive formation of metallatetrahedrane **147**, which is without any parallel in the literature (*vide supra*).

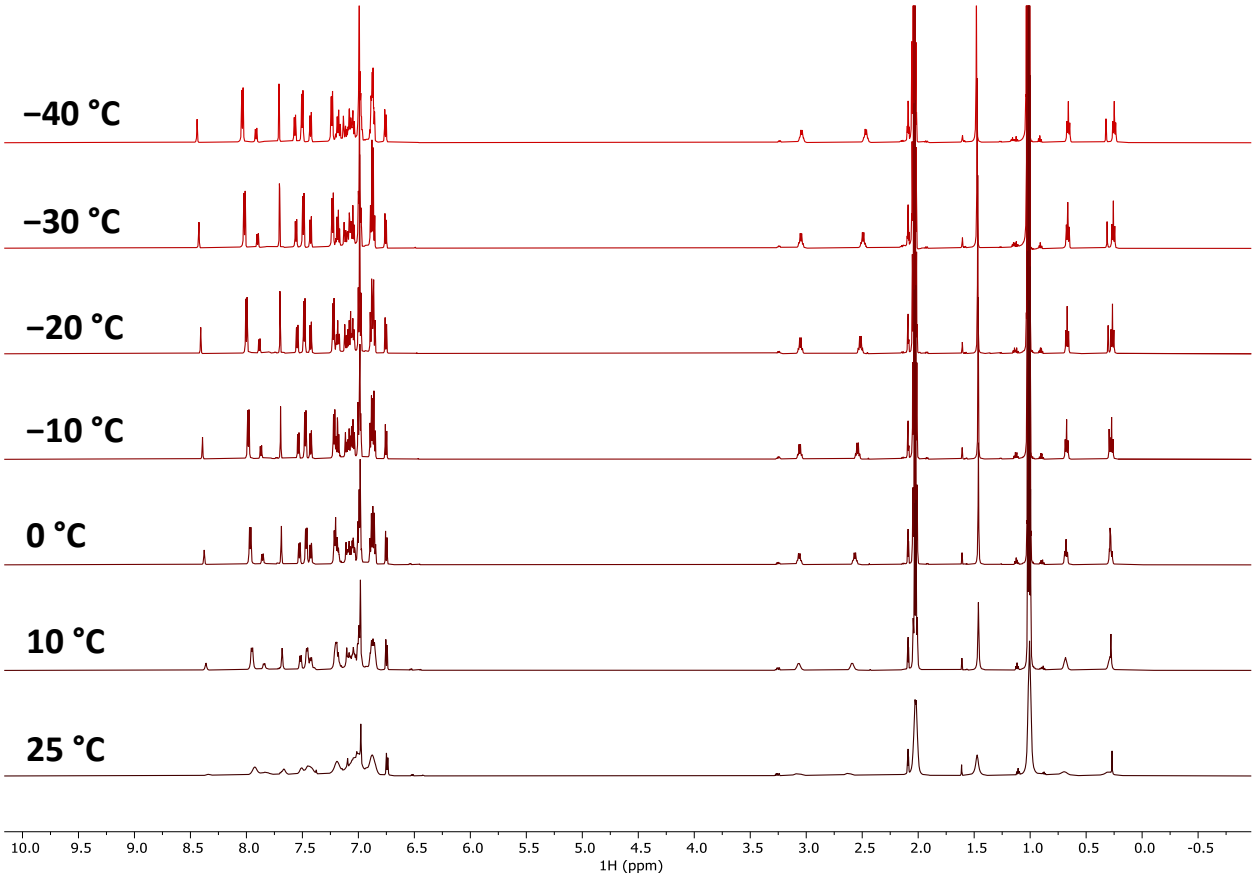


**Figure 58.** Low-temperature NMR study in [$D_8$]-toluene reveal a sharp single set of signals for mixed tungstenacyclobutadiene complex **203** at -40 °C.

The inertia of the mixed tungstenacyclobutadiene complex **203** made it possible to confirm the proposed structure by crystal structure analysis. Red crystals suitable for single crystal X-ray diffraction were obtained from a concentrated diethyl ether solution of **203** at –20 °C (**Figure 59**). Strikingly, the coordination geometry of **203** is much closer to square pyramidal ($\tau_5 \approx 0.14$) than to trigonal bipyramidal, which might also explain the low reactivity of complex **203**. The short W–O bond of the equatorial siloxide (1.903(2) Å) and of both axial siloxide (1.988(1) Å, 1.952(1) Å) bear witness for a tightly bound donor.

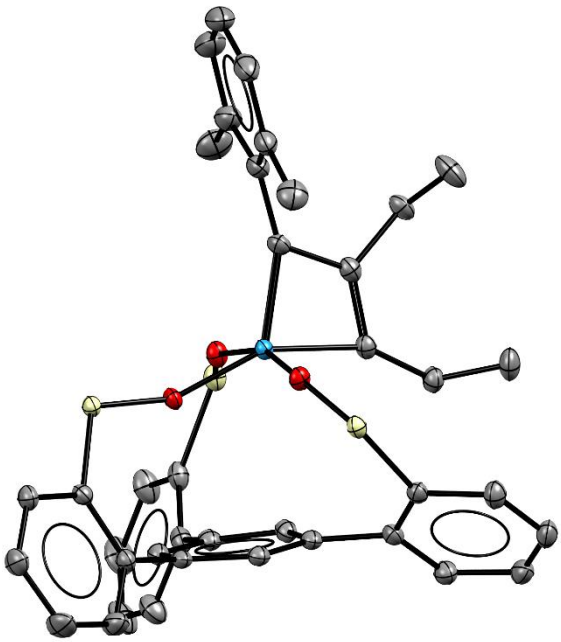

**Figure 59.** Truncated solid state structure of truncated tungstenacyclobutadiene complex **203**. Phenyl rings on silicon and all hydrogen atoms omitted for clarity.

In the solid state, the tungstenacyclobutadiene core is highly distorted in all bonds and angles. This distortion persists in solution as judged by NMR experiments (**Figure 60**). The $C_{\alpha}/C_{\alpha'}$ atoms of tungstenacyclobutadiene **203** have significantly different W–C bond distances, which results in two $^{13}C$ NMR signals and corresponds to one of the two tautomeric extremes. We were also able to deduce the $^{1}J_{C,W}$ coupling constants from the $^{13}C$ NMR spectrum of **203**. The $^{1}J_{C,W}$ coupling constants mainly arise from Fermi contact interaction, which couples two nuclear spins *via* *s*-electron density (s(C), s(W), σ(W-C), σ(C-C)). Therefore, the shorter W–C bond (1.877(2) Å) with a larger $^{1}J_{C,W}$ coupling constant of 153 Hz indicated the double bond character in the tungstenacyclobutadiene and the longer W–C bond (1.965(2) Å) with a smaller $^{1}J_{C,W}$ coupling constant of 86.8 Hz showed the single bond character.

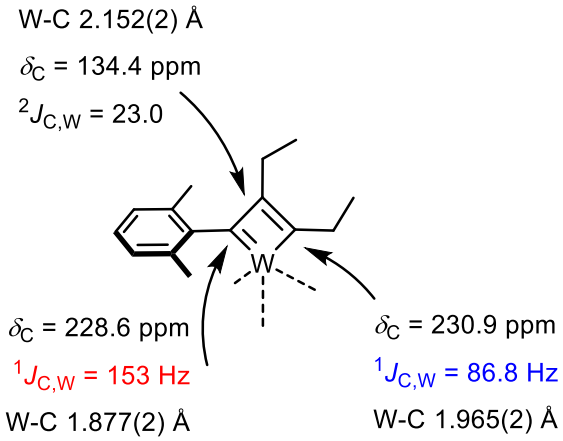


**Figure 60.** NMR analysis of tungstenacyclobutadiene complex **203**.

Surprisingly, tungstenacyclobutadiene **204** gave rise to three distinct NMR signal sets for each ethyl substituent. We observed the mutual interconversion of the ethyl substituents at $C_{\alpha}$- and $C_{\alpha'}$-atoms by exchange NMR spectroscopy (ROESY) (**Scheme 73**). Since, in this particular case, there is no competing exchange with free 3-hexyne or any other species we were able to deduce the activation

parameters of this dynamic exchange process from line-shape analysis and Eyring plots ($\Delta H^{\ddagger}$ = 13.6±0.1 kcal·mol$^{-1}$, $\Delta S^{\ddagger}$ = 1.24±0.29 cal·mol$^{-1}$·K$^{-1}$). These data support the notion of an intramolecular reorganization of the π-system (**Scheme 74**). Interestingly, only the $C_{\alpha}/C_{\alpha'}$ positions of **204** gave broad/dynamic $^{1}$H NMR signals, whereas $C_{\beta}$ gave sharp static signals. Hence, the intermediate structure for the interconversion $C_{\alpha}/C_{\alpha'}$ positions process is not $C_3$-symmetric and therefore excludes a metallatetrahedrane.

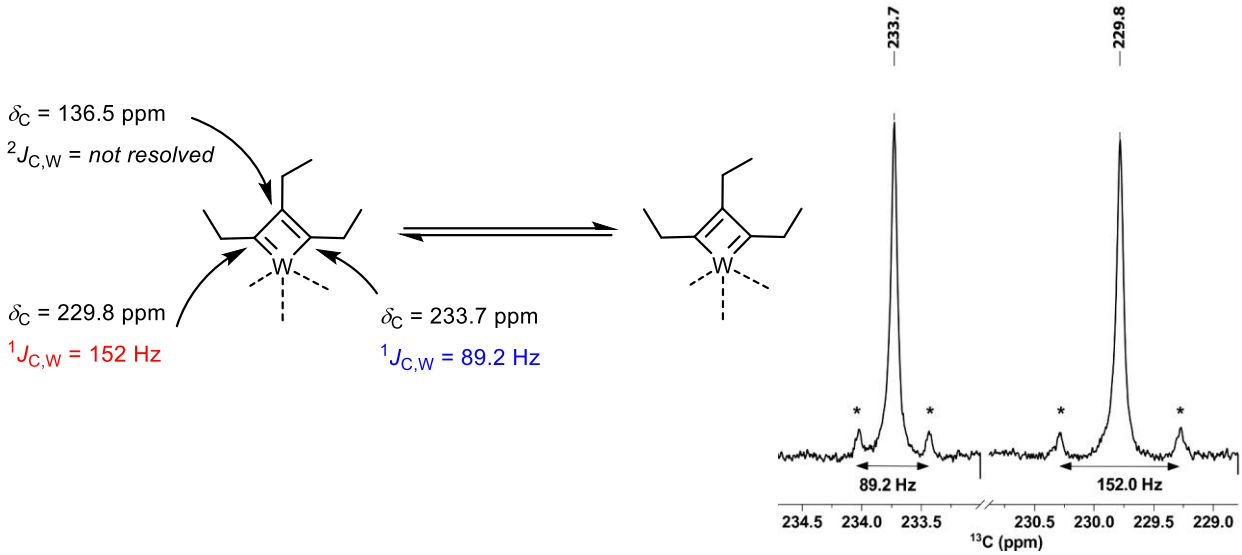


**Scheme 73.** NMR analysis of tungstenacyclobutadiene **204** and satellite peaks for the $C_{\alpha}/C_{\alpha'}$ in the $^{13}$C NMR spectrum.

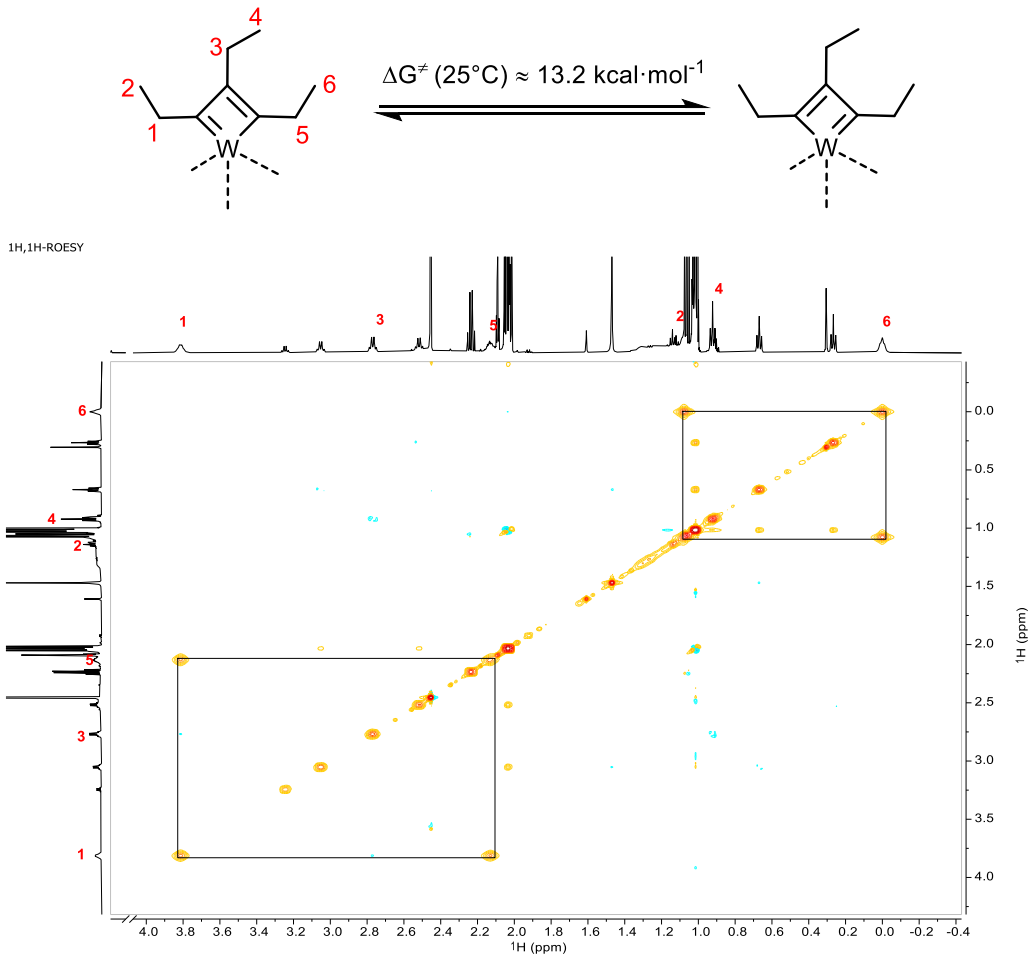


**Scheme 74.** Dynamic exchange processes of **204** observed by ROESY NMR spectroscopy in [D$_8$]-toluene at -20°C.

Due to the unfavorably high Lewis-acidity of triarylsilanolate-based complex **202**, we prepared complexes **206a-c** with more electron-releasing aliphatic substituents on silicon. Stirring of a solution of precatalyst **201** and trisilanol ligand **205** in toluene at ambient temperature gave complexes **206a-c** in excellent yield (**Scheme 75**).

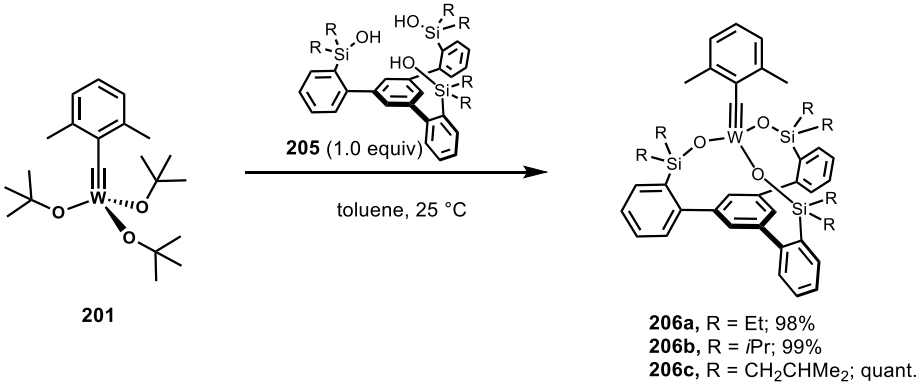


**Scheme 75.** Preparation of tripodal tungsten complexes **206**.

Next, we prepared complex **207** by addition of three equivalents of $LiOSi(OtBu)_3$ to a solution of precursor **200** in $CH_2Cl_2$ (**Scheme 76**).[79, 80]

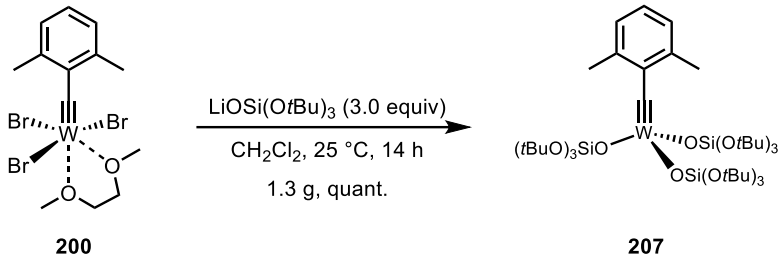


**Scheme 76.** Preparation of complex **207**.

Yellow crystals suitable for single-crystal X-ray diffraction were grown from a concentrated diethyl ether solution of **207** upon slow evaporation of the solvent at ambient temperatures (**Figure 61**).

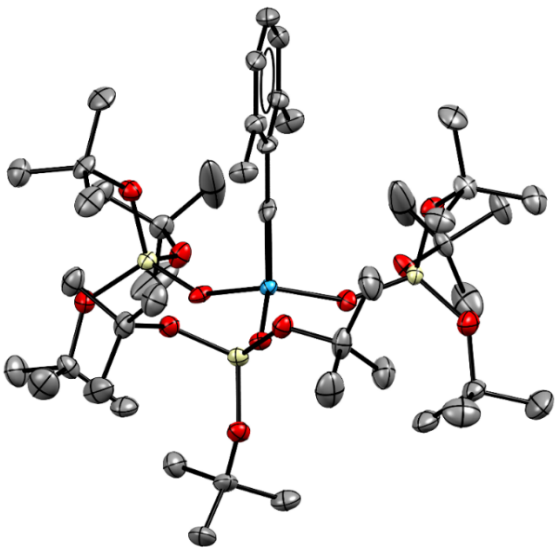

**Figure 61.** Solid state structure of catalyst **207**.

Previous attempts to prepare the neutral silanolate based complex **208** had failed and exclusively gave ate-complex **209**.[58, 150, 167] The promising results obtained with 2,6 dimethlybenzylidyne complexes encouraged us to prepare the monodentate triphenylsilanolate complex **208** *via* salt metathesis or protonolysis (**Scheme 77**). Treatment of a solution of tribromide precursor **200** in toluene with three equivalents of triphenylsilanolate salt gave the desired neutral complex **208** and ate-complex **209** in about 1:1 ratio (judged by $^{1}$H NMR). Recrystallization of an ethereal solution at -85 °C enabled us to separate both complexes. The neutral complex **208** was stored at low-temperature for crystallization but quickly decomposed to form more ate-complex **209** and free ligand as evidenced by NMR analysis. The high Lewis acidity of the neutral complex **208** might explain the instability of this complex. In contrast, the protonolysis protocol gave neutral complex **208** as major product in 41% yield with roughly 15% of an unknown side product and no formation of ate-complex **209**. Attempts to separate both complexes were not successful.

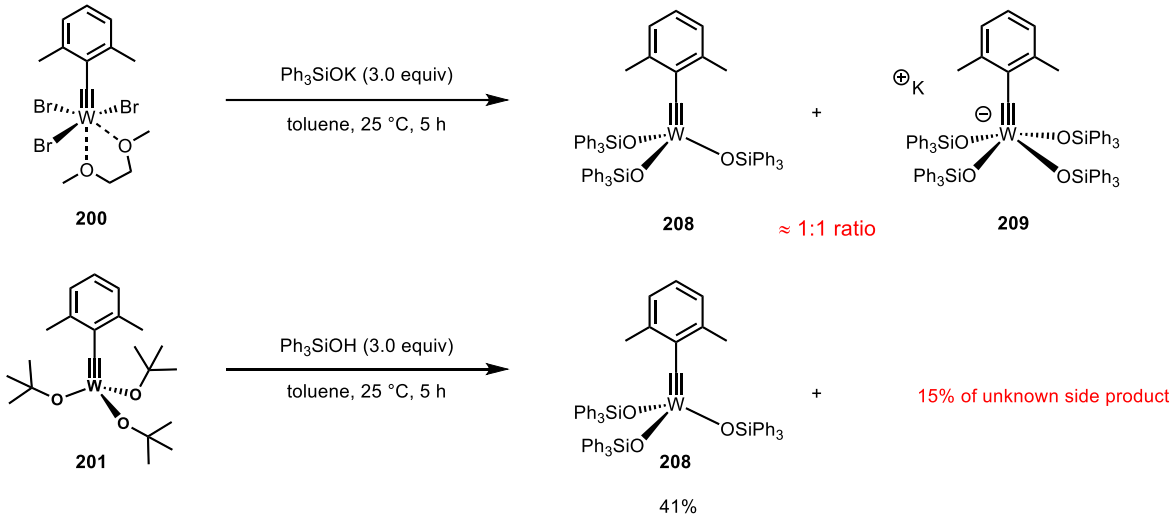


**Scheme 77.** Preparation of tungsten alkylidyne complex **208** by salt-metathesis and protonolysis.

Several attempts to obtain crystals of **208** for single-crystal X-ray diffraction failed and furnished instead benzyl tungsten-oxo complex **210** depicted in **Figure 62**, which was formed by the addition of one equivalent of water.

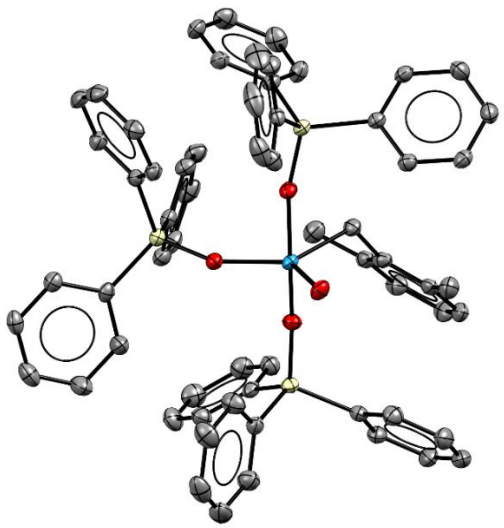

**Figure 62.** Benzyl tungsten-oxo complex **210** in the solid state; all hydrogens omitted for clarity.

Indeed, deliberate addition of one equivalent of water to a solution of **208** in toluene gave benzyl tungsten-oxo complex **210** (**Scheme 78**). Complex **210** is the first monomeric oxo-complex of tungsten; we are aware of a single prior report on a controlled double-protonation, which gave an alkylidyne complex.[68, 164, 165, 168-175]

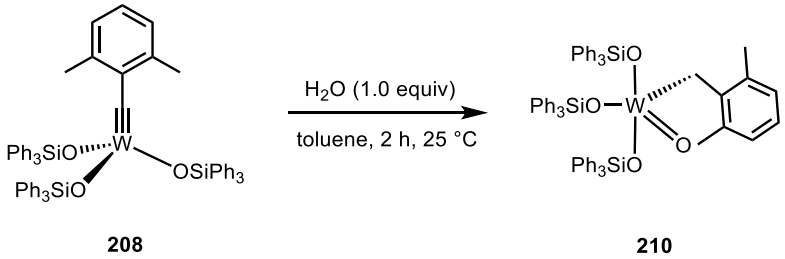


**208** **210**

**Scheme 78.** Hydrolysis of tungsten alkylidyne complex **208** with one equivalent of water.

Additionally, we prepared complex **212** endowed with fluorinated alkoxides by an adapted procedure (**Scheme 79**).[98, 176] The addition of alkoxide salt to the stirred solution of complex **211** in THF afforded complex **212** in 93% yield as a THF adduct.

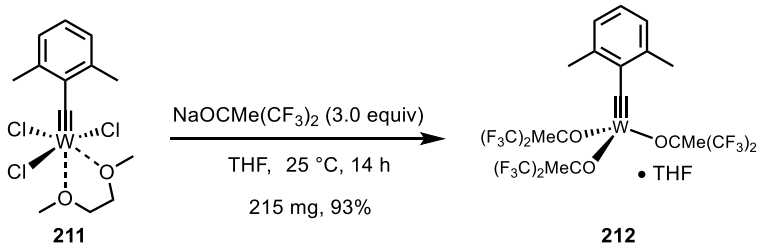


**211** **212**

**Scheme 79.** Preparation of complex **212**.

### 3.2.2 Benchmarking of the Catalytic Activity

With various tungsten complexes in hand, we investigated the catalytic performance in the homo-metathesis reaction of **145** (**Scheme 80**).

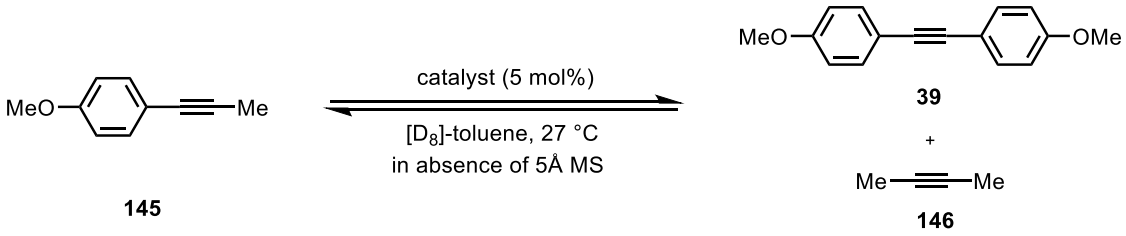


**145** **39** **146**

**Scheme 80.** Benchmark catalytic activity of various complexes by $^{1}H$ NMR spectroscopy.

Disappointingly, all tested complexes **202**, **206a-c**, **207** and **212** gave similarly poor results at ambient temperature (**Figure 63**). All reaction profiles were not well-behaved, in that the mass balance was invariably off. The reaction did not reach equilibrium, the starting material was almost entirely consumed and the released 2-butyne was channeled off during the reaction. The recorded NMR spectra provided evidence for competing polymerization independent of whether MS 5 Å was added or not (**Table 6**).

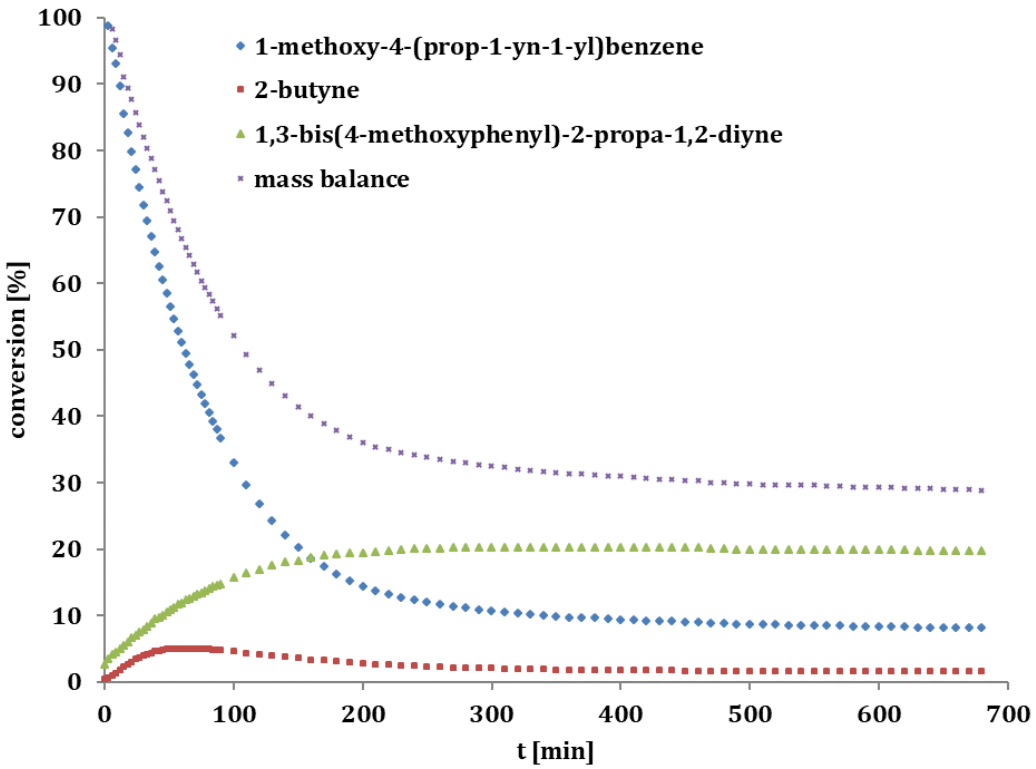


**Figure 63.** Conversion-time diagram of homo-metathesis with 5 mol% of complex **206a**.

**Table 6.** Homo-metathesis of 1-methoxy-4-(prop-1yn-1-yl)benzene (**145**) in toluene (0.2 M), 5 mol% of different tungsten catalysts.

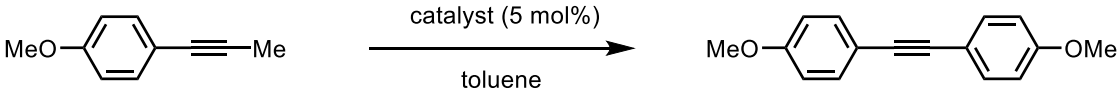


**145** **39**

| complex | additive | T (°C) | reaction time (h) | yield (% NMR) |
|---|---|---|---|---|
| **201** | 5 Å mol. sieves | 25 | 14 | 30 |
| **208** | 5 Å mol. sieves | 25 | 14 | no reaction |
| **202** | 5 Å mol. sieves | 25 | 14 | no reaction |
| **206a** | 5 Å mol. sieves | 25 | 14 | 56 |
| **206c** | 5 Å mol. sieves | 25 | 14 | 53 |
| **206b** | 5 Å mol. sieves | 25 | 14 | no reaction |
| **207** | 5 Å mol. sieves | 25 | 14 | 53 |
| **214** | 5 Å mol. sieves | 25 | 14 | 69 |
| **214** | – | 25 | 4 | 76 |
| **214** | silanized 5 Å mol. sieves | 25 | 2 | 85 |

### 3.2.3 $^{1}$H, $^{183}$W HMBC NMR Experiments

As described above, $^{95}$Mo NMR spectroscopy had turned out to be a very useful tool for guiding catalyst design. In this context, we again wanted to take advantage of measuring the NMR signal of the metal center in order to understand the poor catalytic performance of the literature-known and new tripodal tungsten complexes. Although the $^{183}$W isotope has a spin of ½, the very poor receptivity makes this nucleus ≈ 49 times less sensitive than the $^{95}$Mo nucleus.[156] 2D shift $^{1}$H,$^{183}$W correlation spectroscopy provides an elegant solution to increase the sensitivity of low-γ nuclei.[177] However, the very small scalar coupling of tungsten complexes to protons/hydrides makes it difficult to detect a signal.[178] Pleasingly, we were able to detect a good $^{183}$W NMR signal of complex **202** ($\delta_W$ =517 ppm) by $^{1}$H, $^{183}$W HMBC experiment exploiting a long-range $^{5}J$-coupling between the $^{183}$W nucleus and the protons on the 2,6-dimethyl benzylidyne unit, which bear testimony for effective orbital overlap between the alkylidyne and the aryl cap (**Figure 64**). In contrast, we were not able to detect $^{183}$W NMR signals of the tungstenacyclobutadiene complexes **203** or **204**.

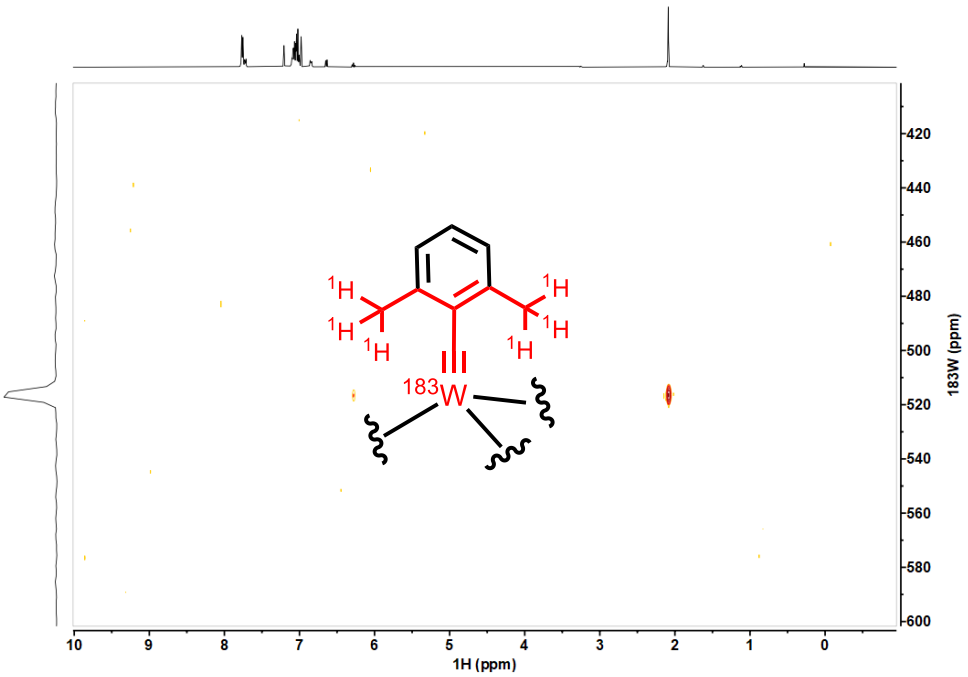


**Figure 64.** $^{1}$H, $^{183}$W HMBC NMR spectrum of complex **202** in [D$_8$]-toluene.

A single prior study by Enemark and co-workers reported the $^{183}$W NMR signal of [(*t*BuO)$_3$W≡CPh] ($\delta_W$ = 2526 ppm) which was recorded by 1D $^{183}$W NMR measurement. However, the closely related complex **201** yielded a very different $^{183}$W NMR signal ($\delta_W$ = 166 ppm) acquired by our $^{1}$H, $^{183}$W HMBC experiment, which cannot be explained by such a subtle change.[157] We had already raised concerns about the $^{95}$Mo NMR signals reported by Enemark and co-workers and assume the striking discrepancy is caused by folding in the direct dimension, a technical problem with older generations of NMR spectrometers. To verify this, we measured spectra with different offset and sweep widths to exclude any possible folding of the signals in our 2D experiments (**Figure 65**). Additionally, we recorded a 1D $^{183}$W NMR spectrum of complex **201** using an INEPT magnetization transfer and proved that the $^{183}$W NMR signals recorded with either methods are identical within ±0.2 ppm.

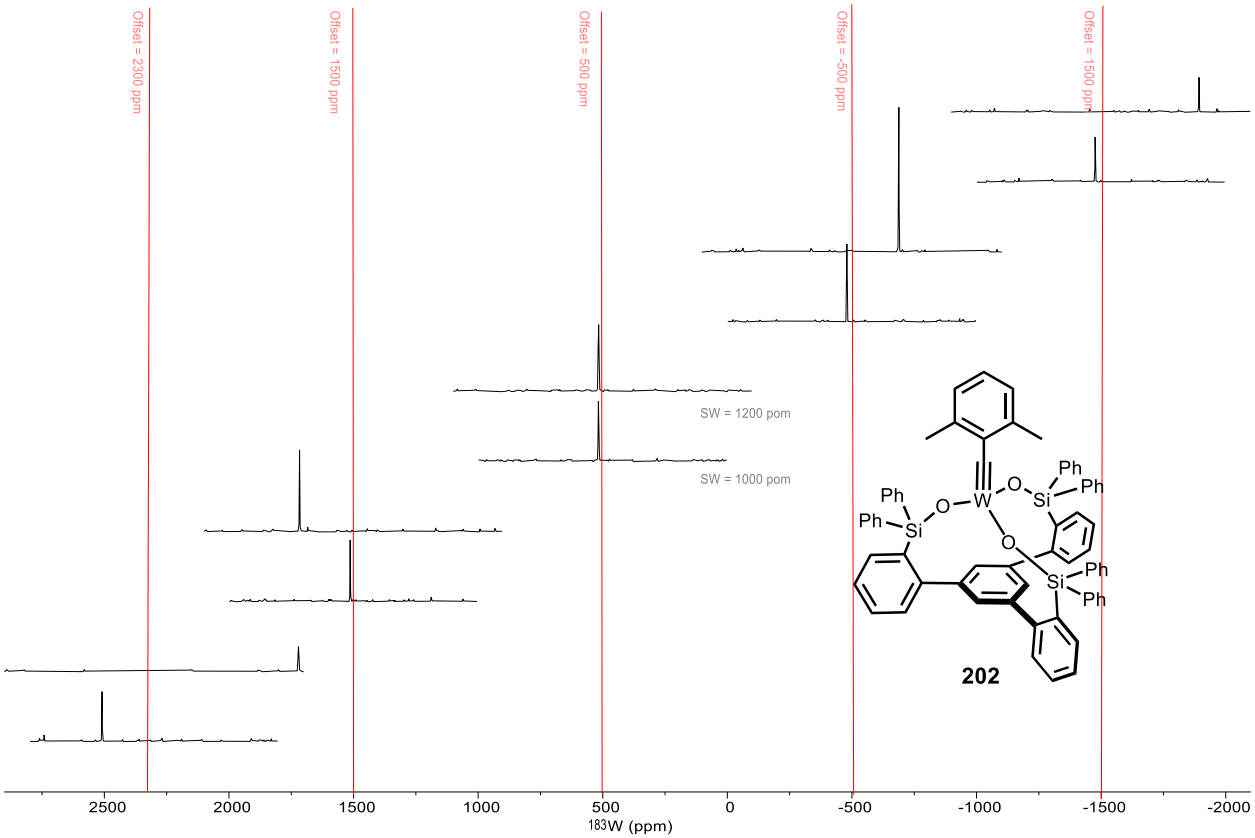


**Figure 65.** Comparison of different $^{183}$W projections extracted from $^{1}$H, $^{183}$W HMBC NMR spectra acquired with different offsets (vertical bars) and two different sweep widths of complex **202**, 400 MHz, [$D_8$]-toluene, 25 °C.

Next, we acquired $^{1}$H, $^{183}$W HMBC spectra of all prepared tungsten complexes in less than 20 min on a Bruker AVIIIHD 400 MHz NMR spectrometer and translated the 2D $^{183}$W NMR signals into 1D NMR signals for comparison (**Figure 66**). The strongly deshielded $^{183}$W NMR nucleus of complex **210** ($\delta_W$ = 758 ppm) nicely fits to a $d^0$ oxo-complex. The tripodal silanolate complex **202** ($\delta_W$ = 517 ppm), which is incompetent for alkyne metathesis, resonated at much lower field in comparison to the classical Schrock catalyst **201** ($\delta_W$ = 166 ppm). Similarly, the $^{183}$W NMR nucleus of monodentate triphenylsilanolate complex **208** was even more deshielded ($\delta_W$ = 548 ppm), which was also poorly active for alkyne metathesis. Overall, silanolate based ligands render the tungsten center too Lewis-acidic, which is reflected by the strongly deshielded $^{183}$W NMR nucleus and results in an over-stabilization of the tungstenacyclobutadiene. Complexes **206a**, **206b** and **206c** with aliphatic substituted silanolates or complex **207** with permethylated siloxides gave more strongly shielded $^{183}$W NMR nuclei but with a similarly poor catalytic performance (*vide supra*). In accordance, complex **212** endowed with fluorinated alkoxides ($\delta_W$ = 396 ppm) matched well with the poor σ- and π-donor properties of silanolate based complexes and gave a similarly deshielded $^{183}$W NMR nucleus; it led to extensive polymerization when applied to the homo-metathesis test reaction.[70]

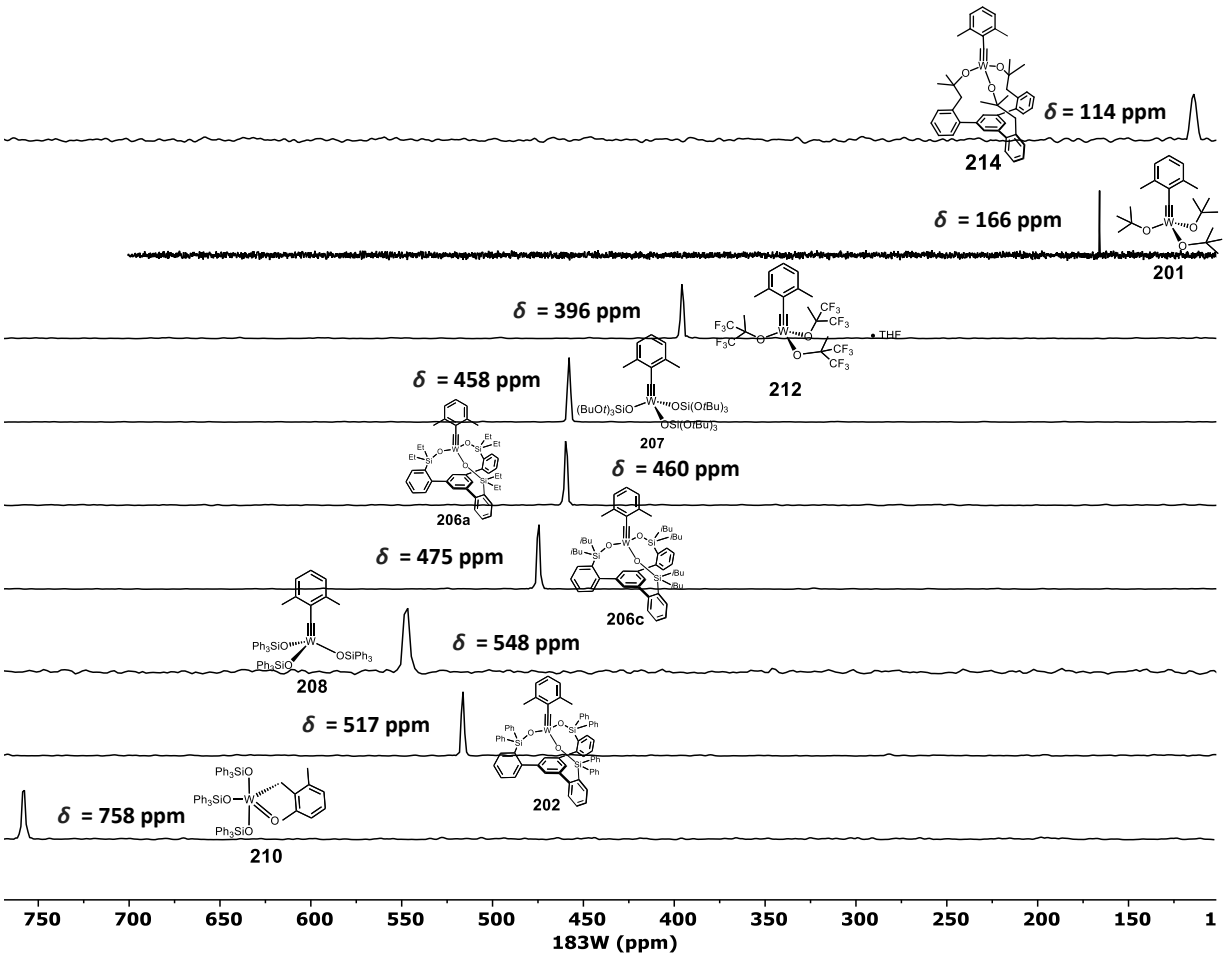


**Figure 66.** $^{183}$W NMR shifts of different tungsten complexes, as determined by $^{1}$H, $^{183}$W HMBC experiments.

Direct comparison of the $^{183}$W, $^{29}$Si, and $^{13}$C-alkylidyne NMR shifts revealed no direct correlation; no general trend can be deduced from the data (**Table 7**).

**Table 7.** $^{183}$W, $^{29}$Si, and $^{13}$C-alkylidyne NMR shifts ([D$_8$]-toluene, 25 °C) of the different complexes.

| complex | $\delta$ ($^{183}$W) [ppm] | $\delta$ ($^{29}$Si) [ppm] | $\delta$ ($^{13}$C) [ppm] |
|---|---|---|---|
| **214** | 114 | – | 264.0 |
| **201** | 166 | – | 271.3 |
| **212**·THF | 396 | – | 289.8 |
| **207** | 458 | –93.2 | 281.2 |
| **206a** | 460 | 12.9 | 281.5 |
| **206b** | 460 | 11.6 | 282.1 |
| **206c** | 475 | 9.90 | 281.9 |
| **202** | 517 | –8.50 | 287.4 |
| **208** | 548 | –8.00 | 283.1 |
| **210** | 758 | –10.4 | 64.30 |

In contrast, the $^{1}J_{C,W}$ coupling values increase for more shielded alkylidyne complexes. However, a generalization is not possible at this point because of missing literature data (**Table 8**).

**Table 8.** $J$-$^{183}$W-$^{13}$C NMR coupling constants [D$_8$]-toluene, 25 °C of different complexes.

| complex | $^{1}J$-$^{183}$W-$^{13}$C [Hz] | $^{2}J$-$^{183}$W-$^{13}$C [Hz] | $\delta$ ($^{13}$C) [ppm] |
|---|---|---|---|
| **214** | 292.7 | 44.2 | 264.0 |
| **201** | 297.3 | 44.8 | 271.3 |
| **212**·THF | 283.9 | 40.6 | 289.8 |
| **207** | 274.8 | 38.7 | 281.2 |
| **206a** | 272.5 | 38.8 | 281.5 |
| **206b** | 274.3 | 38.7 | 282.1 |
| **206c** | 272.8 | 38.6 | 281.9 |
| **202** | 270.1 | 37.1 | 287.4 |
| **208** | 273.0 | 38.1 | 283.1 |
| **210** | 101.9 | n. d. | 64.3 |

### 3.2.4 Tripodal Carbinol Tungsten Complexes

Struck by this fundamental problem, we thought to prepare a more strongly donating tripodal ligand sphere to compensate the intrinsic high Lewis acidity of tungsten and leverage catalytic activity. However, carbinol ligand **135** is not $C_3$-symmetric and resulted in a bidentate-binding motif in the molybdenum complex **138**. Stirring of a solution of precatalyst **201** and triol **135** in toluene at ambient temperature gave only ill-defined mixtures as judged by $^{1}$H NMR (**Scheme 81**).

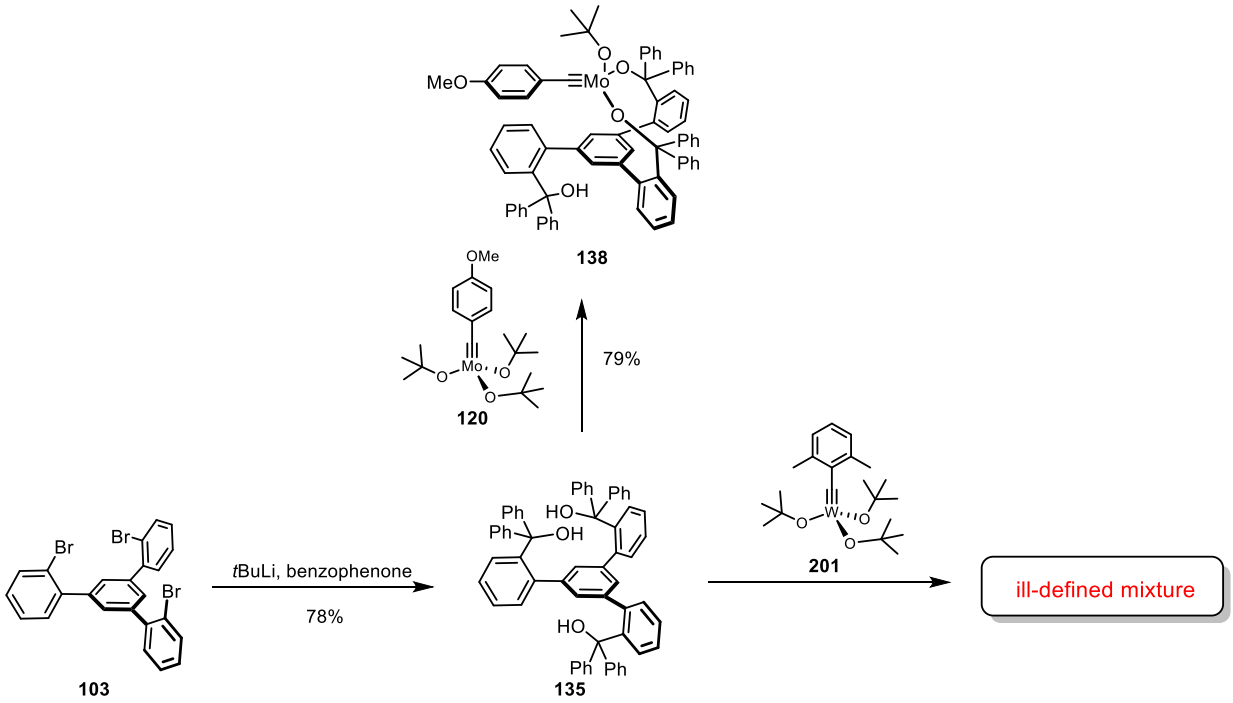


**Scheme 81.** Initial experimentations with carbinol ligand **135**.

Therefore, a new ligand design was developed, which resembles a tripodal *tert*-butoxy ligand. The ligand can be prepared in two simple operations without flash column chromatography in good overall yield (**Scheme 82**).

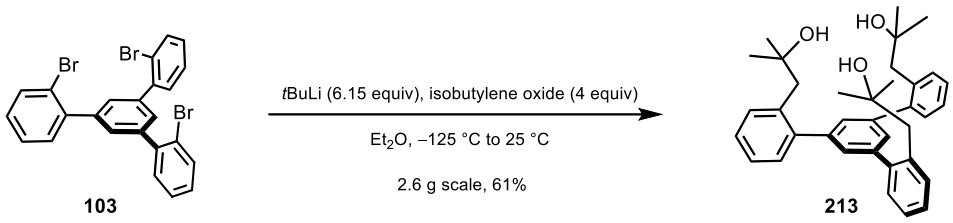


**Scheme 82**. Ligand preparation of $C_3$-symmetic carbinol ligand **213**.

The solid state structure of ligand **213** confirmed the all "upward" oriented conformation (**Figure 67**). The $C_3$-symmetry is maintained in solution, as evidenced by the $^1$H NMR spectrum.

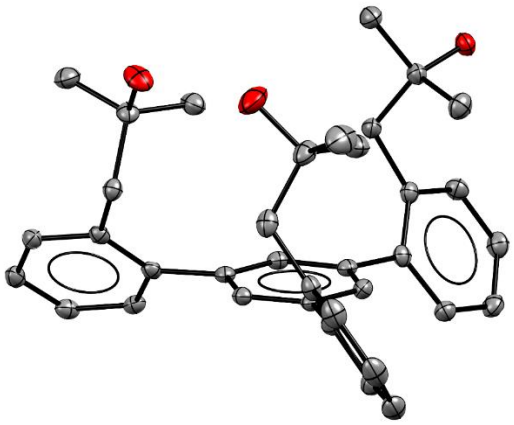

**Figure 67.** Solid state structure of carbinol ligand **213**; hydrogen-atoms and water molecules omitted for clarity.

Stirring of a solution of precatalyst **201** and carbinol ligand **213** in toluene at ambient temperature and evaporation of the solvent gave complex **214** in essentially quantitative yield (**Scheme 83**).

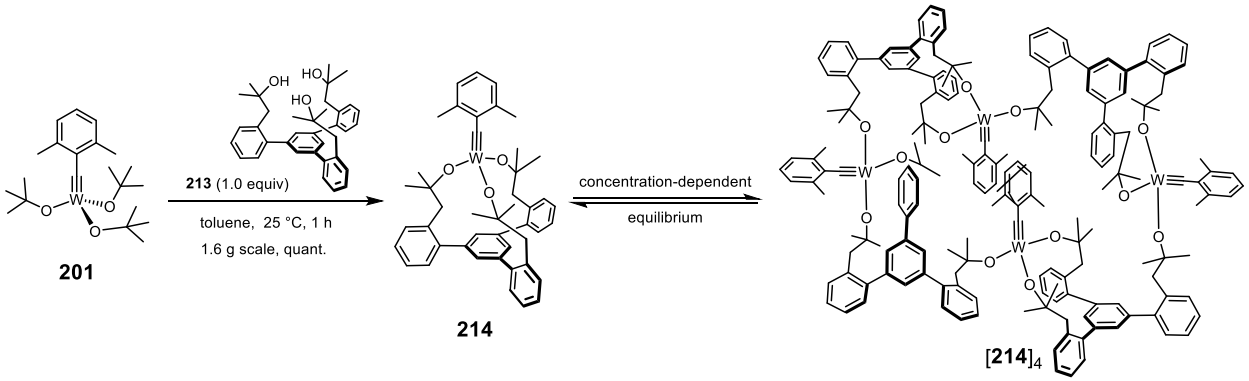


**Scheme 83.** Preparation of tungsten catalyst **214** and concentration-dependent formation of [**214**]$_4$.

This material was only moderately soluble in [D$_8$]-toluene: although the recorded spectra speak for the $C_3$-symmetric monomeric complex **214**, a second minor signal set was present that showed broad NMR shifts of lower symmetry as evident by the diastereotopic benzylic protons ($\delta_H$ = 4.0–3.6) (**Figure 68**). A concentration series from 0.025 mM to 0.005 mM in [D$_8$]-toluene revealed a strong concentration dependency: Under catalytic, low concentration (0.005 mM) conditions only monomeric complex **214** was present, whereas higher concentrations favored the specie of lower symmetry. In contrast to the molybdenum agglomerates such as [**108**]$_2$, heating of this solution did not interconvert both species. The recorded DOSY NMR data confirmed that two compounds of considerably different molecular weights/sizes ($D_{exp.}$ = 6.62·10$^{-10}$ m$^2$/s$^{-1}$; $D_{exp.}$ = 9.02·10$^{-10}$ m$^2$/s$^{-1}$) were present. $^{13}$C NMR and $^1$H, $^{183}$W-HMBC NMR experiments confirmed this conclusion ($\delta_c$ = 264 ppm and 260 ppm; $\delta_W$ = 114 ppm and 27 ppm).

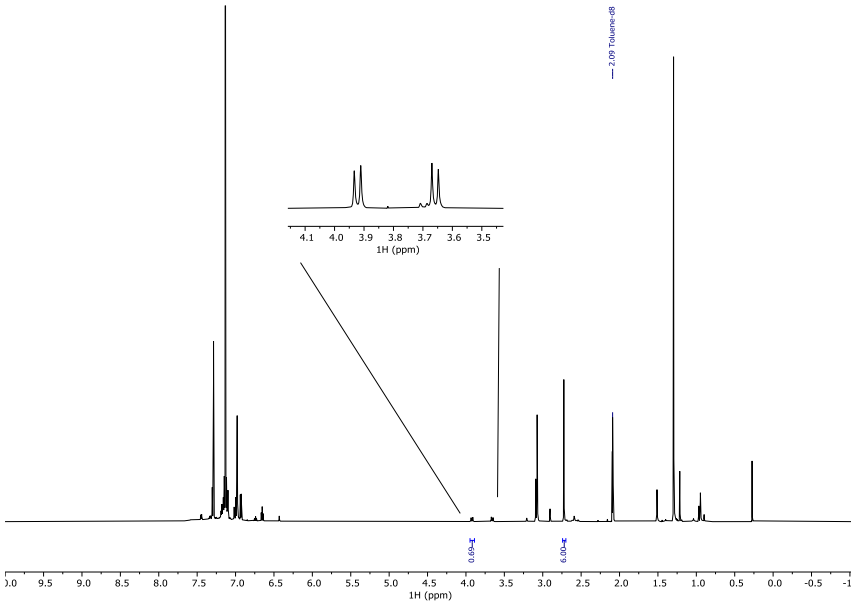


**Figure 68**. $^{1}$H NMR spectra of tungsten alkylidyne complex **214** in [$D_8$]-toluene; insert: diastereotopic benzylic protons.

Due to the concentration-dependent equilibrium, multiple crystallization attempts with various solvents and conditions failed to give crystalline material for X-ray diffraction. Finally, a concentrated fluorobenzene solution of **214** gave small crystals at -20 °C, which were suitable for X-ray diffraction and were measured at the DESY in Hamburg. Surprisingly, the solid state structure shows tetrameric [**214**]$_4$ (**Figure 69**). In comparison to tetrameric molybdenum complex [**214**]$_4$, the unit cell of [**214**]$_4$ with a volume of 9691 Å$^3$ is roughly three times smaller. Intriguingly, all four tungsten centers are arranged in a parallelogram and reside on the same plane.

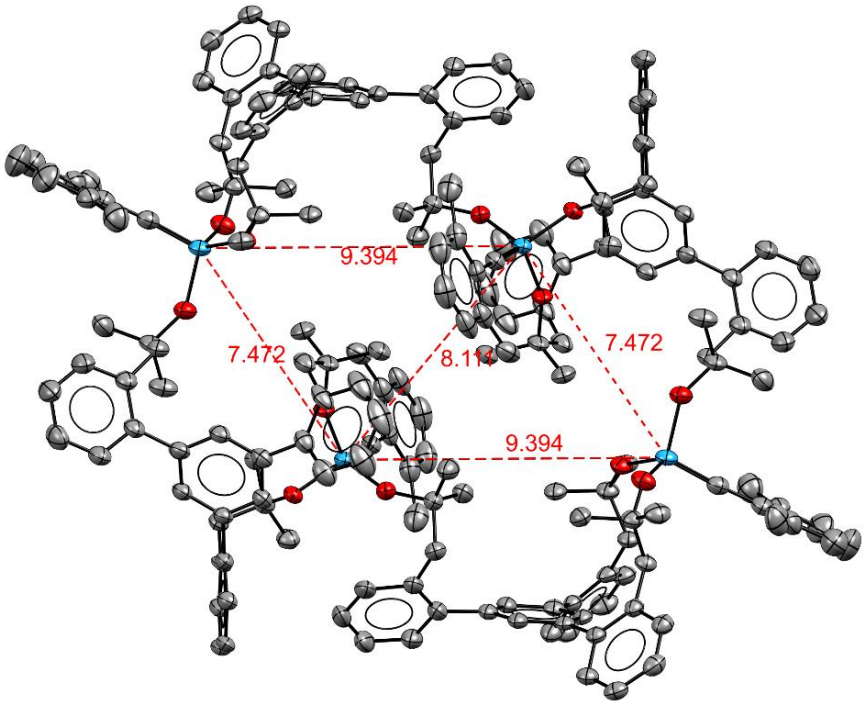


**Figure 69.** Solid state structure of [**214**]$_4$**;** Hydrogen and fluorobenzene omitted for clarity.

Overall, the crystal structures of tetrameric molybdenum and tungsten alkylidyne complexes provided experimental evidence for the likelihood that tripodal ligand spheres can cross-link to give well-defined tetramers. High concentration or addition of coordinating solvent favored the formation

of such tetramers over the monomeric $C_3$-symmetric complexes. The $^{183}W$ nucleus of monomeric **214** at $\delta_W$ = 114 ppm was notably shielded in comparison to the Schrock catalyst **201** ($\delta_W$ = 166 ppm) (**Figure 66**). Although the coordination sphere consists of formally *tert*-butoxy groups, the chelated structure resulted in an overall stronger donor.

### 3.2.5 Computational Studies

The calculated energies of the canonical MO's were notably different: the tripodal ligand **213** as the better donor raised the energy of the π-symmetric orbitals. This effect was slightly manifested in the π(W–C) orbitals (HOMO, HOMO-1) but particularly notable in the energy of the π*(W–C) orbitals. An important consequence of this uplifting of the π*(W–C) levels is the fact that the canonical LUMO of **214** is almost entirely ligand-based, with the largest lobes on the phenyl group that forms the basal plane (**Figure 70**).

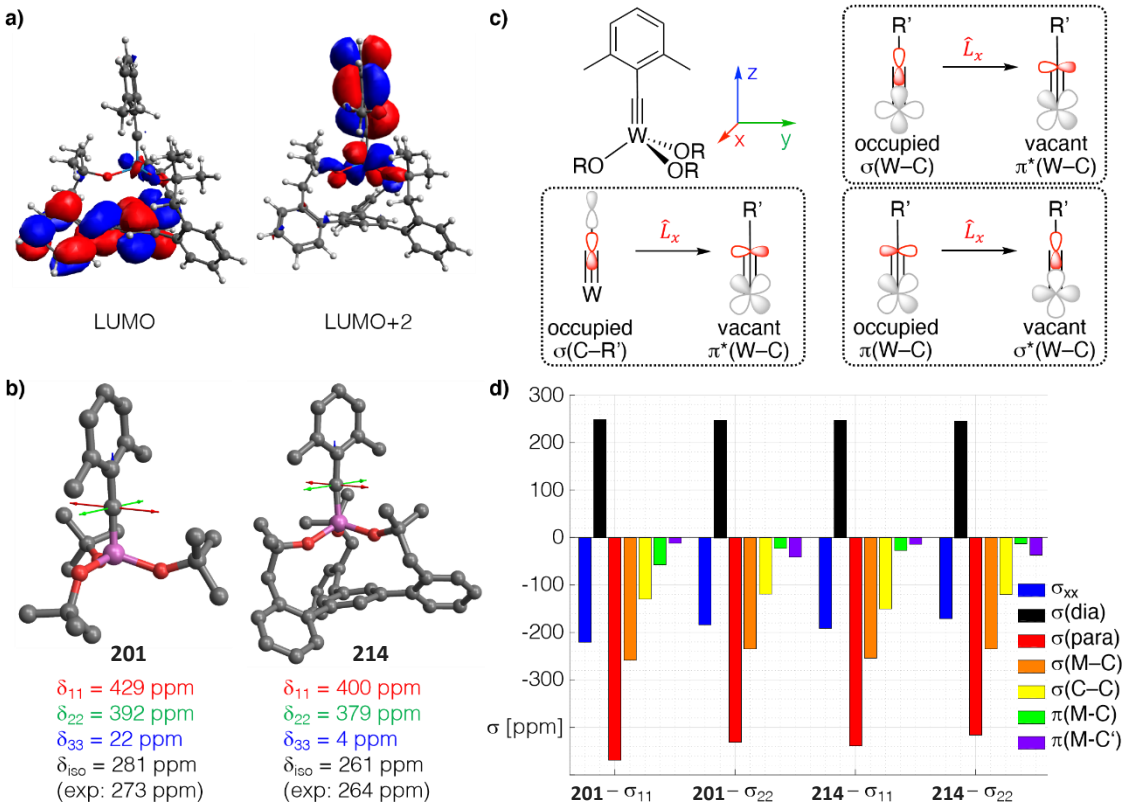


**Figure 70.** a) Canonical LUMO and LUMO+2 of the tripodal chelate complex **214**; b) Graphical representation of the shielding tensors of the Schrock complex **201** and **214**, which is more shielded in all three principle components; c) the three most relevant orbital couplings of a metal alkylidyne; d) Chemical Shift Tensor (CST) analysis for the alkylidyne C-atom of both complexes based on Natural Localized Molecular Orbitals (NLMOs) (Christopher Gordon and Prof. Dr. Christophe Copéret).

The calculated isotropic $^{13}C$ NMR shifts and $^{1}J_{W,C}$ and $^{2}J_{W,C}$ coupling constants match very well with the experimentally obtained values (**Table 9**). Tripodal silanolate complex **202** resulted in deshielding in comparison to monodentate triphenylsilanolate complex **208**. Intriguingly, the newly developed complex **214** is strongly shielded in comparison to the monodentate *tert*-butoxide complex **201**. Next, a Natural Chemical Shielding (NCS) analysis was performed to get further insight. The contributions arising from π(M–C) orbitals (and to a lesser extent those of the σ(M–C) orbitals) decreased upon going from **201** to **214**. This reflected the higher-lying π*(M–C) orbitals that render **214** less electrophilic, as well as the equally higher-lying σ*(M–C) orbital induced by the tripodal ligand.

**Table 9.** Tabulation of recorded and computed NMR data ([D8]-toluene) of the alkylidyne unit of different tungsten 2,6-dimethylbenzylidyne complexes (Christopher Gordon and Prof. Dr. Christophe Copéret).

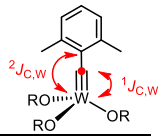


| Complex | $\delta_W$ (ppm) | $\delta_C$ (ppm) | | $^1J_{W,C}$ (Hz) | | $^2J_{W,C}$ (Hz) | |
|---|---|---|---|---|---|---|---|
| | | exp. | computed | exp. | computed | exp. | computed |
| **202** | 517 | 287 | 285 | 270 | 282 | 37.1 | 37.3 |
| **208** | 548 | 283 | 274 | 273 | 289 | 30.1 | 38.9 |
| **207** | 458 | 281 | 280 | 274 | n.d. | 38.7 | n.d. |
| **201** | 166 | 273 | 281 | 297 | 310 | 44.8 | 43.4 |
| **214** | 114 | 264 | 262 | 293 | 304 | 44.4 | 43.4 |

n.d. = not determined

It is also interesting to note that the lowering of the π*(M–C) orbitals in **201** and **214** is associated with the less-deshielding $\sigma_{22}$ component. This presumably resulted from the delocalization of the π(M–C) system over the dimethylphenyl moiety, which decreased the efficiency of the orbital overlap. The component oriented along the M–C axis ($\sigma_{33}$) was particularly shielded in **214** and pointed to a highly cylindrical electron density distribution around this M–C bond, as was observed for acetylene and molecules with a $C_\infty$ axis,[179] making it difficult to draw a direct relation to the HOMO-LUMO gap for this component. The relatively high-lying metal-centered π*(W–C) orbital (LUMO+2) and the canonical LUMO delocalized on the ligand framework will destabilize the metallacycle: a good level of activity and selectivity may therefore result.

### 3.2.6 Catalytic Activity, Scope and Applications

In the absence of 5 Å molecular sieves the homo-metathesis reaction of **145** with 5 mol% of classical Schrock catalyst **201** reached the equilibrium very slowly at 27 °C and the mass balance is again off (**Scheme 84**).

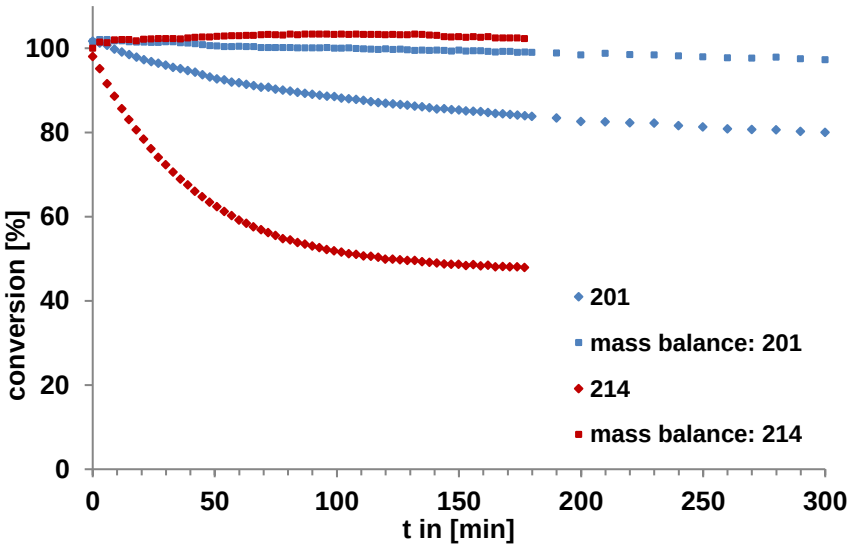


**Scheme 84.** Conversion-time diagram of homo-metathesis of **145** with 5 mol% of complexes **201** and **214** in [D8]-toluene (0.1 M) at 27 °C.

In contrast, the conversion-time diagram with 5 mol% of tripodal complex **214** was well behaved and outperformed the Schrock catalyst **201** in terms of rate and selectivity. No evidence for polymerization was observed during the reaction. When the concentrated solution was kept

overnight (~ 14h) at ambient temperature, small amounts of polymer were visible in the NMR spectra. Next, we independently ran the same homo-metathesis reaction in the presence of ordinary 5 Å molecular sieves to reach full conversion. However, tripodal complex **214** seemed to react with the protic Si–OH groups on the surface of the 5 Å molecular sieves and decomposes. We therefore treated the 5 Å molecular sieves with $Me_3SiCl$ to cap the reactive surface sites.[180] When performed in the presence of silanized MS 5 Å to sequester the released 2-butyne, the reaction furnished the desired homo-metathesis product in 85% yield (NMR). At elevated temperature and in the absence of 5 Å molecular sieves several demanding ring closing alkyne metathesis (RCAM) reactions were successfully achieved (**Scheme 85**). Sensitive epoxides, aldol subunits and many heteroatoms donor sites were well tolerated by the tripodal complex **214**, that have been beyond the scope of classical Schrock catalyst **201**.[105, 181]

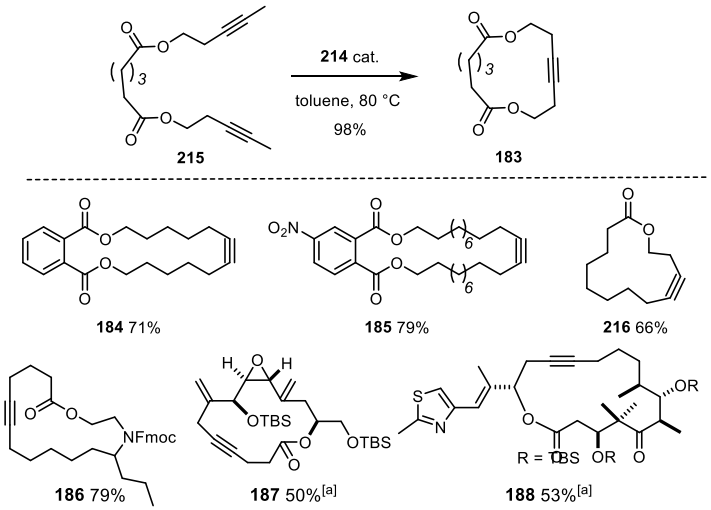


**Scheme 85.** Representative RCAM reactions; unless stated otherwise, all reactions were performed with 5 mol% of catalyst **214**; [a] with 30 mol%

The tempered Lewis-acidity of tripodal tungsten catalyst **214** resulted in high catalytic performance and in a good application profile. Overall, the new catalyst design provides new opportunities for further catalyst development in the tungsten series.

### 3.2.7 Future Directions

Trisamido molybdenum alkylidyne complexes proved to give efficient catalysts for alkyne metathesis. Guided by $^{183}W$ NMR spectroscopy a new generation of tungsten alkylidyne complexes endowed with trisamido ligands seems worth investigating.

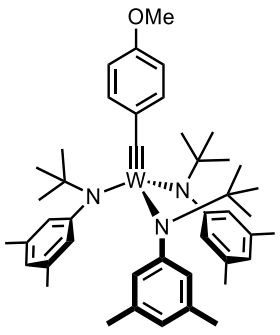


**217**

**Figure 71.** Trisamido tungsten complex **217** as a promising alkyne metathesis catalyst.

## 3.3 Isolation of a Mo(V) Alkoxide Complex and Activation of Acetonitrile by Mo(III) Alkoxide Complex

This chapter summarizes our discovery of an entirely new Mo(V) alkoxide complex and the unprecedented activation of acetonitrile by an Mo(III) alkoxide complex. We coincidently isolated both complexes during the synthesis of dinuclear Mo(III) complex [(*t*BuO)$_3$Mo≡Mo(O*t*Bu)$_3$] (**218**). The preparation of [MoCl$_3$(THF)$_3$] (**56**) is well described in the literature and starts from [MoCl$_5$] (**219**) (**Scheme 86**).[182] Reduction with acetonitrile and ligand substitution with THF affords [MoCl$_4$(THF)$_2$] (**221**). Subsequent reduction with granular tin in THF gives access to the desired [MoCl$_3$(THF)$_3$] (**56**). The visual color change from dark-blue [MoCl$_5$] (**219**) to yellow/orange [MoCl$_3$(THF)$_3$] (**56**) can be followed over the entire sequence. However, every reaction step is heterogeneous and all complexes are paramagnetic, highly sensitive and require rigorous Schlenk-techniques.

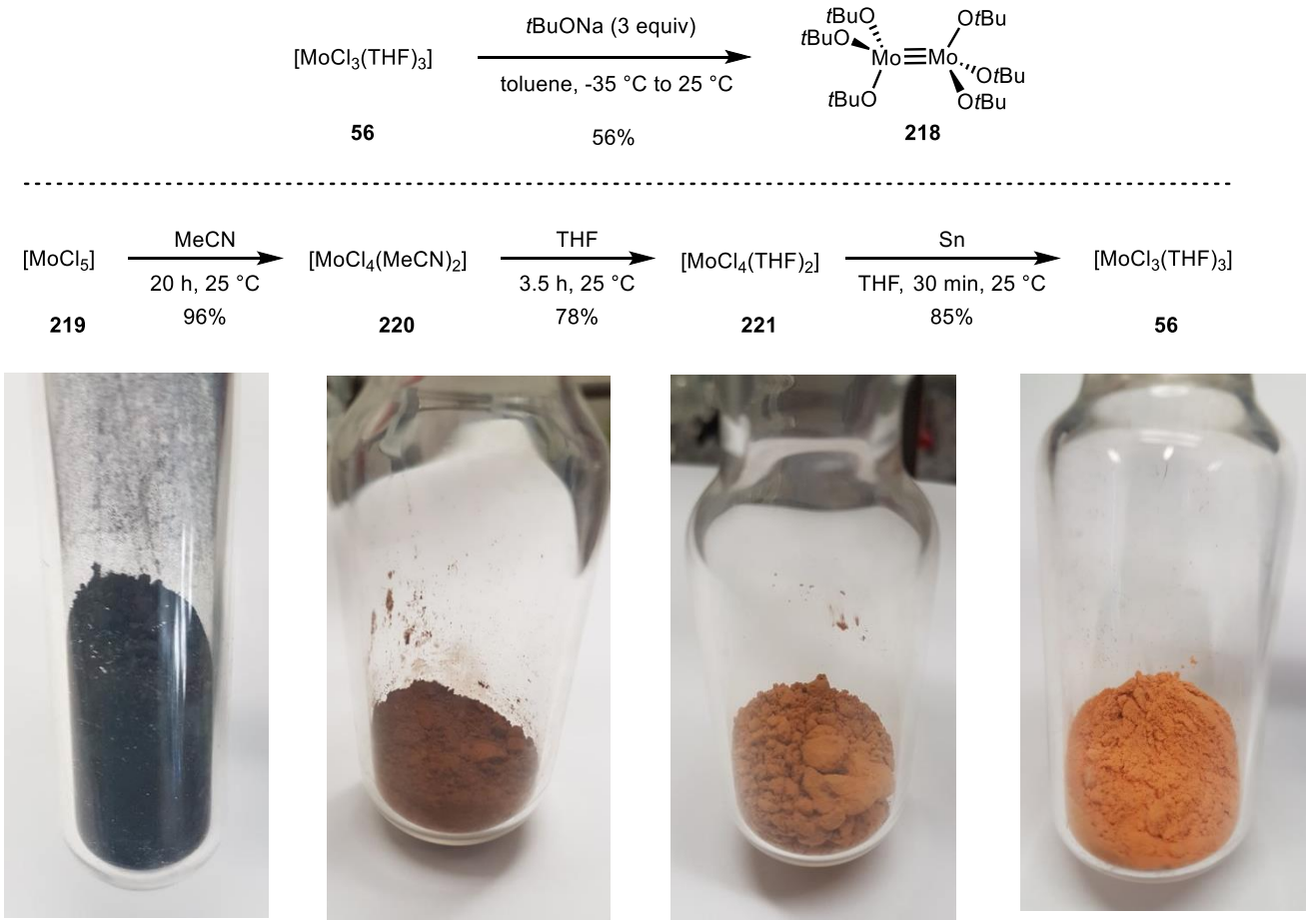


**Scheme 86.** Synthetic procedure to access [MoCl$_3$(THF)$_3$] (**56**). The photos show the color change during the synthesis.

We successfully reproduced the entire protocol on a small scale (~2 g of [MoCl$_5$] (**219**)) and prepared the dinuclear Mo(III) complex [(*t*BuO)$_3$Mo≡Mo(O*t*Bu)$_3$] (**218**) in high purity (**Figure 72** A). Upon scale-up (~17 g of [MoCl$_5$] (**219**)) and treatment of "[MoCl$_3$(THF)$_3$] (**56**)" with sodium *tert*-butoxide, we identified several other products in the $^1$H NMR spectrum after removal of the solvent (**Figure 72**, B).

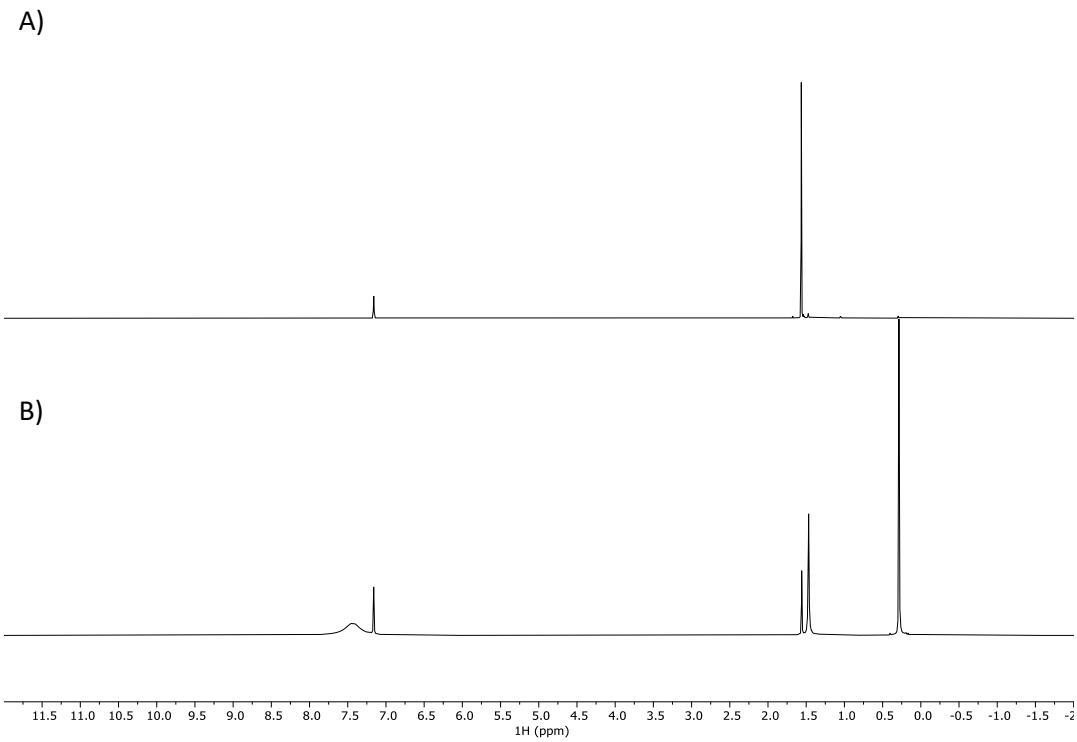


**Figure 72**. Initial observation: $^{1}H$ NMR spectra in $C_6D_6$ at 25 °C. A) $[(tBuO)_3Mo{\equiv}Mo(OtBu)_3]$ (**218**) on a small scale B) $[(tBuO)_3Mo{\equiv}Mo(OtBu)_3]$ (**218**) on a large scale.

Driven by curiosity, we intended to elucidate the structure of the formed side products by single-crystal X-ray diffraction. Indeed, crystallization at −35 °C in diethyl ether yielded two different crops of crystals. A green crop of crystals consisted Mo(V) alkoxide complex **222**, which was confirmed by several independent measurements. The second crop of orange crystals gave the literature known Mo(VI) nitrido complex **223** (**Figure 73**).[183]

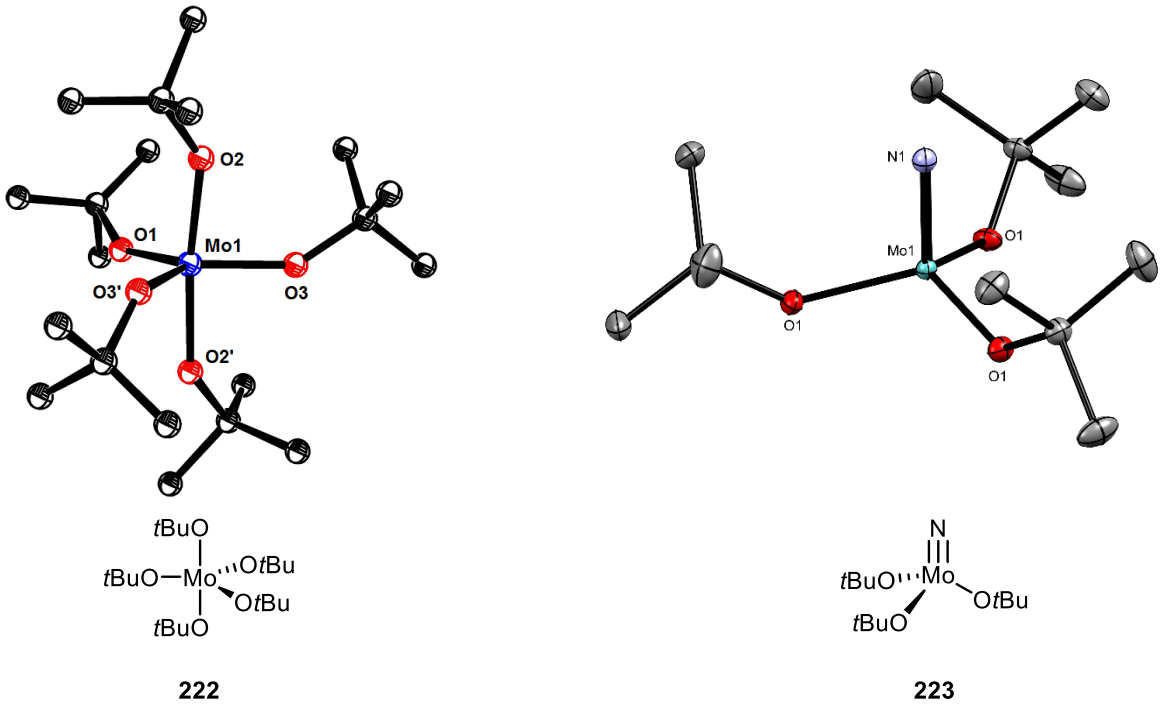


**Figure 73.** Solid state structure of Mo(V) complex **222** and Mo(VI) nitrido complex **223**.

At this point, it was unclear how both complexes might be formed. Therefore, we further analyzed the obtained mixture (**Figure 72**, B) by NMR spectroscopy and could additionally identify [Sn(O*t*Bu)$_4$] and1-chloro-4-(4-chlorobutoxy)butane. $^{1}$H, $^{13}$C and $^{119}$Sn NMR confirmed without doubt that [Sn(O*t*Bu)$_4$] is present, which presumably resulted from [SnCl$_4$] substitution with *tert*-butoxide and was not efficiently removed after the tin reduction step.[184] We also confirmed that 1-chloro-4-(4-chlorobutoxy)butane was present in small quantities, which is a known product of THF cleavage by high-valent molybdenum complexes.[185] Although [MoCl$_3$(THF)$_3$] (**56**) dimerizes in $CD_2Cl_2$ to give broad paramagnetic $^{1}$H NMR signals,[186] we further analyzed the starting material "[MoCl$_3$(THF)$_3$] (**56**)" and observed the characteristic signals for [MoCl$_4$(THF)$_2$] (**221**) ($\delta_H$ = 12.60 (s, 8H), –35.13 (s, 8H)). It became clear that the heterogeneous tin reduction did not run to completion and that prolonged stirring is particularly important for the large-scale reaction. Hence, we recommend to check the conversion by $^{1}$H NMR spectroscopy and to repeat the reduction with tin, if necessary.

### 3.3.1 Isolation of a Homoleptic Non-Oxo Mo(V) Alkoxide Complex

The puzzling formation of [Mo(O*t*Bu)$_5$] (**222**) could be traced back to the disproportionation of [MoCl$_4$(THF)$_2$] (**221**) in the presence of three equivalents of sodium *tert*-butoxide in toluene (**Scheme 87**). After 4 h reaction time, the solvent was removed *in vacuo* and both disproportionation products [Mo(O*t*Bu)$_5$] (**222**) and [Mo$_2$(O*t*Bu)$_6$] (**218**) were isolated by extraction with *n*-pentane to give a deep green solution. The [Mo(O*t*Bu)$_5$] (**222**) complex can be purified by sublimation (25 °C, $10^{-7}$ mbar).

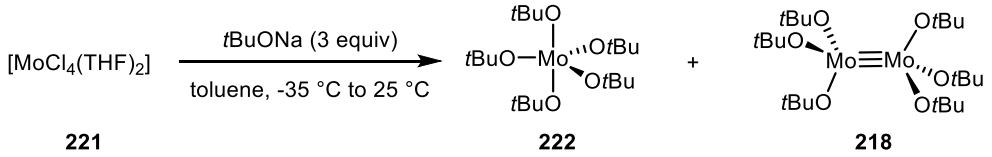


**Scheme 87.** Alkoxide-promoted disproportionation of [MoCl$_4$(THF)$_2$] (**221**).

[Mo(O*t*Bu)$_5$] (**222**) is the first monomeric, homoleptic, five-coordinated alkoxide, non-oxo 4d$^1$ Mo(V) complex and represents the first example of this new class of compounds. High-valent molybdenum complexes endowed with alkoxide ligands are prone to dimerize or form molybdenum-oxo complexes. **Scheme 88** summarizes the literature precedence for high-valent molybdenum alkoxide complexes.[187]

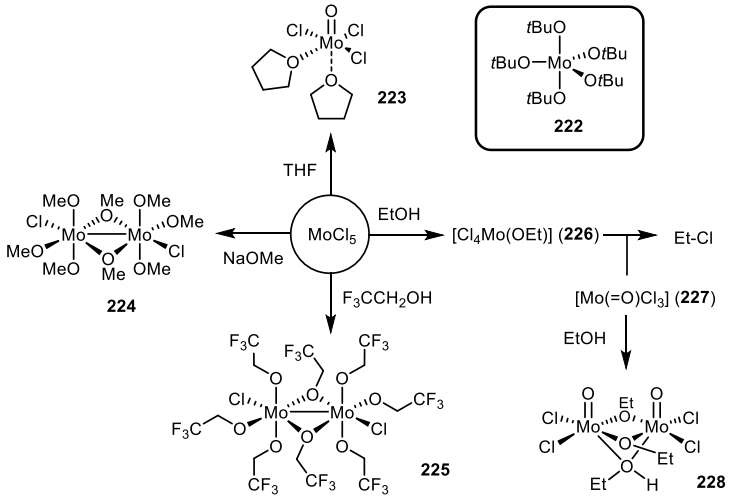


**Scheme 88.** Overview of high-valent molybdenum alkoxide complexes in the literature.

Complex **222** is a green, paramagnetic, air-sensitive solid, which can be stored for several days (~ 4 days) at ambient temperatures. At ≥ 50°C the complex decomposed in [$D_8$]-toluene to give isobutylene and an insoluble precipitate. The complex is well soluble in *n*-pentane, benzene, toluene and $CH_2Cl_2$ but readily decomposes in acetonitrile at ambient temperature. The experimentally found elementary analysis matched reasonably well with the calculated one (Anal. Calc. for $C_{20}H_{45}O_5Mo$: C, 52.05; H, 9.83, Mo, 20.79. Found C, 52.33; H, 10.01; Mo, 19.58). Interestingly, Mo(V) complex **222** was only formed under specific reaction conditions (**Table 10**). Three equivalents of sodium *tert*-butoxide gave the highest yield. Changing the solvent from toluene to THF gave only ~ 5% of the desired complex; changing to *n*-pentane the disproportionation pathway shut down. The specific conditions to form this unusual metal complex might in part explain why it has not been described before.

**Table 10.** Conditions for alkoxide-promoted disproportionation of [$MoCl_4(THF)_2$] (**221**).

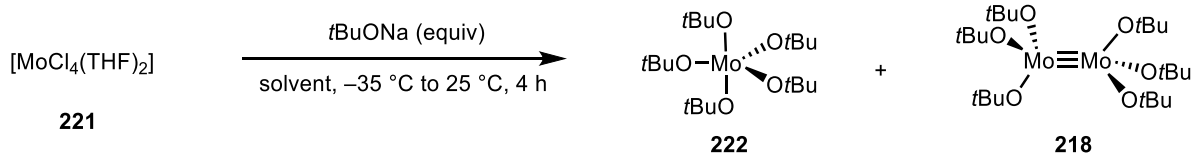


| entry | equiv. | solvent | observation |
|---|---|---|---|
| 1 | 2 | toluene | new species |
| 2 | 3 | toluene | 30% of [Mo(O*t*Bu)$_5$] (**222**) |
| 3 | 4 | toluene | 15% of [Mo(O*t*Bu)$_5$] (**222**) |
| 4 | 5 | toluene | 5% of [Mo(O*t*Bu)$_5$] (**222**) |
| 5 | 3 | THF | 5% of [Mo(O*t*Bu)$_5$] (**222**) |
| 6 | 3 | *n*-pentane | no conversion |

Green crystals suitable for single-crystal X-ray diffraction were grown by storing a concentrated *n*-pentane solution at –35 °C for three days. Complex **222** crystallized in the orthorhombic crystal system, space group *P*nc2. Two independent molecules reside in the unit cell. Single-crystal X-ray diffraction data were collected at 200 K since the crystals broke at lower temperature. [Mo(O*t*Bu)$_5$] (**222**) exhibits a trigonal bipyramidal geometry with slight deviations from the idealized structure. The equatorial angles (O1–Mo–O2 = 119.9(3)°, O1–Mo–O2' = 115.2(3)°, O2–Mo–O2' = 122.6(4)°) are close to 120°, while the axial angle (O3–Mo–O3' = 178.4(7)°) is slightly smaller than 180°. The molybdenum oxygen bond length in the axial position (Mo–O3 = 1.881(6) Å) is slightly longer than the equatorial positions (Mo–O1 = 1.858 Å, Mo–O2 = 1.870(5) Å), which have similar bond lengths as the reported octahedral [Mo(OMe)$_6$] complex (1.862(4)–1.909(4) Å).[188] By NMR spectroscopy we identified two characteristic signals for the paramagnetic complex (in $C_6D_6$: broad $\delta_H$ = 7.43 ppm; broad $\delta_C$ = 54.9, 30.3 ppm).

However, the formation of [Mo(O*t*Bu)$_5$] (**222**) was surprising since the alkoxide substitution of [$MoCl_4(THF)_2$] (**221**) has been reported to give [Mo(O*t*Bu)$_4$] (**229**).[189] When we reproduced the described protocol for the preparation of [Mo(O*t*Bu)$_4$] (**229**) by Poli and co-workers, we only

obtained [Mo(O*t*Bu)$_5$] (**222**) and [Mo$_2$(O*t*Bu)$_6$] (**218**) as judged by $^1$H, $^{13}$C and $^{95}$Mo NMR spectroscopy (**Scheme 89**).[157] The literature report provided only an elementary analysis and a $^1$H NMR shift (in $C_6D_6$: $\delta_H$ = 1.55 ppm) of presumed [Mo(O*t*Bu)$_4$] (**229**),[189] which is in good agreement with that of dimeric [Mo$_2$(O*t*Bu)$_6$] (**218**).[190] In our hands, several independent runs with either NaO*t*Bu or LiO*t*Bu invariably gave both disproportionation products; we are not able to confirm or exclude the formation of [Mo(O*t*Bu)$_4$] (**229**).

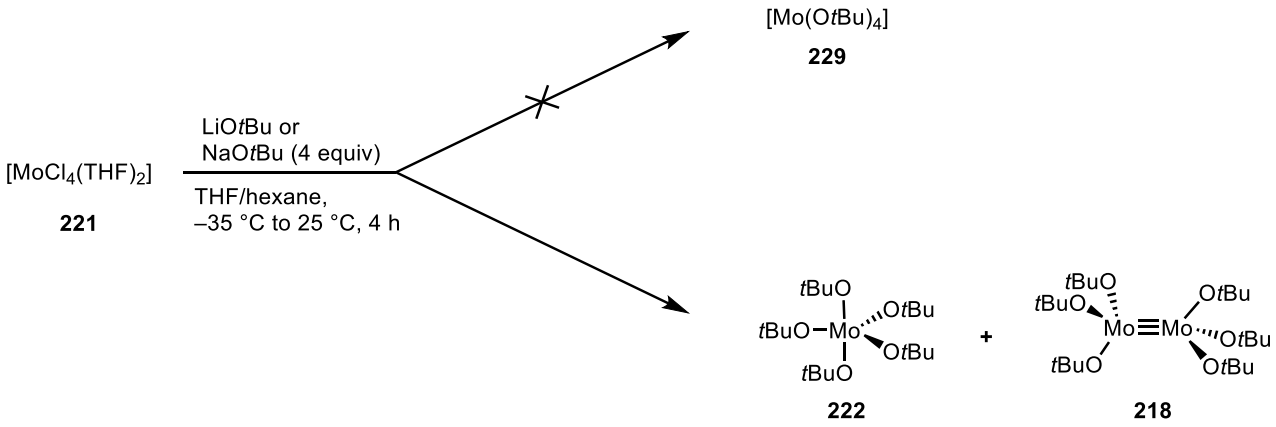


**Scheme 89.** Attempt to reproduce the reported metathetic ligand exchange of [MoCl$_4$(THF)$_2$] (**221**) with *tert*-butoxide salts.

Similarly, we reproduced the protonolysis of tetrakis(dimethylamide)molybdenum(IV) complex (**230**) with *tert*-butyl alcohol described by Chisholm and co-workers (**Scheme 90**).[191] Upon addition of four equivalents *tert*-butyl alcohol to the purple solution of tetrakis(dimethylamide)molybdenum(IV) (**230**) at 0 °C, the solution instantly turned green. After 6 h the green-brown suspension was evaporated to dryness, $^1$H, $^{13}$C NMR spectra of the crude material again confirmed the formation of [Mo(O*t*Bu)$_5$] (**222**) and a new paramagnetic complex **231**. Extraction of the crude mixture with *n*-pentane gave purified dinuclear complex **231**.

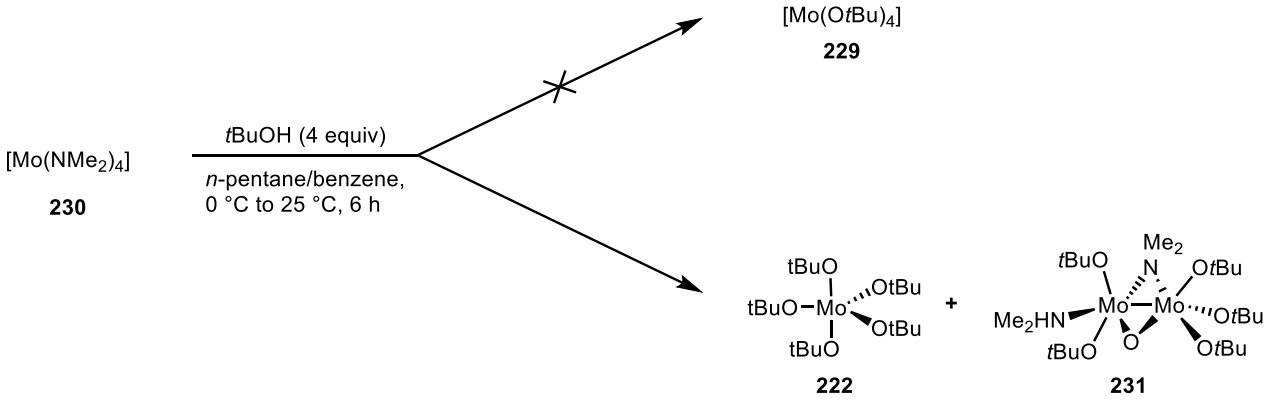


**Scheme 90.** Reproducing the literature reported protonolysis of [Mo(NMe$_2$)$_4$] (**230**) with *t*BuOH.

Orange crystals suitable for single-crystal X-ray diffraction were grown by storing a concentrated *n*-pentane solution of **231** at –20 °C for three days (**Figure 74**). The dinuclear complex **231** is bridged by an oxo- and an amide-ligand. Additionally, a molecule of dimethylamine occupies a coordination site, which must have been released during the reaction. Solely based on the short Mo1–Mo2 bond distance (2.486(3)Å) it is problematic to derive a bond order. However, the paramagnetic nature of **231** makes it unlikely to be a double bond. Related diamagnetic Mo≡Mo complexes with a Mo1–Mo2 bond distance (2.449(1)Å and 2.523(1)Å) have been assigned with a double bond.[192, 193]

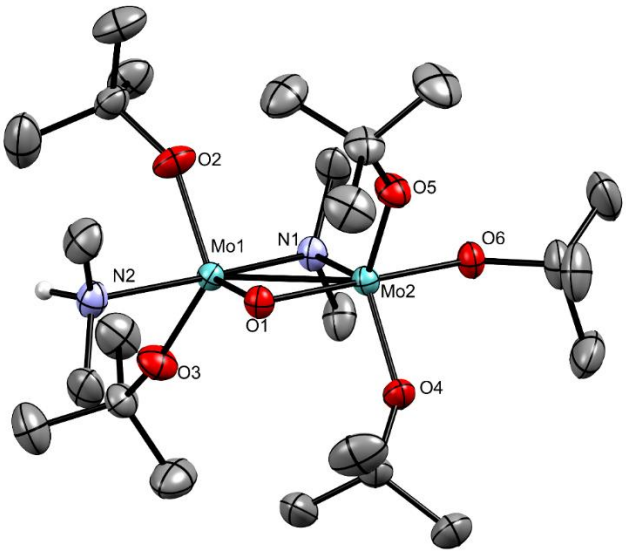


**Figure 74.** Solid state structure of dinuclear complex **231**; hydrogen atoms, except for the NH atom and disorder omitted for clarity.

Finally, we investigated whether $[MoCl_4(THF)_2]$ (**221**) is prone to disproportionation in the absence of alkoxides (**Scheme 91**). Indeed, $[MoCl_4(THF)_2]$ (**221**) disproportionated in a solution of $CH_2Cl_2$ over 4 days at 25 °C. The solid state structure confirmed the formation of complex $[MoOCl_3(THF)(H_2O)]$ (**232**)[194] and dimeric $[Mo_2Cl_6(THF)_3]$ (**233**)[195]. Interestingly, both molecules occupy the same unit cell and thus provided proof for the disproportionation event (**Figure 75**). Although $[MoCl_4(THF)_2]$ (**221**) had previously described as an unstable complex (even under nitrogen atmosphere), the decomposition products had never been identified.[182]

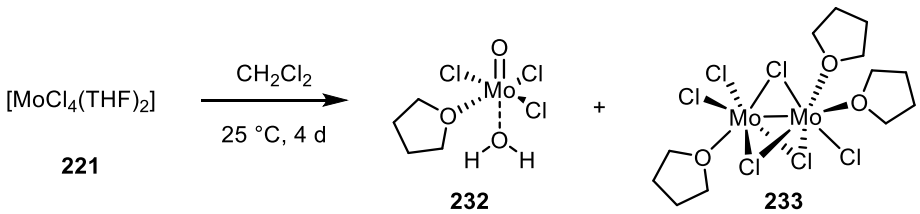


**Scheme 91.** Disproportionation of Mo(IV) in the absence of alkoxides.

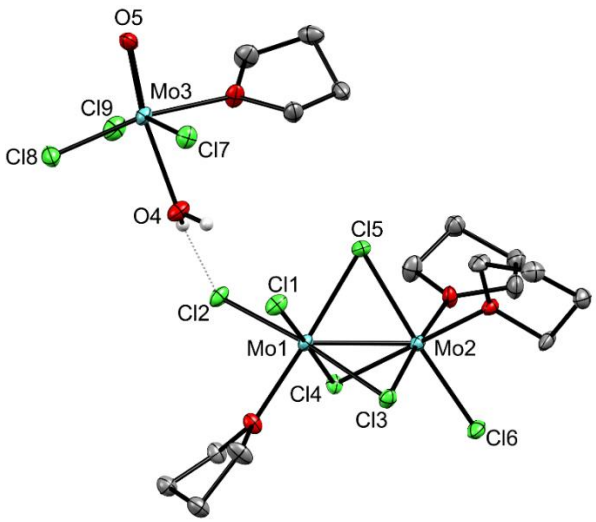


**Figure 75.** Unit cell occupied by $[MoOCl_3(THF)(H_2O)]$ (**232**) and $[Mo_2Cl_6(THF)_3]$ (**233**).

### 3.3.2 Activation of Acetonitrile by a Mo(III) Alkoxide Complex

Next, we investigated the peculiar formation of the nitrido complex **223**. A single synthetic protocol is described in the literature and starts with azide decomposition by $[MoCl_4(MeCN)_2]$ (**220**) to give $[N{\equiv}MoCl_3]$ (**234**).[183] After repeating the described protocol, we further confirmed the formation of **234** by $^{95}$Mo NMR spectroscopy in $CD_3CN$ ($\delta_{Mo}$ = 1106.9 ppm). However, the literature reported $^{95}$Mo NMR shift ($\delta_{Mo}$ = 952 ppm) in $CD_3CN$ did not match and was presumably mixed up in the reported table.[196] Treatment of complex **234** with three equivalents of sodium *tert*-butoxide gave, after purification by sublimation, the desired complex $[N{\equiv}Mo(O\mathit{t}Bu)_3]$ (**223**) in 40% yield over two steps. The $^{95}$Mo NMR shift ($\delta_{Mo}$ = 53.7 ppm) in $CD_2Cl_2$ matched the literature reported shift ($\delta_{Mo}$ = 55 ppm) in $CD_2Cl_2$.[196] In principle three conceptually different routes are conceivable to access $[N{\equiv}Mo(O\mathit{t}Bu)_3]$ (**223**) (**Scheme 92**). A spectacular reaction would be the triple bond metathesis of dinuclear Mo(III) complex $[(\mathit{t}BuO)_3Mo{\equiv}Mo(O\mathit{t}Bu)_3]$ (**218**) with dinitrogen or acetonitrile. While the cleavage of alkynes or nitriles by dinuclear W(III) complex $[(\mathit{t}BuO)_3W{\equiv}W(O\mathit{t}Bu)_3]$ (**11**) is well-known to be facile, attempts to cleave dinitrogen at ambient conditions or high pressures and elevated temperature failed.[197] In contrast, dinuclear complex $[(\mathit{t}BuO)_3Mo{\equiv}Mo(O\mathit{t}Bu)_3]$ (**218**) only cleaved terminal acetylene but failed to metathesize internal acetylenes or nitriles.[197, 198]

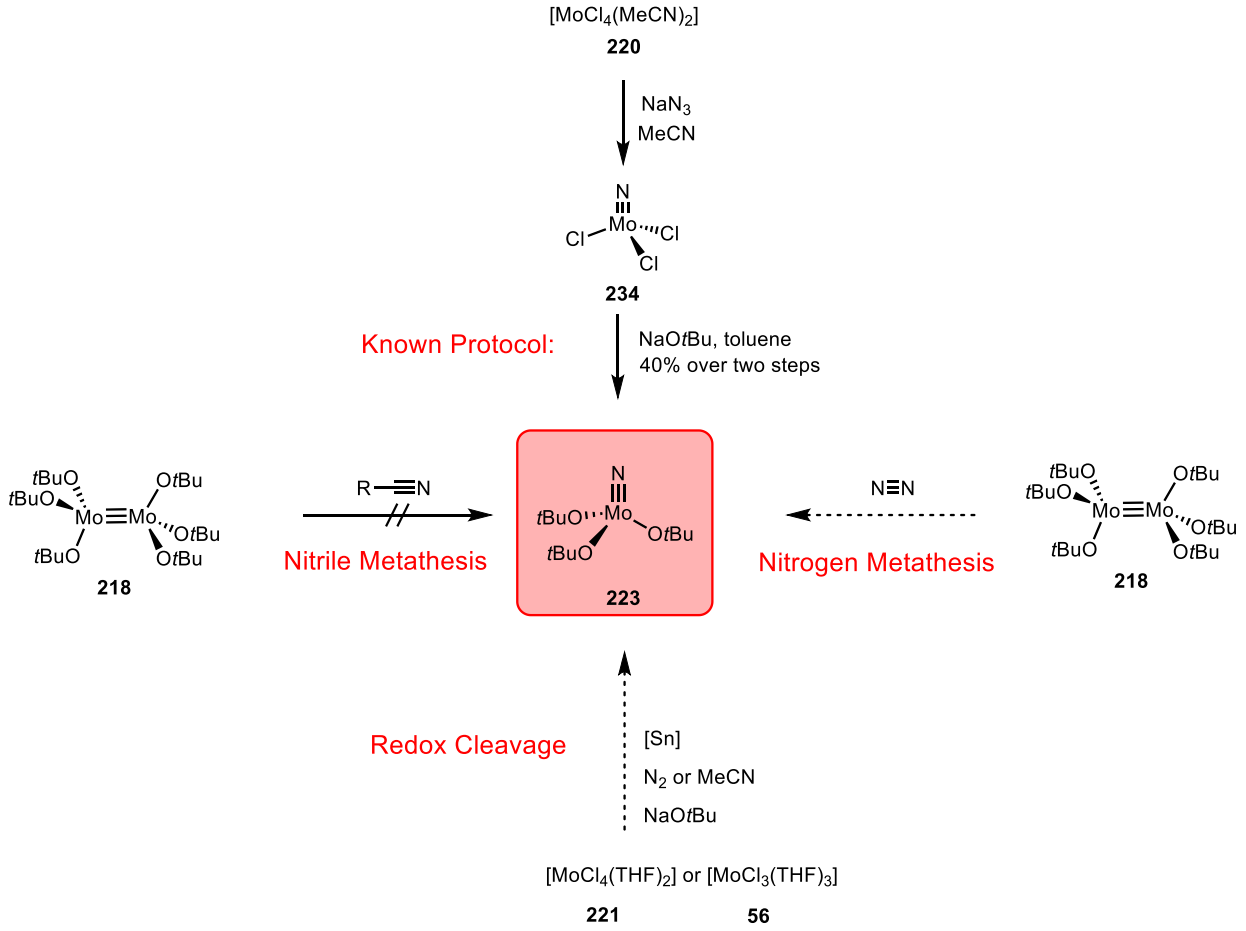


**Scheme 92.** Overview of synthetic and potential routes to access $[N{\equiv}Mo(O\mathit{t}Bu)_3]$ (**223**).

Although the metathesis of molecular dinitrogen has not been reported in the literature, a solution of $[(\mathit{t}BuO)_3Mo{\equiv}Mo(O\mathit{t}Bu)_3]$ (**218**) in toluene was stirred for 6 days at 25 °C under continuous dinitrogen atmosphere (Linde gas 99.999%). Removal of the solvent *in vacuo* and analysis of the crude material by NMR spectroscopy gave no evidence for the formation of $[N{\equiv}Mo(O\mathit{t}Bu)_3]$ (**223**) (**Scheme 93**).

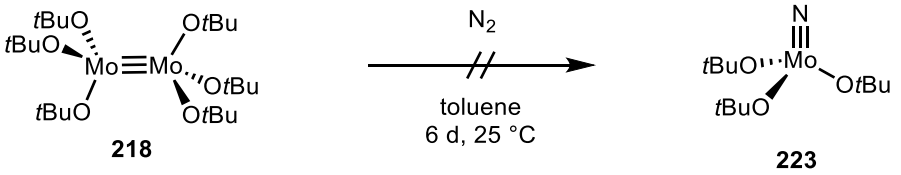


**Scheme 93.** Attempt for dinitrogen metathesis.

Another access to nitrido complex **223** could be the direct activation of dinitrogen or acetonitrile by $[MoCl_4(MeCN)_2]$ (**220**) or $[MoCl_4(THF)_2]$ (**221**) to form $[N{\equiv}MoCl_3]$ (**234**), in the presence of a reductant such as $SnCl_2$ or $Sn(OtBu)_2$. Richards and co-workers reported on the reaction of $[MoCl_4(THF)_2]$ (**221**) with a dinitrogen rhenium complex to form a μ-dinitrogen complex $[(PMe_2Ph)_4ClReN_2MoCl_4(OMe)]$.[199] Stirring of a solution of $[MoCl_4(THF)_2]$ (**221**) in toluene or $CH_2Cl_2$ in the presence of $SnCl_2$ or $Sn(OtBu)_2$ under continuous dinitrogen atmosphere (Linde gas 99.999%) gave no $^{95}Mo$ NMR signal corresponding to $[N{\equiv}MoCl_3]$ (**234**) (**Scheme 94**).

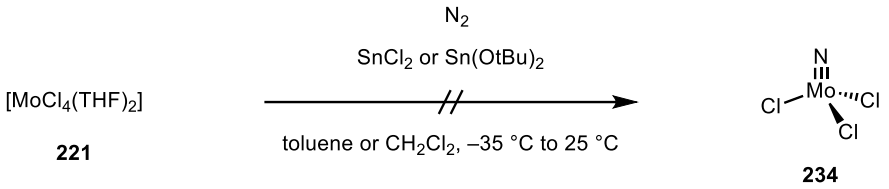


**Scheme 94.** Attempted dinitrogen activation to form nitrido complex **234**.

Stirring of a solution of $[MoCl_4(MeCN)_2]$ (**220**) in acetonitrile in the presence of $SnCl_2$ gave no $^{95}Mo$ NMR signal corresponding to $[N{\equiv}MoCl_3]$ (**234**) but gave access to an unusual dicationic $[MoCl_2(MeCN)_4SnCl_6]$ complex **235** (**Scheme 95**). Crystal structure analysis confirmed the proposed structure (**Figure 76**).

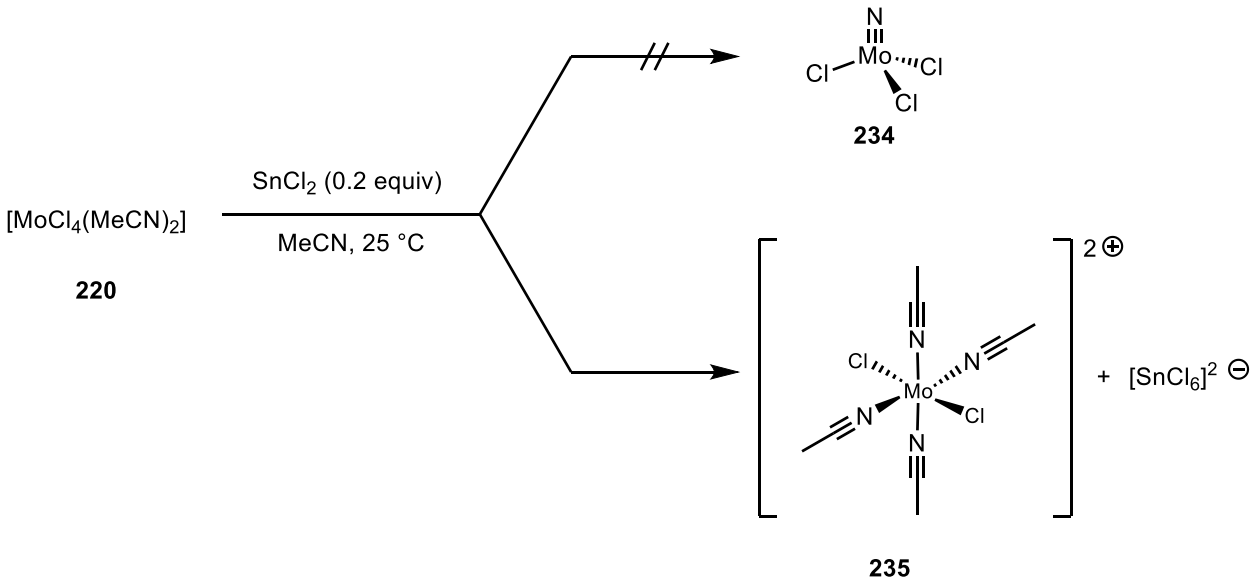


**Scheme 95.** Attempt acetonitrile activation to form nitrido complex **234**.

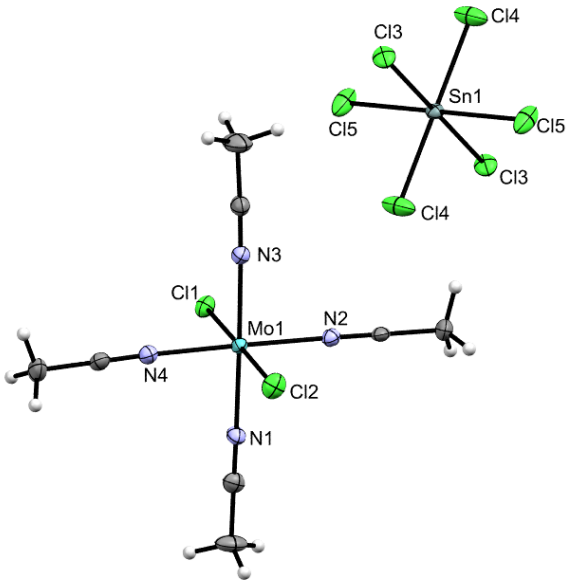


**Figure 76.** Solid state structure of complex **235**.

Molybdenum(III) trisamide complex [Mo(N*t*BuAr)$_3$)] (**58**) has first been synthesized by Cummins and co-workers in 1995 and represents the first and only monomeric Mo(III) complex that can be isolated and characterized. The high reactivity of Mo(III) complex **58** was demonstrated by a plethora of small molecule activations, including dinitrogen splitting.[104] In this context, complex **58** reductively dimerized organic nitriles such as benzonitrile to give a $d^2/d^2$ dimerized product **237**, but did not fragment to release the nitrido complex **236** and alkyne **4** at ambient temperature or even 100 °C (**Scheme 96**).[200]

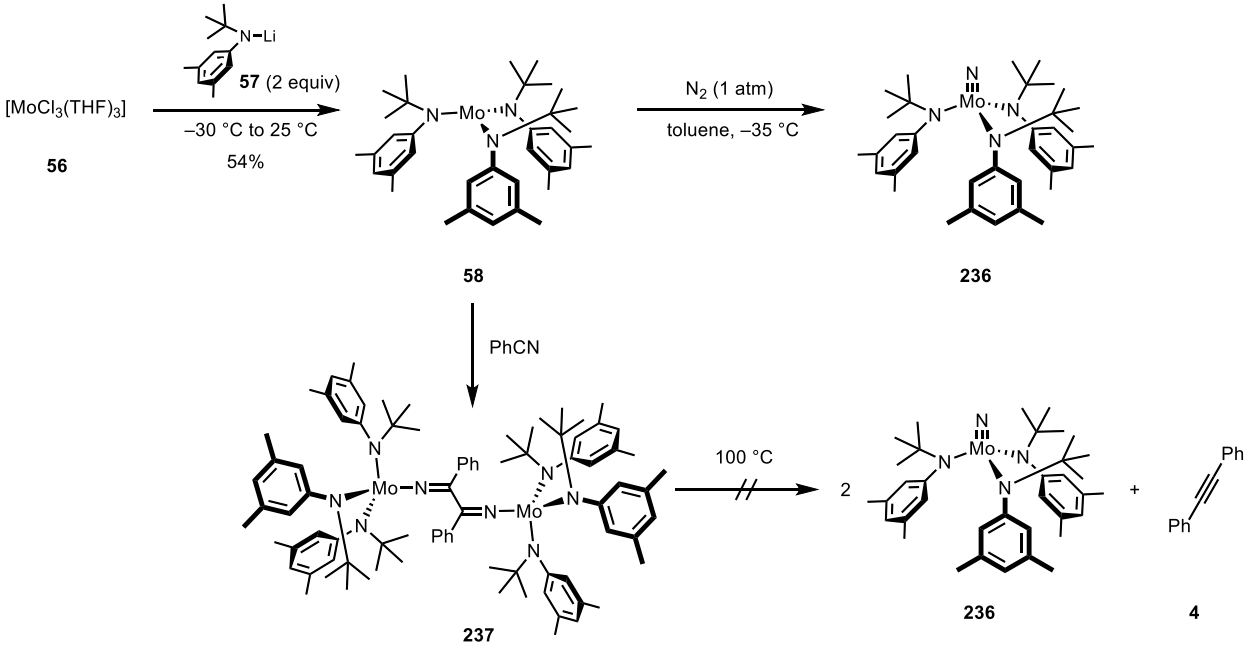


**Scheme 96.** Reactivity of Mo(III) complex **58** with dinitrogen and benzonitrile.

Ligation with *N*-isopropylanilide gave instead cyclometalated complex **238** that underwent reversible β-hydride elimination.[200, 201] Addition of benzonitrile gave the $\eta^2$-adduct **239** and resulted in the formation of dinuclear complex **242**. In contrast, slow addition of PhCN to a solution of **239** in a 1:3 ratio cleaved the nitrile to give benzylidyne complex **240** and dimerized nitrido complex **241**.[201]

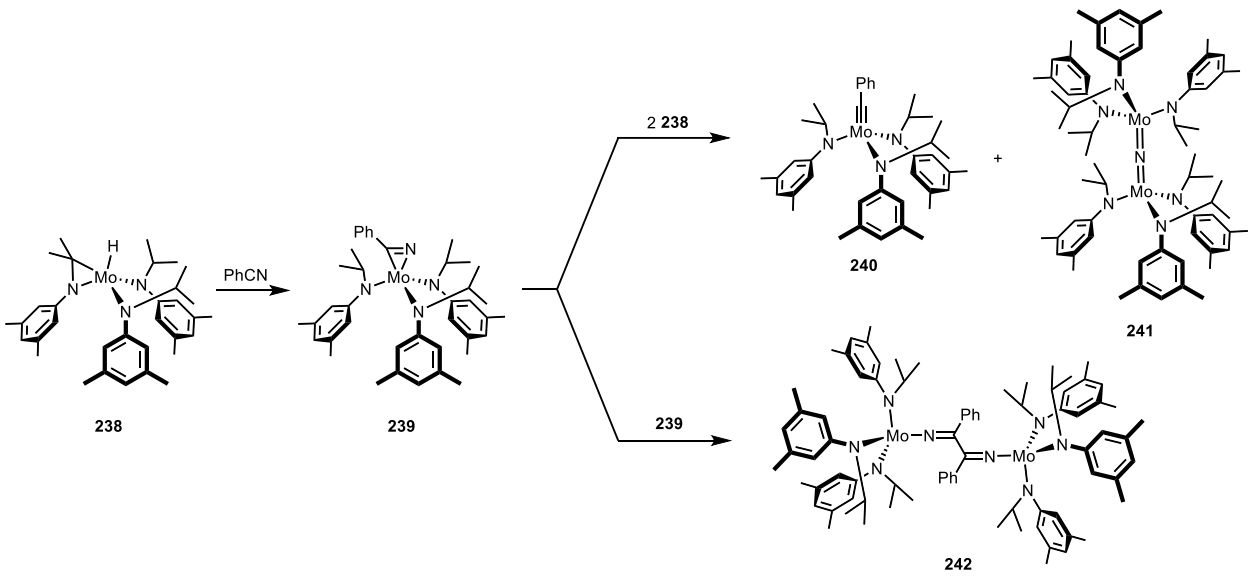


**Scheme 97.** Reactivity of Mo(III) complex **238** with benzonitrile.

Yet, it has not been possible to prepare a monomeric Mo(III) complex endowed with alkoxide ligands. Since *tert*-butoxide ligands are not efficiently shielding the metal center, treatment of $[MoCl_3(THF)_3]$ (**56**) with sodium *tert*-butoxide resulted in the formation of dinuclear complex $[(t\text{BuO})_3\text{Mo}{\equiv}\text{Mo}(\text{O}t\text{Bu})_3]$ (**218**) (*vide supra*). However, Cummins and co-workers provided indirect evidence that alkoxide-ligated Mo(III) complexes might be involved in dinitrogen splitting.[202] Inspired by this report, we treated $[MoCl_3(THF)_3]$ (**56**) with sodium *tert*-butoxide in the presence of two equivalents of acetonitrile. Removal of the solvent gave no evidence for nitrido complex **223**.

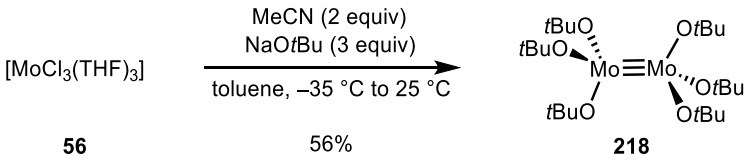


**Scheme 98.** Attempted acetonitrile activation with two equivalents of acetonitrile.

Because dimerization in toluene is too fast, we prepared the corresponding $[MoCl_3(MeCN)_3]$ (**243**) and treated it with sodium *tert*-butoxide in acetonitrile. Upon addition of sodium *tert*-butoxide the yellow solution of $[MoCl_3(MeCN)_3]$ (**243**) instantly turned black and after 4 h the solvent was removed *in vacuo*. $^1$H, $^{13}$C and $^{95}$Mo NMR of the crude product confirmed the successful formation of $[\text{N}{\equiv}\text{Mo}(\text{O}t\text{Bu})_3]$ (**223**) as the major product in 87% yield (NMR). In small quantities we also identified $[(t\text{BuO})_3\text{Mo}{\equiv}\text{Mo}(\text{O}t\text{Bu})_3]$ (**218**) as a byproduct in 13% yield (NMR) that might have been formed through competing dimerization. Complex $[\text{N}{\equiv}\text{Mo}(\text{O}t\text{Bu})_3]$ (**223**) could be purified by sublimation as described in the literature.[183]

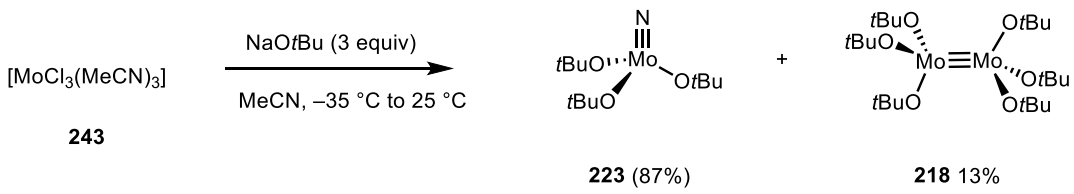


**Scheme 99.** Acetonitrile activation by Mo(III) alkoxide complex.

In accordance with the literature precedence, two mechanistic scenarios are conceivable: Ligand substitution with *tert*-butoxide affords intermediate **244**, which reacts with a second equivalent of **244** *via* cleavage of the carbon nitrogen triple bond to form nitrido complex **223** and alkylidyne complex **245**; alternatively a reductive coupling to form nitrido complex **223** and 2-butyne (**146**) might take place. Each molybdenum center acts as a three-electron reductant, resulting in an overall six-electron reduction process. However, neither the alkylidyne complex **245** nor 2-butyne (**146**) was traceable by NMR spectroscopy or GC-MS analysis.

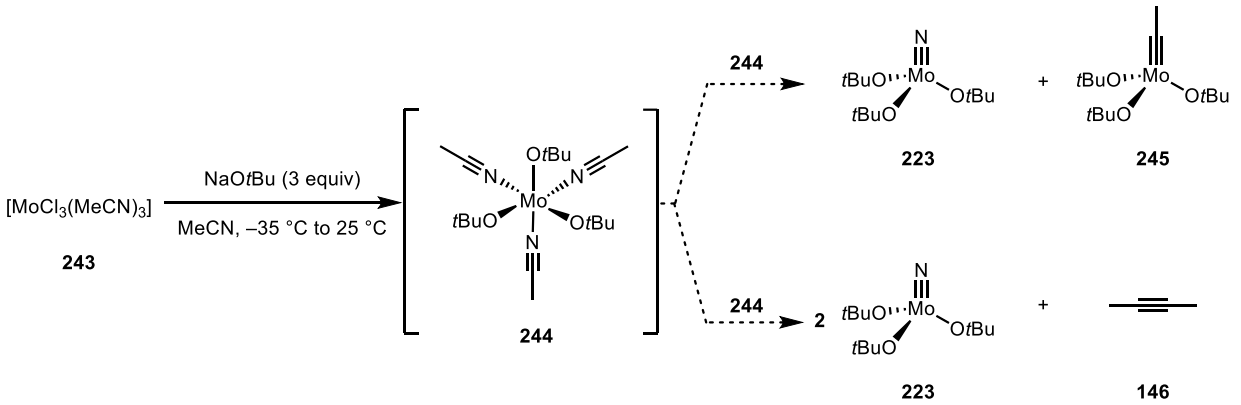


**Scheme 100.** Proposed reaction pathways for formation of nitrido complex **223**.

The ethylidyne complex **245** is prone to decompose by retro-metathesis to give [(*t*BuO)$_3$Mo≡Mo(O*t*Bu)$_3$] (**218**) and is therefore difficult to isolate. Schrock and co-workers have addressed this issue by adding excess quinuclidine to stabilize unstable alkylidyne complexes.[198] However, adding four equivalents of quinuclidine, did not result in the formation of quinuclidine adduct **246** (**Scheme 101**).

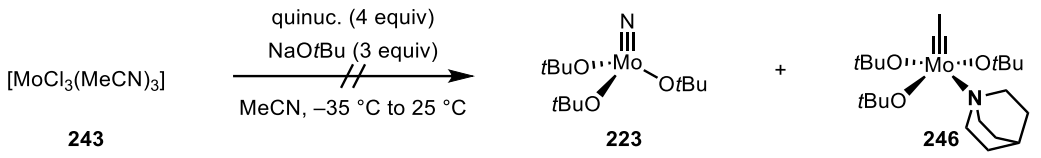


**Scheme 101.** Addition experiment with quinuclidine.

It is well described in the literature that 2-butyne is prone to polymerization and hence difficult to detect. Instead of acetonitrile we used benzonitrile or pivalonitrile to detect the corresponding byproducts but were not successful either. Therefore, we prepared the benzonitrile precursor [MoCl$_3$(PhCN)$_3$] (**247**) by stirring [MoCl$_3$(MeCN)$_3$] (**243**) in excess benzonitrile under vacuum to facilitate the equilibrium exchange and remove the more volatile acetonitrile (**Scheme 102**). After 3 h, we obtained a yellow suspension, filtered off the yellow supernatant solution and obtained a yellow solid. However, by NMR spectroscopy it was not possible to determine whether the desired complex **247** remained in solution or in the solid material. To clear this up we used crystal structure analysis: therefore, the yellow solid material was dissolved in $CH_2Cl_2$, filtered and carefully layered with excess *n*-pentane. After three days we obtained yellow crystals suitable for crystal structure analysis, which revealed the composition of [MoCl$_3$(MeCN)$_2$(PhCN)] (**248**). Next, we analyzed the supernatant solution of the reaction, which was directly layered with excess *n*-pentane. After three days we obtained yellow crystals suitable for crystal structure analysis, which had the composition of [MoCl$_3$(PhCN)$_3$] (**247**) (**Figure 77**).

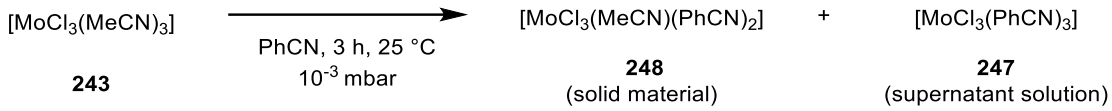


**Scheme 102.** Preparation of $[MoCl_3(PhCN)_3]$ complex (**247**).

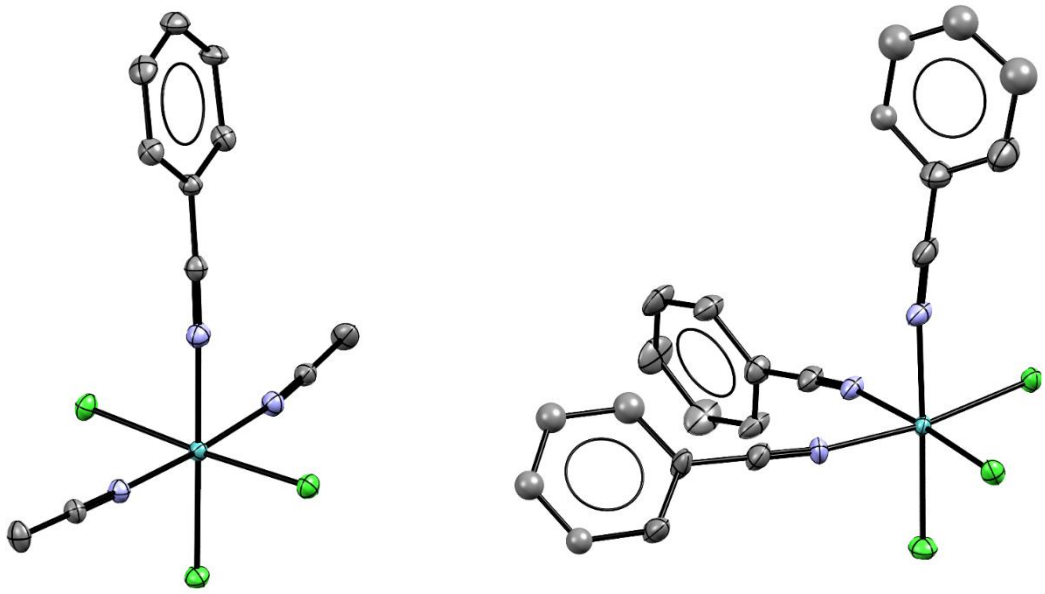

**Figure 77.** Solid state structure of $[MoCl_3(MeCN)_2(PhCN)]$ (**248**) and $[MoCl_3(PhCN)_3]$ complex (**247**); disorder, solvent and hydrogen-atoms omitted for clarity.

With complex $[MoCl_3(PhCN)_3]$ (**247**) in hand, we treated the material with sodium *tert*-butoxide in benzonitrile. However, we did not observe the formation of alkylidyne complex **249**, diphenylacetylene (**4**), $[N{\equiv}Mo(O\mathit{t}Bu)_3]$ (**223**), nor $[(\mathit{t}BuO)_3Mo{\equiv}Mo(O\mathit{t}Bu)_3]$ (**218**) (**Scheme 103**).

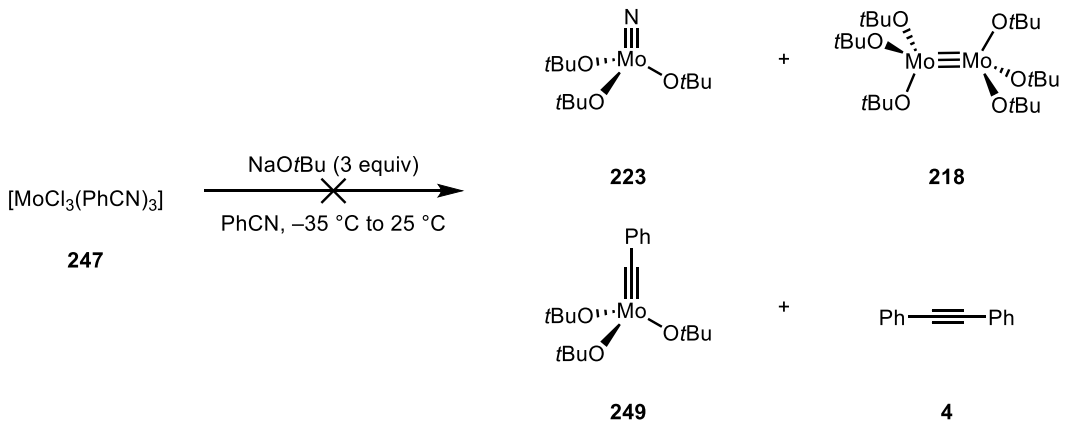


**Scheme 103.** Attempted reaction with $[MoCl_3(PhCN)_3]$ (**247**).

In conclusion, treatment of $[MoCl_3(MeCN)_3]$ (**243**) with three equivalents of sodium *tert*-butoxide in acetonitrile yielded $[N{\equiv}Mo(O\mathit{t}Bu)_3]$ (**223**) as the major product. Although extensive efforts have been made to clarify the peculiar formation of nitrido complex **233**, neither an alkylidyne complex nor an alkyne was detected. Therefore, the mechanism of this puzzling redox chemistry remains unclear.

## 3.4 Miscellaneous Ligand Designs

### 3.4.1 Preparation of a Tripodal Aniline Ligand

In a first foray, we prepared the tripodal aniline ligand **250** by adapting a literature procedure (**Scheme 104**).[103, 203] A solution of the lithiated ligand **250** was added dropwise to a solution of precatalyst **106**. The recorded $^1$H NMR spectrum shows broad NMR signals, indicating undesired oligomerization.[204, 205] In respect to the newly developed complexation *via* protonolysis (*vide supra*), it is worthwhile to test the complexation with either [(*t*BuO)$_3$Mo≡Ar] or [(R$_2$N)$_3$Mo≡Ar].[47]

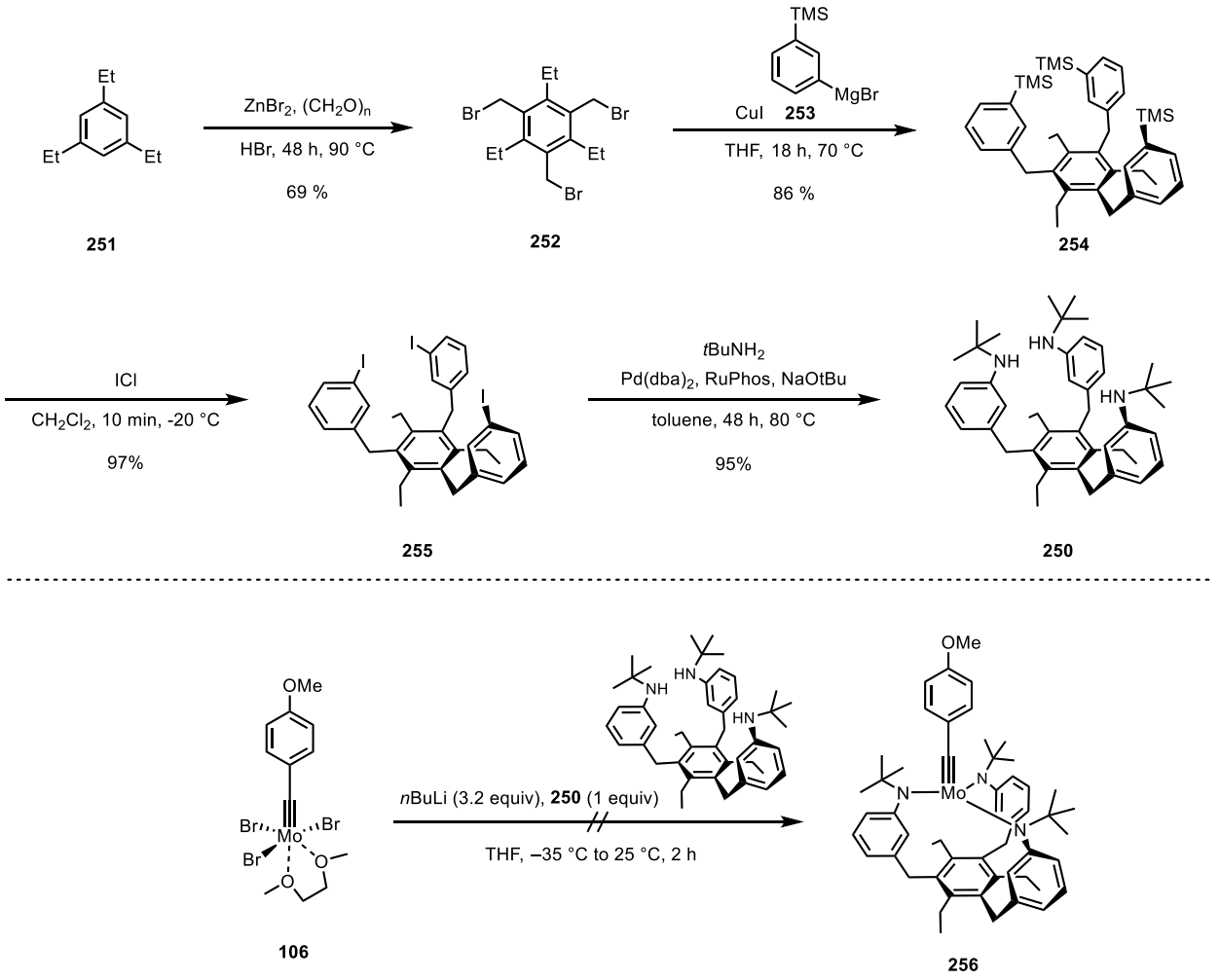


**Scheme 104.** Preparation of tripodal anilide ligand **250** and attempted complexation to molybdenum alkylidyne complex.

### 3.4.2 Attempted Preparation of an Alternative Tripodal Silanol Ligand

Cyclotriveratrylene-based ligand frameworks have been extensively used for self-assembled coordination complexes.[206] Inspired by tripodal carboxylate copper complexes (**Figure 78**), we envisioned to prepare the corresponding trisilanol **257** by adapting the procedure (**Scheme 105**).[207-211]

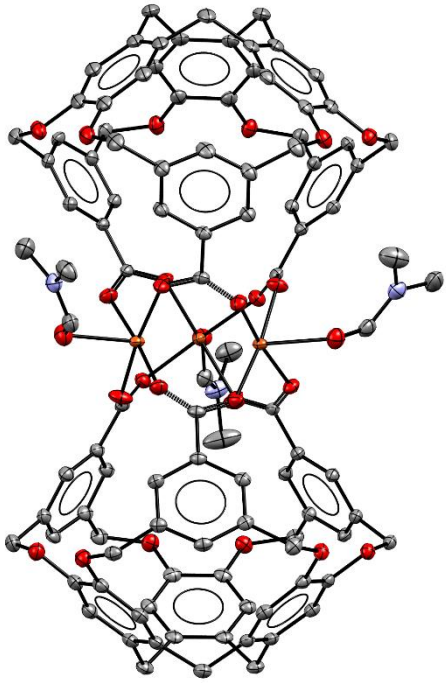

**Figure 78.** Solid state structure of tripodal carboxylate copper complex.[207]

Preparation of hexol **260** worked well but the subsequent substitution with bis-benzyl bromide **261** gave only low yield of the desired compound **262**. The poor solubility of compound **262** and the base sensitivity of DMF leave room for improvement. Simple solvent change to dimethylacetamide and introducing aliphatic chains similar to Tiefenbachers work should give the opportunity to improve the yield.[212, 213] Colorless crystals suitable for single-crystal X-ray diffraction were grown by slow evaporation of a solution of compound **262** in $CH_2Cl_2$ at ambient temperature. The cavity is occupied by a molecule of water and the bromide substituted aryl rings are orientated inward/outward, highlighting the flexibility of the linker. Several different halogen-metal exchange conditions with compound **262** were tested but failed, after quenching with diphenylchlorsilane, to give the desired product **263** (monitored by HPLC). Again, we observed solubility issues.

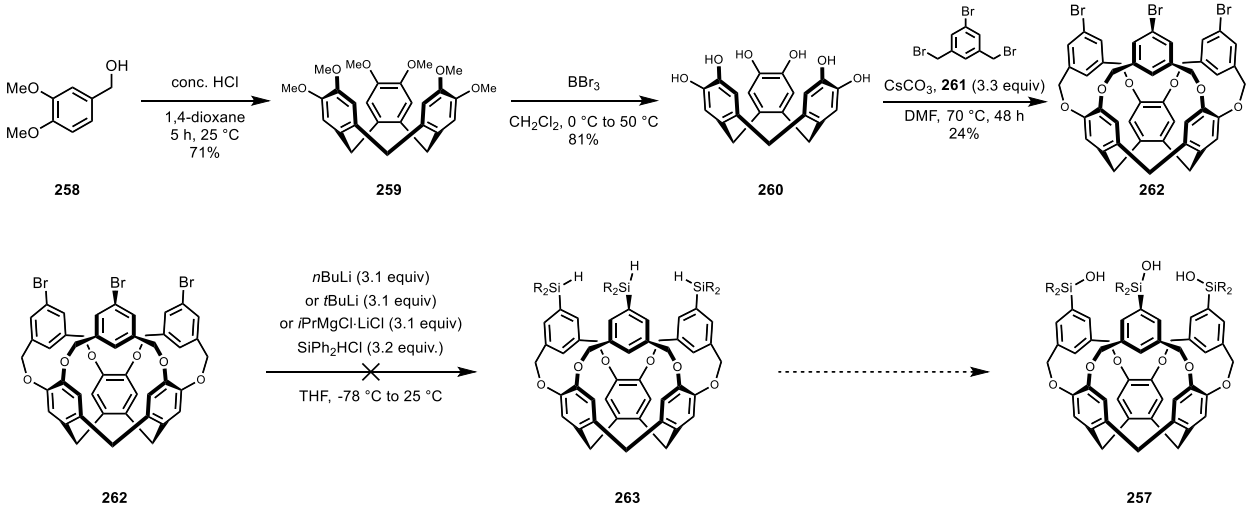


**Scheme 105.** Preparation of tribromide **262** and attempted synthesis of trisilanol **257**.

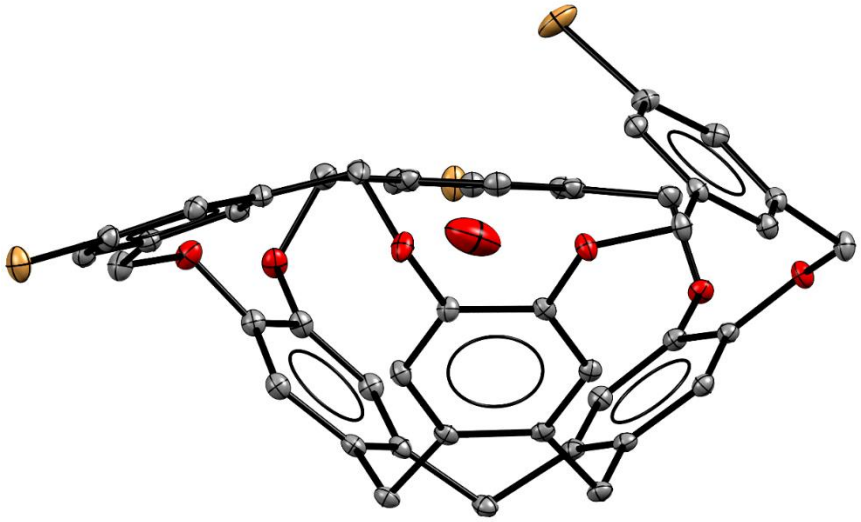

**Figure 79.** Solid state structure of compound **262**·$H_2O$; hydrogen-atoms and free $CH_2Cl_2$ omitted for clarity.

### 3.4.3 Boroxide Ligands for Alkyne Metathesis

The limited number of ligands (alkoxide, siloxide and anilide) for alkyne metathesis catalysts sparked our interest to find a new class of competent ligands. The adaptive ligand properties of silanolates efficiently modulate the frontier orbitals of molybdenum alkylidyne complexes to give excellent catalysts. In accordance, borinic acids feature an empty p-orbital and compete for the oxygen π-bonding. Overall, the Lewis acidic boron atom makes borinic acids weak σ- and π-donors. Although borinic acids are potentially competent ligands, they are difficult to prepare, readily decompose and are rarely used in organic synthesis. Due to the high Lewis acidity, borinic acids are readily attacked by nucleophiles, condensate and decompose by protodeboration.[214] Additionally, the trigonal planar geometry of borinic acids does not guarantee the necessary steric protection of the molybdenum center and may facilitate decomposition once ligated to a metal. One approach to suppress the aforementioned limitations is to make use of sterically encumbered aryl substituents such as mesityl or trip (trip = 2,4,6-triisopropylphenyl). Ligation can be either accomplished by salt metathesis or by protonolysis (**Scheme 106**).[215, 216] Interestingly, Olivier-Bourbigou and co-workers showed by $^{95}$Mo NMR spectroscopy that a single boroxide ligand lowered the electron density of molybdenum based alkene metathesis catalysts.[217]

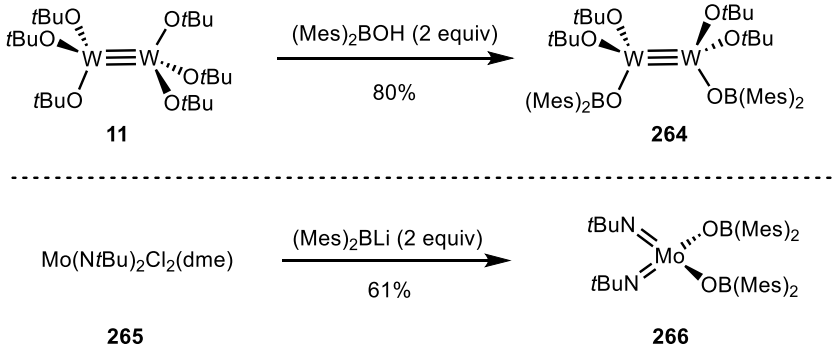


**Scheme 106.** Literature examples of tungsten and molybdenum ligated boroxide complexes.

Previously, treatment of precursor **106** with three equivalents of potassium boroxide afforded complex **267**. Due to isolation problems, ligation to 1,10-phenanthroline gave the corresponding adduct **268** in 41% yield over two steps.[150] However, both complexes **267** and **268** showed low

catalytic activity for alkyne metathesis and readily decomposed in the presence of metal salts (**Scheme 107**).

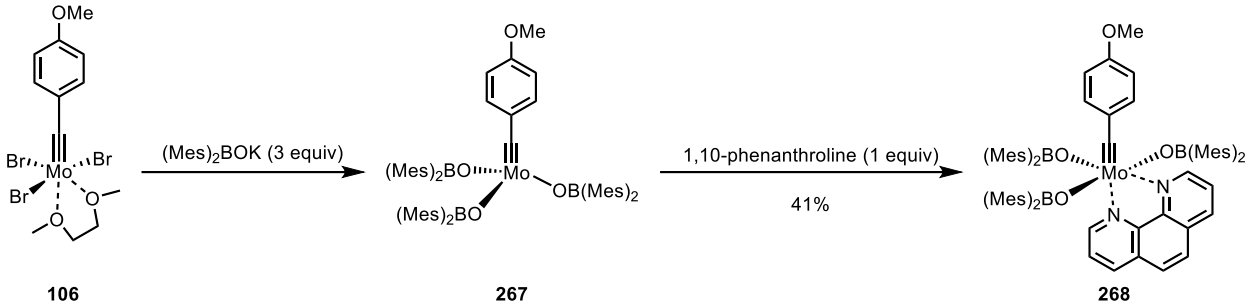


**Scheme 107.** Preparation of boroxide ligated molybdenum alkylidyne complexes.[150]

To circumvent the aforementioned challenges with borinic acids, we envisioned to prepare compound **269**, **270** and **271** with an additional donor site in order to reversibly occupy the empty p-orbital, increase the stability and modulate the donor properties of the borinic acid. Moreover, our protonolysis protocol could also be advantageous in this case (**Scheme 108**).

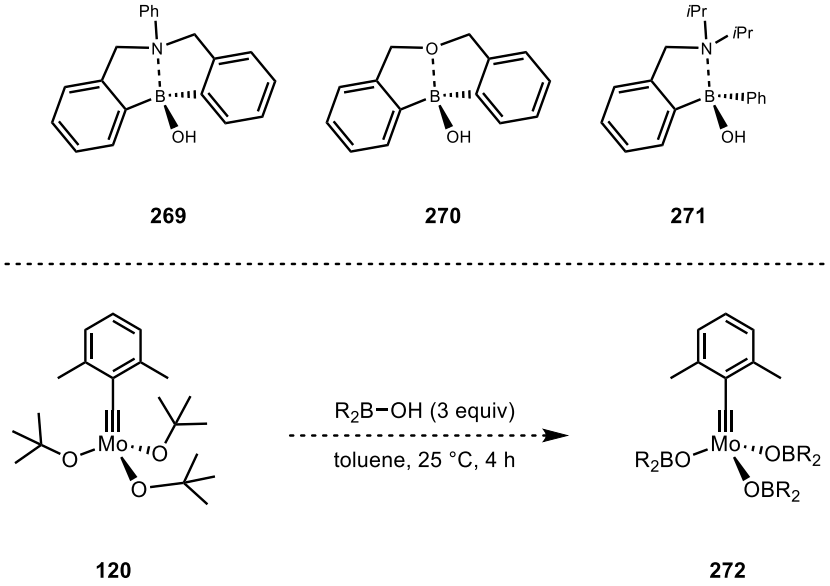


**Scheme 108.** New approach for the preparation of molybdenum alkylidyne complexes endowed with boroxide ligands.

Wang and co-workers reported on the preparation of **274** by treatment of compound **273** with butyl lithium and quenching with TipB(OMe2) (Tip = 2,4, 6-triisopropylphenyl).[218]

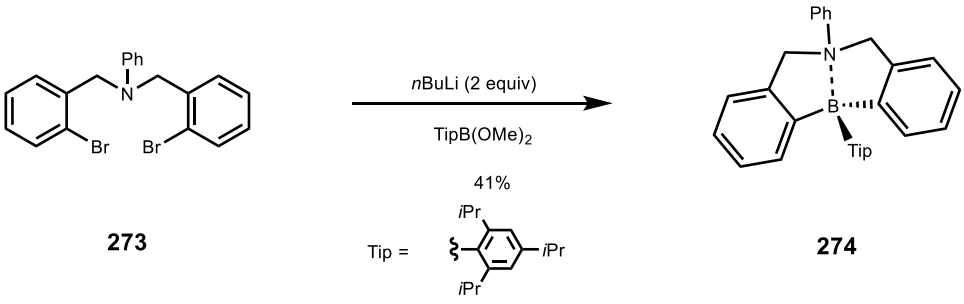


**Scheme 109.** Preparation of compound **274**.[218]

The solid state structure of **274** confirmed the desired B/N Lewis pair adduct with a B–N bond distance of 1.808(2) Å (**Figure 80**).

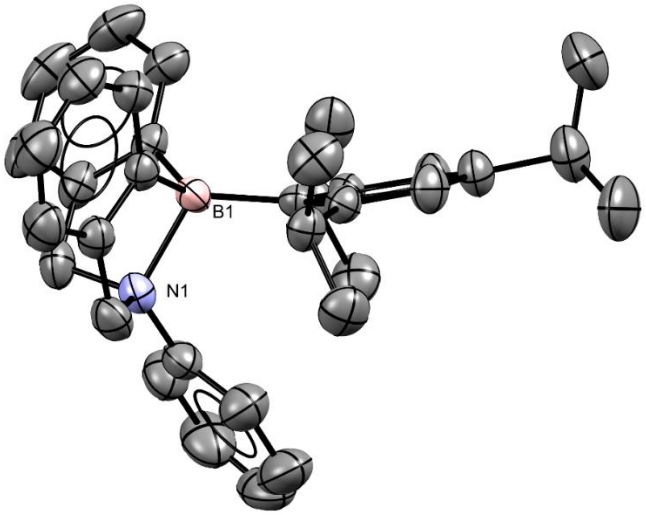


**Figure 80.** Solid state structure of **274**.[218]

Similarly, we treated compound **273** with *n*BuLi and quenched with either trimethyl borate, triethyl borate or boron trichloride. After aqueous work-up, we did not obtain the desired borinic acid **275** (**Scheme 110**).

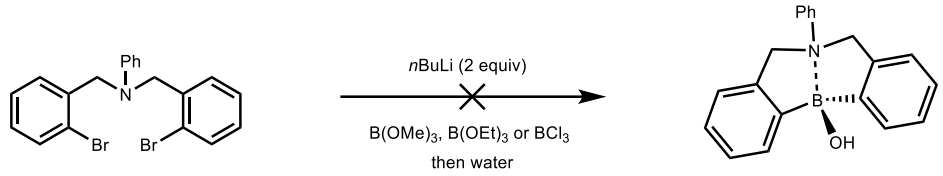


**273** **275**

**Scheme 110.** Attempted synthesis of borinic acid **275**.

In accordance with the work of Pucheault and co-workers, treatment of **273** with amine-borane complex, catalytic amount of phenyl magnesium bromide and excess magnesium gave bench-stable compound **276** in 30% yield. [219]

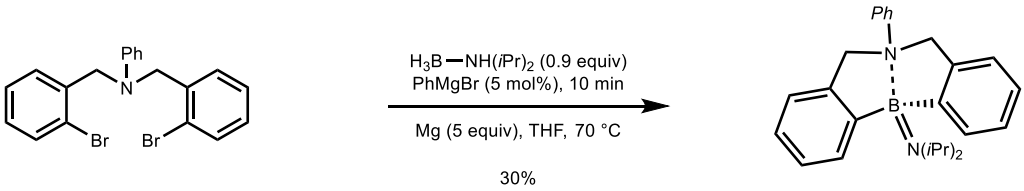


**273** **276**

**Scheme 111.** Preparation of compound **276**.

Colorless crystals suitable for single-crystal X-ray diffraction were grown by slow evaporation of a solution of **276** in $CH_2Cl_2$ at ambient temperature. The B–N2 bond distance of 2.567(2) Å is significantly elongated and signifies a weaker B/N2 Lewis pair adduct. This goes along with the "double" bond character of the very short B–N1 bond distance of 1.405(2) Å and the trigonal planar coordination geometry of the N(*i*Pr)$_2$ unit (**Figure 81**).

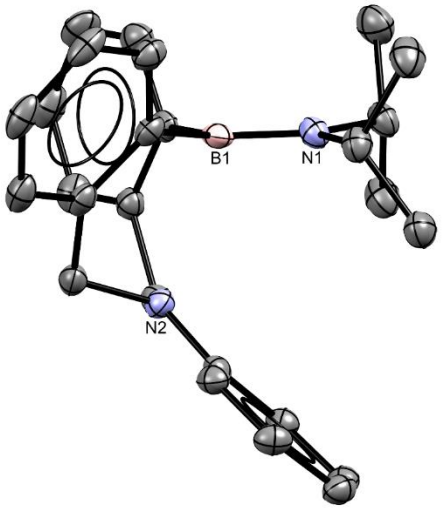


**Figure 81.** Solid state structure of compound **276**.

However, the reported hydrolysis conditions did not afford the desired borinic acid **277**.[219, 220] A more systematic investigation into the hydrolysis conditions is recommended.

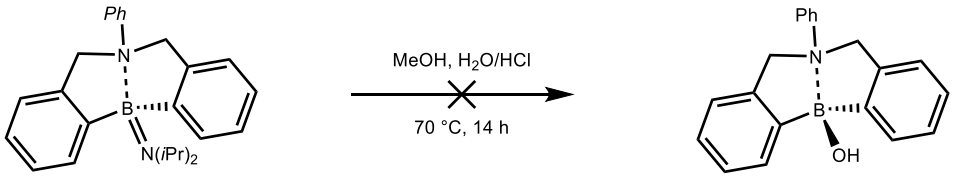


**276** **277**

**Scheme 112.** Failed hydrolysis to form borinic acid **277**.

Tetrahedral borinic acid **279** could be accessible by lithiation of precursor **278**, quenching with commercially available dichlorophenylborane and subsequent hydrolysis (**Scheme 113**). Minoura and co-workers prepared the corresponding borinic acid **281** and confirmed the tetrahedral geometry by X-Ray analysis (**Figure 82**).[221]

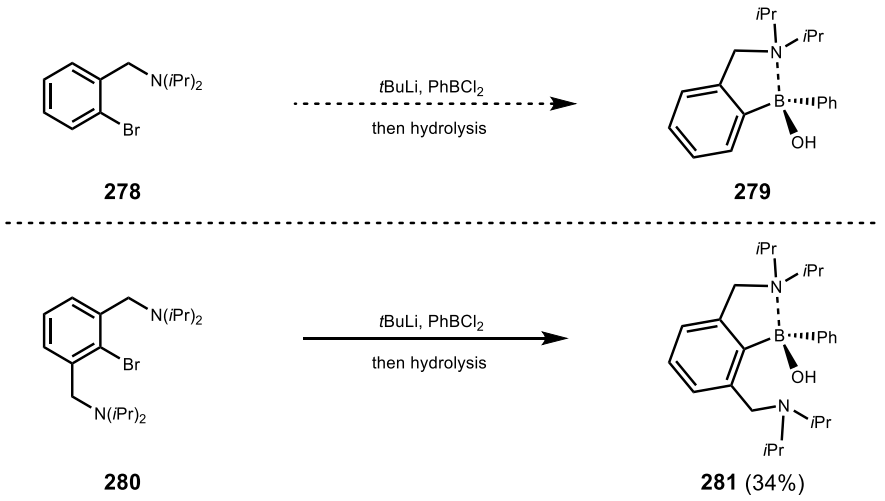


**Scheme 113.** Proposed synthesis of borinic acid **279** and relevant literature precedence.

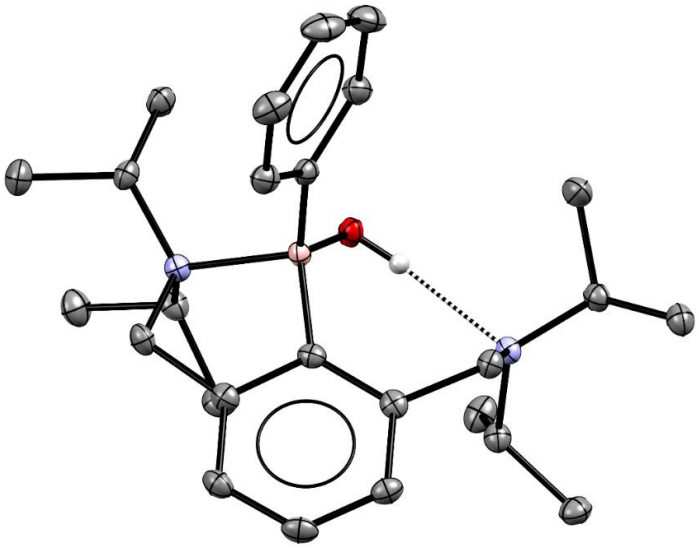

**Figure 82.** Solid state structure of literature-known borinic acid **281**.[221]

### 3.4.4 Future Directions

Inspired by tripodal carboxylate ligands for first-row transition metals (**Figure 83**),[222] another conceivable tripodal ligand design is depicted in **Scheme 114**.

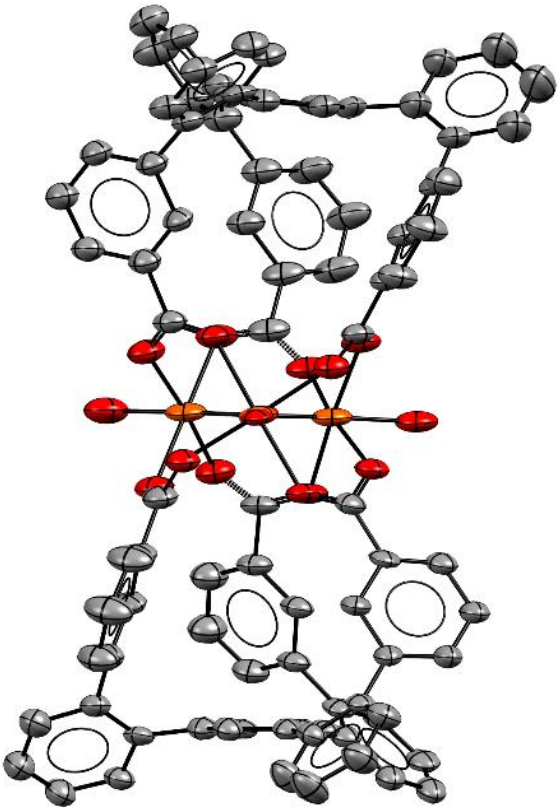

**Figure 83.** Solid state structure of tripodal carboxylate iron complex.[222]

Compound **285** can be prepared by a literature-known procedure starting from the tribromide **282**. Exhaustive lithiation of **285** and quenching with an electrophile gives access to trisilanol **286**.[223]

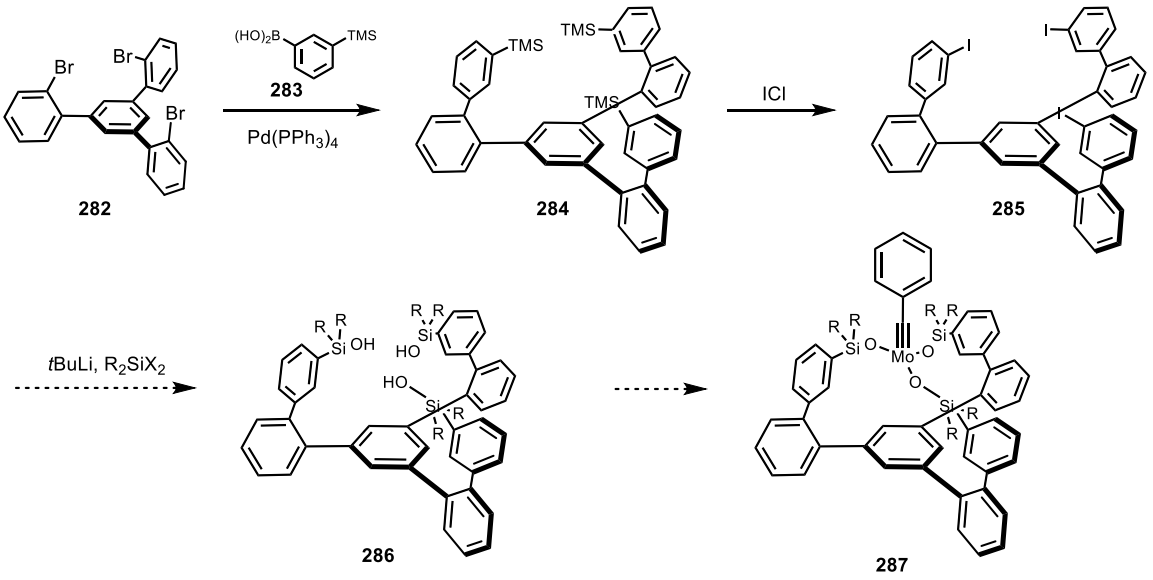


**Scheme 114.** Proposed synthetic procedure to access trisilanol **286** and complexation to molybdenum alkylidyne.

Another trisilanol **292** can be prepared in four steps by the depicted route in **Scheme 115**. The solid state structure of **292** shows the desired "upward/inward"-orientation of all three Si–OH groups (**Figure 84**). The $C_3$-symmetric conformation is stabilized by a hydrogen-bonding array and sets the necessary level of preorganization to form a well-defined podand complex. The actual complexation has not been tried yet.

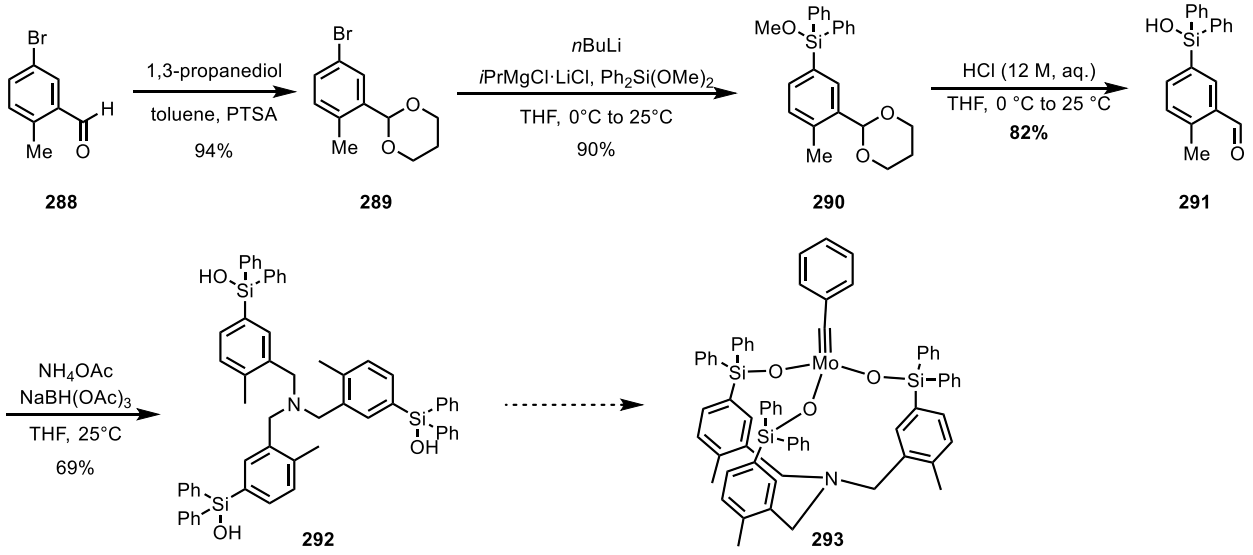


**Scheme 115.** Preparation of trisilanol **292** with Christian Wille and Dr. Takahiro Fukino.

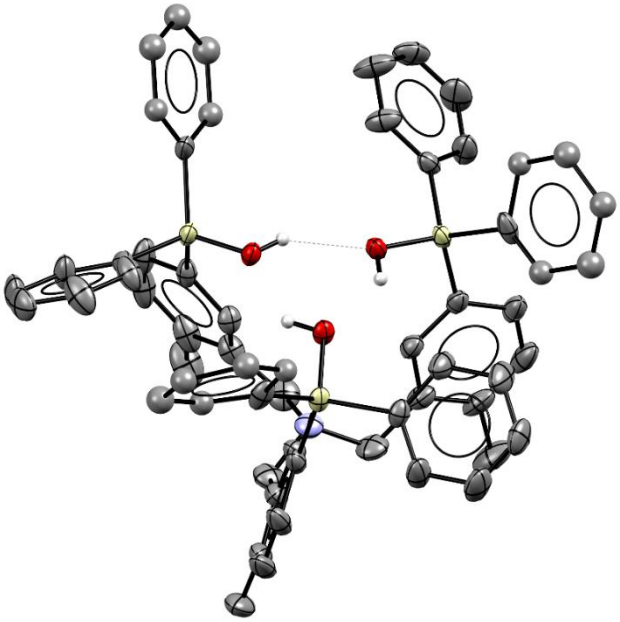

**Figure 84.** Solid state structure of **292**; disorder omitted for clarity; only H-atoms involved in hydrogen bonding are shown.

# 4 Summary

In recent years, molybdenum alkylidyne catalysts with triphenylsilanolate ligands set new standards in the field of alkyne metathesis. However, important limitations remained. Catalysts of this type are largely unable to cope with protic functional groups such as unprotected alcohols and sterically congested substrates. Several approaches to address this issue by developing a molybdenum alkylidyne complex with a tripodal ligand framework failed to give well-defined complexes (**Scheme 116**).

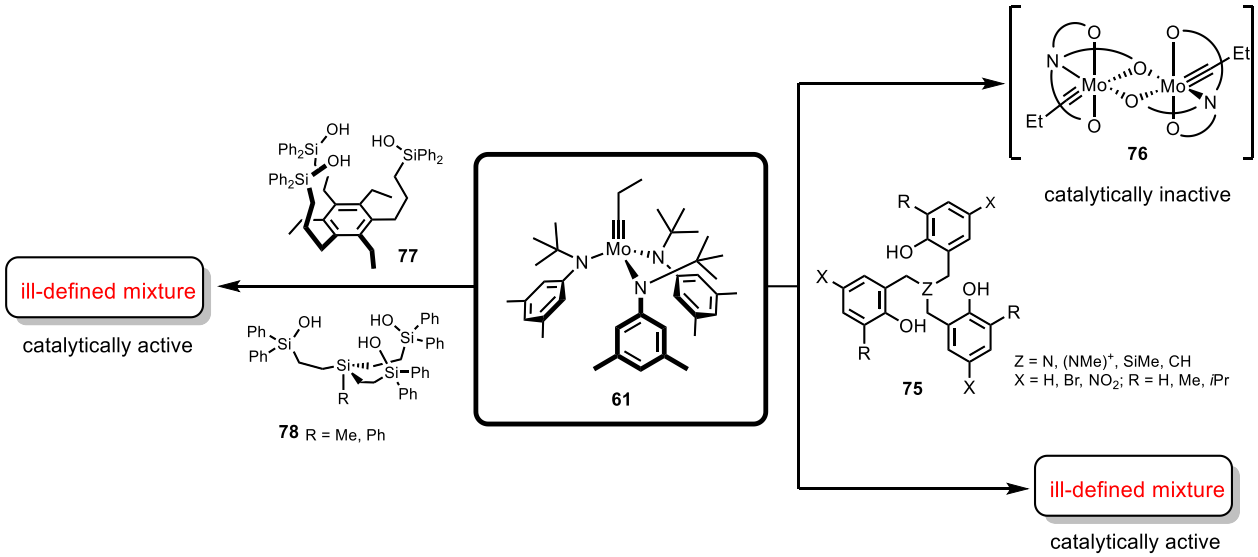


**Scheme 116.** Previous attempts to prepare well-defined molybdenum alkylidyne complexes.

Herein, we report a new generation of structurally well-defined molybdenum alkylidyne catalysts with a tripodal ligand framework for alkyne metathesis. The scalable and modular ligand design allowed us to prepare a library of different tripodal ligands and to study the steric and electronic impact on the catalytic activity (**Scheme 117**). The desired preorganized and $C_3$-symmetric geometry of trisilanol **126** was confirmed by X-ray crystallography. With regard to the actual complexation reaction, we developed a more practical precatalyst **107**, which is readily accessible on scale and improved the isolation of the desired tripodal catalysts.

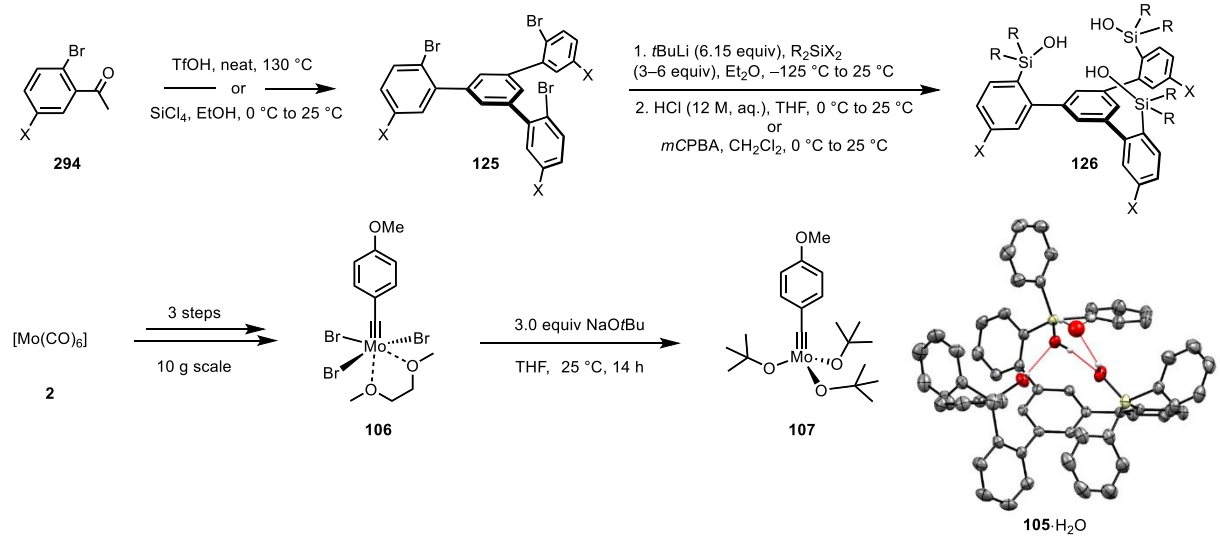


**Scheme 117.** Ligand and molybdenum precatalyst **107** synthesis on gram scale; solid state structure of ligand **105**·$H_2O$.

Stirring of a solution of precatalyst **107** and triarylsilanol **105** in toluene at ambient temperature gave complex [**108**]$_2$ (**Scheme 118**). VT NMR and DOSY NMR studies confirmed the notion of an equilibrium between monomer **108** and aggregate [**108**]$_2$, which is likely dimeric. The monomeric molybdenum alkylidyne structure was confirmed in the form of adduct **108**·MeCN.

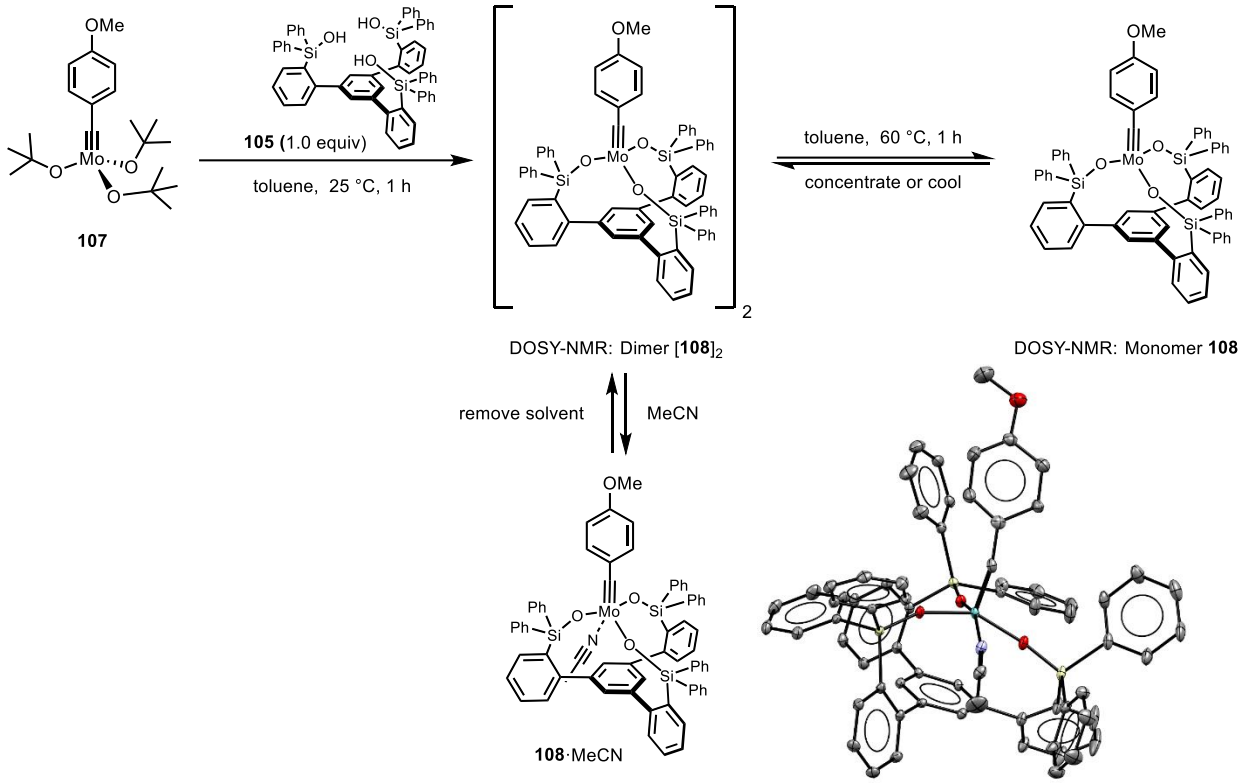


**Scheme 118.** Preparation of structurally well-defined alkyne metathesis catalyst **108** and solid state structure of **108**·MeCN.

Similarly, reaction of precatalyst **107** and triarylsilanol **112** gave a mixture of monomeric complex **116** and aggregate [**116**]$_2$ (**Scheme 119**). Surprisingly, addition of pyridine gave the tetrameric pyridine adduct [**116**·py]$_4$. Removal of excess pyridine *in vacuo*, released monomeric complex **116** and provided compelling evidence that this process is reversible. The crystal structure of tetrameric molybdenum alkylidyne complex [**116**·py]$_4$ provided experimental evidence for the likelihood that tripodal ligand spheres can covalently cross-link to give well-defined tetramers such as [**116**·py]$_4$.

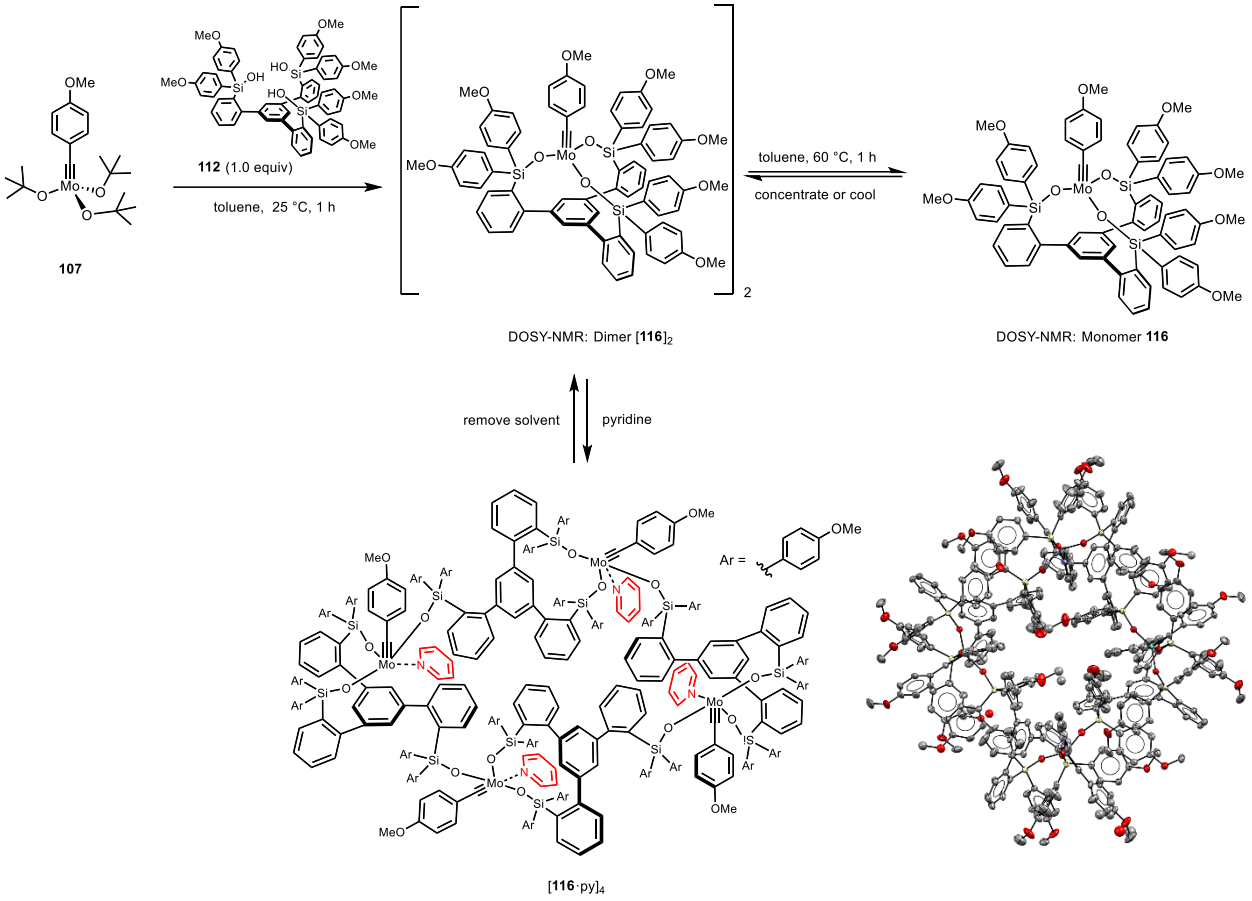


**Scheme 119.** Preparation of structurally well-defined alkyne metathesis catalyst **116** and isolation of tetrameric [**116**·py]$_4$; solid state structure of [**116**·py]$_4$.

In order to circumvent this aggregation issue, we substituted the *ortho*-benzylidyne protons with sterically bulky groups or replaced the phenyl groups on the silanolate ligand. Indeed, stirring of a solution of precatalyst **120** and triarylsilanol **105** gave complex **124**. The monomeric composition was confirmed by DOSY NMR and X-ray structure analysis (**Scheme 120**).

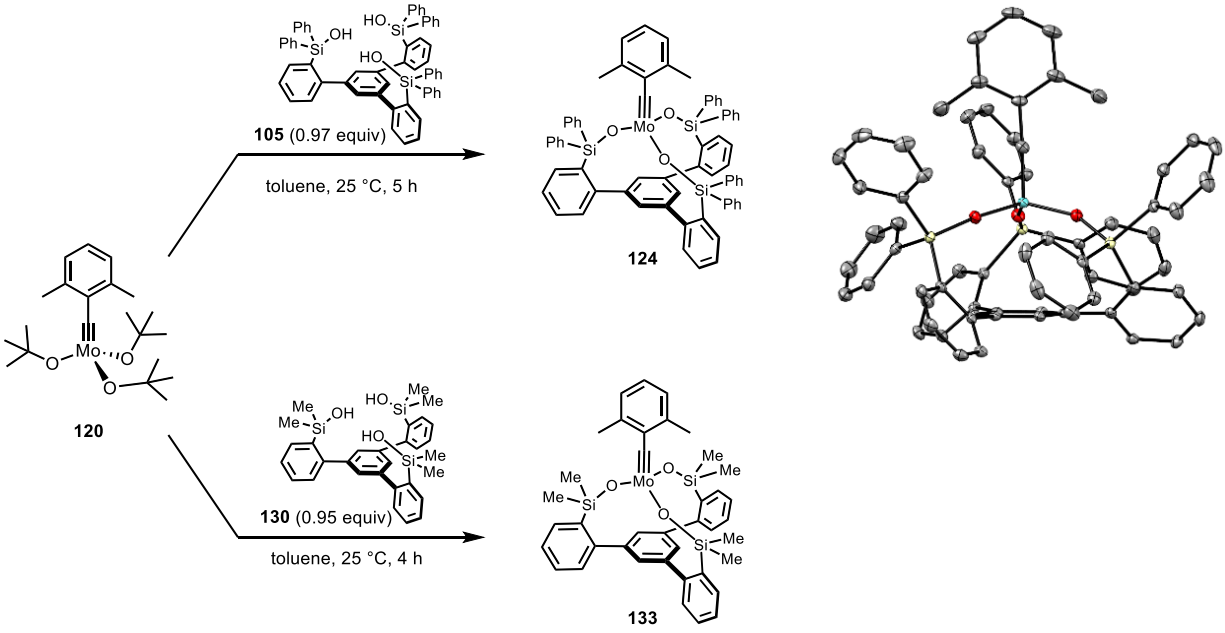


**Scheme 120.** Preparation of the well-defined monomeric complex **124** and **133**; solid state structure of **124**.

The newly developed protocol enabled us to prepare a library of tripodal molybdenum alkylidyne complexes and to investigate the critical parameter for efficient alkyne metathesis. Previously, $^{95}$Mo NMR spectroscopy has been rarely used for analytical purposes in organometallic chemistry. Herein, we uncovered the full potential of $^{95}$Mo NMR spectroscopy and demonstrated its application to catalyst design. Chemical shift tensor analysis of the alkylidyne carbon atom revealed an increased electrophilicity imparted by the tripodal ligand sphere. Benchmarking of the catalytic activity with a series of different catalysts showed that catalyst **133** with a methyl substituted silanolate ligand is by far the most active catalyst in the entire new series (**Scheme 120**). Since the influence of the different ligand spheres on the catalytic activity was dramatic, we sought to investigate this aspect in more detail. Intriguingly, addition of excess 3-hexyne either formed a metallacyclobutadiene **154** with $Ph_3SiO$ ligands or a metallatetrahedrane **147** with tridentate ligand **105**. Molybdenacyclobutadienes are scarce in the literature and the poor quality of X-ray data of competent alkyne metathesis catalysts precluded a detailed structure analysis. It is therefore remarkable that we obtained the solid state structure of molybdenacyclobutadiene **154**, derived from a very active alkyne metathesis catalyst, in good quality (**Scheme 121**).

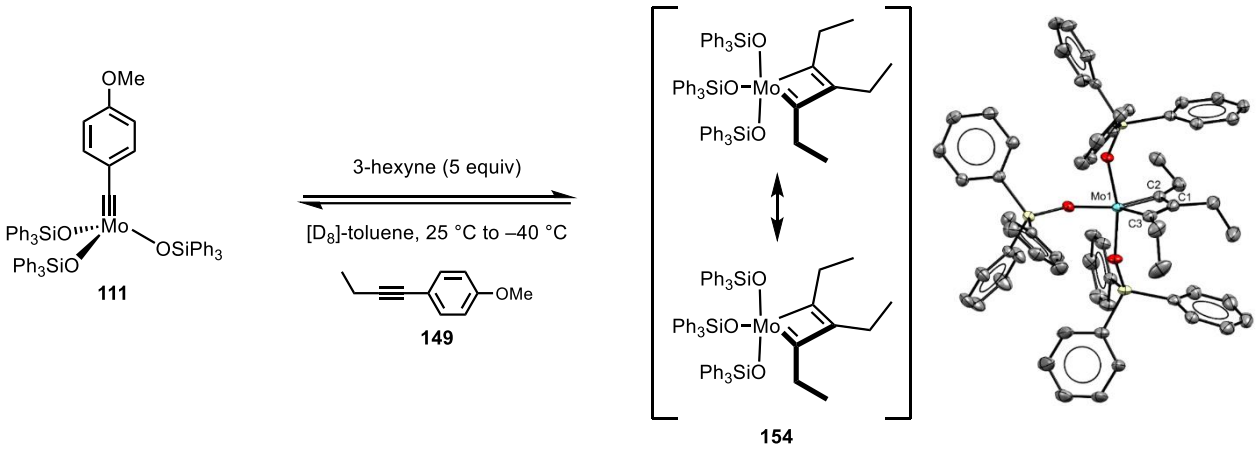


**Scheme 121.** Formation of molybdenacyclobutadiene complex **154** and solid state structure thereof.

Yet, the alkyne itself played a vital role in determining which intermediate is formed and observable. Addition of excess 2-butyne to a solution of complex **108** in [$D_8$]-toluene gave a mixture of molybdenatetrahedrane **155** and molybdenacyclobutadiene **156** (**Scheme 122**). An EXSY NMR study proved that both intermediates are interconverting.

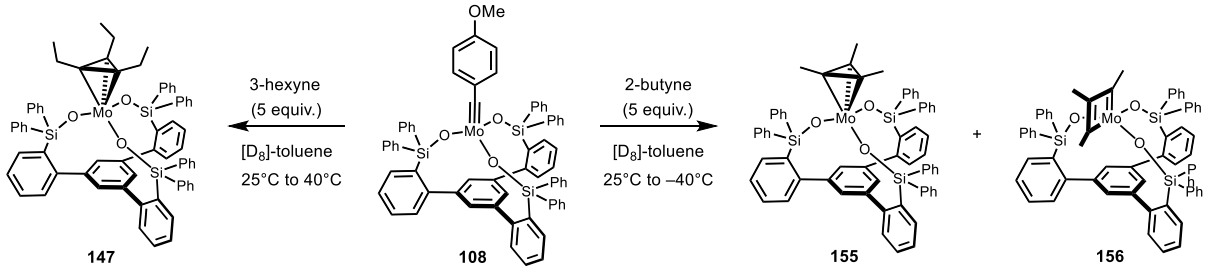


**Scheme 122.** Formation of molybdenacyclobutadiene **156** and molybdenatetrahedrane **155**.

Moreover, we noticed that the $C_\alpha/C_{\alpha'}$ atoms of the metallacyclobutadiene complex **156** are inequivalent and exchanging on the NMR timescale, which was interpreted as interconversion of the two tautomers. In consequence thereof, both tautomeric molybdenacyclobutadiene forms need to overcome an energetic barrier to release the product. A pseudorotation for productive alkyne metathesis with canopy catalysts is necessary and a revisited mechanism is proposed (**Scheme 123**).

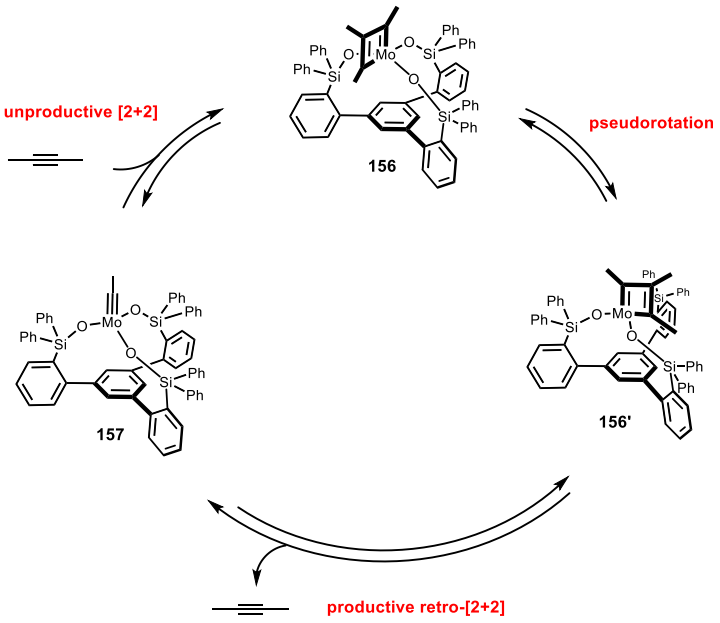


**Scheme 123.** Revised alkyne metathesis mechanism for canopy catalysts.

The newly developed catalysts show an unrivaled functional group tolerance, tolerate protic functional groups such as unprotected alcohols and entail even a certain stability towards water. Furthermore, the excellent application profile has been demonstrated by application to challenging ring-closing alkyne metathesis reaction leading to polyfunctionalized (natural) products (**Scheme 124**). Overall, this work is deemed to mark an important milestone in the field of alkyne metathesis.

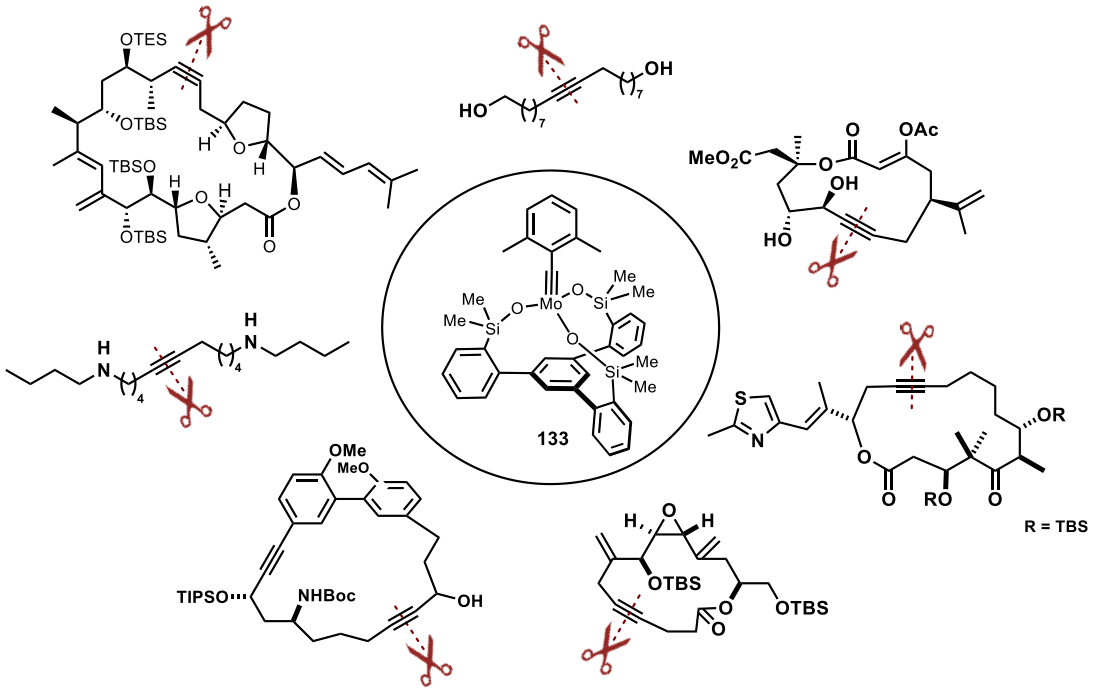


**Scheme 124.** Application profile of canopy catalysts.

In the second part of this work, we extended the coverage to tripodal tungsten alkylidyne complexes and developed a new competent tungsten-based catalyst for alkyne metathesis that outperformed the classical Schrock catalyst. Again, we took advantage of the 2,6-dimethylbenzyldiyne substitution,

which turned out to be ultimately important to form monomeric tungsten alkylidyne complexes. Stirring of a solution of precatalyst **201** and triarylsilanol **105** in toluene gave complex **202** (**Scheme 125**).

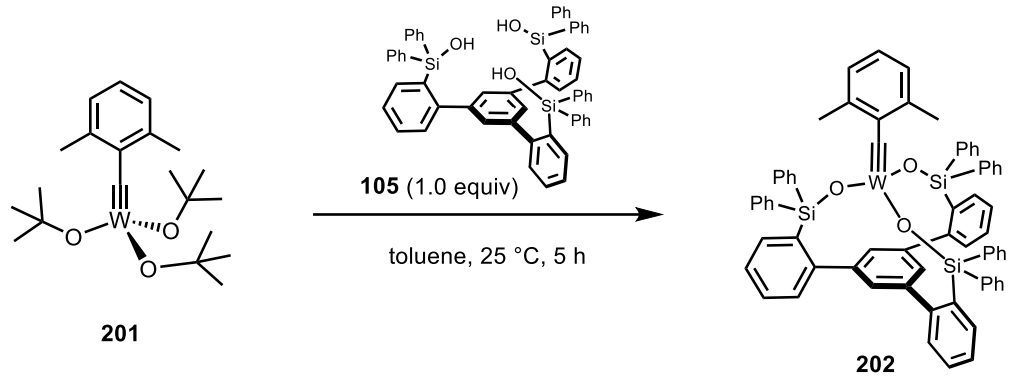


**Scheme 125.** Preparation of tungsten alkylidyne complex **202**.

However, complex **202** is not a competent catalyst for alkyne metathesis. In contrast to the analogous molybdenum complex, treatment with excess 3-hexyne resulted in the formation of the mixed tungstenacyclobutadiene complex **203**, which could be isolated and characterized by NMR spectroscopy and crystal structure analysis (**Scheme 126**). As evident by the slow conversion to the "all-ethyl" substituted metallacyclobutadiene complex **204**, the tungsten center is too Lewis acidic in that the release of alkyne becomes rate-limiting. This experiment provided compelling evidence that tripodal silanolate ligands give catalytically incompetent tungsten complexes for alkyne metathesis.

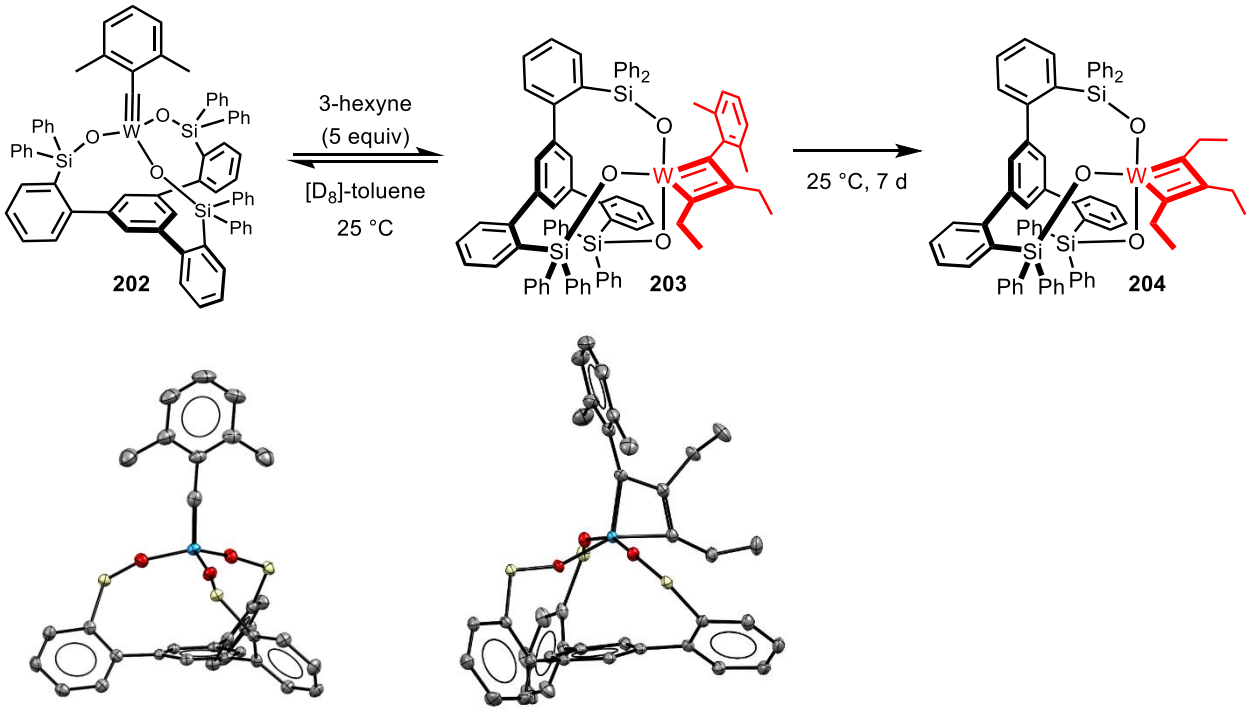


**Scheme 126.** Formation of mixed and tri-ethyl substituted tungstenacyclobutadiene complexes; truncated solid state structure of tungsten alkylidyne complex **202** and mixed tungstenacyclobutadiene complex **203**.

In accordance to the tripodal molybdenacyclobutadiene complex **156**, we noticed that the $C_{\alpha}/C_{\alpha'}$ atoms of the tungstenacyclobutadiene complex **204** are inequivalent and exchanging on the NMR timescale, which was interpreted as interconversion of the two tautomers. The activation parameters

were deduced from line-shape analysis and Eyring plots ($\Delta H^{\ddagger}$ = 13.6±0.1 kcal·mol$^{-1}$, $\Delta S^{\ddagger}$ = 1.24±0.29 cal·mol$^{-1}$·K$^{-1}$) and support the proposed intramolecular isomerization. Interestingly, only the $C_{\alpha}/C_{\alpha'}$ positions gave broad/dynamic $^{1}$H NMR signals, whereas $C_{\beta}$ gave sharp rather static signals. Hence, the intermediate structure for the interconversion of **204** is not $C_3$-symmetric and therefore excludes a metallatetrahedrane as transient intermediate. A library of different tripodal silanolate and literature-known catalysts was prepared and their activity tested with simple homo-metathesis reactions. Disappointingly, all tested complexes gave similarly poor results. 2D-$^{1}$H, $^{183}$W HMBC experiments revealed that tripodal silanolate ligands upregulate the Lewis acidity of tungsten alkylidyne complexes, in that the tungstenacyclobutadiene intermediate gets over-stabilized and catalytic activity is shut down. To overcome this fundamental mismatch, we developed the more strongly donating tripodal alkoxide ligand **213**, which gave upon complexation tripodal tungsten catalyst **214** (**Scheme 127**). Indeed, the $^{183}$W nucleus of **214** was strongly shielded, and bearing witness for an overall stronger donor character, which was further supported by chemical shift tensor analysis.

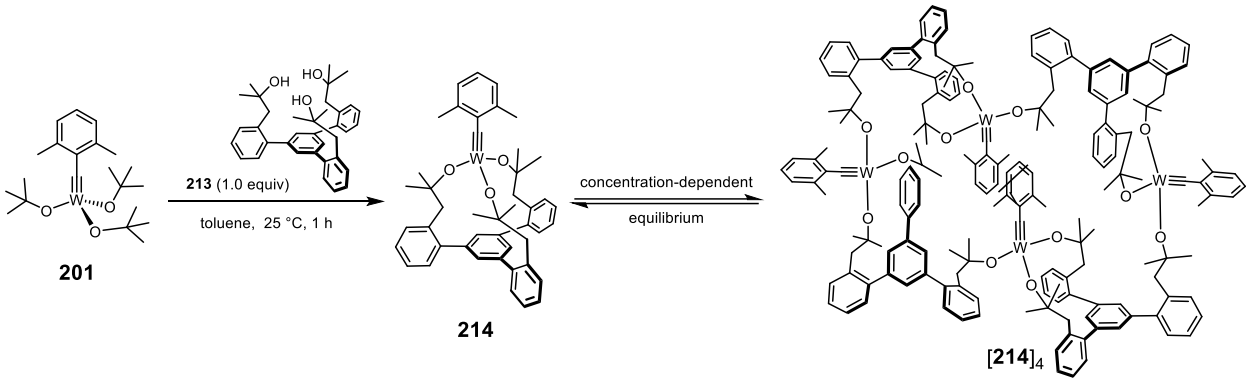


**Scheme 127.** Preparation of tungsten catalyst **214** and concentration-dependent formation of [**214**]$_4$.

Under catalytic conditions only monomeric complex **214** was present, whereas higher concentrations favored the tetrameric complex [**214**]$_4$. The solid state structure of [**214**]$_4$ was confirmed by X-ray diffraction (**Figure 85**). The newly developed tripodal tungsten catalyst **214** outperformed all tungsten-based catalysts known to date in terms of activity and selectivity, and gave promising results for several demanding ring-closing alkyne metathesis reactions.

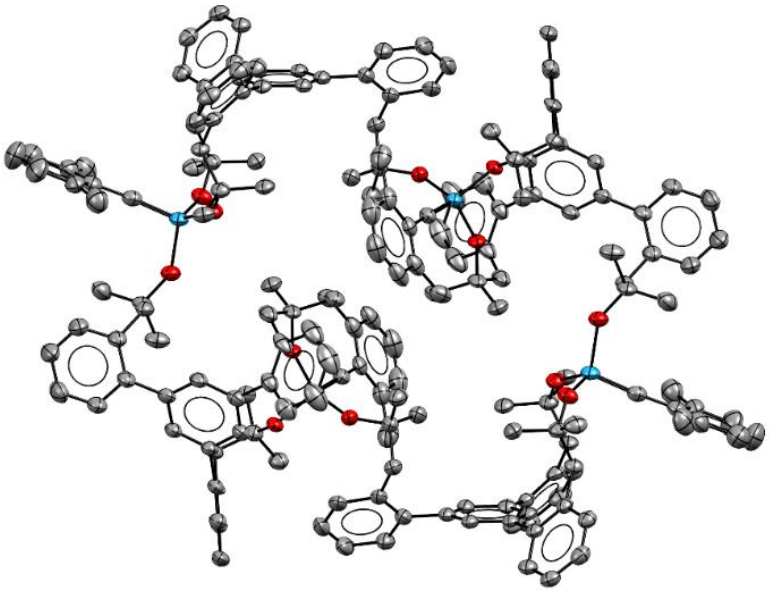

**Figure 85.** Solid state structure of [**214**]$_4$.

In the third chapter we report on the isolation of the first monomeric, homoleptic, five-coordinated alkoxide, non-oxo $4d^1$ Mo(V) complex. High-valent molybdenum complexes endowed with alkoxide ligands are prone to dimerize and/or form molybdenum-oxo complexes. [Mo(O*t*Bu)$_5$] (**222**) represents the first example of an entirely new class of high-valent $d^1$ molybdenum complexes (**Figure 86**).

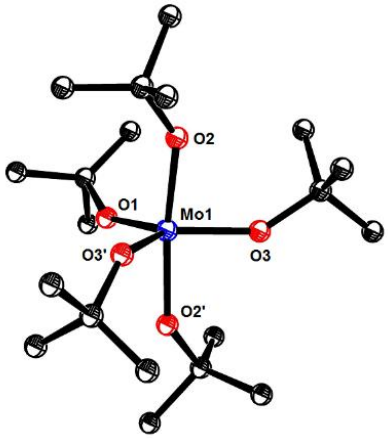


**Figure 86.** Solid state structure of [Mo(OtBu)$_5$] (**222**).

[Mo(O*t*Bu)$_5$] (**222**) was formed together with the well-known [Mo$_2$(O*t*Bu)$_6$] (**218**) complex by disproportionation of [MoCl$_4$(THF)$_2$] (**221**) in the presence of three equivalents of sodium *tert*-butoxide (**Scheme 128**).

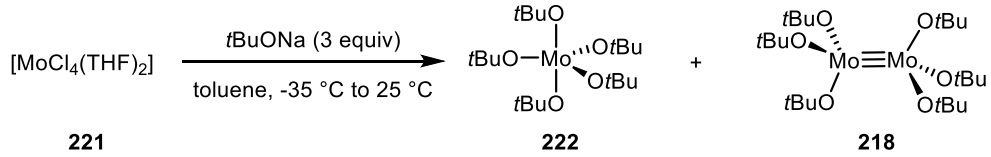


**Scheme 128.** Alkoxide-promoted disproportionation of [MoCl$_4$(THF)$_2$] (**221**).

This result was surprising since the alkoxide substitution of [MoCl$_4$(THF)$_2$] (**221**) has previously been reported to give [Mo(O*t*Bu)$_4$] (**229**). Several independent runs with either NaO*t*Bu or LiO*t*Bu invariably gave [Mo(O*t*Bu)$_5$] (**222**) and [Mo$_2$(O*t*Bu)$_6$] (**218**) as judged by $^1$H, $^{13}$C and $^{95}$Mo NMR spectroscopy (**Scheme 129**). Similarly, the reported protonolysis of tetrakis(dimethylamide)molybdenum(IV) (**230**) with *tert*-butyl alcohol to form [Mo(O*t*Bu)$_4$] (**229**) only gave, in our hands, [Mo(O*t*Bu)$_5$] (**222**) and the new dinuclear complex **231** (**Figure 87**).

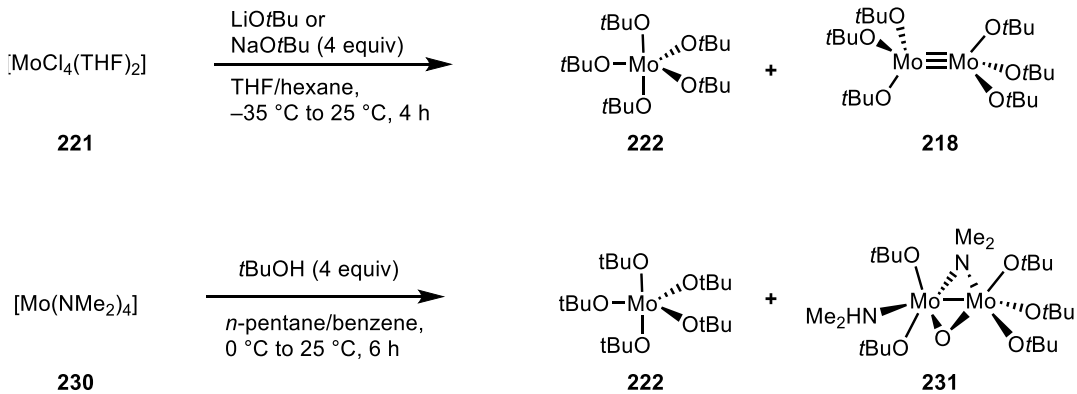


**Scheme 129.** Attempted salt metathesis and protonolysis reaction described in the literature.

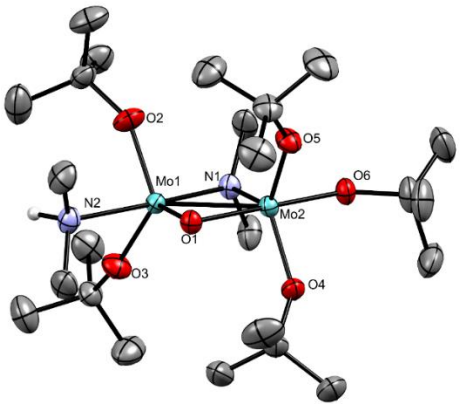


**Figure 87.** Solid state structure of dinuclear complex **231**; hydrogen atoms, except for the NH atom and disorder omitted for clarity.

Finally, we confirmed the propensity of $[MoCl_4(THF)_2]$ (**221**) to disproportionate. In the absence of alkoxides, $[MoCl_4(THF)_2]$ (**221**) disproportionated in $CH_2Cl_2$ solution over 4 days at 25 °C to give complex $[MoOCl_3(THF)(H_2O)]$ (**232**) and dimeric $[Mo_2Cl_6(THF)_3]$ (**233**) (**Scheme 130**).

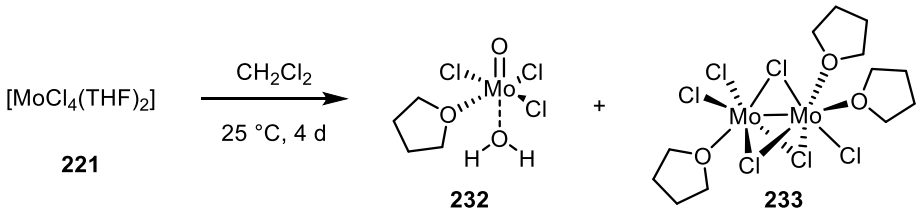


**Scheme 130**. Disproportionation of Mo(IV) in the absence of alkoxides.

Both complexes occupy the same unit cell and hence provided proof for the inherent instability of Mo(IV) (**Figure 88**).

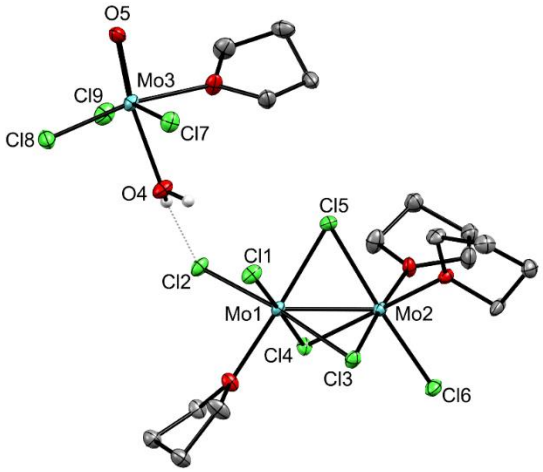


**Figure 88.** Unit cell occupied by $[MoOCl_3(THF)(H_2O)]$ (**232**) and $[Mo_2Cl_6(THF)_3]$ (**233**).

Treatment of $[MoCl_3(MeCN)_3]$ (**243**) with three equivalents of sodium *tert*-butoxide in acetonitrile yielded $[N{\equiv}Mo(O\mathit{t}Bu)_3]$ (**223**) as the major product (**Scheme 131**), the structure of which was confirmed by crystal structure analysis (**Figure 89**).

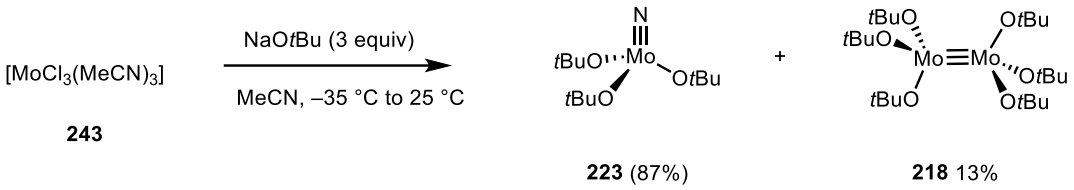


**Scheme 131.** Acetonitrile activation by Mo(III) alkoxide complex.

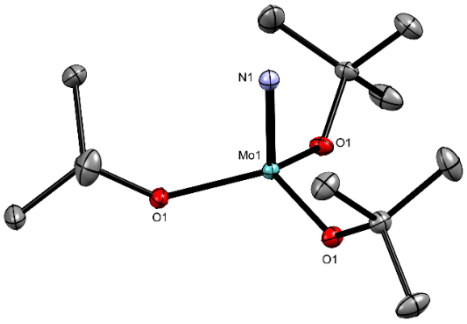


**Figure 89.** Solid state structure of Mo(VI) nitrido complex **223**.

Previously, low-valent Mo(III) alkoxide complexes have not been sterically encumbered enough to suppress dimerization and their reactivity for small molecule activation remained unknown. Intriguingly, the molybdenum nitrido complex was formed by the direct activation of acetonitrile by a transient low-valent Mo(III) alkoxide complex.

# 5 Experimental Section

## 5.1 General Experimental Methods

Unless stated otherwise, all reactions were carried out under Ar in flame-dried glassware. The solvents used were purified by distillation over the drying agents indicated and were transferred under Ar: THF (Na/K), $Et_2O$ (Na/K), DME ($CaH_2$), $CH_2Cl_2$ ($CaH_2$), MeCN ($CaH_2$), *n*-pentane (Na/K), benzene (Na/K), toluene (Na/K), *t*BuOH ($CaH_2$). Flash chromatography on silica gel (FC): Merck silica gel 60 (230–400 mesh). All commercially available compounds (Fluka, Lancaster, Aldrich) were used as received, unless stated otherwise. The molecular sieves used in this investigation were dried for 24 h at 150°C (sand bath) under vacuum prior to use and were stored and transferred under argon atmosphere.

NMR: Spectra were acquired on Bruker AvanceIII 300, 400, 500 MHz or Avance Neo 600 MHz NMR spectrometers in the solvents indicated; chemical shifts (δ) are given in ppm relative to TMS, coupling constants (*J*) in Hz. The solvent signals were used as references and the chemical shifts converted to the TMS scale ($CDCl_3$: $\delta_C \equiv 77.0$ ppm; residual $CHCl_3$ in $CDCl_3$: $\delta_H \equiv 7.26$ ppm; $CD_2Cl_2$: $\delta_C \equiv 53.8$ ppm; residual 1H: $\delta_H \equiv 5.32$ ppm; [$D_8$]-toluene: $\delta_C \equiv 20.7$ ppm; residual $D_5C_6CD_2H$: $\delta_H = 2.09$ ppm).

$^{95}$Mo NMR spectra were acquired with the aring pulse sequence to minimize acoustic ringing from the NMR probe. The π/2 pulse was calibrated for a 2 M $Na_2MoO_4$ in $D_2O$ and had a typical length of 22.5 µs at a power of 85W. Chemical shifts were referenced indirectly to the $^1$H chemical shift of the solvent.[224] For broad signals high sample amount (>40 mg) were necessary. Dependent on the line width of the signal, 8000 to 150000 FID containing 8192 complex data points were averaged to obtain a reasonable signal-to-noise ratio. The acquisition time of a single FID was around 150 ms. The data was Fourier-transformed with zero-filling to 8192 data points and with a line broadening lb = 20 Hz, unless noted otherwise.

$^{183}$W NMR shifts were extracted from the indirect dimension of a $^1$H,$^{183}$W HMBC experiment. For the measurement, a standard Bruker BBFO probe ($^{31}$P-$^{119}$Ag) of a AVIIIHD 400 MHz NMR spectrometer could be tuned to the $^{183}$W resonance frequency (16.67 MHz). The standard parameters for the experiment are shown in **Table 11**:

**Table 11.** Standard parameters for $^1$H,$^{183}$W HMBC experiments.

| | F1 | F2 |
|---|---|---|
| **ULPROG** | hmbcgpndqf | |
| **Nuc1** | 1H | 183W |
| **TD** | 2048 | 512 |
| **Offset (ppm)** | 5 | 500 |
| **SW (ppm)** | 12.98 | 997.4 |
| **CNST13** | 4 | |
| **DS** | 4 | |

| | F1 | F2 |
|---|---|---|
| **NS** | 16 | |
| **GPNAM** | SMSQ10.100 | |
| **GPZ1(%)** | 70 | |
| **GPZ2(%)** | 30 | |
| **GPZ3(%)** | 44.17 | |
| **NUS** | 25% | |
| **Expt** | 16 min 16 sec | |

The π/2 pulse was calibrated for a solution of $Na_2WO_4$ in $D_2O$ (1 M) and had a typical length of 35 µs with a pulse power of 85 W. Data points in the indirect dimension (F1) were sparsely sampled with 25% NUS to reduce the measurement time. A second HMBC (10% NUS) with the same offset O2, but different SW in the indirect dimension was acquired to make sure that the observed peak is not folded. Raw data were Fourier-transformed with zero-filling and linear-prediction in the indirect dimension giving to a total matrix size of 1024 x 1024 datapoints. Unless denoted otherwise 1D $^{183}$W spectra shown in the manuscript were generated from the 2D spectrum as a sum of all slices that contained a $^{183}$W signal. The 1D $^{183}$W spectrum of compound **201** was acquired with a standard ineptrd sequence optimized for the same long range coupling (4 Hz) as the HMBC spectra. Data from AvanceNEO 600 MHz NMR spectrometer was acquired Bruker BBO CryoProbe, which significantly reduced the measurement time of most of the spectra, especially the 1D $^{13}$C spectrum. A good SNR in the $^{13}$C spectra was crucial to extract the $^{183}$W-$^{13}$C coupling constants of the complexes.

Data on the AVneo 600 MHz NMR spectrometer was acquired with a Bruker BBO CryoProbe, which significantly reduced the measurement time of most of the spectra, especially the 1D $^{13}$C NMR data.

Diffusion coefficients were obtained from a double stimulated echo sequence with bipolar gradient pulses, convection compensation, longitudinal eddy current delay (LED) and three spoiler gradients (Bruker sequence: dstebpgp3s). The gradient pulse strength G was incremented from 2% to 98% of the maximum $G_{max}$ with a squared gradient ramp in 60 steps. The diffusion time (Δ) used was 71 ms and the length of a gradient pulse gradient pulse (δ/2) of the encoding gradient was 1.3 ms. The maximum gradient strength $G_{max}$ of the NMR probe (PA BBO 400S1 BBF-H-D-05 Z PLUS) was 53.5 G·cm$^{-1}$. Diffusion coefficients were obtained by averaging three diffusion coefficients obtained from fitting the signal decay of three different resonance integrals to the Stejskal-Tanner equation (I) in the Bruker TOPSPIN T1T2 relaxation module.

$$I(G) = I_0 e^{-D(\gamma G\delta)^2(\Delta-\delta/3)} \qquad \text{(I)}$$

Diffusion values were predicted using an EXCEL spreadsheet Stokes–Einstein Gierer-Wirtz Estimation (SEGWE) method.[146]

IR: Spectrum One (Perkin-Elmer) spectrometer, wavenumbers ($\tilde{\nu}$) in cm$^{-1}$. MS (EI): Finnigan MAT 8200 (70 eV), ESI-MS: ESQ3000 (Bruker), accurate mass determinations: Bruker APEX III FT-MS (7 T magnet) or Mat 95 (Finnigan). Elemental analysis: H. Kolbe, Mülheim/Ruhr.

Measurements of mass spectra were conducted by the mass spectrometry department of the Max-Planck-Institut für Kohlenforschung. EI-spectra were acquired on a Finnigan MAT 8200 (70 eV) or on a Finnigan MAT 8400 (70 eV) spectrometer. ESI-spectra were measured on a Bruker ESQ 3000 spectrometer. All values are given in mass units per elementary charge (m/z). Intensities are given in percent relative to the basis peak. High resolution mass spectra (HRMS) were recorded on a Finnigan MAT 95 spectrometer (EI) or a Bruker APEX III FT-ICR-MS (7 Tesla magnet, ESI).

X-ray diffraction measurements were conducted by the department “Chemical Crystallography and Electron Microscopy” of the Max-Planck-Institut für Kohlenforschung. The measurements were done on a Bruker-AXS X8 Proteum diffractometer.

Melting points were measured in open capillary on a Büchi (B-540) melting point device.

## 5.2 Ligand Preparation

**1,3,4-Tris-2'-bromophenylbenzene (103)**

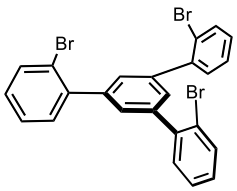


A two-necked, round-bottomed flask was equipped with a magnetic stir bar and a gas inlet connected to an argon-vacuum manifold. The flame-dried flask was filled with argon and charged with a solution of 2-bromoacetophenone (**102**) (20.0 g, 100 mmol) in EtOH (164 mL). The flask was cooled to 0°C and connected to a washing bottle containing aqueous KOH solution. Then silicon tetrachloride (34.5 mL, 301 mmol) was added dropwise over 1 min. The resulting yellow mixture was stirred for 1.5 h at 0°C and then allowed to warm to ambient temperature. After 24 h, the mixture was again cooled to 0°C and the reaction quenched with water (800 mL). The orange-yellow slurry obtained was extracted with $CHCl_3$ (3 x 250 mL). The combined extracts were dried over $MgSO_4$, filtered and concentrated in vacuo. The red syrup obtained was triturated with hexanes (100 mL) and filtered with suction to give the title compound as a yellow flaky solid (16 g, 90%). $^1$H NMR (400 MHz, $CDCl_3$): δ = 7.69 (dd, *J* = 8.0, 1.2 Hz, 3H), 7.50 (s, 3H), 7.46 (dd, *J* = 7.6, 1.7 Hz, 3H), 7.38 (td, J = 7.5, 1.2 Hz, 3H), 7.22 (ddd, *J* = 8.0, 7.4, 1.8 Hz, 3H). $^{13}$C NMR (100 MHz, $CDCl_3$): δ = 141.9, 140.4, 133.2, 131.5, 129.6, 128.9, 127.4, 122.7. The analytical and spectroscopic data are in agreement with those reported in the literature.[143]

**2,2''-Dibromo-5'-(2-bromo-5-fluorophenyl)-5,5''-difluoro-1,1':3',1''-terphenyl (125)[225]**

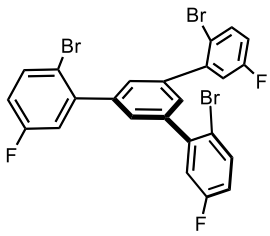


A two-necked, round-bottomed flask was equipped with a magnetic stir bar, a reflux condenser and a gas inlet connected to an argon-vacuum manifold. The flame-dried flask was filled with argon and charged with 2-bromo-5-fluoroacetophenone (**294**) (1.00 g, 4.60 mmol). Trifluoromethanesulfonic acid (0.041 mL, 0.460 mmol) was added dropwise to the neat stirred solution at 25 °C. The mixture was heated with stirring to 140°C for 6 h in a microwave oven. The black mixture was allowed to cool to ambient temperature, the reaction was quenched by adding water (20 mL) and mixture extracted with $CH_2Cl_2$ (3 x 20 mL). The combined organic layers were washed with brine (20 mL), dried over $MgSO_4$, filtered and concentrated *in vacuo*. The residue was purified by flash chromatography on silica gel (hexanes/ethyl acetate, 95:5) to give the title compound as a yellow solid (0.50 g, 55%). $^1$H NMR (300 MHz, $CDCl_3$): δ = 7.65 (dd, *J* = 8.8, 5.3 Hz, 3H), 7.48 (s, 3H), 7.18 (dd, *J* = 9.0, 3.1 Hz, 3H), 6.98 (ddd, *J* = 8.7, 7.8, 3.0 Hz, 3H). $^{19}$F NMR (282 MHz, $CDCl_3$): δ = –115.0. $^{13}$C NMR (100 MHz, $CDCl_3$): δ =162.0 (d, *J* = 248.0 Hz), 143.4 (d, *J* = 8.0 Hz), 134.6 (d, *J* = 8.1 Hz), 118.6 (d, *J* = 23.0 Hz), 117.0 (d, *J* = 3.2 Hz), 116.5 (d, *J* = 22.2 Hz). IR (film): $\tilde{\nu}$ 3067, 2921, 2854, 1876, 1748, 1573, 1594, 1471, 1429, 1405, 1380, 1330, 1256, 1284, 1175, 1195, 1117, 1089, 1069, 1030, 950, 907, 871, 811, 732, 759, 705, 716, 651, 666, 602, 628, 592, 526, 460, 436,419

$cm^{-1}$. HRMS-ESI (m/z): calculated for $C_{24}H_{12}Br_3F_3Na^+$ $[M+Na]^+$, 593.84416; found, 593.84402. The analytical and spectroscopic data are in agreement with those reported in the literature.[225]

***Caution:*** **Pyrophoric materials (*tert*-butyllithium) should be carefully quenched, especially on large scale! Use a 2M solution of isopropanol in heptanes is recommended!**

**(5'-(2-(Methoxydiphenylsilyl)phenyl)-[1,1':3',1''-terphenyl]-2,2''-diyl)bis(methoxydiphenylsilane) (104)**

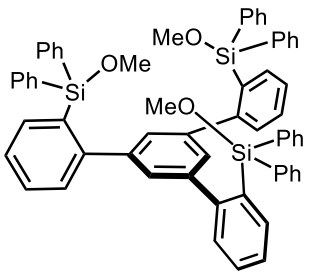


A three-necked, round-bottomed flask was equipped with a magnetic stir bar and a gas inlet connected to an argon-vacuum manifold. The flame-dried flask was filled with argon and charged with 1,3,4-tris-2'-bromophenylbenzene (**103**) (4.00 g, 7.37 mmol). $Et_2O$ (90 mL) was added and the stirred suspension was cooled to −125°C. A solution of *tert*-butyllithium (28.3 mL, 45.3 mmol, 1.7 M in *n*-pentane) was added over 10 min while the suspension was stirring. The mixture was allowed to warm to ambient temperature and stirring was continued for 1.5 h. The obtained brown suspension was again cooled to −125°C and a solution of diphenyldimethoxysilane (5.17 mL, 22.1 mmol) in $Et_2O$ (30 mL) was added dropwise over 15 min. The reaction mixture was allowed to warm to ambient temperature and stirred for 12 h. The reaction was carefully quenched with water and the mixture was transferred into a separation funnel. The organic phase was separated and the aqueous solution was extracted with $CH_2Cl_2$ (3 x 50 mL). The combined organic layers were dried over $MgSO_4$, filtered and concentrated *in vacuo*. Hexanes (50 mL) was added to precipitate the title compound as a white solid (7.53 g, 75%). $^1H$ NMR (500 MHz, $CDCl_3$): δ = 7.62 (dd, *J* = 7.4, 1.4 Hz, 3H), 7.38 (td, *J* = 7.5, 1.5 Hz, 3H), 7.35 (dd, *J* = 7.6, 1.3 Hz, 12H), 7.30 (td, *J* = 7.4, 1.3 Hz, 3H), 7.24 (tt, *J* = 7.4, 1.4 Hz, 6H), 7.14 (t, *J* = 7.5, 7.1 Hz, 12H), 6.98 (dd, *J* = 7.6, 1.3 Hz, 3H), 6.95 (s, 3H), 3.01 (s, 9H). $^{13}C$ NMR (126 MHz, $CDCl_3$): δ = 149.6, 141.5, 137.3, 135.2, 135.1, 131.6, 130.9, 129.6, 129.4, 129.2, 127.5, 125.7, 50.9. $^{29}Si$ NMR (99 MHz, $CDCl_3$): δ = −11.6. IR (film): $\tilde{\nu}$ 3045, 2930, 2830, 1582, 1557, 1471, 1427, 1409, 1263, 1183, 1108, 1082, 998, 877, 830, 760, 735, 697, 621, 499, 477, 411 $cm^{-1}$. HRMS-ESI (m/z): calc'd. for $C_{36}H_{54}O_3Si_3Na^+$ $[M+Na]^+$, 965.32730; found, 965.32862.

**(5,5''-Difluoro-5'-(5-fluoro-2-(methoxydiphenylsilyl)phenyl)-[1,1':3',1''-terphenyl]-2,2''-diyl)bis-(methoxydiphenylsilane) (S1)**

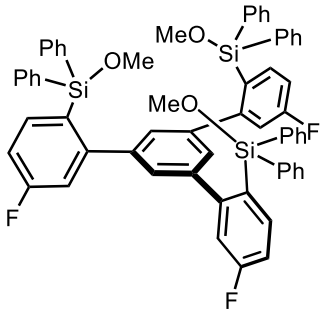


A three-necked, round-bottomed flask was equipped with a magnetic stir bar and a gas inlet connected to an argon-vacuum manifold. The flame-dried flask was filled with argon and charged with 2,2''-dibromo-5'-(2-bromo-5-fluorophenyl)-5,5''-difluoro-1,1':3',1''-terphenyl (**125**) (0.50 g, 0.837 mmol). $Et_2O$ (23 mL) was added and the stirred suspension was cooled to −125°C. A solution of *tert*-butyllithium (3.00 mL, 5.15 mmol, 1.7 M in *n*-pentane) was added over 10 min while the suspension was stirring. The mixture was allowed to warm to ambient temperature and stirring was continued for 1.5 h. The obtained brown suspension was again cooled to −125°C and a solution of diphenyldimethoxysilan (0.57 mL, 2.51 mmol) in $Et_2O$ (8 mL) was added dropwise over 15 min. The reaction mixture was allowed to warm to ambient temperature and stirred for 12 h. The reaction was carefully quenched with water and the resulting mixture was transferred into a separation funnel. The organic phase was separated and the aqueous solution was extracted with ethyl acetate (3 x 50 mL). The combined organic layers were dried over $MgSO_4$, filtered and concentrated *in vacuo*. The residue was purified by flash chromatography on silica gel (hexanes/ethyl acetate, 95:5) to give the title compound as a white solid (0.80 g, 86%). $^1$H NMR (500 MHz, $C_6D_6$): δ =7.64 (dd, *J* = 8.4, 6.6 Hz, 3H), 7.50 – 7.45 (m, 12H), 7.17 (s, 3H), 7.13 – 7.09 (m, 6H), 7.09 – 7.04 (m, 12H), 7.02 (dd, *J* = 10.2, 2.6 Hz, 3H), 6.83 (td, *J* = 8.5, 2.6 Hz, 3H), 3.00 (s, 9H). $^{19}$F NMR (470 MHz, $C_6D_6$): δ = −111.0. $^{13}$C NMR (126 MHz, $C_6D_6$): δ = 164.1 (d, *J* = 249.9 Hz), 152.3 (d, *J* = 7.5 Hz), 140.7 (d, *J* = 1.8 Hz), 140.0 (d, *J* = 7.9 Hz), 118.1 (d, *J* = 20.1 Hz), 112.9 (d, *J* = 19.2 Hz). $^{29}$Si NMR (99 MHz, $C_6D_6$): δ = −11.5. IR (film): $\tilde{\nu}$ 3068, 3011, 2933, 2833, 1568, 1588, 1473, 1427, 1376, 1329, 1276, 1224, 1172, 1082, 1108, 1055, 1029, 998, 952, 870, 894, 820, 772, 736, 698, 687, 618, 633, 643, 569, 495, 442, 421 cm$^{-1}$. HRMS-ESI (m/z): calculated for $C_{63}H_{51}F_3O_3Si_3Na^+$ $[M+Na]^+$, 1019.29904; found, 1019.29849.

**Dimethoxybis(4-methoxyphenyl)silane (113)**

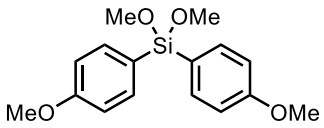


A two-necked, round-bottomed flask was equipped with a magnetic stir bar, a reflux condenser and a gas inlet connected to an argon/vacuum manifold. The flame-dried flask was charged with magnesium turnings (851 mg, 35.0 mmol, 5.00 equiv) and THF (6 mL) under argon atmosphere. 1,2-Dibromoethane (3 drops) was added to the stirred mixture, which was quickly heated up to 60°C for 5 min to activate the magnesium. After reaching ambient temperature, 4-bromoansiole (2.19 mL, 17.5 mmol, 2.5 equiv.) was added dropwise and the resulting green-grey suspension was stirred for 1h at 25 °C until full conversion was indicated by GC-MS analysis.

A three-necked, round-bottomed flask was equipped with a magnetic stir bar, a dropping funnel and a gas inlet connected to an argon/vacuum manifold. The flame-dried flask was filled with argon and charged with tetramethylorthosilicate (1.03 mL, 7.00 mmol, 1.00 equiv). THF (23 mL) was added and the colorless solution was cooled to 0°C. The solution of the freshly prepared Grignard reagent was diluted with THF (8 mL) and transferred into the dropping funnel, using additional THF (8 mL) to rinse the flask. This solution was added dropwise to the cooled solution of the orthosilicate. Once the addition was complete, the mixture was allowed to warm to ambient temperature and stirring was continued for 4 h. The mixture was poured into a separation funnel charged with *n*-pentane (50 mL) and was washed with water (3 x 50 mL).The organic layer was dried over $MgSO_4$, filtered and concentrated *in vacuo*. The residue was purified by flash chromatography on silica gel (hexanes/EtOAc 98:2) to give the title compound as a colorless oil (1.05 g, 49%). $^1$H NMR (400 MHz, $C_6D_6$): δ = 7.85 – 7.74 (m, 4H), 6.91 – 6.82 (m, 4H), 3.54 (s, 6H), 3.27 (d, *J* = 0.9 Hz, 6H). $^{13}$C NMR (100 MHz, $C_6D_6$): δ = 162.1, 137.1, 124.3, 114.1, 54.6, 50.6. IR (film): $\tilde{\nu}$ 2937, 2836, 1593, 1565, 1503, 1461, 1399, 1309, 1279, 1245, 1179, 1123, 1069, 1028, 737, 719, 658, 631, 601, 529, 508, 444 cm$^{-1}$. HRMS-ESI (*m/z*): calcd. for $C_{16}H_{20}O_4SiNa^+$ [M+Na]$^+$, 327.1023; found, 327.1023.

**(5'-(2-(Methoxybis(4-methoxyphenyl)silyl)phenyl)-[1,1':3',1''-terphenyl]-2,2''-diyl)bis(methoxybis(4-methoxyphenyl)silane) (114) and Isomer 115**

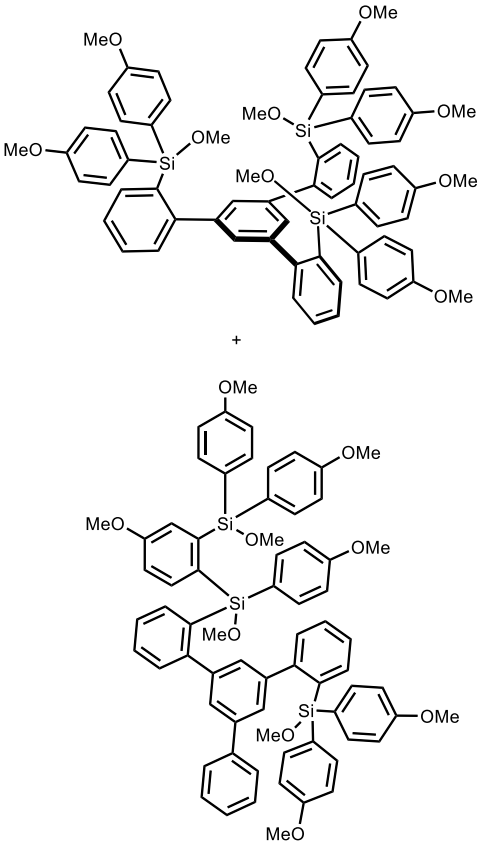

A three-necked, round-bottomed flask was equipped with a magnetic stir bar and a gas inlet connected to an argon-vacuum manifold. The flame-dried flask was filled with argon and charged with 1,3,4-tris-2'-bromophenylbenzene (**103**) (1.63 g, 3.00 mmol). Diethyl ether (60 mL) was added and the stirred suspension was cooled to −125°C. A solution of *tert*-butyllithium (10.9 mL, 18.5 mmol, 1.7 M in pentane) was added over 10 min while the suspension was stirring. The mixture was allowed to warm to ambient temperature and stirring was continued for 1.5 h. The obtained brown suspension was again cooled to −125°C and a solution of dimethoxybis(4-methoxyphenyl)silane **113** (4.30 g, 14.1 mmol) in diethyl ether (5 mL) was added dropwise over 15 min. The reaction mixture was allowed to warm to ambient temperature. After stirring for 8 h, the mixture was carefully quenched with water and was transferred into a separation funnel. The organic phase was separated and the aqueous solution extracted with $CH_2Cl_2$ (3 x 50 mL). The combined organic layers were dried over $MgSO_4$,

filtered and concentrated *in vacuo*. The residue was purified by high-performance liquid chromatography with MeCN as the eluent to afford compound **114** as a white solid (400 mg, 12%) as well as a constitutional isomer **115** (1.63 g, 47%). $^{1}$H NMR (400 MHz, $CDCl_3$): δ = 7.70 – 7.62 (m, 3H), 7.37 (td, *J* = 7.5, 1.6 Hz, 3H), 7.31 (dd, *J* = 7.4, 1.3 Hz, 3H), 7.27 – 7.23 (m, 12H), 6.99 – 6.95 (m, 3H), 6.92 (s, 3H), 6.70 – 6.64 (m, 12H), 3.71 (s, 18H), 3.00 (s, 9H). $^{13}$C NMR (126 MHz, $CDCl_3$): δ = 160.7, 149.8, 141.6, 137.3, 136.9, 132.6, 131.0, 129.6, 129.3, 126.4, 125.7, 113.3, 55.0, 50.8. $^{29}$Si NMR (99 MHz, $CDCl_3$): δ = −11.3. IR (film): $\tilde{\nu}$ 2932, 2832, 1592, 1562, 1501, 1461, 1440, 1398, 1276, 1244, 1178, 1027, 815, 797, 719, 689, 649, 629, 609, 531, 463 cm$^{-1}$. HRMS-ESI (*m/z*): calcd. for $C_{69}H_{66}O_9Si_3Na^+$ $[M+Na]^+$, 1145.39069; found, 1145.39091.

Data of the constitutional isomer **115**: $^{1}$H NMR (500 MHz, $CDCl_3$): δ = 7.99 (ddd, *J* = 7.4, 1.6, 0.7 Hz, 1H), 7.60 (dd, *J* = 7.0, 1.9 Hz, 1H), 7.41 (tdd, *J* = 7.4, 1.4, 0.6 Hz, 1H), 7.38 – 7.30 (m, 7H), 7.30 – 7.22 (m, 6H), 7.22 – 7.15 (m, 4H), 7.10 (t, *J* = 7.6 Hz, 2H), 7.04 – 7.02 (m, 1H), 6.97 (td, *J* = 1.7, 0.7 Hz, 1H), 6.83 – 6.76 (m, 7H), 6.72 – 6.69 (m, 2H), 6.68 – 6.64 (m, 3H), 6.59 – 6.56 (m, 1H), 6.55 (dd, *J* = 2.7, 0.6 Hz, 1H), 6.54 – 6.53 (m, 0H), 6.51 (s, 3H), 3.82 (d, *J* = 0.4 Hz, 3H), 3.76 – 3.75 (m, 6H), 3.74 (d, *J* = 0.4 Hz, 3H), 3.69 (s, 3H), 3.59 (d, *J* = 0.5 Hz, 3H), 3.36 (d, *J* = 0.7 Hz, 3H), 2.92 (s, 3H), 2.82 (s, 3H). $^{13}$C NMR (126 MHz, $CDCl_3$): δ = 160.8, 160.7, 160.7, 160.5, 160.4, 160.3, 158.9, 149.8, 148.8, 143.8, 143.7, 142.8, 140.2, 139.2, 138.3, 137.9, 137.6, 137.3, 137.0, 137.0, 137.0, 137.0, 136.9, 136.8, 136.8, 136.5, 135.3, 133.2, 130.1, 129.8, 129.5, 129.1, 129.0, 129.0, 129.0, 128.4, 128.3, 128.2, 128.2, 128.1, 126.8, 126.7, 126.6, 126.4, 126.3, 126.3, 126.0, 125.7, 125.6, 125.6, 125.3, 123.2, 113.4, 113.4, 113.4, 113.2, 113.0, 113.0, 112.7, 77.3, 77.0, 76.8, 72.8, 54.9, 54.9, 54.9, 54.9, 54.9, 54.8, 54.8, 54.8, 54.8, 54.8, 54.8, 54.8, 54.6, 54.6, 54.6, 54.6, 51.0, 51.0, 51.0, 50.8, 50.8, 50.6, 49.5, 27.0, 27.0, 27.0, 27.0, 27.0, 27.0, 27.0, 27.0, 21.5. $^{29}$Si NMR (99 MHz, $CDCl_3$): δ = −11.1, −11.3, −11.7. HRMS-ESI (m/z): calcd. for $C_{69}H_{66}O_9Si_3Na^+$ $[M+Na]^+$, 1145.39069; found, 1145.39080.

**(5'-(2-(Dimethylsilyl)phenyl)-[1,1':3',1''-terphenyl]-2,2''-diyl)bis(dimethylsilane) (S2)**

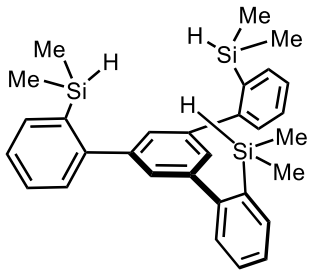


A two-necked, round-bottomed flask was equipped with a magnetic stir bar and a gas inlet connected to an argon-vacuum manifold. The flame-dried flask was filled with argon and charged with 1,3,4-tris-2'-bromophenylbenzene (**103**) (1.00 g, 1.84 mmol) and $Et_2O$ (39 mL). The resulting mixture was cooled to −125°C. A solution of *tert*-butyllithium (7.08 mL, 11.3 mmol, 1.7 M in *n*-pentane) was added dropwise and the resulting mixture was allowed to warm to ambient temperature. After stirring at ambient temperature for 1 h, the mixture was cooled to −125°C and dimethylchlorosilane (1.29 mL, 11.1 mmol) was added dropwise. The mixture was allowed to warm to ambient temperature and stirred overnight. The reaction was carefully quenched with water and the solvent was removed *in vacuo*. The residue was purified by flash chromatography on silica gel

(hexanes/ethyl acetate, 4:1) to give the title compound as a pale yellow foam (807 mg, 91%). $^{1}$H NMR (500 MHz, $CDCl_3$): 7.55 – 7.50 (m, 3H), 7.36 – 7.30 (m, 3H), 7.28 – 7.24 (m, 8H), 7.16 (s, 3H), 4.34 (hept, *J* = 3.8 Hz, 3H), 0.05 (d, *J* = 3.8 Hz, 18H). $^{13}$C NMR (126 MHz, $CDCl_3$): δ = 148.94, 143.03, 135.84, 135.03, 129.41, 129.11, 128.81, 126.44, - 2.80. $^{29}$Si NMR (99 MHz, $CDCl_3$): δ = –19.1. IR (film): ṽ 3051, 2956, 2117, 1583, 1558, 1468, 1409, 1247, 1124, 1100, 1063, 893, 833, 967, 707, 524, 426, 448 cm$^{-1}$. HRMS-ESI (m/z): calculated for $C_{30}H_{36}Si_3$ $[M]^{\cdot+}$,480.21229; found, 480.21249.

**(5'-(2-(Diethylsilyl)phenyl)-[1,1':3',1''-terphenyl]-2,2''-diyl)bis(diethylsilane) (S3)**

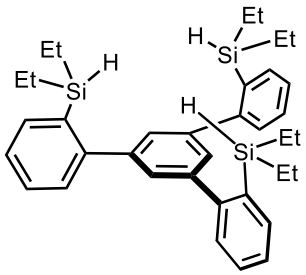


A two-necked, round-bottomed flask was equipped with a magnetic stir bar and a gas inlet connected to an argon-vacuum manifold. The flame-dried flask was filled with argon and charged with 1,3,4-tris-2'-bromophenylbenzene (**103**) (2.00 g, 3.68 mmol) and $Et_2O$ (77 mL). The resulting mixture was cooled to −125 °C. A solution of *tert*-butyllithium (14.2 mL, 22.6 mmol, 1.6 M in *n*-pentane) was added drophwise and the mixture was allowed to warm to ambient temperature. After stirring for 1 h stirring, the mixture was cooled to −125 °C and diethylsilane (2.86 mL, 22.1 mmol) was added dropwise. The mixture was then warmed to ambient temperature and stirring was continued overnight. The reaction was carefully quenched by adding water and the resulting mixture was transferred into a separation funnel. The organic phase was separated and the aqueous solution was extracted with ethyl acetate (3 x 50 mL). The combined organic layers were dried over $MgSO_4$, filtered and concentrated in vacuo. The residue was purified by flash chromatography on silica gel (hexanes/ethyl acetate, 10:1) to give the title compound as a colorless solid (1.9 g, 91%). $^{1}$H NMR (400 MHz, $CD_3Cl$): δ = 7.58 – 7.54 (m, 3H), 7.42 – 7.36 (m, 3H), 7.35 – 7.28 (m, 6H), 7.22 (s, 3H), 4.13 (p, *J* = 3.4 Hz, 3H), 0.84 (t, *J* = 7.8 Hz, 18H), 0.60 (m, 12H). $^{13}$C NMR (101 MHz, $CDCl_3$): δ = 149.4, 143.1, 136.0, 134.2, 129.6, 129.1, 128.9, 126.4, 8.5, 4.2. IR (film): ṽ 3051, 2952, 2872, 2102, 1583, 1558, 1460, 1409, 1378, 1260, 1230, 1124, 1098, 1063, 1006, 970, 891, 873, 736, 686, 640, 623, 607, 527, 458 cm$^{-1}$. HRMS-APPI (m/z): calcd. for $C_{36}H_{48}Si_3$ $[M]^{\cdot+}$, 564.30584; found, 564.30642.

**5'-(2-(Diisopropylsilyl)phenyl)-[1,1':3',1''-terphenyl]-2,2''-diyl)bis(diisopropylsilane) (S4)**

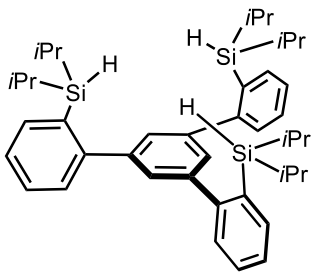


A two-necked, round-bottomed flask was equipped with a magnetic stir bar and a gas inlet connected to an argon-vacuum manifold. The flame-dried flask was filled with argon and charged with 1,3,4-tris-2'-bromophenylbenzene (**103**) (1.50 g, 2.57 mmol) and $Et_2O$ (58 mL). The resulting mixture was cooled to −125°C and a solution of *tert*-butyllithium (10.6 mL, 17.0 mmol, 1.7 M in *n*-pentane) was added dropwise. The reaction mixture was allowed to warm to ambient temperature and stirring

continued for 1 h. After cooling to −125°C, diisopropylchlorosilane (2.92 mL, 16.6 mmol) was added dropwise and the resulting mixture was allowed to warm to ambient temperature while stirring overnight. The reaction was carefully quenched with water, the solvent was removed *in vacuo*, and the residue was purified by flash chromatography on silica gel (hexanes/ethyl acetate, 4:1) to give the title compound as a pale yellow foam (1.50 g, 81%). $^{1}$H NMR (500 MHz, $CDCl_3$): δ = 7.57 (ddd, *J* = 7.3, 1.5, 0.6 Hz, 3H), 7.41 (td, *J* = 7.7, 7.1, 1.5 Hz, 3H), 7.36 (ddd, *J* = 7.7, 1.5, 0.6 Hz, 3H), 7.32 (td, *J* = 7.3, 1.5 Hz, 3H), 7.20 (s, 3H), 3.87 (t, *J* = 3.7 Hz, 3H), 1.07 (heptd, *J* = 7.2, 3.7 Hz, 6H), 0.95 (d, *J* = 7.2 Hz, 18H), 0.89 (d, *J* = 7.3 Hz, 18H). $^{13}$C NMR (126 MHz, $CDCl_3$): δ = 149.7, 142.6, 135.8, 129.6, 129.4, 128.7, 125.9, 77.2, 77.0, 76.7, 19.2, 18.9, 11.6. $^{29}$Si NMR (99 MHz, $CDCl_3$): δ = 2.1. IR (film): ṽ 3051, 2939, 2889, 2862, 2132, 1583, 1557, 1461, 1409, 1383, 1364, 1259, 1122, 1098, 1065, 1001, 919, 877, 811, 773, 734, 686, 656, 631, 603, 527, 481, 458 cm$^{-1}$. HRMS-ESI (m/z): calculated for $C_{42}H_{61}Si_3$ $[M+H]^+$, 649.40756; found, 649.40680.

**(5'-(2-(Di-isobutylsilyl)phenyl)-[1,1':3',1''-terphenyl]-2,2''-diyl)bis(diisobutylsilane) (S5)**

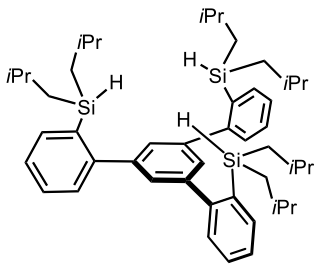


A two-necked, round-bottomed flask was equipped with a magnetic stir bar and a gas inlet connected to an argon-vacuum manifold. The flame-dried flask was filled with argon and charged with 1,3,4-tris-2'-bromophenylbenzene (**103**) (1.50 g, 2.76 mmol)[1] and $Et_2O$ (58 mL). The resulting mixture was cooled to −125 °C. A solution of *tert*-butyllithium (8.94 mL, 17.0 mmol, 1.9 M in *n*-pentane) was added dropwise and the mixture was allowed to warm to ambient temperature. After stirring for 1 h at ambient temperature, the mixture was cooled to −125 °C and di-*iso*-butylchlorosilane (3.07 mL, 16.6 mmol) was added dropwise. The mixture was warmed to ambient temperature and stirring was continued overnight. The reaction was carefully quenched by adding water and the resulting mixture was transferred into a separation funnel. The organic phase was separated and the aqueous solution extracted with ethyl acetate (3 x 50 mL). The combined organic layers were dried over $MgSO_4$, filtered and concentrated in vacuo. The residue was purified by flash chromatography on silica gel (hexanes/*t*-butyl methyl ether, 99:1) and the product dried in high vacuum (70°C, $10^{-3}$ mbar, 3 h) to give silane **S5** as a colorless oil (1.56 g, 77%). $^{1}$H NMR (600 MHz, $CD_3Cl$): δ = 7.64 (ddd, *J* = 7.4, 1.4, 0.6 Hz, 3H), 7.40 – 7.36 (m, 6H), 7.35 – 7.31 (m, 3H), 7.27 (s, 3H), 4.35 – 4.28 (m, 3H), 1.68 – 1.57 (m, 6H), 0.82 – 0.75 (m, 36H), 0.68 – 0.56 (m, 12H). $^{13}$C NMR (151 MHz, $CDCl_3$): δ = 149.3, 143.0, 136.3, 135.1, 129.6, 129.1, 129.0, 126.4, 26.1, 25.7, 25.5, 24.3. $^{29}$Si NMR (119 MHz, $CDCl_3$): δ = −14.4. IR (film): ṽ 3053, 2952, 2895, 2867, 2826, 2113, 1584, 1558, 1463, 1408, 1382, 1364, 1328, 1261, 1203, 1163, 1124, 1085, 1034, 950, 891, 849, 759, 740, 723, 637, 623, 527, 461, 417 cm$^{-1}$. HRMS-APPI (m/z): calcd. for $C_{48}H_{72}Si_3$ $[M]^+$, 732.49364; found, 732.49398.

**Ligand 105**

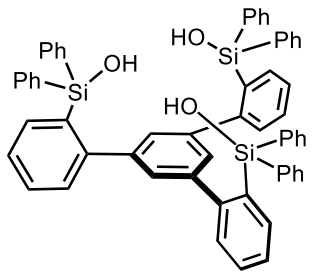

A two-necked, round-bottomed flask was equipped with a magnetic stir bar and a dropping funnel. The flask was charged with compound **104** (4.97 g, 5.27 mmol) and THF (120 mL). The solution was cooled to 0°C before concentrated aqueous HCl (39.5 mL, 474 mmol) was added dropwise. The mixture was allowed to warm to ambient temperature and stirring was continued for 1 h. After cooling to 0°C, the mixture was carefully neutralized by dropwise addition of saturated aqueous $NaHCO_3$ solution. The organic phase was separated and the aqueous solution extracted with $CH_2Cl_2$ (3 x 100 mL). The combined organic layers were washed with water (200 mL), dried over $MgSO_4$, filtered and concentrated *in vacuo* to give the title compound as a white solid (4.74 g, quant.). $^1$H NMR (400 MHz, $CDCl_3$): δ = 7.55 – 7.51 (m, 12H), 7.48 – 7.43 (m, 3H), 7.30 – 7.22 (m, 12H), 7.21 – 7.13 (m, 12H), 6.92 – 6.87 (m, 6H), 4.36 (s, 3H). $^{13}$C NMR (126 MHz, $CDCl_3$): δ = 149.0, 143.8, 137.5, 137.0, 134.6, 133.9, 130.1, 129.7, 129.4, 128.6, 127.9, 126.0. IR (film): $\tilde{\nu}$ 3046, 1582, 1471, 1427, 1263, 1204, 1112, 1087, 997, 900, 824, 762, 735, 698, 622, 471, 411 cm$^{-1}$. HRMS-ESI (*m/z*): calcd. for $C_{60}H_{48}O_3Si_3Na^+$ [M+Na]$^+$, 923.28035; found, 923.28182.

**Ligand 127**

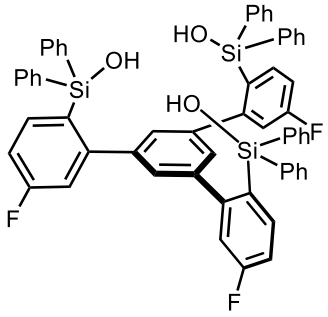

A two-necked, round-bottomed flask was equipped with a magnetic stir bar and a dropping funnel. The flask was charged with compound **S1** (200 mg, 0.201 mmol) and THF (3 mL). The solution was cooled to 0°C before concentrated aqueous HCl (0.5 mL, 6.02 mmol) was added dropwise. The mixture was allowed to warm to ambient temperature and stirring was continued for 1.5 h. After cooling to 0°C, the mixture was carefully neutralized by adding saturated aqueous $NaHCO_3$ solution. The organic phase was separated and the aqueous solution was extracted with $CH_2Cl_2$ (3 x 5 mL). The combined organic layers were washed with water (20 mL), dried over $MgSO_4$, filtered and concentrated *in vacuo* to give the title compound as a white solid (150 mg, 78%). $^1$H NMR (500 MHz, [$D_7$]-DMF): δ = 7.49 (dd, *J* = 8.5, 6.6 Hz, 3H), 7.49 – 7.45 (m, 12H), 7.38 – 7.33 (m, 6H), 7.32 – 7.26 (m, 12H), 7.20 (td, *J* = 8.9, 8.4, 2.6 Hz, 3H), 6.88 (s, 3H), 6.69 (dd, *J* = 10.2, 2.6 Hz, 3H), 6.65 (s, 3H). $^{19}$F NMR (470 MHz, [$D_7$]-DMF): δ = −112.6. $^{13}$C NMR (126 MHz, [$D_7$]-DMF): δ = 163.5 (d, *J* = 248.4 Hz), 151.8 (d, *J* = 7.4 Hz), 141.3, 139.3 (d, *J* = 8.1 Hz), 137.7, 134.5, 130.7 (d, *J* = 3.4 Hz), 129.5, 128.8, 127.7, 116.9 (d, *J* = 20.2 Hz), 112.9 (d, *J* = 19.4 Hz). $^{29}$Si NMR (99 MHz, [$D_7$]-DMF): δ = -16.0. IR (film): $\tilde{\nu}$ 3407, 3067, 3018, 1737, 1588, 1569, 1475, 1428, 1380, 1329, 1307, 1276, 1262, 1249, 1228, 1186, 1174, 1112, 1091, 1054, 1028, 998, 954, 918, 872, 860, 814, 762, 740, 700, 660, 641, 634, 614,

573, 493, 416 $cm^{-1}$. HRMS-ESI (m/z): calculated for $C_{60}H_{44}F_3O_3Si_3^-$ $[M-H]^-$, 953.25559; found, 953.25501.

**Ligand 115**

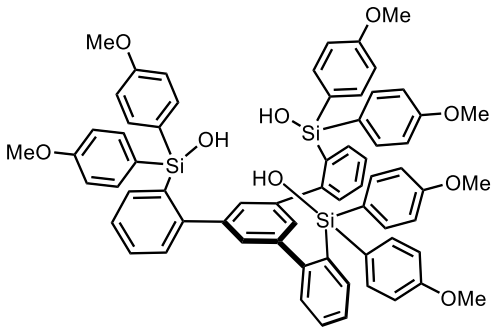


A two-necked, round-bottomed flask was equipped with a magnetic stir bar and a dropping funnel. The flask was charged with compound **115** (400 mg, 2.22 mmol) and THF (7.6 mL). The resulting solution was cooled to 0°C before concentrated aqueous HCl (2.60 mL, 31.2 mmol) was added dropwise. The mixture was allowed to warm to ambient temperature and stirring was continued for 1 h. After cooling to 0°C, the solution was carefully neutralized by dropwise addition of saturated aqueous $NaHCO_3$. The organic phase was separated and the aqueous solution was extracted with $CH_2Cl_2$ (3 x 10 mL). The combined organic layers were washed with water (50 mL), dried over $MgSO_4$, filtered and concentrated *in vacuo* to give the title compound as a white solid (380 mg, 99%). Colorless crystals suitable for single-crystal X-ray diffraction were grown by storing a concentrated toluene solution at 5°C for three days. M. p. = 250–253°C. $^1$H NMR (500 MHz, $CDCl_3$): δ = 7.49 – 7.45 (m, 3H), 7.45 – 7.42 (m, 12H), 7.28 – 7.25 (m, 6H), 6.92 (d, *J* = 7.0 Hz, 6H), 6.72 – 6.68 (m, 12H), 3.74 (s, 18H). $^{13}$C NMR (126 MHz, $CDCl_3$): δ = 160.7, 148.9, 143.5, 137.3, 136.0, 134.7, 129.7, 129.3, 128.5, 128.3, 125.7, 113.4, 54.9. $^{29}$Si NMR (99 MHz, $CDCl_3$): δ = −11.6. IR (film): $\tilde{\nu}$ 1592, 1562, 1501, 1437, 1276, 1244, 1180, 1111, 1030, 897, 811, 795, 764, 722, 690, 650, 628, 612, 529, 464, 428, 410 $cm^{-1}$. HRMS-ESI (*m/z*): calcd. for $C_{66}H_{60}O_9Si_3Na^+$ $[M+Na]^+$, 1103.3437; found, 1103.3435.

**Ligand 130**

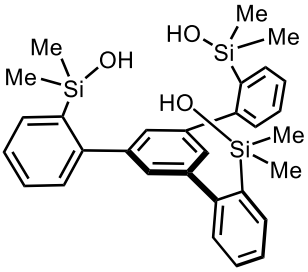


A one-neck round bottomed flask equipped with a stir bar was charged with compound 10d (1.00 g, 2.08 mmol) and $CH_2Cl_2$ (28 mL). The resulting mixture was cooled to 0°C. *m*CPBA (1.54 g, 6.86 mmol, 77% w/w) was added portionwise and the resulting mixture stirred at ambient temperature for 4 h. The mixture was diluted with $CH_2Cl_2$ (370 mL), carefully transferred to a separation funnel, and washed with sat. $NaHCO_3$ (3 x 150 mL) and brine (3 x 100 mL). The organic phase was dried over $MgSO_4$, filtered and concentrated *in vacuo* to give the title compound as a pale colorless fluffy solid (1.03 g, 94%). $^1$H NMR (500 MHz, $CDCl_3$): δ = 7.55 (d, *J* = 8.4 Hz, 3H), 7.43 – 7.34 (m, 6H), 7.33 – 7.28 (m, 6H), 3.30 (s, 3H), 0.31 (s, 18H). $^{13}$C NMR (126 MHz, $CDCl_3$): δ = 147.9, 143.8, 137.9, 134.2, 129.6, 128.9, 127.9, 126.4, 2.1. $^{29}$Si NMR (99 MHz, $CDCl_3$): δ = 6.9. IR (film): ν̃ 3262, 3050, 2898, 1699, 1558, 1409, 1430,

1408, 1252, 1161, 1126, 1065, 830, 778, 759, 694, 664, 623, 580, 530, 460, 440 $cm^{-1}$. HRMS-ESI (m/z): calculated for $C_{30}H_{35}O_3Si_3^-$[M-H]$^-$, 527.18996; found, 527.19076.

**Ligand 129**

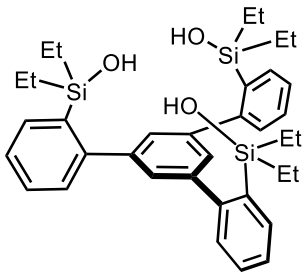

A one-neck round bottomed flask equipped with a stir bar was charged with silane **S2** (222 mg, 0.393 mmol) and $CH_2Cl_2$ (5 mL). The resulting mixture was cooled to 0 °C. *m*-Chloroperbenzoic acid (291 mg, 1.30 mmol, 77% *w/w*) was added portionwise and the reaction mixture was allowed to warm to ambient temperature. After 4 h, the mixture was carefully transferred to a separation funnel, diluted with $CH_2Cl_2$ (10 mL) and washed with sat. $NaHCO_3$ (4 x 15 mL) and brine (3 x 10 mL). The organic phase was then dried over $MgSO_4$, filtered and concentrated *in vacuo* to give ligand **129** as a colorless solid (240 mg, 99%). $^1$H NMR (400 MHz, $CDCl_3$): δ = 7.51 – 7.47 (m, 3H), 7.43 – 7.33 (m, 6H), 7.33 – 7.30 (m, 3H), 7.24 (s, 3H), 0.90 – 0.85 (m, 18H), 0.75 (m, 12H). $^{13}$C NMR (101 MHz, $CDCl_3$): δ = 149.0, 144.1, 135.9, 134.6, 129.9, 128.9, 127.6, 126.4, 8.2, 6.9. $^{29}$Si NMR (119 MHz, $CDCl_3$): δ = 7.7. IR (film): ṽ 3318, 3051, 2955, 2912, 2875, 1583, 1558, 1461, 1410, 1378, 1260, 1235, 1162, 1124, 1090, 1065, 1005, 959, 908, 888, 822, 760, 711, 615, 530, 512, 465 $cm^{-1}$. HRMS-ESI (m/z): calcd. for $C_{36}H_{47}O_3Si_3$ [M-H]$^-$, 611.28386; found, 611.28383.

**Ligand 128**

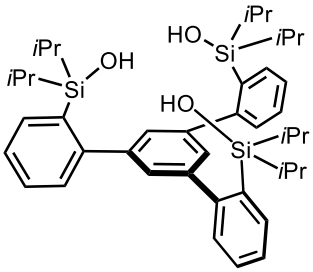

A round bottomed flask equipped with a stir bar was charged with compound **S3** (843 mg, 1.30 mmol) and THF (14 mL). *m*CPBA (1.75 g, 7.79 mmol, 77% *w/w*) was added portionwise and the resulting mixture was stirred at ambient temperature overnight before it was concentrated *in vacuo*. The residue was purified by flash chromatography on silica gel (hexanes/ethyl acetate, 4:1) to give the title compound as a white powdery solid (786 mg, 87%). $^1$H NMR (400 MHz, $CDCl_3$): δ = 7.48 (dd, *J* = 7.4, 1.6 Hz, 3H), 7.40 – 7.29 (m, 6H), 7.29 – 7.25 (m, 3H), 7.21 (s, 3H), 2.97 (s, 3H), 1.12 (ddt, *J* = 13.5, 8.4, 6.5 Hz, 6H), 0.99 (d, *J* = 7.2 Hz, 18H), 0.95 (d, *J* = 7.4 Hz, 18H). $^{13}$C NMR (101 MHz, $CDCl_3$): δ = 149.3, 143.6, 135.0, 134.3, 130.2, 128.5, 127.7, 126.0, 18.1, 17.9, 14.1. $^{29}$Si NMR (99 MHz, $CDCl_3$): δ = 7.7. IR (film): ṽ 3473, 3044, 2943, 2864, 2182, 2021, 1966, 1583, 1557, 1462, 1410, 1381, 1363, 1259, 1242, 1023, 1088, 1064, 997, 950, 919, 884, 760, 740, 738, 720, 653, 633, 495, 467 $cm^{-1}$. HRMS-ESI (m/z): calculated for $C_{42}H_{59}O_3Si_3^-$[M-H]$^-$, 695.37776; found, 695.37766.

**Ligand S6**

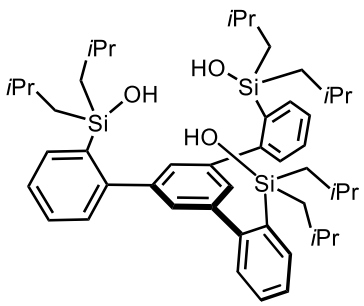


A two-neck round bottomed flask equipped with a stir bar was charged with silane **S5** (563 mg, 0.768 mmol) and $CH_2Cl_2$ (10 mL). The resulting mixture was cooled to 0 °C. *m*-Chloroperbenzoic acid (568 mg, 2.53 mmol, 77% w/w) was added in portions and the reaction mixture was allowed to warm to ambient temperature. After 4 h, the mixture was carefully transferred to a separation funnel, diluted with $CH_2Cl_2$ (10 mL) and washed with sat. $NaHCO_3$ (4 x 15 mL) and brine (3 x 10 mL). The organic phase was then dried over $MgSO_4$, filtered and concentrated *in vacuo* to give ligand **S6** as a colorless solid (584 mg, 97%). $^1$H NMR (600 MHz, $CDCl_3$): δ = 7.54 – 7.51 (m, 3H), 7.40 – 7.36 (m, 3H), 7.34 – 7.32 (m, 6H), 7.27 (s, 3H), 1.75 (hept, *J* = 6.6 Hz, 6H), 0.80 (m, 36H), 0.78 – 0.69 (m, 12H). $^{13}$C NMR (151 MHz, $CDCl_3$): δ = 148.5, 144.1, 137.4, 135.0, 129.7, 128.9, 127.9, 126.2, 28.5, 26.6, 26.3, 24.3. $^{29}$Si NMR (119 MHz, $CDCl_3$): δ = 4.5. IR (film): $\tilde{\nu}$ 3449, 2951, 2924, 2894, 2866, 1584, 1463, 1435, 1409, 1381, 1364, 1328, 1219, 1163, 1123, 1088, 1064, 1033, 951, 908, 889, 830, 814, 759, 733, 667, 643, 622, 528, 487, 468 cm$^{-1}$. HRMS-ESI (m/z): calcd. for $C_{48}H_{72}O_3Si_3Na$ $[M+Na]^+$, 803.46815; found, 803.46891.

**Ligand 135**

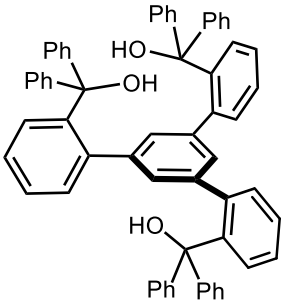


A two-necked, round-bottomed flask was equipped with a magnetic stir bar and a gas inlet connected to an argon-vacuum manifold. The flame-dried flask was filled with argon and charged with compound **103** (2.00 g, 3.86 mmol). $Et_2O$ (78 mL) was added and the resulting bright yellow mixture was cooled to –125°C. A solution of *tert*-butyllithium (14.2 mL, 22.6 mmol, 1.6 M in *n*-pentane) was added over 10 min and the mixture was allowed to warm to ambient temperature. After stirring for another 1 h, the heterogeneous dark brown mixture was again cooled to –125°C. A solution of benzophenone (2.01 g, 11.0 mmol) in $Et_2O$ (10 mL) was added and the resulting mixture was allowed to warm to ambient temperature while stirring overnight. The reaction was carefully quenched with water and the solution transferred into a separation funnel. The organic phase was separated and the aqueous solution was extracted with $CH_2Cl_2$ (3 x 100 mL). The combined organic layers were dried over $MgSO_4$, filtered and concentrated *in vacuo*. The residue was purified by trituration with ice-cold MeOH (3 x 20 mL) to afford the title compound as a pale pink powdery solid (2.46 g, 78%). $^1$H NMR (600 MHz, $CD_2Cl_2$): δ = 7.25 (m, 8H), 7.21 (m, 4H), 7.18 (m, 4H), 7.12 (m, 12H), 7.04 (t, *J* = 7.7 Hz, 1H), 7.00 (d, *J* = 7.6 Hz, 4H), 6.95 (d, *J* = 7.7 Hz, 4H), 6.91 (d, *J* = 7.4 Hz, 2H), 6.59 (d, *J* = 7.9 Hz, 2H), 6.45 (d, *J* = 7.9 Hz, 1H), 6.04 (d, *J* = 7.5 Hz, 1H), 5.62 (d, *J* = 1.6 Hz, 2H), 3.25 (s, 2H), 2.81 (s, 1H). $^{13}$C NMR (151 MHz, $CD_2Cl_2$): δ = 147.6, 147.5, 147.1, 144.4, 143.9, 141.2, 140.7, 139.3, 139.2, 133.8, 132.5,

129.9, 129.6, 129.4, 129.2, 128.2, 127.9, 127.9, 127.8, 127.6, 127.4, 127.3, 127.1, 127.0, 126.8, 126.3, 126.1, 126.0, 83.0, 82.9. IR (film): $\tilde{\nu}$ 3537, 3057, 1980, 1587, 147, 1445, 1414, 1317, 1262, 1154, 1014, 896, 750, 728, 706, 636, 583, 508, 446, 416 $cm^{-1}$. HRMS-ESI (m/z): calculated for $C_{63}H_{48}O_3Na^+$ $[M+Na]^+$, 875.34956; found, 875.34907.

**Ligand 213**

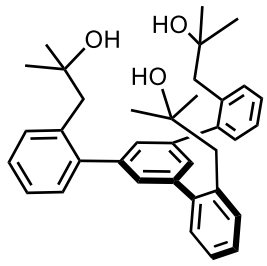


A two-necked, round-bottomed flask was equipped with a magnetic stir bar and a gas inlet connected to an argon-vacuum manifold. The flame-dried flask was filled with argon and charged with compound **103** (2.64 g, 4.86 mmol). $Et_2O$ (102 mL) was added and the resulting suspension was cooled to –125°C. A solution of *tert*-butyllithium (18.7 mL, 29.9 mmol, 1.6 M in *n*-pentane) was added over 10 min and the mixture was allowed to warm to ambient temperature once the addition was complete. After stirring for another 1 h, the heterogeneous dark brown mixture was again cooled to –125°C. 1,1-Dimethyloxirane (1.76 mL, 19.4 mmol) was added dropwise and the resulting mixture was allowed to warm to ambient temperature. After 8 h, the reaction was carefully quenched by adding water and the resulting mixture was transferred into a separation funnel. The organic phase was separated and the aqueous solution was extracted with ethyl acetate (4 x 50 mL). The combined organic layers were dried over $MgSO_4$, filtered and concentrated *in vacuo*. Hexanes (50 mL) was added to precipitate ligand **213** in the form of a white solid material (1.55 g, 61%). Colorless crystals suitable for single-crystal X-ray diffraction were grown from a concentrated $CH_2Cl_2$ solution (5 mL) layered with *n*-pentane (5 mL). $^1H$ NMR (400 MHz, $CDCl_3$): δ = 7.4 – 7.3 (m, 15H), 3.0 (s, 6H), 1.1 (s, 18H). $^{13}C$ NMR (101 MHz, $CDCl_3$): δ = 142.7, 142.6, 135.6, 131.8, 130.8, 129.9, 127.4, 126.8, 72.2, 45.9, 29.5. IR (film): $\tilde{\nu}$ 3404, 2971, 2929, 1591, 1488, 1465, 1412, 1364, 1302, 1202, 1138, 1083, 971, 901, 850, 757, 725, 639, 624, 613, 543, 513, 461 $cm^{-1}$. HRMS-ESI (m/z): calcd. for $C_{36}H_{41}O_3^-$ $[M-H]^-$, 521.30502; found, 521.30639.

**Ligand 140**

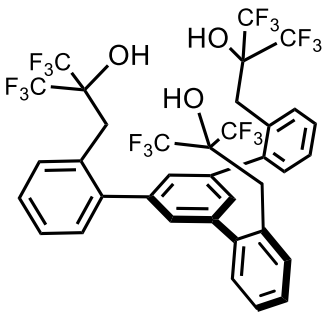


A two-necked, round-bottomed flask was equipped with a magnetic stir bar and a gas inlet connected to an argon-vacuum manifold. The flame-dried flask was filled with argon and charged with compound **103** (1.00 g, 1.84 mmol). $Et_2O$ (40 mL) was added and the resulting suspension was cooled to –125°C. A solution of *tert*-butyllithium (6.67 mL, 11.3 mmol, 1.6 M in *n*-pentane) was added over 10 min and the mixture was allowed to warm to ambient temperature once the addition was complete. After stirring for another 1 h, the heterogeneous dark brown mixture was again cooled to –125°C. Copper(I) iodide (150 mg, 0.788 mmol) was added and then 3,3,3-trifluoro-

2-(trifluoromethyl)-1,2,-propenoxide (**139**) (0.8 mL, 6.45 mmol) was added dropwise and the resulting mixture was allowed to warm to ambient temperature. After 14 h, the reaction was carefully quenched by adding water and the resulting mixture was transferred into a separation funnel. The organic phase was separated and the aqueous solution was extracted with ethyl acetate (4 x 50 mL). The combined organic layers were dried over $MgSO_4$, filtered and concentrated *in vacuo* to give the desired product in the crude mixture in 41% (NMR). The residue was purified by flash chromatography on silica gel (hexanes/ethyl acetate, 5:1) and subsequently by high-performance liquid chromatography with MeOH/$H_2O$ (8:2) as the eluent to afford compound **140** as a white solid . $^1$H NMR (400 MHz, $CDCl_3$): δ = 7.48 – 7.45 (m, 3H), 7.44 – 7.36 (m, 6H), 7.30 (dd, *J* = 7.0, 2.1 Hz, 3H), 7.25 (m, 3H), 3.47 (s, 6H), 2.72 (s, 3H). $^{13}$C NMR (101 MHz, $CDCl_3$): δ = 143.1, 141.8, 132.1, 131.4, 129.7, 128.7, 128.5, 128.2, 122.9 (q, *J* = 287.3 Hz), 77.4 – 75.6 (m), 31.6. $^{19}$F NMR (470 MHz, $CDCl_3$): δ = -76.6. IR (film): $\tilde{\nu}$ 3528, 1492, 1447, 1209, 1145, 1010, 1048, 975, 775, 761, 714, 652 cm$^{-1}$. HRMS-ESI (m/z): calcd. for $C_{36}H_{24}F_{18}O_3Na^+$ [M+Na]$^+$, 869.133027; found, 869.132760.

## 5.3 Catalyst Preparation

**Complex 107**

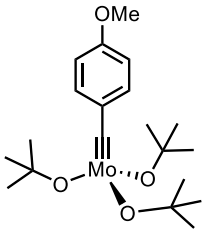


A 250 mL Schlenk flask was equipped with a magnetic stir bar and was flame dried under vacuum. The flask was filled with argon and charged with Mo(≡CAr)$Br_3$(dme) (**106**, Ar = 4-methoxyphenyl)[113] (3.02 g, 5.55 mmol) and THF (62 mL). A solution of NaOtBu (1.62 g, 16.5 mmol) in THF (15 mL) was added dropwise at ambient temperature and stirring was continued for 14 h before the solvent was removed *in vacuo* to obtain a dark brown solid. A second, flame dried 250 mL Schlenk flask was equipped with a magnetic stir bar and a Celite® (2 cm) packed argon frit. The dark brown solid was suspended in *n*-pentane (4 x 20 mL) and was filtered through the Celite® pad. The resulting filtrate was concentrated and the residue dried under vacuum ($10^{-3}$ mbar) to give complex **107** as a brown sticky solid (2.00 g, 83%) free of any residual THF. $^1$H NMR (400 MHz, $C_6D_5CD_3$): δ = 7.44 – 7.35 (m, 2H), 6.77 – 6.49 (m, 2H), 3.26 (s, 3H), 1.51 (s, 27H). $^{13}$C NMR (101 MHz, $C_6D_5CD_3$): δ = 276.0, 158.2, 140.4, 130.8, 113.1, 79.5, 54.2, 32.4. $^{95}$Mo NMR (26 MHz, 60°C, $C_6D_5CD_3$): δ = 79.6. IR (film): $\tilde{\nu}$ 2969, 1595, 1502, 1466, 1358, 1281, 1244, 1166, 1037, 933, 827, 785, 585, 562, 503, 480 cm$^{-1}$. HRMS-EI (m/z): calculated for $C_{20}H_{34}MoO_4^+$ [M]$^+$, 436.15122; found, 436.15181.

**Complex [Li·$(Et_2O)_{3/5}$]Mo$(CO)_5$(COAr) (Ar = 2,6-dimethylphenyl) (119)**

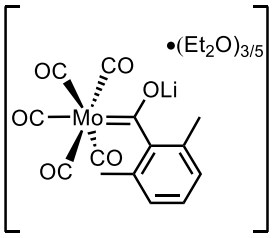


A two-neck 250 mL round-bottom flask is equipped with a Teflon-coated magnetic stirring bar and an Argon-vacuum manifold. The flask is charged with 2-bromo-1,3-dimethylbenzene (3.59 g, 19.0 mmol) and diethyl ether (80 mL). The solution is cooled to −25°C and a solution of *tert*-butyllithium (23.8 mL, 38.0 mmol, 1.6 M in *n*-pentane) was added over 10 min. Once the addition is complete, stirring is continued for 3 h at −20°C. A 500 mL, three-neck round-bottom flask is equipped with a Teflon-coated magnetic stirring bar, a reflux condenser, a pressure-equalizing dropping funnel fitted with a rubber stopper and an Argon-vacuum manifold. The flask is charged with [$Mo(CO)_6$] (**2**) (5.12 g, 19.0 mmol) and diethyl ether (60 mL) and the mixture is cooled to 0°C. The cold (−20 °C) solution of 2,6-dimethylphenyl lithium is added via the dropping funnel over 5 min to the suspension, causing an immediate color change to orange-brown and a slight exotherm. Once the addition is complete, the resulting orange-brown solution is stirred at ambient temperature for 4 h. The dropping funnel and the reflux condenser are replaced by glass stoppers. A solvent trap is connected to the Argon-vacuum manifold and the solvent is removed under reduced pressure. A flame-dried three-neck 250 mL round-bottom flask is equipped with a magnetic stir bar, an Argon-vacuum manifold and an argon frit. The frit is loaded with Celite® (3 cm), slurried and packed with $CH_2Cl_2$. The orange solid was suspended in $CH_2Cl_2$ (4 x 20 mL) and was filtered through the Celite® pad. The resulting filtrate was concentrated under vacuum ($10^{-3}$ mbar) until 10 mL of the orange solution remained. Pentane (200 mL) was added to the vigorously stirred solution to precipitate a yellow microcrystalline material. The solid was isolated through filtration over an argon frit, washed with n-pentane (3x 10 mL) and dried under high vacuum ($10^{-3}$ mbar) to give complex **119** as a pale orange microcrystalline solid (6.78 g, 78%). The complex is still contaminated with starting complex [$Mo(CO_6)$], which can't be removed due to its low solubility, but turned out not to be problematic in the next step. $^1$H NMR (600 MHz, $CD_2Cl_2$): δ = 6.99 – 6.95 (m, 1H), 6.91 (d, *J* = 7.6 Hz, 2H), 2.98 (q, *J* = 7.0 Hz, 3H), 2.23 (s, 6H), 0.69 (t, *J* = 7.0 Hz, 4H). $^{13}$C NMR (151 MHz, $CD_2Cl_2$): δ = 353.1, 213.5, 208.8, 201.2, 159.6, 128.4, 126.5, 126.5, 65.9, 18.5, 13.4.

**Complex [Mo(≡CAr)$Br_3$(dme)] (Ar = 2,6-dimethylphenyl) (117)**

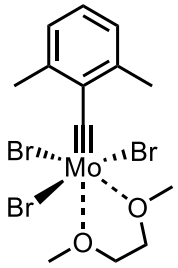


A 500 mL, three-neck round-bottom flask is equipped with a Teflon-coated magnetic stirring bar, an internal thermometer, a rubber stopper and an Argon-vacuum manifold. The flask is charged with complex **119** (6.48 g, 14.2 mmol) and $CH_2Cl_2$ (300 mL). The mixture is cooled to −78 °C and stirred for 15 min before a solution of oxalyl bromide (1.40 mL, 14.6 mmol) in $CH_2Cl_2$ (6 mL) is added dropwise over 10 min. Once the addition is complete, stirring is continued for 15 min at −78 °C. The mixture is then allowed to warm until a rapid color change to light brown is observed (at an internal

temperature of ca. −40 °C, not warmer!). At this point, the reaction flask is quickly re-cooled to −78 °C. A 1 L, three-neck jacketed cooling flask is equipped with a Teflon-coated magnetic stirring bar, a jacketed cooling filter frit (diameter: 4.5 cm; height: 20 cm; porosity: 4) containing a 3 cm-length pad of Celite®, a 20 mL pressure-equalizing dropping funnel connected to an Argon-vacuum manifold. The Celite® in the jacketed filter is slurried with $CH_2Cl_2$ and cooled to −78 °C using a cryostat. The 1 L, three-neck jacketed flask is loaded with 1, 2-dimethoxyethane (7.40 mL, 71.2 mmol) and cooled to −78 °C. The cold light brownish mixture is filtered through the Celite® packed filter frit, resulting in a bright yellow filtrate. Upon contact with DME in the 1 L receiving flask, a color change from yellow to dark red is observed. The mixture is stirred for 10 min before a solution of $Br_2$ (0.75 mL, 14.7 mmol) in $CH_2Cl_2$ (5 mL) is added dropwise over a period of 5 min via the dropping funnel. Once the addition is complete, the mixture is stirred for 15 min. The resulting brown-orange mixture is allowed to reach ambient temperature over the course of 1 h, during which time the color intensifies. Stirring is continued for 1 h at ambient temperature before the dropping funnel and the jacketed cooling filter frit are replaced by glass stoppers. The reaction mixture is filtered through a pad of Celite® and the filtrate is concentrated at ambient temperature under reduced pressure. For further purification, the solid material is washed with $Et_2O$ (3 x 10 mL) to give complex **117** as a brown solid (6.84 g, 89%). $^1$H NMR (400 MHz, $C_6D_6$): δ = 6.76 (d, *J* = 7.6 Hz, 2H), 6.45 (t, *J* = 7.6 Hz, 1H), 3.49 (s, 3H), 3.36 (s, 6H), 3.07 (m, 5H), 2.89 (s, 2H). The analytical and spectroscopic data are in agreement with those reported in the literature.[113]

**Complexes 120, 121, 122 and 123.**

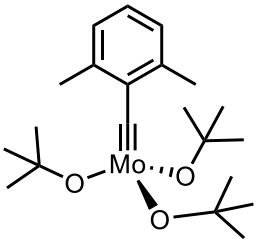


A 250 mL Schlenk flask was equipped with a magnetic stir bar and was flame dried under vacuum. The flask was filled with argon and charged with Mo(≡CAr)$Br_3$(dme) (**117**, Ar = 2,6-dimethylphenyl) (1.05 g, 1.93 mmol) and THF (21 mL). A solution of NaOtBu (563 mg, 5.74 mmol) in THF (5 mL) was added dropwise at 25 °C and stirring was continued for 14 h before the solvent was removed *in vacuo* to obtain a dark brown solid. A second, flame dried 250 mL Schlenk flask was equipped with a magnetic stir bar and a Celite® (2 cm) packed argon frit. The dark brown solid was suspended in *n*-pentane (4 x 15 mL) and was filtered through the Celite® pad. The resulting filtrate was concentrated and the residue dried under vacuum ($10^{-3}$ mbar) to give complex **120** as a brown solid containing **121**, dinuclear complex **122** and 1,2-bis(2,6-dimethylphenyl)ethyne (**123**) and (769 mg, 92%). Neopentylidyne complex **121** was separated from this mixture by sublimation at 60 °C for 3 h under high vacuum ($10^{-3}$ mbar). The remaining mixture was dissolved in minimum of *n*-pentane (20 mL) and filtered via cannula into a flame dried 50 mL Schlenk flask under Ar. The brown/purple solution was stored for 6 h on dry ice (–85°C) to give red/purple crystals. The brown supernatant solution was filtered off via cannula and the solvent of this solution was removed *in*

*vacuo* to give pure complex **120**. $^{1}$H NMR (400 MHz, $C_6D_6$): δ = 6.90 (dd, *J* = 7.3, 0.8 Hz, 2H), 6.80 (dd, *J* = 8.2, 6.8 Hz, 2H), 2.86 (s, 6H), 1.44 (s, 27H). $^{13}$C NMR (101 MHz, $C_6D_6$): δ = 297.1, 145.5, 139.4, 127.4, 127.1, 78.7, 33.2, 32.3. $^{95}$Mo NMR (26 MHz, 60°C, $C_6D_5CD_3$): δ = 259. IR (film): $\tilde{\nu}$ 2969, 2923, 1461, 1359, 1383, 1236, 1162, 1099, 1025, 946, 895, 765, 788, 732, 640, 575, 591, 475, 412 cm$^{-1}$. Elemental analysis (%) calculated for $C_{21}H_{36}MoO_3$: C 58.32, H 8.39, Mo 22.19; found: C 58.32, H 8.66, Mo 21.77. HRMS: not detectable (decomp.).

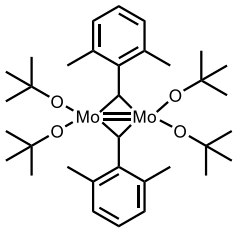


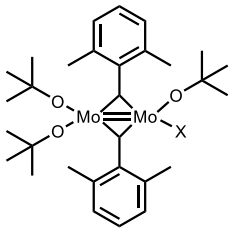


The remaining red/purple crystals were redissolved in $Et_2O$ (5 mL) and the concentrated $Et_2O$ solution was filtered via cannula into a 10 mL Schlenk flask. This solution was cooled from ambient temperature to –75°C over 10 h to give red crystals suitable for single-crystal X-ray diffraction. NMR spectroscopy confirmed the dinuclear complex **122** but it was also observed that a chemically very similar unsymmetric complex was also present in solution. Also free *tert*-butanol as well as 1,2-bis(2,6-dimethylphenyl)ethyne were present in solution. Symmetric dinuclear complex **122**: $^{1}$H NMR (600 MHz, $C_6D_5CD_3$): δ = 7.18 (m, 4H), 7.02 (m, 2H), 2.98 (s, 12H), 0.98 (s, 36H). $^{13}$C NMR (151 MHz, $C_6D_5CD_3$): δ = 341.3, 151.4, 131.9, 128.6, 126.6, 80.8, 31.9, 24.7. HRMS was not detectable (decomposition observed). Unsymmetric dinuclear complex: $^{1}$H NMR (400 MHz, $C_6D_5CD_3$): δ = 7.18 (m, 4H), 7.05 (t, *J* = 7.3 Hz, 2H), 3.38 (s, 12H), 1.06 (s, 9H), 1.06 (s, 9H), 0.42 (s, 9H) . $^{13}$C NMR (151 MHz, $C_6D_5CD_3$): δ = 339.5, 146.0, 134.1, 129.2, 127.0, 81.4, 81.0, 79.4, 32.1, 31.8, 30.9, 26.2. HRMS: not detectable (decomp.).

**Complex 109**

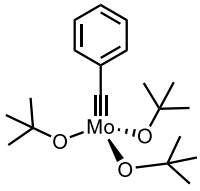


A 100 mL Schlenk flask was equipped with a magnetic stir bar and was flame dried under vacuum. The flask was filled with argon and Mo(≡CPh)$Br_3$(dme) (**S7**)[113] (1.20 g, 2.20 mmol) was dissolved in THF (25 mL). Then a solution of NaO*t*Bu (633 mg, 6.59 mmol) in THF (10 mL) was added dropwise at 25°C to the stirred solution. Stirring was continued for 14 h at ambient temperature before the solvent was removed *in vacuo* to obtain a dark brown solid. A second, flame dried 50 mL Schlenk flask was equipped with a magnetic stir bar and a Celite® (2 cm) packed argon frit. The dark brown solid was suspended in *n*-pentane (4 x 5 mL) and was filtered through the Celite® pad. The resulting filtrate was concentrated and the residue dried under vacuum ($10^{-3}$ mbar) to give complex **109** as a brown solid (717 mg, 80%) free of any residual THF. $^{1}$H NMR (400 MHz, $C_6D_6$): δ = 7.52 – 7.49 (m, 2H), 7.13 – 7.07 (m, 2H), 6.88 (tt, *J* = 7.2, 1.3 Hz, 1H), 1.49 (s, 27H). $^{13}$C NMR (101 MHz, $C_6D_6$): δ = 276.6, 146.7, 129.7, 128.4, 127.0, 80.3, 32.8. $^{95}$Mo NMR (26 MHz, 60°C, $C_6D_5CD_3$): δ = 62.0. The analytical and spectroscopic data are in agreement with those reported in the literature.[95]

**Complex 108**

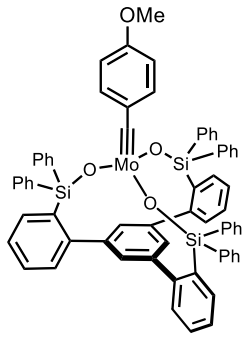


A 250 mL Schlenk flask was equipped with a magnetic stir bar and was flame dried under vacuum. The flask was filled with argon and charged with ligand **105** (968 mg, 1.07 mmol), which was azeotropically dried with benzene (3 x 5 mL) to remove residual water. Then toluene (81 mL) was added and the mixture was vigorously stirred for 10 min to obtain a clear solution. A solution of complex **107** (467 mg, 1.07 mmol) in toluene (16 mL) was added dropwise under vigorous stirring at 25 °C. After stirring for an additional 1 h, the solvent was removed *in vacuo* to give a yellow powder (1.14 g, 95%, mixture of monomer **108** and dimer [**108**]$_2$), which was used in the next step.

A 10 mL Schlenk flask was equipped with a magnetic stir bar and was flame dried under vacuum. The flask was filled with argon and then charged with complex [**108**]$_2$ (94.0 mg, 42.2 µmol) and $C_6D_5CD_3$ (2 mL). The resulting yellow suspension was vigorously stirred at 60°C for 1 h to give an orange solution containing only monomeric complex **108** which showed the following analytical and spectral data: $^1$H NMR (400 MHz, $C_6D_5CD_3$): δ = 7.86 – 7.77 (m, 12H), 7.78 – 7.69 (m, 3H), 7.25 (s, 3H), 7.13 – 7.00 (m, 24H), 6.87 (dd, *J* = 6.3, 2.5 Hz, 3H), 6.21 (d, *J* = 8.8 Hz, 2H), 6.13 (d, *J* = 8.6 Hz, 2H), 3.05 (s, 3H). $^{13}$C NMR (101 MHz, $C_6D_5CD_3$): δ = 310.4, 158.7, 149.1, 143.6, 140.6, 137.7, 137.0, 137.0, 135.0, 134.6, 130.1, 130.0, 129.6, 129.3, 128.9, 128.8, 128.0, 127.7, 125.8, 112.1, 53.9. $^{29}$Si NMR (79 MHz, $C_6D_6$): δ = −9.9. $^{95}$Mo NMR (26 MHz, 60°C, $C_6D_5CD_3$): δ = 421.8. $^1$H-DOSY NMR ($C_6D_5CD_3$): $D_{exp.}$ = 5.557·10$^{-10}$ m$^2$/s$^{-1}$. HRMS-ESI (*m/z*): calculated for $C_{68}H_{53}MoO_4Si_3^+$ [M+H]$^+$, 1115.23002; found, 1115.23153; Elemental analysis (%) calculated for $C_{68}H_{52}MoO_4Si_3$: C 73.36, H 4.71, Mo 8.62, Si 7.57; found: C 71.10, H 4.92, Mo 8.31, Si 7.51.

**Complex 131**

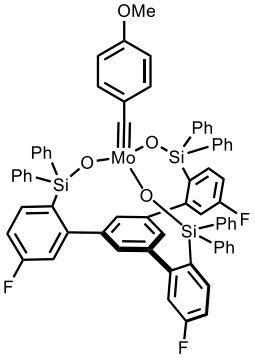


A 100 mL Schlenk flask was equipped with a magnetic stir bar and was flame dried under vacuum. The flask was filled with argon and charged with ligand **127** (571 mg, 0.598 mmol), which was azeotropically dried with benzene (3 x 5 mL) to remove residual water. Toluene (45 mL) was added and the mixture vigorously stirred for 10 min to obtain a clear solution. A solution of complex **107** (260 mg, 0.598 mmol) in toluene (9 mL) was added dropwise to the vigorously stirred solution at 25 °C. After stirring for 1 h, the solvent was removed *in vacuo* to give a bright yellow powder (350 mg, 50%, mixture of monomer **131** and dimer [**131**]$_2$), which was used in the next step.

A 10 mL Schlenk flask was equipped with a magnetic stir bar and flame dried under vacuum. The flask was filled with argon and charged with the crude mixture of **131**/[**131**]$_2$ (70.0 mg, 59.9 µmol) and $C_6D_5CD_3$ (1 mL) to give a yellow suspension. The mixture was vigorously stirred at 60°C for 3 h to give an orange solution containing only monomeric complex **131**. $^1$H NMR (400 MHz, $C_6D_5CD_3$): δ = 7.74 (d, *J* = 7.1 Hz, 12H), 7.56 (dd, *J* = 8.3, 6.5 Hz, 3H), 7.18 – 7.01 (m, 21H), 6.74 (td, *J* = 8.5, 2.6 Hz, 3H), 6.57 (dd, *J* = 10.1, 2.5 Hz, 3H), 6.24 (d, *J* = 8.5 Hz, 2H), 6.14 (d, *J* = 8.6 Hz, 2H), 3.05 (s, 3H). $^{13}$C NMR (101 MHz, $C_6D_5CD_3$): δ = 311.4, 164.0 (d, *J* = 250.2 Hz), 158.9, 151.3 (d, *J* = 7.5 Hz), 142.4, 140.6, 139.3 (d, *J* = 8.1 Hz), 137.4, 134.4, 130.7 (d, *J* = 3.4 Hz), 130.0, 129.5, 128.9, 127.8, 117.0 (d, *J* = 20.3 Hz), 112.8 (d, *J* = 19.5 Hz), 112.2, 53.9. $^{19}$F NMR (376 MHz, $C_6D_5CD_3$): δ = −111.2. $^{29}$Si NMR (79 MHz, $C_6D_5CD_3$): δ = −9.8. $^{95}$Mo NMR (26 MHz, 60°C, $C_6D_5CD_3$): δ = 433.6. IR (film): $\tilde{\nu}$ 1590, 1569, 1505, 1474, 1247, 1428, 1172, 1112, 1030, 995, 871, 826, 762, 740, 697, 635, 493, 461, 422 cm$^{-1}$. HRMS-APPI (m/z): calculated for $C_{68}H_{49}F_3MoO_4Si_3^+$ [M]$^+$, 1168.19478; found, 1168.19393. Elemental analysis (%) calculated for $C_{68}H_{49}F_3MoO_4Si_3$: C 69.97, H 4.23, F 4.88, Mo 8.22, Si 7.22; found: C 67.87, H 4.59, F 4.69, Mo 7.91, Si 6.95.

**Complex 116**

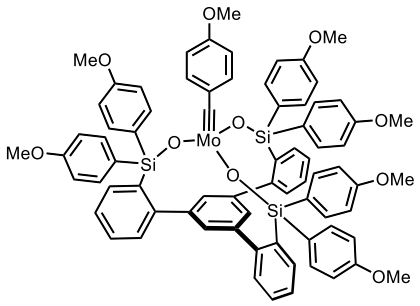


A 50 mL Schlenk flask was equipped with a magnetic stir bar and flame dried under vaccum. The flask was filled with argon and charged with ligand **112** (329 mg, 0.304 mmol), which was azeotropically dried with benzene (3 x 5 mL) to remove residual water. Toluene (23 mL) was added and the resulting mixture vigorously stirred for 10 min to obtain a clear solution. A solution of complex 14a (132 mg, 0.304 mmol) in toluene (5 mL) was added dropwise and stirring was continued for 1 h. The solvent was removed *in vacuo* to give a yellow powder (299 mg, 76%, mixture of monomer 16b and dimer [16b]$_2$), which was used in the next step. A 10 mL Schlenk flask was equipped with a magnetic stir bar and flame dried under vacuum. The flask was filled with argon and charged with the crude mixture of [**116**]$_2$/**116** (60.0 mg, 46.4 µmol) and $C_6D_5CD_3$ (1 mL). The resulting yellow suspension was vigorously stirred at 60°C for 1 h to give an orange solution containing only monomeric complex **116**. $^1$H NMR (400 MHz, $C_6D_5CD_3$): δ = 7.85 (dd, *J* = 6.9, 1.9 Hz, 3H), 7.81 – 7.73 (m, 9H), 7.36 (s, 3H), 7.15 (dd, *J* = 7.1, 1.8 Hz, 3H), 7.13 – 7.08 (m, 3H), 6.97 – 6.93 (m, 3H), 6.73 – 6.58 (m, 12H), 6.28 – 6.23 (m, 3H), 6.20 – 6.10 (m, 3H), 3.31 (s, 18H), 3.06 (s, 3H). $^{13}$C NMR (101 MHz, $C_6D_5CD_3$): δ = 309.3, 161.0, 158.5, 149.3, 143.6, 140.7, 136.2, 136.1, 130.2, 130.0, 129.4, 129.1, 128.9, 125.6, 113.6, 112.0, 53.9, 53.9. $^{29}$Si NMR (79 MHz, $C_6D_6$): δ = −9.1. $^{95}$Mo NMR (26 MHz, 60°C, $C_6D_5CD_3$): δ = 414.3. $^1$H-DOSY NMR ($C_6D_5CD_3$): $D_{exp.}$ = 5.557·10$^{-10}$ m$^2$/s$^{-1}$. IR (film): $\tilde{\nu}$ 2834, 1592, 1563, 1501, 1461, 1439, 1409, 1397, 1277, 1244, 1179, 1113, 1063, 1030, 994, 868, 820, 796, 759, 731, 692, 647, 622, 530, 502, 464, 426, 408 cm$^{-1}$. HRMS-APPI (*m/z*): calculated

for $C_{74}H_{64}MoO_{10}Si_3^+$ [M+H]$^+$, 1294.28559; found, 1294.28623. Elemental analysis (%) calculated for $C_{74}H_{64}MoO_{10}Si_3$: C 68.71, H 4.99, Mo 7.42, Si 6.51; found: C 68.37, H 5.12, Mo 7.33, Si 6.41.

**Complex [116·py]$_4$**

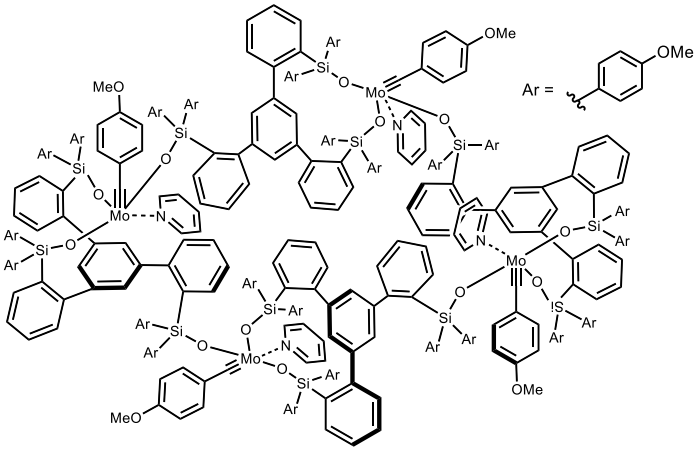


A 10 mL Schlenk flask was equipped with a magnetic stir bar and was flame dried under vacuum. The flask was filled with argon, charged with [**116**]$_2$ (18.0 mg, 13.9 µmol) and pyridine (2.5 mL) to give a purple solution, which was filtered into a second, flame dried and argon filled 10 mL Schlenk flask. This purple solution was layered with *n*-pentane (5 mL) and gave violet crystals suitable for single-crystal X-ray after 3 days storing at ambient temperature.

$^1$H NMR (400 MHz, $C_6D_5CD_3$): δ = broaden shifts (NMR attached). IR (film): $\tilde{\nu}$ 1591, 1562, 1500, 1438, 1243, 1275, 1179, 1107, 1030, 987, 886, 822, 796, 757, 719, 689, 649, 625, 500, 532, 460 cm$^{-1}$. HRMS-ESI (m/z): calculated for $C_{296}H_{258}Mo_4O_{40}Si_{12}^+$ [M–4·($C_5H_5N$)]$^+$, 2589.57955; found, 2589.589890. Elemental analysis (%) calculated for $C_{316}H_{276}Mo_4N_4O_{40}Si_{12}$: C 69.13, H 5.07, N 1.02, Mo 6.99, Si 6.14; found: C 67.81, H 4.92, N 0.98, Mo 6.91, Si 6.01.

**Complex 132**

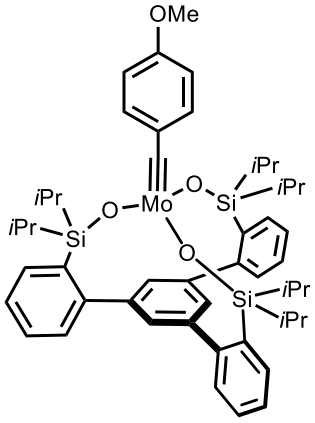


A 50 mL Schlenk flask was equipped with a magnetic stir bar and was flame dried under vacuum. The flask was filled with argon and charged with ligand **128** (264 mg, 0.379 mmol), which was azeotropically dried with benzene (3 x 5 mL) to remove residual water. Toluene (28 mL) was added and the mixture vigorously stirred for 10 min to obtain a clear solution. Then a solution of complex **107** (158 mg, 0.365 mmol) in toluene (6 mL) was added dropwise at 25 °C and stirring continued for 3 h. The solvent was removed *in vacuo* to give a yellow/orange powder containing only monomeric complex **132** (340 mg, 99%). Yellow crystals suitable for single-crystal X-ray diffraction were grown from a concentrated $Et_2O$ solution at –30°C. $^1$H NMR (400 MHz, $C_6D_5CD_3$): δ = 7.45 – 7.38 (m, 6H), 7.28 – 7.21 (m, 3H), 7.17 (td, *J* = 6.6, 5.6, 3.7 Hz, 6H), 7.13 – 7.06 (m, 2H), 6.54 (d, *J* = 8.8 Hz, 2H), 3.16 (s, 3H), 1.29 (hept, *J* = 7.1 Hz, 6H), 1.24 (d, *J* = 6.8 Hz, 18H), 1.11 (d, *J* = 7.1 Hz, 18H). $^{13}$C NMR (101 MHz, $C_6D_5CD_3$): δ = 303.3, 158.7, 149.6, 143.6, 140.9, 135.0, 133.8, 130.8, 129.6, 128.3 (t, *J* = 23.8 Hz), 127.6, 125.9, 112.7, 54.1, 18.1, 17.7, 15.0. $^{29}$Si NMR (79 MHz, $C_6D_5CD_3$): δ = 10.2. $^{95}$Mo NMR (26 MHz, 60°C, $C_6D_5CD_3$): δ = 358.0. $^1$H-DOSY NMR ($C_6D_5CD_3$): $D_{predicted.}$ = 6.08·10$^{-10}$ m$^2$/s$^{-1}$;

$D_{exp.}$ = 6.80·10$^{-10}$ m$^2$/s$^{-1}$. IR (film): $\tilde{\nu}$ 2941, 2862, 1591, 1503, 1462, 1408, 1259, 1243, 1171, 1088, 1017, 919, 875, 799, 757, 738, 722, 671, 651, 627, 518, 471 cm$^{-1}$. HRMS-ESI (m/z): calculated for $C_{50}H_{65}MoO_4Si_3^+$ $[M+H]^+$, 911.32392; found, 911.32409. Elemental analysis (%) calculated for $C_{50}H_{64}MoO_4Si_3$: C 66.05, H 7.09, Mo 10.55, Si 9.27; found: C 62.02, H 6.82, Mo 9.93, Si 8.72.

**Complex 134**

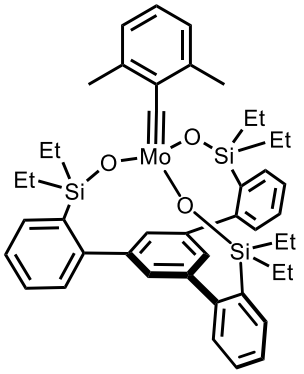


A 100 mL Schlenk flask was equipped with a magnetic stir bar and flame dried under vacuum. The flask was filled with argon and charged with ligand **129** (1.23 g, 2.01 mmol), which was azeotropically dried with benzene (3 x 5 mL) to remove residual water. Toluene (28 mL) was added and the mixture vigorously stirred for 10 min to obtain a clear solution. Then a solution of complex **120** (925 mg, 2.14 mmol) in toluene (15 mL) was added dropwise and stirring was continued for 4 h at ambient temperature. The solvent was removed *in vacuo* and the crude solid was extracted with *n*-pentane (5 x 15 mL) to give a yellow/orange powder containing only monomeric complex **134** (1.63 g, 99%). Yellow crystals suitable for single-crystal X-ray diffraction were grown from a concentrated $Et_2O$ solution at –20°C. $^1$H NMR (600 MHz, $C_6D_5CD_3$): δ = 7.44 (s, 3H), 7.43 – 7.39 (m, 3H), 7.26 – 7.21 (m, 3H), 7.20 – 7.14 (m, 6H), 6.80 – 6.76 (m, 2H), 6.65 (t, *J* = 7.5 Hz, 1H), 2.68 (s, 6H), 1.01 – 0.96 (m, 18H), 0.95 – 0.86 (m, 12H). $^{13}$C NMR (151 MHz, $C_6D_5CD_3$): δ = 305.8, 149.2, 145.0, 144.2, 137.9, 135.9, 134.2, 130.4, 128.6, 127.6, 127.0, 126.3, 126.2, 20.4, 9.1, 6.8. $^{29}$Si NMR (119 MHz, $C_6D_5CD_3$): δ = 11.8. $^{95}$Mo NMR (26 MHz, 60°C, $C_6D_5CD_3$): δ = 416.9 . IR (film): $\tilde{\nu}$ 3051, 2952, 2931, 2909, 2872, 1581, 1557, 1460, 1429, 1407, 1375, 1259, 1232, 1161, 1122, 1088, 1063, 1044, 1012, 1002, 912, 761, 725, 697, 668, 624, 584, 552, 528, 513, 479, 460, 420 cm$^{-1}$. HRMS-ESI (m/z): calculated for $C_{45}H_{54}MoO_3Si_3^+$ $[M]^+$, 824.24293; found, 824.24333. Elemental analysis (%) calculated for $C_{45}H_{54}MoO_3Si_3$: C 65.66, H 6.61, Mo 11.66, Si 10.24; found: C 64.10, H 6.47, Mo 11.27, Si 9.87.

**Complex 124**

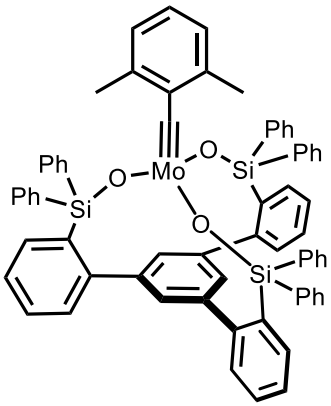


A 100 mL Schlenk flask was equipped with a magnetic stir bar and flame dried under vacuum. The flask was filled with argon and charged with ligand **105** (388 mg, 0.431 mmol), which was azeotropically dried with benzene (3 x 5 mL) to remove residual water. Toluene (32 mL) was added and the mixture vigorously stirred for 10 min to obtain a clear solution. Then a solution of complex **120** (192 mg, 0.444 mmol) in toluene (6 mL) was added dropwise and stirring was continued for 6 h at ambient temperature. The solvent was removed *in vacuo* and the yellow/orange solid was washed with *n*-pentane (3 x 5 mL) and $Et_2O$ (3 x 5 mL) to give a yellow/orange powder

containing only the monomeric complex **124** (312 mg, 65%). Yellow crystals suitable for single-crystal X-ray diffraction were grown from a concentrated $Et_2O$ solution at –20°C. $^1$H NMR (400 MHz, $C_6D_5CD_3$): δ = 7.81 – 7.76 (m, 12H), 7.76 – 7.72 (m, 3H), 7.23 (s, 3H), 7.13 – 7.00 (m, 24H), 6.87 – 6.81 (m, 3H), 6.37 (s, 3H), 1.95 (s, 6H). $^{13}$C NMR (101 MHz, $C_6D_5CD_3$): δ = 312.2, 149.2, 144.8, 143.8, 138.6, 137.5, 137.1, 134.8, 134.6, 130.1, 129.7, 129.4, 128.7, 127.6, 127.2, 125.8, 125.6, 19.7. $^{29}$Si NMR (79 MHz, $C_6D_5CD_3$): δ = −9.4. $^{95}$Mo NMR (26 MHz, 60°C, $C_6D_5CD_3$): δ = 466.8. $^1$H-DOSY NMR ($C_6D_5CD_3$): $D_{predicted.}$ = $5.56\cdot10^{-10}$ $m^2/s^{-1}$; $D_{exp.}$ = $5.56\cdot10^{-10}$ $m^2/s^{-1}$. IR (film): $\tilde{\nu}$ 1428, 1112, 1086, 1020, 1032, 997, 875, 849, 736, 772, 443, 413 $cm^{-1}$. HRMS-ESI (m/z): calculated for $C_{69}H_{55}MoO_3Si_3^+$ $[M+H]^+$, 1113.25076; found, 1113.25104. Elemental analysis (%) calculated for $C_{69}H_{54}MoO_3Si_3$: C 74.57, H 4.90, Mo 8.63; found: C 74.45, H 5.06, Mo 9.13.

**Complex 110**

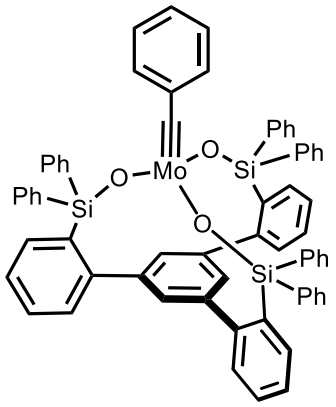


A 250 mL Schlenk flask was equipped with a magnetic stir bar and flame dried under vacuum. The flask was filled with argon and charged with ligand **105** (964 mg, 1.07 mmol), which was azeotropically dried with benzene (3 x 5 mL) to remove residual water. Toluene (81 mL) was added and the mixture vigorously stirred for 10 min to obtain a clear solution. Then a solution of complex **109** (454 mg, 1.12 mmol) in toluene (16 mL) was added dropwise and stirring was continued for 3 h at ambient temperature. The solvent was removed *in vacuo* and the yellow/orange solid was washed with *n*-pentane (3 x 5 mL) and $Et_2O$ (3 x 5 mL) to give a yellow/orange powder containing crude mixture of **110**/[**110**]$_2$ (1.14 g, 98%). A 10 mL Schlenk flask was equipped with a magnetic stir bar and flame dried under vacuum. The flask was filled with argon and charged with the crude mixture of **110**/[**110**]$_2$ (70.0 mg, 64.6 µmol) and $C_6D_5CD_3$ (1 mL) to give a yellow suspension. The mixture was vigorously stirred at 60°C for 1 h to give an orange solution containing only monomeric complex **110**. $^1$H NMR (600 MHz, $C_6D_5CD_3$): δ = 7.81 – 7.77 (m, 12H), 7.75 – 7.73 (m, 3H), 7.25 (s, 3H), 7.12 – 7.06 (m, 12H), 7.06 – 7.01 (m, 12H), 6.89 – 6.85 (m, 3H), 6.58 (t, *J* = 7.7 Hz, 2H), 6.49 (tt, *J* = 6.9, 1.1 Hz, 1H), 6.24 – 6.19 (m, 2H). $^{13}$C NMR (151 MHz, $C_6D_5CD_3$): δ = 310.7, 149.5, 146.3, 144.1, 138.0, 137.4, 135.3, 135.0, 130.5, 130.1, 129.8, 129.3, 128.6, 128.2, 127.3, 127.2, 126.2, 20.4. $^{29}$Si NMR (79 MHz, $C_6D_5CD_3$): δ = −9.6. $^{95}$Mo NMR (26 MHz, 60°C, $C_6D_5CD_3$): δ = 377.2. IR (film): $\tilde{\nu}$ 3045, 1583, 1484, 1427, 1409, 1261, 1112, 1063, 1029, 1001, 871, 830, 759, 738, 696, 622, 566, 548, 528, 506, 464 $cm^{-1}$. HRMS-ESI (m/z): calculated for $C_{67}H_{50}MoO_3Si_3^+$ $[M]^+$, 1084.21163; found, 1084.212010. Elemental analysis (%) calculated for $C_{67}H_{50}MoO_3Si_3$: C 74.28, H 4.65, Mo 8.86, Si 7.78; found: C 74.31, H 4.67, Mo 8.80, Si 7.71.

**Complex 133**

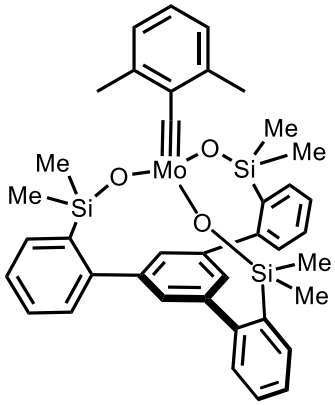


A 250 mL Schlenk flask was equipped with a magnetic stir bar and flame dried under vacuum. The flask was filled with argon and charged with ligand **130** (468 mg, 0.885 mmol), which was azeotropically dried with benzene (3 x 5 mL) to remove residual water. Toluene (70 mL) was added and the mixture was vigorously stirred for 10 min to obtain a clear solution. Then a solution of complex **120** (403 mg, 0.932 mmol) in toluene (14 mL) was added dropwise and stirring was continued for 4 h at ambient temperature. The solvent was removed *in vacuo* and the crude solid was extracted with *n*-pentane (5 x 5 mL) to give a yellow/orange powder containing monomeric complex **133** and a minor (oligomeric) impurity (550 mg, 84%). $^{1}$H NMR (400 MHz, $C_6D_5CD_3$): δ 7.44 (s, 3H), 7.43 – 7.40 (m, 3H), 7.25 – 7.13 (m, 9H), 6.77 (d, *J* = 7.5 Hz, 2H), 6.71 – 6.62 (m, 1H), 2.63 (s, 6H), 0.41 (s, 18H). $^{13}$C NMR (101 MHz, $C_6D_5CD_3$): δ = 304.7, 148.4, 145.0, 144.2, 138.4, 138.0, 134.2, 130.1, 128.7, 127.9, 127.1, 126.4, 126.3, 20.3, 3.0. $^{29}$Si NMR (79 MHz, $C_6D_5CD_3$): δ = 9.4. $^{95}$Mo NMR (26 MHz, 60°C, $C_6D_5CD_3$): δ = 421.8. $^{1}$H-DOSY NMR ($C_6D_5CD_3$): $D_{predicted.}$ = 6.69·10$^{-10}$ m$^2$/s$^{-1}$; $D_{exp.}$ = 7.09·10$^{-10}$ m$^2$/s$^{-1}$. IR (film): $\tilde{\nu}$ 2964, 2037, 1259, 1124, 1094, 1020, 987, 886, 877, 832, 806, 781, 759, 743, 728, 695, 653, 633, 605, 592, 581, 562, 529, 518, 509, 493, 474, 463, 454, 430, 412 cm$^{-1}$. HRMS-ESI (m/z): calculated for $C_{39}H_{43}MoO_3Si_3^+$ [M+H]$^+$, 741.15686; found, 741.15690.

**Complex 136**

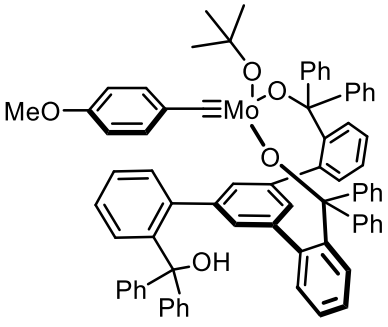


A 50 mL Schlenk flask was equipped with a magnetic stir bar and flame dried under vacuum. The flask was filled with argon and charged with ligand **135** (153 mg, 0.179 mmol), which was azeotropically dried with benzene (3 x 5 mL) to remove residual water. Toluene (13 mL) was added and the mixture vigorously stirred for 10 min to obtain a clear solution. A solution of complex **107** (86.0 mg, 0.198 mmol) in toluene (3 mL) was added dropwise and stirring continued for 14 h. The solvent was removed *in vacuo* and the brown residue was washed with *n*-pentane (3 x 5 mL) to give complex **136** as a bright brown powder (156 mg, 82%). $^{1}$H NMR (600 MHz, $C_6D_5CD_3$): 7.71 (dd, *J* = 7.5, 1.5 Hz, 1H), 7.57 (dd, *J* = 8.4, 1.3 Hz, 4H), 7.38 (dd, *J* = 8.4, 1.3 Hz, 4H), 7.32 – 7.29 (m, 4H), 7.28 (td, *J* = 7.4, 1.3 Hz, 1H), 7.11 (dd, *J* = 8.4, 7.0 Hz, 4H), 7.04 – 7.00 (m, 9H), 6.97 – 6.89 (m, 8H), 6.89 – 6.84 (m, 5H), 6.75 (t, *J* = 1.7 Hz, 1H), 6.71 (d, *J* = 1.7 Hz, 2H), 6.66 (dd, *J* = 7.6, 1.5 Hz, 2H), 6.36 – 6.27 (m, 2H), 5.46 – 5.40 (m, 2H), 3.66 (s, 1H), 3.09 (s, 3H), 1.46 (s, 9H). $^{13}$C NMR (151 MHz, $C_6D_5CD_3$): δ = 287.1, 158.3, 149.3, 149.0, 148.7, 145.2, 144.9, 144.5, 141.2, 141.1, 139.2, 138.8, 133.9, 132.5, 131.0, 130.8, 130.0, 129.3, 128.7, 128.5, 127.7, 127.6, 127.5, 127.5, 127.5, 127.4, 127.0, 126.7, 126.5, 126.1, 126.1, 125.7, 112.1, 94.2, 83.6, 82.7, 53.9, 32.8. $^{95}$Mo NMR (26 MHz,

60°C, $C_6D_5CD_3$): δ = 118.3. $^1$H-DOSY NMR ($C_6D_5CD_3$): $D_{predicted.}$ = 5.50·10$^{-10}$ m$^2$/s$^{-1}$; $D_{exp.}$ = 5.58·10$^{-10}$ m$^2$/s$^{-1}$. IR (film): $\tilde{\nu}$ 3533, 3058, 2968, 1593, 1503, 1445, 1360, 1283, 1243, 1168, 1040, 1013, 922, 908, 828, 804, 787, 755, 729, 696, 637, 607, 591, 515, 498, 454, 430, 412 cm$^{-1}$. HRMS-ESI (m/z): calculated for $C_{75}H_{62}MoO_5Na^+$ [M+Na]$^+$, 1163.35435; found, 1163.35514. Elemental analysis (%) calculated for $C_{75}H_{62}MoO_5$: C 79.07, H 5.49, Mo 8.42; found: C 79.25, H 5.66, Mo 8.12.

**Complex 147**

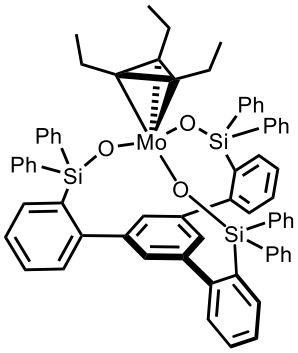


A 10 mL Schlenk flask was equipped with a magnetic stir bar and was flame dried under vacuum. The flask was filled with argon, charged with [**108**]$_2$ (13.5 mg, 0.012 mmol) and suspended in [D$_8$]-toluene (0.6 mL) to give a yellow suspension. A flame dried *J. Young* NMR tube was filled with argon, charged with the suspension and heated to 60°C until full conversion to monomeric complex **108** was observed. After cooling to 25°C, 3-hexyne (6.9 µL, 61 µmol) was added to the yellow solution and an instant color change to black was observed. The full characterization of **147** was conducted by NMR spectroscopy at 25°C. $^1$H NMR (600 MHz, $C_6D_5CD_3$): δ = 7.81 – 7.76 (m, 12H), 7.68 – 7.64 (m, 3H), 7.27 (s, 3H), 7.18 – 7.13 (m, 6H), 7.10 – 7.06 (m, 12H), 6.93 – 6.89 (m, 3H), 7.13 – 6.98 (m, 6H), 1.75 (m, 6H), 0.48 (t, *J* = 7.4 Hz, 9H). $^{13}$C NMR (151 MHz, $C_6D_5CD_3$): δ = 150.3, 144.0, 139.1, 137.2, 136.7, 135.2, 129.6, 129.3, 129.2, 128.3, 127.4, 125.2, 83.9, 18.5, 15.4. $^{29}$Si NMR (119 MHz, $C_6D_5CD_3$): δ = -8.48. The spectroscopic data are in agreement with those reported in the literature.[159]

**Complex 111: Optimized Procedure and Alternative Protonolysis Protocol**

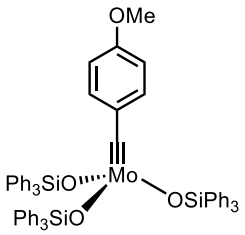


A 250 mL, three neck round-bottom flask was equipped with a magnetic stirring bar, a pressure-equalizing dropping funnel fitted with a rubber stopper and a gas inlet connected to an argon/vacuum manifold. The flask was loaded with [Mo(≡CAr)Br$_3$(dme)] (Ar = 4-Methoxyphenyl) **106** (1.50 g, 2.75 mmol) and THF (46 mL). The stirring brown solution was cooled to 0 °C before a solution of potassium triphenylsilanolate (2.58 g, 8.21 mmol) in THF (54 mL) was added via the addition funnel over 4 h. When the addition was complete, the cooling bath was removed and stirring continued for an additional 1 h. The solvent was removed *in vacuo*, the residue was slurried in toluene (30 mL) and the mixture filtered under Ar through a pad of compressed Celite® (2 cm), rinsing with toluene (15 mL). The brown filtrate was concentrated to dryness and the residue was dissolved in $Et_2O$ (40 mL). The solution was stirred for 30 min at 0°C and a yellow solid precipitated. The yellow crystalline material was collected by filtration, washed with cold $Et_2O$ (20 mL) and was dried under high vacuum to give the title complex as a yellow powder (repeated seven times, average yield: 1.43 g, 50%).

**Protonolysis:**

A 250 mL Schlenk flask was equipped with a magnetic stir bar and flame dried under vacuum. The flask was filled with argon and charged with complex **107** (0.75 g, 1.73 mmol) and dissolved in toluene (60 mL). Then a solution of triphenylsilanol (1.47 g, 5.33 mmol) in toluene (30 mL) was added dropwise to the stirred solution within 10 min. The solution was stirred for 16 h at ambient temperature before the solvent was removed *in vacuo* to obtain a yellow foam. The solid was fully dissolved in *n*-pentane (23 mL) and $Et_2O$ (8 mL), then excess *n*-pentane (150 mL) was added to precipitate the desired complex. The yellow crystalline material was collected by filtration, washed with *n*-pentane (3x 10 mL) and $Et_2O$ (1x 3mL) and was dried under high vacuum to give the title complex as a yellow powder (repeated six times, average yield: 1.08 g, 60%). $^1$H NMR (400 MHz, $C_6D_5CD_3$): δ = 7.79 – 7.72 (m, 18H), 7.22 – 7.15 (m, 9H), 7.10 (t, *J* = 7.4 Hz, 18H), 6.18 – 6.13 (m, 2H), 5.57 – 5.49 (m, 2H), 3.19 (s, 3H). $^{13}$C NMR (101 MHz, $C_6D_5CD_3$): δ = 300.5, 158.7, 140.3, 136.4, 135.8, 131.1, 130.0, 128.1, 112.0, 54.4. $^{29}$Si NMR (79 MHz, $C_6D_6$): δ = −8.0. $^{95}$Mo NMR (26 MHz, 25 °C, $C_6D_5CD_3$): δ = 385.8. $^{95}$Mo NMR (26 MHz, 60°C, $C_6D_5CD_3$): δ = 397.6. The analytical and spectroscopic data are in agreement with those reported in the literature.[58, 113]

**Complex 154**

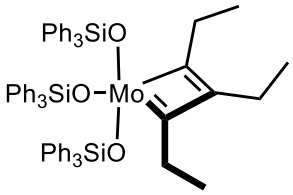


A 10 mL Schlenk flask was equipped with a magnetic stir bar and was flame dried under vacuum. The flask was filled with argon, charged with **111** (27.1 mg, 0.026 mmol) and dissolved in $Et_2O$ (1 mL) to give a yellow solution. Upon addition of 3-hexyne (10.7 mg, 14.8 µL) the color instantly changed to a green/blue solution. This solution was cannula filtered under Ar and stored at –85 °C for one week to obtain very sensitive, steel-blue crystals suitable for single-crystal X-ray diffraction.

A 10 mL Schlenk flask was equipped with a magnetic stir bar and was flame dried under vacuum. The flask was filled with argon, charged with complex **111** (12.6 mg, 0.012 mmol) and dissolved in $C_6D_5CD_3$ (0.6 mL) to give a yellow solution. This solution was transferred into a *J. Young* NMR Tube and a $^1$H-NMR spectrum was measured. Upon addition of 3-hexyne (10.7 mg, 6.9 µL) the color instantly change to a green/blue solution. Complex **154** was fully characterized in this mixture by NMR spectroscopy at -40 °C. $^1$H NMR (600 MHz, $C_6D_5CD_3$, -40°C): δ = 8.07 (d, *J* = 7.3 Hz, 6H), 7.45 – 7.42 (m, 12H), 7.11 (t, *J* = 7.5 Hz, 9H), 7.02 (t, *J* = 7.3 Hz, 18H), 2.61 (q, *J* = 7.5 Hz, 4H), 1.87 (q, *J* = 7.8 Hz, 2H), 1.52 (t, *J* = 7.5 Hz, 6H), -0.13 (t, *J* = 7.7 Hz, 3H). $^{13}$C NMR (151 MHz, $C_6D_5CD_3$, -40°C): δ = 248.8, 144.8, 138.5, 137.3, 136.1, 135.4, 129.4, 128.6, 127.3, 127.3, 31.2, 26.0, 14.4, 11.2. $^{29}$Si NMR (119 MHz, $C_6D_5CD_3$, -40°C): = δ –15.6, –22.3.

**Complex 197**

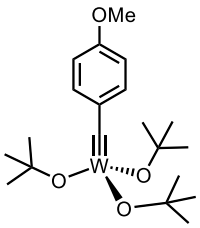


A 25 mL Schlenk flask was equipped with a magnetic stir bar and was flame dried under vacuum. The flask was filled with argon and W(≡CAr)$Br_3$(dme) (Ar = 4-methoxyphenyl) (**196**)[167] (503 mg, 0.795 mmol) was dissolved in THF (9 mL). Then a solution of NaO*t*Bu (232 mg, 2.37 mmol) in THF (2 mL) was added dropwise at 25 °C to the stirred solution. Stirring was continued for 14 h at ambient temperature before the solvent was removed *in vacuo* to obtain a dark brown solid. A second, flame dried 50 mL Schlenk flask was equipped with a magnetic stir bar and a Celite® (2 cm) packed argon frit. The dark brown solid was suspended in *n*-pentane (4 x 5 mL) and was filtered through the Celite® pad. The resulting filtrate was concentrated and the residue dried under vacuum ($10^{-3}$ mbar) to give complex **197** as a brown solid (376 mg, 91%) free of any residual THF. $^1$H NMR (400 MHz, $C_6D_6$): δ = 7.31 – 7.25 (m, 2H), 6.87 – 6.72 (m, 2H), 3.31 (d, *J* = 1.0 Hz, 3H), 1.52 (d, *J* = 0.8 Hz, 27H). $^{13}$C NMR (101 MHz, $C_6D_6$): δ = 257.2, 158.4, 142.2, 133.5, 113.2, 81.0, 54.8, 32.8. IR (film): $\tilde{\nu}$ 2969, 1580, 1505, 1468, 1359, 1277, 1239, 1166, 1042, 935, 826, 788, 590, 547, 481 $cm^{-1}$. HRMS-EI (m/z): calcd. for $C_{20}H_{34}WO_4^+$ $[M]^+$, 522.19670; found, 522.19707. Elemental analysis (%) calcd for $C_{20}H_{34}WO_4$: C 45.99, H 6.56; found: C 45.77, H 6.31.

**Complex $[NMe_4]W(CO)_5(COAr)$ (Ar = 2,6-dimethlyphenyl) (198)**

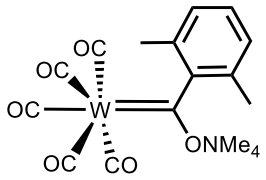


A two-neck round-bottom flask is equipped with a Teflon-coated magnetic stirring bar and an Argon-vacuum manifold. The flask is charged with 2-bromo-1,3-dimethylbenzene (3.02 g, 16.0 mmol) and diethyl ether (67 mL). The solution is cooled to −25°C and a solution of *tert*-butyllithium (21.0 mL, 33.6 mmol, 1.6 M in *n*-pentane) was added over 10 min. Once the addition is complete, stirring is continued for 1 h at −20°C. A 250 mL, three-neck round-bottom flask is equipped with a Teflon-coated magnetic stirring bar, a reflux condenser, a pressure-equalizing dropping funnel fitted with a rubber stopper and an Argon-vacuum manifold. The flask is charged with $[W(CO)_6]$ (**12**) (5.63 g, 16.0 mmol) and diethyl ether (51 mL) and the mixture is cooled to 0°C. The cold (−20 °C) solution of 2,6-dimethylphenyl lithium is added via the dropping funnel over 5 min to the suspension, causing an immediate color change to orange-brown and a slight exotherm. Once the addition is complete, the resulting orange-brown solution is stirred at ambient temperature for 2 h. The dropping funnel and the reflux condenser are replaced by a glass stopper and the solvent is removed at ambient temperature under reduced pressure. A solution of $Me_4NBr$ (3.84 g, 24.4 mmol) in deionized water (20 mL) is added to the remaining dark yellow residue, causing the formation of an orange solid. The resulting suspension is vigorously stirred for 15 min at ambient temperature before the precipitate is filtered off in air, washed once with deionized water (5 mL), twice with cold (0 °C) diethyl ether (20 mL) and dried under high vacuum ($10^{-3}$ mbar) to give complex **198** as a pale

orange microcrystalline solid (5.45 g, 64%). The complex is still contaminated with starting complex $W(CO_6)$, which can't be removed due to its low solubility, but turned out not to be problematic in the next step. $^1$H NMR (600 MHz, $CCl_2D_2$): δ = 6.91 – 6.77 (m, 3H), 3.12 (s, 12H), 2.18 (s, 6H). $^{13}$C NMR (151 MHz, $CCl_2D_2$): δ = 298.1 ($^1J$-$^{183}$W-$^{13}$C = 82.4 Hz), 208.3 ($^1J$-$^{183}$W-$^{13}$C = 134.1 Hz), 203.5 ($^1J$-$^{183}$W-$^{13}$C = 127.9 Hz), 162.4 ($^2J$-$^{183}$W-$^{13}$C = 13.3 Hz), 128.3, 127.9, 125.0, 56.6 ($^1J$-$^{14}$N-$^{13}$C = 3.9 Hz), 18.8, 18.6. IR (film): $\tilde{\nu}$ 2028, 1859, 1552, 1519, 1485, 1438, 947, 849, 767, 693, 636, 596, 576, 534, 485, 440, 419 cm$^{-1}$. HRMS-ESI (m/z): calcd. for $C_{14}H_9O_6W^+$ $[M\text{-}C_4H_{12}N]^+$, 456.99139; found, 456.99199. Elemental analysis (%) calcd. for $C_{18}H_{21}NO_6W$: C 40.70, H 3.98, N 2.64; found: C 40.81, H 4.11, N 2.37.

**Complex [W(≡CAr)Br$_3$(dme)] (Ar = 2,6-dimethlyphenyl) (200)**

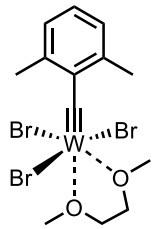


A 250 mL, three-neck round-bottom flask is equipped with a Teflon-coated magnetic stirring bar, a thermometer adapter, a rubber stopper and an Argon-vacuum manifold. The flask is charged with complex **198** (5.82 g, 10.9 mmol) and $CH_2Cl_2$ (93 mL). The mixture is cooled to −78 °C and stirred for 15 min before a solution of oxalyl bromide (1.03 mL, 11.0 mmol) in $CH_2Cl_2$ (6 mL) is added dropwise over 10 min. Once the addition is complete, stirring is continued for 15 min at −78 °C. The mixture is then allowed to warm until a rapid color change to light brown is observed (at an internal temperature of ca. −40 °C). At this point, the reaction flask is quickly re-cooled to −78 °C. A 1 L, three-neck jacketed cooling flask is equipped with a Teflon-coated magnetic stirring bar, a jacketed cooling filter frit (diameter: 4.5 cm; height: 20 cm; porosity: 4) containing a 3 cm-length pad of Celite®, a 20 mL pressure-equalizing dropping funnel connected to an Argon-vacuum manifold. The Celite® in the jacketed filter is slurried with $CH_2Cl_2$ and cooled to −78 °C using a cryostat. The 1 L, three-neck jacketed flask is loaded with 1, 2-dimethoxyethane (5.64 mL, 54.3 mmol) and cooled to −78 °C. The cold light brownish mixture is filtered onto the Celite® packed filter frit, resulting in a bright yellow filtrate. Upon contact with DME in the 1 L receiving flask, a color change from yellow to dark red is observed. The mixture is stirred for 10 min before a solution of $Br_2$ (0.56 mL, 11.0 mmol) in $CH_2Cl_2$ (5 mL) is added dropwise over a period of 15 min via the dropping funnel. Once the addition is complete, the mixture is stirred for 15 min. The resulting brown-orange mixture is allowed to reach ambient temperature over the course of 1 h, during which time the color intensifies. Stirring is continued for 1 h at ambient temperature before the dropping funnel and the filter are replaced by glass stoppers. The reaction mixture is filtered through a pad of Celite® and the filtrate is concentrated at ambient temperature under reduced pressure to give complex **200** as a green microcrystalline solid (6.28 g, 92%). $^1$H NMR (600 MHz, $C_6D_6$): δ = 7.12 (dp, $J$ = 7.7, 0.7 Hz, 2H), 6.15 (t, $J$ = 7.6 Hz, 1H), 3.62 (d, $J$ = 0.8 Hz, 6H), 3.47 (s, 3H), 3.38 (s, 3H), 2.96 – 2.92 (m, 2H), 2.89 – 2.85 (m, 2H). $^{13}$C NMR (151 MHz, $C_6D_6$): δ = 337.4, 150.4, 136.9, 132.1, 125.2, 78.2, 75.5, 69.4, 60.2, 20.6.

IR (film): $\tilde{\nu}$ 2935, 1445, 1080, 1030, 1010, 982, 855, 818, 775, 736, 422 $cm^{-1}$. Elemental analysis (%) calcd for $C_{13}H_{19}Br_3O_2W$: C 24.75, H 3.04, Br 38.00, W 29.14, O 5.07; found: C 24.63, H 3.00, Br 37.85, W 29.17.

**Complex 201**

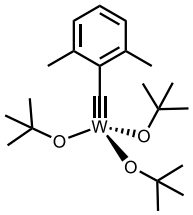

A 50 mL Schlenk flask was equipped with a magnetic stir bar and was flame dried under vaccum. The flask was filled with argon and complex **200** (1.00 g, 1.60 mmol) was dissolved in THF (18 mL). Then a solution of NaO*t*Bu (467 mg, 4.76 mmol) in THF (4 mL) was added dropwise at 25 °C to the stirred brown solution. Stirring was continued for 14 h at ambient temperature before the solvent was removed *in vacuo* to obtain a dark brown solid.

A second, flame dried 100 mL Schlenk flask was equipped with a magnetic stir bar and a Celite® (2 cm) packed argon frit. The dark brown solid was suspended in *n*-pentane (4 x 15 mL) and was filtered through the Celite® pad. The resulting filtrate was concentrated and dried under vacuum ($10^{-3}$ mbar) to give complex **201** as a brown solid (743 mg, 89%) free of any residual THF. Yellow crystals suitable for single-crystal X-ray diffraction were grown from a concentrated *n*-pentane solution (5 mL) stored at −85°C for one week. $^1$H NMR (600 MHz, $C_6D_5CD_3$): δ = 7.01 (d, *J* = 7.5 Hz, 2H), 6.70 (t, *J* = 7.5 Hz, 1H), 2.87 (s, 6H), 1.40 (s, 27H). $^{13}$C NMR (151 MHz, $C_6D_5CD_3$): δ = 271.3 ($^1J$-$^{183}$W-$^{13}$C = 297.3 Hz), 145.3 ($^2J$-$^{183}$W-$^{13}$C = 44.8 Hz), 140.7, 126.8, 125.9, 79.6, 32.1, 21.7. $^{183}$W NMR (17 MHz, $C_6D_5CD_3$): δ = 166.0. IR (film): $\tilde{\nu}$ 2970, 2925, 1462, 1385, 1360, 1239, 1161, 1099, 1026, 944, 913, 895, 791, 780, 762, 734, 628, 597, 558, 512, 478 $cm^{-1}$. Elemental analysis (%) calcd for $C_{21}H_{36}WO_3$: C 48.47, H 6.97, W 35.33; found: C 47.99, H 7.02, W 34.94.

**Complex 212**

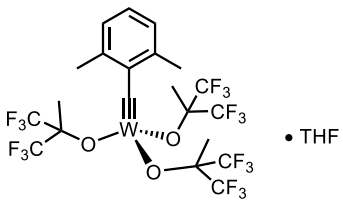

A 25 mL Schlenk flask was equipped with a magnetic stir bar and was flame dried under vaccum. The flask was filled with argon and charged with W(≡CAr)$Cl_3$(dme) (Ar = 2,6-$Me_2C_6H_3$) **211**[176] and THF (4 mL) to give a blue solution. A solution of NaOCMe$(CF_3)_3$ (153 mg, 0.814 mmol) in THF (2 mL) was then added dropwise at 25 °C to give a pink suspension. Stirring was continued for 14 h at ambient temperature before the solvent was removed *in vacuo*. The solid material was extracted with *n*-pentane (4 x 1 mL) and the supernatant transferred via cannula into a second flame dried 10 mL Schlenk flask. The combined filtrates were concentrated and the residue was dried under vacuum ($10^{-3}$ mbar) and co-evaporated with toluene (2 x 2 mL) to give complex **212** as a THF adduct (215 mg, 93%). $^1$H NMR (600 MHz, $C_6D_5CD_3$): δ = 6.90 (dp, *J* = 7.6, 0.7 Hz, 2H), 6.56 (tp, *J* = 7.6, 0.4 Hz, 1H), 3.80 (t, *J* = 6.3 Hz, 4H), 2.68 (s, 6H), 1.62 (s, 9H), 1.37 – 1.26 (m, 4H). $^{13}$C NMR (151 MHz, $C_6D_5CD_3$): δ = 289.8 ($^1J$-$^{183}$W-$^{13}$C = 283.9 Hz), 144.7, 141.5 ($^2J$-$^{183}$W-$^{13}$C =

40.6 Hz), 129.6, 126.8, 124.7 (q, *J* = 288.6 Hz), 83.4 (hept, *J* = 29.0 Hz), 74.4, 25.6, 20.7, 18.5. $^{19}$F NMR (565 MHz, $C_6D_5CD_3$): δ = −76.6. $^{183}$W NMR (17 MHz, $C_6D_5CD_3$): δ = 395.7. HRMS-ESI (m/z): calcd. for $C_{21}H_{18}F_{18}O_3W^+$ [M-THF]$^+$: 844.04724; found, 844.04815.

**Complex 202**

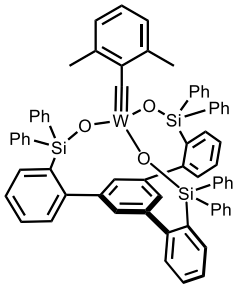


A 100 mL Schlenk flask was equipped with a magnetic stir bar and was flame dried under vacuum. The flask was filled with argon, charged with ligand **105** (617 mg, 0.685 mmol) which was azeotropically dried with benzene (3 x 5 mL) to remove any residual water. Toluene (51 mL) was then added and the mixture vigorously stirred for 10 min to obtain a clear solution. A solution of complex **201** (374 mg, 0.719 mmol) in toluene (10 mL) was added dropwise to the vigorously stirred mixture at 25 °C. After 3 h stirring at ambient temperature, the solvent was removed *in vacuo* and the yellow/orange solid was washed with diethyl ether (4 x 5 mL) to give complex **202** as a yellow/orange powder (646 mg, 79%). Yellow crystals suitable for single-crystal X-ray diffraction were grown from a concentrated $Et_2O$ solution (5 mL) stored at –85°C for 1 week. $^1$H NMR (600 MHz, $C_6D_5CD_3$): δ = 7.81 – 7.78 (m, 12H), 7.77 – 7.74 (m, 3H), 7.24 (s, 3H), 7.11 – 7.04 (m, 12H), 7.03 – 7.00 (m, 12H), 6.86 – 6.82 (m, 3H), 6.66 (m, 2H), 6.32 (t, *J* = 7.5 Hz, 1H), 2.07 (s, 6H). $^{13}$C NMR (151 MHz, $C_6D_5CD_3$): δ = 287.4 ($^1J$-$^{183}$W-$^{13}$C = 270.1 Hz), 149.2, 144.1, 143.6 ($^2J$-$^{183}$W-$^{13}$C = 37.1 Hz), 141.2, 137.5, 136.8, 134.9, 134.5, 130.3, 130.2, 130.0, 129.0, 128.0, 126.6, 126.2, 125.1, 20.1. $^{29}$Si NMR (79 MHz, $C_6D_5CD_3$): δ = −8.5 ($^2J$-$^{183}$W-$^{29}$Si = 19.4 Hz). $^{183}$W NMR (17 MHz, $C_6D_5CD_3$): δ = 516.5. $^1$H-DOSY NMR ($C_6D_5CD_3$): $D_{predicted.}$ = 5.37·10$^{-10}$ m$^2$/s$^{-1}$; $D_{exp.}$ = 5.79·10$^{-10}$ m$^2$/s$^{-1}$. IR (film): $\tilde{\nu}$ 1468, 1428, 1113, 1087, 1038, 1048, 998, 943, 900, 765, 735, 721, 696, 623, 576, 545, 508, 436, 409 cm$^{-1}$. HRMS-ESI (m/z): calcd. for $C_{69}H_{55}O_3Si_3W^+$ [M+H]$^+$, 1199.2963; found, 1199.2971. Elemental analysis (%) calcd. for $C_{69}H_{54}O_3Si_3W$: C 69.10, H 4.54, Si 7.03, W 15.33; found: C 68.89, H 4.53, Si 6.94, W 15.13.

**Complex 206a**

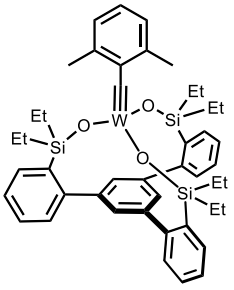


A 100 mL Schlenk flask was equipped with a magnetic stir bar and was flame dried under vacuum. The flask was filled with argon and charged with ligand **129** (204 mg, 0.333 mmol), which was azeotropically dried with benzene (3 x 5 mL) to remove any residual water. Toluene (25 mL) was added and the mixture vigorously stirred for 10 min to obtain a clear solution before a solution of complex **201** (173 mg, 0.333 mmol) in toluene (5 mL) was added dropwise with vigorous stirring. After 2 h stirring at ambient temperature, the solvent was removed *in vacuo* and the yellow/orange solid was extracted with *n*-pentane (4 x 5 mL). The solvent was removed *in vacuo* to give complex **206a** as a yellow/orange solid (298 mg, 98%). $^1$H NMR (600 MHz, $C_6D_5CD_3$): δ = 7.41 (s, 3H), 7.40 – 7.34 (m, 3H), 7.25 – 7.20 (m, 3H), 7.20 – 7.13 (m, 6H), 7.01 (d, *J* = 7.5 Hz, 2H),

6.55 (t, *J* = 7.5 Hz, 1H), 2.83 (s, 6H), 1.00 – 0.91 (m, 18H), 0.98 – 0.83 (m, 12H). $^{13}$C NMR (151 MHz, $C_6D_5CD_3$): δ = 281.5 ($^{1}J$-$^{183}$W-$^{13}$C = 272.5 Hz), 149.4, 144.7, 144.6 ($^{2}J$-$^{183}$W-$^{13}$C = 38.8 Hz), 140.5, 135.7, 134.6, 130.8, 129.2, 128.0, 126.7, 126.4, 125.9, 21.0, 9.2, 7.1. $^{29}$Si NMR (119 MHz, $C_6D_5CD_3$): δ = 12.9. $^{183}$W NMR (17 MHz, $C_6D_5CD_3$): δ = 460.0. $^{1}$H-DOSY NMR ($C_6D_5CD_3$): $D_{predicted.}$ = 6.08·10$^{-10}$ m$^2$/s$^{-1}$; $D_{exp.}$ = 6.94·10$^{-10}$ m$^2$/s$^{-1}$. IR (film): $\tilde{\nu}$ 3049, 2953, 2910, 2873, 1583, 1557, 1459, 1408, 1377, 1260, 1232, 1123, 1090, 1046, 1027, 1005, 932, 881, 760, 712, 672, 623, 575, 553, 527, 508, 460 cm$^{-1}$. Elemental analysis (%) calcd. for $C_{45}H_{54}O_3Si_3W$: C 59.33, H 5.97, Si 9.25, W 20.18; found: C 58.87, H 5.83, Si 9.21, W 19.98.

**Complex 206c**

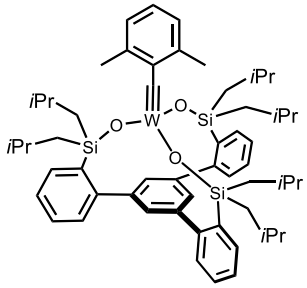


A 100 mL Schlenk flask was equipped with a magnetic stir bar and was flame dried under vacuum. The flask was filled with argon and charged with ligand **S6** (296 mg, 0.379 mmol), which was azeotropically dried with benzene (3 x 5 mL) to remove any residual water. Toluene (29 mL) was added and the mixture vigorously stirred for 10 min to obtain a clear solution before a solution of complex **201** (199 mg, 0.382 mmol) in toluene (6 mL) was added to the vigorously stirred mixture. After 2 h stirring at ambient temperature, the solvent was removed *in vacuo* and the yellow/orange solid was extracted with *n*-pentane (4 x 5 mL). The solvent was removed *in vacuo* to give complex **206c** as a yellow/orange powder (407 mg, quant.). $^{1}$H NMR (600 MHz, $C_6D_5CD_3$): δ = 7.55 – 7.49 (m, 3H), 7.47 (s, 3H), 7.26 – 7.21 (m, 3H), 7.20 – 7.15 (m, 6H), 6.99 (dm, *J* = 7.6 Hz, 2H), 6.53 (t, *J* = 7.5 Hz, 1H), 2.86 (s, 6H), 2.06 – 1.98 (m, *J* = 6.6 Hz, 6H), 1.08 – 0.98 (m, 12H), 0.88 (d, *J* = 6.6 Hz, 18H), 0.87 (d, *J* = 6.6 Hz, 18H). $^{13}$C NMR (151 MHz, $C_6D_5CD_3$): δ = 281.9 ($^{1}J$-$^{183}$W-$^{13}$C = 272.8 Hz), 148.9, 144.7, 144.4 ($^{2}J$-$^{183}$W-$^{13}$C = 38.6 Hz), 140.5, 137.1, 135.2, 130.8, 129.2, 128.0, 126.5, 126.4, 125.8, 29.7, 26.9, 26.5, 24.5, 21.5. $^{29}$Si NMR (119 MHz, $C_6D_5CD_3$): δ = 9.9. $^{183}$W NMR (17 MHz, $C_6D_5CD_3$): δ = 475.2. IR (film): $\tilde{\nu}$ 2950, 2924, 2895, 2864, 1584, 1557, 1462, 1408, 1381, 1363, 1327, 1260, 1215, 1162, 1123, 1088, 1047, 1019, 925, 829, 758, 733, 661, 622, 576, 552, 505, 475, 408 cm$^{-1}$. HRMS-ESI (m/z): calcd. for $C_{57}H_{79}O_3Si_3W^+$ $[M+H]^+$, 1079.48409; found, 1079.48429. Elemental analysis (%) calcd. for $C_{57}H_{78}O_3Si_3W$: C 63.43, H 7.28, Si 7.81, W 17.03; found: C 63.59, H 7.31, Si 7.74, W 16.71.

**Complex 206b**

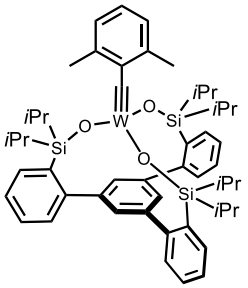


A 100 mL Schlenk flask was equipped with a magnetic stir bar and was flame dried under vacuum. The flask was filled with argon and charged with ligand **128** (291 mg, 0.471 mmol), which was azeotropically dried with benzene (3 x 5 mL) to remove any residual water. Toluene (31 mL) was added and the mixture vigorously stirred for 10 min to obtain a clear solution, before a

solution of complex **201** (217 mg, 0.417mmol) in toluene (6 mL) was added dropwise to the vigorously stirred mixture. After 2 h stirring at ambient temperature, the solvent was removed *in vacuo* and the yellow/orange solid was extracted with *n*-pentane (4 x 5 mL). The solvent was removed *in vacuo* to give complex **206b** as yellow/orange powder (413 mg, 99%). $^{1}$H NMR (600 MHz, $C_6D_5CD_3$): δ = 7.45 – 7.42 (m, 3H), 7.38 (s, 3H), 7.23 – 7.19 (m, 3H), 7.18 – 7.12 (m, 6H), 6.98 (d, *J* = 7.5 Hz, 2H), 6.53 (t, *J* = 7.5 Hz, 1H), 2.86 (s, 6H), 1.37 (hept, *J* = 7.5 Hz, 6H), 1.11 (d, *J* = 7.5 Hz, 18H), 1.10 (d, *J* = 7.4 Hz, 18H). $^{13}$C NMR (151 MHz, $C_6D_5CD_3$): δ = 282.1 ($^{1}J$-$^{183}$W-$^{13}$C = 274.3 Hz), 149.7, 144.5 ($^{2}J$-$^{183}$W-$^{13}$C = 38.7 Hz), 144.3, 140.5, 134.4, 134.3, 131.2, 128.9, 127.7, 126.5, 126.3, 125.9, 21.5, 18.3, 17.9, 15.1. $^{29}$Si NMR (119 MHz, $C_6D_5CD_3$): δ = 11.6 ($^{2}J$-$^{183}$W-$^{29}$Si = 8.1 Hz). $^{183}$W NMR (17 MHz, $C_6D_5CD_3$): δ = 460.0. $^{1}$H-DOSY NMR ($C_6D_5CD_3$): $D_{predicted.}$ = 5.84·10$^{-10}$ m$^2$/s$^{-1}$; $D_{exp.}$ = 6.79·10$^{-10}$ m$^2$/s$^{-1}$. IR (film): $\tilde{\nu}$ 3050, 2943, 2864, 1705, 1583, 1556, 1462, 1408, 1384, 1364, 1293, 1259, 1241, 1162, 1123, 1089, 1065, 1045, 1017, 1005, 924, 880, 759, 735, 722, 693, 666, 653, 626, 596, 577, 535, 513, 497, 466 cm$^{-1}$. HRMS-ESI (m/z): calcd. for $C_{51}H_{67}O_3Si_3W$ [M+H]$^+$ 995.39018; found, 995.39051. Elemental analysis (%) calcd. for $C_{51}H_{66}O_3Si_3W$: C 61.55, H 6.69, Si 8.47, W 18.47; found: C 58.85, H 6.89, Si 8.12, W 17.66.

**Complex 208**

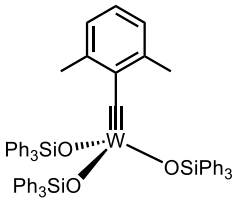


A 100 mL Schlenk flask was equipped with a magnetic stir bar and was flame dried under vacuum. The flask was filled with argon and charged with triphenylsilanol (510 mg, 1.81 mmol), which was azeotropically dried with benzene (3 x 5 mL) to remove any residual water. Toluene (45 mL) was added and the mixture vigorously stirred for 10 min to obtain a clear solution bwefore a solution of complex **201** (345 mg, 0.663 mmol) in toluene (9 mL) was added dropwise to the vigorously stirred mixture. After stirring for 3 h at ambient temperature, the solvent was removed *in vacuo* to obtain a yellow/orange foam. Addition of diethyl ether (10 mL) gave a yellow solid and an orange-brown supernatant solution. The suspension was stored for 14 h at −85° before the orange-brown supernatant solution was removed by cannula filtration. The yellow solid was washed with *n*-pentane (3 x 5 mL) to give complex **208** (305 mg, 41%) and an impurity (~28%), which could not be fully removed due to its similar solubility. $^{1}$H NMR (600 MHz, $C_6D_5CD_3$): δ = 7.68 – 7.64 (m, 18H), 7.17 – 7.11 (m, 9H), 7.07 – 7.02 (m, 18H), 6.71 (d, *J* = 7.5 Hz, 2H), 6.45 (t, *J* = 7.5 Hz, 1H), 2.00 (s, 6H). $^{13}$C NMR (151 MHz, $C_6D_5CD_3$): δ = 283.1 ($^{1}J$-$^{183}$W-$^{13}$C = 273.0 Hz), 143.5 ($^{2}J$-$^{183}$W-$^{13}$C = 38.1 Hz), 141.8, 135.7, 135.5, 130.2, 128.1, 126.7, 125.5, 20.3. $^{29}$Si NMR (79 MHz, $C_6D_5CD_3$): δ = -8.03 ($^{2}J$-$^{183}$W-$^{29}$Si = 13.6 Hz). $^{183}$W NMR (17 MHz, $C_6D_5CD_3$): δ = 548.0. HRMS-ESI (m/z): calcd. for $C_{63}H_{55}O_3Si_3W^+$ [M+H]$^+$ 1127.29628; found, 1127.29847.

**Complex 210**

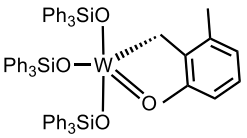


A 100 mL Schlenk flask was equipped with a magnetic stir bar and was flame dried under vacuum. The flask was filled with argon, charged with complex **201** (269 mg, 0.518 mmol) and toluene (39 mL). A solution of triphenylsilanol (438 mg, 1.56 mmol) in toluene (8 mL) was added dropwise to the vigorously stirred mixture at 25 °C. After stirring for 2.5 h at ambient temperature, water (9.3 µL, 0.518 mmol) was added and stirring was continued for 2 h before the solvent was removed *in vacuo*. The reaction mixture containing complex **210** was analyzed by NMR spectroscopy. Orange crystals suitable for single-crystal X-ray diffraction were grown from a concentrated $Et_2O$ solution (5 mL) store at –18°C for one week.

$^{1}$H NMR (600 MHz, $C_6D_6$): δ = 7.58 – 7.52 (m, 18H), 7.15 – 7.11 (m, 9H), 7.03 – 6.96 (m, 18H), 6.68 (d, *J* = 7.5 Hz, 2H), 6.48 (t, *J* = 7.5 Hz, 1H), 3.70 ($^{2}J$-$^{183}$W-$^{1}$H = 13.3 Hz, s, 2H), 2.10 (s, 6H). $^{13}$C NMR (151 MHz, $C_6D_6$): δ = 146.1, 136.1, 135.0, 134.9, 130.2, 128.1, 127.3, 125.5, 64.4 ($^{1}J$-$^{183}$W-$^{13}$C = 101.9 Hz), 20.8. $^{29}$Si NMR (79 MHz, $C_6D_6$): δ = –0.4 ($^{2}J$-$^{183}$W-$^{29}$Si = 11.5 Hz). $^{183}$W NMR (17 MHz, $C_6D_6CD_3$): δ = 758.1. HRMS: decomp.

**Complex 207**

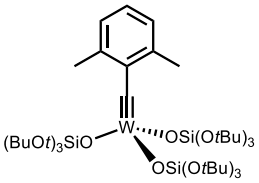


A 50 mL Schlenk flask was equipped with a magnetic stir bar and was flame dried under vacuum. The flask was filled with argon, charged with complex **200** (757 mg, 1.20 mmol) and dissolved in $CH_2Cl_2$ (14 mL). Then a solution of $LiOSi(OtBu)_3$[226] (973 mg, 3.60 mmol) in $CH_2Cl_2$ (7 mL) was added dropwise to the vigorously stirred green solution at 25 °C, which turned instantly into a yellow suspension. After stirring for 14 h at ambient temperature, the solvent was removed *in vacuo* and the yellow/orange solid was extracted with *n*-pentane (4 x 5 mL). The solvent was removed *in vacuo* to give complex **207** as yellow crystalline material (1.31 g, 99%). Yellow crystals suitable for single-crystal X-ray diffraction were obtained from a concentrated $Et_2O$ solution (5 mL) upon slow evaporation of the solvent. $^{1}$H NMR (600 MHz, $C_6D_5CD_3$): δ 7.05 – 7.02 (m, 2H), 6.59 (t, *J* = 7.5 Hz, 1H), 3.08 (s, 6H), 1.43 (s, 81H). $^{13}$C NMR (151 MHz, $C_6D_5CD_3$): δ = 281.2 ($^{1}J$-$^{183}$W-$^{13}$C = 274.8 Hz), 144.0 ($^{2}J$-$^{183}$W-$^{13}$C = 38.7 Hz), 142.1, 126.7, 125.6, 73.3, 31.9, 22.3. $^{29}$Si NMR (119 MHz, $C_6D_5CD_3$): δ = –93.2 ($^{2}J$-$^{183}$W-$^{29}$Si = 10.4 Hz). $^{183}$W NMR (17 MHz, $C_6D_5CD_3$): δ = 458.1. $^{1}$H-DOSY NMR ($C_6D_5CD_3$): $D_{predicted.}$ = $5.60 \cdot 10^{-10}$ $m^2/s^{-1}$; $D_{exp.}$ = $7.216 \cdot 10^{-10}$ $m^2/s^{-1}$. IR (film): $\tilde{\nu}$ 2972, 2930, 2872, 1470, 1389, 1364, 1241, 1188, 1053, 1026, 906, 829, 765, 734, 697, 649, 580, 510, 536, 470, 429 $cm^{-1}$. HRMS: decomp.; Elemental analysis (%) calcd. for $C_{45}H_{90}O_{12}Si_3W$: C 49.53, H 8.31, Si 7.72, W 16.85; found: C 48.89, H 8.41, Si 7.41, W 16.39.

**Complex 214**

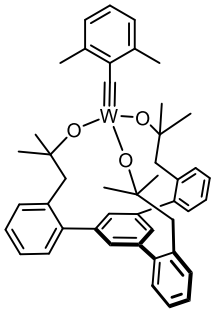

A 500 mL Schlenk flask was equipped with a magnetic stir bar and was flame dried under vacuum. The flask was filled with argon and charged with ligand **213** (1.03 g, 1.98 mmol), which was azeotropically dried with benzene (3 x 5 mL) to remove any residual water. Toluene (148 mL) was added and the mixture was vigorously stirred for 10 min to obtain a clear solution. A solution of complex **201** (1.03 g, 1.98 mmol) in toluene (30 mL) was then added dropwise to the vigorously stirred mixture. After stirring for 2 h at ambient temperature, the solvent was removed in vacuo to give complex **214** as an orange powder (1.62 g, quant.). 1H NMR (600 MHz, C6D5CD3): δ 7.30 (dd, J = 7.4, 1.7 Hz, 3H), 7.29 (s, 3H), 7.15 (td, J = 7.4, 1.6 Hz, 3H), 7.12 (td, J = 7.3, 1.7 Hz, 3H), 6.99 (d, J = 7.5 Hz, 2H), 6.93 (dd, J = 7.4, 1.6 Hz, 3H), 6.65 (t, J = 7.5 Hz, 1H), 3.07 (s, 6H), 2.73 (s, 6H), 1.30 (s, 18H). 13C NMR (151 MHz, C6D5CD3): δ = 264.0 (1J-183W-13C = 292.7 Hz), 145.6 (2J-183W-13C = 44.2 Hz), 144.5, 143.3, 139.5, 136.4, 133.4, 132.6, 128.3, 127.1, 127.0, 126.8, 125.2, 83.9, 49.3, 31.4, 22.1. 183W NMR (17 MHz, C6D5CD3): δ = 114.2. IR (film): ṽ 3032, 2973, 2922, 1458, 1478, 1363, 1377, 1207, 1227, 1170, 1124, 1098, 972, 984, 999, 940, 896, 872, 786, 814, 757, 739, 675, 624, 639, 572, 590, 535, 558, 512, 472, 415 cm-1. HRMS: decomp.; Elemental analysis (%) calcd. for C45H48O3W: C 65.86, H 5.90, W 22.40; found C 65.63, H 5.93, W 22.19.

**Complex 203**

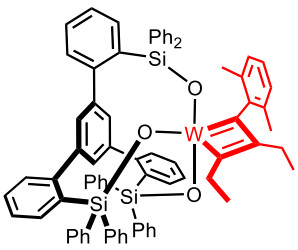

A 10 mL Schlenk flask was equipped with a magnetic stir bar and was flame dried under vacuum. The flask was filled with argon and charged with complex **202** (32.3 mg, 0.027 mmol) and $Et_2O$ (1 mL) to give a yellow suspension. Upon addition of 3-hexyne (10.7 mg, 14.8 µL) the color instantly changed to deep red. This solution was filtered via cannula and the filtrate was stored at –20°C for one week to obtain very sensitive, red crystals suitable for single-crystal X-ray diffraction. NMR analysis: A 10 mL Schlenk flask was equipped with a magnetic stir bar and was flame dried under vacuum. The flask was filled with argon and charged with complex **203** (29.3 mg, 0.025 mmol) and $C_6D_5CD_3$ (0.5 mL) to give a deep orange solution. This solution was transferred into a flame-dried *J. Young* NMR tube under Ar. Upon addition of 3-hexyne (13.9 µL, 0.122 mmol) the color instantly changed to deep red. The signals of the new complex were as follows: $^1$H NMR (600 MHz, $C_6D_5CD_3$): δ = 8.41 (t, *J* = 1.7 Hz, 1H), 8.02 – 7.97 (m, 4H), 7.90 – 7.87 (m, 1H), 7.70 (d, *J* = 1.6 Hz, 2H), 7.57 – 7.52 (m, 2H), 7.51 – 7.46 (m, 4H), 7.43 (dt, *J* = 7.7, 1.0 Hz, 2H), 7.24 – 7.21 (m, 4H), 7.19 (td, *J* = 7.3, 1.3 Hz, 3H), 7.18 (td, *J* = 7.6, 1.5 Hz, 1H), 7.13 – 7.03 (m, 4H), 7.01 – 6.96 (m, 8H), 6.86 (s, 9H), 6.75 (d, *J* = 7.6 Hz, 2H), 3.05 (q, *J* = 7.3 Hz, 2H), 2.52 (q, *J* = 7.6 Hz, 2H), 1.47 (s, 6H), 0.67 (t, *J* = 7.6 Hz, 3H), 0.26 (t, *J* = 7.6 Hz, 3H). $^{13}$C NMR (151 MHz, $C_6D_5CD_3$): δ = 231.2 ($^1J$-$^{183}$W-$^{13}$C = 86.8 Hz), 228.9 ($^1J$-$^{183}$W-$^{13}$C = 153.0 Hz), 149.8, 148.8, 147.0, 143.7, 142.7, 140.1, 139.4,

139.2, 138.7, 138.1, 137.2, 136.7, 135.8, 135.8, 135.6, 135.1, 134.6 ($^{2}J$-$^{183}$W-$^{13}$C = 23.0 Hz), 131.2, 131.0, 129.4, 129.2, 129.2, 129.1, 129.0, 128.7, 128.0, 127.6, 127.6, 127.4, 127.2, 126.2, 126.2, 125.3, 29.2, 27.1, 20.9, 15.3, 13.2. $^{29}$Si NMR (119 MHz, $C_6D_5CD_3$): = –18.02 ($^{2}J$-$^{183}$W-$^{29}$Si = 15.6 Hz), –18.81 ($^{2}J$-$^{183}$W-$^{29}$Si = 16.6 Hz). A $^{183}$W-NMR signal could not be detected; HRMS: decomp.; because of the sensitivity of the material, a correct elemental analysis has not been obtained.

### Complex 204

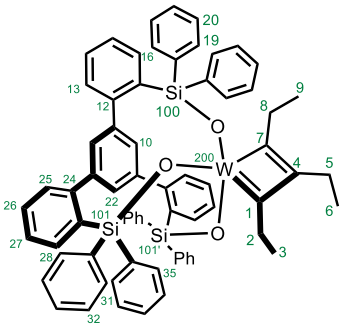


The NMR sample of complex **203** was stored for one week at ambient temperatures upon which time complex **204** was formed. Not all shifts of the new complex **204** in the $^{1}$H and $^{13}$C NMR NMR could be assigned due to signal broadening and overlaps with complex **203** (see attached spectra for more details) (**Table 12**).

**Table 12.** Assigned NMR signals of complex **204**.

| Atom | δ (ppm) | J | COSY | HSQC | NOESY | Atom | δ (ppm) | J | COSY | HSQC | NOESY |
|---|---|---|---|---|---|---|---|---|---|---|---|
| 1 C | 233.72 | 89.20(200) | | | | 20 C | | | | | |
| 2 C | 28.25 | | | 2 | | H | 6.93 | | 19 | | |
| H2 | 2.13 | | 3 | 2 | 5, 10, 22 | 22 C | 125.73 | | | 22 | |
| 3 C | 15.5 | | | 3 | | H | 8.23 | | 10 | 22 | 2, 8, 13, 25 |
| H3 | 0 | | 2 | 3 | 5, 19, 31, 35 | 24 C | 149.45 | | | | |
| 4 C | 136.58 | | | | | 25 C | 130.98 | | | 25 | |
| 5 C | 26.06 | | | 5 | | H | 7.35 | | 26 | 25 | 22 |
| H2 | 2.77 | | 6 | 5 | 2, 3, 8, 9, 19, 31, 35 | 26 C | | | | | |
| 6 C | 13.36 | | | 6 | | H | 7.15 | | 25 | | |
| H3 | 0.92 | | 5 | 6 | 8, 19, 31, 35 | 27 C | | | | | |
| 7 C | 229.77 | 152.00(200) | | | | H | 7.04 | | 28 | | |
| 8 C | 29.91 | | | 8 | | 28 C | 137.08 | | | 28 | |
| H2 | 3.81 | | 9 | 8 | 5, 6, 10, 19, 22, 31, 35 | H | 7.75 | | 27 | 28 | |
| 9 C | 16.28 | | | 9 | | 31 C | 134.8 | | | 31 | |
| H3 | 1.08 | | 8 | 9 | 5, 19, 31, 35 | H | 7.6 | | 32 | 31 | 3, 5, 6, 8, 9 |
| 10 C | 130.55 | | | 10 | | 32 C | | | | | |
| H | 7.56 | | 22 | 10 | 2, 8 | H | 6.91 | | 31 | | |
| 12 C | 148.34 | | | | | 35 C | | | | 35 | |
| 13 C | | | | 13 | | H | 7.13 | | | 35 | 3, 5, 6, 8, 9 |
| H | 7.04 | | | 13 | 22 | 100 Si | -18.08 | | | | |
| 16 C | 134.96 | | | 16 | | 101 Si | -20.71 | | | | |
| H | 7.66 | | | 16 | | 101' Si | -20.71 | | | | |
| 19 C | 135.94 | | | 19 | | 200 W | | 152.00(7), 89.20(1) | | | |
| H | 8.15 | | 20 | 19 | 3, 5, 6, 8, 9 | | | | | | |

## 5.4 Alkyne Metathesis Reactions

**Representative Procedure for Alkyne Homo-Metathesis. 4,4'-(Ethyne-1,2-diyl)diphenol (161b)**

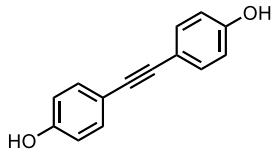


4-(Prop-1-yn-1-yl)phenol (33.0 mg, 25.0 µmol) was added to a stirred suspension of complex **108** (13.9 mg, 12.5 µmol, 5 mol%) and powdered molecular sieves 5Å (250 mg) in toluene (1.25 mL) at 60 °C under argon atmosphere. The mixture was stirred for 14 h at this temperature before it was filtered through a short pad of Celite® which was carefully rinsed with ethyl acetate (20 mL). The combined filtrates were evaporated and the residue was purified by flash chromatography on silica gel (hexanes/toluene/EA, 6:2:2) to give the title compound as a white solid (24.3 mg, 93%). $^{1}$H NMR (400 MHz, $CD_3CN$): δ = 7.39 – 7.31 (m, 4H), 7.27 (s, 2H), 6.85 – 6.77 (m, 4H). $^{13}$C NMR (101 MHz, $CD_3CN$): δ = 158.1, 133.8, 116.5, 115.6, 88.4. The analytical and spectroscopic data are in agreement with those reported in the literature.[123]

**1,2-Bis(4-methoxyphenyl)ethyne (161a)**

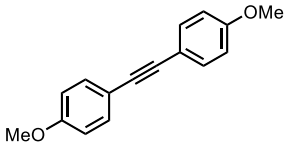


Prepared analogously with complex **108** (13.9 mg, 12.5 µmol, 5 mol%) at 25 °C; white solid (27.3 mg, 92%). $^{1}$H NMR (400 MHz, $CDCl_3$): δ = 7.45 (d, *J* = 8.8 Hz, 3H), 6.87 (d, *J* = 8.8 Hz, 4H), 3.82 (s, 6H). $^{13}$C NMR (101 MHz, $CDCl_3$): δ = 159.5, 133.0, 115.9, 114.1, 88.1, 55.4. The analytical and spectroscopic data are in agreement with those reported in the literature.[227]

**1,2-Bis(4-(trifluoromethyl)phenyl)ethyne (161c)**

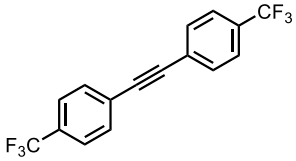


Prepared analogously with complex **108** (13.9 mg, 12.5 µmol, 5 mol%) at 60 °C; white solid (35.5 mg, 90%). $^{1}$H NMR (400 MHz, $CDCl_3$): δ = 7.68 – 7.59 (m, 8H). $^{13}$C NMR (101 MHz, $CDCl_3$): δ = 132.1, 131.1, 130.8, 130.5, 130.2, 128.0, 126.5, 125.6, 125.5, 125.5, 125.3, 122.6, 119.9, 90.3. $^{19}$F NMR (282 MHz, $CDCl_3$): δ = −62.9. The analytical and spectroscopic data are in agreement with those reported in the literature.[58]

**4,4'-(Ethyne-1,2-diyl)dibenzonitrile (161d)**

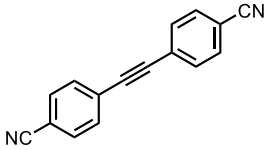


Prepared analogously with complex **108** (13.9 mg, 12.5 µmol, 5 mol%) at 60 °C ; white solid (22.0 mg, 77%). $^{1}$H NMR (400 MHz, $CDCl_3$): δ = 7.67 (d, *J* = 8.6 Hz, 2H), 7.63 (d, *J* = 8.8 Hz, 2H). $^{13}$C NMR (101 MHz, $CDCl_3$): δ = 132.7, 132.6, 127.5, 118.7, 112.9, 92.0. The analytical and spectroscopic data are in agreement with those reported in the literature.[58]

**1,1'-(Ethyne-1,2-diylbis(4,1-phenylene))bis(ethan-1-one) (161e)**

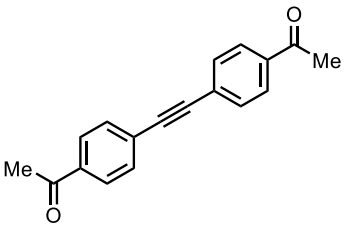

Prepared analogously with complex **108** (13.9 mg, 12.5 µmol, 5 mol%) at 25 °C; white solid (32.0 mg, 98%). $^{1}$H NMR (400 MHz, $CDCl_3$): δ = 7.96 (d, *J* = 8.6 Hz, 4H), 7.64 (d, *J* = 8.6 Hz, 4H), 2.63 (s, 6H). $^{13}$C NMR (101 MHz, $CDCl_3$): δ = 197.2, 136.6, 131.8, 128.3, 127.5, 91.7, 26.7. The analytical and spectroscopic data are in agreement with those reported in the literature.[58]

**1,2-Bis(2-(methylthio)phenyl)ethyne (162)**

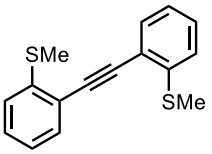

Prepared analogously with complex **133** (9.7 mg, 12.5 µmol, 5 mol%) at 90 °C; white solid (31.0 mg, 92%). $^{1}$H NMR (400 MHz, $CDCl_3$): δ = 7.57 – 7.53 (m, 2H), 7.33 – 7.28 (m, 2H), 7.21 – 7.18 (m, 2H), 7.14 – 7.10 (m, 2H), 2.52 (s, 6H). $^{13}$C NMR (101 MHz, $CDCl_3$): δ = 141.6, 132.6, 128.9, 124.2, 121.4, 92.2, 77.2, 15.3. The analytical and spectroscopic data are in agreement with those reported in the literature.[58]

**1,2-Di(pyridin-3-yl)ethyne (163)**

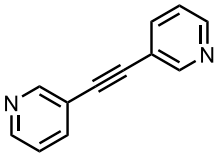

Prepared analogously with either complex **108** (13.9 mg, 12.5 µmol, 5 mol%) or complex **133** (9.7 mg, 12.5 µmol, 5 mol%) at 90 °C; pale yellow solid (14.0 mg, 62%; 17.0 mg, 76%). $^{1}$H NMR (400 MHz, $CDCl_3$): δ = 8.86 – 8.77 (m, 2H), 8.67 – 8.55 (m, 2H), 7.87 (dt, *J* = 6.1 Hz, 2H), 7.35 (m, 2H). $^{13}$C NMR (101 MHz, $CDCl_3$): δ = 151.8, 148.6, 138.96, 123.3, 119.8, 89.2. The analytical and spectroscopic data are in agreement with those reported in the literature.[58]

**1,2-Di(thiophen-2-yl)ethyne (164)**

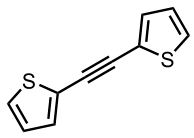

Prepared analogously with either complex **108** (13.9 mg, 12.5 µmol, 5 mol%) or complex **133** (9.7 mg, 12.5 µmol, 5 mol%) at 25 °C; white solid (22.3 mg, 94%; 20.2 mg, 85%). $^{1}$H NMR (400 MHz, $CDCl_3$): δ = 7.33 – 7.27 (m, 4H), 7.02 (dd, *J* = 5.2, 3.7 Hz, 2H). $^{13}$C NMR (101 MHz, $CDCl_3$): δ = 132.1, 127.6, 127.1, 122.9, 86.2. The analytical and spectroscopic data are in agreement with those reported in the literature.[58]

**Dimethyl oct-4-ynedioate (165)**

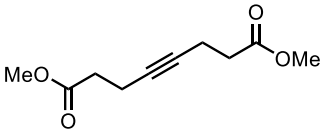

Prepared analogously with complex **108** (13.9 mg, 12.5 µmol, 5 mol%) at 25 °C; colorless oil (28.0 mg, 72%). $^{1}$H NMR (400 MHz, $CDCl_3$): δ = 3.63 (s, 6H), 2.56 – 2.27 (m, 8H). $^{13}$C NMR (101 MHz, $CDCl_3$): δ = 171.5, 77.9,

50.7, 32.7, 13.7. The analytical and spectroscopic data are in agreement with those reported in the literature.[58]

### *N*[1],*N*[12]-Dibutyldodec-6-yne-1,12-diamine (166)

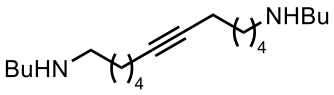


*N*-Butyloct-6-yn-1-amine (45.3 mg, 25.0 µmol) was added to a stirred suspension of complex **108** (13.9 mg, 12.5 µmol, 5 mol%) and powdered molecular sieves 5Å (250 mg) in toluene (1.25 mL) at 60 °C under argon atmosphere. After stirring for 12 h, the mixture was filtered through a short pad of Celite®, which was rinsed with MeOH (20 mL). The combined filtrates were evaporated and the residue was dissolved in $CHCl_3$ (1 mL). Ethyl acetate (20 mL) was added to precipitate the product. The supernatant solution was decanted and the remaining solid was dissolved in $CH_2Cl_2$ (10 mL). The organic layer was washed with sat. aq. $NaHCO_3$ (10 mL), dried over $MgSO_4$, filtered and concentrated *in vacuo* to give the title compound as a beige solid (38.6 mg, 71%). $^1$H NMR (400 MHz, $CDCl_3$): δ = 2.59 (td, *J* = 7.3, 1.9 Hz, 8H), 2.18 – 2.09 (m, 4H), 1.55 – 1.29 (m, 20H), 0.90 (t, *J* = 7.3 Hz, 6H). $^{13}$C NMR (101 MHz, $CDCl_3$): δ = 80.3, 50.1, 49.9, 32.4, 29.8, 29.2, 26.8, 20.7, 18.9, 14.2. IR (film): $\tilde{\nu}$ 3260, 2930, 2851, 1460, 1414, 1052, 1023, 995, 725, 420 cm$^{-1}$. HRMS-ESI (m/z): calcd. for $C_{20}H_{40}N_2$ $[M+H]^+$,309.32642; found,309.32602. The analytical and spectroscopic data are in agreement with those reported in the literature.[123]

### 1,12-Di(piperidin-1-yl)dodec-6-yne (167).

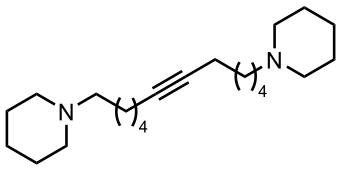


Prepared analogously with complex **108** (13.9 mg, 12.5 µmol, 5 mol%) at 25 °C; white solid (36.7 mg, 88%). $^1$H NMR (400 MHz, $CDCl_3$): δ =2.42 – 2.31 (m, 8H), 2.32 – 2.24 (m, 4H), 2.16 – 2.07 (m, 4H), 1.57 (p, *J* = 5.6 Hz, 8H), 1.49 – 1.33 (m, 16H). $^{13}$C NMR (101 MHz, $CDCl_3$): δ = 80.3, 59.5, 54.7, 29.2, 27.1, 26.5, 26.0, 24.6, 18.8. The analytical and spectroscopic data are in agreement with those reported in the literature.[123]

### 1,10-Bis(dodecylthio)dec-5-yne (168)

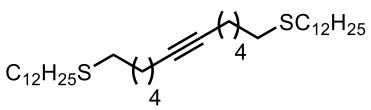


Prepared analogously with complex **108** (13.9 mg, 12.5 µmol, 5 mol%) at 25 °C; white solid (64.0 mg, 95%). $^1$H NMR (400 MHz, $CD_2Cl_2$): δ = 2.46 – 2.42 (m, 8H), 2.10 – 2.06 (m, 4H),1.54 – 1.46 (m, 16H), 1.30 – 1.18 (m, 32H), 0.83 – 0.79 (m, 6H). $^{13}$C NMR (101 MHz, $CD_2Cl_2$): δ = 80.5, 32.6, 32.5, 32.5, 30.7, 30.4, 30.3, 30.2, 30.1, 30.0, 29.9, 29.9, 29.5, 29.4, 28.7, 23.3, 19.2, 14.5. The analytical and spectroscopic data are in agreement with those reported in the literature.[123]

### *N*¹,*N*⁸-Dimethoxy-*N*¹,*N*⁸-dimethyloct-4-ynediamide (169)

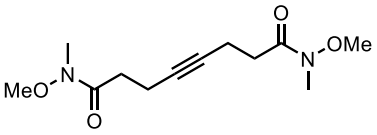

Prepared analogously with complex **108** (13.9 mg, 12.5 µmol, 5 mol%) at 25 °C; white solid (16.7 mg, 52%). $^{1}$H NMR (400 MHz, $CDCl_3$): δ = 3.69 (s, 6H), 3.18 (s, 6H), 2.63 (t, *J* = 7.3 Hz, 4H), 2.47 (dd, *J* = 8.7, 6.7 Hz, 4H). $^{13}$C NMR (101 MHz, $CDCl_3$): δ = 172.9, 79.6, 61.4, 32.3, 31.7, 14.4. The analytical and spectroscopic data are in agreement with those reported in the literature.[123]

### Hex-3-yne-1,6-diyl bis(4-methylbenzenesulfonate) (170)

Prepared analogously with complex **108** (13.9 mg, 12.5 µmol, 5 mol%) at 25 °C; white solid (43.8 mg, 83%). $^{1}$H NMR (400 MHz, $CDCl_3$): δ = 7.82 – 7.75 (m, 4H), 7.35 (d, *J* = 8.0 Hz, 4H), 4.04 – 3.97 (m, 4H), 2.45 (m, 10H). $^{13}$C NMR (101 MHz, $CDCl_3$): δ = 145.1, 133.0, 130.0, 128.1, 76.9, 67.9, 21.8, 19.8. The analytical and spectroscopic data are in agreement with those reported in the literature.[58]

### 1,12-Diiodododec-6-yne (171)

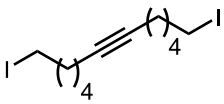

Prepared analogously with complex 108 (13.9 mg, 12.5 µmol, 5 mol%) at 25 °C; pale orange oil (43.0 mg, 82%). $^{1}$H NMR (400 MHz, $CDCl_3$): δ = 3.21 (t, *J* = 7.0 Hz, 4H), 2.17 (m, 4H), 1.85 (m, 4H), 1.50 (m, 8H). $^{13}$C NMR (101 MHz, $CDCl_3$): δ = 80.1, 33.1, 29.7, 27.9, 18.6, 6.9. IR (film): ṽ 2931, 2855, 1606, 1509, 1456, 1428, 1368, 1347, 1333, 1290, 1246, 1202, 1164, 1120, 1077, 1032, 891, 832, 805, 765, 723, 593, 532, 503 cm$^{-1}$. HRMS-CI (m/z): calculated for $C_{12}H_{21}I_2^+$ [M+H]$^+$, 418.97272; found, 418.97282.

### 2,2'-(Octadec-9-yne-1,18-diyl)bis(isoindoline-1,3-dione) (172)

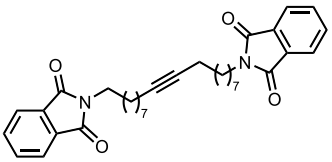

Prepared analogously with complex **108** (13.9 mg, 12.5 µmol, 5 mol%) at 25 °C; white solid (60.0 mg, 89%). $^{1}$H NMR (400 MHz, $CDCl_3$): δ = 7.81 (dt, *J* = 7.2, 3.6 Hz, 4H), 7.68 (dd, *J* = 5.4, 3.0 Hz, 4H), 3.65 (t, *J* = 7.3 Hz, 4H), 2.14 – 2.05 (m, 4H), 1.64 (t, *J* = 7.2 Hz, 4H), 1.43 (t, *J* = 7.3 Hz, 4H), 1.34 – 1.25 (m, 16H). $^{13}$C NMR (101 MHz, $CDCl_3$): δ = 168.5, 133.9, 132.3, 123.2, 80.3, 38.1, 29.2, 29.1, 28.9, 28.7, 26.9, 18.8. The analytical and spectroscopic data are in agreement with those reported in the literature.[123]

### Dodec-6-yne-1,12-diol (173a)

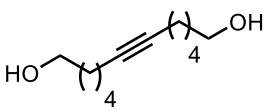

Prepared analogously with either complex **108** (13.9 mg, 12.5 µmol, 5 mol%) or complex **133** (9.72 mg, 12.5 µmol, 5 mol%) at 25 °C; colorless oil (16.0 mg, 69%; 18.0 mg, 73%). $^{1}$H NMR (400 MHz, $CDCl_3$): δ = 3.64 – 3.54 (m, 4H), 2.14

– 2.03 (m, 4H), 1.58 – 1.33 (m, 12H). $^{13}$C NMR (101 MHz, $CDCl_3$): δ = 80.2, 62.9, 32.3, 28.8, 24.9, 18.7.The analytical and spectroscopic data are in agreement with those reported in the literature.[228]

**Tetradec-7-yne-1,14-diol (173b)**

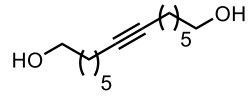

Prepared analogously with either complex **108** (13.9 mg, 12.5 µmol, 5 mol%) or complex **133** (9.7 mg, 12.5 µmol, 5 mol%) at 25 °C; white solid (18.0 mg, 66%; 20.1 mg, 71%). $^{1}$H NMR (400 MHz, $CDCl_3$): δ = 3.58 (t, *J* = 6.6 Hz, 4H), 2.09 (td, *J* = 5.9, 5.0, 2.0 Hz, 4H), 1.58 – 1.26 (m, 16 H). $^{13}$C NMR (101 MHz, $CDCl_3$): δ = 80.2, 62.9, 32.7, 29.0, 28.6, 25.3, 18.7.The analytical and spectroscopic data are in agreement with those reported in the literature.[123]

**Hexadec-8-yne-1,16-diol (173c)**

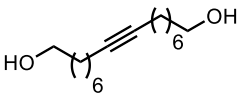

Prepared analogously with either complex **108** (13.9 mg, 12.5 µmol, 5 mol%) or complex **133** (9.7 mg, 12.5 µmol, 5 mol%) at 25 °C; white solid (25.0 mg, 83%; 28.0 mg, 88%). $^{1}$H NMR (400 MHz, $CDCl_3$): δ =3.57 (t, *J* = 6.6 Hz, 4H), 2.19 – 1.96 (m, 4H), 1.62 – 1.13 (m, 20H). $^{13}$C NMR (101 MHz, $CDCl_3$): δ = 80.2, 63.0, 32.7, 29.0, 28.9, 28.8, 25.7, 18.7. The analytical and spectroscopic data are in agreement with those reported in the literature.[229]

**Octadec-9-yne-1,18-diol (173d)**

Prepared analogously with either complex **108** (13.9 mg, 12.5 µmol, 5 mol%) or complex **133** (9.7 mg, 12.5 µmol, 5 mol%) at 25 °C; white solid (32.2 mg, 91%; 30.7 mg, 87%). $^{1}$H NMR (400 MHz, $CDCl_3$): δ = 3.63 (t, *J* = 6.6 Hz, 4H), 2.19 – 2.06 (m, 4H), 1.61 – 1.42 (m, 8H), 1.37 – 1.27 (m, 16H). $^{13}$C NMR (101 MHz, $CDCl_3$): δ = 80.4, 63.2, 32.9, 29.5, 29.3, 29.2, 28.9, 25.8, 18.9. IR (film): $\tilde{\nu}$ 3260, 2930, 2851, 1460, 1414, 1052, 1023, 995, 725, 420 cm$^{-1}$. HRMS-ESI (*m/z*): calcd. for $C_{18}H_{34}O_{32}$ $[M]^+$, 283.263155; found, 283.26328.

**(2S,17S)-octadec-9-yne-2,17-diol (174)**

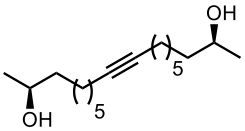

Prepared analogously with complex **108** (9.2 mg, 12.5 µmol, 5 mol%) at 25 °C; pale yellow oil (33.1 mg, 94%). $^{1}$H NMR (400 MHz, $CDCl_3$): δ = 3.83 – 3.70 (m, 2H), 2.18 – 2.08 (m, 4H), 1.66 (s, 2H), 1.53 – 1.24 (m, 20H), 1.17 (d, *J* = 6.2 Hz, 6H). $^{13}$C NMR (101 MHz, $CDCl_3$): δ = 80.3, 68.2, 39.4, 29.3, 29.2, 28.9, 25.8, 23.6, 18.8. The analytical and spectroscopic data are in agreement with those reported in the literature.[123]

**4-(Methoxymethoxy)cyclotetradec-2-yn-1-ol (175)**

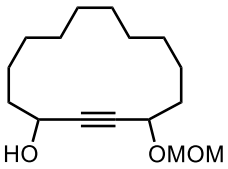


To a stirred suspension of 15-(methoxymethoxy)octadeca-2,16-diyn-4-ol (9.60 mg, 29.8 μmol) and powdered molecular sieves 5Å (200 mg) in toluene (13 mL) at 110 °C was added a solution of complex **133** (2.2 mg, 3.0 μmol, 10 mol%) in toluene (2.0 mL) under argon atmosphere. The mixture was stirred for 2 h at this temperature before it was cooled to ambient temperatures and filtered through a short pad of Celite® and rinsed with ethyl acetate (20 mL). The filtrate was evaporated and the residue was purified by flash chromatography on silica gel (hexanes/*t*-butyl methyl ether 8:2 to 7:3) to give the title compound as an oil (5.4 mg, 68%). $^{1}$H NMR (400 MHz, $CDCl_3$) δ 4.92 (dd, *J* = 6.8, 5.0 Hz, 1H), 4.60 (dd, *J* = 6.8, 1.6 Hz, 1H), 4.55 – 4.35 (m, 2H), 3.38 (d, *J* = 0.7 Hz, 3H), 1.79 – 1.62 (m, 4H), 1.57 – 1.25 (m, 16H). $^{13}$C NMR (101 MHz, $CDCl_3$) δ 94.3, 87.1, 87.1, 84.1, 83.9, 66.3, 66.2, 63.1, 63.0, 55.8, 37.2, 37.1, 35.1, 35.0, 26.6, 26.5, 25.9, 25.9, 25.8, 25.8, 23.9, 23.8, 22.5, 22.4, 22.3, 22.3. The analytical and spectroscopic data are in agreement with those reported in the literature.[123]

**Compound (176)**

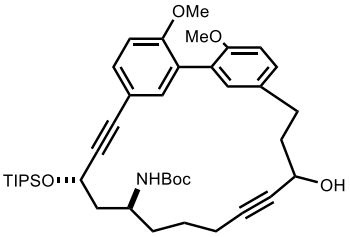


To a stirred suspension of diyne (17.3 mg, 23.2 μmol) and powdered molecular sieves 5Å (200 mg) in toluene (10 mL) at 80 °C was added a solution of complex **133** (3.4 mg, 4.6 μmol, 20 mol%) in toluene (2.0 mL) under argon atmosphere. The mixture was stirred for 3 h at this temperature before it was cooled to ambient temperatures and filtered through a short pad of Celite® and rinsed with ethyl acetate (20 mL). The filtrate was evaporated and the residue was purified by flash chromatography on silica gel (hexanes/*t*-butyl methyl ether 6:4 to 7:3) to give the title compound as an oil (10.5 mg, 66%). $^{1}$H NMR (mixture of conformers 400 MHz, $CDCl_3$): δ = 7.39 – 7.27 (m, 2H), 7.21 – 7.13 (m, 1H), 7.07 (d, *J* = 2.3 Hz, 1H), 6.93 – 6.83 (m, 2H), 5.17 – 5.08 (m, 1H), 4.90 – 4.81 (m, 1H), 4.71 (ddd, *J* = 19.1, 10.5, 3.4 Hz, 1H), 4.51 (d, *J* = 8.2 Hz, 1H), 4.07 (ddd, *J* = 16.1, 9.9, 4.0 Hz, 1H), 3.93 (d, *J* = 20.6 Hz, 1H), 3.79 (dd, *J* = 14.1, 2.8 Hz, 7H), 3.65 (q, *J* = 2.0 Hz, 1H), 2.93 – 2.65 (m, 2H), 2.42 – 2.16 (m, 1H), 2.17 – 1.88 (m, 2H), 1.88 – 1.53 (m, 2H), 1.41 (d, *J* = 9.3 Hz, 9H), 1.22 – 0.95 (m, 18H). The analytical and spectroscopic data are in agreement with those reported in the literature.[123]

**Compound 177**

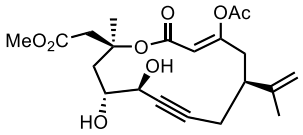

Diyne (50.0 mg, 83.1 µmol) was added to a stirred suspension of complex **108** (27.8 mg, 24.9 µmol, 30 mol%) and powdered molecular sieves 5Å (20 mg) in toluene (42 mL) at 110 °C under Ar. The mixture was stirred for 45 min at this temperature before it was filtered through a short pad of Celite®, which was carefully rinsed with ethyl acetate(100 mL). The combined filtrates were evaporated and the residue was purified by flash chromatography on silica (hexanes/ethyl acetate,3:1).

Zinc dust (217 mg, 332 µmol) was added to a solution of this compound in HOAc/THF/$H_2O$ (0.3 mL, 3:1:1). The suspension was vigorously stirred for 3 h at room temperature before all insoluble materials were filtered off through a pad of Celite®. The filtrate was diluted with sat. aq. $NaHCO_3$ (10 mL), the aqueous phase was extracted with ethyl acetate (3 x 20 mL), the combined organic layers were washed with brine, dried over $MgSO_4$, filtered and concentrated. The residue was purified by flash chromatography on silica (hexanes/ethyl acetate, 2:1 to 1:1) to afford the title compound as a colorless oil (23.0 mg, 68% over two steps). $^1$H NMR (400 MHz, $CDCl_3$): δ = 5.61 (s, 1H), 4.82 (p, *J* = 1.6 Hz, 1H), 4.78 – 4.73 (m, 1H), 4.58 (q, *J* = 2.3 Hz, 1H), 4.18 – 4.11 (m, 1H), 3.84 – 3.77 (m, 1H), 3.75 (d, *J* = 1.7 Hz, 1H), 3.72 (s, 3H), 3.42 (dd, *J* = 14.4, 5.0 Hz, 1H), 3.06 (d, *J* = 14.6 Hz, 1H), 2.74 – 2.69 (m, 1H), 2.67 (d, *J* = 1.9 Hz, 1H), 2.63 (d, *J* = 1.4 Hz, 1H), 2.48 (tt, *J* = 9.0, 4.6 Hz, 1H), 2.39 (dd, *J* = 4.1, 1.7 Hz, 1H), 2.34 (dd, *J* = 4.1, 1.7 Hz, 1H), 2.30 (dd, *J* = 8.8, 3.0 Hz, 1H), 2.11 (s, 3H), 2.05 (dd, *J* = 16.2, 8.4 Hz, 1H), 1.71 (s, 3H), 1.69 (t, *J* = 1.0 Hz, 3H). $^{13}$C NMR (101 MHz, $CDCl_3$): δ = 172.9, 168.1, 165.1, 163.2, 144.9, 114.2, 112.9, 85.7, 83.2, 81.4, 71.6, 67.3, 52.4, 44.7, 42.6, 40.1, 33.6, 25.8, 24.0, 21.2, 20.1. The analytical and spectroscopic data are in agreement with those reported in the literature.[161]

**Dimethyl 2,7-diacetyloct-4-ynedioate (178)**

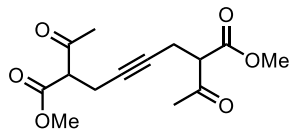

Prepared analogously with catalyst **108** (27.8 mg, 0.025 mmol, 10 mol%) at 90 °C; colorless oil (28.0 mg, 79%). $^1$H NMR (400 MHz, $CDCl_3$): δ = 3.75 (s, 3H), 3.65 – 3.56 (m, 1H), 2.67 – 2.61 (m, 2H), 2.27 (s, 3H). $^{13}$C NMR (101 MHz, $CDCl_3$): δ = 201.4, 168.8, 78.4, 58.5, 52.8, 29.6, 17.9. IR (film): $\tilde{\nu}$ 2956, 2163, 2002, 1745, 1719, 1435, 1361, 1266, 1226, 1151, 1004, 904, 510, 424 cm$^{-1}$. HRMS-ESI (m/z): calculated for $C_{14}H_{18}O_6Na^+$ $[M+Na]^+$, 305.09956; found, 305.09970.

***O*,*O*'-(Dodec-6-yne-1,12-diyl) dimethyl dimalonate (179)**

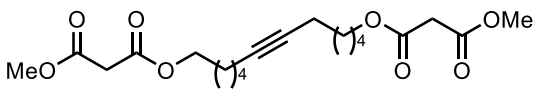

Prepared analogously with complex **108** (13.9 mg, 12.5 µmol, 5 mol%) at 25 °C; white solid (45.3 mg, 91%). $^1$H NMR (400 MHz, $CDCl_3$): δ = 4.11 (t, *J* = 6.7 Hz, 4H), 3.71 (s, 6H), 3.35 (s, 4H), 2.19 – 2.05 (m, 4H), 1.72 – 1.59 (m, 4H), 1.44 (ddt, *J* = 15.0, 8.0, 4.3

Hz, 8H). $^{13}$C NMR (101 MHz, $CDCl_3$): δ = 167.1, 166.6, 80.1, 65.6, 52.5, 41.4, 28.7, 28.0, 25.1, 18.7. The analytical and spectroscopic data are in agreement with those reported in the literature.[123]

**Dimethyl 2,7-diacetamidooct-4-ynedioate (180)**

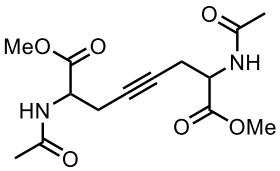

Prepared analogously with complex **108** (13.9 mg, 12.5 μmol, 5 mol%) at 25 °C; white solid (26.2 mg, 67%). $^1$H NMR (400 MHz, $CDCl_3$): δ = 7.16 (d, *J* = 9.1 Hz, 2H), 6.57 (d, *J* = 8.5 Hz, 2H), 4.88 (dt, *J* = 9.1, 3.7 Hz, 2H), 4.79 (dt, *J* = 7.8, 3.9 Hz, 2H), 3.80 – 3.76 (m, 13H), 2.64 (dtd, *J* = 17.4, 4.5, 2.8 Hz, 8H), 2.12 – 2.11 (m, 13H). $^{13}$C NMR (101 MHz, $CDCl_3$): δ = 172.6, 171.5, 170.4, 170.4, 78.6, 78.0, 52.9, 50.7, 50.4, 23.5, 23.2, 23.2, 22.9. The analytical and spectroscopic data are in agreement with those reported in the literature.[123]

**Di-*tert*-butyl (1,10-bis(phenylsulfonyl)dec-5-yne-1,10-diyl)dicarbamate (181)**

Prepared analogously with either complex **108** (13.9 mg, 12.5 μmol, 5 mol%) at 25 °C; white solid (62 mg, 76%). $^1$H NMR (Diastereomer 1, 600 MHz, $C_6D_6$): δ = 8.15 – 8.10 (m, 4H), 7.09 – 7.03 (m, 6H), 6.38 (d, *J* = 10.7 Hz, 2H), 5.19 (td, *J* = 10.4, 5.1 Hz, 2H), 2.52 – 2.37 (m, 1H), 2.13 – 2.02 (m, 4H), 1.97 – 1.90 (m, 3H), 1.52 – 1.34 (m, 4H), 1.15 (s, 18H). $^1$H NMR (Diastereomer 2, 600 MHz, $C_6D_6$): δ = 8.08 (dt, *J* = 7.4, 1.9 Hz, 4H), 6.99 (td, *J* = 5.8, 5.1, 2.9 Hz, 6H), 5.30 (d, *J* = 10.8 Hz, 2H), 5.13 (td, *J* = 10.9, 3.5 Hz, 2H), 2.52 – 2.46 (m, 1H), 1.93 (td, *J* = 5.1, 3.9, 2.1 Hz, 4H), 1.85 (d, *J* = 4.2 Hz, 1H), 1.30 – 1.21 (m, 4H), 1.16 (s, 18H). $^{13}$C NMR (Diastereomer 1, 151 MHz, $C_6D_6$): δ = 154.3, 138.1, 133.1, 129.7, 128.5, 80.3, 79.4, 71.2, 27.7, 26.4, 24.4, 18.3. $^{13}$C NMR (Diastereomer 2, 151 MHz, $C_6D_6$): δ = 153.9, 138.1, 133.0, 129.5, 128.6, 80.0, 79.5, 70.7, 27.7, 25.4, 24.5, 17.9. IR (film): $\tilde{\nu}$ 3339, 2977, 2933, 1718, 1514, 1447, 1393, 1367, 1307, 1284, 1242, 1164, 1138, 1081, 1048, 1025, 999, 864, 812, 776, 754, 732, 715, 687, 592, 545, 517, 498, 428 cm$^{-1}$. HRMS-ESI (m/z): calcd. for $C_{32}H_{44}N_2O_8S_2Na$ $[M+Na]^+$, 671.243131; found, 671.243520.

**Representative Procedure for Ring Closing Alkyne Metathesis. 1,6-Dioxacyclododec-9-yne-2,5-dione (182)**

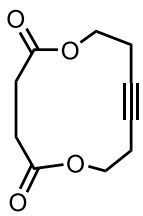

Di(pent-3-yn-1-yl) succinate (25.0 mg, 0.100 mmol) was added to a stirred suspension of complex **108** (5.57 mg, 0.5 μmol, 5 mol%) and powdered molecular sieves 5Å (200 mg) in toluene (50 mL) at 60 °C under argon atmosphere. The mixture was stirred for 14 h at this temperature before it was filtered through a short pad of Celite® which was carefully rinsed with ethyl acetate (20 mL). The combined filtrates were evaporated and the residue was purified by flash chromatography on silica gel (hexanes/*t*-butyl methyl ether 6:4 to 1:4) to give the title compound as a white solid (18.6 mg, 95%). $^1$H NMR (400 MHz, $CDCl_3$): δ = 4.34

– 4.16 (m, 4H), 2.69 (s, 4H), 2.58 – 2.34 (m, 4H). $^{13}$C NMR (101 MHz, $CDCl_3$): δ = 171.8, 78.9, 61.5, 30.1, 19.8. The analytical and spectroscopic data are in agreement with those reported in the literature.[58]

**1,8-Dioxacyclotetradec-11-yne-2,7-dione (183)**

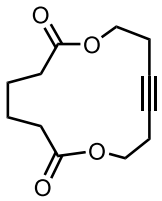

Prepared analogously with complex **108** (13.9 mg, 12.5 µmol, 5 mol%) at 25 °C; white solid (19.1 mg, 85%). $^1$H NMR (400 MHz, $CDCl_3$): δ = 4.18 – 4.10 (m, 4H), 2.56 – 2.49 (m, 4H), 2.39 (ddt, *J* = 6.0, 3.8, 1.8 Hz, 4H), 1.79 – 1.69 (m, 4H). $^{13}$C NMR (101 MHz, $CDCl_3$): δ = 173.3, 78.1, 62.7, 35.1, 25.2, 19.3. The analytical and spectroscopic data are in agreement with those reported in the literature.[58]

**Compound 184**

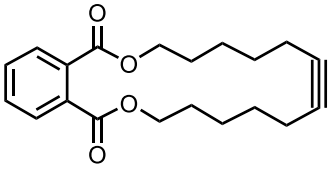

Prepared analogously with complex **108** (13.9 mg, 12.5 µmol, 5 mol%) at 25 °C; white solid (32.1 mg, 98%). $^1$H NMR (400 MHz, $CDCl_3$): δ =7.77 – 7.69 (m, 2H), 7.58 – 7.49 (m, 2H), 4.35 (t, *J* = 6.1 Hz, 4H), 2.24 – 2.15 (m, 4H), 1.79 (dq, *J* = 9.0, 5.8 Hz, 4H), 1.64 – 1.45 (m, 8H). $^{13}$C NMR (101 MHz, $CDCl_3$): δ = 167.9, 132.4, 131.1, 129.0, 80.8, 66.5, 28.5, 28.2, 26.0, 18.8. The analytical and spectroscopic data are in agreement with those reported in the literature.[58]

**Compound 185**

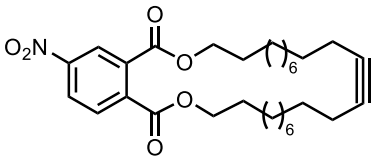

Prepared analogously with complex **108** (13.9 mg, 12.5 µmol, 5 mol%) at 60 °C; white solid (51.4 mg, 98%). $^1$H NMR (400 MHz, $CDCl_3$): δ = 8.61 (d, *J* = 2.3 Hz, 1H), 8.38 (dd, *J* = 8.5, 2.3 Hz, 1H), 7.85 (d, *J* = 8.5 Hz, 1H), 4.33 (td, *J* = 7.0, 4.7 Hz, 4H), 2.17 (h, *J* = 2.1 Hz, 4H), 1.75 (h, *J* = 7.2 Hz, 4H), 1.48 – 1.28 (m, 28H). $^{13}$C NMR (101 MHz, $CDCl_3$): δ = 166.5, 165.4, 148.9, 138.4, 133.4, 130.3, 126.0, 124.6, 80.7, 66.8, 29.8, 29.8, 29.7, 29.6, 29.5, 29.3, 29.3, 26.0, 25.9, 18.7. The analytical and spectroscopic data are in agreement with those reported in the literature.[58]

**Compound 186**

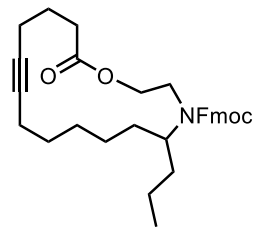

Prepared analogously with complex **108** (13.9 mg, 12.5 µmol, 5 mol%) at 25 °C ; white solid (26.8 mg, 99%). $^1$H NMR (rotamers, 400 MHz, $CDCl_3$): δ = 7.76 (dd, *J* = 7.7, 2.2 Hz, 2H), 7.63 – 7.53 (m, 2H), 7.45 – 7.27 (m, 4H), 4.73 – 4.49 (m, 2H), 4.22 (q, *J* = 5.2 Hz, 2H), 3.92 – 3.66 (m, 1H), 3.42 (s, 0H), 2.99 (s, 1H), 2.70 – 2.35 (m, 1H), 2.32 – 2.13 (m, 3H), 2.13 – 2.01 (m, 1H), 1.86 – 1.69 (m, 2H), 1.61 – 0.77 (m, 14H), 0.70 (s, 2H). $^{13}$C NMR (rotamers, 101 MHz, $CDCl_3$): δ = 173.5, 173.4, 144.3, 144.2, 144.1, 141.6, 141.6, 127.8, 127.8, 127.7, 127.3, 127.2, 127.2, 127.1, 124.8, 124.7, 120.1, 120.1, 120.0, 120.0, 79.8, 79.6, 77.4, 66.6, 66.4, 63.6, 47.8, 47.5, 35.1, 34.8, 34.7, 32.6, 32.5, 28.6, 28.4,

26.9, 26.8, 23.7, 23.6, 19.7, 18.4, 17.9, 14.2, 14.0. The analytical and spectroscopic data are in agreement with those reported in the literature.[58, 125]

**Compound 188**

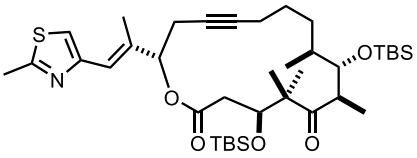


Prepared analogously with complex **108** (13.9 mg, 12.5 µmol, 5 mol%) at 60 °C; white solid (5.30 mg, 75%). $^1$H NMR (400 MHz, $CDCl_3$): δ = 6.96 (s, 1H), 6.55 (s, 1H), 5.34 (dd, *J* = 7.3, 3.4 Hz, 1H), 4.70 (dd, *J* = 6.4, 4.8 Hz, 1H), 3.94 (dd, *J* = 6.6, 1.9 Hz, 1H), 3.31 – 3.12 (m, 1H), 2.83 – 2.74 (m, 1H), 2.71 (s, 3H), 2.71 – 2.53 (m, 3H), 2.18 (d, *J* = 1.3 Hz, 3H), 2.39 – 1.94 (m, 3H), 1.81 – 1.35 (m, 1H), 1.17 (s, 3H), 1.15 (s, 3H), 1.11 (s, 3H), 0.95 – 0.94 (m, 3H), 0.92 (s, 9H), 0.87 (s, 9H), 0.10 (s, 6H), 0.09 (s, 3H), 0.07 (d, *J* = 2.2 Hz, 6H). $^{13}$C NMR (101 MHz, $CDCl_3$): δ = 216.7, 170.2, 164.9, 152.6, 137.0, 120.7, 116.9, 82.3, 78.2, 77.4, 76.5, 72.8, 54.7, 53.5, 44.6, 41.8, 39.1, 29.9, 26.4, 26.2, 26.1, 24.3, 21.2, 20.7, 19.4, 18.8, 18.7, 18.5, 17.1, 15.2, −3.1, −3.6, −3.9, −3.9. The analytical and spectroscopic data are in agreement with those reported in the literature.[105]

**Compound 187**

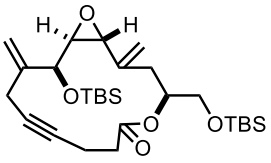


Prepared analogously with complex **108** (13.9 mg, 12.5 µmol, 5 mol%) at 25 °C; white solid (4.42 mg, 85%). $^1$H NMR (400 MHz, $CDCl_3$): δ 5.19 (p, *J* = 1.1 Hz, 1H), 5.14 (d, *J* = 1.2 Hz, 1H), 5.12 – 5.06 (m, 1H), 5.05 (t, *J* = 1.5 Hz, 1H), 5.01 (p, *J* = 1.2 Hz, 1H), 4.12 (d, *J* = 4.8 Hz, 1H), 3.71 (dd, *J* = 10.4, 5.0 Hz, 1H), 3.60 (dd, *J* = 10.4, 5.7 Hz, 1H), 3.31 (dd, *J* = 2.1, 0.8 Hz, 1H), 3.19 (d, *J* = 17.6 Hz, 1H), 3.14 (dd, *J* = 4.8, 2.1 Hz, 1H), 2.93 (d, *J* = 17.6 Hz, 1H), 2.55 – 2.32 (m, 6H), 0.91 (s, 9H), 0.89 (s, 9H), 0.14 (s, 3H), 0.05 (d, *J* = 0.8 Hz, 9H). $^{13}$C NMR (101 MHz, $CDCl_3$): δ = 171.7, 143.9, 141.2, 114.2, 114.1, 80.4, 78.8, 74.9, 72.6, 64.5, 62.7, 57.0, 34.3, 34.1, 26.0, 25.9, 22.7, 18.4, 18.4, 15.3, –4.7, –4.9, –5.3, –5.3. The analytical and spectroscopic data are in agreement with those reported in the literature.[162]

**Compound 189**

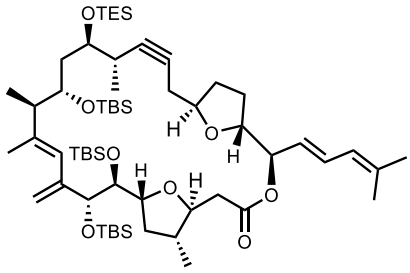


To a stirred suspension of diyne (8.1 mg, 7.3 µmol) and powdered molecular sieves 5Å (30 mg) in toluene (3.5 mL) at 80 °C was added a solution of complex **133** (1.8 mg, 2.2 µmol, 30 mol%) in toluene (1.0 mL) under argon atmosphere. The mixture was stirred for 5 h at this temperature before it was filtered through a short pad of Celite® and rinsed with ethyl acetate (10 mL). The filtrate was evaporated and the residue was purified by flash chromatography on silica gel (hexanes/*t*-butyl methyl ether 97:3 to 9:1) to give the title compound as an oil (6.3 mg, 81%). $^1$H NMR (600 MHz, $C_6D_6$, broad signals due to slowly equilibrating conformers): δ = 6.65 (m, 1H), 6.48 (s, 1H),

5.77 (m, 1H), 5.48 (m, 1H), 5.43 (m, 1H), 5.10 (s, 1H), 5.04 (s, 1H), 4.26 (bs, 1H), 4.15 (s, 1H), 4.12 (m, 1H), 4.10 (m, 1H), 4.03 (m, 1H), 4.00 (m, 1H), 3.80 (d, *J* = 7 Hz, 1H), 3.58 (bs, 1H), 2.86 (m, 1H), 2.82 (m, 1H), 2.73 (bs, 1H), 2.57 (m, 1H), 2.53 (m, 1H), 2.40 (m, 1H), 2.33 (d, *J* = 13 Hz, 1H), 2.18 (m, 1H), 2.13 (m, 3H), 2.07 (m, 1H), 2.06 (m, 1H), 1.83 (m, 1H), 1.60 (m, 1H), 1.57 (m, 1H), 1.54 (s, 3H), 1.48 (s, 3H), 1.45 (m, 3H), 1.43 (m, 1H), 1.34 (m, 3H), 1.29 (s, 9H), 1.13 (m, 1H), 1.07 (m, 9H), 1.05 (s, 9H), 1.01 (s, 9H), 0.82 (m, 3H), 0.70 (q, *J* = 8 Hz, 6H), 0.49 (s, 3H), 0.43 (s, 3H), 0.25 (s, 3H), 0.22 (s, 3H), 0.13 (s, 3H), 0.12 (s, 3H). $^{13}$C NMR (151 MHz, $CDCl_3$, broad signals due to slowly equilibrating rotamer): δ = 169.2, 147.3, 140.9, 137.2, 132.1, 129.4, 126.0, 125.0, 115.0, 83.8, 83.1, 81.4, 80.3, 80.0, 79.4, 77.8, 76.3, 73.9, 72.6, 47.7, 38.8, 37.8, 33.0, 31.3, 27.8, 27.0, 26.9, 26.3, 26.0, 19.2, 18.7, 18.4, 18.3, 17.6, 16.4, 16.3, 14.4, 7.3, 5.6, –3.8, –3.9, –4.3, –4.3. The analytical and spectroscopic data are in agreement with those reported in the literature.[117]

**Compound 216**

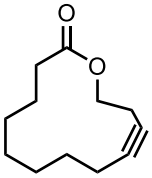

Pent-3-yn-1-yl undec-9-ynoate (25.6 mg, 0.100 mmol) was added to a stirred solution of complex **214** (4.1 mg, 0.5 µmol, 5 mol%) in toluene (50 mL) at 80 °C under argon atmosphere. The mixture was stirred for 4 h at this temperature before it was allowed to cool to ambient temperature and filtered through a short pad of Celite®, which was carefully rinsed with ethyl acetate (20 mL). The combined filtrates were evaporated and the residue was purified by flash chromatography on silica gel (hexanes/*t*-butyl methyl ether, 9:1 to 6:4) to give the title compound as a white solid (12.8 mg, 66%). $^1$H NMR (400 MHz, $CDCl_3$): δ = 4.20 – 4.13 (m, 2H), 2.52 (tt, *J* = 5.3, 2.5 Hz, 2H), 2.42 – 2.34 (m, 2H), 1.80 – 1.68 (m, 2H), 1.51 – 1.33 (m, 8H). $^{13}$C NMR (101 MHz, $CDCl_3$): δ = 174.1, 82.9, 77.0, 62.8, 34.6, 27.8, 27.3, 27.1, 26.8, 24.8, 19.5, 18.9. The analytical and spectroscopic data are in agreement with those reported in the literature.[125]

## 5.5 Preparation of Complexes

**$[MoCl_4(THF)_2]$ (221)[103, 182]**

A 25-mL, two-necked, round-bottomed flask was equipped with a magnetic stir bar and was flame dried under vacuum. The flask was filled with argon and charged with acetonitrile (10 mL). $[MoCl_5]$ (**219**) (2.00 g, 7.32 mmol) was added in portions. The resulting red-brown suspension was stirred for 14 h at ambient temperature before the solid was filtered off and washed with additional acetonitrile (3 x 1 mL). The solid material was dried under vacuum ($10^{-3}$ mbar) and was transferred into a flame-dried 25 mL Schlenk flask to give $[MoCl_4(MeCN)_2]$ (**220**) as a red-brown solid (2.24 g, 96%). THF (8 mL) was added and the orange suspension was stirred for 3.5 h at ambient temperature. The resulting solid material was filtered off, washed with pentane (3 x 20 mL) and dried under vacuum ($10^{-3}$ mbar) to give $[MoCl_4(THF)_2]$ (**221**) as an orange solid (2.19 g, 78%). $^1$H NMR

(400 MHz, $CD_2Cl_2$): δ = 12.60 (s, 8H), −35.13 (s, 8H). IR (film): $\tilde{\nu}$ 2949, 1457, 1342, 1245, 1042, 989, 918, 948, 840, 689 $cm^{-1}$. Elemental analysis (%) calcd for $C_8H_{14}Cl_4MoO_2$: C 25.29, H 3.71, Cl 37.32, Mo 25.26; found: C 25.02, H 4.30, Cl 36.99, Mo 25.02. The analytical and spectroscopic data are in agreement with those reported in the literature.[189]

**[Mo(O*t*Bu)$_5$] (222)**

A 50 mL Schlenk flask was equipped with a magnetic stir bar and was flame dried under vacuum. The flask was filled with argon before it was charged with [$MoCl_4(THF)_2$] (**221**) (500 mg, 1.31 mmol) and toluene (16 mL) to give an orange suspension. The flask was capped with a rubber septum and the mixture was stirred for 30 min at −35°C. The septum was removed and NaO*t*Bu (377 mg, 3.93 mmol) was added all at once. The mixtures was allowed to warm to ambient temperature and stirring was continued for 4 h to give a brown suspension. The solvent was removed *in vacuo* and the residue was extracted with *n*-pentane (5 x 5 mL). A green solution was transferred via cannula into a flame-dried, argon-filled 50 mL Schlenk flask and the solvent was removed *in vacuo*. The product was further purified by sublimation (25 °C, $10^{-7}$ mbar, −30°C cold finger) to yield [Mo(O*t*Bu)$_5$] (**222**) as a fine green powder (181 mg, 30%). Green crystals suitable for single-crystal X-ray diffraction were grown by storing a concentrated solution in *n*-pentane at −18°C for three days. $^1$H NMR (400 MHz, $C_6D_6$): δ = 7.98 – 7.06 (*br*, paramagnetic). $^{13}$C NMR (101 MHz, $C_6D_6$): δ = 55.4 – 53.9 (*br*, paramagnetic), 30.7 – 29.8 (*br*, paramagnetic). IR (film): 1462, 1360, 1232, 1163, 970, 910, 775, 562, 468 $\tilde{\nu}$ $cm^{-1}$. Elemental analysis (%) calcd for $C_{20}H_{45}MoO_5$: C 52.05, H 9.83, Mo 20.79; found: C 52.33, H 10.01, Mo 20.58.

**Metathetic ligand exchange of [$MoCl_4(THF)_2$] (221) with LiO*t*Bu[189]**

A 50 mL Schlenk flask was equipped with a magnetic stir bar and was flame dried under vacuum. The flask was filled with argon before it was charged with [$MoCl_4(THF)_2$] (**221**) (531 mg, 1.39 mmol) and THF (15 mL) to give an orange suspension. The flask was capped with a rubber septum and the mixture was stirred at 0°C (ice bath). A solution of LiO*t*Bu in THF/hexane (1 M, 5.55 mL, 5.55 mmol) was added dropwise. The reaction was stirred for 1 h at 0°C, before it was slowly warmed to ambient temperature and stirring was continued for additional 14 h. The solvent was removed *in vacuo* and the residue was extracted with *n*-pentane (5 x 5 mL). The solution was filtered via cannula into a flame-dried, argon-filled 50 mL Schlenk flask and the solvent was removed *in vacuo*. The solid was dissolved in $C_6D_6$ and the solution was transferred into a NMR tube for NMR-analysis. $^1$H NMR (400 MHz, $C_6D_6$): δ = 7.98 – 7.06 (*br*, paramagnetic [Mo(O*t*Bu)$_5$]), 1.56 (s, [$Mo_2$(O*t*Bu)$_6$]). $^{13}$C NMR (101 MHz, $C_6D_6$): δ = 55.4 – 53.9 (*br*, paramagnetic [Mo(O*t*Bu)$_5$]), 30.7 – 29.8 (*br*, paramagnetic [Mo(O*t*Bu)$_5$]), 79.2 ([$Mo_2$(O*t*Bu)$_6$]), 33.2 ([$Mo_2$(O*t*Bu)$_6$]). $^{95}$Mo NMR (26 MHz, 25°C, $C_6D_6$): δ = 2640 ([$Mo_2$(O*t*Bu)$_6$]). The spectroscopic data are in agreement with those reported for [Mo(O*t*Bu)$_5$] and for [$Mo_2$(O*t*Bu)$_6$] as reported in the literature.[157]

**Protonolysis of [Mo(NMe$_2$)$_4$] (230) with *t*BuOH[191]**

A 25 mL Schlenk flask was equipped with a magnetic stir bar and was flame dried under vacuum. The flask was filled with argon before it was charged with [Mo(NMe$_2$)$_4$] (**230**) (500 mg, 1.83 mmol) and *n*-pentane (6.3 mL) to give a purple solution. The flask was capped with a rubber septum and the mixture was stirred at 0°C (ice bath). After 15 min, a solution of *t*BuOH (0.704 mL, 7.36 mmol) in benzene (1.3 mL) was added dropwise and the reaction mixture turned into a green suspension. The mixture was allowed to warm to ambient temperature and stirring was continued for additional 6 h. The solvent was removed *in vacuo*, the crude solid was dissolved in $C_6D_6$ and the solution was transferred into a NMR tube for NMR-analysis. $^1$H NMR (400 MHz, $C_6D_6$): δ = 12.02 – 9.31 (*br*, paramagnetic [Mo$_2$O(O*t*Bu)$_5$(NMe$_2$)(NHMe$_2$)]), 7.99 – 7.10 (*br*, paramagnetic [Mo(O*t*Bu)$_5$]), 4.75 – 3.78 (*br*, paramagnetic [Mo$_2$O(O*t*Bu)$_5$(NMe$_2$)(NHMe$_2$)]), 3.82 – 3.11 (*br*, paramagnetic [Mo$_2$O(O*t*Bu)$_5$(NMe$_2$)(NHMe$_2$)]), 1.70 – 1.10 (*br*, paramagnetic [Mo$_2$O(O*t*Bu)$_5$(NMe$_2$)(NHMe$_2$)]). $^{13}$C NMR (101 MHz, $C_6D_6$): δ = 55.2 – 54.2 (*br*, paramagnetic [Mo(O*t*Bu)$_5$]), 32.9 – 31.7 (*br*, paramagnetic [Mo(O*t*Bu)$_5$]). The spectroscopic data are in agreement with those reported for [Mo(O*t*Bu)$_5$].

The crude solid was cooled to –30°C and was further purified by extraction with cold *n*-pentane (–30°C, 3 x 5 mL). A green solution was filtered via cannula into a flame-dried, argon-filled 25 mL Schlenk flask and the solvent was removed *in vacuo*. The remaining purple solid is only moderately soluble in *n*-pentane and was filtered via cannula into a flame-dried, argon-filled 25 mL Schlenk flask. This solution was stored at –20°C for 3 d, upon which time purple crystals of dinuclear complex (**231**) suitable for single-crystal X-ray diffraction studies had grown. $^1$H NMR (400 MHz, $C_6D_6$): δ = 12.02 – 9.31 (*br*, paramagnetic [Mo$_2$O(O*t*Bu)$_5$(NMe$_2$)(NHMe$_2$)]), 4.75 – 3.78 (*br*, paramagnetic [Mo$_2$O(O*t*Bu)$_5$(NMe$_2$)(NHMe$_2$)]), 3.82 – 3.11 (*br*, paramagnetic [Mo$_2$O(O*t*Bu)$_5$(NMe$_2$)(NHMe$_2$)]), 1.70 – 1.10 (*br*, paramagnetic [Mo$_2$O(O*t*Bu)$_5$(NMe$_2$)(NHMe$_2$)]). IR (film): $\tilde{\nu}$ 2966, 2923, 1455, 1356, 1381, 1228, 1260, 1163, 1100, 1020, 992, 936, 779, 807, 563, 536, 508, 477 cm$^{-1}$. Elemental analysis (%) calcd for $C_{24}H_{58}Mo_2N_2O_6$: C 43.50, H 8.82, Mo 28.96, N 4.23; found: C 44.68, H 8.20, Mo 30.12, N 27.70.

**Disproportionation of Mo(IV) in the Absence of Alkoxides: Complexes [MoOCl$_3$(THF)(H$_2$O)] (232) and [Mo$_2$Cl$_6$(THF)$_3$] (233)**

A 25 mL Schlenk flask was equipped with a magnetic stir bar and was flame-dried under vacuum. The flask was filled with argon before it was charged with [MoCl$_4$(THF)$_2$] (**221**) (294 mg, 0.770 mmol) and $CH_2Cl_2$ (12 mL). The flask was capped with a rubber septum and the mixture was stirred for 4 d at 25 °C under argon atmosphere, upon which time the color of the solution changed from orange, green to deep red. The solvent was removed *in vacuo* to give a deep red solid. Crystals suitable for single-crystal X-ray diffraction were grown by layering a concentrated solution of the crude solid in $CH_2Cl_2$ (2 mL) with *n*-pentane (5 mL) at 5°C. $^1$H NMR (400 MHz, $C_2Cl_2$): δ = 7.4, 7.3, 6.7, 6.7, 6.5, 6.2,

6.1, 6.0, 5.9, 5.9, 5.7, 4.6, 2.5, 2.4, 2.3, 2.1, 1.3, 0.9. IR (film): $\tilde{\nu}$ 3232, 2962, 2887, 1620, 1455, 1364, 1261, 1041, 996, 919, 848, 795, 719, 520, 470 $cm^{-1}$. Elemental analysis (%) calcd for $C_{16}H_{34}Cl_9Mo_3O_6$: C 20.68, H 3.69, Cl 34.33, Mo 30.98; found: C 20.49, H 3.65, Cl 34.37, Mo 31.04. The spectroscopic data are in agreement with $[Mo_2Cl_6(THF)_3]$ (**233**) as reported in the literature.[195]

**[N≡Mo(O*t*Bu)$_3$] (223)**

A 50 mL Schlenk flask was equipped with a magnetic stir bar and was flame dried under vacuum. The flask was filled with argon before it was charged with $[MoCl_3(MeCN)_3]$ (**243**) (500 mg, 1.54 mmol) and MeCN (19 mL) to give an orange suspension. The flask was capped with a rubber septum and the mixture was stirred for 30 min at –35°C. Then NaO*t*Bu (444 mg, 4.62 mmol) was added all at once and an instant color change to black was observed. The mixtures was allowed to warm to ambient temperature and stirring was continued for 4 h to give a suspension. The solvent was removed *in vacuo* to yield $[N{\equiv}Mo(O\textit{t}Bu)_3]$ (**223**) (87% by NMR) and $[(\textit{t}BuO)_3Mo{\equiv}Mo(O\textit{t}Bu)_3]$ (**218**) as a byproduct (13% by NMR). $[N{\equiv}Mo(O\textit{t}Bu)_3]$ (**223**) could be further purified by sublimation as described in the literature.[183] $^1$H NMR (400 MHz, $CD_2Cl_2$): δ = 1.48 ($N{\equiv}Mo(O\textit{t}Bu)_3$), 1.42 ($(\textit{t}BuO)_3Mo{\equiv}Mo(O\textit{t}Bu)_3$). $^{13}$C NMR (101 MHz, $CD_2Cl_2$): δ = 80.9 ($N{\equiv}Mo(O\textit{t}Bu)_3$), 79.2 ($(\textit{t}BuO)_3Mo{\equiv}Mo(O\textit{t}Bu)_3$), 33.0 ($(\textit{t}BuO)_3Mo{\equiv}Mo(O\textit{t}Bu)_3$), 31.2 ($N{\equiv}Mo(O\textit{t}Bu)_3$). $^{95}$Mo NMR (26 MHz, 25°C, $CD_2Cl_2$): δ = 53.7 ($N{\equiv}Mo(O\textit{t}Bu)_3$). The spectroscopic data are in agreement with those reported for $[N{\equiv}Mo(O\textit{t}Bu)_3]$ and for $[Mo_2(O\textit{t}Bu)_6]$ as reported in the literature.[157, 183, 196]

## 5.6 Miscellaneous Ligand Designs

**Compound 259**

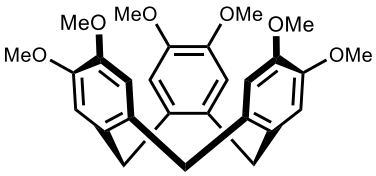


A 250 mL one-necked, round-bottomed flask was equipped with a magnetic stir bar and charged with 3,4-dimethoxybenzyl alcohol (**258**) (5.00 g, 29.7 mmol). 1,4-Dioxane was added (50 mL) and the colorless solution was vigorously stirred at ambient temperature. Then concentrated HCl (90 mL) was added dropwise over 5 min causing an immediate color change to pink and a slight exotherm. After 5 min stirring a perciptate crushed out and the pink suspension was stirred for 5 h at ambient temperature. The reaction mixture was transferred into a separation funnel and was extracted with ethyl acetate (3 x 100 mL). The combined extracts were washed with saturated aqueous NaCl (2 x 300 mL), dried over $MgSO_4$, filtered and concentrated in vacuo. The crude material was redissolved in 10% MeOH/DCM (50 mL) and hexanes (100 mL) was added to precipitate the desired product as a white solid (3.17 g, 72%). $^1$H NMR (400 MHz, $CDCl_3$): δ = 6.83 (s, 6H), 4.77 (d, *J* = 13.7 Hz, 3H), 3.84 (s, 18H), 3.55 (d, *J* = 13.7 Hz, 3H). $^{13}$C NMR (100 MHz, $CDCl_3$): δ =

147.9, 131.9, 113.3, 56.2, 36.7. The analytical and spectroscopic data are in agreement with those reported in the literature.[210]

**Compound 260**

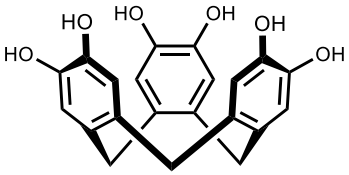


A 100 mL three-necked, round-bottomed flask was equipped with a magnetic stir bar, a reflux condenser, an argon-vacuum manifold and was flame dried under vacuum. The flask was filled with argon and charged with compound **259** (1.50 g, 3.33 mmol), methylene chloride (26 mL) and was cooled to 0 °C. Then a solution of boron tribromide (23.3 mL, 1 M in methylene chloride) was added dropwise over 10 min causing an immediate color change to green/purple/grey. After stirring at 0 °C for 15 min and then at ambient temperature for 10 min, the reaction mixture was heated to 40 °C for 5 h. The reaction mixture was cooled to 0 °C and was carefully quenched by the slow addition of water (25 mL). The resulting slurry was filtered through a Büchner filter and was washed with water (5 mL) and pentane (25 mL) to give the desired product as a brown solid (988 mg, 81%). $^1$H NMR (300 MHz, DMSO): δ = 6.65 (s, 6H), 6.57 – 6.24 (br, 6H), 4.48 (d, *J* = 13.5 Hz, 3H), 3.20 (d, *J* = 13.5 Hz, 3H). The analytical and spectroscopic data are in agreement with those reported in the literature.[211]

**Compound 261**

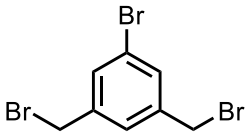


A 250 mL three-necked, round-bottomed flask was equipped with a magnetic stir bar, a reflux condenser, an argon-vacuum manifold and was flame dried under vacuum. The flask was filled with argon and charged with 1-bromo-3,5-dimethylbenzene (1.84 mL, 13.5 mmol) and benzene (81 mL). This solution was heated to 80 °C for 6 h, during which time *N*-bromosuccinimide (14.4 g, 81.1 mmol) and benzoyl peroxide (425 mg, 1.76 mmol) was added in three equal portions (at the beginning, after 2 h and after 4 h) to the reaction mixture. After 6 h, full conversion of the starting material was indicated by TLC and the mixture was cooled to ambient temperature. The mixture was filtered and washed with pentane (100 mL). The filtrate was transferred to a separation funnel, washed with saturated aqueous $NaHCO_3$ solution (40 mL) and saturated aqueous NaCl (40 mL), dried over $MgSO_4$, filtered and concentrated in vacuo. A 250 mL three-necked, round-bottomed flask was equipped with a magnetic stir bar, a glas stopper, connected to an argon-vacuum manifold and was flame dried under vacuum. The flask was filled with argon and the crude material was transferred and redissolved in THF (27 mL). This solution was stirred at 0 °C and a solution of diethyl phosphite (20.9 mL, 162 mmol) and *N*-ethyldiisopropylamine (27.8 mL, 159 mmol) was added. The cooling bath was removed and the reaction mixture was stirred at ambient temperature for 14 h. The mixture was poured into separation funnel loaded with ice water and extracted with ethyl acetate (3 x 50 mL). The combined

extracts were washed with a solution of aqueous HCl (1M, 100 mL) and subsequently with a solution of saturated aqueous NaCl (100 mL), dried over $MgSO_4$, filtered and concentrated in vacuo. The residue was purified by flash chromatography on silica gel with pentane to give the title compound as a white solid (3.08 g, 66%). $^1$H NMR (400 MHz, $CDCl_3$): δ = 7.47 (d, *J* = 1.6 Hz, 2H), 7.34 (d, *J* = 1.6 Hz, 1H), 4.41 (s, 4H). $^{13}$C NMR (100 MHz, $CDCl_3$): δ = 140.4, 132.1, 128.4, 122.8, 31.6. The analytical and spectroscopic data are in agreement with those reported in the literature.[208, 209]

**Compound 262**

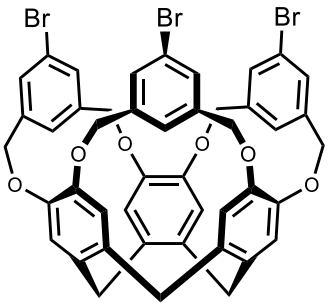


A 1 L three-necked, round-bottomed flask was equipped with a magnetic stir bar, a reflux condenser, a 100 mL dropping funnel, an argon-vacuum manifold and was flame dried under vacuum. The flask was filled with argon and charged with $Cs_2CO_3$ (4.48 g, 13.8 mmol) and DMF (350 mL). This suspension was vigorously stirred at 70 °C and a solution of compound **260** (300 mg, 0.819 mmol), compound **261** (926 mg, 2.70 mmol) and DMF (100 mL) was added dropwise to it. The mixture was stirred for 48 h at 70 °C, before it was cooled to ambient temperature and the DMF was removed in in vacuo. The residue was poured into separation funnel loaded with water (200 mL) and methylene chloride (200 mL). The organic layer was separated and the aqueous layer was extracted with methylene chloride (3 x 100 mL). The combined extracts were washed with water (5 x 100 mL), dried over $MgSO_4$, filtered and concentrated in vacuo. The residue was purified by flash chromatography on silica gel (MeOH/methylene chloride, 5:95) to afford the title compound as a white solid (180 mg, 24%). Colorless crystals suitable for single-crystal X-ray diffraction were grown by slow evaporation from a concentrated methylene chloride solution at ambient temperature. $^1$H NMR (400 MHz, $CD_2Cl_2$): δ = 7.49 (d, *J* = 1.3 Hz, 6H), 7.31 (s, 3H), 6.52 (s, 6H), 5.08 (d, *J* = 12.9 Hz, 6H), 5.00 (d, *J* = 12.9 Hz, 7H), 4.43 (d, *J* = 13.6 Hz, 3H), 3.23 (d, *J* = 13.6 Hz, 3H). $^{13}$C NMR (101 MHz, $CD_2Cl_2$): δ = 146.1, 138.6, 132.7, 132.5, 132.4, 124.0, 118.4, 70.6, 35.9. HRMS-ESI (m/z): calculated for $C_{45}H_{34}O_6Br_3^+$ $[M+H]^+$, 906.990041; found, 906.991030.

# 6 Appendix

## 6.1 Relevant NMR Data

$^1$H NMR of Complex **141**, $CDCl_3$, 25 °C

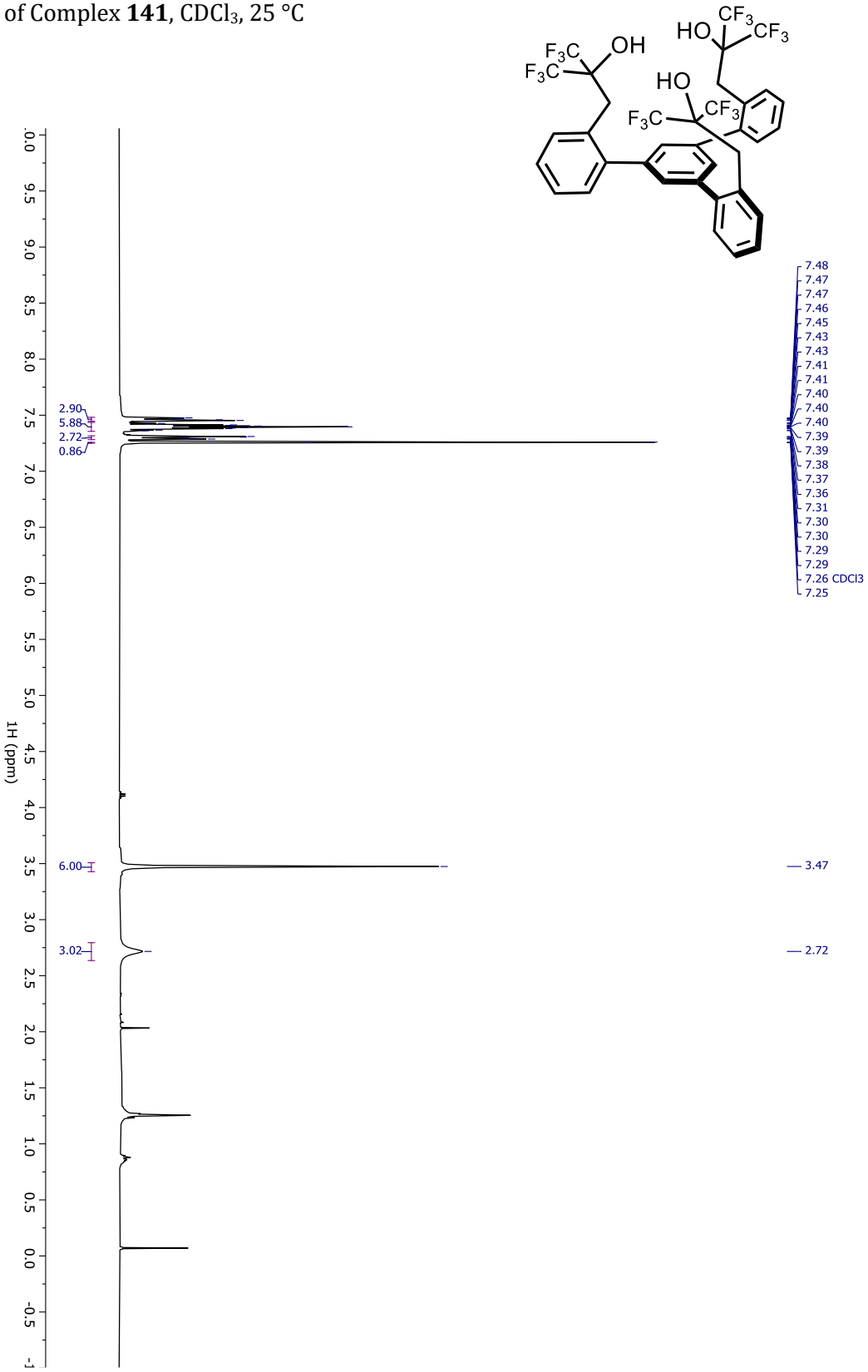

$^{13}C$ NMR of Complex **141**, $CDCl_3$, 25 °C

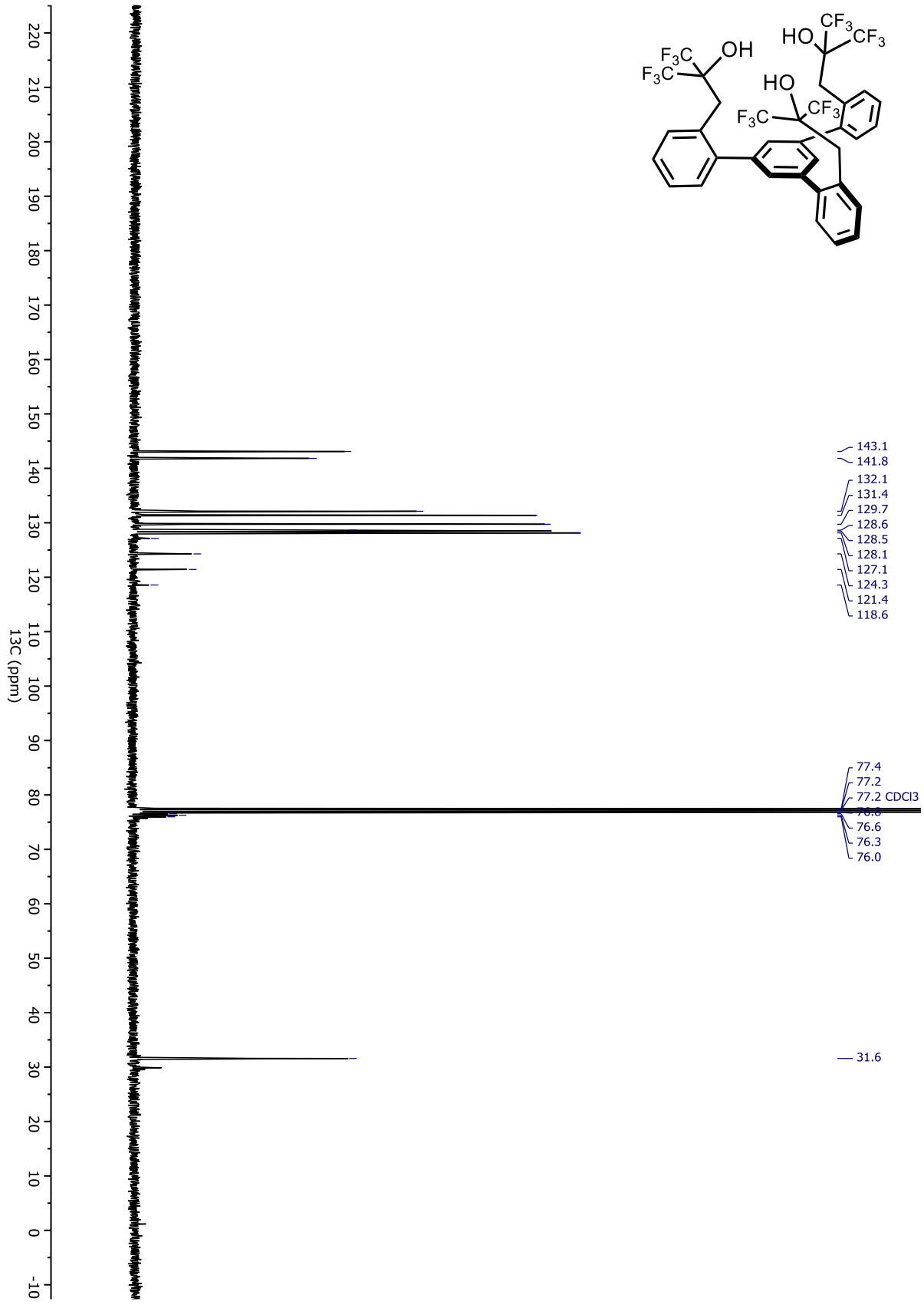

$^{19}F$ NMR of Complex **141**, $CDCl_3$, 25 °C

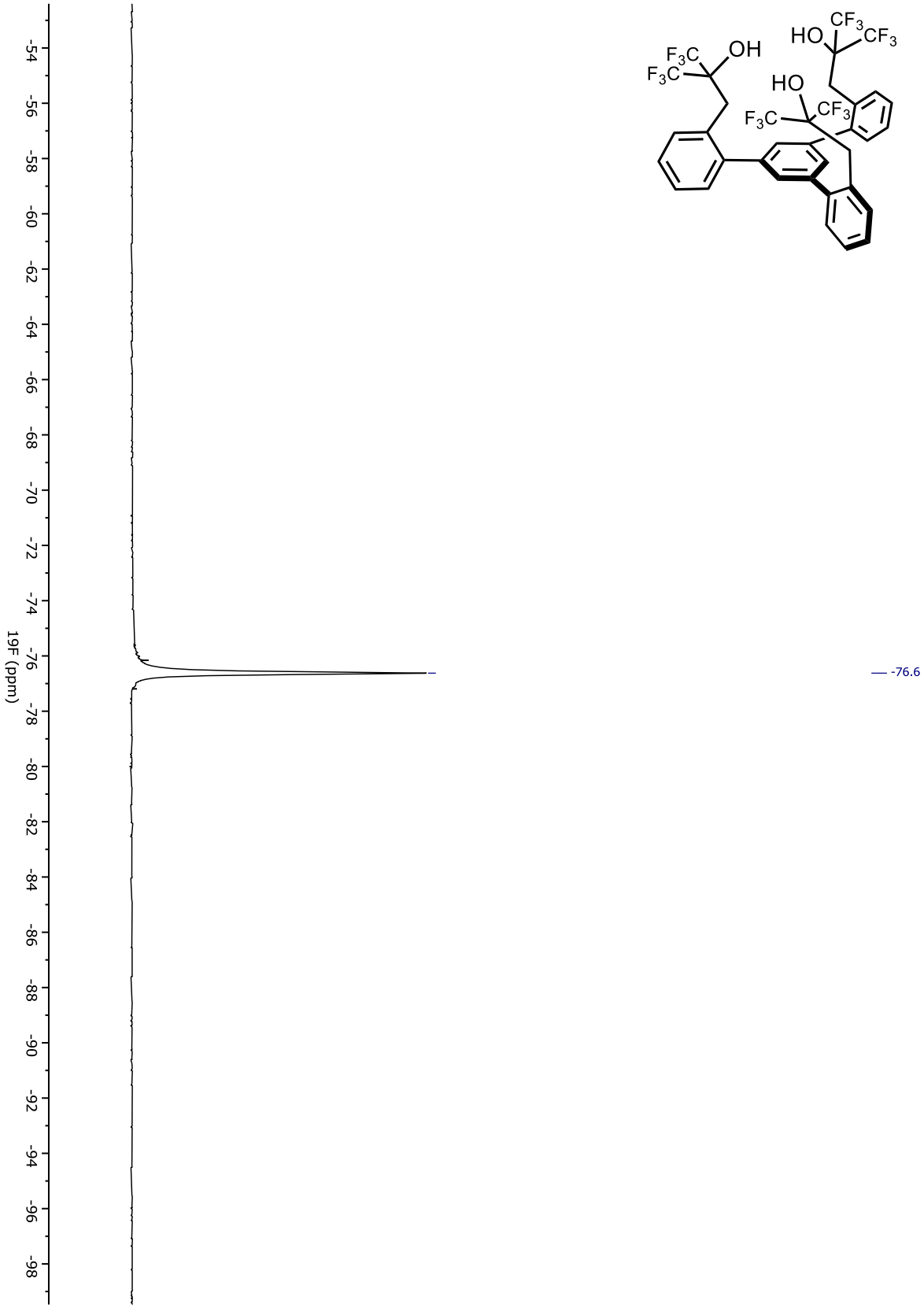

$^1$H NMR of Complex **119**, $CD_2Cl_2$, 25 °C

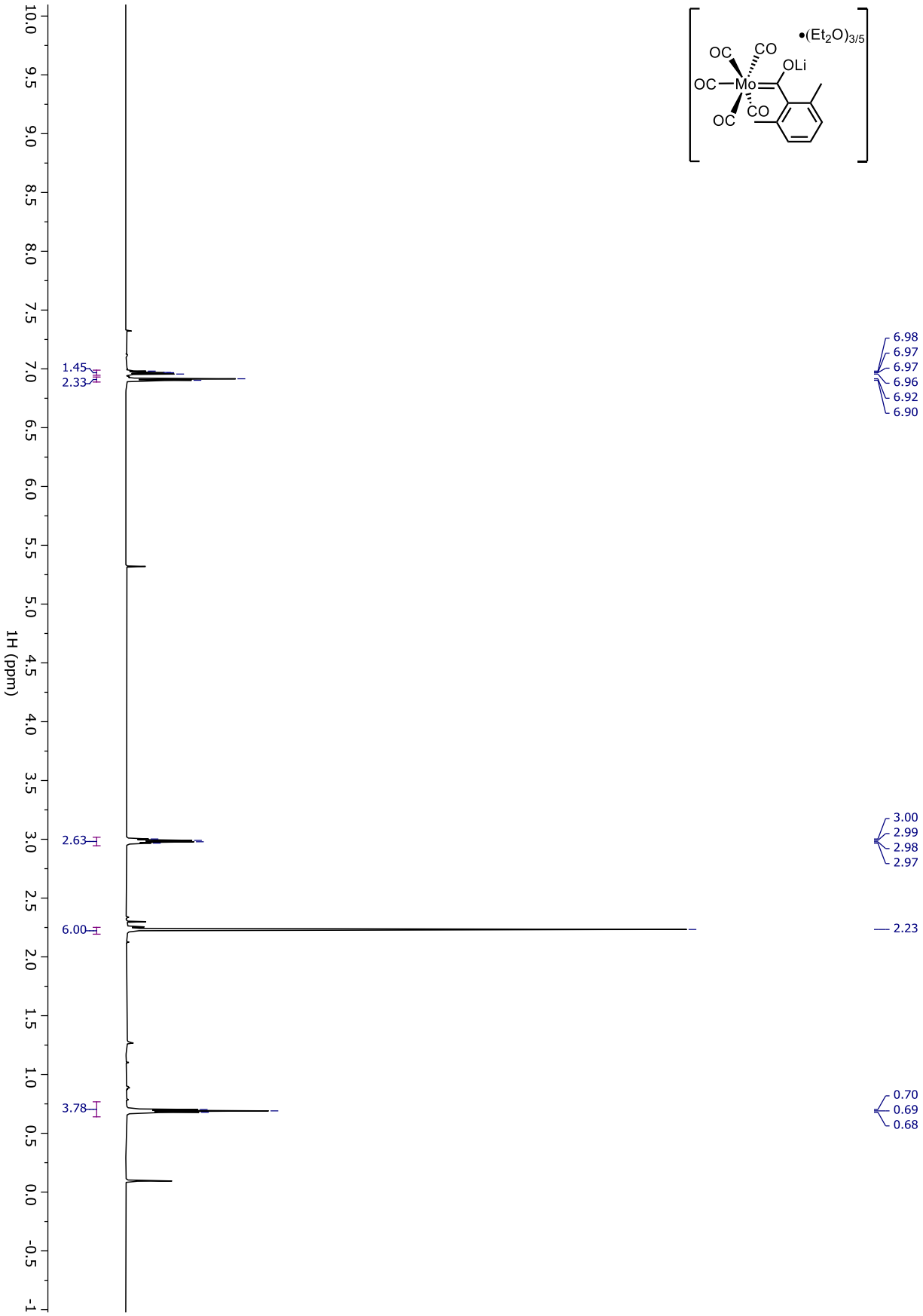

$^{13}C$ NMR of Complex **119**, $CD_2Cl_2$, 25 °C

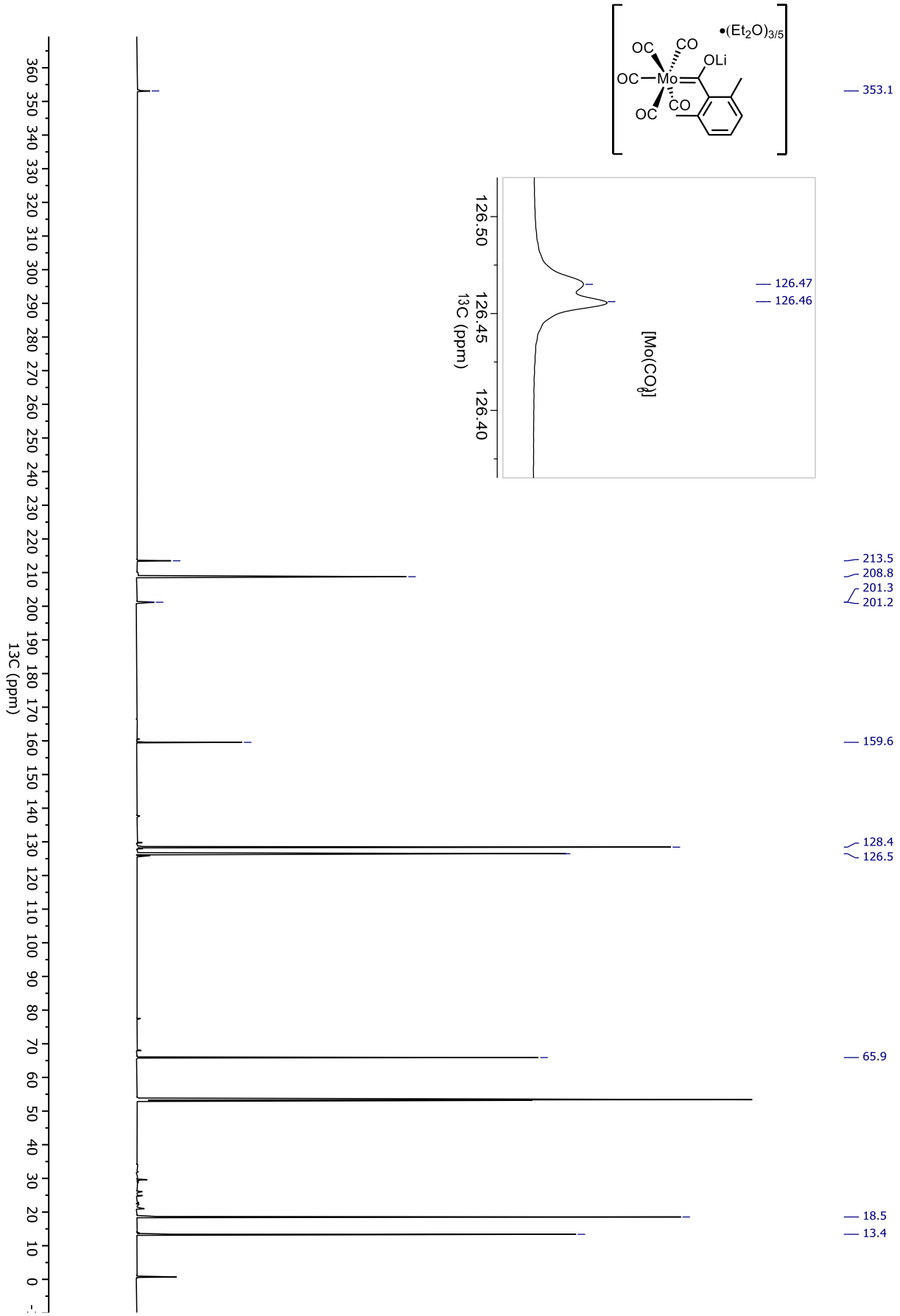

$^{1}$H NMR of Complex **109**, $C_6D_6$, 25 °C

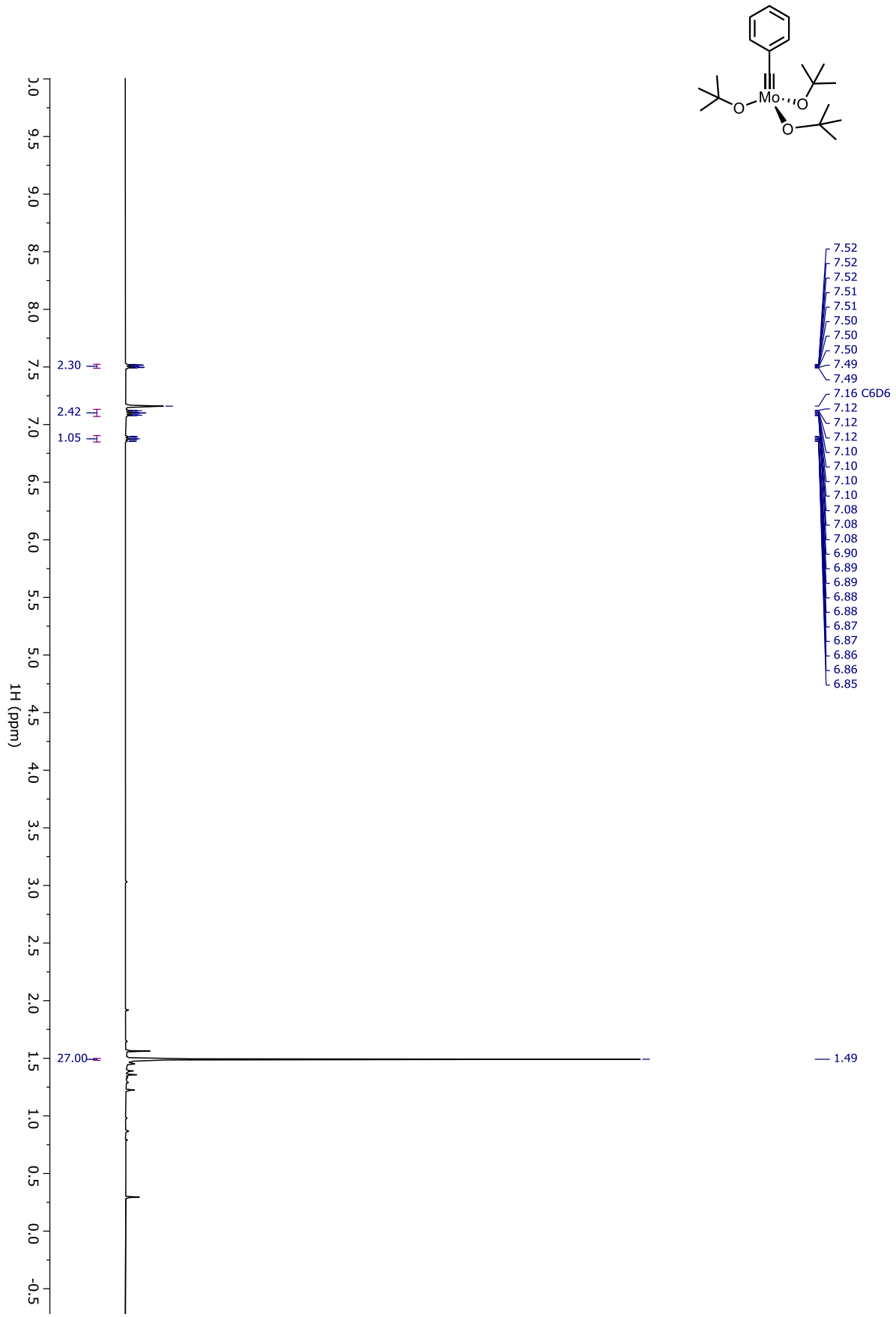

$^{13}C$ NMR of Complex **109**, $C_6D_6$, 25 °C

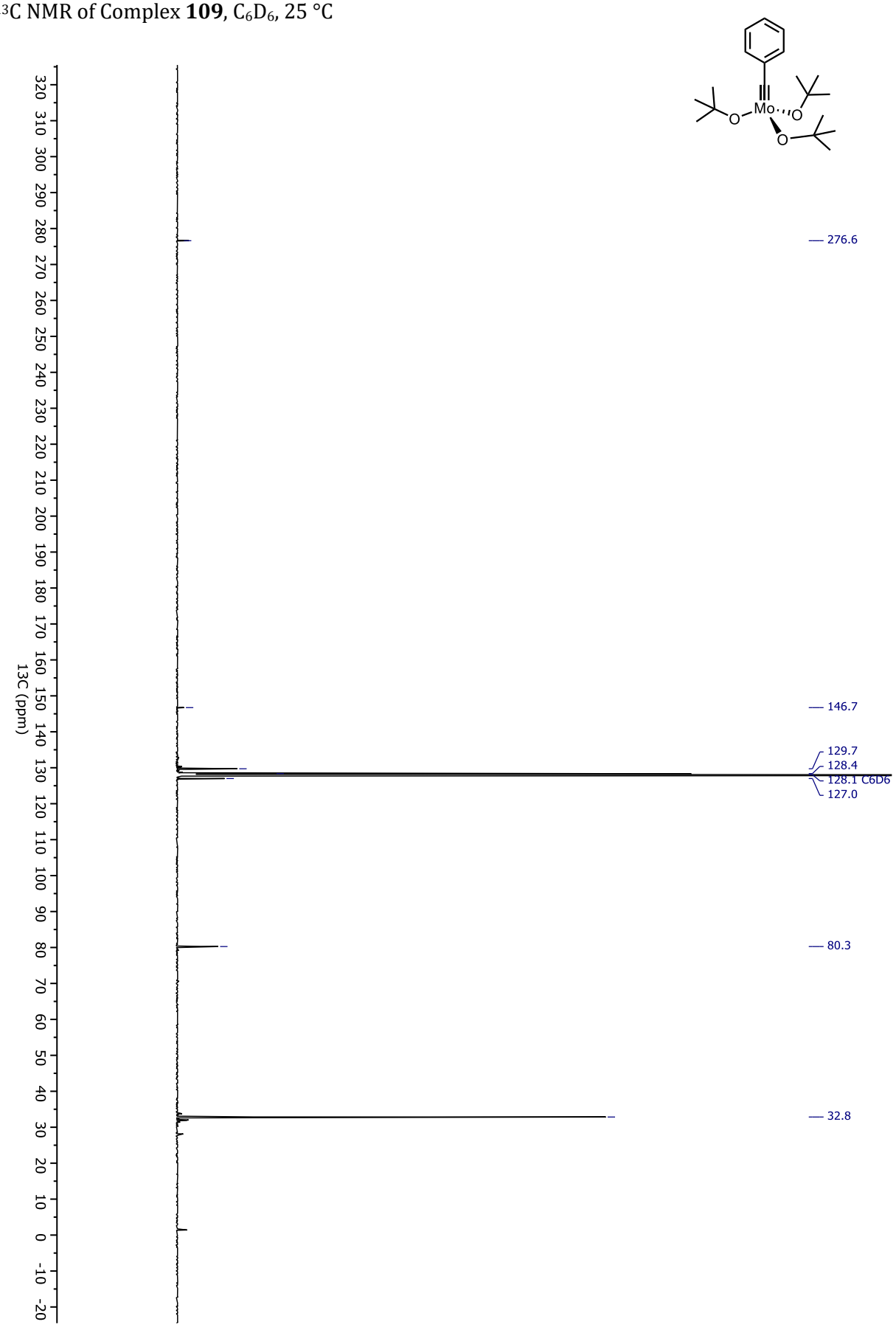

$^{95}$Mo NMR of Complex **109**, $C_6D_5CD_3$, 60 °C

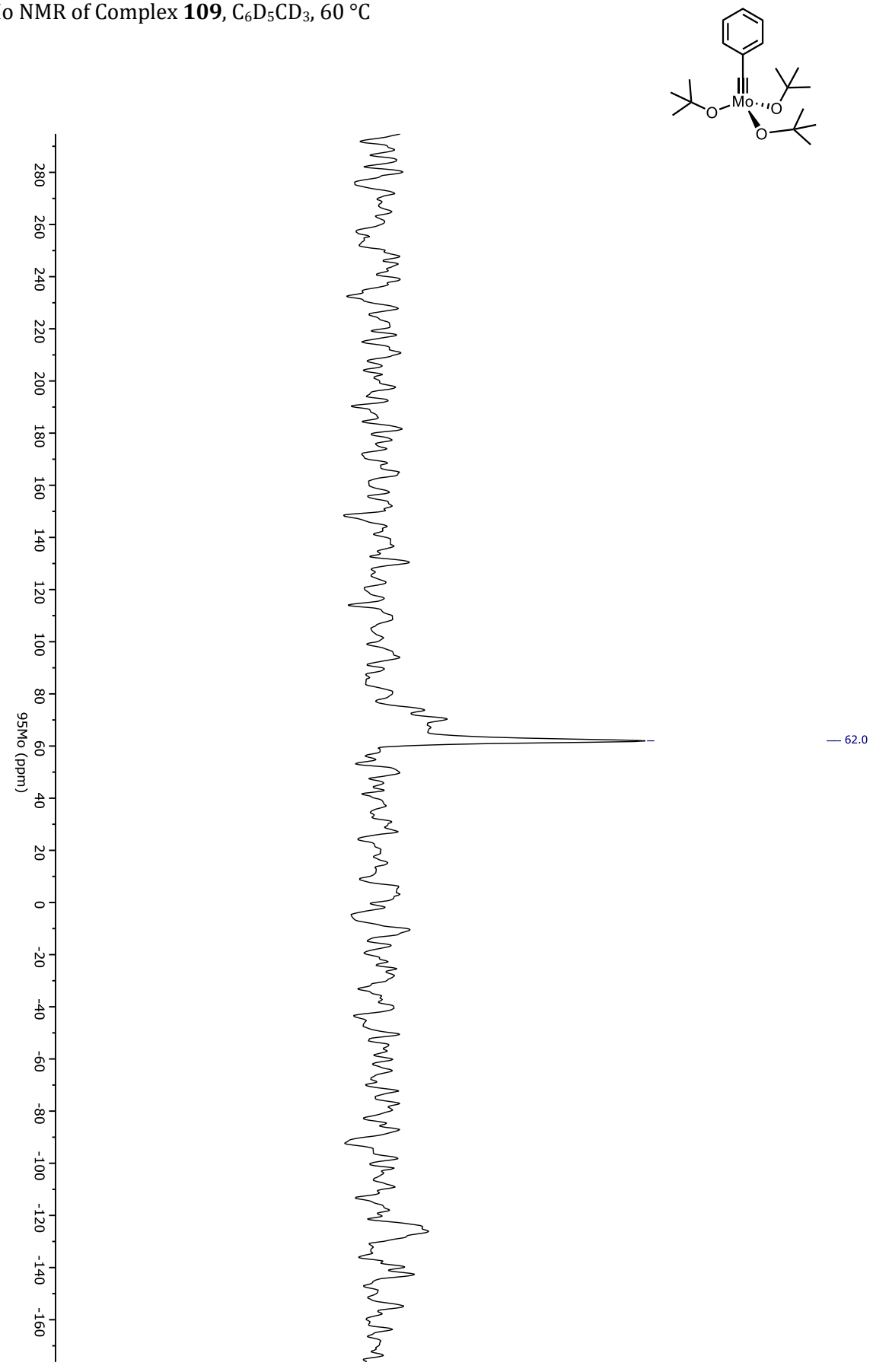

$^1$H NMR of Complex **110**, $C_6D_5CD_3$, 25 °C

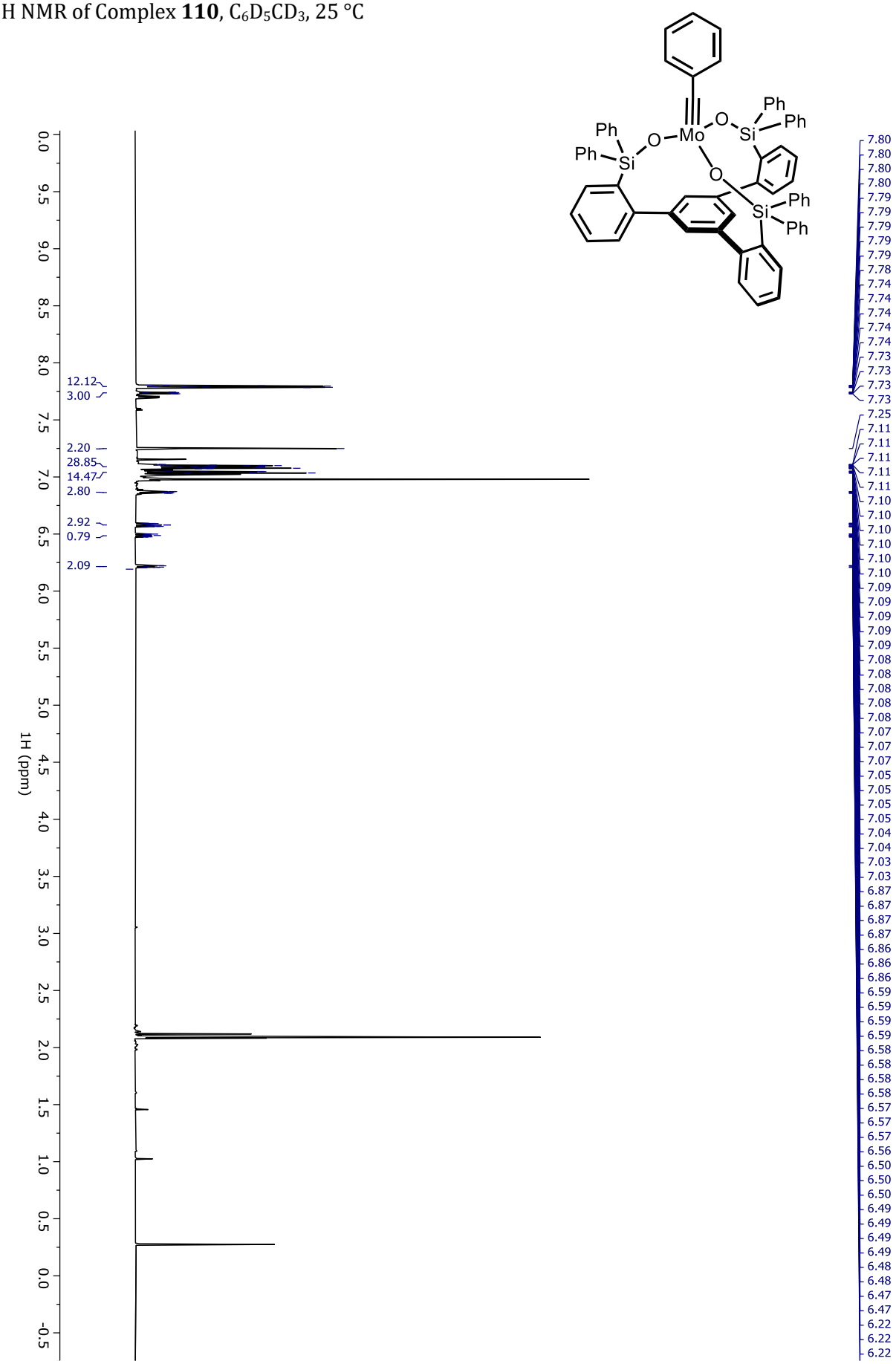

$^{13}C$ NMR of Complex **110**, $C_6D_5CD_3$, 25 °C

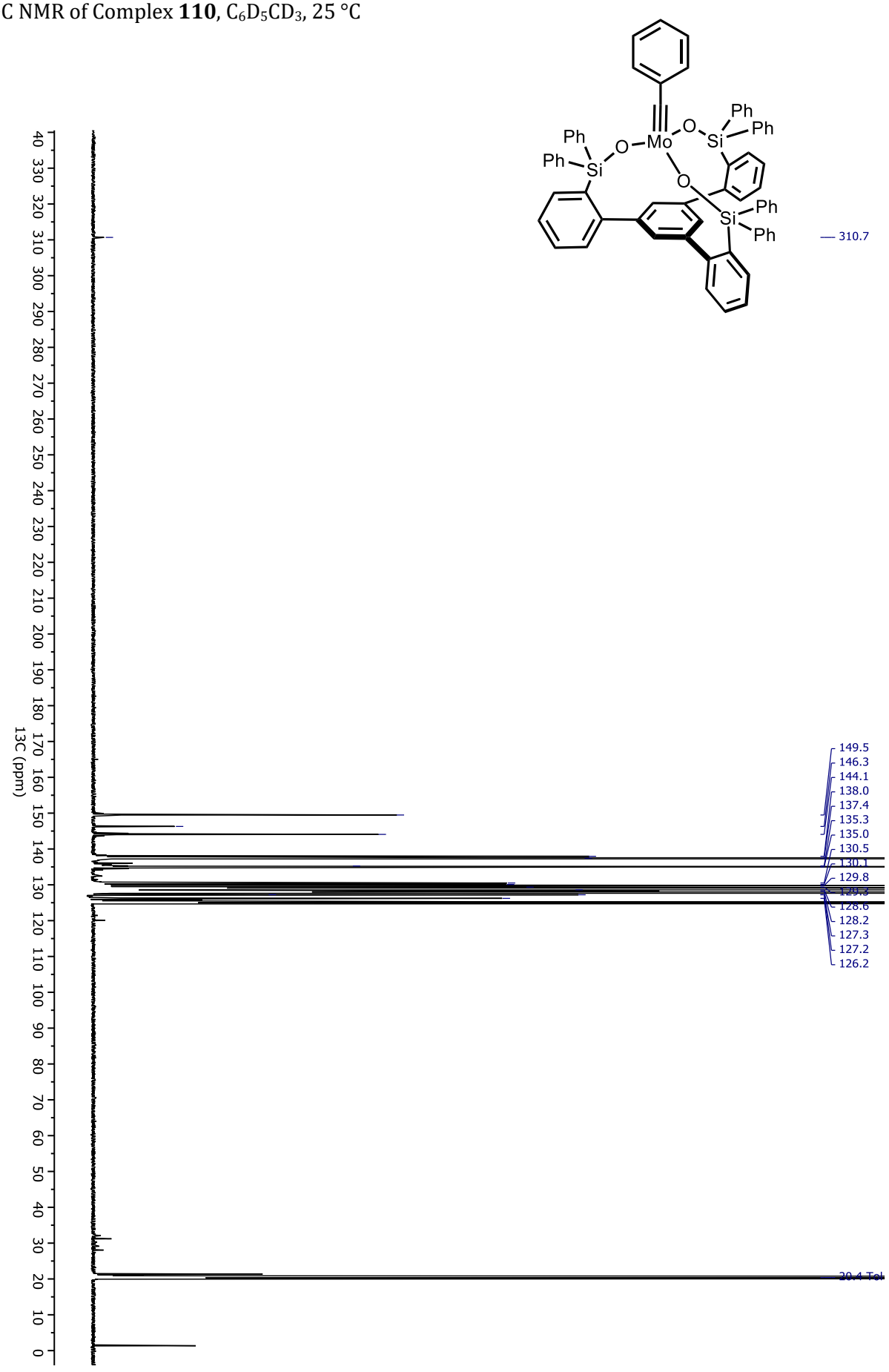

$^{29}$Si NMR of Complex **110**, $C_6D_5CD_3$, 25 °C

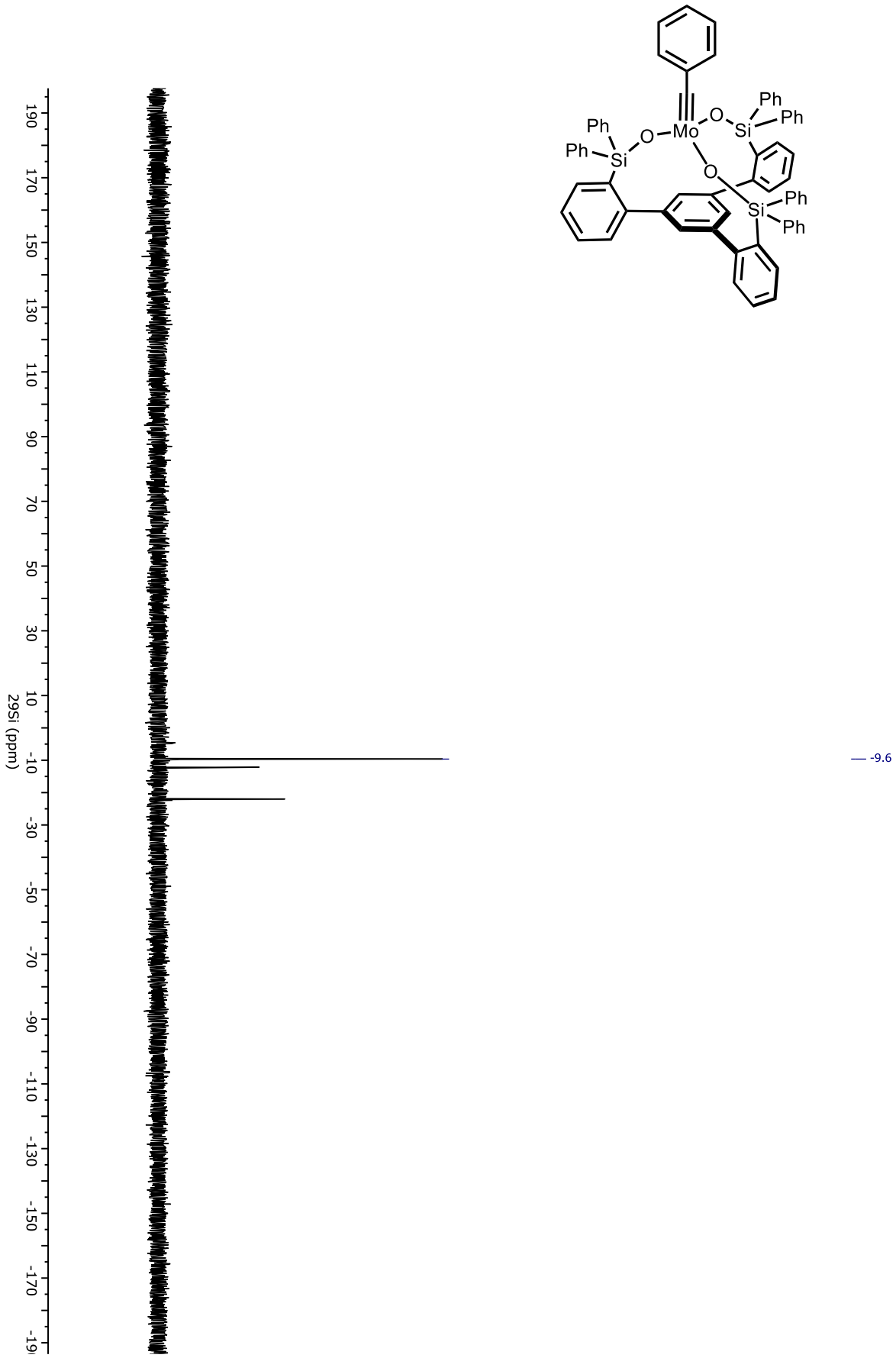

$^{95}$Mo NMR of Complex **110**, $C_6D_5CD_3$, 60 °C

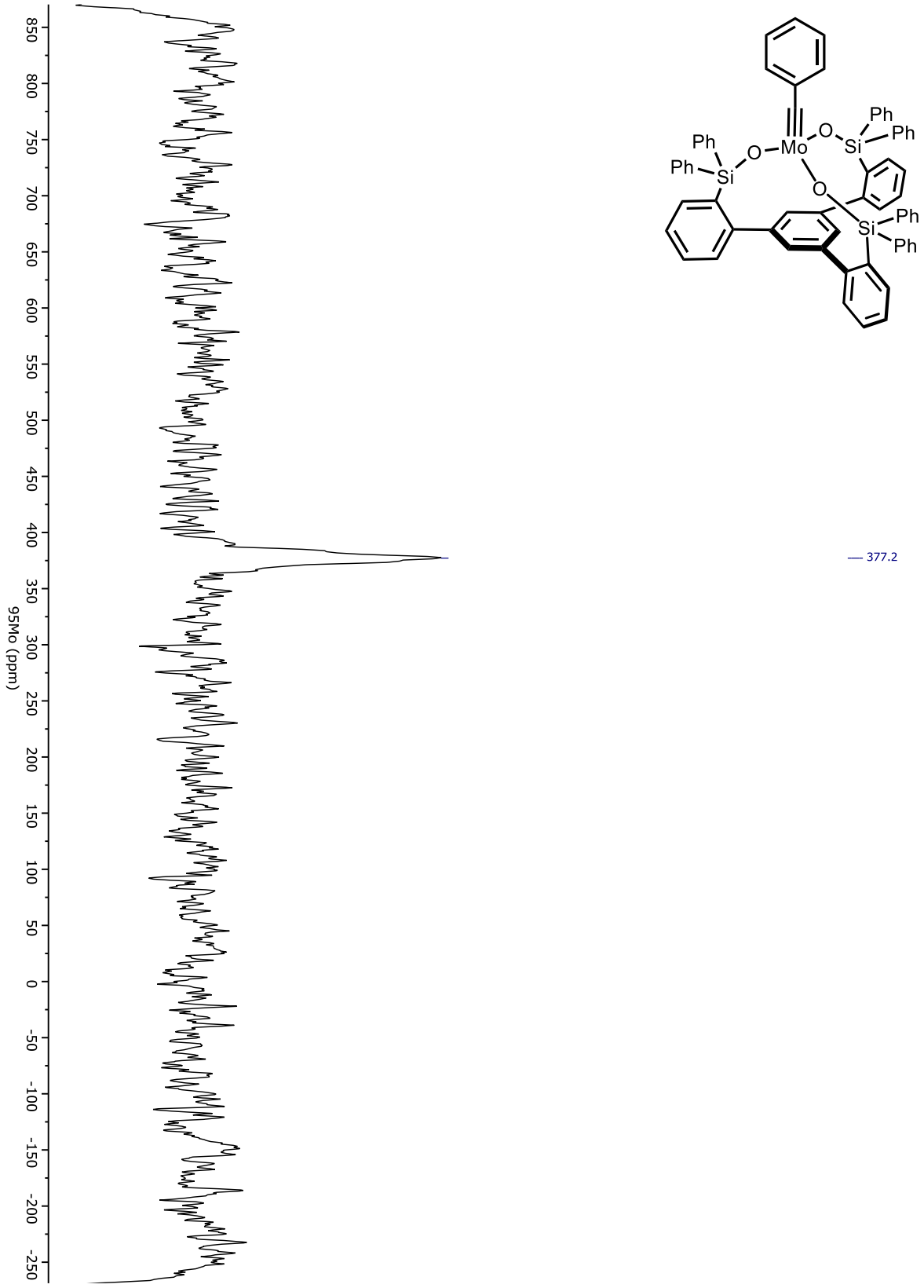

$^{1}$H NMR of Complex **134**, $C_6D_5CD_3$, 25 °C

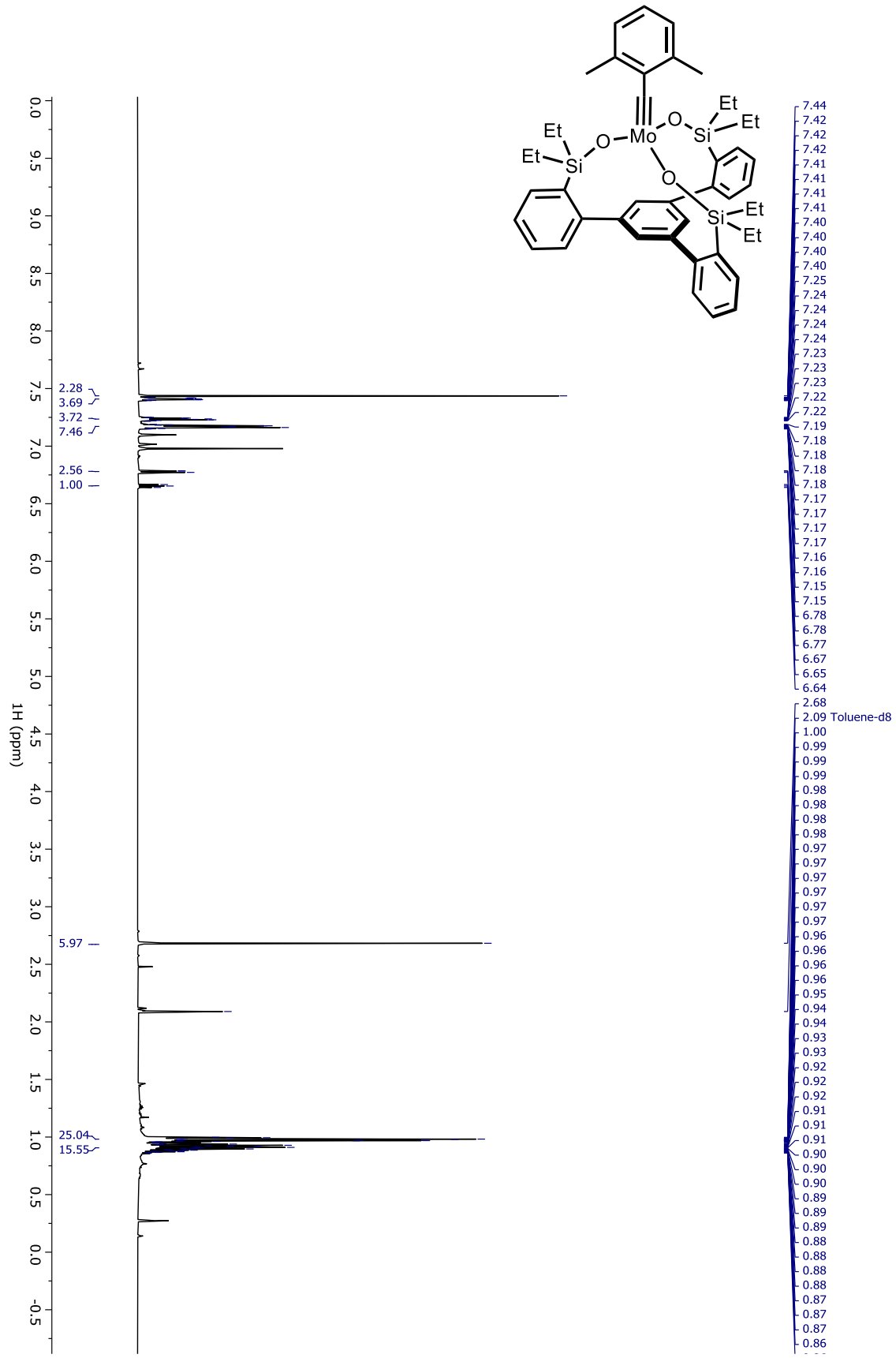

$^{13}C$ NMR of Complex **134**, $C_6D_5CD_3$, 25 °C

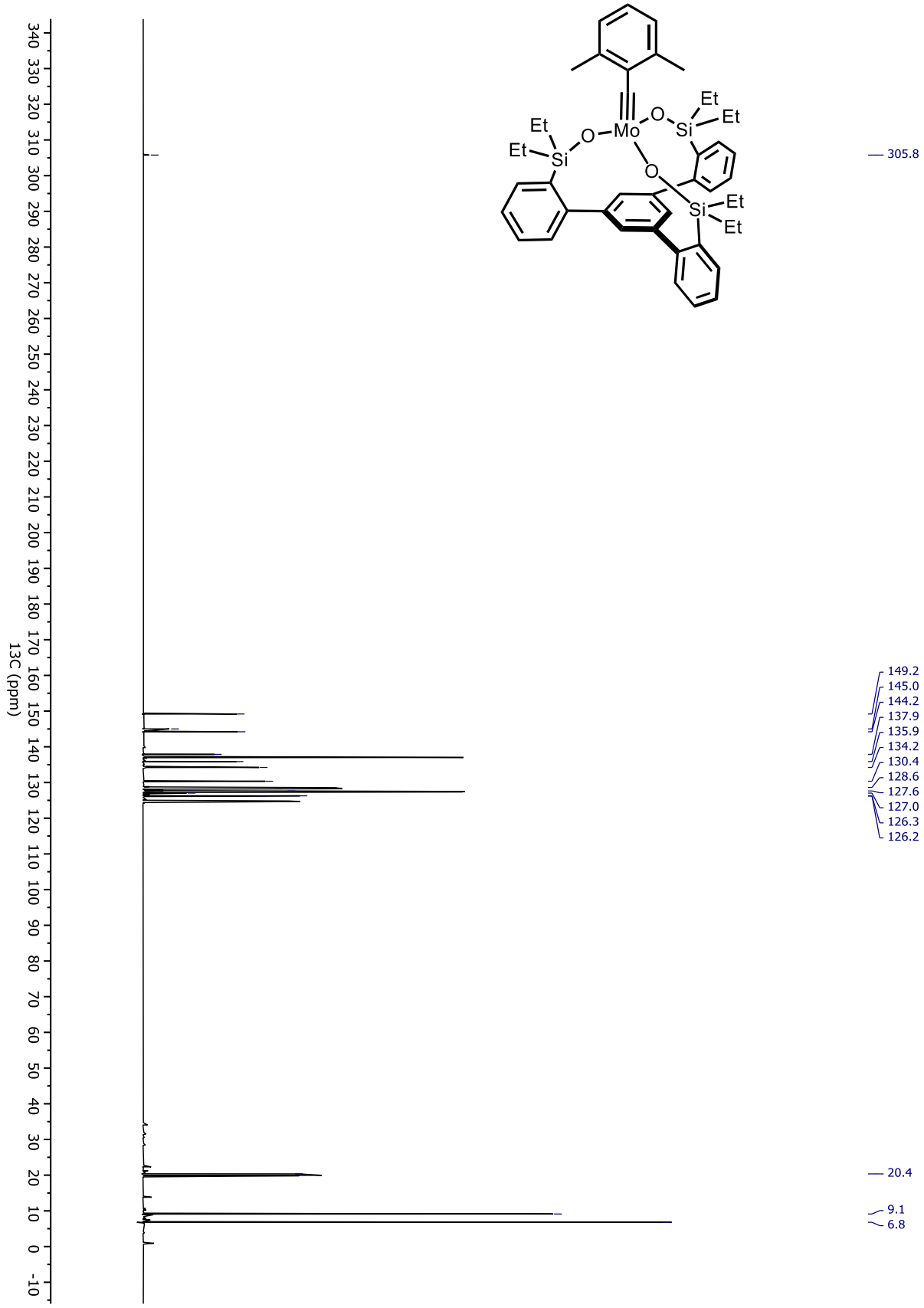

$^{29}$Si NMR of Complex **134**, $C_6D_5CD_3$, 25 °C

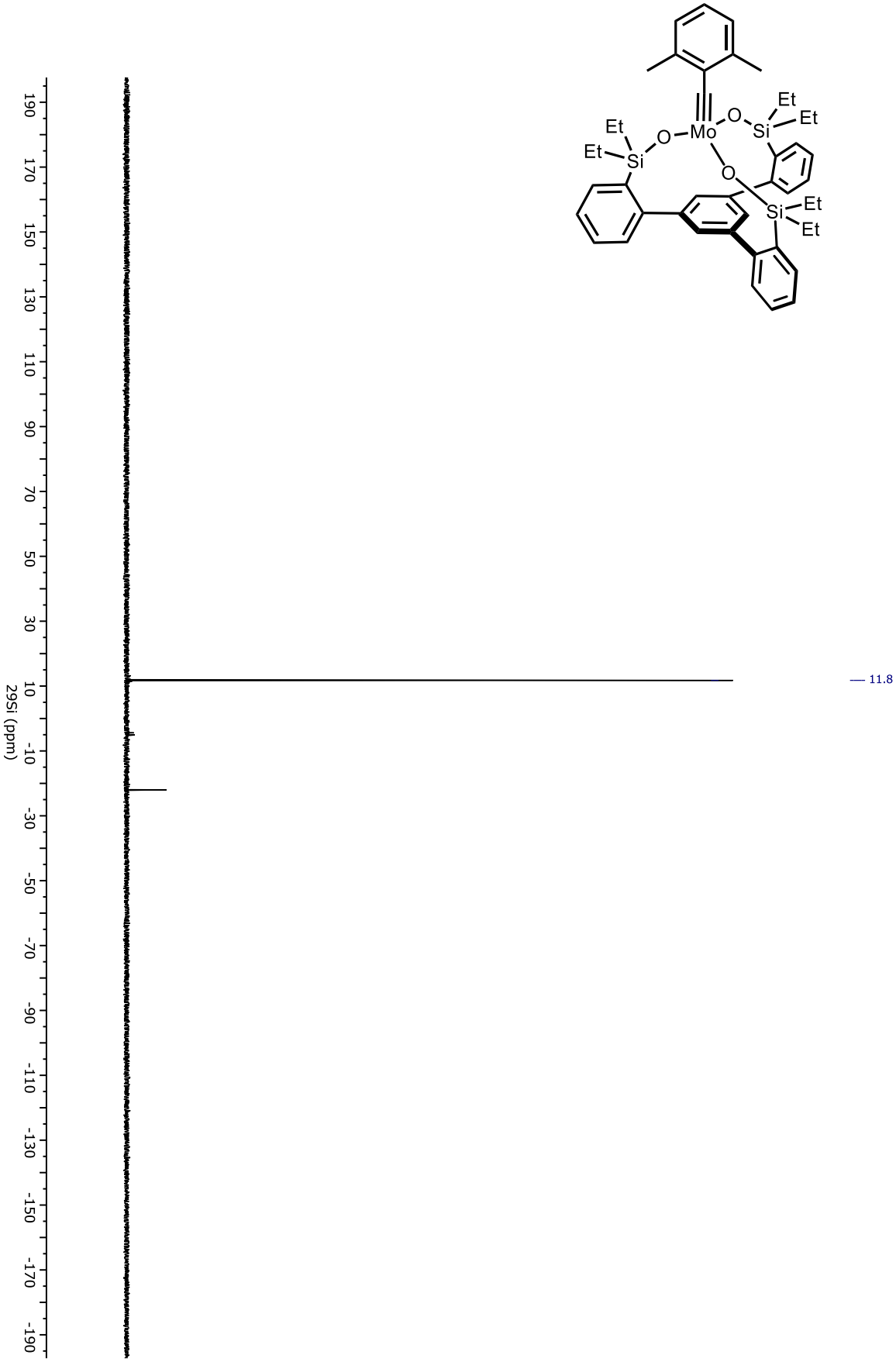

$^{95}$Mo NMR of Complex **134**, $C_6D_5CD_3$, 60 °C

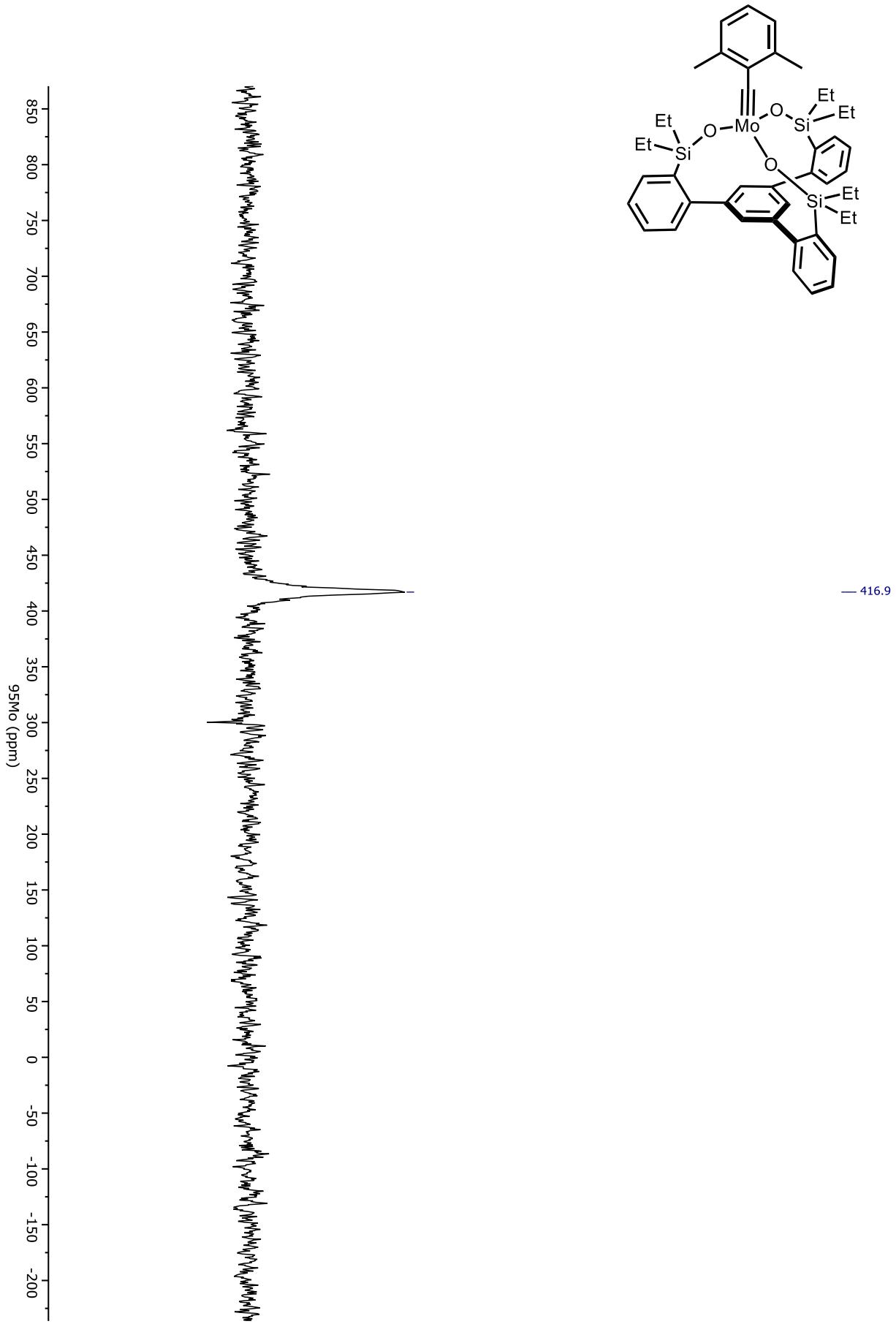

VT NMR Studies of Metallacyclobutadiene Complex **154**, $C_6D_5CD_3$, 25 °C to –40 °C

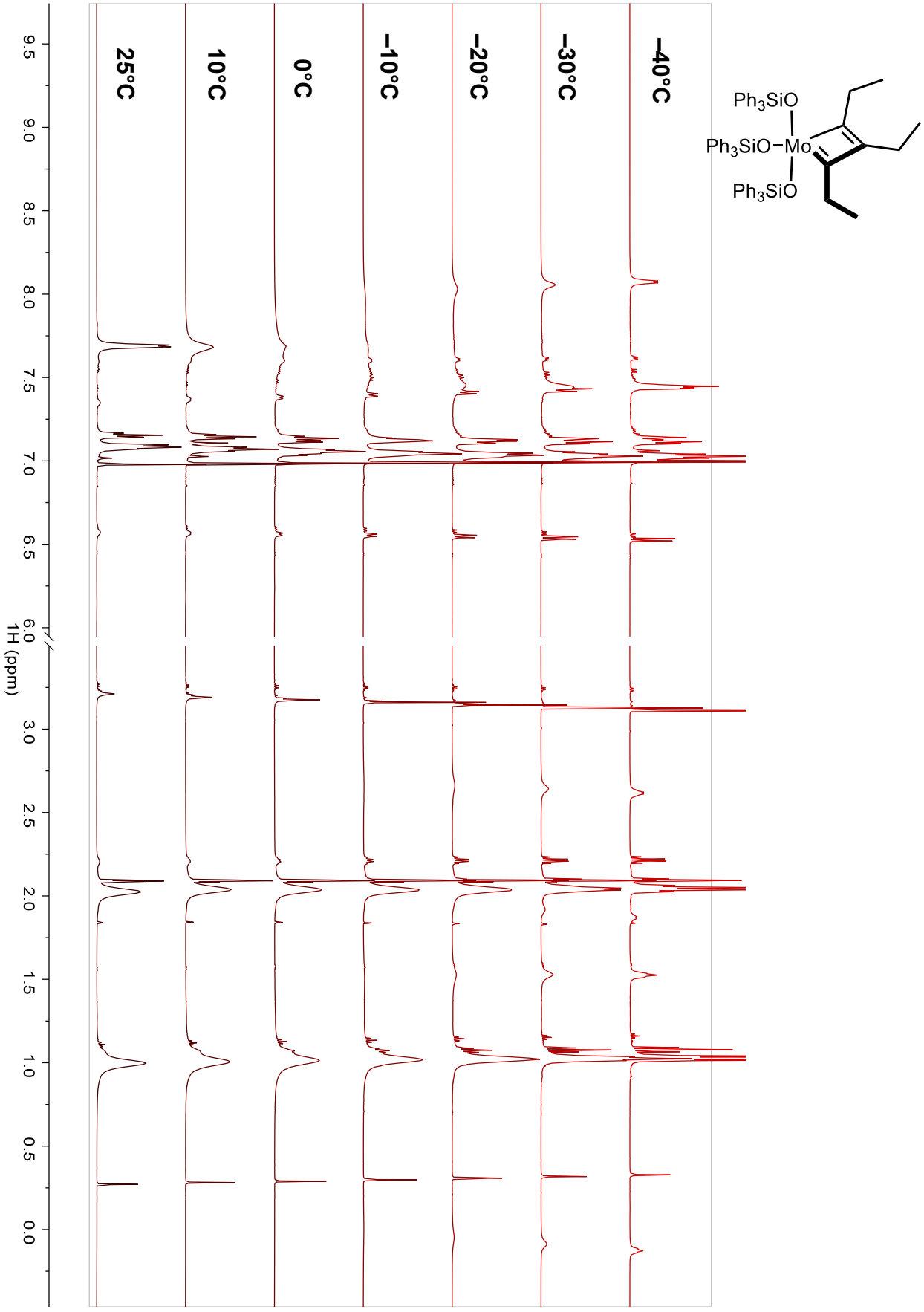

NMR assignment table of Metallacyclobutadiene Complex **154**, $C_6D_5CD_3$, –40 °C

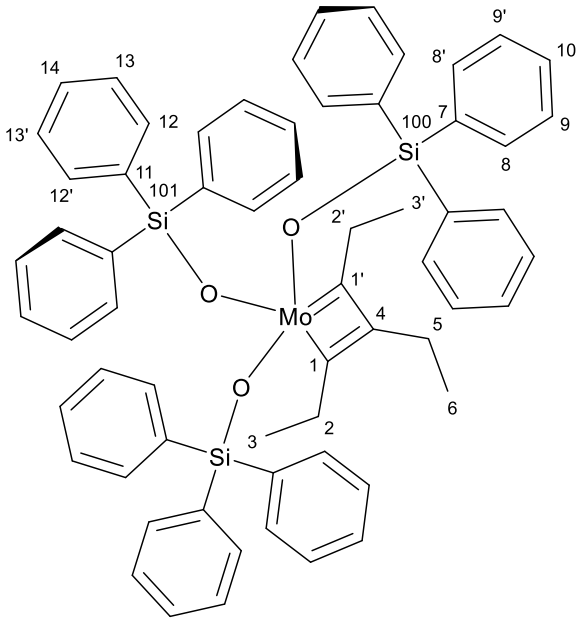


| Atom | δ (ppm) | COSY | HSQC | HMBC | Si-HMBC | Atom | δ (ppm) | COSY | HSQC | HMBC | Si-HMBC |
|---|---|---|---|---|---|---|---|---|---|---|---|
| **1 C** | 248.84 | | | 2, 3 | | **9 C** | 127.3 | | 9 | 9' | |
| **1' C** | 248.84 | | | 3' | | **H** | 7.02 | 8 | 9 | 7, 9' | 100 |
| **2 C** | 31.22 | | 2 | 3 | | **9' C** | 127.3 | | 9' | 9 | |
| **H2** | 2.61 | 3 | 2 | 1, 3, 4 | | **H** | 7.02 | 9' | 9' | 7, 9 | 100 |
| **2' C** | 31.22 | | 2' | 3' | | **10 C** | 128.59 | | 10 | 8, 8' | |
| **H2** | 2.61 | 3' | 2' | | | **H** | 7.11 | | 10 | 8, 8' | |
| **3 C** | 14.36 | | 3 | 2 | | **11 C** | 137.33 | | | 12, 13, 13' | |
| **H3** | 1.52 | 2 | 3 | 1, 2 | | **12 C** | 136.14 | | 12 | 14 | |
| **3' C** | 14.36 | | 3' | | | **H** | 8.07 | 13 | 12 | 11, 12', 14 | 101 |
| **H3** | 1.52 | 2' | 3' | 1', 2' | | **12' C** | 136.14 | | 12' | 12, 14 | |
| **4 C** | 144.79 | | | 2, 5, 6 | | **H** | 8.07 | 13' | 12' | | 101 |
| **5 C** | 25.96 | | 5 | 6 | | **13 C** | 127.3 | | 13 | 13' | |
| **H2** | 1.87 | 6 | 5 | 4, 6 | | **H** | 7.02 | 12 | 13 | 11, 13' | |
| **6 C** | 11.2 | | 6 | 5 | | **13' C** | 127.3 | | 13' | 13 | |
| **H3** | -0.13 | 5 | 6 | 4, 5 | | **H** | 7.02 | 12' | 13' | 11, 13 | |
| **7 C** | 138.51 | | | 8, 8', 9, 9' | | **14 C** | 129.36 | | 14 | 12 | |
| **8 C** | 135.43 | | 8 | 8', 10 | | **H** | 7.11 | | 14 | 12, 12' | |
| **H** | 7.44 | 9 | 8 | 7, 8', 10 | 100 | **100 Si** | -22.34 | | | | 8, 8', 9, 9' |
| **8' C** | 135.43 | | 8' | 8, 10 | | **101 Si** | -15.56 | | | | 12, 12' |
| **H** | 7.44 | | 8' | 7, 8, 10 | 100 | | | | | | |

$^1$H NMR Studies of Metallacyclobutadiene Complex **154**, $C_6D_5CD_3$, –40 °C

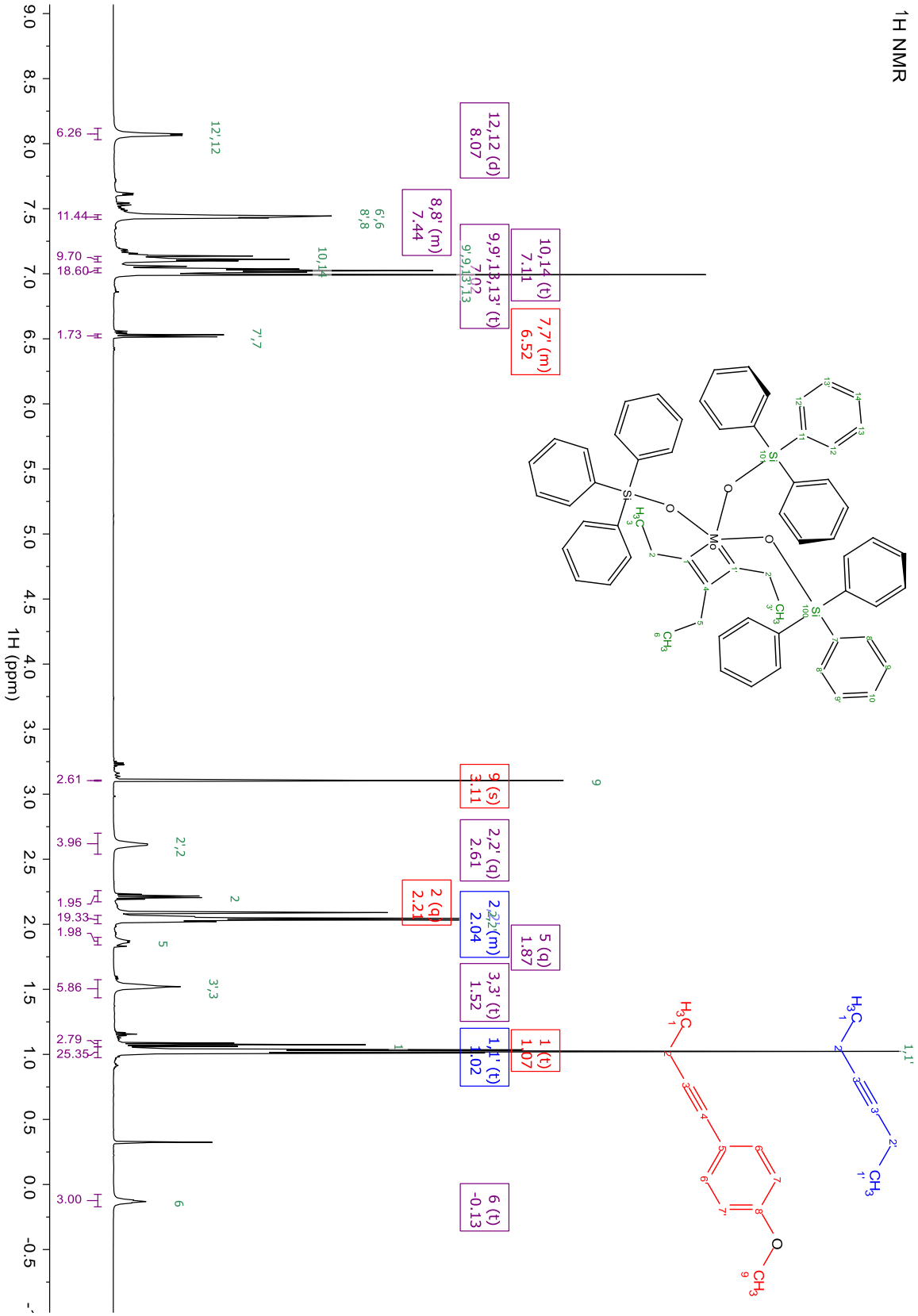

$^1$H CLIP COSY NMR Studies of Metallacyclobutadiene Complex **154**, $C_6D_5CD_3$, –40 °C

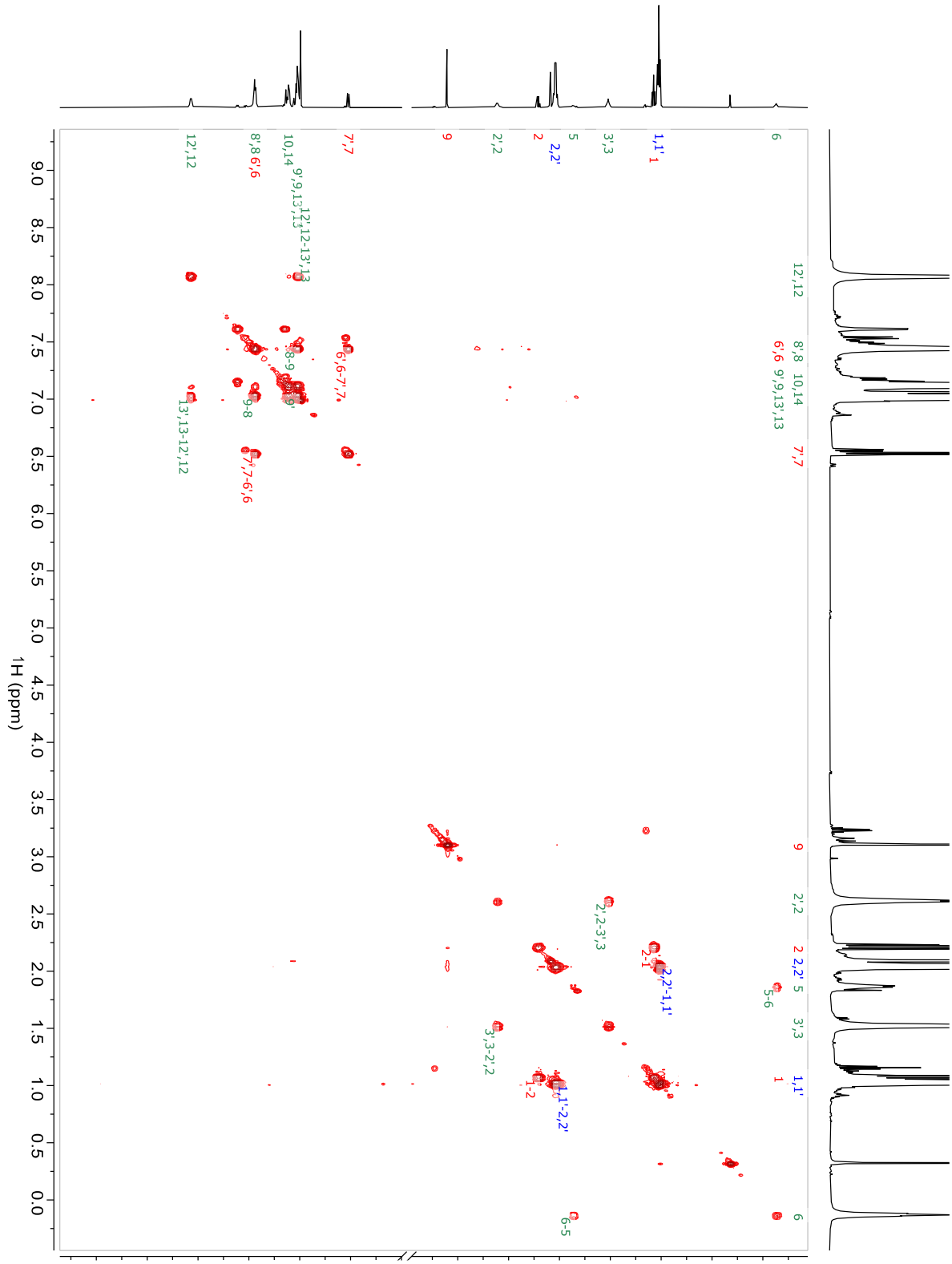

$^1$H EASY ROESY NMR Studies of Metallacyclobutadiene Complex **154**, $C_6D_5CD_3$, –40 °C

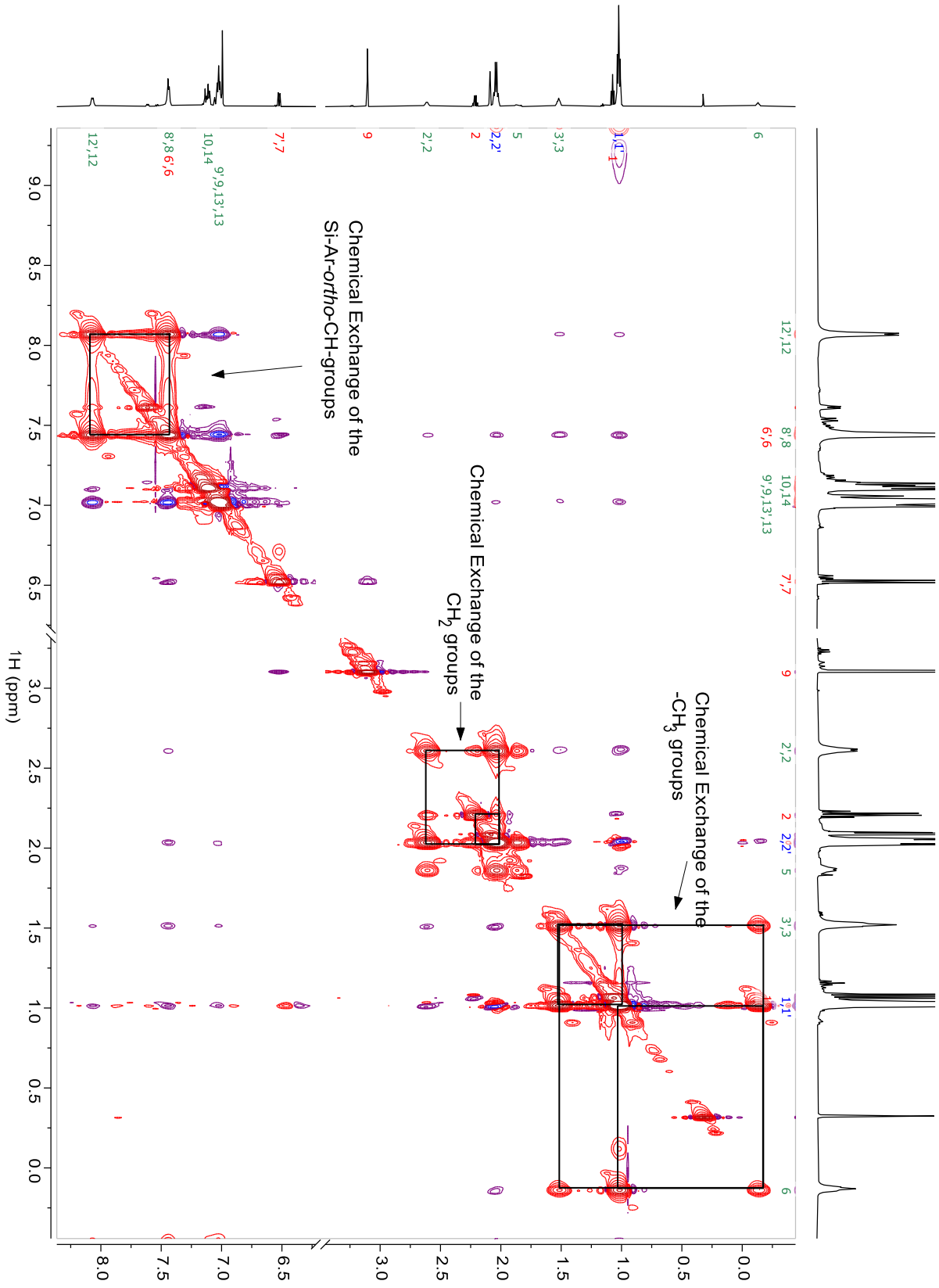

$^{13}$C NMR Studies of Metallacyclobutadiene Complex **154**, $C_6D_5CD_3$, –40 °C

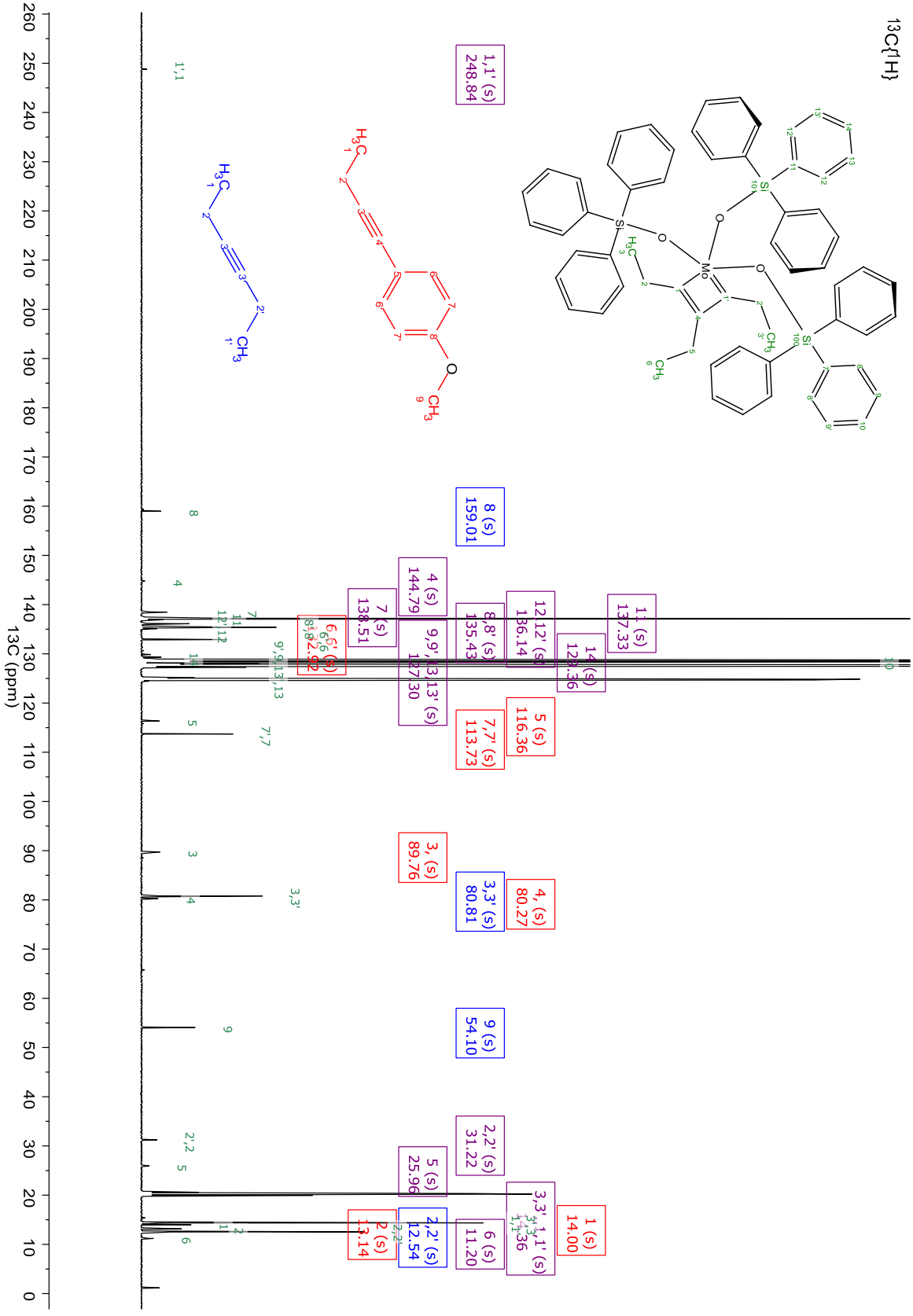

$^{1}$H-$^{13}$C edited HSQC NMR Studies of Metallacyclobutadiene Complex **154**, $C_6D_5CD_3$, –40 °C

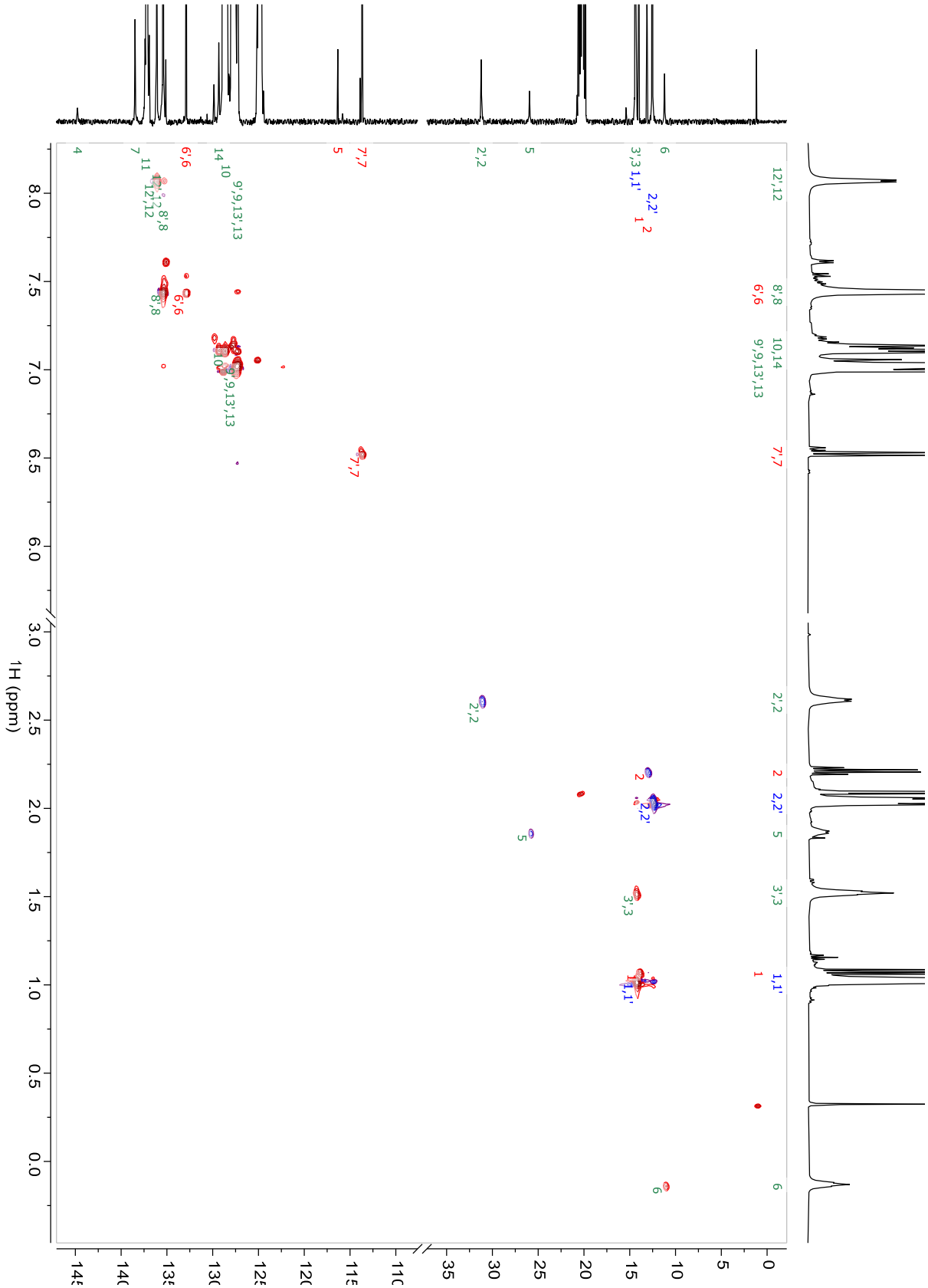

$^{1}$H-$^{13}$C HMBC NMR Studies of Metallacyclobutadiene Complex **154**, $C_6D_5CD_3$, –40 °C

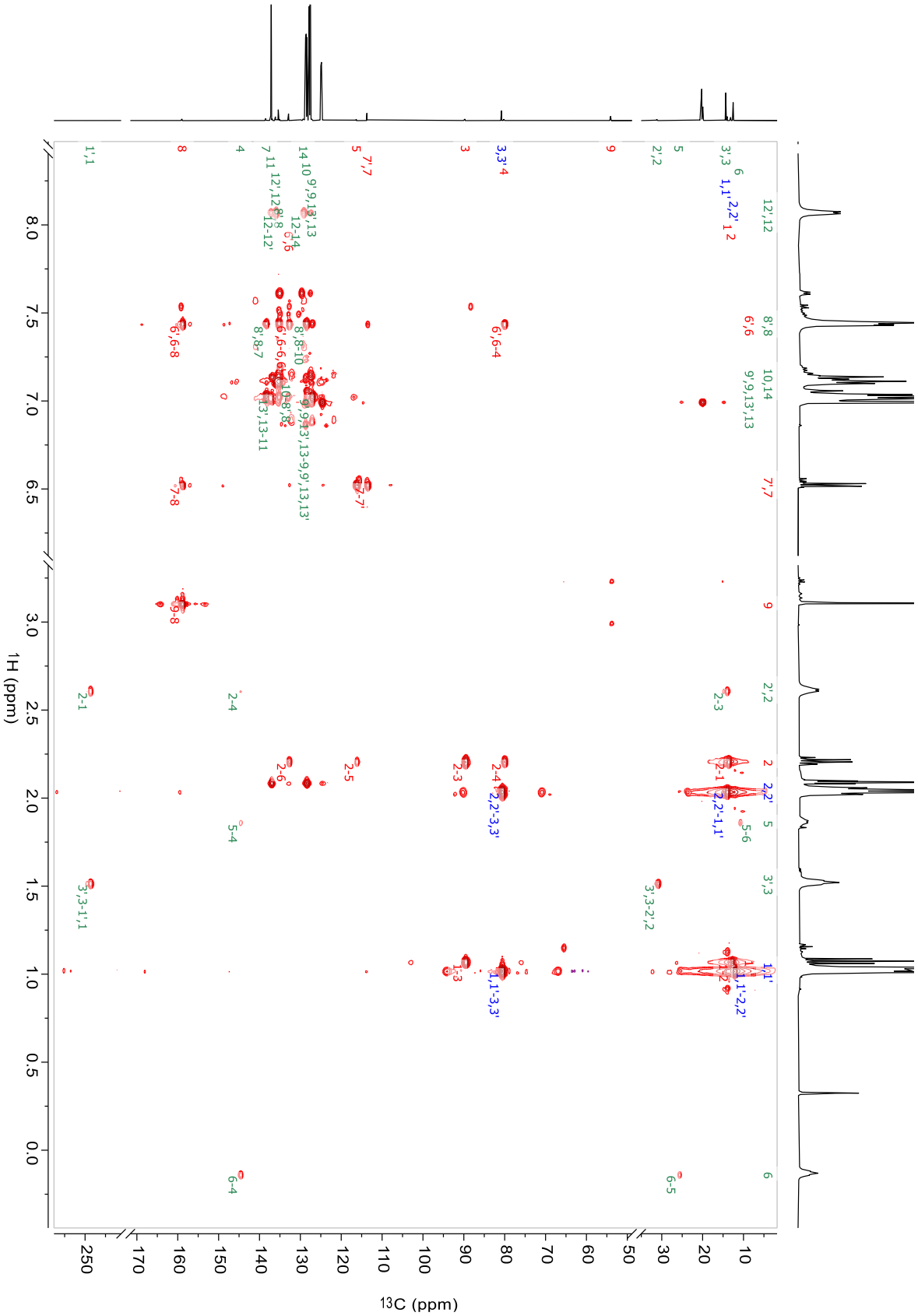

$^{29}$Si NMR Studies of Metallacyclobutadiene Complex **154**, $C_6D_5CD_3$, –40 °C

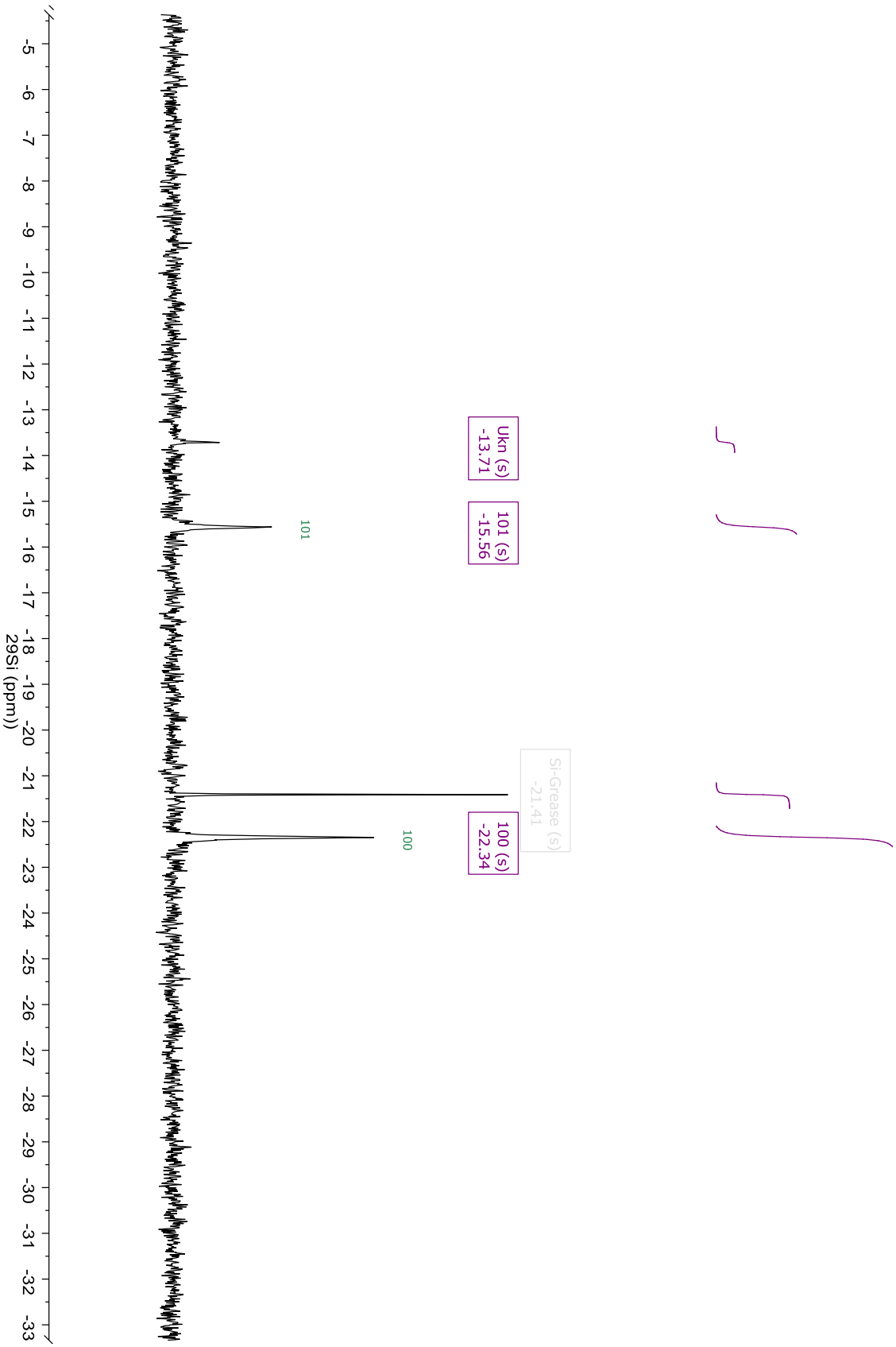

$^1$H NMR of Complex [**116**·py]$_4$ crystals, $C_6D_5CD_3$, 25 °C

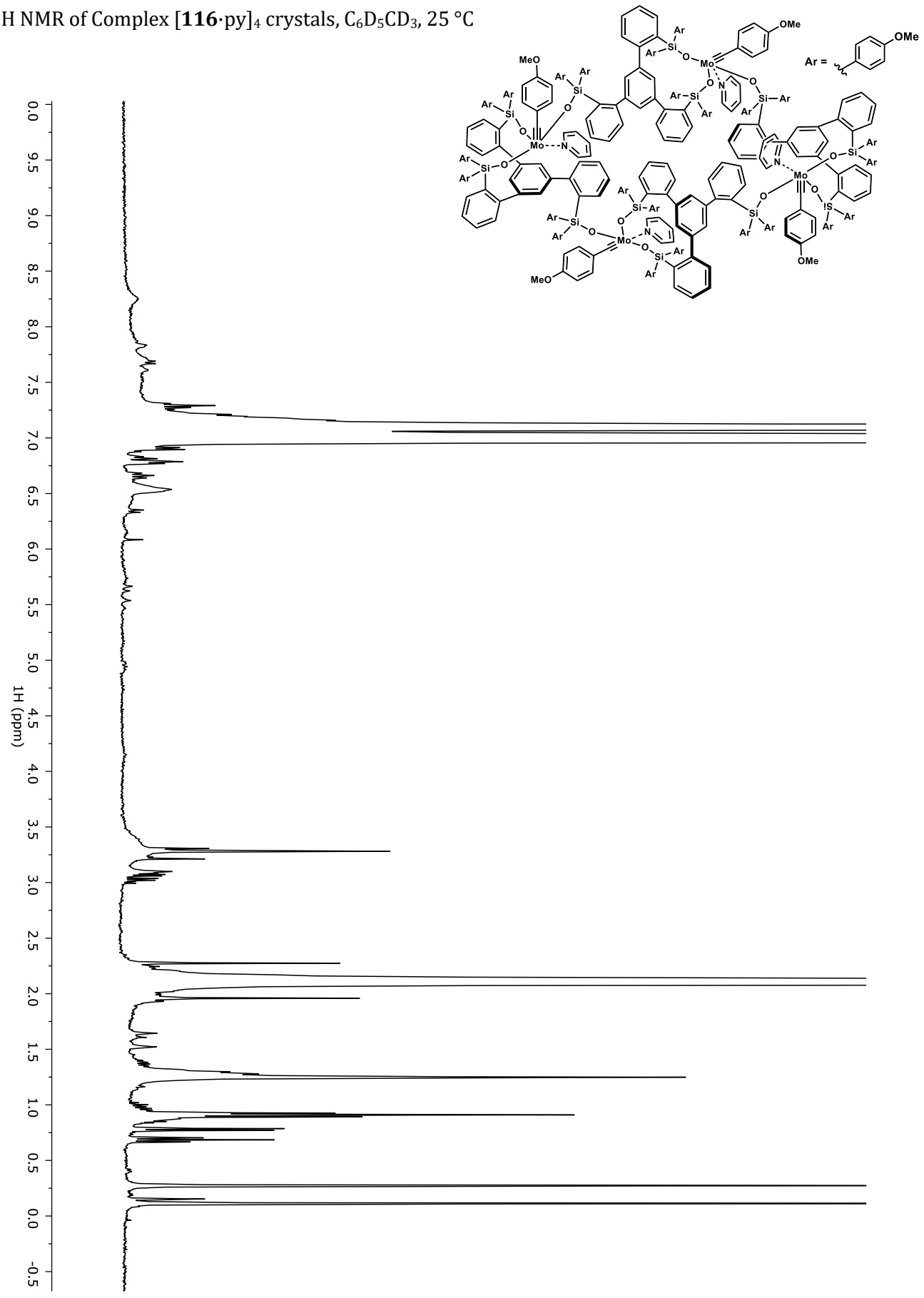

$^1$H EASY ROESY NMR Studies of Metallacyclobutadiene Complex **156** with 2-butyne, $C_6D_5CD_3$, .40°C

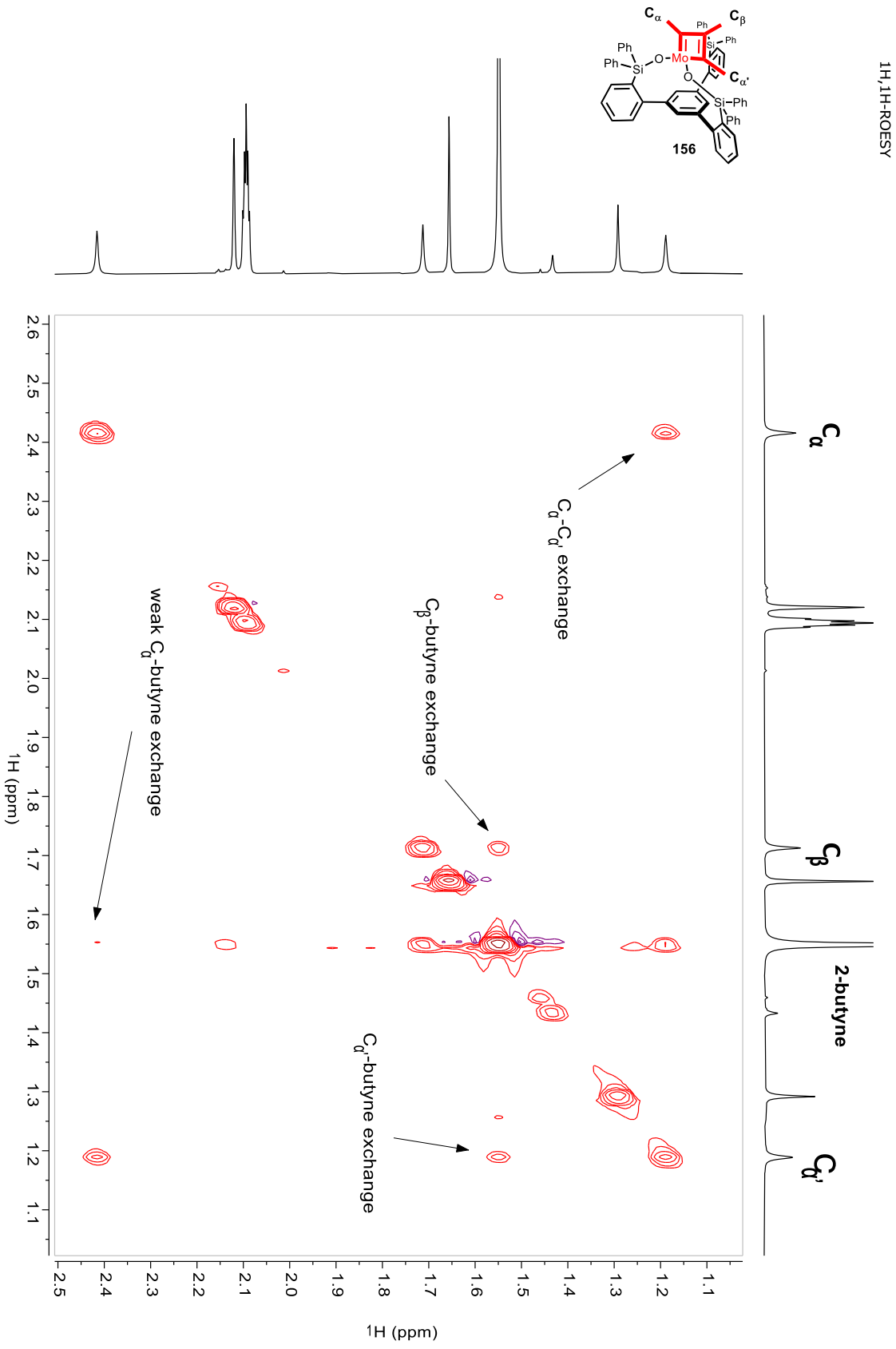

$^1$H NMR of Complex **223** and **218**, $CD_2Cl_2$, 25 °C

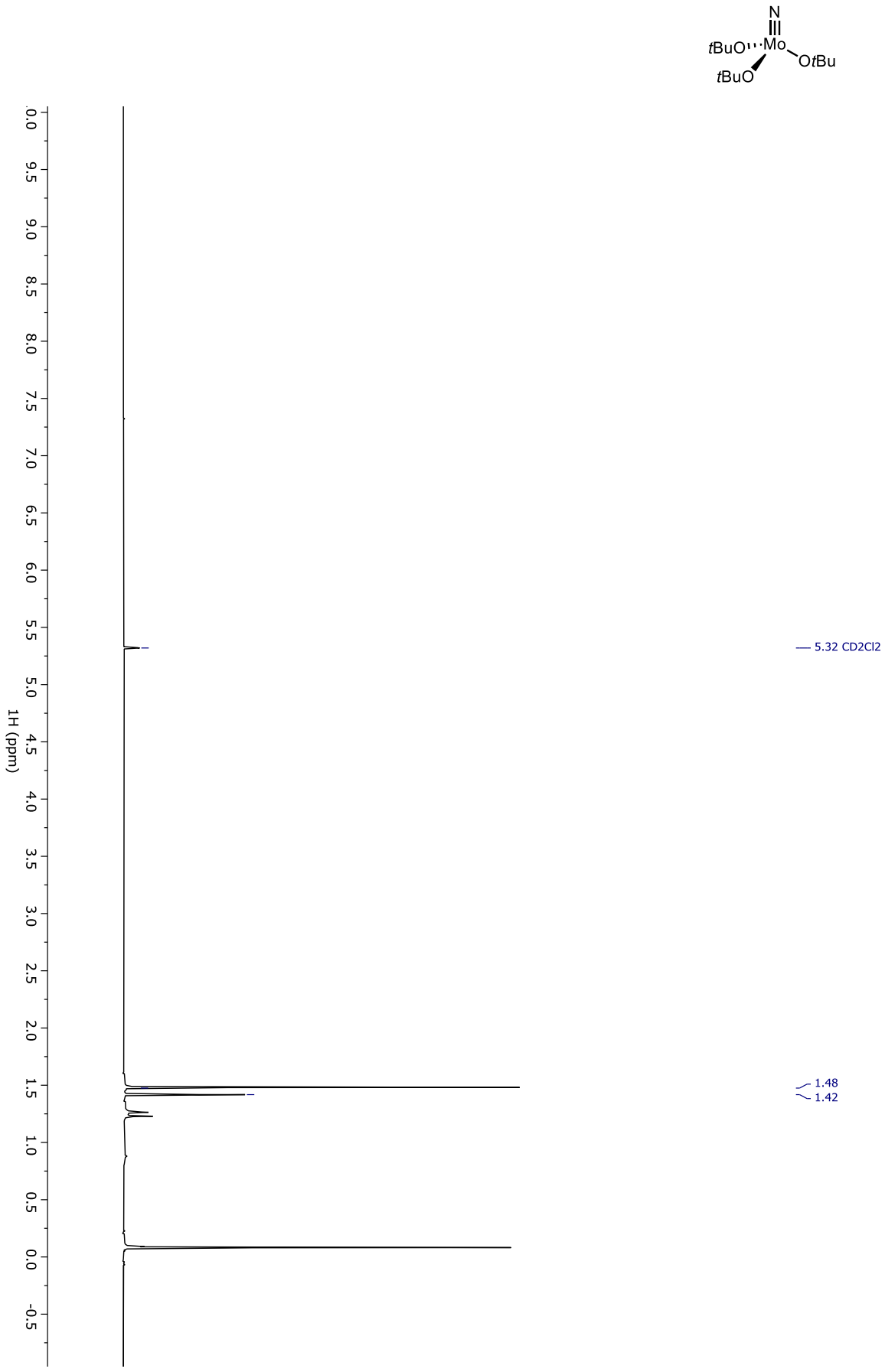

$^{13}C$ NMR of Complex **223** and **218**, $CD_2Cl_2$, 25 °C

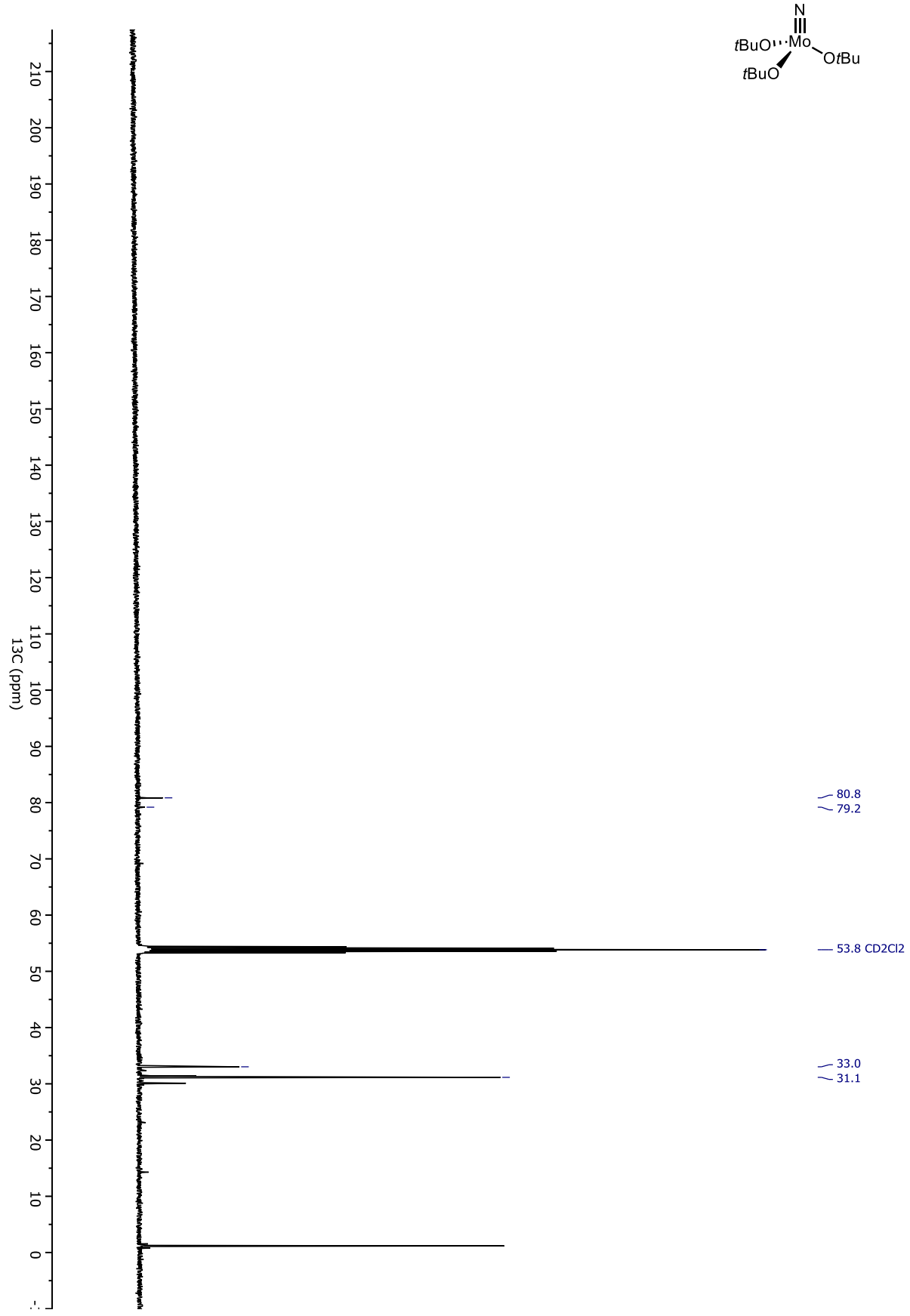

$^{95}$Mo NMR of Complex **223**, $CD_2Cl_2$, 25 °C

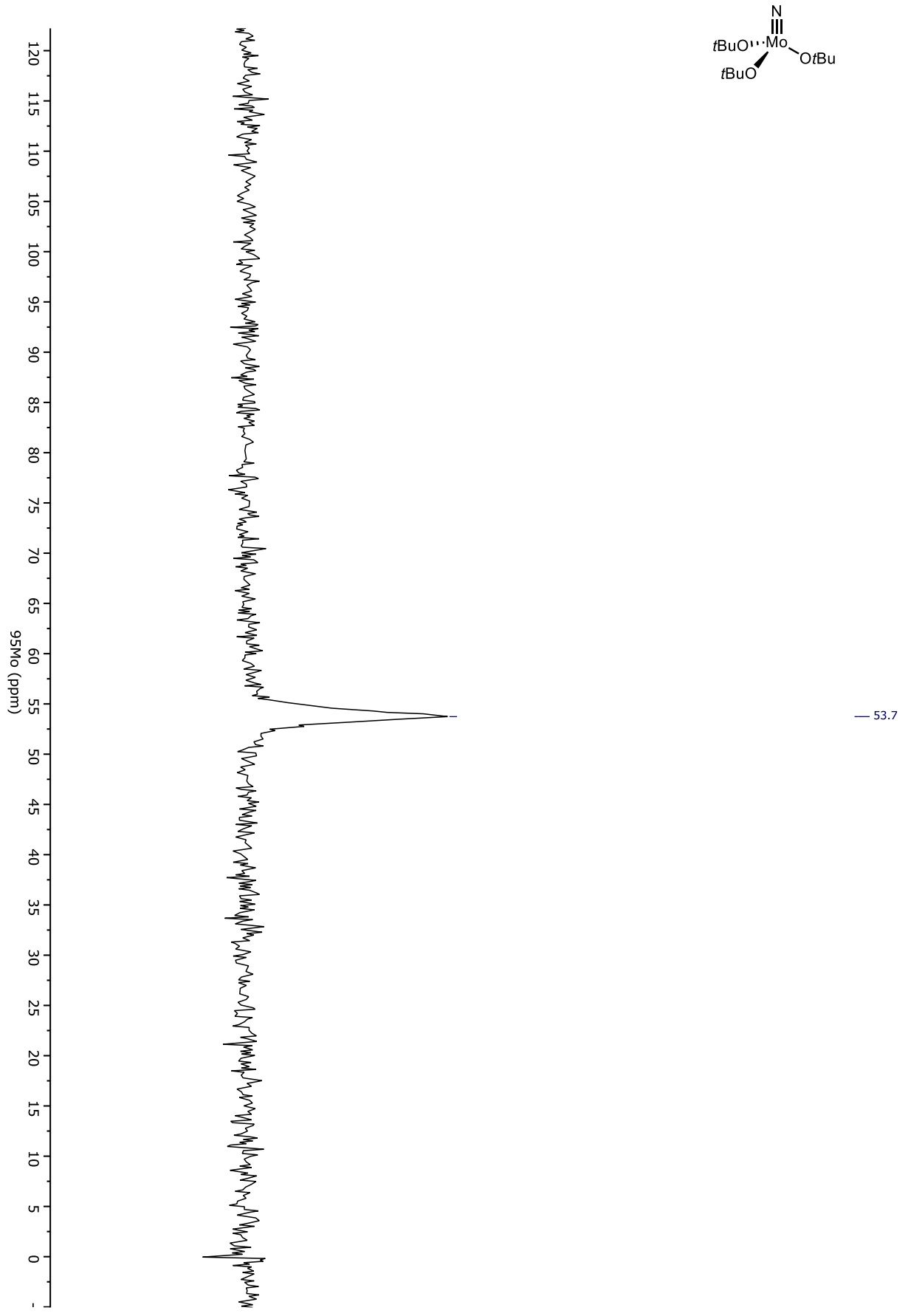

$^1$H NMR of Compound **262**, $CD_2Cl_2$, 25 °C

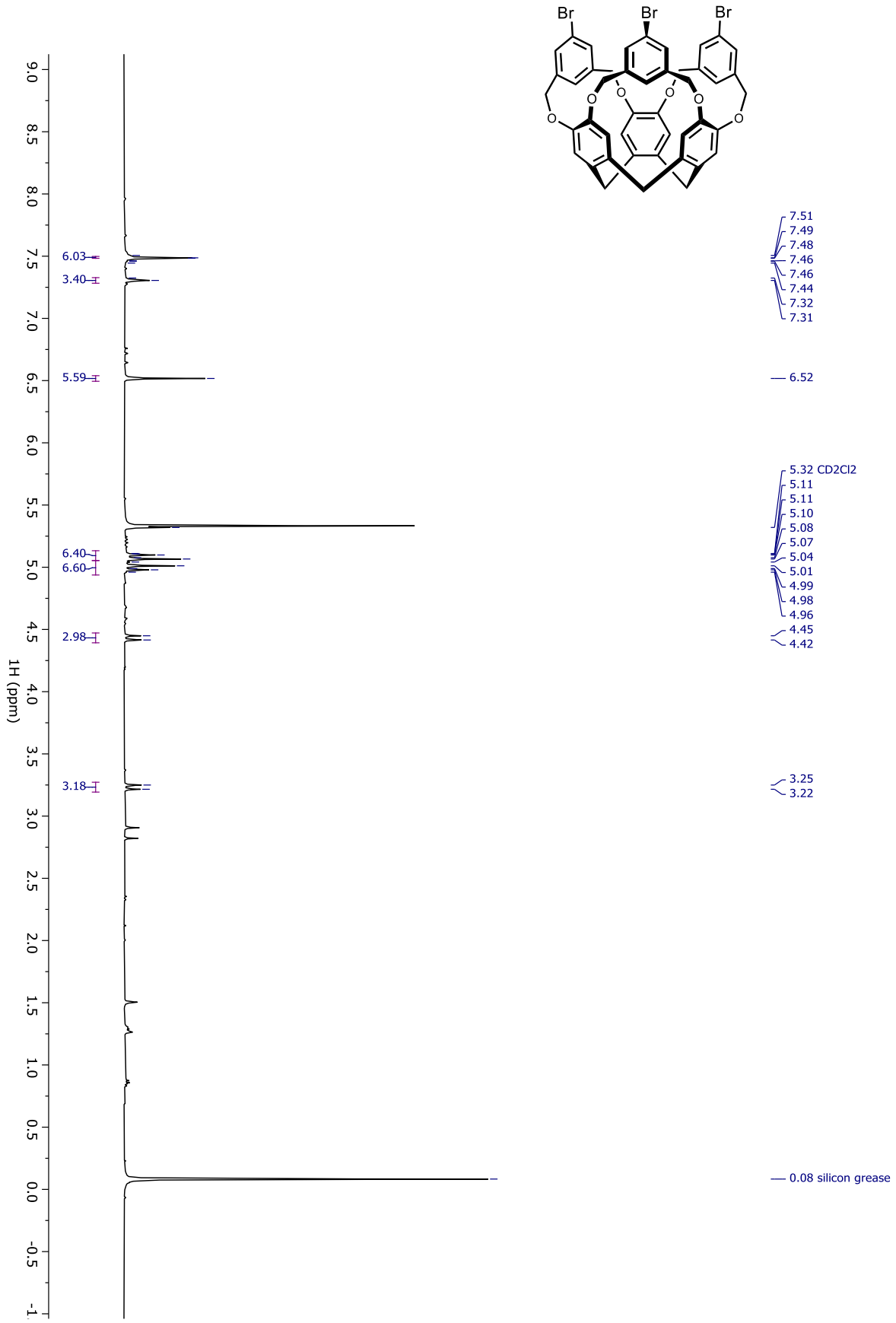

$^{13}C$ NMR of Compound **262**, $CD_2Cl_2$, 25 °C

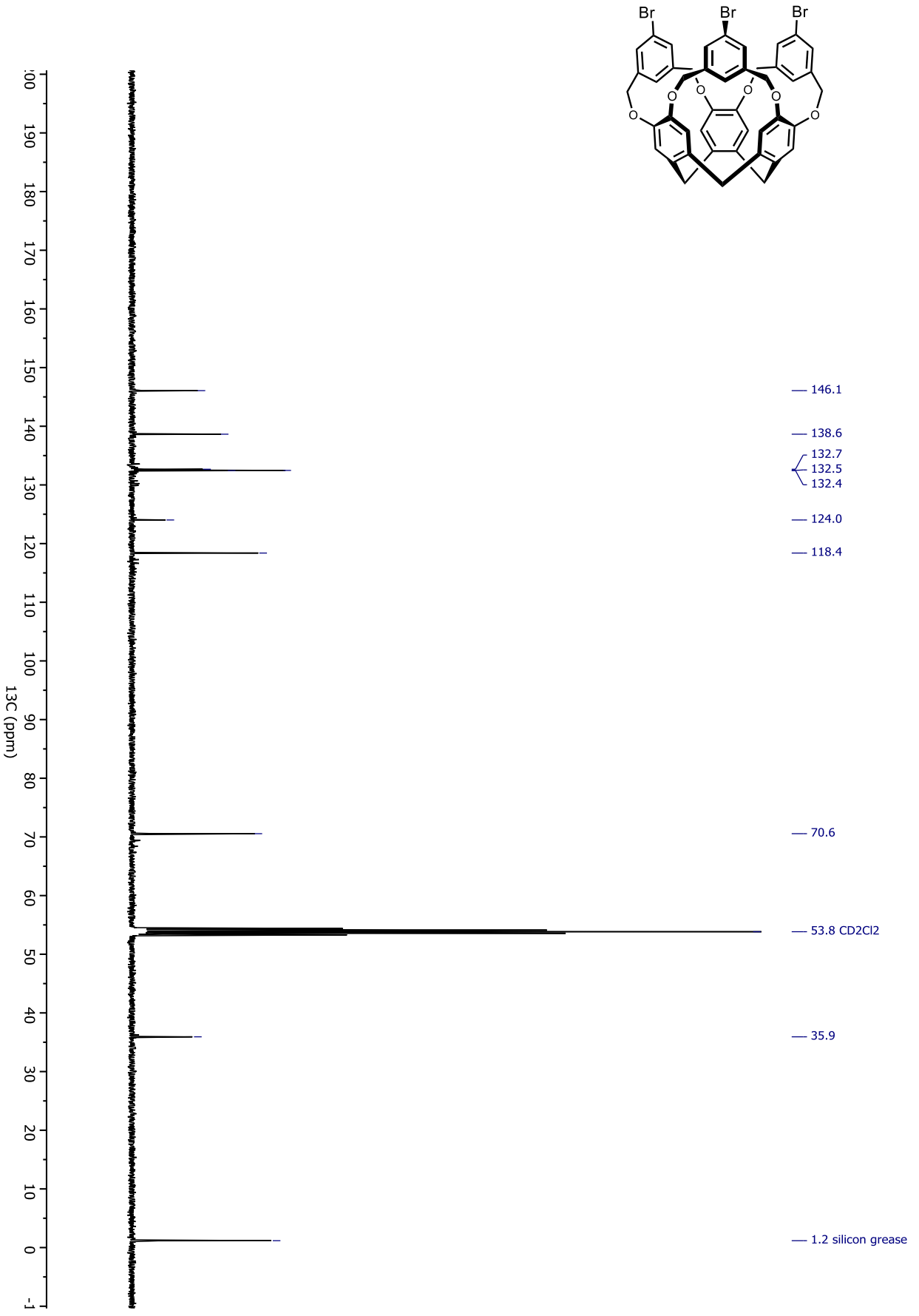

## 6.2 Crystallographic Data

### 6.2.1 Crystallographic Data of 103

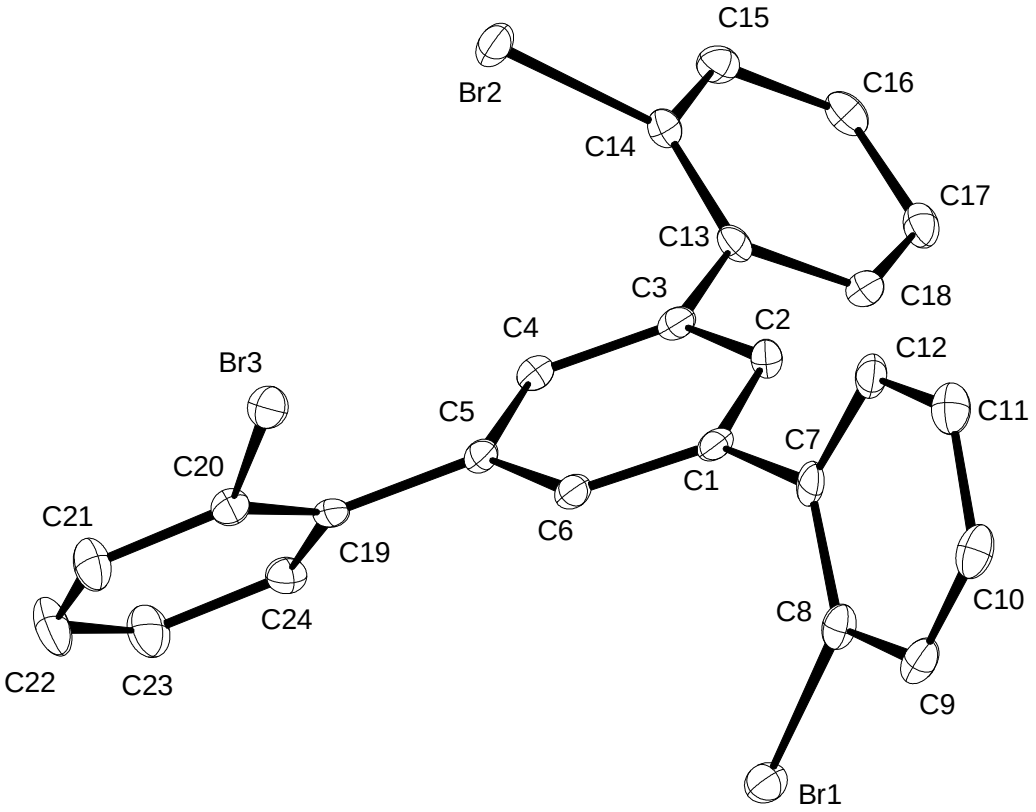


| | | |
|---|---|---|
| Identification code | 12633 | |
| Empirical formula | $C_{24}H_{15}Br_3$ | |
| Color | lightgreen | |
| Formula weight | 543.09 $g \cdot mol^{-1}$ | |
| Temperature | 100(2) K | |
| Wavelength | 1.54178 Å | |
| Crystal system | TRICLINIC | |
| Space group | $\mathbf{P\bar{1}}$, (**no. 2**) | |
| Unit cell dimensions | a = 9.9442(4) Å | α= 111.2510(10)°. |
| | b = 10.9266(4) Å | β= 99.0800(10)°. |
| | c = 11.1792(4) Å | γ = 112.6310(10)°. |

| | | |
|---|---|---|
| Volume | 980.54(6) $Å^3$ | |
| Z | 2 | |
| Density (calculated) | 1.839 $Mg \cdot m^{-3}$ | |
| Absorption coefficient | 7.663 $mm^{-1}$ | |
| F(000) | 528 e | |
| Crystal size | 0.208 x 0.174 x 0.100 $mm^3$ | |
| θ range for data collection | 4.522 to 63.667°. | |
| Index ranges | $-11 \leq h \leq 11, -12 \leq k \leq 12, -12 \leq l \leq 12$ | |
| Reflections collected | 18480 | |
| Independent reflections | 3076 [$R_{int}$ = 0.0392] | |
| Reflections with I>2σ(I) | 3053 | |
| Completeness to θ = 63.667° | 95.1 % | |
| Absorption correction | Gaussian | |
| Max. and min. transmission | 0.56 and 0.36 | |
| Refinement method | Full-matrix least-squares on $F^2$ | |
| Data / restraints / parameters | 3076 / 0 / 244 | |
| Goodness-of-fit on $F^2$ | 1.138 | |
| Final R indices [I>2σ(I)] | $R_1$ = 0.0232 | $wR^2$ = 0.0597 |
| R indices (all data) | $R_1$ = 0.0235 | $wR^2$ = 0.0598 |
| Largest diff. peak and hole | 0.4 and -0.5 $e \cdot Å^{-3}$ | |

### 6.2.2 Crystallographic Data of 104

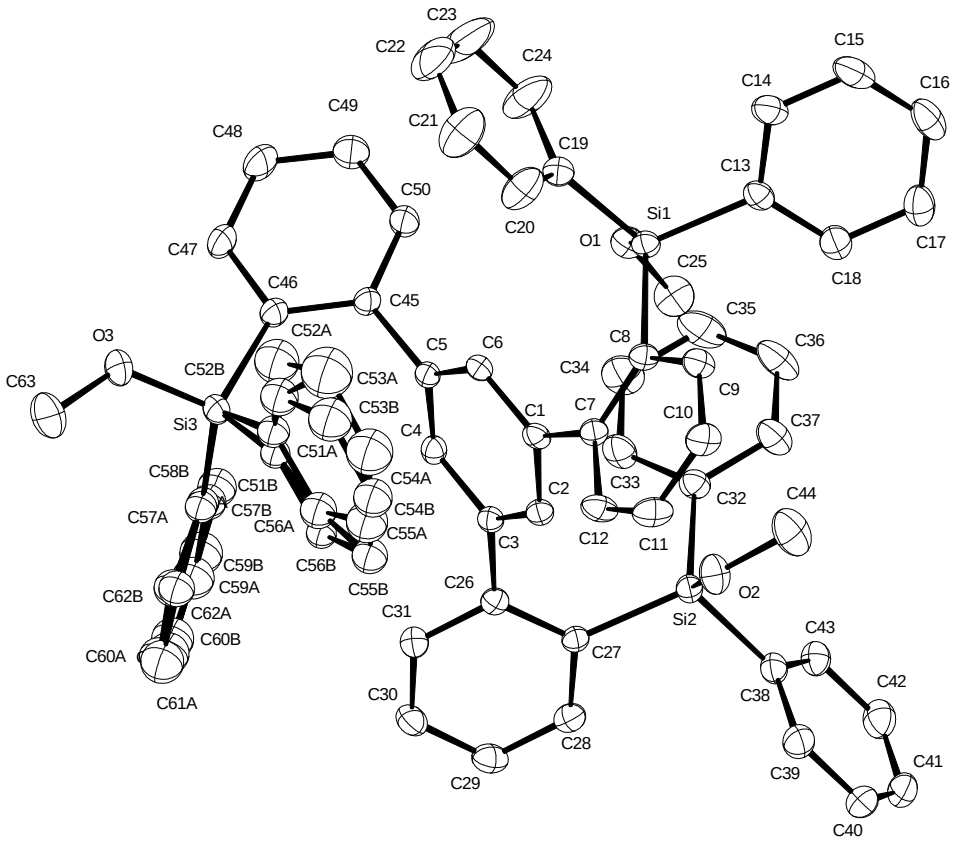


| | | |
|---|---|---|
| Identification code | 12284 | |
| Empirical formula | $C_{63}\,H_{54}\,O_3\,Si_3$ | |
| Color | colourless | |
| Formula weight | 943.33 $g \cdot mol^{-1}$ | |
| Temperature | 150(2) K | |
| Wavelength | 0.71073 Å | |
| Crystal system | TRICLINIC | |
| Space group | $\mathbf{P\bar{1}}$, (**no. 2**) | |
| Unit cell dimensions | a = 9.2600(5) Å | α= 82.152(3)°. |
| | b = 11.8325(7) Å | β= 80.757(2)°. |
| | c = 25.7130(14) Å | γ = 85.908(3)°. |
| Volume | 2751.2(3) $Å^3$ | |

| | | |
|---|---|---|
| Z | 2 | |
| Density (calculated) | 1.139 $Mg \cdot m^{-3}$ | |
| Absorption coefficient | 0.130 $mm^{-1}$ | |
| F(000) | 996 e | |
| Crystal size | 0.124 x 0.095 x 0.041 $mm^3$ | |
| θ range for data collection | 0.809 to 31.351°. | |
| Index ranges | $-13 \leq h \leq 13, -17 \leq k \leq 17, -36 \leq l \leq 37$ | |
| Reflections collected | 92135 | |
| Independent reflections | 17920 [$R_{int}$ = 0.0559] | |
| Reflections with I>2σ(I) | 12594 | |
| Completeness to θ = 25.242° | 99.7 % | |
| Absorption correction | Gaussian | |
| Max. and min. transmission | 1.00 and 0.99 | |
| Refinement method | Full-matrix least-squares on $F^2$ | |
| Data / restraints / parameters | 17920 / 0 / 613 | |
| Goodness-of-fit on $F^2$ | 1.081 | |
| Final R indices [I>2σ(I)] | $R_1$ = 0.0770 | $wR^2$ = 0.1941 |
| R indices (all data) | $R_1$ = 0.1085 | $wR^2$ = 0.2102 |
| Largest diff. peak and hole | 1.2 and -0.6 $e \cdot Å^{-3}$ | |

### 6.2.3 Crystallographic Data of 105

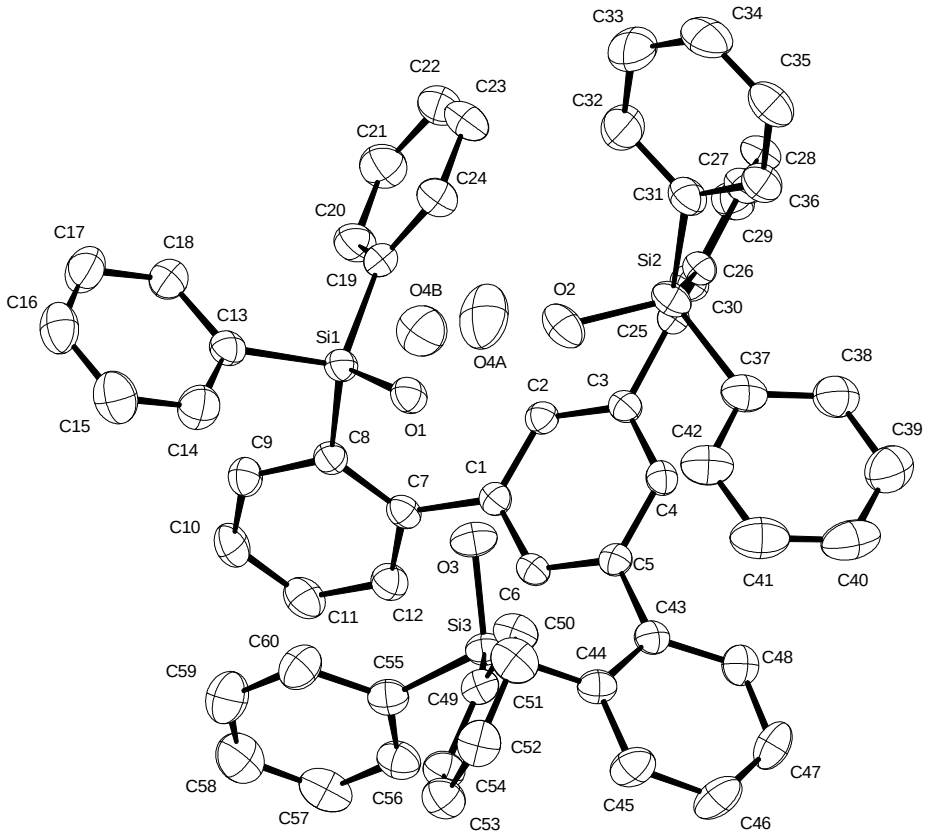


| | | |
|---|---|---|
| Identification code | 12303 | |
| Empirical formula | $C_{60}\,H_{50}\,O_4\,Si_3$ | |
| Color | colourless | |
| Formula weight | 919.27 g · mol$^{-1}$ | |
| Temperature | 150(2) K | |
| Wavelength | 1.54178 Å | |
| Crystal system | TRICLINIC | |
| **Space group** | **$P\bar{1}$, (no. 2)** | |
| Unit cell dimensions | a = 13.2599(5) Å | α= 95.490(2)°. |
| | b = 13.9312(5) Å | β= 100.576(2)°. |
| | c = 15.4657(5) Å | γ = 116.665(2)°. |

| | | |
|---|---|---|
| Volume | 2457.62(16) $Å^3$ | |
| Z | 2 | |
| Density (calculated) | 1.242 $Mg \cdot m^{-3}$ | |
| Absorption coefficient | 1.266 $mm^{-1}$ | |
| F(000) | 968 e | |
| Crystal size | 0.371 x 0.205 x 0.100 $mm^3$ | |
| θ range for data collection | 2.968 to 72.366°. | |
| Index ranges | $-16 \leq h \leq 15, -17 \leq k \leq 17, -18 \leq l \leq 19$ | |
| Reflections collected | 91024 | |
| Independent reflections | 9135 [$R_{int}$ = 0.0409] | |
| Reflections with I>2σ(I) | 7824 | |
| Completeness to θ = 67.679° | 95.2 % | |
| Absorption correction | Gaussian | |
| Max. and min. transmission | 0.91 and 0.78 | |
| Refinement method | Full-matrix least-squares on $F^2$ | |
| Data / restraints / parameters | 9135 / 0 / 623 | |
| Goodness-of-fit on $F^2$ | 1.092 | |
| Final R indices [I>2σ(I)] | $R_1$ = 0.0409 | $wR^2$ = 0.1009 |
| R indices (all data) | $R_1$ = 0.0501 | $wR^2$ = 0.1058 |
| Largest diff. peak and hole | 0.4 and -0.4 $e \cdot Å^{-3}$ | |

### 6.2.4 Crystallographic Data of 108·MeCN

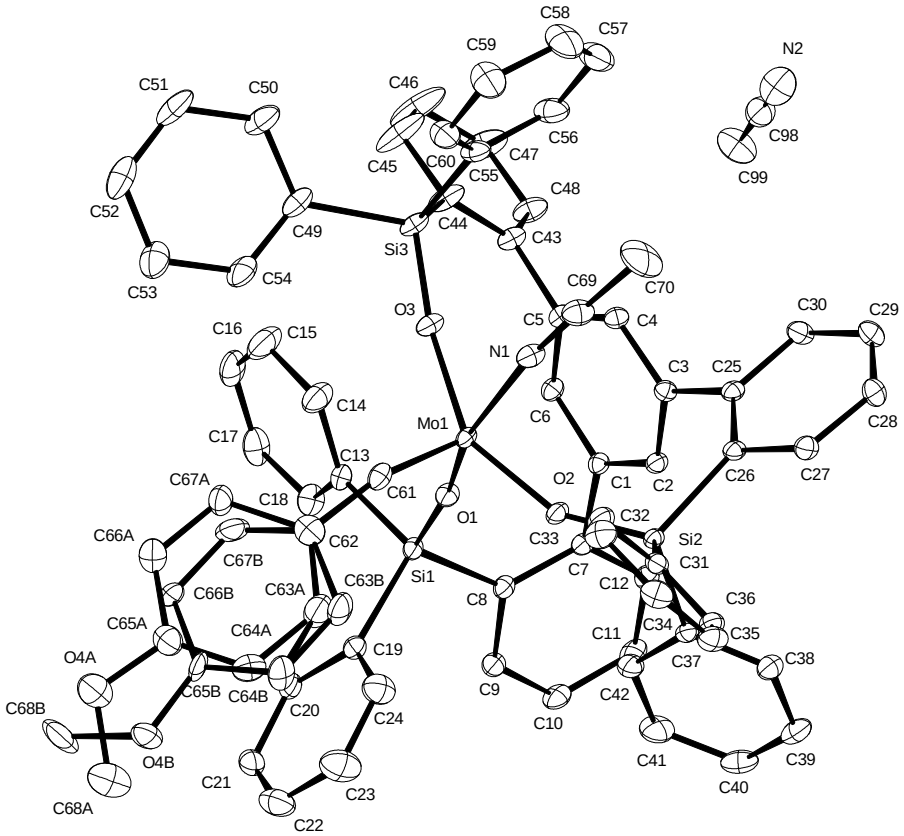


| | | |
|---|---|---|
| Identification code | 12438 | |
| Empirical formula | $C_{72}\,H_{58}\,Mo\,N_2\,O_4\,Si_3$ | |
| Color | blue | |
| Formula weight | 1195.41 g·mol$^{-1}$ | |
| Temperature | 100(2) K | |
| Wavelength | 0.71073 Å | |
| Crystal system | MONOCLINIC | |
| Space group | **$P2_1/c$, (no. 14)** | |
| Unit cell dimensions | a = 17.6003(8) Å | α= 90°. |
| | b = 13.1720(5) Å | β= 95.230(2)°. |
| | c = 25.0014(11) Å | γ = 90°. |

| | | |
|---|---|---|
| Volume | 5772.0(4) $Å^3$ | |
| Z | 4 | |
| Density (calculated) | 1.376 $Mg \cdot m^{-3}$ | |
| Absorption coefficient | 0.344 $mm^{-1}$ | |
| F(000) | 2480 e | |
| Crystal size | 0.130 x 0.049 x 0.031 $mm^3$ | |
| θ range for data collection | 1.162 to 33.381°. | |
| Index ranges | $-27 \leq h \leq 27, -20 \leq k \leq 20, -38 \leq l \leq 38$ | |
| Reflections collected | 227517 | |
| Independent reflections | 22353 [$R_{int}$ = 0.0885] | |
| Reflections with I>2σ(I) | 15858 | |
| Completeness to θ = 25.242° | 99.9 % | |
| Absorption correction | Gaussian | |
| Max. and min. transmission | 0.99 and 0.97 | |
| Refinement method | Full-matrix least-squares on $F^2$ | |
| Data / restraints / parameters | 22353 / 0 / 806 | |
| Goodness-of-fit on $F^2$ | 1.034 | |
| Final R indices [I>2σ(I)] | $R_1$ = 0.0451 | $wR^2$ = 0.0948 |
| R indices (all data) | $R_1$ = 0.0808 | $wR^2$ = 0.1086 |
| Largest diff. peak and hole | 1.2 and -1.1 $e \cdot Å^{-3}$ | |

### 6.2.5 Crystallographic Data of 112

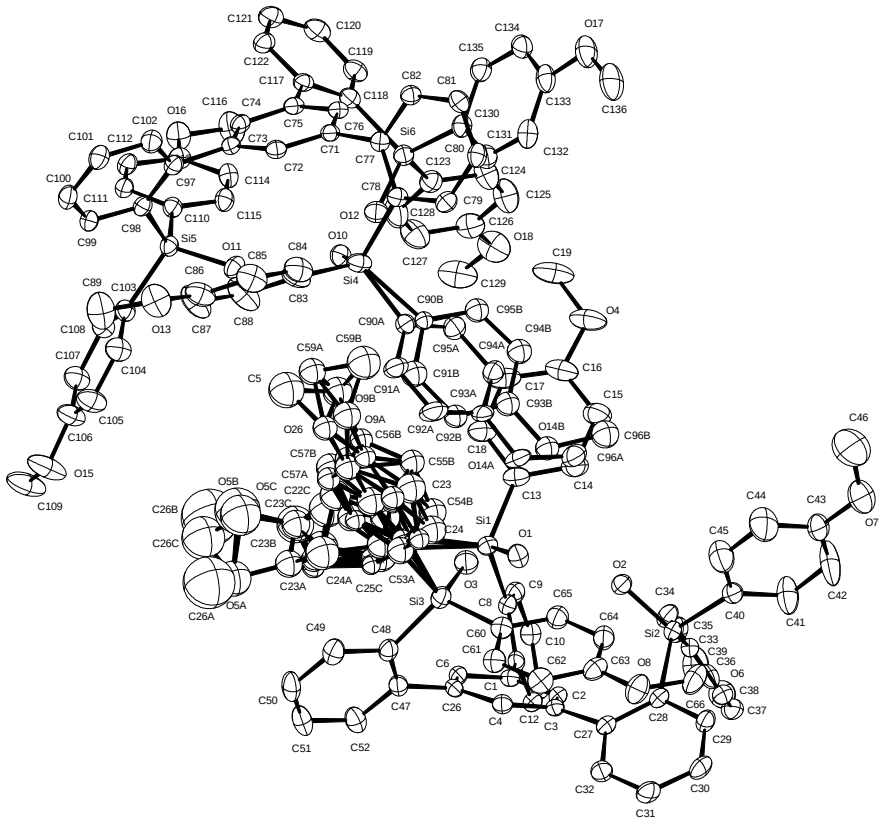

| | | |
|---|---|---|
| Identification code | 12687 | |
| Empirical formula | $C_{66}H_{60}O_9Si_3$ | |
| Color | colourless | |
| Formula weight | 1081.41 g · mol$^{-1}$ | |
| Temperature | 100(2) K | |
| Wavelength | 0.71073 Å | |
| Crystal system | TRICLINIC | |
| Space group | $\mathbf{P\bar{1}}$, (**no. 2**) | |
| Unit cell dimensions | a = 14.3600(8) Å | α= 64.756(8)°. |
| | b = 20.7942(18) Å | β= 77.870(5)°. |
| | c = 23.1783(16) Å | γ = 78.137(7)°. |
| Volume | 6067.6(9) Å$^3$ | |

| | | |
|---|---|---|
| Z | 4 | |
| Density (calculated) | 1.184 Mg · $m^{-3}$ | |
| Absorption coefficient | 0.133 $mm^{-1}$ | |
| F(000) | 2280 e | |
| Crystal size | 0.21 x 0.20 x 0.10 $mm^3$ | |
| Θ range for data collection | 2.605 to 27.500°. | |
| Index ranges | $-18 \leq h \leq 18, -26 \leq k \leq 27, -30 \leq l \leq 30$ | |
| Reflections collected | 76645 | |
| Independent reflections | 27319 [$R_{int}$ = 0.0470] | |
| Reflections with I>2σ(I) | 18846 | |
| Completeness to Θ = 25.242° | 98.6 % | |
| Absorption correction | Gaussian | |
| Max. and min. transmission | 0.99 and 0.98 | |
| Refinement method | Full-matrix least-squares on $F^2$ | |
| Data / restraints / parameters | 27319 / 6 / 1448 | |
| Goodness-of-fit on $F^2$ | 1.030 | |
| Final R indices [I>2σ(I)] | $R_1$ = 0.0668 | $wR^2$ = 0.1639 |
| R indices (all data) | $R_1$ = 0.1035 | $wR^2$ = 0.1933 |
| Remarks | **SQUEEZE was applied!** | |
| Largest diff. peak and hole | 1.7 and -0.6 e · $Å^{-3}$ | |

### 6.2.6 Crystallographic Data of [116·py]$_4$

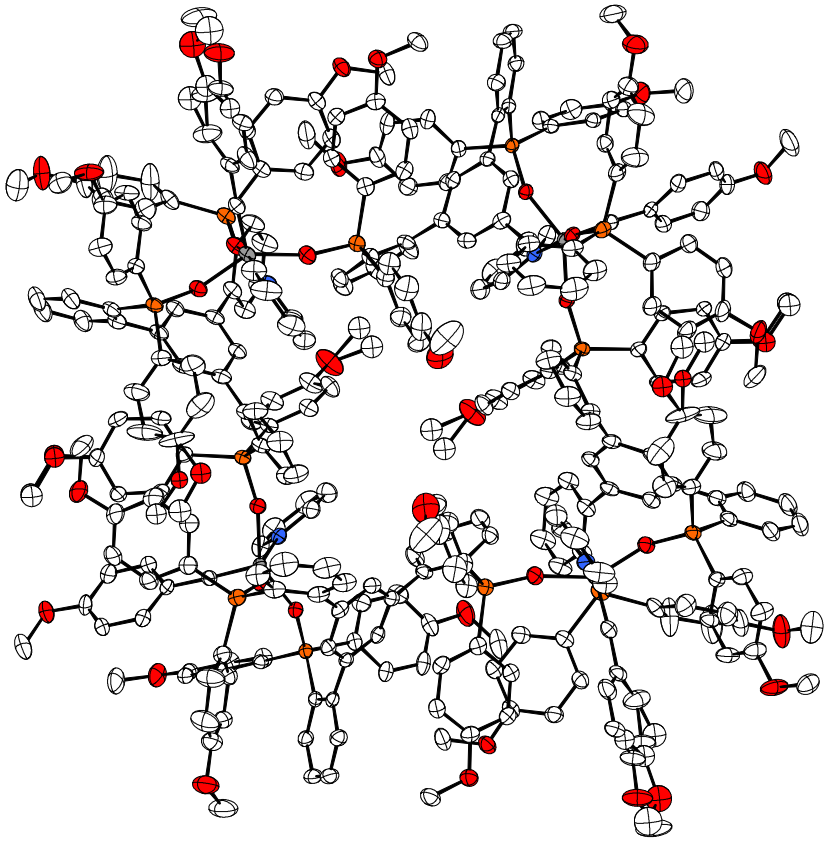

| | | |
|---|---|---|
| Identification code | 12766 | |
| Empirical formula | $C_{79}\,H_{69.15}\,Mo\,N\,O_{10}\,Si_3$ | |
| Color | violet | |
| Formula weight | 1372.71 g · mol$^{-1}$ | |
| Temperature | 100(2) K | |
| Wavelength | 0.71073 Å | |
| Crystal system | MONOCLINIC | |
| Space group | **C2/c, (no. 15)** | |
| Unit cell dimensions | a = 25.6416(12) Å | α= 90°. |
| | b = 29.0265(13) Å | β= 92.816(2)°. |
| | c = 47.213(2) Å | γ = 90°. |
| Volume | 35098(3) Å$^3$ | |

| | | |
|---|---|---|
| Z | 16 | |
| Density (calculated) | 1.039 $Mg \cdot m^{-3}$ | |
| Absorption coefficient | 0.238 $mm^{-1}$ | |
| F(000) | 11426 e | |
| Crystal size | 0.257 x 0.105 x 0.100 $mm^3$ | |
| θ range for data collection | 0.864 to 26.287°. | |
| Index ranges | $-31 \leq h \leq 31, -36 \leq k \leq 36, -58 \leq l \leq 58$ | |
| Reflections collected | 575157 | |
| Independent reflections | 35471 [$R_{int}$ = 0.0715] | |
| Reflections with I>2σ(I) | 28987 | |
| Completeness to θ = 25.242° | 99.9 % | |
| Absorption correction | Gaussian | |
| Max. and min. transmission | 0.98 and 0.96 | |
| Refinement method | Full-matrix least-squares on $F^2$ | |
| Data / restraints / parameters | 35471 / 1 / 1726 | |
| Goodness-of-fit on $F^2$ | 1.072 | |
| Final R indices [I>2σ(I)] | $R_1$ = 0.0606 | $wR^2$ = 0.1394 |
| R indices (all data) | $R_1$ = 0.0762 | $wR^2$ = 0.1473 |
| Remarks | **SQUEEZE was applied!!** | |
| Largest diff. peak and hole | 1.178 and -0.911 e · $Å^{-3}$ | |

### 6.2.7 Crystallographic Data of 122

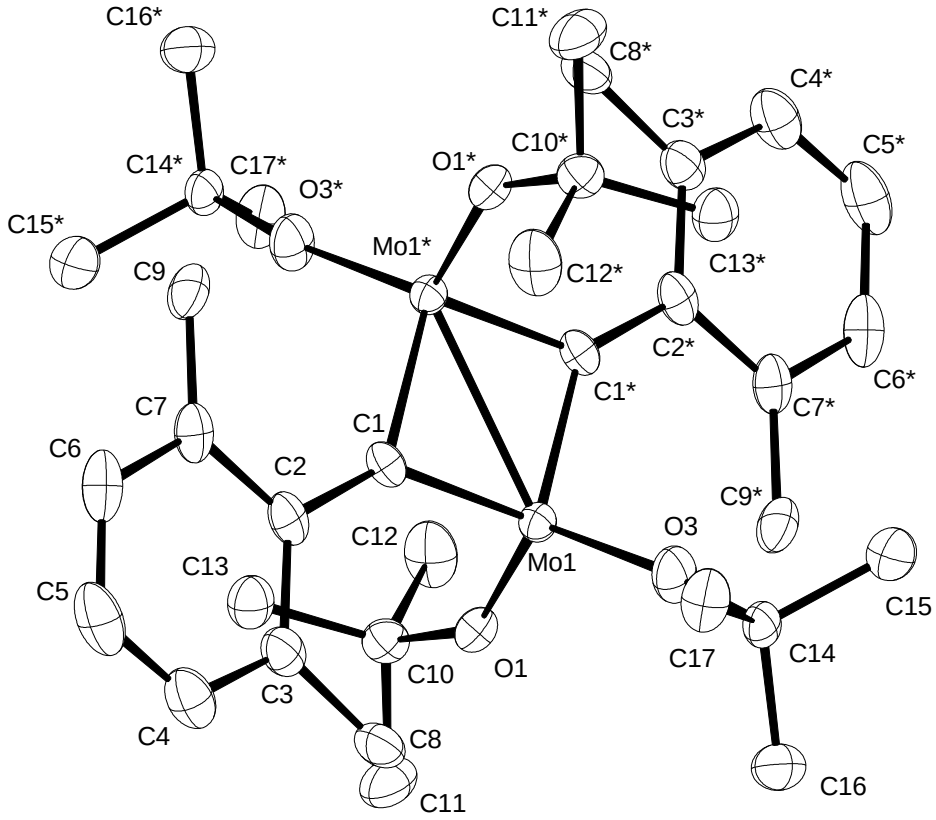


| | | |
|---|---|---|
| Identification code | 12947 | |
| Empirical formula | $C_{17}H_{27}MoO_2$ | |
| Color | red | |
| Formula weight | 359.32 $g \cdot mol^{-1}$ | |
| Temperature | 100(2) K | |
| Wavelength | 0.71073 Å | |
| Crystal system | MONOCLINIC | |
| Space group | **$P2_1/c$, (no. 14)** | |
| Unit cell dimensions | a = 9.096(4) Å | α= 90°. |
| | b = 16.677(16) Å | β= 105.59(6)°. |
| | c = 11.573(11) Å | γ = 90°. |
| Volume | 1691(2) $Å^3$ | |

| | | |
|---|---|---|
| Z | 4 | |
| Density (calculated) | 1.411 $Mg \cdot m^{-3}$ | |
| Absorption coefficient | 0.775 $mm^{-1}$ | |
| F(000) | 748 e | |
| Crystal size | 0.06 x 0.03 x 0.01 $mm^3$ | |
| θ range for data collection | 2.626 to 30.521°. | |
| Index ranges | $-12 \leq h \leq 12, -23 \leq k \leq 23, -16 \leq l \leq 16$ | |
| Reflections collected | 23980 | |
| Independent reflections | 5156 [$R_{int}$ = 0.2246] | |
| Reflections with I>2σ(I) | 2934 | |
| Completeness to θ = 25.242° | 99.9 % | |
| Absorption correction | Gaussian | |
| Max. and min. transmission | 0.99 and 0.96 | |
| Refinement method | Full-matrix least-squares on $F^2$ | |
| Data / restraints / parameters | 5156 / 0 / 189 | |
| Goodness-of-fit on $F^2$ | 1.022 | |
| Final R indices [I>2σ(I)] | $R_1$ = 0.0672 | $wR^2$ = 0.1362 |
| R indices (all data) | $R_1$ = 0.1447 | $wR^2$ = 0.1710 |
| Largest diff. peak and hole | 1.0 and -1.4 $e \cdot Å^{-3}$ | |

### 6.2.8 Crystallographic Data of 123

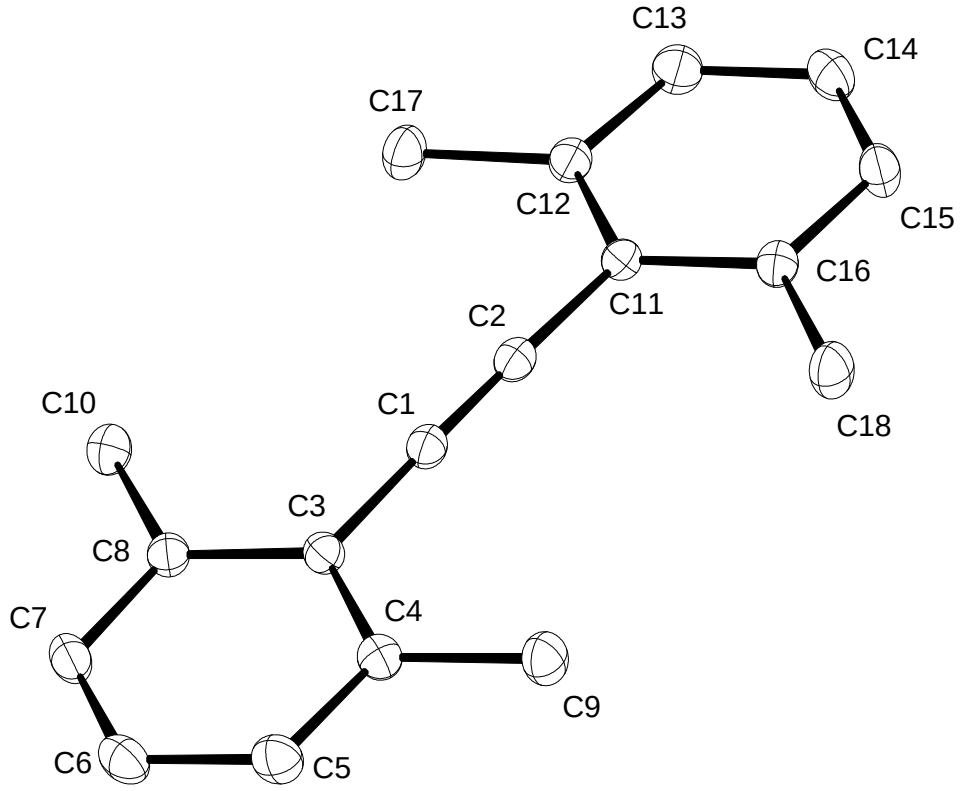


| | | |
|---|---|---|
| Identification code | 12944 | |
| Empirical formula | $C_{18}H_{18}$ | |
| Color | light yellow | |
| Formula weight | 234.32 $g \cdot mol^{-1}$ | |
| Temperature | 100(2) K | |
| Wavelength | 0.71073 Å | |
| Crystal system | MONOCLINIC | |
| Space group | **$P2_1/c$, (no. 14)** | |
| Unit cell dimensions | a = 5.6223(2) Å | α= 90°. |
| | b = 12.6521(5) Å | β= 92.518(2)°. |
| | c = 18.5302(8) Å | γ = 90°. |
| Volume | 1316.85(9) $Å^3$ | |

| | | |
|---|---|---|
| Z | 4 | |
| Density (calculated) | 1.182 $Mg \cdot m^{-3}$ | |
| Absorption coefficient | 0.066 $mm^{-1}$ | |
| F(000) | 504 e | |
| Crystal size | 0.120 x 0.045 x 0.031 $mm^3$ | |
| θ range for data collection | 1.950 to 31.447°. | |
| Index ranges | $-8 \leq h \leq 8, -18 \leq k \leq 18, -27 \leq l \leq 27$ | |
| Reflections collected | 44365 | |
| Independent reflections | 4340 [$R_{int}$ = 0.0417] | |
| Reflections with I>2σ(I) | 3127 | |
| Completeness to θ = 25.242° | 100.0 % | |
| Absorption correction | Gaussian | |
| Max. and min. transmission | 0.98 and 0.94 | |
| Refinement method | Full-matrix least-squares on $F^2$ | |
| Data / restraints / parameters | 4340 / 0 / 167 | |
| Goodness-of-fit on $F^2$ | 1.040 | |
| Final R indices [I>2σ(I)] | $R_1$ = 0.0501 | $wR^2$ = 0.1358 |
| R indices (all data) | $R_1$ = 0.0755 | $wR^2$ = 0.1525 |
| Largest diff. peak and hole | 0.4 and -0.3 $e \cdot Å^{-3}$ | |

### 6.2.9 Crystallographic Data of 124

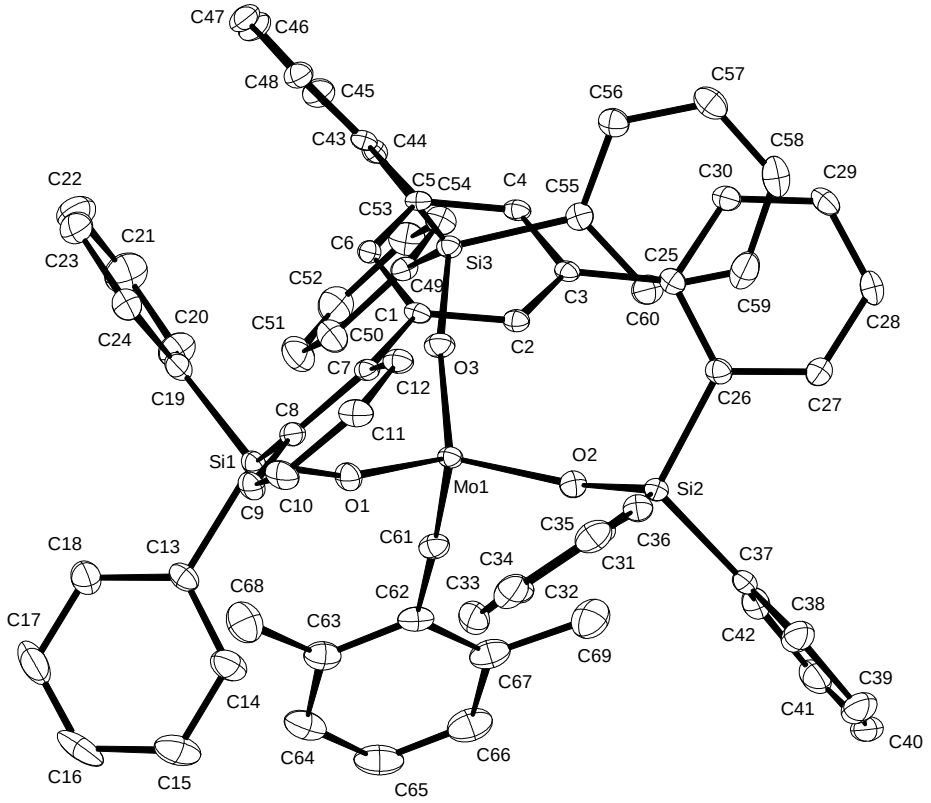


| | | |
|---|---|---|
| Identification code | 12919 | |
| Empirical formula | $C_{69}H_{54}MoO_3Si_3$ | |
| Color | yellow | |
| Formula weight | 1111.33 $g \cdot mol^{-1}$ | |
| Temperature | 100(2) K | |
| Wavelength | 0.71073 Å | |
| Crystal system | TRICLINIC | |
| Space group | $\mathbf{P\bar{1}}$, (**no. 2**) | |
| Unit cell dimensions | a = 13.9667(5) Å | α= 83.661(2)°. |
| | b = 14.1087(5) Å | β= 72.572(2)°. |
| | c = 16.4977(6) Å | γ = 61.763(2)°. |
| Volume | 2730.67(18) $Å^3$ | |

| | | |
|---|---|---|
| Z | 2 | |
| Density (calculated) | 1.352 $Mg \cdot m^{-3}$ | |
| Absorption coefficient | 0.356 $mm^{-1}$ | |
| F(000) | 1152 e | |
| Crystal size | 0.110 x 0.097 x 0.011 $mm^3$ | |
| θ range for data collection | 1.295 to 30.514°. | |
| Index ranges | $-19 \leq h \leq 19, -20 \leq k \leq 20, -23 \leq l \leq 23$ | |
| Reflections collected | 86764 | |
| Independent reflections | 16547 [$R_{int}$ = 0.0577] | |
| Reflections with I>2σ(I) | 12420 | |
| Completeness to θ = 25.242° | 100.0 % | |
| Absorption correction | Gaussian | |
| Max. and min. transmission | 1.00 and 0.97 | |
| Refinement method | Full-matrix least-squares on $F^2$ | |
| Data / restraints / parameters | 16547 / 0 / 687 | |
| Goodness-of-fit on $F^2$ | 1.041 | |
| Final R indices [I>2σ(I)] | $R_1$ = 0.0404 | $wR^2$ = 0.0876 |
| R indices (all data) | $R_1$ = 0.0690 | $wR^2$ = 0.0972 |
| Largest diff. peak and hole | 0.6 and -0.9 $e \cdot Å^{-3}$ | |

### 6.2.10 Crystallographic Data of 127

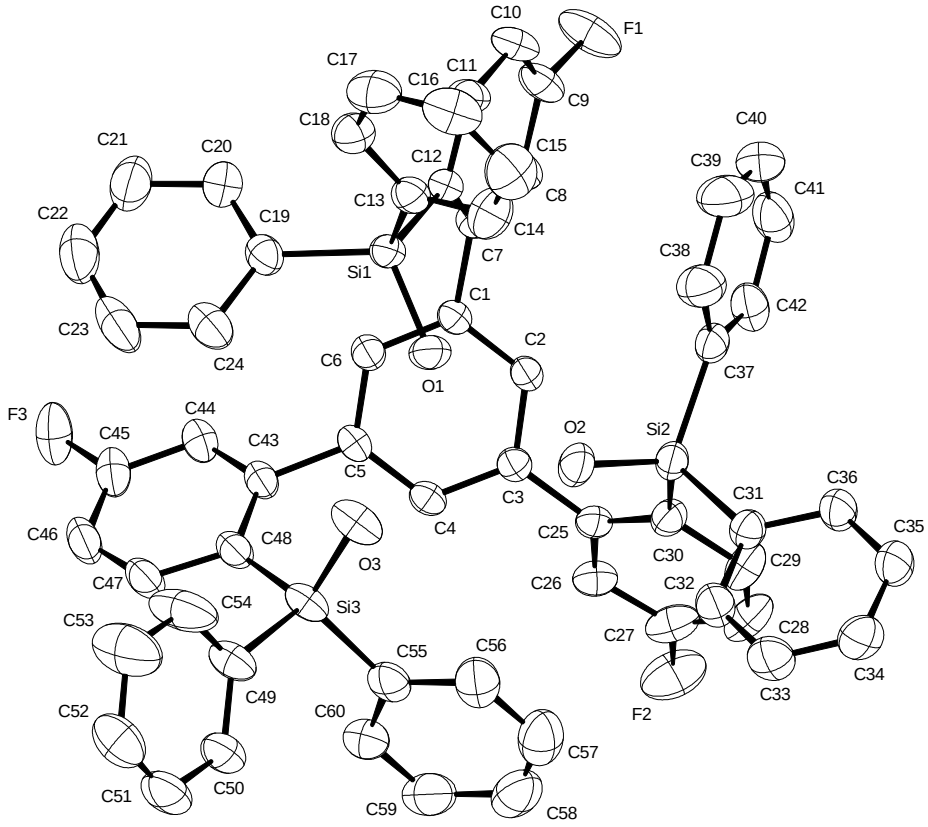


| | | |
|---|---|---|
| Identification code | 12698 | |
| Empirical formula | $C_{60}\,H_{45}\,F_3\,O_3\,Si_3$ | |
| Color | colourless | |
| Formula weight | 955.23 $g \cdot mol^{-1}$ | |
| Temperature | 200(2) K | |
| Wavelength | 0.71073 Å | |
| Crystal system | TRICLINIC | |
| Space group | $\mathbf{P\bar{1}}$, (**no. 2**) | |
| Unit cell dimensions | a = 13.4432(5) Å | α= 94.388(2)°. |
| | b = 13.9609(5) Å | β= 101.719(2)°. |
| | c = 15.6464(6) Å | γ = 117.6550(10)°. |
| Volume | 2496.95(16) $Å^3$ | |

| | | |
|---|---|---|
| Z | 2 | |
| Density (calculated) | 1.271 $Mg \cdot m^{-3}$ | |
| Absorption coefficient | 0.152 $mm^{-1}$ | |
| F(000) | 996 e | |
| Crystal size | 0.203 x 0.074 x 0.050 $mm^3$ | |
| θ range for data collection | 2.812 to 30.842°. | |
| Index ranges | $-19 \leq h \leq 19, -19 \leq k \leq 20, -22 \leq l \leq 20$ | |
| Reflections collected | 77584 | |
| Independent reflections | 15632 [$R_{int}$ = 0.0293] | |
| Reflections with I>2σ(I) | 11148 | |
| Completeness to θ = 25.242° | 99.8 % | |
| Absorption correction | Gaussian | |
| Max. and min. transmission | 0.99 and 0.98 | |
| Refinement method | Full-matrix least-squares on $F^2$ | |
| Data / restraints / parameters | 15632 / 3 / 634 | |
| Goodness-of-fit on $F^2$ | 1.031 | |
| Final R indices [I>2σ(I)] | $R_1$ = 0.0457 | $wR^2$ = 0.1141 |
| R indices (all data) | $R_1$ = 0.0711 | $wR^2$ = 0.1281 |
| Remarks | **SQUEEZE was applied!** | |
| Largest diff. peak and hole | 0.4 and -0.4 $e \cdot Å^{-3}$ | |

### 6.2.11 Crystallographic Data of 132

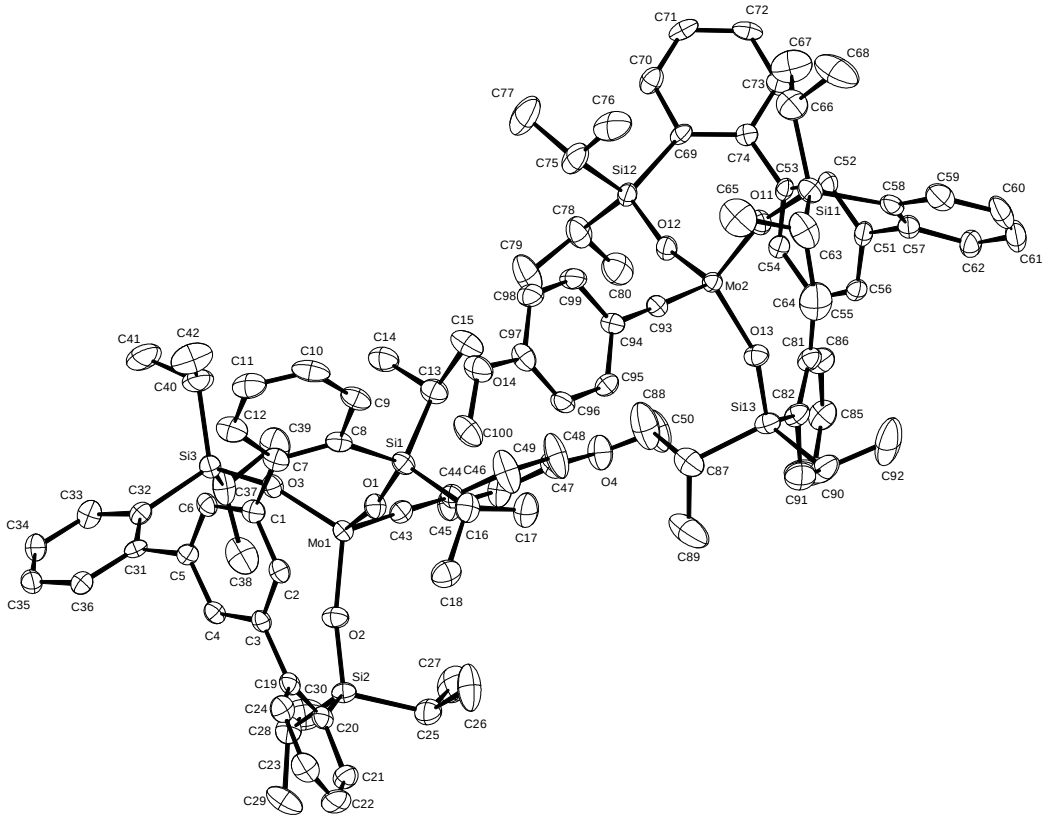


| | | |
|---|---|---|
| Identification code | 12849 | |
| Empirical formula | $C_{50}\,H_{64}\,Mo\,O_4\,Si_3$ | |
| Color | yellow | |
| Formula weight | 909.22 g · mol$^{-1}$ | |
| Temperature | 100(2) K | |
| Wavelength | 0.71073 Å | |
| Crystal system | MONOCLINIC | |
| Space group | **$P2_1$, (no. 4)** | |
| Unit cell dimensions | a = 11.3831(10) Å | α= 90°. |
| | b = 40.159(3) Å | β= 91.474(7)°. |
| | c = 11.6138(12) Å | γ= 90°. |
| Volume | 5307.3(8) Å$^3$ | |

| | | |
|---|---|---|
| Z | 4 | |
| Density (calculated) | 1.138 $Mg \cdot m^{-3}$ | |
| Absorption coefficient | 0.352 $mm^{-1}$ | |
| F(000) | 1920 e | |
| Crystal size | 0.19 x 0.08 x 0.07 $mm^3$ | |
| θ range for data collection | 2.674 to 32.069°. | |
| Index ranges | $-16 \leq h \leq 16$, $-58 \leq k \leq 58$, $-17 \leq l \leq 17$ | |
| Reflections collected | 128378 | |
| Independent reflections | 33802 [$R_{int}$ = 0.0889] | |
| Reflections with I>2σ(I) | 22677 | |
| Completeness to θ = 25.242° | 99.9 % | |
| Absorption correction | Gaussian | |
| Max. and min. transmission | 0.98 and 0.95 | |
| Refinement method | Full-matrix least-squares on $F^2$ | |
| Data / restraints / parameters | 33802 / 1 / 1071 | |
| Goodness-of-fit on $F^2$ | 1.027 | |
| Final R indices [I>2σ(I)] | $R_1$ = 0.0556 | $wR^2$ = 0.1080 |
| R indices (all data) | $R_1$ = 0.1084 | $wR^2$ = 0.1223 |
| Absolute structure parameter | -0.002(13) | |
| Remarks | **SQUEEZE was applied!** | |
| Largest diff. peak and hole | 0.4 and -0.9 $e \cdot Å^{-3}$ | |

### 6.2.12 Crystallographic Data of 134

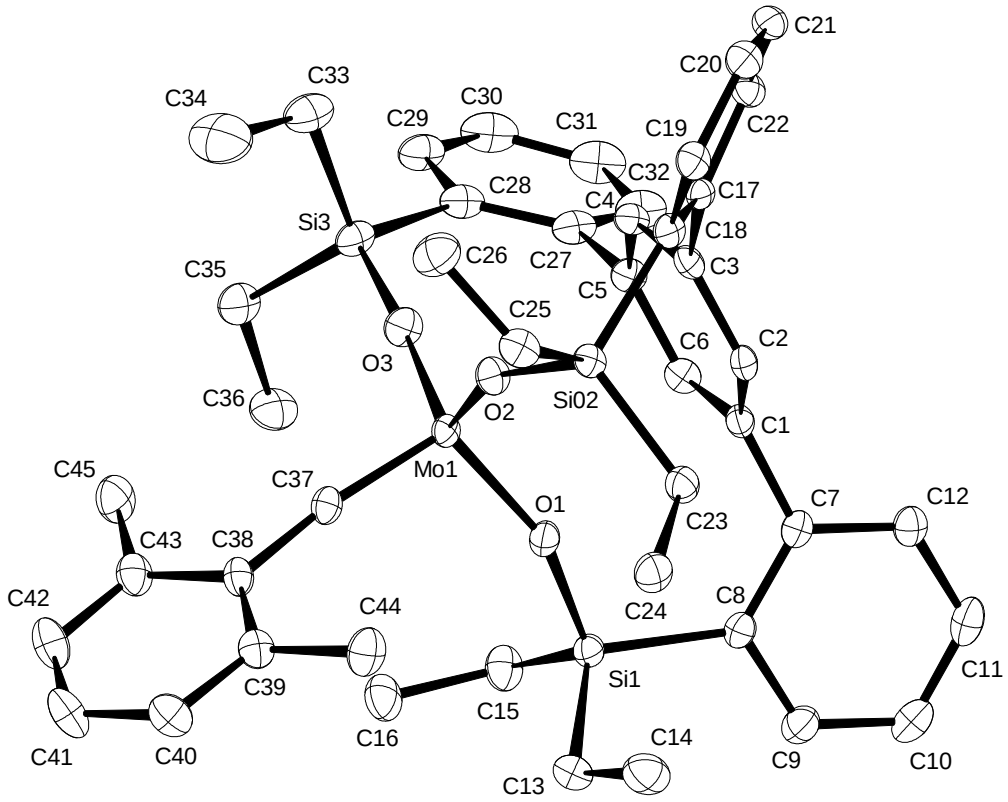


| | | |
|---|---|---|
| Identification code | 13437 | |
| Empirical formula | $C_{45}\,H_{54}\,Mo\,O_3\,Si_3$ | |
| Color | yellow | |
| Formula weight | 823.09 g·mol$^{-1}$ | |
| Temperature | 100(2) K | |
| Wavelength | 0.71073 Å | |
| Crystal system | TRICLINIC | |
| Space group | $\mathbf{P\bar{1}}$, (**no. 2**) | |
| Unit cell dimensions | a = 10.1902(8) Å | α= 95.927(14)°. |
| | b = 11.108(3) Å | β= 97.963(15)°. |
| | c = 20.652(5) Å | γ = 114.883(13)°. |
| Volume | 2065.9(7) Å$^3$ | |

| | | |
|---|---|---|
| Z | 2 | |
| Density (calculated) | 1.323 $Mg \cdot m^{-3}$ | |
| Absorption coefficient | 0.443 $mm^{-1}$ | |
| F(000) | 864 e | |
| Crystal size | 0.12 x 0.10 x 0.06 $mm^3$ | |
| θ range for data collection | 2.613 to 33.195°. | |
| Index ranges | $-15 \leq h \leq 15, -17 \leq k \leq 17, -31 \leq l \leq 31$ | |
| Reflections collected | 75169 | |
| Independent reflections | 15720 [$R_{int}$ = 0.0915] | |
| Reflections with I>2σ(I) | 10751 | |
| Completeness to θ = 25.242° | 99.8 % | |
| Absorption correction | Gaussian | |
| Max. and min. transmission | 0.98 and 0.95 | |
| Refinement method | Full-matrix least-squares on $F^2$ | |
| Data / restraints / parameters | 15720 / 0 / 477 | |
| Goodness-of-fit on $F^2$ | 1.055 | |
| Final R indices [I>2σ(I)] | $R_1$ = 0.0522 | $wR^2$ = 0.1294 |
| R indices (all data) | $R_1$ = 0.0928 | $wR^2$ = 0.1439 |
| Largest diff. peak and hole | 1.1 and -1.8 $e \cdot Å^{-3}$ | |

### 6.2.13 Crystallographic Data of 135

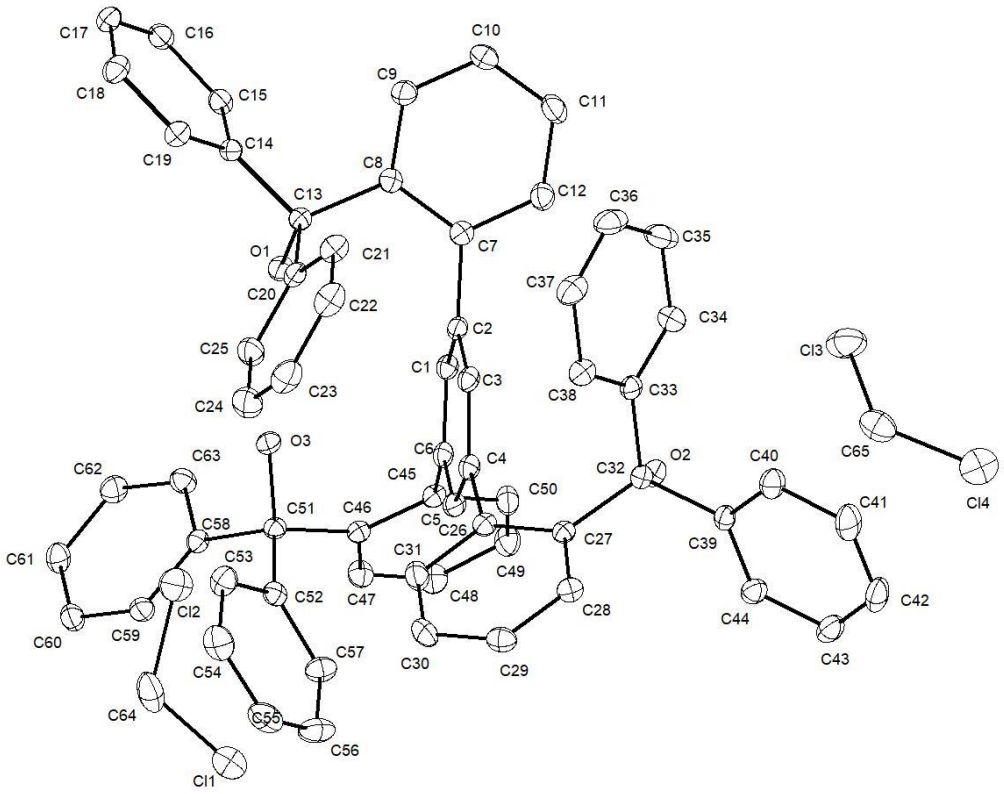


| | |
|---|---|
| Identification code | 12855 |
| Empirical formula | $C_{65}\,H_{52}\,Cl_4\,O_3$ |
| Color | colourless |
| Formula weight | 1022.86 g·mol$^{-1}$ |
| Temperature | 100(2) K |
| Wavelength | 0.71073 Å |
| Crystal system | Triclinic |
| Space group | ***P*-1, (No. 2)** |
| Unit cell dimensions | a = 13.1915(14) Å α= 88.176(5)°. |
| | b = 13.5990(15) Å β= 82.096(4)°. |
| | c = 14.5650(15) Å γ = 86.176(5)°. |
| Volume | 2581.6(5) Å$^3$ |
| Z | 2 |
| Density (calculated) | 1.316 Mg·m$^{-3}$ |
| Absorption coefficient | 0.278 mm$^{-1}$ |
| F(000) | 1068 e |
| Crystal size | 0.154 x 0.141 x 0.104 mm$^3$ |
| θ range for data collection | 2.097 to 30.508°. |
| Index ranges | $-18 \le h \le 18$, $-19 \le k \le 19$, $-20 \le l \le 20$ |
| Reflections collected | 85349 |

| | | |
|---|---|---|
| Independent reflections | 15745 [$R_{int}$ = 0.0324] | |
| Reflections with I>2σ(I) | 12687 | |
| Completeness to θ = 25.242° | 99.9 % | |
| Absorption correction | Gaussian | |
| Max. and min. transmission | 0.98113 and 0.96631 | |
| Refinement method | Full-matrix least-squares on $F^2$ | |
| Data / restraints / parameters | 15745 / 0 / 667 | |
| Goodness-of-fit on $F^2$ | 1.026 | |
| Final R indices [I>2σ(I)] | $R_1$ = 0.0451 | $wR^2$ = 0.1171 |
| R indices (all data) | $R_1$ = 0.0595 | $wR^2$ = 0.1264 |
| Extinction coefficient | n/a | |
| Largest diff. peak and hole | 0.592 and -0.897 e·$Å^{-3}$ | |

### 6.2.14 Crystallographic Data of 138

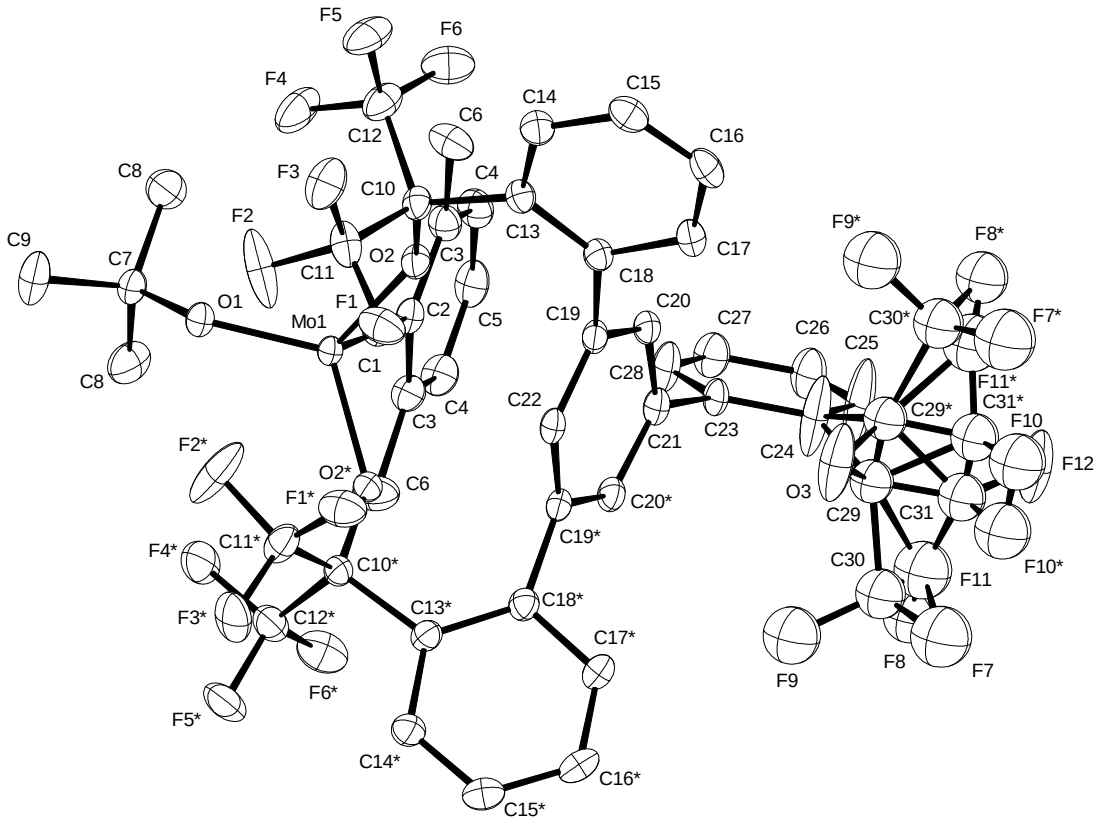


| | | |
|---|---|---|
| Identification code | 13107 | |
| Empirical formula | $C_{46}H_{33}F_{18}MoO_4$ | |
| Color | yellow-orange | |
| Formula weight | 1087.66 $g \cdot mol^{-1}$ | |
| Temperature | 100(2) K | |
| Wavelength | 0.71073 Å | |
| Crystal system | MONOCLINIC | |
| Space group | **$P2_1/m$, (no. 11)** | |
| Unit cell dimensions | a = 12.3046(15) Å | α= 90°. |
| | b = 14.5461(19) Å | β= 111.977(7)°. |
| | c = 13.2803(15) Å | γ= 90°. |
| Volume | 2204.2(5) $Å^3$ | |

| | | |
|---|---|---|
| Z | 2 | |
| Density (calculated) | 1.639 $Mg \cdot m^{-3}$ | |
| Absorption coefficient | 0.418 $mm^{-1}$ | |
| F(000) | 1090 e | |
| Crystal size | 0.12 x 0.06 x 0.05 $mm^3$ | |
| θ range for data collection | 2.801 to 30.964°. | |
| Index ranges | $-17 \leq h \leq 17, -21 \leq k \leq 21, -19 \leq l \leq 19$ | |
| Reflections collected | 44575 | |
| Independent reflections | 7231 [$R_{int}$ = 0.0705] | |
| Reflections with I>2σ(I) | 5453 | |
| Completeness to θ = 25.242° | 99.8 % | |
| Absorption correction | Gaussian | |
| Max. and min. transmission | 0.98 and 0.95 | |
| Refinement method | Full-matrix least-squares on $F^2$ | |
| Data / restraints / parameters | 7231 / 0 / 342 | |
| Goodness-of-fit on $F^2$ | 1.054 | |
| Final R indices [I>2σ(I)] | $R_1$ = 0.0610 | $wR^2$ = 0.1253 |
| R indices (all data) | $R_1$ = 0.0915 | $wR^2$ = 0.1401 |
| Largest diff. peak and hole | 1.9 and -1.0 $e \cdot Å^{-3}$ | |

## 6.2.15 Crystallographic Data of 154

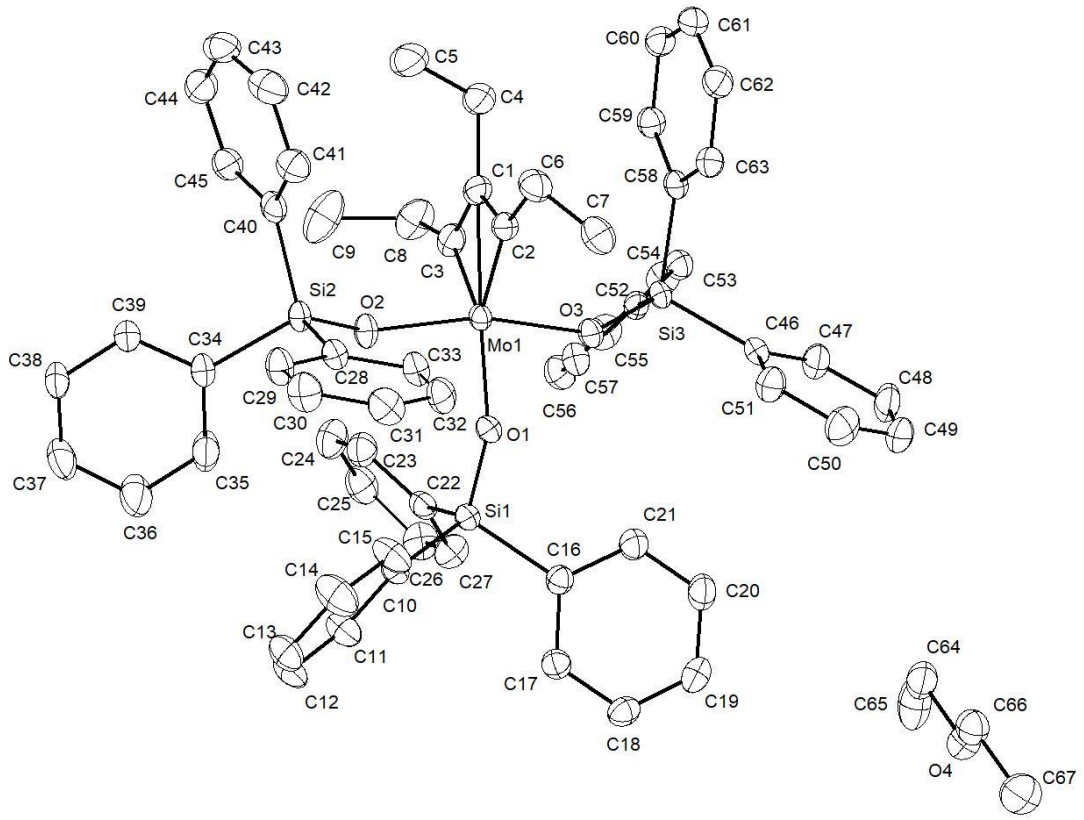


| | | |
|---|---|---|
| Identification code | 12905 | |
| Empirical formula | $C_{67}$ $H_{70}$ Mo $O_4$ $Si_3$ | |
| Color | blue | |
| Formula weight | 1119.44 g·mol$^{-1}$ | |
| Temperature | 100(2) K | |
| Wavelength | 0.71073 Å | |
| Crystal system | Monoclinic | |
| Space group | **P $2_1$/n, (No. 14)** | |
| Unit cell dimensions | a = 11.515(3) Å | α= 90°. |
| | b = 17.3173(16) Å | β= 94.723(11)°. |
| | c = 29.157(4) Å | γ = 90°. |
| Volume | 5794.3(16) Å$^3$ | |
| Z | 4 | |
| Density (calculated) | 1.283 Mg·m$^{-3}$ | |
| Absorption coefficient | 0.336 mm$^{-1}$ | |
| F(000) | 2352 e | |
| Crystal size | 0.22 x 0.16 x 0.15 mm$^3$ | |
| θ range for data collection | 2.628 to 33.193°. | |
| Index ranges | -17 ≤ h ≤ 17, -26≤ k ≤ 26, -44 ≤ l ≤ 43 | |
| Reflections collected | 125041 | |

| | | |
|---|---|---|
| Independent reflections | 22074 [$R_{int}$ = 0.0658] | |
| Reflections with I>2σ(I) | 15242 | |
| Completeness to θ = 25.242° | 99.8 % | |
| Absorption correction | Gaussian | |
| Max. and min. transmission | 0.95898 and 0.93429 | |
| Refinement method | Full-matrix least-squares on $F^2$ | |
| Data / restraints / parameters | 22074 / 0 / 689 | |
| Goodness-of-fit on $F^2$ | 1.064 | |
| Final R indices [I>2σ(I)] | $R_1$ = 0.0484 | $wR^2$ = 0.1037 |
| R indices (all data) | $R_1$ = 0.0864 | $wR^2$ = 0.1192 |
| Extinction coefficient | n/a | |
| Largest diff. peak and hole | 0.789 and -0.993 e·$Å^{-3}$ | |

### 6.2.16 Crystallographic Data of 201

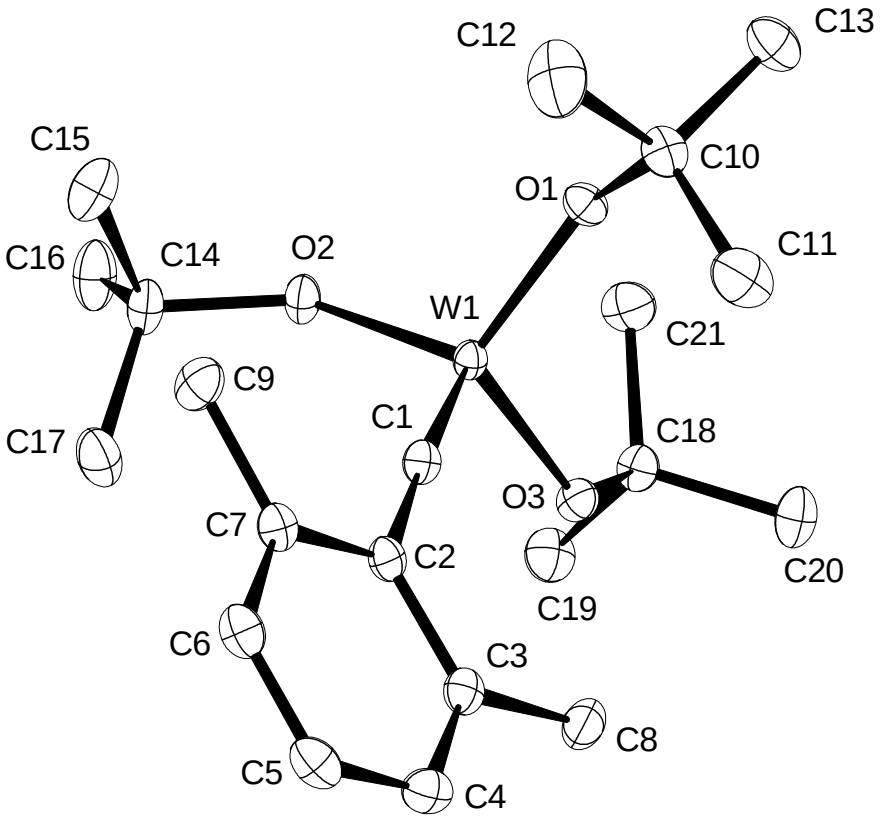


| | | |
|---|---|---|
| Identification code | 13141 | |
| Empirical formula | $C_{21}H_{36}O_3W$ | |
| Color | yellow | |
| Formula weight | 520.35 $g \cdot mol^{-1}$ | |
| Temperature | 100(2) K | |
| Wavelength | 0.71073 Å | |
| Crystal system | TRICLINIC | |
| Space group | $\mathbf{P\bar{1}}$, (**no. 2**) | |
| Unit cell dimensions | a = 9.6983(9) Å | α= 98.969(5)°. |
| | b = 10.9563(13) Å | β= 102.942(9)°. |
| | c = 11.7039(13) Å | γ = 105.650(7)°. |
| Volume | 1135.7(2) $Å^3$ | |

| | | |
|---|---|---|
| Z | 2 | |
| Density (calculated) | 1.522 $Mg \cdot m^{-3}$ | |
| Absorption coefficient | 5.100 $mm^{-1}$ | |
| F(000) | 520 e | |
| Crystal size | 0.17 x 0.16 x 0.08 $mm^3$ | |
| θ range for data collection | 2.993 to 27.500°. | |
| Index ranges | $-12 \leq h \leq 12, -14 \leq k \leq 14, -15 \leq l \leq 15$ | |
| Reflections collected | 24688 | |
| Independent reflections | 5219 [$R_{int}$ = 0.0343] | |
| Reflections with I>2σ(I) | 5101 | |
| Completeness to θ = 25.242° | 99.8 % | |
| Absorption correction | Gaussian | |
| Max. and min. transmission | 0.69 and 0.44 | |
| Refinement method | Full-matrix least-squares on $F^2$ | |
| Data / restraints / parameters | 5219 / 0 / 237 | |
| Goodness-of-fit on $F^2$ | 1.058 | |
| Final R indices [I>2σ(I)] | $R_1$ = 0.0144 | $wR^2$ = 0.0362 |
| R indices (all data) | $R_1$ = 0.0149 | $wR^2$ = 0.0365 |
| Largest diff. peak and hole | 0.8 and -1.2 $e \cdot Å^{-3}$ | |

### 6.2.17 Crystallographic Data of 202

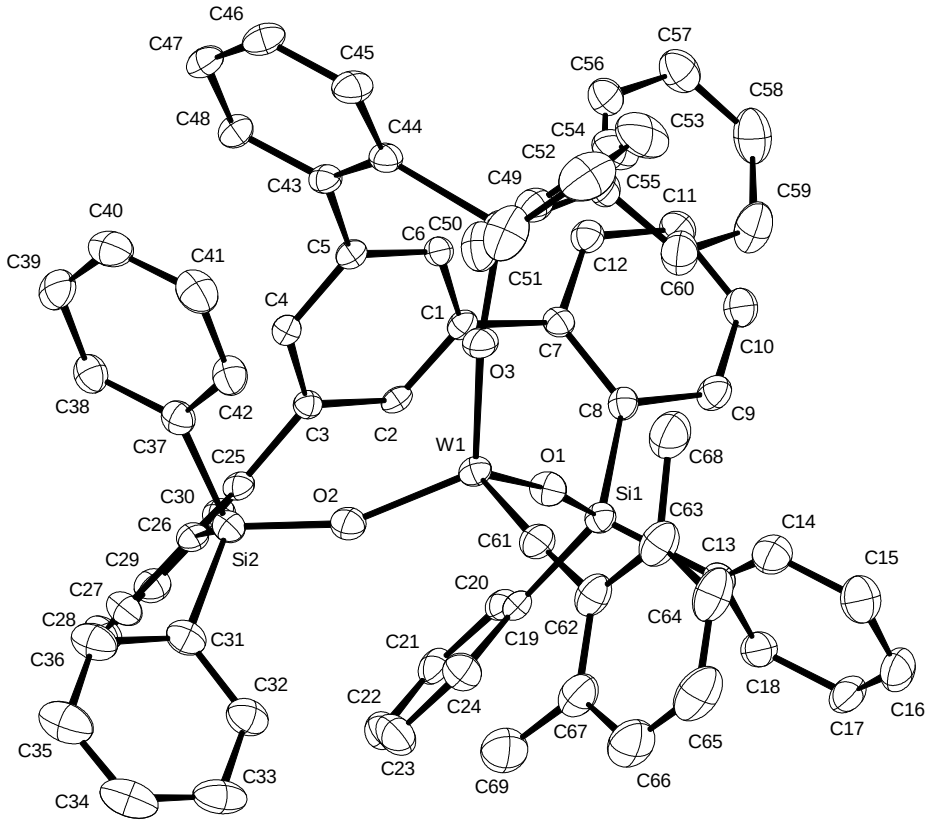


| | | |
|---|---|---|
| Identification code | 12884 | |
| Empirical formula | $C_{69}H_{54}O_3Si_3W$ | |
| Color | yellow | |
| Formula weight | 1199.24 $g \cdot mol^{-1}$ | |
| Temperature | 100(2) K | |
| Wavelength | 0.71073 Å | |
| Crystal system | TRICLINIC | |
| Space group | $\mathbf{P\bar{1}}$, (**no. 2**) | |
| Unit cell dimensions | a = 13.9825(6) Å | α= 83.475(2)°. |
| | b = 14.0803(6) Å | β= 72.892(2)°. |
| | c = 16.5360(7) Å | γ = 61.767(2)°. |

| | | |
|---|---|---|
| Volume | 2740.1(2) $Å^3$ | |
| Z | 2 | |
| Density (calculated) | 1.454 $Mg \cdot m^{-3}$ | |
| Absorption coefficient | 2.223 $mm^{-1}$ | |
| F(000) | 1216 e | |
| Crystal size | 0.083 x 0.071 x 0.021 $mm^3$ | |
| θ range for data collection | 1.289 to 31.789°. | |
| Index ranges | $-20 \leq h \leq 20, -20 \leq k \leq 20, -24 \leq l \leq 24$ | |
| Reflections collected | 89053 | |
| Independent reflections | 18570 [$R_{int}$ = 0.0770] | |
| Reflections with I>2σ(I) | 13207 | |
| Completeness to θ = 25.242° | 100.0 % | |
| Absorption correction | Gaussian | |
| Max. and min. transmission | 0.97 and 0.88 | |
| Refinement method | Full-matrix least-squares on $F^2$ | |
| Data / restraints / parameters | 18570 / 0 / 687 | |
| Goodness-of-fit on $F^2$ | 1.006 | |
| Final R indices [I>2σ(I)] | $R_1$ = 0.0425 | $wR^2$ = 0.0779 |
| R indices (all data) | $R_1$ = 0.0817 | $wR^2$ = 0.0897 |
| Largest diff. peak and hole | 2.6 and -3.4 $e \cdot Å^{-3}$ | |

### 6.2.18 Crystallographic Data of 203

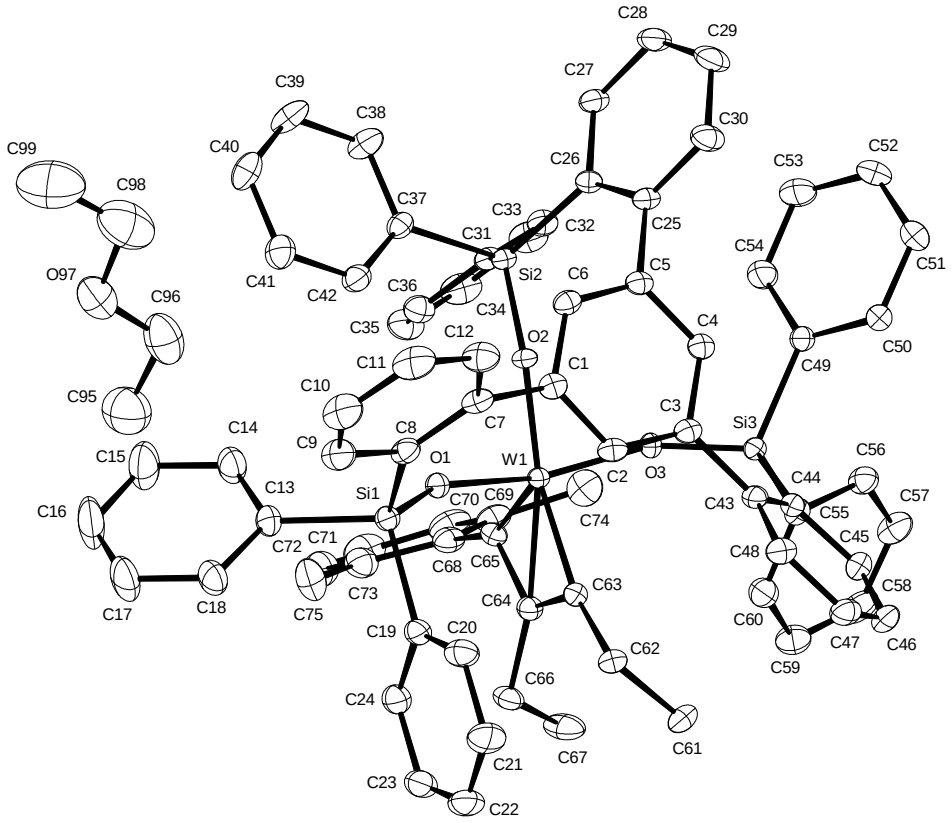


| | | |
|---|---|---|
| Identification code | 12926 | |
| Empirical formula | $C_{79}H_{74}O_4Si_3W$ | |
| Color | red | |
| Formula weight | 1355.50 $g \cdot mol^{-1}$ | |
| Temperature | 100(2) K | |
| Wavelength | 0.71073 Å | |
| Crystal system | TRICLINIC | |
| Space group | $\mathbf{P\bar{1}}$, (**no. 2**) | |
| Unit cell dimensions | a = 12.785(3) Å | α= 81.047(10)°. |
| | b = 13.8712(19) Å | β= 86.292(17)°. |
| | c = 20.155(3) Å | γ = 87.448(14)°. |
| Volume | 3521.2(10) $Å^3$ | |

| | | |
|---|---|---|
| Z | 2 | |
| Density (calculated) | 1.278 $Mg \cdot m^{-3}$ | |
| Absorption coefficient | 1.739 $mm^{-1}$ | |
| F(000) | 1392 e | |
| Crystal size | 0.14 x 0.13 x 0.11 $mm^3$ | |
| θ range for data collection | 2.711 to 32.577°. | |
| Index ranges | $-19 \leq h \leq 19, -21 \leq k \leq 21, -30 \leq l \leq 30$ | |
| Reflections collected | 114388 | |
| Independent reflections | 25571 [$R_{int}$ = 0.0492] | |
| Reflections with I>2σ(I) | 21228 | |
| Completeness to θ = 25.242° | 99.6 % | |
| Absorption correction | Gaussian | |
| Max. and min. transmission | 0.85 and 0.80 | |
| Refinement method | Full-matrix least-squares on $F^2$ | |
| Data / restraints / parameters | 25571 / 0 / 790 | |
| Goodness-of-fit on $F^2$ | 1.050 | |
| Final R indices [I>2σ(I)] | $R_1$ = 0.0293 | $wR^2$ = 0.0616 |
| R indices (all data) | $R_1$ = 0.0438 | $wR^2$ = 0.0645 |
| Remarks | **SQUEEZE was applied!** | |
| Largest diff. peak and hole | 1.3and -1.6 e · $Å^{-3}$ | |

### 6.2.19 Crystallographic Data of 207

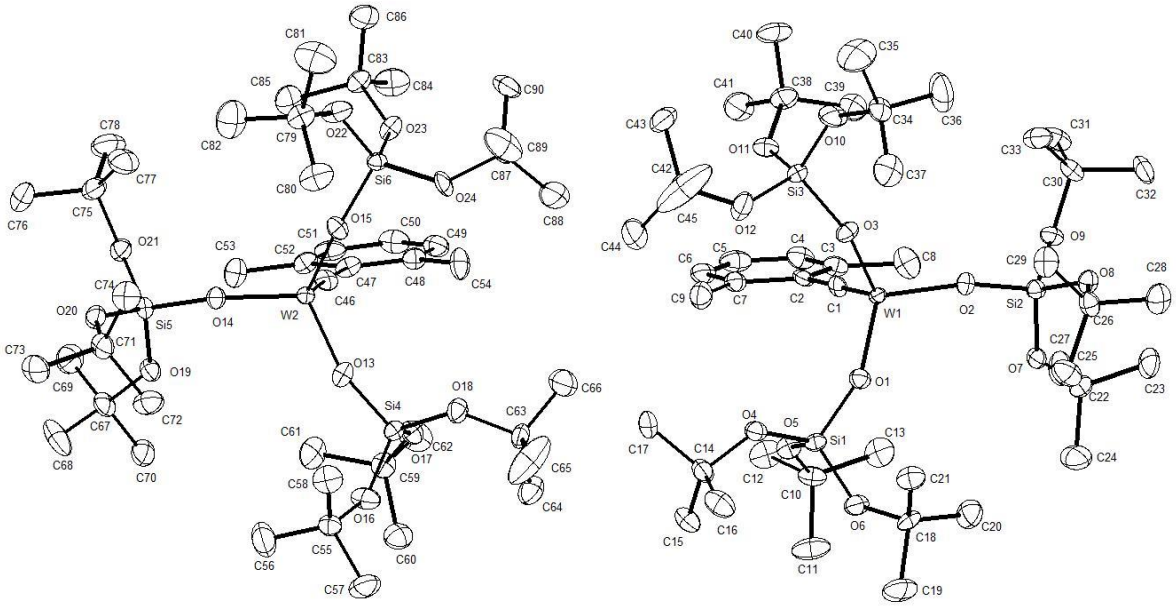


| | |
|---|---|
| Identification code | 13064 |
| Empirical formula | $C_{45}\ H_{90}\ O_{12}\ Si_3\ W$ |
| Color | yellow |
| Formula weight | 1091.28 g·mol$^{-1}$ |
| Temperature | 100(2) K |
| Wavelength | 0.71073 Å |
| Crystal system | Orthorhombic |
| Space group | **P c a 2$_1$, (No. 29)** |
| Unit cell dimensions | a = 26.7662(17) Å α= 90°.<br>b = 9.6231(16) Å β= 90°.<br>c = 44.027(5) Å γ = 90°. |
| Volume | 11340(2) Å$^3$ |
| Z | 8 |
| Density (calculated) | 1.278 Mg·m$^{-3}$ |
| Absorption coefficient | 2.151 mm$^{-1}$ |
| F(000) | 4576 e |
| Crystal size | 0.26 x 0.08 x 0.02 mm$^3$ |
| θ range for data collection | 2.607 to 30.508°. |
| Index ranges | -38 ≤ h ≤ 38, -13≤ k ≤ 13, -62 ≤ l ≤ 62 |
| Reflections collected | 221877 |
| Independent reflections | 34108 [$R_{int}$ = 0.0845] |
| Reflections with I>2σ(I) | 27986 |

| | | |
|---|---|---|
| Completeness to θ = 25.242° | 99.9 % | |
| Absorption correction | Gaussian | |
| Max. and min. transmission | 0.1861 and 0.0199 | |
| Refinement method | Full-matrix least-squares on $F^2$ | |
| Data / restraints / parameters | 34108 / 1 / 1158 | |
| Goodness-of-fit on $F^2$ | 1.152 | |
| Final R indices [I>2σ(I)] | $R_1$ = 0.0515 | $wR^2$ = 0.0916 |
| R indices (all data) | $R_1$ = 0.0730 | $wR^2$ = 0.0986 |
| Absolute structure parameter | 0.000(4) | |
| Extinction coefficient | n/a | |
| Largest diff. peak and hole | 1.343 and -2.665 e·$Å^{-3}$ | |

### 6.2.20 Crystallographic Data of 210

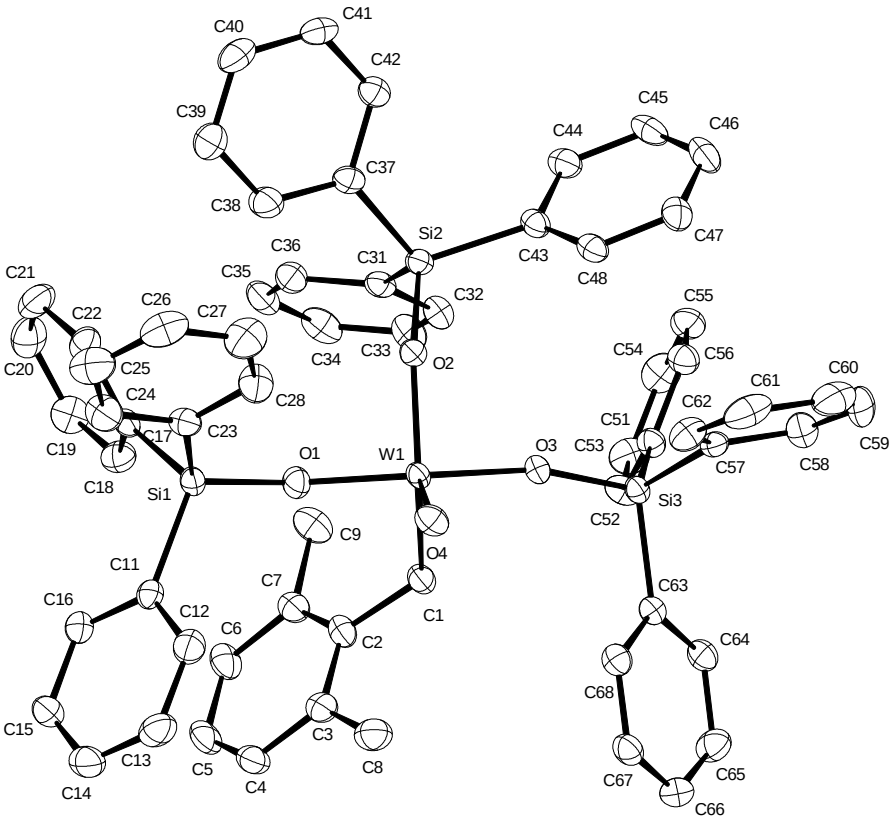


| | | |
|---|---|---|
| Identification code | 13039 | |
| Empirical formula | $C_{63}H_{56}O_4Si_3W$ | |
| Color | orange | |
| Formula weight | 1145.19 $g \cdot mol^{-1}$ | |
| Temperature | 100(2) K | |
| Wavelength | 0.71073 Å | |
| Crystal system | MONOCLINIC | |
| Space group | **$P2_1/n$, (no. 14)** | |
| Unit cell dimensions | a = 9.705(2) Å | α= 90°. |
| | b = 20.153(4) Å | β= 99.930(14)°. |
| | c = 27.244(6) Å | γ = 90°. |
| Volume | 5248.5(19) $Å^3$ | |

| | | |
|---|---|---|
| Z | 4 | |
| Density (calculated) | 1.449 $Mg \cdot m^{-3}$ | |
| Absorption coefficient | 2.318 $mm^{-1}$ | |
| F(000) | 2328 e | |
| Crystal size | 0.16 x 0.10 x 0.10 $mm^3$ | |
| θ range for data collection | 2.838 to 27.500°. | |
| Index ranges | $-12 \leq h \leq 11$, $-26 \leq k \leq 26$, $-35 \leq l \leq 35$ | |
| Reflections collected | 62702 | |
| Independent reflections | 12028 [$R_{int}$ = 0.0551] | |
| Reflections with I>2σ(I) | 9770 | |
| Completeness to θ = 25.242° | 99.6 % | |
| Absorption correction | Gaussian | |
| Max. and min. transmission | 0.88 and 0.77 | |
| Refinement method | Full-matrix least-squares on $F^2$ | |
| Data / restraints / parameters | 12028 / 0 / 650 | |
| Goodness-of-fit on $F^2$ | 1.170 | |
| Final R indices [I>2σ(I)] | $R_1$ = 0.0398 | $wR^2$ = 0.0769 |
| R indices (all data) | $R_1$ = 0.0572 | $wR^2$ = 0.0831 |
| Largest diff. peak and hole | 2.1 and -1.4 $e \cdot Å^{-3}$ | |

## 6.2.21 Crystallographic Data of 213

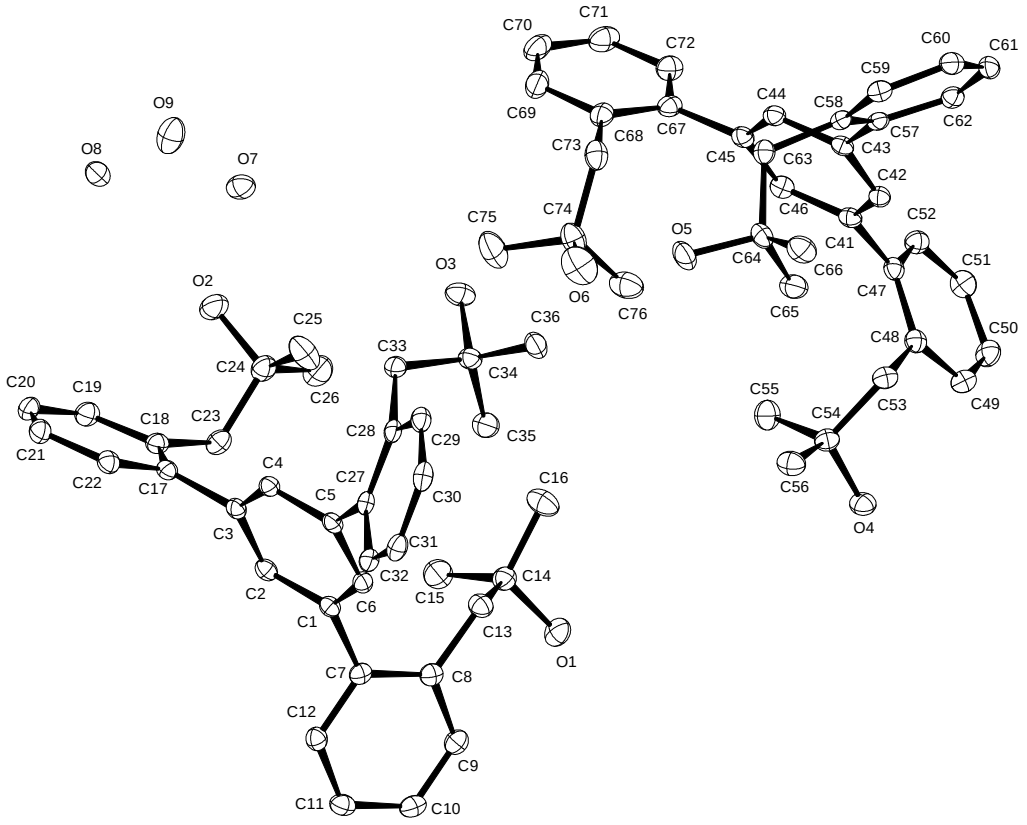


| | | |
|---|---|---|
| Identification code | 13164 | |
| Empirical formula | $C_{36}H_{45}O_{4.50}$ | |
| Color | colourless | |
| Formula weight | 549.72 g · mol$^{-1}$ | |
| Temperature | 100(2) K | |
| Wavelength | 1.54178 Å | |
| Crystal system | TRICLINIC | |
| Space group | $\mathbf{P\bar{1}}$, (**no. 2**) | |
| Unit cell dimensions | a = 11.7759(5) Å | α= 88.641(2)°. |
| | b = 16.2630(7) Å | β= 72.8940(10)°. |
| | c = 17.1108(7) Å | γ = 89.1000(10)°. |
| Volume | 3130.9(2) Å$^3$ | |

| | | |
|---|---|---|
| Z | 4 | |
| Density (calculated) | 1.166 $Mg \cdot m^{-3}$ | |
| Absorption coefficient | 0.592 $mm^{-1}$ | |
| F(000) | 1188 e | |
| Crystal size | 0.674 x 0.301 x 0.160 $mm^3$ | |
| θ range for data collection | 2.702 to 68.240°. | |
| Index ranges | $-13 \leq h \leq 14$, $-19 \leq k \leq 19$, $-20 \leq l \leq 20$ | |
| Reflections collected | 94837 | |
| Independent reflections | 10904 [$R_{int}$ = 0.0379] | |
| Reflections with I>2σ(I) | 10372 | |
| Completeness to θ = 67.679° | 94.9 % | |
| Absorption correction | Gaussian | |
| Max. and min. transmission | 0.93 and 0.80 | |
| Refinement method | Full-matrix least-squares on $F^2$ | |
| Data / restraints / parameters | 10904 / 0 / 790 | |
| Goodness-of-fit on $F^2$ | 1.043 | |
| Final R indices [I>2σ(I)] | $R_1$ = 0.0381 | $wR^2$ = 0.0923 |
| R indices (all data) | $R_1$ = 0.0397 | $wR^2$ = 0.0933 |
| Largest diff. peak and hole | 0.2 and -0.2 $e \cdot Å^{-3}$ | |

## 6.2.22 Crystallographic Data of [214]$_4$

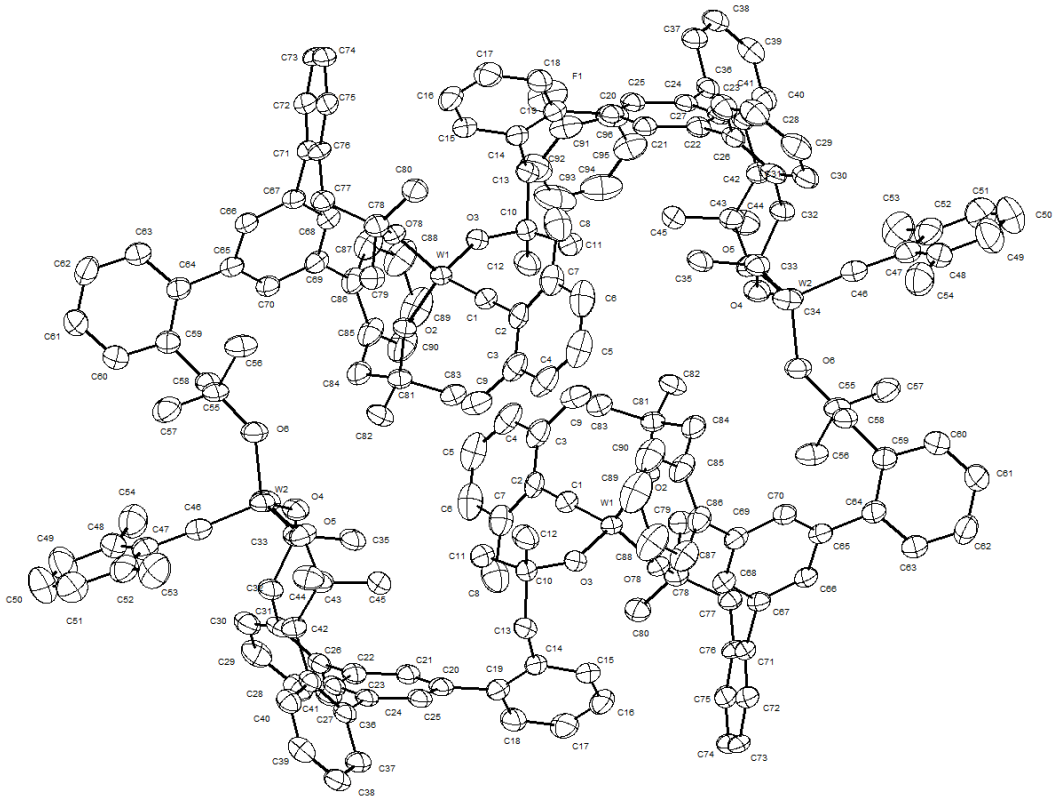

| | | |
|---|---|---|
| Identification code | 13359Petra | |
| Empirical formula | $C_{96}\,H_{100}\,F\,O_6\,W_2$ | |
| Color | yellow | |
| Formula weight | 1736.45 g·mol$^{-1}$ | |
| Temperature | 100(2) K | |
| Wavelength | 0.619900 Å | |
| Crystal system | Monoclinic | |
| Space group | ***P* 2$_1$/n, (No. 14)** | |
| Unit cell dimensions | a = 15.609(11) Å | α= 90°. |
| | b = 29.629(4) Å | β= 96.054(19)°. |
| | c = 21.072(8) Å | γ = 90°. |
| Volume | 9691(8) Å$^3$ | |
| Z | 4 | |
| Density (calculated) | 1.190 Mg·m$^{-3}$ | |
| Absorption coefficient | 1.701 mm$^{-1}$ | |
| F(000) | 3524 e | |
| Crystal size | 0.02 x 0.01 x 0.01 mm$^3$ | |
| θ range for data collection | 1.038 to 24.410°. | |
| Index ranges | -20 ≤ h ≤ 18, -39≤ k ≤ 39, -28 ≤ l ≤ 28 | |
| Reflections collected | 156310 | |

| | | |
|---|---|---|
| Independent reflections | 23363 [$R_{int}$ = 0.0947] | |
| Reflections with I>2σ(I) | 17196 | |
| Completeness to θ = 21.835° | 97.9 % | |
| Absorption correction | None | |
| Max. and min. transmission | 0.8620 and 0.7097 | |
| Refinement method | Full-matrix least-squares on $F^2$ | |
| Data / restraints / parameters | 23363 / 0 / 962 | |
| Goodness-of-fit on $F^2$ | 1.051 | |
| Final R indices [I>2σ(I)] | $R_1$ = 0.0532 | $wR^2$ = 0.1326 |
| R indices (all data) | $R_1$ = 0.0738 | $wR^2$ = 0.1422 |
| Extinction coefficient | n/a | |
| Largest diff. peak and hole | 2.350 and -2.171 e·$Å^{-3}$ | |

### 6.2.23 Crystallographic Data of 222

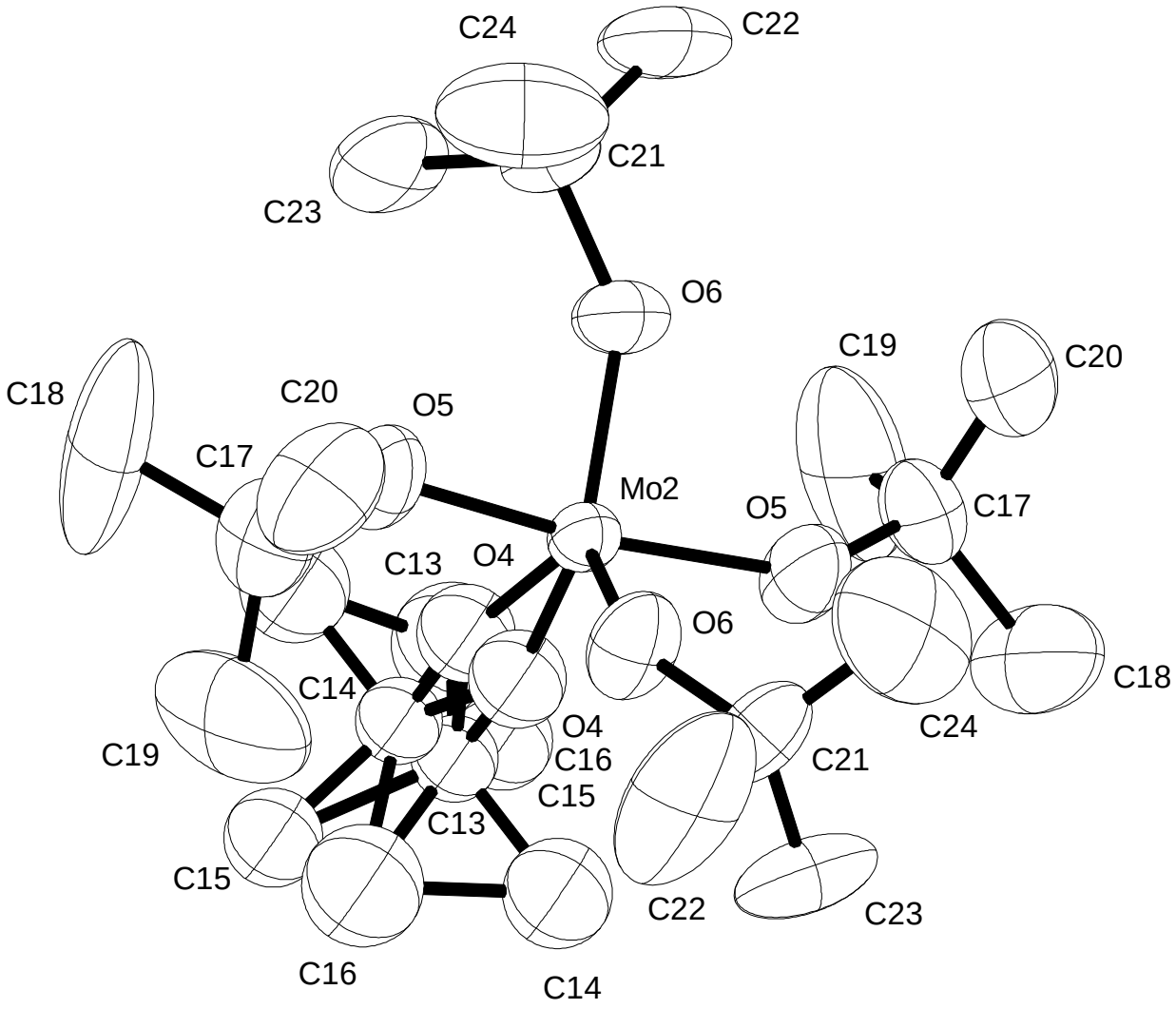


| | | |
|---|---|---|
| Identification code | 12008 | |
| Empirical formula | $C_{20}$ $H_{45}$ Mo $O_5$ | |
| Color | blue | |
| Formula weight | 461.50 g·mol$^{-1}$ | |
| Temperature | 200(2) K | |
| Wavelength | 0.71073 Å | |
| Crystal system | Orthorhombic | |
| Space group | ***P* n c 2, (No. 30)** | |
| Unit cell dimensions | a = 16.275(2) Å | α= 90°. |
| | b = 16.297(2) Å | β= 90°. |
| | c = 9.8512(13) Å | γ = 90°. |
| Volume | 2613.0(6) Å$^3$ | |
| Z | 4 | |
| Density (calculated) | 1.173 Mg·m$^{-3}$ | |
| Absorption coefficient | 0.524 mm$^{-1}$ | |

| | | |
|---|---|---|
| F(000) | 988 e | |
| Crystal size | 0.095 x 0.085 x 0.052 $mm^3$ | |
| θ range for data collection | 1.249 to 33.803°. | |
| Index ranges | $-25 \leq h \leq 25, -25 \leq k \leq 25, -15 \leq l \leq 15$ | |
| Reflections collected | 81521 | |
| Independent reflections | 10730 [$R_{int}$ = 0.0576] | |
| Reflections with I>2σ(I) | 7342 | |
| Completeness to θ = 25.242° | 100.0 % | |
| Absorption correction | Gaussian | |
| Max. and min. transmission | 0.96833 and 0.93673 | |
| Refinement method | Full-matrix least-squares on $F^2$ | |
| Data / restraints / parameters | 10730 / 0 / 249 | |
| Goodness-of-fit on $F^2$ | 1.020 | |
| Final R indices [I>2σ(I)] | $R_1$ = 0.0388 | $wR^2$ = 0.0929 |
| R indices (all data) | $R_1$ = 0.0687 | $wR^2$ = 0.1087 |
| Absolute structure parameter | 0.42(3) | |
| Extinction coefficient | n/a | |
| Largest diff. peak and hole | 0.807 and -0.586 e·$Å^{-3}$ | |

### 6.2.24 Crystallographic Data of 231

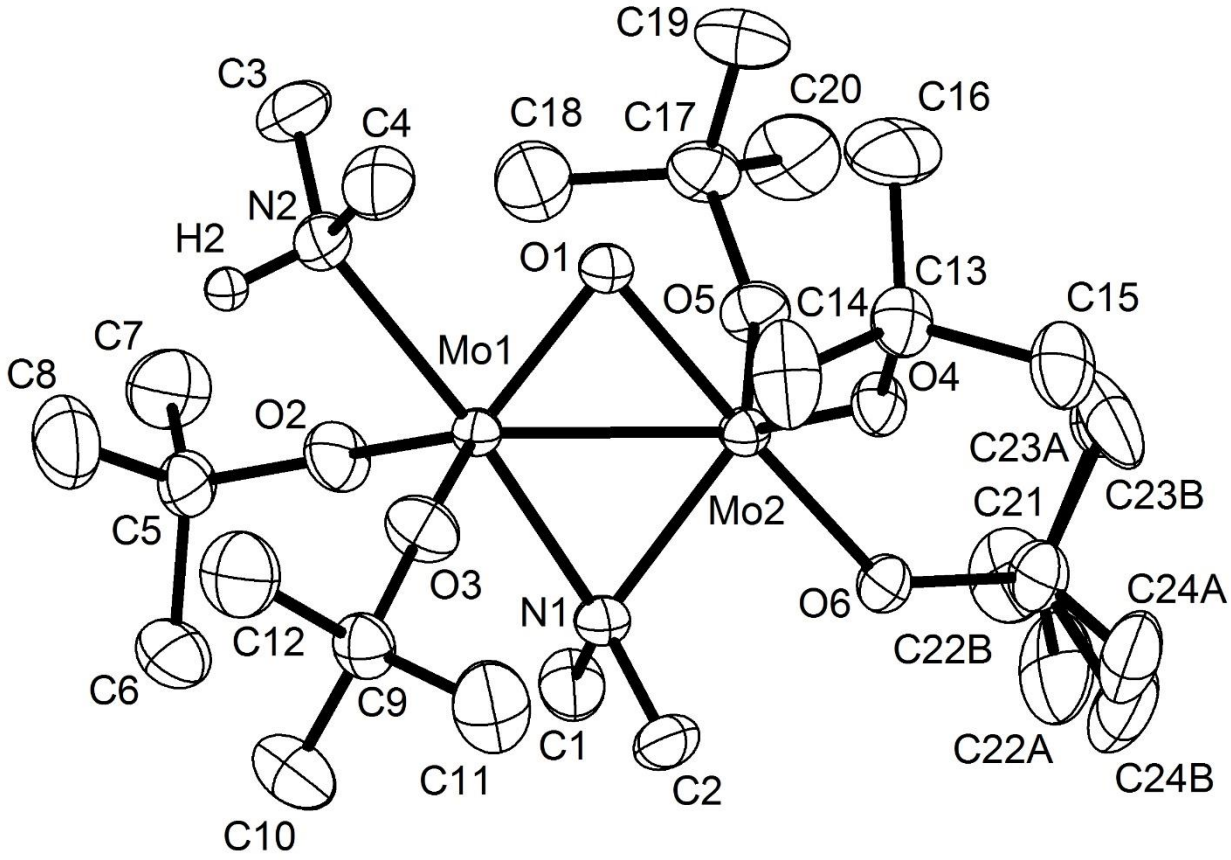


| | |
|---|---|
| Identification code | 12225 |
| Empirical formula | $C_{24}H_{58}Mo_2N_2O_6$ |
| Color | orange |
| Formula weight | 662.60 g·mol$^{-1}$ |
| Temperature | 200(2) K |
| Wavelength | 0.71073 Å |
| Crystal system | triclinic |
| Space group | $\mathbf{P\bar{1}}$, (**no. 2**) |
| Unit cell dimensions | a = 9.0540(9) Å α= 73.800(7)°.<br>b = 11.2385(7) Å β= 85.071(6)°.<br>c = 17.5263(15) Å γ = 72.601(6)°. |
| Volume | 1634.2(2) Å$^3$ |
| Z | 2 |
| Density (calculated) | 1.347 Mg·m$^{-3}$ |
| Absorption coefficient | 0.801 mm$^{-1}$ |
| F(000) | 696 e |
| Crystal size | 0.28 x 0.16 x 0.12 mm$^3$ |

| | | |
|---|---|---|
| Θ range for data collection | 2.683 to 33.073°. | |
| Index ranges | $-13 \leq h \leq 13$, $-17 \leq k \leq 17$, $-26 \leq l \leq 26$ | |
| Reflections collected | 46964 | |
| Independent reflections | 12372 [$R_{int}$ = 0.0333] | |
| Reflections with I>2σ(I) | 10546 | |
| Completeness to θ = 25.242° | 99.8 % | |
| Absorption correction | Gaussian | |
| Max. and min. transmission | 0.92121 and 0.82572 | |
| Refinement method | Full-matrix least-squares on $F^2$ | |
| Data / restraints / parameters | 12372 / 0 / 356 | |
| Goodness-of-fit on $F^2$ | 1.164 | |
| Final R indices [I>2σ(I)] | $R_1$ = 0.0322 | $wR^2$ = 0.0757 |
| R indices (all data) | $R_1$ = 0.0413 | $wR^2$ = 0.0796 |
| Extinction coefficient | 0 | |
| Largest diff. peak and hole | 1.007 and -0.837 e·$Å^{-3}$ | |

### 6.2.25 Crystallographic Data of 232 and 233

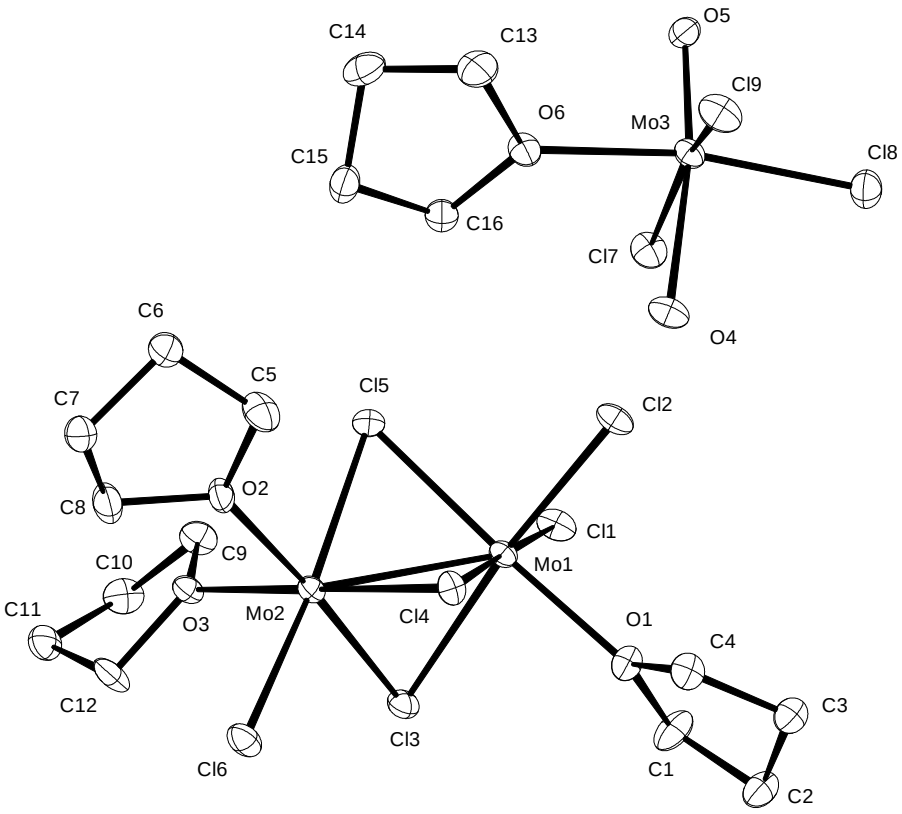


| | |
|---|---|
| Identification code | 12146 |
| Empirical formula | $C_{16}H_{34}Cl_9Mo_3O_6$ |
| Color | orange |
| Formula weight | 929.30 g · mol$^{-1}$ |
| Temperature | 100(2) K |
| Wavelength | 0.71073 Å |
| Crystal system | MONOCLINIC |
| Space group | **$P2_1/c$, (no. 14)** |
| Unit cell dimensions | a = 12.7817(17) Å $\alpha$= 90°. |
| | b = 11.6601(16) Å $\beta$= 92.439(2)°. |
| | c = 20.715(3) Å $\gamma$ = 90°. |

| | | |
|---|---|---|
| Volume | 3084.5(7) $Å^3$ | |
| Z | 4 | |
| Density (calculated) | 2.001 $Mg \cdot m^{-3}$ | |
| Absorption coefficient | 2.010 $mm^{-1}$ | |
| F(000) | 1828 e | |
| Crystal size | 0.050 x 0.036 x 0.024 $mm^3$ | |
| θ range for data collection | 2.536 to 27.499°. | |
| Index ranges | $-16 \leq h \leq 16, -15 \leq k \leq 15, -26 \leq l \leq 26$ | |
| Reflections collected | 59479 | |
| Independent reflections | 7092 [$R_{int}$ = 0.0889] | |
| Reflections with I>2σ(I) | 5204 | |
| Completeness to θ = 25.242° | 99.9 % | |
| Absorption correction | Gaussian | |
| Max. and min. transmission | 0.98 and 0.89 | |
| Refinement method | Full-matrix least-squares on $F^2$ | |
| Data / restraints / parameters | 7092 / 0 / 315 | |
| Goodness-of-fit on $F^2$ | 1.152 | |
| Final R indices [I>2σ(I)] | $R_1$ = 0.0387 | $wR^2$ = 0.0778 |
| R indices (all data) | $R_1$ = 0.0658 | $wR^2$ = 0.0887 |
| Largest diff. peak and hole | 0.8 and -0.9 $e \cdot Å^{-3}$ | |

## 6.2.26 Crystallographic Data of 235

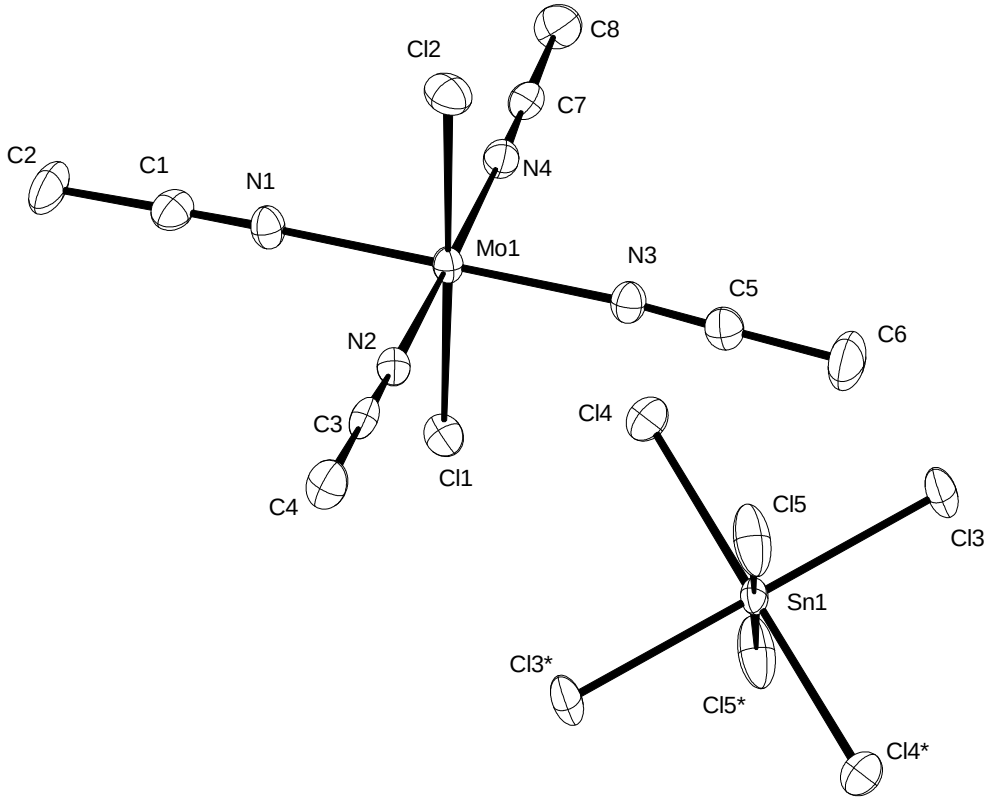


| | | |
|---|---|---|
| Identification code | 12193 | |
| Empirical formula | $C_{16}H_{24}Cl_{10}Mo_2N_8Sn$ | |
| Color | colourless | |
| Formula weight | 993.50 $g \cdot mol^{-1}$ | |
| Temperature | 100(2) K | |
| Wavelength | 0.71073 Å | |
| Crystal system | TRICLINIC | |
| Space group | $\mathbf{P\bar{1}}$, (**no. 2**) | |
| Unit cell dimensions | a = 8.2821(4) Å | α= 98.003(2)°. |
| | b = 9.7907(5) Å | β= 96.691(2)°. |
| | c = 14.7384(8) Å | γ = 92.660(2)°. |

| | | |
|---|---|---|
| Volume | 1173.02(10) $Å^3$ | |
| Z | 1 | |
| Density (calculated) | 1.406 $Mg \cdot m^{-3}$ | |
| Absorption coefficient | 1.641 $mm^{-1}$ | |
| F(000) | 480 e | |
| Crystal size | 0.063 x 0.030 x 0.018 $mm^3$ | |
| θ range for data collection | 2.355 to 31.445°. | |
| Index ranges | $-11 \leq h \leq 12, -14 \leq k \leq 14, -21 \leq l \leq 21$ | |
| Reflections collected | 40534 | |
| Independent reflections | 7718 [$R_{int}$ = 0.0555] | |
| Reflections with I>2σ(I) | 5897 | |
| Completeness to θ = 25.242° | 99.8 % | |
| Absorption correction | Gaussian | |
| Max. and min. transmission | 1.00 and 0.93 | |
| Refinement method | Full-matrix least-squares on $F^2$ | |
| Data / restraints / parameters | 7718 / 0 / 173 | |
| Goodness-of-fit on $F^2$ | 1.053 | |
| Final R indices [I>2σ(I)] | $R_1$ = 0.0334 | $wR^2$ = 0.0696 |
| R indices (all data) | $R_1$ = 0.0524 | $wR^2$ = 0.0740 |
| Largest diff. peak and hole | 0.8 and -0.8 $e \cdot Å^{-3}$ | |

### 6.2.27 Crystallographic Data of 223

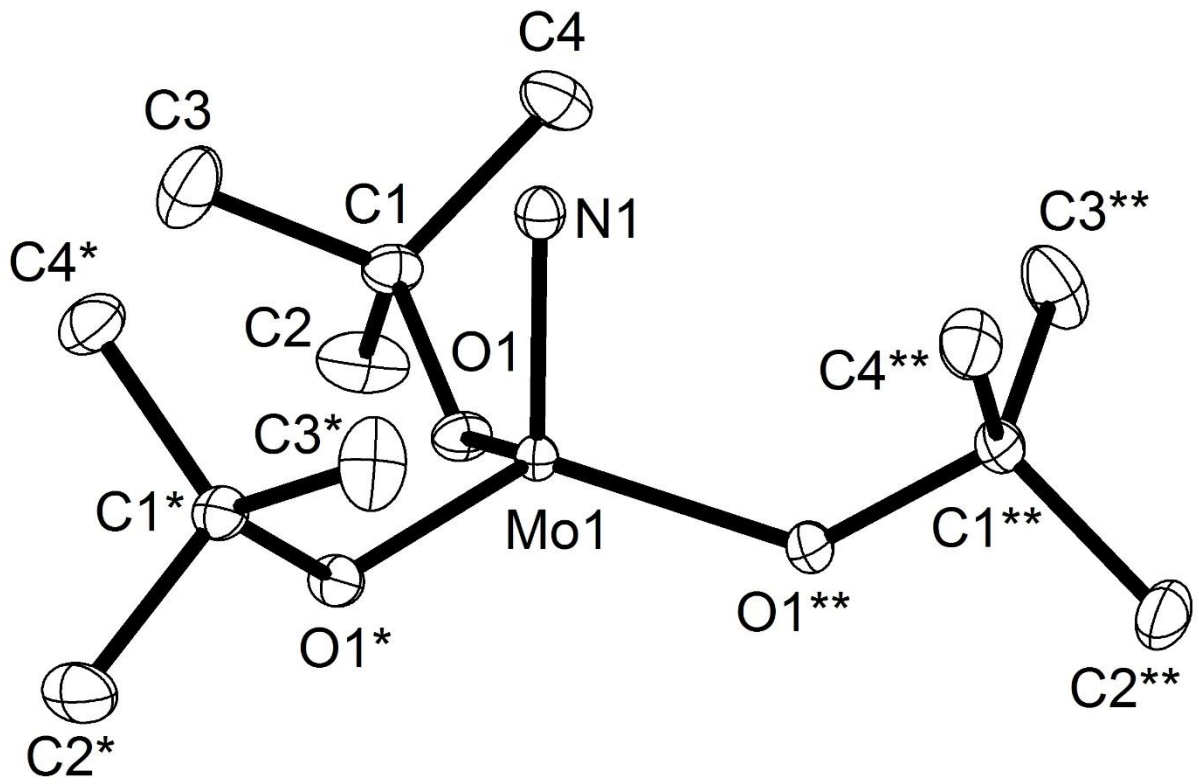


| | | |
|---|---|---|
| Identification code | HIJ-HB-177 (11977) | |
| Empirical formula | $C_{12}\ H_{27}\ Mo\ N\ O_3$ | |
| Color | orange | |
| Formula weight | 329.28 g·mol$^{-1}$ | |
| Temperature | 100(2) K | |
| Wavelength | 0.71073 Å | |
| Crystal system | hexagonal | |
| Space group | ***P* 6$_3$, (no. 173)** | |
| Unit cell dimensions | a = 10.0413(8) Å | α= 90°. |
| | b = 10.0413(8) Å | β= 90°. |
| | c = 9.0168(7) Å | γ = 120°. |
| Volume | 787.34(14) Å$^3$ | |
| Z | 2 | |
| Density (calculated) | 1.389 Mg·m$^{-3}$ | |
| Absorption coefficient | 0.831 mm$^{-1}$ | |
| F(000) | 344 e | |
| Crystal size | 0.102 x 0.042 x 0.041 mm$^3$ | |
| θ range for data collection | 2.259 to 37.439°. | |

| | | |
|---|---|---|
| Index ranges | $-16 \leq h \leq 16$, $-16 \leq k \leq 16$, $-15 \leq l \leq 15$ | |
| Reflections collected | 21950 | |
| Independent reflections | 2687 [$R_{int} = 0.0198$] | |
| Reflections with $I>2\sigma(I)$ | 2531 | |
| Completeness to $\theta = 25.242°$ | 99.8 % | |
| Absorption correction | Gaussian | |
| Max. and min. transmission | 0.97958 and 0.95299 | |
| Refinement method | Full-matrix least-squares on $F^2$ | |
| Data / restraints / parameters | 2687 / 1 / 56 | |
| Goodness-of-fit on $F^2$ | 1.112 | |
| Final R indices [$I>2\sigma(I)$] | $R_1 = 0.0173$ | $wR^2 = 0.0434$ |
| R indices (all data) | $R_1 = 0.0198$ | $wR^2 = 0.0451$ |
| Absolute structure parameter | ? | |
| Extinction coefficient | 0 | |
| Largest diff. peak and hole | 2.062 and -0.637 $e \cdot Å^{-3}$ | |

### 6.2.28 Crystallographic Data of 248

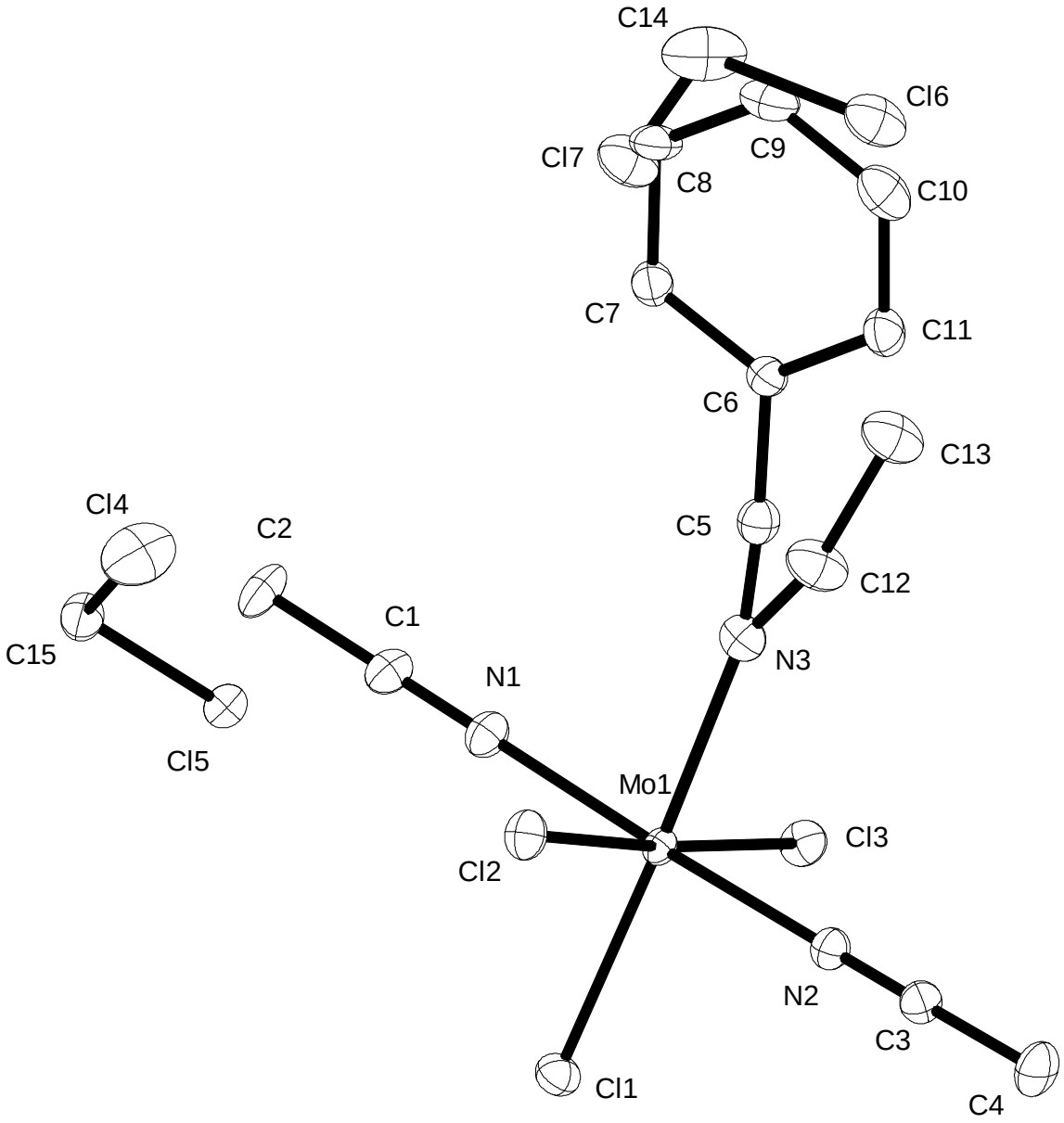


| | | |
|---|---|---|
| Identification code | 12295 | |
| Empirical formula | $C_{11.59}\,H_{12.95}\,Cl_{5.23}\,Mo\,N_3$ | |
| Color | yellow | |
| Formula weight | 475.50 g·mol$^{-1}$ | |
| Temperature | 100(2) K | |
| Wavelength | 0.71073 Å | |
| Crystal system | Monoclinic | |
| Space group | ***P* 2$_1$/c, (No. 14)** | |
| Unit cell dimensions | a = 7.5806(4) Å | α= 90°. |
| | b = 13.0108(7) Å | β= 99.2600(10)°. |

| | |
|---|---|
| | c = 18.9763(11) Å  γ = 90°. |
| Volume | 1847.24(18) Å$^3$ |
| Z | 4 |
| Density (calculated) | 1.710 Mg·m$^{-3}$ |
| Absorption coefficient | 1.460 mm$^{-1}$ |
| F(000) | 937 e |
| Crystal size | 0.117 x 0.073 x 0.062 mm$^3$ |
| θ range for data collection | 1.906 to 36.882°. |
| Index ranges | -12 ≤ h ≤ 12, -21≤ k ≤ 21, -29 ≤ l ≤ 31 |
| Reflections collected | 69260 |
| Independent reflections | 9191 [$R_{int}$ = 0.0256] |
| Reflections with I>2σ(I) | 8071 |
| Completeness to θ = 25.242° | 99.9 % |
| Absorption correction | Gaussian |
| Max. and min. transmission | 0.94314 and 0.88341 |
| Refinement method | Full-matrix least-squares on F$^2$ |
| Data / restraints / parameters | 9191 / 0 / 226 |
| Goodness-of-fit on F$^2$ | 1.152 |
| Final R indices [I>2σ(I)] | $R_1$ = 0.0282  wR$^2$ = 0.0559 |
| R indices (all data) | $R_1$ = 0.0360  wR$^2$ = 0.0580 |
| Extinction coefficient | n/a |
| Largest diff. peak and hole | 0.625 and -0.628 e·Å$^{-3}$ |

## 6.2.29 Crystallographic Data of 247

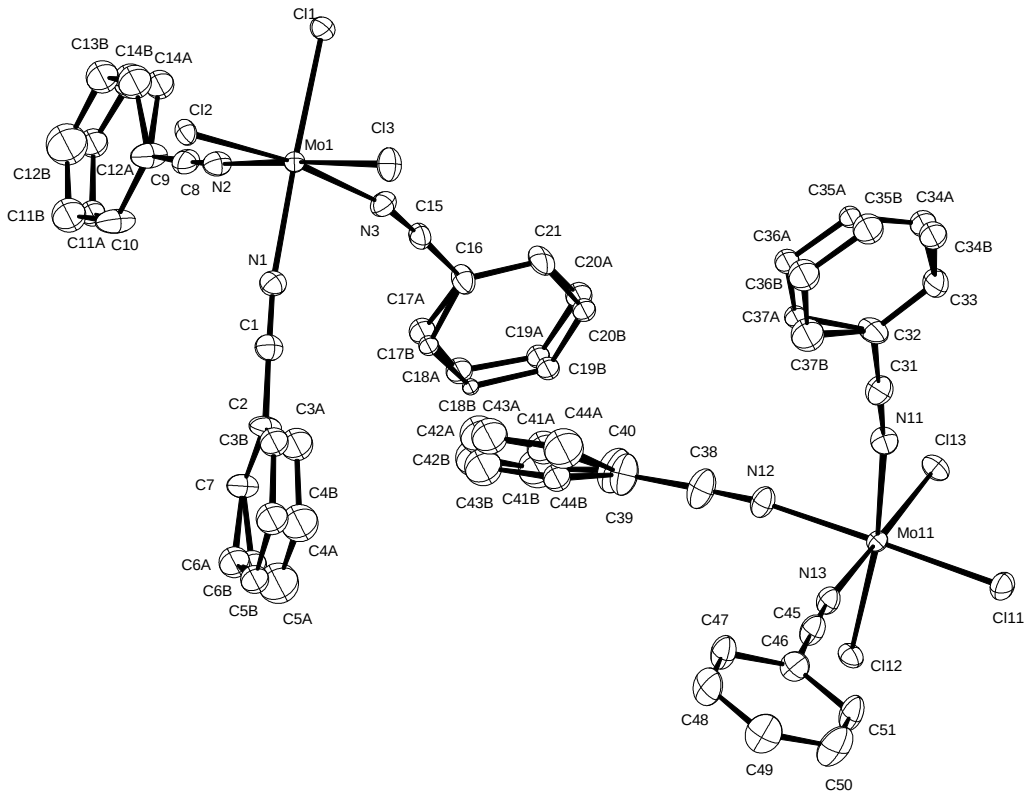


| | |
|---|---|
| Identification code | 12296 |
| Empirical formula | $C_{21}\,H_{15}\,Cl_3\,Mo\,N_3$ |
| Color | yellow |
| Formula weight | 511.65 $g \cdot mol^{-1}$ |
| Temperature | 100(2) K |
| Wavelength | 0.71073 Å |
| Crystal system | ORTHORHOMBIC |
| Space group | **$Pca2_1$, (no. 29)** |
| Unit cell dimensions | a = 23.7539(13) Å $\alpha$= 90°. |
| | b = 18.3629(10) Å $\beta$= 90°. |
| | c = 11.4146(6) Å $\gamma$ = 90°. |

| | | |
|---|---|---|
| Volume | 4978.9(5) $Å^3$ | |
| Z | 8 | |
| Density (calculated) | 1.365 $Mg \cdot m^{-3}$ | |
| Absorption coefficient | 0.859 $mm^{-1}$ | |
| F(000) | 2040 e | |
| Crystal size | 0.120 x 0.071 x 0.050 $mm^3$ | |
| θ range for data collection | 1.109 to 30.508°. | |
| Index ranges | $-33 \leq h \leq 30, -26 \leq k \leq 26, -16 \leq l \leq 16$ | |
| Reflections collected | 126162 | |
| Independent reflections | 15195 [$R_{int}$ = 0.0460] | |
| Reflections with I>2σ(I) | 11971 | |
| Completeness to θ = 25.242° | 99.9 % | |
| Absorption correction | Gaussian | |
| Max. and min. transmission | 0.95 and 0.88 | |
| Refinement method | Full-matrix least-squares on $F^2$ | |
| Data / restraints / parameters | 15195 / 1 / 486 | |
| Goodness-of-fit on $F^2$ | 1.027 | |
| Final R indices [I>2σ(I)] | $R_1$ = 0.0341 | $wR^2$ = 0.0681 |
| R indices (all data) | $R_1$ = 0.0542 | $wR^2$ = 0.0747 |
| Absolute structure parameter | 0.49(5) | |
| Largest diff. peak and hole | 0.5 and -0.4 $e \cdot Å^{-3}$ | |

### 6.2.30 Crystallographic Data of 262

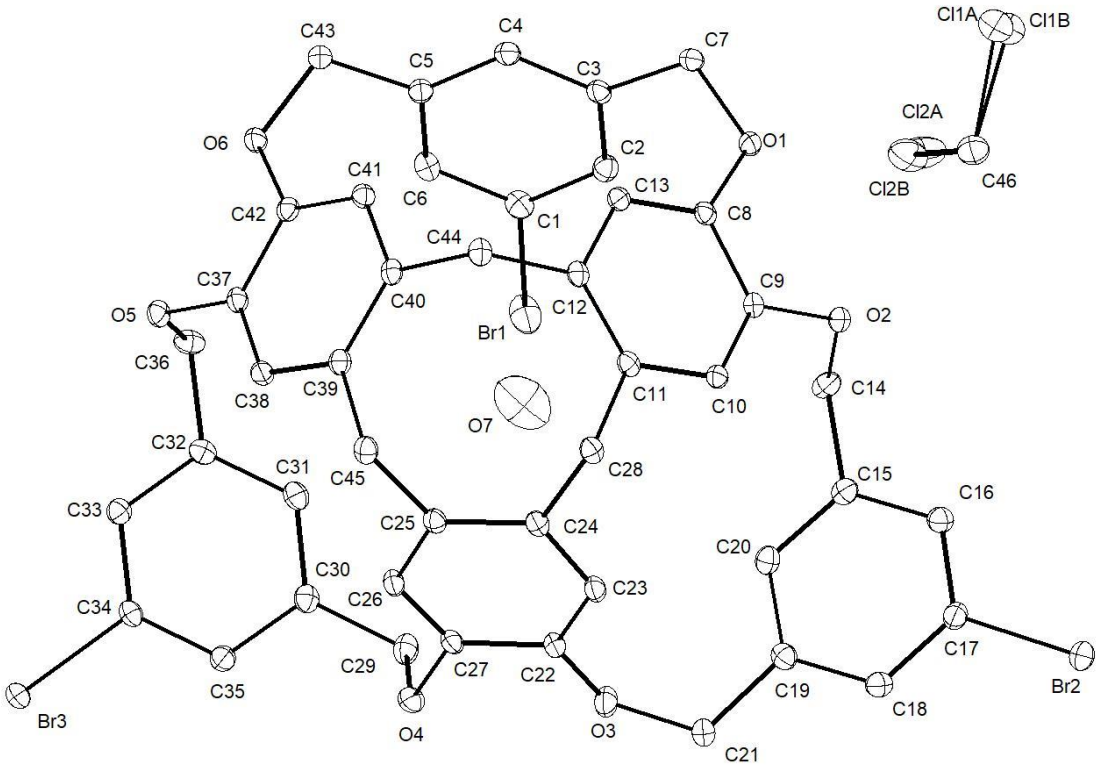


| | | |
|---|---|---|
| Identification code | 12876 | |
| Empirical formula | $C_{46}\ H_{34.86}\ Br_3\ Cl_2\ O_{6.25}$ | |
| Color | colourless | |
| Formula weight | 998.23 g·mol$^{-1}$ | |
| Temperature | 100(2) K | |
| Wavelength | 0.71073 Å | |
| Crystal system | Monoclinic | |
| Space group | **P 2$_1$/n, (No. 14)** | |
| Unit cell dimensions | a = 11.6360(7) Å | α= 90°. |
| | b = 13.7293(9) Å | β= 101.055(2)°. |
| | c = 25.1038(15) Å | γ = 90°. |
| Volume | 3936.0(4) Å$^3$ | |
| Z | 4 | |
| Density (calculated) | 1.685 Mg·m$^{-3}$ | |
| Absorption coefficient | 3.263 mm$^{-1}$ | |
| F(000) | 1999 e | |
| Crystal size | 0.112 x 0.097 x 0.065 mm$^3$ | |
| θ range for data collection | 2.320 to 30.508°. | |

| | | |
|---|---|---|
| Index ranges | $-16 \leq h \leq 16, -19 \leq k \leq 19, -35 \leq l \leq 35$ | |
| Reflections collected | 311272 | |
| Independent reflections | 12027 [$R_{int}$ = 0.0289] | |
| Reflections with I>2σ(I) | 11181 | |
| Completeness to θ = 25.242° | 99.9 % | |
| Absorption correction | Gaussian | |
| Max. and min. transmission | 0.83549 and 0.76009 | |
| Refinement method | Full-matrix least-squares on $F^2$ | |
| Data / restraints / parameters | 12027 / 0 / 543 | |
| Goodness-of-fit on $F^2$ | 1.040 | |
| Final R indices [I>2σ(I)] | $R_1$ = 0.0249 | $wR^2$ = 0.0661 |
| R indices (all data) | $R_1$ = 0.0275 | $wR^2$ = 0.0676 |
| Extinction coefficient | n/a | |
| Largest diff. peak and hole | 2.794 and -0.791 e·$Å^{-3}$ | |

### 6.2.31 Crystallographic Data of 276

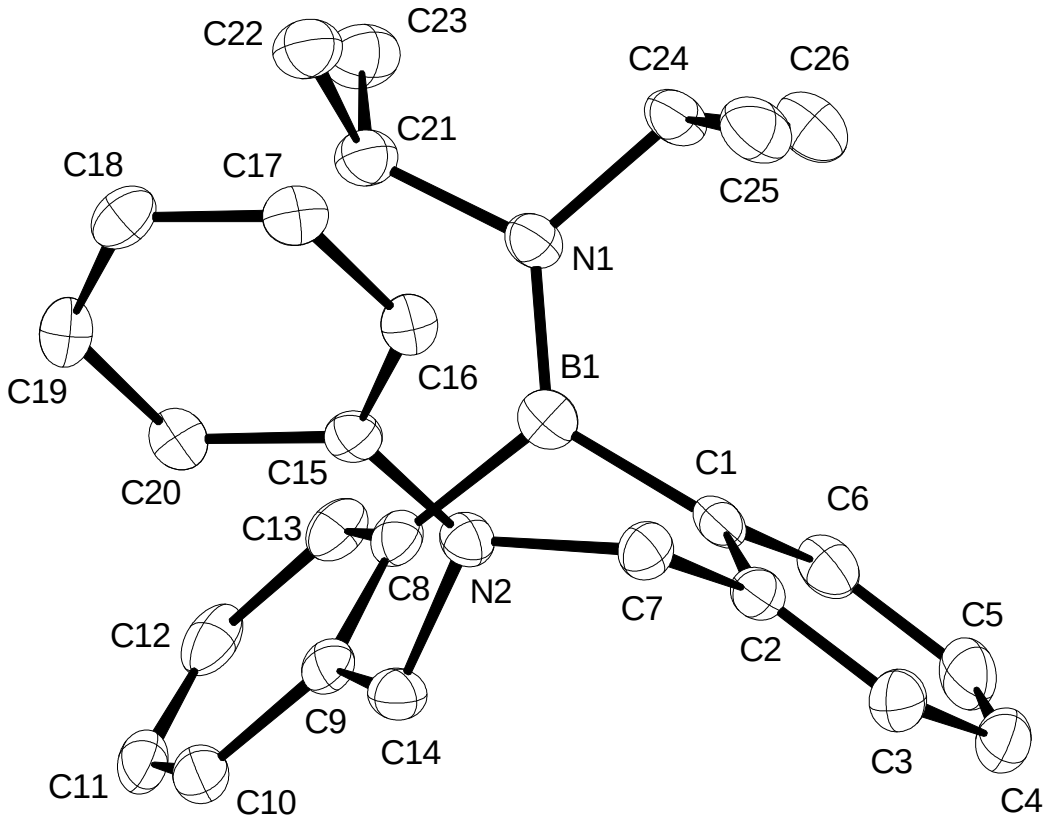


| | | |
|---|---|---|
| Identification code | 12669 | |
| Empirical formula | $C_{26}H_{31}BN_2$ | |
| Color | colourless | |
| Formula weight | 382.34 g · mol$^{-1}$ | |
| Temperature | 100(2) K | |
| Wavelength | 0.71073 Å | |
| Crystal system | ORTHORHOMBIC | |
| Space group | **Pbca, (no. 61)** | |
| Unit cell dimensions | a = 9.2359(16) Å | α= 90°. |
| | b = 16.059(2) Å | β= 90°. |
| | c = 29.694(4) Å | γ = 90°. |

| | | |
|---|---|---|
| Volume | 4404.2(11) $Å^3$ | |
| Z | 8 | |
| Density (calculated) | 1.153 $Mg \cdot m^{-3}$ | |
| Absorption coefficient | 0.066 $mm^{-1}$ | |
| F(000) | 1648 e | |
| Crystal size | 0.15 x 0.07 x 0.07 $mm^3$ | |
| θ range for data collection | 2.884 to 26.732°. | |
| Index ranges | $-11 \leq h \leq 11, -20 \leq k \leq 19, -37 \leq l \leq 37$ | |
| Reflections collected | 61023 | |
| Independent reflections | 4681 [$R_{int}$ = 0.1215] | |
| Reflections with I>2σ(I) | 3166 | |
| Completeness to θ = 25.242° | 99.8 % | |
| Absorption correction | Gaussian | |
| Max. and min. transmission | 1.00 and 0.99 | |
| Refinement method | Full-matrix least-squares on $F^2$ | |
| Data / restraints / parameters | 4681 / 0 / 278 | |
| Goodness-of-fit on $F^2$ | 1.101 | |
| Final R indices [I>2σ(I)] | $R_1$ = 0.0540 | $wR^2$ = 0.0942 |
| R indices (all data) | $R_1$ = 0.0986 | $wR^2$ = 0.1127 |
| Largest diff. peak and hole | 0.2 and -0.2 $e \cdot Å^{-3}$ | |

## 6.3 List of Abbreviations

| | |
|---|---|
| Ac | acetyl |
| ACM | alkyne cross metathesis |
| Anal. | analytically |
| aq. | aqueous |
| Bn | benzyl |
| bp | boiling point |
| br | broad |
| Bu | butyl |
| Bz | benzoyl |
| calc. | calculated |
| cat. | catalytic |
| CI | chemical ionization |
| conc. | concentrated |
| $\delta$ | chemical shift |
| d | day |
| d | doublet |
| diff. | difference |
| dme | dimethoxyethane |
| DMF | *N*,*N*-dimethylformamide |
| DMSO | dimethyl sulfoxide |
| EI | electron ionization |
| ESI | electronspray ionization |
| Et | ethyl |
| equiv | equivalents |
| eV | electronvolt |
| GC | gas chromatography |
| h | hour |

| | |
|---|---|
| HMBC | heteronuclear multiple bond correlation |
| HPLC | high pressure liquid chromatography |
| HRMS | high resolution mass spectroscopy |
| Hz | hertz, 1 Hz = 1 s−1 |
| *i* | *iso* |
| IR | infrared spectroscopy |
| *J* | coupling constant |
| Lit. | literature |
| MeCN | acetonitrile |
| *m* | meta |
| m | multiplet |
| M | molar: mol·l-1 |
| m/z | mass per charge |
| Me | methyl |
| MOM | methoxymethyl |
| Mp. | melting point |
| MS | mass spectrometry |
| MS | molecular sieves |
| MTBE | methyl *tert*-butyl ether |
| n | normal |
| NACM | nitrile alkyne cross metathesis |
| NBS | *N*-bromosuccinimide |
| *n*BuLi | *n*-butyllithium |
| n.d. | not detected |
| NMR | nuclear magnetic resonance |
| NOE | nuclear overhauser effect |
| NR | no reaction |
| *p* | *para* |
| Ph | phenyl |

| | |
|---|---|
| phen | 1,10-phenanthroline |
| PMB | *para*-methoxybenzyl |
| ppm | parts per million |
| PPTS | pyridinium *p*-toluenesulfonate |
| PTSA | *p*-toluenesulfonic acid |
| py | pyridine |
| q | quartet |
| quant. | quantitative |
| quinuc | quinuclidine |
| R | organic substituent |
| rac | Racemic |
| RCAM | ring-closing alkyne metathesis |
| rt | ambient temperature |
| s | singlet |
| sat. | saturated |
| sm | starting material |
| *t* | *tert* |
| t | triplet |
| T | temperature |
| Tab. | table |
| TBS | *tert*-butyldimethylsilyl |
| TBDPS | *tert*-butyldiphenylsilyl |
| *t*BuLi | *tert*-butyllithium |
| *tert* | tertiary |
| TES | triethylsilyl |
| Theor. | theoretical |
| THF | tetrahydrofuran |
| TLC | thin layer chromatography |
| TMS | trimethylsilyl |

| | |
|---|---|
| Ts | tosyl |
| VT | variable temperature |

# 7 References


1. Schrock, R. R., *Chem. Rev.* **2002,** *102*, 145-180.
2. Schrock, R. R., *Science* **1983,** *219*, 13-18.
3. Trnka, T. M.; Grubbs, R. H., *Acc. of Chem. Res.* **2001,** *34*, 18-29.
4. Samojłowicz, C.; Bieniek, M.; Grela, K., *Chem. Rev.* **2009,** *109*, 3708-3742.
5. Fürstner, A., *Angew. Chem., Int. Ed*. **2000,** *39*, 3012-3043.
6. Mol, J. C., *J. Mol. Catal. Chem.* **2004,** *213*, 39-45.
7. Fürstner, A., *Angew. Chem., Int. Ed*. **2013,** *52*, 2794-2819.
8. Fürstner, A., *Science* **2013,** *341*, 1229713.
9. Ehrhorn, H.; Tamm, M., *Chem. Eur. J.* **2019,** *25*, 3190-3208.
10. Chauvin, Y., *Angew. Chem., Int. Ed*. **2006,** *45*, 3740-3747.
11. Grubbs, R. H., *Angew. Chem., Int. Ed*. **2006,** *45*, 3760-3765.
12. Schrock, R. R., *Angew. Chem., Int. Ed*. **2006,** *45*, 3748-3759.
13. Pennella, F.; Banks, R. L.; Bailey, G. C., *Chem. Commun.* **1968,** 1548-1549.
14. Moulijn, J. A.; Reitsma, H. J.; Boelhouwer, C., *J. Catal.* **1972,** *25*, 434-436.
15. Mortreux, A.; Petit, F.; Blanchard, M., *J. Mol. Catal.* **1980,** *8*, 97-106.
16. Mortreux, A.; Blanchard, M., *J. Chem. Soc., Chem. Commun.* **1974,** 786-787.
17. Mortreux, A.; Dy, N.; Blanchard, M., *J. Mol. Catal.* **1976,** *1*, 101-109.
18. Mortreux, A.; Petit, F.; Blanchard, M., *Tetrahedron Lett.* **1978,** *19*, 4967-4968.
19. Bencheick, A.; Petit, M.; Mortreux, A.; Petit, F., *J. Mol. Catal.* **1982,** *15*, 93-101.
20. Mortreux, A.; Delgrange, J. C.; Blanchard, M.; Lubochinsky, B., *J. Mol. Catal.* **1977,** *2*, 73-82.
21. Du Plessis, J. A. K.; Vosloo, H. C. M., *J. Mol. Catal.* **1991,** *65*, 21-24.
22. Vosloo, H. C. M.; Du Plessis, J. A. K., *J. Mol. Catal. A: Chem.* **1998,** *133*, 205-211.
23. Devarajan, S.; Walton, D. R. M.; Leigh, G. J., *J. Organomet. Chem.* **1979,** *181*, 99-104.
24. Villemin, D.; Cadiot, P., *Tetrahedron Lett.* **1982,** *23*, 5139-5140.
25. Kaneta, N.; Hirai, T.; Mori, M., *Chem. Lett.* **1995,** *24*, 627-628.
26. Kaneta, N.; Hikichi, K.; Asaka, S.; Uemura, M.; Mori, M., *Chem. Lett.* **1995,** *24*, 1055-1056.
27. Kloppenburg, L.; Song, D.; Bunz, U. H. F., *J. Am. Chem. Soc.* **1998,** *120*, 7973-7974.
28. Pschirer, N. G.; Bunz, U. H. F., *Tetrahedron Lett.* **1999,** *40*, 2481-2484.
29. Bly, R. K.; Dyke, K. M.; Bunz, U. H. F., *J. Organomet. Chem.* **2005,** *690*, 825-829.
30. Grela, K.; Ignatowska, J., *Org. Lett.* **2002,** *4*, 3747-3749.
31. Sashuk, V.; Ignatowska, J.; Grela, K., *J. Org. Chem.* **2004,** *69* , 7748-7751.
32. Huc, V.; Weihofen, R.; Martin-Jimenez, I.; Oulié, P.; Lepetit, C.; Lavigne, G.; Chauvin, R., *New J. Chem.* **2003,** *27*, 1412-1414.
33. Maraval, V.; Lepetit, C.; Caminade, A.-M.; Majoral, J.-P.; Chauvin, R., *Tetrahedron Lett.* **2006,** *47*, 2155-2159.
34. Brizius, G.; Bunz, U. H. F., *Org. Lett.* **2002,** *4*, 2829-2831.
35. Fürstner, A.; Stelzer, F.; Rumbo, A.; Krause, H., *Chem. Eur. J.* **2002,** *8* , 1856-1871.
36. Fürstner, A.; Grela, K.; Mathes, C.; Lehmann, C. W., *J. Am. Chem. Soc.* **2000,** *122*, 11799-11805.
37. Fritch, J. R.; Vollhardt, K. P. C., *Angew. Chem., Int. Ed*. **1979,** *18*, 409-411.
38. Nishida, M.; Shiga, H.; Mori, M., *J. Org. Chem.* **1998,** *63*, 8606-8608.
39. Woo, T.; Folga, E.; Ziegler, T., *Organometallics* **1993,** *12*, 1289-1298.
40. Sancho, J.; Schrock, R. R., *J. Mol. Catal.* **1982,** *15*, 75-79.
41. Katz, T. J.; McGinnis, J., *J. Am. Chem. Soc.* **1975,** *97*, 1592-1594.
42. Fischer, E. O.; Kreis, G.; Kreiter, C. G.; Müller, J.; Huttner, G.; Lorenz, H., *Angew. Chem., Int. Ed*. **1973,** *12*, 564-565.
43. Schrock, R. R., *J. Am. Chem. Soc.* **1974,** *96*, 6796-6797.
44. Guggenberger, L. J.; Schrock, R. R., *J. Am. Chem. Soc.* **1975,** *97*, 2935-2935.
45. Wengrovius, J. H.; Sancho, J.; Schrock, R. R., *J. Am. Chem. Soc.* **1981,** *103*, 3932-3934.
46. Clark, D. N.; Schrock, R. R., *J. Am. Chem. Soc.* **1978,** *100*, 6774-6776.
47. Schrock, R. R.; Clark, D. N.; Sancho, J.; Wengrovius, J. H.; Rocklage, S. M.; Pedersen, S. F., *Organometallics* **1982,** *1*, 1645-1651.

48. Schrock, R. R., Sancho, J., Pederson, S.F., Virgil, S.C. and Grubbs, R.H, *Inorg. Synth.* **2007,** 44-51.
49. Chisholm, M. H., Martin, J.D., Hill, J.E. and Rothwell, I.P. , *Inorg. Synth.* **2007,** 137-140.
50. Akiyama, M.; Chisholm, M. H.; Cotton, F. A.; Extine, M. W.; Haitko, D. A.; Little, D.; Fanwick, P. E., *Inorg. Chem.* **1979,** *18*, 2266-2270.
51. Chisholm, M. H.; Cotton, F. A.; Extine, M.; Stults, B. R., *J. Am. Chem. Soc.* **1976,** *98*, 4477-4485.
52. Schrock, R. R.; Listemann, M. L.; Sturgeoff, L. G., *J. Am. Chem. Soc.* **1982,** *104*, 4291-4293.
53. Listemann, M. L.; Schrock, R. R., *Organometallics* **1985,** *4*, 74-83.
54. Fischer, E. O.; Maasböl, A., *Chem. Ber.* **1967,** *100*, 2445-2456.
55. Mayr, A.; McDermott, G. A., *J. Am. Chem. Soc.* **1986,** *108*, 548-549.
56. McDermott, G. A.; Dorries, A. M.; Mayr, A., *Organometallics* **1987,** *6*, 925-931.
57. Haberlag, B.; Wu, X.; Brandhorst, K.; Grunenberg, J.; Daniliuc, C. G.; Jones, P. G.; Tamm, M., *Chem. Eur. J.* **2010,** *16*, 8868-8877.
58. Heppekausen, J.; Stade, R.; Goddard, R.; Fürstner, A., *J. Am. Chem. Soc.* **2010,** *132*, 11045-11057.
59. Stevenson, M. A.; Hopkins, M. D., *Organometallics* **1997,** *16*, 3572-3573.
60. Schrock, R. R.; Pedersen, S. F.; Churchill, M. R.; Ziller, J. W., *Organometallics* **1984,** *3*, 1574-1583.
61. Pedersen, S. F.; Schrock, R. R.; Churchill, M. R.; Wasserman, H. J., *J. Am. Chem. Soc.* **1982,** *104*, 6808-6809.
62. Murdzek, J. S.; Blum, L.; Schrock, R. R., *Organometallics* **1988,** *7*, 436-441.
63. Schrock, R. R.; Murdzek, J. S.; Freudenberger, J. H.; Churchill, M. R.; Ziller, J. W., *Organometallics* **1986,** *5*, 25-33.
64. Churchill, M. R.; Ziller, J. W.; Freudenberger, J. H.; Schrock, R. R., *Organometallics* **1984,** *3*, 1554-1562.
65. Schrock, R. R., *Polyhedron* **1995,** *14* , 3177-3195.
66. Chisholm, M. H.; Hoffman, D. M.; Huffman, J. C., *Inorg. Chem* **1983,** *22*, 2903-2906.
67. Freudenberger, J. H.; Schrock, R. R., *Organometallics* **1986,** *5*, 398-400.
68. Feinstein-Jaffe, I.; Pedersen, S. F.; Schrock, R. R., *J. Am. Chem. Soc.* **1983,** *105*, 7176-7177.
69. Feinstein-Jaffe, I.; Dewan, J. C.; Schrock, R. R., *Organometallics* **1985,** *4*, 1189-1193.
70. Freudenberger, J. H.; Schrock, R. R.; Churchill, M. R.; Rheingold, A. L.; Ziller, J. W., *Organometallics* **1984,** *3*, 1563-1573.
71. Churchill, M. R.; Ziller, J. W.; McCullough, L.; Pedersen, S. F.; Schrock, R. R., *Organometallics* **1983,** *2*, 1046-1048.
72. Churchill, M. R.; Fettinger, J. C., *J. Am. Chem. Soc.* **1984,** *106*, 3356-3357.
73. Beer, S.; Hrib, C. G.; Jones, P. G.; Brandhorst, K.; Grunenberg, J.; Tamm, M., *Angew. Chem., Int. Ed*. **2007,** *46*, 8890-8894.
74. Beer, S.; Brandhorst, K.; Grunenberg, J.; Hrib, C. G.; *Org. Lett.* **2008,** *10*, 981-984.
75. Beer, S.; Brandhorst, K.; Hrib, C. G.; Wu, X.; Haberlag, B.; Grunenberg, J.; Jones, P. G.; Tamm, M., *Organometallics* **2009,** *28*, 1534-1545.
76. Tonzetich, Z. J.; Lam, Y. C.; Müller, P.; Schrock, R. R., *Organometallics* **2007,** *26*, 475-477.
77. Wu, X.; Daniliuc, C. G.; Hrib, C. G.; Tamm, M., *J. Organomet. Chem.* **2011,** *696*, 4147-4151.
78. Haberlag, B.; Freytag, M.; Jones, P. G.; Tamm, M., *Adv. Synth. Catal.* **2014,** *356*, 1255-1265.
79. Lysenko, S.; Haberlag, B.; Daniliuc, C. G.; Jones, P. G.; Tamm, M., *ChemCatChem* **2011,** *3*, 115-118.
80. Lysenko, S.; Volbeda, J.; Jones, P. G.; Tamm, M., *Angew. Chem., Int. Ed.* **2012,** *51*, 6757-6761.
81. Elser, I.; Groos, J.; Hauser, P. M.; Koy, M.; van der Ende, M.; Wang, D.; Frey, W.; Wurst, K.; Meisner, J.; Ziegler, F.; Kästner, J.; Buchmeiser, M. R., *Organometallics* **2019,** *38*, 4133-4146.
82. Hauser, P. M.; van der Ende, M.; Groos, J.; Frey, W.; Wang, D.; Buchmeiser, M. R., *Chem. Eur. J.* **2020,** *2020*, 3070-3082.
83. Atagi, L. M.; Critchlow, S. C.; Mayer, J. M., *J. Am. Chem. Soc.* **1992,** *114*, 9223-9224.
84. Atagi, L. M.; Mayer, J. M., *Organometallics* **1994,** *13*, 4794-4803.
85. Mayr, A., *Comments Inorg. Chem.* **1990,** *10* , 227-266.
86. H. Fischer, P. H., F. R. Kreißl, R. R. Schrock, U. Schubert und K. Weiss, Carbyne Complexes. *VCH, Weinheim* **1988**.

87. Geyer, A. M.; Gdula, R. L.; Wiedner, E. S.; Johnson, M. J. A., Catalytic Nitrile-Alkyne Cross-Metathesis. *J. Am. Chem. Soc.* **2007,** *129*, 3800-3801.
88. Geyer, A. M.; Wiedner, E. S.; Gary, J. B.; Gdula, R. L.; Kuhlmann, N. C.; Johnson, M. J. A.; Dunietz, B. D.; Kampf, J. W., *J. Am. Chem. Soc.* **2008,** *130*, 8984-8999.
89. Schrock, R. R.; Weinstock, I. A.; Horton, A. D.; Liu, A. H.; Schofield, M. H., *J. Am. Chem. Soc.* **1988,** *110*, 2686-2687.
90. Weinstock, I. A.; Schrock, R. R.; Davis, W. M., *J. Am. Chem. Soc.* **1991,** *113*, 135-144.
91. Bai, W.; Lee, K.-H.; Sung, H. H. Y.; Williams, I. D.; Lin, Z.; Jia, G., *Organometallics* **2016,** *35*, 3808-3815.
92. Bai, W.; Wei, W.; Sung, H. H. Y.; Williams, I. D.; Lin, Z.; Jia, G., *Organometallics* **2018,** *37*, 559-569.
93. Cui, M.; Bai, W.; Sung, H. H. Y.; Williams, I. D.; Jia, G., *J. Am. Chem. Soc.* **2020,** *142*, 13339-13344.
94. McCullough, L. G.; Schrock, R. R., *J. Am. Chem. Soc.* **1984,** *106*, 4067-4068.
95. McCullough, L. G.; Schrock, R. R.; Dewan, J. C.; Murdzek, J. C., *J. Am. Chem. Soc.* **1985,** *107*, 5987-5998.
96. Blackwell, J. M.; Figueroa, J. S.; Stephens, F. H.; Cummins, C. C., *Organometallics* **2003,** *22*, 3351-3353.
97. Tsai, Y.-C.; Diaconescu, P. L.; Cummins, C. C., *Organometallics* **2000,** *19*, 5260-5262.
98. Haberlag, B.; Freytag, M.; Daniliuc, C. G.; Jones, P. G.; Tamm, M., *Angew. Chem., Int. Ed*. **2012,** *51*, 13019-13022.
99. Estes, D. P.; Gordon, C. P.; Fedorov, A.; Liao, W.-C.; Ehrhorn, H.; Bittner, C.; Zier, M. L.; Bockfeld, D.; Chan, K. W.; Eisenstein, O.; Raynaud, C.; Tamm, M.; Copéret, C., *J. Am. Chem. Soc.* **2017,** *139*, 17597-17607.
100. Bittner, C.; Ehrhorn, H.; Bockfeld, D.; Brandhorst, K.; Tamm, M., *Organometallics* **2017,** *36*, 3398-3406.
101. Ehrhorn, H.; Bockfeld, D.; Freytag, M.; Bannenberg, T.; Kefalidis, C. E.; Maron, L.; Tamm, M., *Organometallics* **2019,** *38*, 1627-1639.
102. Fürstner, A.; Mathes, C.; Lehmann, C. W., *J. Am. Chem. Soc.* **1999,** *121*, 9453-9454.
103. Zhang, W., Lu, Y. and Moore, J. S., *Org. Synth.* **2007**, 163-176.
104. Cummins, C., *Chem. Commun.* **1998,** 1777-1786.
105. Fürstner, A.; Mathes, C.; Lehmann, C. W., *Chem. Eur. J.* **2001,** *7*, 5299-5317.
106. Zhang, W.; Kraft, S.; Moore, J. S., *Chem. Commun.* **2003,** 832-833.
107. Zhang, W.; Kraft, S.; Moore, J. S., *J. Am. Chem. Soc.* **2004,** *126*, 329-335.
108. Fürstner, A.; Davies, P. W., *Chem. Commun.* **2005,** 2307-2320.
109. Gdula, R. L.; Johnson, M. J. A.; Ockwig, N. W., *Inorg. Chem* **2005,** *44*, 9140-9142.
110. Gdula, R. L.; Johnson, M. J. A., *J. Am. Chem. Soc.* **2006,** *128*, 9614-9615.
111. Wiedner, E. S.; Gallagher, K. J.; Johnson, M. J. A.; Kampf, J. W., *Inorg. Chem* **2011,** *50*, 5936-5945.
112. Bindl, M.; Stade, R.; Heilmann, E. K.; Picot, A.; Goddard, R.; Fürstner, A., *J. Am. Chem. Soc.* **2009,** *131*, 9468-9470.
113. Heppekausen, J.; Stade, R.; Kondoh, A.; Seidel, G.; Goddard, R.; Fürstner, A., *Chem. Eur. J.* **2012,** *18*, 10281-10299.
114. Krempner, C., *Chem. Eur. J.* **2011,** *2011*, 1689-1698.
115. Mayer, J. M., *Polyhedron* **1995,** *14*, 3273-3292.
116. Chisholm, M. H.; Folting, K.; Huffman, J. C.; Kirkpatrick, C. C., *Inorg. Chem* **1984,** *23*, 1021-1037.
117. Valot, G.; Regens, C. S.; O'Malley, D. P.; Godineau, E.; Takikawa, H.; Fürstner, A., *Angew. Chem., Int. Ed.* **2013,** *52*, 9534-9538.
118. Valot, G.; Mailhol, D.; Regens, C. S.; O'Malley, D. P.; Godineau, E.; Takikawa, H.; Philipps, P.; Fürstner, A., *Chem. Eur. J.* **2015,** *21* (6), 2398-2408.
119. Jyothish, K.; Zhang, W., *Angew. Chem., Int. Ed.* **2011,** *123*, 3497-3500.
120. Paley, D. W.; Sedbrook, D. F.; Decatur, J.; Fischer, F. R.; Steigerwald, M. L.; Nuckolls, C., *Angew. Chem., Int. Ed.* **2013,** *52*, 4591-4594.

121. Jyothish, K.; Wang, Q.; Zhang, W., *Adv. Synth. Catal.* **2012,** *354*, 2073-2078.
122. Yang, H.; Liu, Z.; Zhang, W., *Adv. Synth. Catal.* **2013,** *355*, 885-890.
123. Schaubach, S.; Gebauer, K.; Ungeheuer, F.; Hoffmeister, L.; Ilg, M. K.; Wirtz, C.; Fürstner, A., *Chem. Eur. J.* **2016,** *22*, 8494-8507.
124. Fürstner, A.; Seidel, G., *Angew. Chem., Int. Ed.* **1998,** *37*, 1734-1736.
125. Fürstner, A.; Guth, O.; Rumbo, A.; Seidel, G., *J. Am. Chem. Soc.* **1999,** *121*, 11108-11113.
126. Lacombe, F.; Radkowski, K.; Seidel, G.; Fürstner, A., *Tetrahedron* **2004,** *60*, 7315-7324.
127. Chuprun, S.; Acosta, C. M.; Mathivathanan, L.; Bukhryakov, K. V., *Organometallics* **2020,** *39*, 3453-3457.
128. Benson, S.; Collin, M.-P.; Arlt, A.; Gabor, B.; Goddard, R.; Fürstner, A., *Angew. Chem., Int. Ed.* **2011,** *50*, 8739-8744.
129. Valot, G.; Regens, C. S.; O'Malley, D. P.; Godineau, E.; Takikawa, H.; Fürstner, A., *Angew. Chem., Int. Ed.* **2013,** *52*, 9534-9538.
130. Ahlers, A.; de Haro, T.; Gabor, B.; Fürstner, A., *Angew. Chem., Int. Ed.* **2016,** *55*, 1406-1411.
131. Karier, P.; Ungeheuer, F.; Ahlers, A.; Anderl, F.; Wille, C.; Fürstner, A., *Angew. Chem., Int. Ed*. **2019,** *58*, 248-253.
132. Rummelt, S. M.; Preindl, J.; Sommer, H.; Fürstner, A., *Angew. Chem., Int. Ed.* **2015,** *54*, 6241-6245.
133. McCullough, L. G.; Listemann, M. L.; Schrock, R. R.; Churchill, M. R.; Ziller, J. W., *J. Am. Chem. Soc.* **1983,** *105*, 6729-6730.
134. Freudenberger, J. H.; Schrock, R. R., *Organometallics* **1986,** *5*, 1411-1417.
135. Bray, A.; Mortreux, A.; Petit, F.; Petit, M.; Szymanska-Buzar, T., *J. Chem. Soc., Chem. Commun.* **1993,** 197-199.
136. Chisholm, M. H.; Folting, K.; Hoffman, D. M.; Huffman, J. C., *J. Am. Chem. Soc.* **1984,** *106*, 6794-6805.
137. Chisholm, M. H., *Acc. Chem. Res.* **1990,** *23*, 419-425.
138. Chisholm, M. H.; Folting, K.; Huffman, J. C.; Rothwell, I. P., *J. Am. Chem. Soc.* **1982,** *104*, 4389-4399.
139. Coutelier, O.; Mortreux, A., *Adv. Synth. Catal.* **2006,** *348*, 2038-2042.
140. Coutelier, O.; Nowogrocki, G.; Paul, J.-F.; Mortreux, A., *Adv. Synth. Catal.* **2007,** *349*, 2259-2263.
141. Lhermet, R.; Fürstner, A., *Chem. Eur. J.* **2014,** *20*, 13188-13193.
142. Tsui, E. Y.; Day, M. W.; Agapie, T., *Angew. Chem., Int. Ed.* **2011,** *50*, 1668-1672.
143. Feng, X.; Wu, J.; Enkelmann, V.; Müllen, K., *Org. Lett.* **2006,** *8*, 1145-1148.
144. Burés, J., *Angew. Chem., Int. Ed.* **2016,** *55*, 2028-2031.
145. Hillenbrand, J.; Leutzsch, M.; Fürstner, A., *Angew. Chem., Int. Ed.* **2019,** *58*, 15690-15696.
146. Evans, R.; Dal Poggetto, G.; Nilsson, M.; Morris, G. A., *Anal. Chem.* **2018,** *90*, 3987-3994.
147. Bart, S. C.; Heinemann, F. W.; Anthon, C.; Hauser, C.; Meyer, K., *Inorg. Chem* **2009,** *48*, 9419-9426.
148. La Pierre, H. S.; Kameo, H.; Halter, D. P.; Heinemann, F. W.; Meyer, K., *Angew. Chem., Int. Ed.* **2014,** *53*, 7154-7157.
149. Manoso, A. S.; Ahn, C.; Soheili, A.; Handy, C. J.; Correia, R.; Seganish, W. M.; DeShong, P., *J. Org. Chem.* **2004,** *69* , 8305-8314.
150. Heppekausen, J., PhD Thesis, TU Dortmund **2012**.
151. Babadzhanova, L. A.; Kirij, N. V.; Yagupolskii, Y. L.; Tyrra, W.; Naumann, D., *Tetrahedron* **2005,** *61*, 1813-1819.
152. Petrov, V. A., *Synthesis* **2002,** *2002*, 2225-2231.
153. Takahashi, O.; Furuhashi, K.; Fukumasa, M.; Hirai, T., *Tetrahedron Lett.* **1990,** *31*, 7031-7034.
154. Auris, S., Final Report. **2019**.
155. Malito, J., Molybdenum-95 NMR Spectroscopy. In *Annual Reports on NMR Spectroscopy*, Webb, G. A., Ed. Academic Press: **1996**, 33, 151-206.
156. Mann, B. E., The Cinderella Nuclei. In *Annual Reports on NMR Spectroscopy*, Webb, G. A., Ed. Academic Press: **1991**, 23, 141-207.
157. Young, C. G.; Kober, E. M.; Enemark, J. H., *Polyhedron* **1987,** *6*, 255-259.

158. Gordon, C. P.; Raynaud, C.; Andersen, R. A.; Copéret, C.; Eisenstein, O., *Acc. Chem. Res.* **2019,** *52*, 2278-2289.
159. Thompson, R. R.; Rotella, M. E.; Du, P.; Zhou, X.; Fronczek, F. R.; Kumar, R.; Gutierrez, O.; Lee, S., *Organometallics* **2019,** *38*, 4054-4059.
160. Suresh, C. H.; Frenking, G., *Organometallics* **2010,** *29*, 4766-4769.
161. Meng, Z.; Fürstner, A., *J. Am. Chem. Soc.* **2019,** *141*, 805-809.
162. Fürstner, A.; Flügge, S.; Larionov, O.; Takahashi, Y.; Kubota, T.; Kobayashi, J. i., *Chem. Eur. J.* **2009,** *15*, 4011-4029.
163. Bukhryakov, K. V.; Schrock, R. R.; Hoveyda, A. H.; Tsay, C.; Müller, P., *J. Am. Chem. Soc.* **2018,** *140*, 2797-2800.
164. Zhai, F.; Bukhryakov, K. V.; Schrock, R. R.; Hoveyda, A. H.; Tsay, C.; Müller, P., *J. Am. Chem. Soc.* **2018,** *140*, 13609-13613.
165. Chen, P.; Zhang, L.; Xue, Z.-L.; Wu, Y.-D.; Zhang, X., *Inorg. Chem* **2017,** *56*, 7111-7119.
166. Ondi, L.; Nagy, G. M.; Czirok, J. B.; Bucsai, A.; Frater, G. E., *Org. Process Res. Dev.* **2016,** *20*, 1709-1716.
167. Lackner, A. D.; Fürstner, A., *Angew. Chem., Int. Ed.* **2015,** *127*, 13005-13009.
168. Feinstein-Jaffe, I.; Gibson, D.; Lippard, S. J.; Schrock, R. R.; Spool, A., *J. Am. Chem. Soc.* **1984,** *106*, 6305-6310.
169. Rocklage, S. M.; Schrock, R. R.; Churchill, M. R.; Wasserman, H. J., *Organometallics* **1982,** *1*, 1332-1338.
170. Zhai, F.; Schrock, R. R.; Hoveyda, A. H.; Müller, P., *Organometallics* **2020,** *39*, 2486-2492.
171. Kress, J. R. M.; Russell, M. J. M.; Wesolek, M. G.; Osborn, J. A., *J. Chem. Soc., Chem. Commun.* **1980,** 431-432.
172. Kress, J.; Wesolek, M.; Le Ny, J.-P.; Osborn, J. A., *Chem. Commun.* **1981,** 1039-1040.
173. Zhang, C.; Schlemper, E. O.; Schrauzer, G. N., *Organometallics* **1990,** *9*, 1016-1020.
174. Lehtonen, A.; Sillanpää, R., *Organometallics* **2005,** *24*, 2795-2800.
175. Rosenfeld, D. C.; Kuiper, D. S.; Lobkovsky, E. B.; Wolczanski, P. T., *Polyhedron* **2006,** *25*, 251-258.
176. Sun, J., Simpson, C.K., Hopkins, M.D., Hock, A.S. and Schrock, R.R., *Inorg. Synth.* **2014**, 36, 134-138.
177. Iggo, J. A.; Liu, J.; Overend, G., In *Annual Reports on NMR Spectroscopy*, Webb, G. A., Ed. Academic Press **2008**, 63, 179-262.
178. Benn, R.; Brenneke, H.; Heck, J.; Rufinska, A., *Inorg. Chem* **1987,** *26*, 2826-2829.
179. Wiberg, K. B.; Hammer, J. D.; Zilm, K. W.; Cheeseman, J. R., *J. Org. Chem.* **1999,** *64*, 6394-6400.
180. Han, X.; Wang, L.; Li, J.; Zhan, X.; Chen, J.; Yang, J., *Appl. Surf. Sci.* **2011,** *257*, 9525-9531.
181. Fürstner, A.; Mathes, C.; Grela, K., *Chem. Commun.* **2001,** 1057-1059.
182. Dilworth, J. R.; Richards, R. L.; Chen, G. J. J.; Mcdonald, J. W., *Inorg. Synth.* **1980**, 20, 119.
183. Chan, D. M. T.; Chisholm, M. H.; Folting, K.; Huffman, J. C.; Marchant, N. S., *Inorg. Chem* **1986,** *25*, 4170-4174.
184. Hampden-Smith, M. J.; Wark, T. A.; Rheingold, A.; Huffman, J. C., *Can. J. Chem.* **1991,** *69*, 121-129.
185. Guo, Q.; Miyaji, T.; Hara, R.; Shen, B.; Takahashi, T., *Tetrahedron* **2002,** *58*, 7327-7334.
186. Poli, R.; Mui, H. D., *J. Am. Chem. Soc.* **1990,** *112*, 2446-2448.
187. Hillenbrand, J.; van Gastel, M.; Bill, E.; Neese, F.; Fürstner, A., *J. Am. Chem. Soc.* **2020,** *142*, 16392-16402.
188. Seisenbaeva, G. A.; Kloo, L.; Werndrup, P.; Kessler, V. G., *Inorg. Chem* **2001,** *40*, 3815-3818.
189. Stoffelbach, F.; Saurenz, D.; Poli, R., *Chem. Eur. J.* **2001,** *2001*, 2699-2703.
190. Broderick, E. M., Browne, S. C., Johnson, M. J., Hitt, T. A. and Girolami, *Org. Synth.* **2014,** *36*, 2014.
191. Chisholm, M. H.; Reichert, W. W.; Thornton, P., *J. Am. Chem. Soc.* **1978,** *100*, 2744-2748.
192. Chisholm, M. H.; Cotton, F. A.; Extine, M. W.; Reichert, W. W., *Inorg. Chem* **1978,** *17*, 2944-2946.
193. Chisholm, M. H.; Huffman, J. C.; Marchant, N. L., *J. Am. Chem. Soc.* **1983,** *105*, 6162-6163.

194. Vitzthumecker, C.; Robinson, F.; Pfitzner, A., *Monatshefte für Chemie - Chemical Monthly* **2017,** *148*, 629-633.
195. Cotton, F. A.; Su, J., *Inorg. Chim. Acta* **1996,** *251*, 101-104.
196. Minelli, M.; Young, C. G.; Enemark, J. H., *Inorg. Chem* **1985,** *24*, 1111-1113.
197. Chisholm, M. H.; Hoffman, D. M.; Huffman, J. C., *Chem. Soc. Rev.* **1985,** *14*, 69-91.
198. Strutz, H.; Schrock, R. R., *Organometallics* **1984,** *3*, 1600-1601.
199. Mercer, M.; Crabtree, R. H.; Richards, R. L., *J. Chem. Soc., Chem. Commun.* **1973,** 808-809.
200. Tsai, Y.-C.; Stephens, F. H.; Meyer, K.; Mendiratta, A.; Gheorghiu, M. D.; Cummins, C. C., *Organometallics* **2003,** *22*, 2902-2913.
201. Tsai, Y.-C.; Johnson, M. J. A.; Mindiola, D. J.; Cummins, C. C.; Klooster, W. T.; Koetzle, T. F., *J. Am. Chem. Soc.* **1999,** *121*, 10426-10427.
202. Laplaza, C. E.; Johnson, A. R.; Cummins, C. C., *J. Am. Chem. Soc.* **1996,** *118*, 709-710.
203. Lee, S.; Yang, A.; Moneypenny, T. P.; Moore, J. S., *J. Am. Chem. Soc.* **2016,** *138*, 2182-2185.
204. Cummins, C. C.; Schrock, R. R.; Davis, W. M., *Inorg. Chem* **1994,** *33*, 1448-1457.
205. Schrock, R. R.; Seidel, S. W.; Mösch-Zanetti, N. C.; Shih, K.-Y.; O'Donoghue, M. B.; Davis, W. M.; Reiff, W. M., *J. Am. Chem. Soc.* **1997,** *119*, 11876-11893.
206. Debata, N. B.; Tripathy, D.; Chand, D. K., *Coord. Chem. Rev.* **2012,** *256*, 1831-1945.
207. Ronson, T. K.; Nowell, H.; Westcott, A.; Hardie, M. J., *Chem. Commun.* **2011,** *47*, 176-178.
208. Deb, S. K.; Maddux, T. M.; Yu, L., *J. Am. Chem. Soc.* **1997,** *119*, 9079-9080.
209. Liu, P.; Chen, Y.; Deng, J.; Tu, Y., *Synthesis* **2001,** *2001*, 2078-2080.
210. Vargas-Rodriguez, Y.; Vargas, M.; Ruvalcaba, R.; Francisco, B.; Noguez, O.; Morales-Serna, J.; Salmón, M., *Org. Commun.* **2012,** *5*.
211. Roche, C.; Sun, H.-J.; Prendergast, M. E.; Leowanawat, P.; Partridge, B. E.; Heiney, P. A.; Araoka, F.; Graf, R.; Spiess, H. W.; Zeng, X.; Ungar, G.; Percec, V., *J. Am. Chem. Soc.* **2014,** *136*, 7169-7185.
212. Zhang, Q.; Tiefenbacher, K., *Nature Chemistry* **2015,** *7*, 197-202.
213. Nemat, S. J.; Jędrzejewska, H.; Prescimone, A.; Szumna, A.; Tiefenbacher, K., *Org. Lett.* **2020,** *22*, 5506-5510.
214. Hawkins, V. F.; Wilkinson, M. C.; Whiting, M., *Org. Process Res. Dev.* **2008,** *12*, 1265-1268.
215. Chisholm, M. H.; Folting, K.; Haubrich, S. T.; Martin, J. D., *Inorg. Chim. Acta* **1993,** *213*, 17-24.
216. Cole, S. C.; Coles, M. P.; Hitchcock, P. B., *J. Chem. Soc., Dalton Trans.* **2002,** 4168-4174.
217. Nasr, A.; Breuil, P.-A. R.; Silva, D. C.; Berthod, M.; Dellus, N.; Jeanneau, E.; Lemaire, M.; Olivier-Bourbigou, H., *Organometallics* **2013,** *32*, 5320-5325.
218. Hou, Q.; Liu, L.; Mellerup, S. K.; Wang, N.; Peng, T.; Chen, P.; Wang, S., *Org. Lett.* **2018,** *20*, 6467-6470.
219. Richard, J.; Birepinte, M.; Charbonnier, J. B.; Liautard, V.; Pinet, S.; Pucheault, M., *Synthesis* **2017,** *49*, 736-744.
220. Xu, S.; Haeffner, F.; Li, B.; Zakharov, L. N.; Liu, S.-Y., *Angew. Chem., Int. Ed.* **2014,** *53*, 6795-6799.
221. Saito, M.; Matsumoto, K.; Fujita, M.; Minoura, M., *Heteroat. Chem* **2014,** *25*, 354-360.
222. Argent, S. P.; Tarassova, I.; Greenaway, A.; Nowell, H.; Barnett, S. A.; Warren, M. R.; Tang, C. C.; Morris, C. G.; Lewis, W.; Champness, N. R.; Schröder, M.; Blake, A. J., *Polyhedron* **2016,** *120*, 18-29.
223. Trawny, D.; Quennet, M.; Rades, N.; Lentz, D.; Paulus, B.; Reissig, H.-U., *Eur. J. Org. Chem.* **2015,** *2015*, 4667-4674.
224. Harris Robin, K.; Becker Edwin, D.; Cabral de Menezes Sonia, M.; Granger, P.; Hoffman Roy, E.; Zilm Kurt, W., *Pure Appl. Chem.* **2008**, 80, 59.
225. Saha, A.; Wu, C.-M.; Peng, R.; Koodali, R.; Banerjee, S., *Eur. J. Org. Chem.* **2019,** *2019*, 104-111.
226. Jarupatrakorn, J.; Coles, M. P.; Tilley, T. D., *Chem. Mater.* **2005,** *17*, 1818-1828.
227. Jin, G.; Zhang, X.; Cao, S., *Org. Lett.* **2013,** *15*, 3114-3117.
228. Ulysse, L. G.; Chmielewski, J., *Bioorg. Med. Chem. Lett.* **1998,** *8*, 3281-3286.
229. Obando, D.; Koda, Y.; Pantarat, N.; Lev, S.; Zuo, X.; Bijosono Oei, J.; Widmer, F.; Djordjevic, J. T.; Sorrell, T. C.; Jolliffe, K. A., *ChemMedChem* **2018,** *13*, 1421-1436.